

University of Warwick institutional repository: <http://go.warwick.ac.uk/wrap>

A Thesis Submitted for the Degree of PhD at the University of Warwick

<http://go.warwick.ac.uk/wrap/58920>

This thesis is made available online and is protected by original copyright.

Please scroll down to view the document itself.

Please refer to the repository record for this item for information to help you to cite it. Our policy information is available from the repository home page.

Novel Strategies in the Synthesis of Functional Glycopolymers

Qiang Zhang

**A thesis submitted in partial fulfilment of the requirements for the
degree of**

Doctor of Philosophy in Chemistry.

Department of Chemistry



July 2013

The most important of my discoveries have been suggested to me by my failures.

Humphry Davy

If you wish to succeed, you should use persistence as your good friend, experience as your reference, prudence as your brother and hopes as your sentry.

Thomas Alva Edison

You should pick up apples at the bottom first and leave others to climb the ladder.

David M Haddleton

Table of Contents

Table of Contents	i
List of Figures	vi
List of Schemes	xviii
List of Tables	xxii
Abbreviations	xxiv
Acknowledgements	xxvii
Declaration	xxviii
Abstract	xxix
Chapter 1 Introduction	1
1.1 Novel strategies in the direct polymerization of glycomonomers	1
1.1.1 Ring-opening polymerization	1
1.1.2 Copper mediated living radical polymerization	2
1.1.3 Reversible addition-fragmentation chain transfer (RAFT) polymerization	6
1.2 Novel strategies in the post-glycosylation of pre-formed polymers	8
1.2.1 Copper-catalyzed azide-alkyne cycloaddition (CuAAC) reaction	8
1.2.2 Thiol-click chemistry	10
1.2.3 Amine chemistry	11
1.3 Novel applications of glycopolymers	13
1.3.1 Therapeutic application: Anti-cancer and Anti-HIV	13
1.3.2 Bio-compatible materials	15
1.4 Conclusion	16
Chapter 2 Terminal functional glycopolymers <i>via</i> a combination of catalytic chain transfer polymerisation (CCTP) followed by three consecutive click reactions	17
2.1 Introduction	18
2.2 Results and discussion	19
2.2.1 Synthesis of alkyne functionalised sugar <i>via</i> Fischer glycosylation	19
2.2.2 Thiol-ene Michael addition reaction of thiol with vinyl terminal CCTP polymers	23
2.2.3 Epoxy ring opening reactions of PGMA with sodium azide	29
2.2.4 CuAAC reactions of azide-containing polymers with alkyne compounds	32
2.2.5 Conclusions	36
2.3 Experimental	36
2.3.1 Materials	36
2.3.2 Instruments and analysis	37

2.3.3 Synthesis of alkyne functionalised sugar <i>via</i> Fischer glycosylation	37
2.3.4 Michael addition reactions of glycidyl methacrylate and PGMA with thiols	42
2.3.5 Epoxy ring opening reaction of PGMA with sodium azide	42
2.3.6 CuAAC reactions of azide-containing polymers with alkyne compounds	42
Chapter 3 Sequence-Controlled Multi-Block Glycopolymers to Inhibit DC-SIGN-gp120 Binding.....	43
3.1 Introduction.....	44
3.2 Results and discussion	46
3.2.1 Synthesis of glycomonomers via CuAAC click reaction.....	46
3.2.2 Homopolymerization of glycomonomers by SET-LRP in DMSO at ambient temperature	47
3.2.3 Synthesis of multiblock glycopolymers <i>via</i> iterative monomer addition by SET-LRP	49
3.2.4 Control of sugar sequence in glycopolymers <i>via</i> iterative monomer addition before full conversion by SET-LRP.....	55
3.2.5 Chain end group functionalization of multiblock glycopolymer by CuAAC	61
3.2.6 Interactions between glycopolymers and DC-SIGN.....	63
3.2.7 Conclusion	68
3.3 Experimental	69
3.3.1 Materials	69
3.3.2 Instruments and analysis	69
3.3.3 Synthesis of 3-azidopropyl acrylate	71
3.3.4 Synthesis of D-glucose glycomonomer via CuAAC	72
3.3.5 Synthesis of D-Mannose Glycomonomer via CuAAC	73
3.3.6 Synthesis of L-Fucose Glycomonomer via CuAAC.....	74
3.3.7 Homopolymerization of D-glucose acrylate glycomonomer via SET-LRP	75
3.3.8 Synthesis of multiblock glycopolymer by iterative addition of glyco monomers after full conversion polymerization.....	76
3.3.9 Synthesis of multiblock glycopolymer by controlled addition of glyco monomers	77
3.3.10 Multiblock copolymerization of DEGEEA and mannose glycomonomer <i>via</i> SET-LRP	78
3.3.11 Multiblock copolymerization of DEGEEA and glucose glycomonomer via SET-LRP	80
3.3.12 Homopolymerization of mannose acrylate glycomonomer via SET-LRP.....	84
3.3.13 Statistical copolymerization of DEGEEA and mannose glycomonomer <i>via</i> SET-LRP	85
3.3.14 Terminal end group modification.....	86

Chapter 4 High-affinity cyclodextrin-based glycoconjugates for HIV-therapeutic and drug delivery	87
4.1 Introduction	88
4.2 Results and Discussion	89
4.2.1 Synthesis and characterization of glycoclusters	89
4.2.2 Synthesis of CD-based initiators and glyco monomers for SET-LRP	92
4.2.3 Synthesis of CD-based glycocluster-smart star polymer hybrids via combination of ATRP and CuAAC	95
4.2.4 Synthesis of cyclodextrin-based star glycopolymers	102
4.2.5 Synthesis of cyclodextrin-based diblock glycopolymers	106
4.2.6 SPR binding test of CD-based glycoconjugates with DC-SIGN	108
4.2.7 Encapsulation ability of the CD-based glycoconjugates	113
4.2.8 Conclusion	117
4.3 Experimental	117
4.3.1 Materials	117
4.3.2 Instruments and analysis	118
4.3.3 Synthesis of <i>Heptkis</i> (6-deoxy-6-bromine)- β -cyclodextrin (β -CD-(Br) ₇)	119
4.3.4 Synthesis of <i>Heptkis</i> -(6-deoxy-6-azido)- β -cyclodextrin (β -CD-(N ₃) ₇)	120
4.3.5 Synthesis of <i>Hepkis</i> -(2, 3, 6-tri-O-(2-bromo-2-methylpropionyl))- β -cyclodextrin (β -CD-(Br) ₁₆)	121
4.3.6 Synthesis of <i>Heptkis</i> -(2, 3-di-O-(2-bromo-2-methylpropionyl)-6-azido)- β -cyclodextrin ((N ₃) ₇ - β -CD-(Br) ₁₀)	122
4.3.7 Synthesis of persubstituted cyclodextrin-based mannose glycocluster via CuAAC (β -CD-(Man) ₇)	123
4.3.8 Synthesis of persubstituted cyclodextrin-based fucose glycocluster via CuAAC (β -CD-(Fuc) ₇)	124
4.3.9 Synthesis of cyclodextrin-based mannose cluster-star PNIPAM hybrid <i>via</i> combination of ATRP and CuAAC	125
4.3.10 Synthesis of cyclodextrin-based mannose cluster-star PDEGMEMMA hybrid <i>via</i> combination of ATRP and CuAAC	127
4.3.11 Cyclodextrin-based star glycopolymers <i>via</i> SET-LRP and chain extension ability test	130
4.3.12 Synthesis of cyclodextrin-centred star mannose glycopolymers (β -CD-[(Mannose) ₂] ₁₆ , β -CD-[(Mannose) ₅] ₁₆ , β -CD-[(Mannose) ₁₀] ₁₆)	131
4.3.13 Synthesis of cyclodextrin-based star diblock mannose glycopolymer (β -CD-[(DEGEEA) ₁₀ - <i>b</i> -(Mannose) ₅] ₁₆)	133
4.3.14 Drug encapsulation ability of the cyclodextrin-based glycoconjugates	134
Chapter 5 Aqueous Copper Mediated Living Polymerization: Exploiting Rapid Disproportionation of CuBr with Me ₆ TREN	135

5.1 Introduction.....	136
5.2 Results and discussion	139
5.2.1 Disproportionation of Cu(I)X (X = Br, Cl) / <i>N</i> -ligand complexes in water.....	139
5.2.2 Synthesis of PNIPAM by ATRP in water.....	144
5.2.3 Cu(0) wire mediated SET-LRP of NIPAM and PEGA ₄₈₀ in water.....	147
5.2.4 Generation of Cu(0) powder and CuBr ₂ <i>via</i> disproportionation of CuBr/Me ₆ TREN in water for SET-LRP of NIPAM under apparent ATRP conditions.	149
5.2.5 Synthesis of PNIPAM by AGET ATRP in water.	152
5.2.6 Synthesis of PNIPAM with varying DP by SET-LRP in water.....	157
5.2.7 Chain end fidelity and chain extension of PNIPAM by SET-LRP in water.	163
5.2.8 Multiblock copolymers by SET-LRP in water.....	174
5.2.9 SET-LRP in PBS buffer, ethanol/water (Tequila) and sheep blood serum.....	178
5.2.10 SET-LRP of hydrophilic monomers mediated by <i>prior</i> disproportionation of CuBr/Me ₆ TREN in pure water.....	184
5.2.11 Synthesis of double hydrophilic diblock glycopolymers via aqueous SET-LRP.	185
5.2.12 Exploration of ligand and solvent effect on the in-situ SET-LRP.	194
5.2.13 Conclusion	198
5.3 Experimental	199
5.3.1 Materials	199
5.3.2 Instruments and analysis	200
5.3.3 Disproportionation of CuBr / Me ₆ TREN into Cu (0) and CuBr ₂ in H ₂ O	201
5.3.4 Disproportionation test of the CuBr / <i>N</i> -ethyl-2-pyridylmethanimine complex in H ₂ O	203
5.3.5 Atom transfer radical polymerization of NIPAM in H ₂ O at ambient temperature	203
5.3.6 Atom transfer radical polymerization of NIPAM in H ₂ O at 0 °C.....	204
5.3.7 SET-LRP of NIPAM in H ₂ O at 0 °C <i>via</i> disproportionation of CuBr / Me ₆ TREN	205
5.3.8 Copper (0) wire mediated SET-LRP of NIPAM and PEGA ₄₈₀ in H ₂ O at ambient temperature	206
5.3.9 Test polymerizations of NIPAM in H ₂ O at ambient temperature <i>via</i> separated copper(0) powder and CuBr ₂ /Me ₆ TREN solution from disproportionation of CuBr/Me ₆ TREN.....	207
5.3.10 SET-LRP of NIPAM (DP=20) in H ₂ O at ambient temperature <i>via</i> disproportionation of CuBr / Me ₆ TREN	209
5.3.11 SET-LRP of NIPAM (DP=8) in H ₂ O at 0 °C and ambient temperature <i>via</i> disproportionation of CuBr/Me ₆ TREN	210

5.3.12 SET-LRP of NIPAM (DP=40) in H ₂ O at ambient temperature <i>via</i> disproportionation of CuBr / Me ₆ TREN	211
5.3.13 SET-LRP of NIPAM (DP = 80) in H ₂ O at different ratios of CuBr / Me ₆ TREN under ambient temperature.....	211
5.3.14 SET-LRP of NIPAM (DP = 160) in H ₂ O at different ratios of CuBr / Me ₆ TREN under ambient temperature and 0 °C.....	212
5.3.15 SET-LRP of NIPAM (DP = 320) <i>via</i> disproportionation of CuBr / Me ₆ TREN in H ₂ O at 0 °C.	214
5.3.16 Chain extension reaction for SET-LRP of NIPAM in H ₂ O at ambient temperature.	214
5.3.17 Chain extension reaction for SET-LRP of NIPAM in H ₂ O at 0 °C.	215
5.3.18 Synthesis of diblock copolymer by SET-LRP in H ₂ O.	217
5.3.19 Synthesis of tri-block copolymer by iterative SET-LRP in H ₂ O.	218
5.3.20 Synthesis of PNIPAM by AGET ATRP in H ₂ O under ambient temperature.	219
5.3.21 Reduction of CuBr ₂ by L-ascorbic acid into CuBr following disproportionation into Cu (0) & CuBr ₂ for SET-LRP of NIPAM in H ₂ O under ambient temperature.	220
5.3.22 SET-LRP of NIPAM (DP=80) <i>via</i> disproportionation of CuBr/Me ₆ TREN in Tequila at 0 °C.	223
5.3.23 SET-LRP of NIPAM <i>via</i> disproportionation of CuBr/Me ₆ TREN in PBS buffer (pH=6.2 & 6.8) at 0 °C.....	224
5.3.24 SET-LRP of NIPAM in sheep serum at 0 °C <i>via</i> disproportionation of CuBr/Me ₆ TREN.....	224
5.3.25 SET-LRP of DMA in sheep serum at 0 °C <i>via</i> disproportionation of CuBr / Me ₆ TREN	225
5.3.26 Synthesis of poly (NIPAM) ₈₀ - <i>b</i> - (DMA) ₈₀ by SET-LRP in sheep serum	226
5.3.27 Synthesis of poly (DMA) ₈₀ - <i>b</i> - (NIPAM) ₈₀ by SET-LRP in sheep serum	227
5.3.28 Aqueous SET-LRP of D-Mannose acrylate glycomonomer at 0 °C <i>via</i> disproportionation of CuBr / Me ₆ TREN	228
5.3.29 Copper(0) wire mediated SET-LRP of D-mannose glycomonomer in H ₂ O.....	229
5.3.30 Aqueous SET-LRP of DEGEAA at 0 °C <i>via</i> disproportionation of CuBr / Me ₆ TREN	229
5.3.31 Synthesis of poly (Mannose) ₁₀ - <i>b</i> - (NIPAM) ₈₀ by aqueous SET-LRP.....	230
5.3.32 Synthesis of poly (Mannose) ₁₀ - <i>b</i> - (DEGEAA) ₈₀ by aqueous SET-LRP.....	231
5.3.33 Optical microscopy characterization of Cu (0) powders from the disproportionation of CuBr / Me ₆ TREN in water and ethanol.....	232
5.3.34 SET-LRP of NIPAM <i>via</i> disproportionation of CuBr / PMDETA or TREN in pure water.....	233
Chapter 6 Overview and Prospect.....	234
Chapter 7 References	236

List of Figures

Figure 1.1 Synthesis of glyco-poly(2-oxazoline)s by ring-opening polymerization.	2
Figure 1.2 Reversible and dynamic equilibrium between active radical growing species and dormant species.....	2
Figure 1.3 Synthesis of glycopolymers via CuAAC of azide sugar with alkyne functional polymer or monomer.....	8
Figure 1.4. Synthesis of glycopolymers via CuAAC of alkyne sugar with azido functional insulin.....	9
Figure 1.5. Synthesis of glycopolymers via simultaneous ATRP and CuAAC using azido monomer and alkyne sugars.....	9
Figure 1.6. Synthesis of glycopolymers via thiol-alkyne click reaction.	10
Figure 1.7. <i>Synthesis of glycopolymers via thiol-halogen click reaction</i>	10
Figure 1.8. Synthesis of glycopolymers by the reaction of ketones with aminooxy sugars. ...	11
Figure 1.9. Synthesis of glycopolymers by reaction of free reducing sugar with hydrazide functional polymer.	11
Figure 1.10. Synthesis of glycopolymers by reaction of poly(pentafluorophenyl methacrylate) with functional amines.	12
Figure 1.11. Synthesis of glycopolymers by reaction of polymers bearing reactive p-nitrophenyl carbonate with amine functional sugar.	12
Figure 1.12. Synthesis of glycopolymers by reaction of poly(azlactone) with amine functional sugar.....	12
Figure 1.13. Synthesis of glycopolymer-dithiocarbamates gold conjugates.....	13
Figure 1.14. Multicopy Multivalent' glycopolymer-stabilized gold nanoparticles as potential synthetic cancer vaccines. ⁵⁹	13
Figure 1.15. High-affinity glycopolymer binding to human-DC-SIGN and disruption of DC-SIGN interactions with gp120. ⁸¹	14
Figure 1.16. Synthesis of hyperbranched glycopolymers via RAFT. ⁵⁴	15
Figure 1.17. Ricin decontamination using biotin-tagged lactose polymer. ⁸²	15
Figure 2. 1. ¹ H NMR (top), ¹³ C NMR (middle) and FT-IR (bottom) spectra of 1-(2'-Propargyl) D-Mannose.....	21
Figure 2. 2. ¹ H NMR (top, middle) and FT-IR (bottom) spectra of 2, 3, 4, 6-tetra- <i>O</i> -acetyl-1-(2'-propargyl)- α -D-mannose and 2, 3, 4, 6-tetra- <i>O</i> -acetyl-1-(2'-propargyl)- β -D-mannose.....	22
Figure 2. 3. Evolution of the ¹ H NMR spectra with time in the reaction of glycidyl methacrylate with benzyl mercaptan (3 equiv) in DMSO- <i>d</i> ₆ at 25 °C. The numbering of the	

typical hydrogen atoms used for the NMR peak assignment is shown in the reaction scheme.	24
Figure 2. 4. ^1H NMR spectra of PGMA 1 (top), benzyl end-functionalised polymer 3 (middle) and ^{13}C NMR spectrum of benzyl end-functionalised polymer 3 (bottom) in $\text{DMSO}-d_6$.	25
Figure 2. 5. FT-IR spectra of CCTP PGMA 1, benzyl end-functionalised polymer 3, azide functionalised polymer 6 and fucose functionalised glycopolymer 12.	26
Figure 2. 6. DMF SEC traces (RI detector) of CCTP PGMA 1, benzyl end-functionalised polymer 3, azide functionalised polymer 6 and fucose functionalised glycopolymer 12.	26
Figure 2. 7. MALDI-ToF MS analysis of CCTP PGMA 1(top), and benzyl end-functionalised polymer 3 (bottom). (Characterization performed by Dr Stacy Slavin).	27
Figure 2. 8. ^1H NMR spectra of PGMA 2 (top), propyl end-functionalised polymer 4 (middle) and benzyl end-functionalised polymer 5 (bottom) in $\text{DMSO}-d_6$.	28
Figure 2. 9. ^1H NMR spectrum of azide functionalised polymer 6 in $\text{DMSO}-d_6$.	29
Figure 2. 10. ^1H NMR spectra of azide functionalised polymer 7 (top) and 8 (bottom) in $\text{DMSO}-d_6$.	30
Figure 2. 11. FT-IR spectra of azide functionalised polymer 7 (top) and 8 (bottom).	31
Figure 2. 12. Molecular weight distributions of polymer 1, 4, 7 and 9 via SEC employing DMF as the eluent.	31
Figure 2. 13. ^1H NMR spectrum of benzyl terminal fucose-functional glycopolymer 12 in $\text{DMSO}-d_6$.	33
Figure 2. 14. ^1H NMR spectrum of benzyl terminal mannose-functional glycopolymer 11 in $\text{DMSO}-d_6$.	33
Figure 2. 15. ^1H NMR spectra of polymer 9 (top) and 10 (bottom) in $\text{DMSO}-d_6$.	34
Figure 2. 16. FT-IR spectra of polymer 11 (top), 9 (middle) and 10 (bottom).	35
Figure 2. 17. Molecular weight distributions of polymer 2, 5, 8, 10 and 11 via SEC employing DMF as the eluent.	35
Figure 3. 1. ^1H (top) and ^{13}C (bottom) NMR spectra of D-glucose acrylate monomer in MeOD.	47
Figure 3. 2. Dependence of M_n and M_w/M_n on conversion (top) and first order kinetic plots (bottom) for the polymerization of D-glucose glycomonomer via SET-LRP in DMSO.	48
Figure 3. 3. ^1H NMR spectrum of D-glucose glycopolymer in $\text{DMSO}-d_6$.	49
Figure 3. 4. Molecular weight distributions (normalized to peak height) of multiblock glycopolymer obtained by SET-LRP <i>via</i> iterative chain extensions ($\text{DP}=2$ for each block).	50
Figure 3. 5. ESI-MS spectra of the 1 st block poly(mannose) ₂ by SET-LRP(top: whole spectra; bottom: zoom of 800-1000 region).	51
Figure 3. 6. ESI-MS spectra of the 2 nd block poly(mannose) ₂ -(glucose) ₂ by SET-LRP(top: whole spectra; bottom: zoom of 800-1800 region).	52

Figure 3. 7. MALDI-ToF MS spectra of the 1 st block poly(mannose) ₂ (top) and 2 nd block poly(mannose) ₂ -(glucose) ₂ (bottom) glycopolymers obtained by SET-LRP.....	53
Figure 3. 8. ¹ H NMR spectrum of multiblock D-mannose/D-Glucose glycopolymer in D ₂ O. 53	
Figure 3. 9. Molecular weight distributions (normalized to peak height) of multiblock glycopolymer obtained by SET-LRP via iterative chain extensions (DP=4 for each block)... 54	
Figure 3. 10. Molecular weight distributions (normalized to peak height) of multiblock glycopolymers obtained by SET-LRP via iterative addition of glyco monomers at defined time period.	56
Figure 3. 11. Molecular weight distributions of multiblock glycopolymer obtained by SET-LRP via iterative addition of DEGEAA and mannose glycomonomer at defined time period.	58
Figure 3. 12. ¹ H NMR spectrum of multiblock DEGEAA-mannose glycopolymer in D ₂ O. ...	59
Figure 3. 13. MALDI-ToF MS spectra of the 1 st block poly(DEGEAA) ₆ (top) and 2 nd block poly(DEGEAA) ₆ - <i>b</i> -(mannose) ₃ (bottom) glycopolymers obtained by SET-LRP.....	60
Figure 3. 14. FT-IR spectra of azide and dibromomaleimide modified multiblock glycopolymer.	62
Figure 3. 15. DMF SEC elution traces of the azide and dibromomaleimide modified glycopolymer via RI detector.....	62
Figure 3. 16. DMF SEC elution traces of the azide and dibromomaleimide modified glycopolymer via UV detector at 400 nm.	63
Figure 3. 17. SPR sensorgrams showing the binding of (a) <i>gp120</i> ; (b) <i>C1 ManMA₅₈</i> ; (c) <i>S1 ManA₂₃</i> ; (d) <i>S2 ManA₁₃-b-OEGA₂</i> ; (e) <i>S3 ManA₉-r-DEGEAA₁₈</i> ; (f) <i>S4 ManA₉-s-DEGEAA₁₈</i> ; (g) <i>S5 GluA₆-s-ManA₄-s-FucA₄</i> ; (h) <i>S6 GluA₄-s-ManA₄-s-GluA₄</i> onto DC-SIGN functionalized surfaces.	66
Figure 3. 18. Competition experiments on <i>gp120</i> functionalized surface between DC-SIGN and (a) <i>gp120</i> ; (b) <i>C1 ManMA₅₈</i> ; (c) <i>S1 ManA₂₃</i> ; (d) <i>S2 ManA₁₃-b-OEGA₂</i> at a concentration range of 0-64 nM for <i>gp120</i> , 0-512 nM for glycopolymer and 4 nM for DC-SIGN.	67
Figure 3. 19. Competition binding experiments on <i>gp120</i> functionalized surface between DC-SIGN and of <i>gp120</i> (black), <i>S1 ManA₂₃</i> (blue) and <i>C1 ManMA₅₈</i> (red) at 4 nM DC-SIGN and different concentration for <i>gp120</i> and the glycopolymers.	67
Figure 3. 20. ¹ H NMR spectrum of multiblock glucose-mannose-fucose glycopolymer in D ₂ O obtained by SET-LRP.	77
Figure 3. 21. MALDI-ToF MS (top) and high resolution ESI-MS (bottom) zooming spectra of the 2 nd block (DEGEAA) ₆ -(mannose) ₃ glycopolymers obtained by SET-LRP.....	79
Figure 3. 22. Molecular weight distributions of multiblock DEGEAA-glucose glycopolymer obtained by SET-LRP via iterative monomer addition at defined time period.....	81
Figure 3. 23. ¹ H NMR spectrum of multiblock DEGEAA-glucose glycopolymer in D ₂ O.	81

Figure 3. 24. MALDI-ToF MS spectra (RP model) of the 1 st block poly(DEGEEA) ₆ (top) and 2 nd block poly(DEGEEA) ₆ - <i>b</i> -(glucose) ₃ (bottom) glycopolymers obtained by SET-LRP.	82
Figure 3. 25. MALDI-ToF MS spectra (LP model) of the 1 st block to 6 th block DEGEEA/glucose (from top to bottom) glycopolymers obtained by SET-LRP. Due to incorporation of more sugar which causes the loss of resolution under LP model, definition of exact structure after 3 rd block is difficult and is for reference only.	83
Figure 3. 26. ¹ H NMR spectrum of home D-mannose glycopolymer in D ₂ O.	84
Figure 3. 27. ¹ H NMR spectrum of random DEGEEA-mannose glycopolymer in D ₂ O.	85
Figure 4. 1. ¹ H NMR (top) and MALDI-ToF MS (bottom) spectra of β-CD-(Man) ₇ & β-CD-(Fuc) ₇ glycoclusters.	91
Figure 4. 2. FT-IR (left) spectra and normalized SEC elution traces (right) of β-CD-(Man) ₇ & β-CD-(Fuc) ₇ glycoclusters.	92
Figure 4. 3. ¹ H (left) and ¹³ C (right) NMR spectra of β-CD-(Br) ₁₆ in DMSO- <i>d</i> ₆	93
Figure 4. 4. MALDI-ToF MS spectrum of β-CD-(Br) ₁₆	94
Figure 4. 5. MALDI-ToF MS spectrum of (N ₃) ₇ -β-CD-(Br) ₈₋₁₂ in linear model.	94
Figure 4. 6. Semi-logarithmic kinetic plots (left) and molecular weight and PDI vs reaction time plots for polymerization of NIPAM from (N ₃) ₇ -β-CD-(Br) ₁₀	96
Figure 4. 7. Semi-logarithmic kinetic plots (left) and molecular weight and PDI vs reaction time plots (right) for ATRP of DEGMEMA from (N ₃) ₇ -β-CD-(Br) ₁₀	97
Figure 4. 8. FT-IR spectra obtained for propargyl mannose, (N ₃) ₇ -β-CD-(PNIPAM) ₁₀ and (Mannose) ₇ -β-CD-(PNIPAM) ₁₀	97
Figure 4. 9. Cloud point measurements of (N ₃) ₇ -β-CD-(PNIPAM) ₁₀ , (Mannose) ₇ -β-CD-(PNIPAM) ₁₀ (left) and (N ₃) ₇ -β-CD-(PDEGMEMA) ₁₀ -(Br) ₁₀ , (N ₃) ₇ -β-CD-(PDEGMEMA) ₁₀ -(N ₃) ₁₀ and (Mannose) ₇ -β-CD-(PNIPAM) ₁₀ -(Mannose) ₁₀ (right) by UV/Vis spectroscopy at 500 nm. The analytes concentrations in water are all 1 mg/mL.	98
Figure 4. 10. Normalized SEC elution traces for (N ₃) ₇ -β-CD-(PNIPAM) ₁₀ and (Mannose) ₇ -β-CD-(PNIPAM) ₁₀ via RI detector. The two samples were injected in sequence at the same time.	98
Figure 4. 11. ¹ H NMR spectra recorded in D ₂ O for (N ₃) ₇ -β-CD-(PNIPAM) ₁₀ (left) and (Mannose) ₇ -β-CD-(PNIPAM) ₁₀ (right).	99
Figure 4. 12. Normalized DMF SEC traces of (N ₃) ₇ -β-CD-(PDEGMEMA) ₁₀ and (Mannose) ₇ -β-CD-(PNIPAM) ₁₀	99
Figure 4. 13. Normalized DMF SEC traces of (N ₃) ₇ -β-CD-(PDEGMEMA) ₁₀ -(Br) ₁₀ , (N ₃) ₇ -β-CD-(PDEGMEMA) ₁₀ -(N ₃) ₁₀ and (Mannose) ₇ -β-CD-(PNIPAM) ₁₀ -(Mannose) ₁₀ . These three samples were injected in sequence at the same time.	99

Figure 4. 14. FT-IR spectra obtained for propargyl mannose, $(N_3)_7\beta\text{-CD-(PDEGMEMA)}_{10}\text{-(Br)}_{10}$, $(N_3)_7\beta\text{-CD-(PDEGMEMA)}_{10}\text{-(N}_3\text{)}_{10}$ and $(mannose)_7\beta\text{-CD-(PNIPAM)}_{10}\text{-(mannose)}_{10}$	100
Figure 4. 15. ^1H NMR spectra recorded in CDCl_3 for $(N_3)_7\beta\text{-CD-(PDEGMEMA)}_{10}\text{-(Br)}_{10}$ (left) and $(Mannose)_7\beta\text{-CD-(PDEGMEMA)}_{10}\text{-(Mannose)}_{10}$ (right).	101
Figure 4. 16. DMF SEC molecular weight distributions (normalized to height, left; black trace: before chain extension; red trace: after chain extension) and ^1H NMR spectra (right) of the diblock CD-based glucose-mannose glycopolymer by SET-LRP.	103
Figure 4. 17. Molecular weight and PDI vs conversion plots (left) and semi-logarithmic kinetic plots (right) for the SET-LRP of mannose glycomonomer from $\beta\text{-CD-(Br)}_{16}$	104
Figure 4. 18. DMF SEC molecular weight distributions (normalized to height, top) and ^1H NMR spectra (bottom) of CD-based mannose glycopolymers obtained by SET-LRP.	105
Figure 4. 19. DMF SEC molecular weight distributions (top) and ^1H NMR spectra (bottom) of CD-based diblock glycopolymer obtained by SET-LRP.	107
Figure 4. 20. FT-IR spectrum (left) of CD-based diblock glycopolymers obtained by SET-LRP and cloud point measurement (right) of $\beta\text{-CD-}[(\text{DEGEEA})_{10}]_{16}$ by UV/vis spectroscopy at 500nm and 1 mg/mL.	108
Figure 4. 21. SPR sensorgrams showing the binding of $\beta\text{-CD}$ based glycol conjugates onto DC-SIGN functionalized surfaces. The concentration for $\beta\text{-CD}$ based glycol conjugates was 4096 nM.	110
Figure 4. 22. Competition experiments on gp120 functionalized surface between DC-SIGN and $\beta\text{-CD}$ based glycol conjugates at a concentration range of 0-4096 nM for glycol conjugates and 4 nM DC-SIGN.	111
Figure 4. 23. SPR sensorgrams showing the binding of $\beta\text{-CD-(Man)}_7$ (a), $\beta\text{-CD-}[(\text{Mannose})_2]_{16}$ (b), $\beta\text{-CD-}[(\text{Mannose})_{4,3}]_{16}$ (c), $\beta\text{-CD-}[(\text{Mannose})_{9,6}]_{16}$ (d) $\beta\text{-CD-}[(\text{DEGEEA})_{10}\text{-b-(Mannose)}_5]_{16}$ (e), $\beta\text{-CD-(Fuc)}_7$ (f) and $(\text{Man})_7\beta\text{-CD-(PNIPAM)}_{10}$ (g) onto DC-SIGN functionalized surfaces. The concentration ranges for all the glycoconjugates were 128-4096 nM. Characterization of sample f and g was performed by Dr Remzi Becer.	112
Figure 4. 24. Competition experiments on gp120 functionalized surface between DC-SIGN and $\beta\text{-CD-(Man)}_7$ (a), $\beta\text{-CD-}[(\text{Mannose})_2]_{16}$ (b), $\beta\text{-CD-}[(\text{Mannose})_{4,3}]_{16}$ (c), $\beta\text{-CD-}[(\text{Mannose})_{9,6}]_{16}$ (d) and $\beta\text{-CD-}[(\text{DEGEEA})_{10}\text{-b-(Mannose)}_5]_{16}$ (e). The concentration ranges for all the glycoconjugates were 4-4096 nM and 4 nM for the DC-SIGN.	113
Figure 4. 25. UV-Vis spectra of DHA solution in the presence of different cyclodextrin products. All measurements with $\beta\text{-CD}$, $\beta\text{-CD-(Man)}_7$ and glycopolymers were performed at a concentration of 1 mg/mL.	114

Figure 4. 26. ^1H NMR spectra of saquinavir mesylate (bottom) and of saquinavir mesylate encapsulated into polymer $\beta\text{-CD-}[(\text{DEGEEA})_{10}\text{-}b\text{-(Mannose)}_5]_{16}$ (top). Both measurements were performed in D_2O with 10 mM DMF as an internal standard.	115
Figure 5. 1. Visual observation of the disproportionation of $\text{CuBr}/\text{Me}_6\text{TREN}$ in H_2O . Conditions: $\text{H}_2\text{O} = 5\text{ mL}$, (a) $\text{CuBr} = 72\text{ mg}$, 0.5 mmol; (b) $\text{CuBr} = 72\text{ mg}$, 0.5 mmol; $\text{Me}_6\text{TREN} = 130\text{ }\mu\text{L}$, 0.5 mmol; (c) zoom of the bottom copper (0) powder of (b). Pictures were taken 1 h after mixing the reagents.	140
Figure 5. 2. Visual observation of the disproportionation of $\text{CuBr}/N\text{-ethyl-2-pyridylmethanimine}$ in H_2O . Conditions: $\text{H}_2\text{O} = 2\text{ mL}$, (a) $\text{CuBr} = 14\text{ mg}$, 0.1 mmol; $N\text{-ethyl-2-pyridylmethanimine} = 27\text{ mg}$, 0.2 mmol; (b) zoom of (a). Pictures were taken 1 h after mixing the reagents.	140
Figure 5. 3. Visual observation of the disproportionation of $\text{CuBr}/\text{Me}_6\text{TREN}$ in H_2O . Conditions: $\text{H}_2\text{O} = 12\text{ mL}$; $\text{CuBr} = 43\text{ mg}$, 0.3 mmol; $\text{Me}_6\text{TREN} = 78\text{ }\mu\text{L}$, 0.3 mmol; nitrogen protection. Picture was taken 45 min after mixing the reagents.	141
Figure 5. 4. Optical microscopy image (top) of copper powders from disproportionation of $\text{CuBr}/\text{Me}_6\text{TREN}$ in H_2O and UV-Vis spectra (bottom) of the solution of $\text{CuBr}_2/\text{Me}_6\text{TREN}$ and filtered disproportionation solution (dashed line). All the samples were diluted ten times before analysis (0.5 mL sample solution into 4.5 mL degassed H_2O). The optical microscopy analysis was helped by Dr Yunhua Chen.	142
Figure 5. 5. Calibration curve based on UV-Vis absorbance at 700 nm (top) and 865 nm (bottom). The intercept for the linear fit was set as 0.	143
Figure 5. 6. Molecular weight distributions of PNIPAM by ATRP at ambient temperature <i>via</i> DMF SEC. Reaction conditions: $\text{H}_2\text{O} = 5\text{ mL}$; NIPAM = 1.13 g, 10 mmol; 2, 3-dihydroxypropyl 2-bromo-2-methylpropanoate = 60 mg, 0.25 mmol; $\text{Me}_6\text{TREN} = 65\text{ }\mu\text{L}$, 0.25 mmol; $\text{CuBr} = 36\text{ mg}$, 0.25 mmol. Note: The gel was not soluble in DMF and was removed by filtration before analysis. So SEC did not reveal the MW of the gel.	145
Figure 5. 7. Visual observation of the ATRP of NIPAM in H_2O under ambient temperature ($\sim 18\text{ }^\circ\text{C}$). Pictures were taken at different time after mixing the reagents. (a) 10 seconds; (b) 2 min; (c) 30 min.	145
Figure 5. 8. Molecular weight distributions of PNIPAM by ATRP and SET-LRP with $[\text{NIPAM}]: [\text{initiator}]: [\text{CuBr}]: [\text{Me}_6\text{TREN}] = 80: 1: 0.8: 0.4$ at $0\text{ }^\circ\text{C}$ as measured <i>via</i> SEC employing DMF as eluent.	146
Figure 5. 9. Dependence of conversion on time for the copper (0) wire mediated SET-LRP of NIPAM in H_2O at ambient temperature.	147
Figure 5. 10. Molecular weight distributions of PNIPAM by copper (0) wire mediated SET-LRP at ambient temperature <i>via</i> DMF SEC.	148

Figure 5. 11. Molecular weight distributions of poly (PEGA ₄₈₀) ₁₀ by copper (0) wire mediated SET-LRP at ambient temperature <i>via</i> DMF SEC.	148
Figure 5. 12. Visual observation of the disproportionation of CuBr/Me ₆ TREN in H ₂ O under strict freeze-pump-thaw degas procedure. Conditions: H ₂ O = 2 mL; CuBr = 10 mg, 0.07 mmol; Me ₆ TREN = 9 μL, 0.035 mmol. Picture was taken 1 min after mixing the reagents <i>via</i> cannula.	149
Figure 5. 13. Molecular weight distributions of PNIPAM (DP=20) catalyzed by separated Cu(0) powder/Me ₆ TREN (black) or Cu (0) powder/CuBr ₂ /Me ₆ TREN (red) in H ₂ O at ambient temperature as measured <i>via</i> SEC employing DMF as eluent.	151
Figure 5. 14. DMF SEC molecular weight distributions for the ARGET ATRP of NIPAM (DP=20) in H ₂ O at ambient temperature with [initiator]: [CuBr ₂]: [Me ₆ TREN]: [Ascorbic acid] = 1: 0.4: 0.4: 0.16.	153
Figure 5. 15. DMF SEC molecular weight distributions for the ARGET ATRP of NIPAM (DP=20) in H ₂ O at ambient temperature with [initiator]: [CuBr ₂]: [Me ₆ TREN]: [Ascorbic acid] = 1: 0.4: 0.8: 0.2.	153
Figure 5. 16. Visual observation of the AGET ATRP of NIPAM in H ₂ O with [initiator]: [CuBr ₂]: [Me ₆ TREN]: [Ascorbic acid] = 1: 0.4: 0.4: 0.16 before (a) and after (b) addition of L-ascorbic acid. Conditions: a) Picture was taken 15 min after nitrogen bubbling. b) Picture was taken 1 min after addition of L-ascorbic acid.	154
Figure 5. 17. Visual observation of the reduction of CuBr ₂ /Me ₆ TREN complex by L-ascorbic acid for AGET ATRP of NIPAM in H ₂ O under ambient temperature with [initiator]: [CuBr ₂]: [Me ₆ TREN]: [Ascorbic acid] = 1: 0.4: 0.4: 0.16. Conditions: a) CuBr ₂ / Me ₆ TREN in H ₂ O; b) picture was taken 1 min after addition of L-Ascorbic acid; c) picture was taken 15 min after addition of L-Ascorbic acid; d) picture was taken 1 min after addition of initiator and monomer.	154
Figure 5. 18. Visual observation of the reduction of CuBr ₂ by L-ascorbic acid into CuBr following disproportionation into Cu (0) & CuBr ₂ for SET-LRP of NIPAM in H ₂ O under ambient temperature with [initiator]: [CuBr ₂]: [Me ₆ TREN]: [Ascorbic acid] = 1: 0.4: 0.4: 0.16. Conditions: a) CuBr ₂ in H ₂ O; b) after addition of L-Ascorbic acid; c) after addition of Me ₆ TREN; d) after addition of initiator and monomer; All pictures were taken 1 min after relative reaction.	155
Figure 5. 19. Molecular weight distributions of PNIPAM (DP=8, 20, 40, 80, 160, 320) catalyzed by the in-situ generated Cu(0) powders/CuBr ₂ /Me ₆ TREN in H ₂ O as measured <i>via</i> SEC employing DMF as eluent.	157
Figure 5. 20. DMF SEC molecular weight distributions at different time for the aqueous SET-LRP of NIPAM (DP=40) at ambient temperature.	158

Figure 5. 21. Dependence of conversion, M_n and M_w / M_n on time for the SET-LRP of NIPAM (DP=40) <i>via</i> disproportionation of CuBr / Me ₆ TREN in H ₂ O at ambient temperature.	158
Figure 5. 22. DMF SEC molecular weight distributions at different time for the SET-LRP of NIPAM (DP=80, left; DP=160, right) in H ₂ O at ambient temperature with [initiator]: [CuBr]: [Me ₆ TREN] = 1: 0.4: 0.4.	159
Figure 5. 23. DMF SEC molecular weight distributions at different time for the SET-LRP of NIPAM (DP=80) in H ₂ O at ambient temperature with [initiator]: [CuBr]: [Me ₆ TREN] = 1: 0.8: 0.4.	159
Figure 5. 24. Visual observations for SET-LRP of NIPAM (DP=160) in H ₂ O at ambient temperature (~18 °C) with [initiator]: [CuBr]: [Me ₆ TREN] = 1: 0.8: 0.4. Conditions: white equipment = time meter; blue equipment = IKA electronic contact thermometer. Video screenshot (d) shows highest temperature as 31.6 °C (3 min 40 s).....	160
Figure 5. 25. DMF SEC molecular weight distributions at 1 h for the SET-LRP of NIPAM (DP=160) in H ₂ O at ambient temperature with [initiator]: [CuBr]: [Me ₆ TREN] = 1: 0.8: 0.4.	161
Figure 5. 26. DMF SEC molecular weight distributions at different time for the SET-LRP of NIPAM (DP=160) in H ₂ O at 0 °C with [initiator]: [CuBr]: [Me ₆ TREN] = 1: 0.8: 0.4.	161
Figure 5. 27. DMF SEC molecular weight distributions at different time for the SET-LRP of NIPAM (DP=320) in H ₂ O at 0 °C with [initiator]: [CuBr]: [Me ₆ TREN] = 1: 0.8: 0.4.	162
Figure 5. 28. DMF SEC molecular weight distributions at different time for the SET-LRP of NIPAM (DP=160) in H ₂ O at ambient temperature with [initiator]: [CuBr]: [Me ₆ TREN] = 1: 1.2: 0.4.	162
Figure 5. 29. Molecular weight distributions of PNIPAM by SET-LRP for chain extension in H ₂ O under ambient temperature as measured <i>via</i> SEC employing DMF as eluent.	163
Figure 5. 30. Molecular weight distributions of PNIPAM (DP=8) by SET-LRP at 0 °C and ambient temperature <i>via</i> DMF SEC.....	164
Figure 5. 31. FTIR spectra of PNIPAM (DP=8) by SET-LRP at 0 °C (left) and ambient temperature (right).	164
Figure 5. 32. ¹ H NMR spectrum of PNIPAM (DP=8) in D ₂ O by SET-LRP at ambient temperature. The numbering of the hydrogen atoms used for the NMR peak assignment is shown in the spectrum. Peak i is overlapped with peak c.	165
Figure 5. 33. ¹³ C NMR spectrum of PNIPAM (DP=8) in D ₂ O by SET-LRP at ambient temperature. The numbering of the carbon atoms used for the NMR peak assignment is shown in the spectrum. Peak f is overlapped with peak i.	165
Figure 5. 34. ¹ H- ¹ H COSY NMR spectrum of PNIPAM (DP=8) in D ₂ O by SET-LRP at ambient temperature.....	166

Figure 5. 35. ^1H - ^{13}C HSQC NMR spectrum of PNIPAM (DP=8) in D_2O by SET-LRP at ambient temperature.....	167
Figure 5. 36. ^1H NMR spectrum of PNIPAM (DP=8) in D_2O by SET-LRP at 0 °C. The numbering of the hydrogen atoms used for the NMR peak assignment is shown in the spectrum. Peak i-OH is overlapped with peak c.	168
Figure 5. 37. ^{13}C NMR spectrum of PNIPAM (DP=8) in D_2O by SET-LRP at 0 °C. The numbering of the carbon atoms used for the NMR peak assignment is shown in the spectrum. Peak f is overlapped with peak i-OH.	168
Figure 5. 38. ^1H - ^1H COSY NMR spectrum of PNIPAM (DP=8) in D_2O by SET-LRP at 0 °C.	169
Figure 5. 39. ^1H - ^{13}C HSQC NMR spectrum of PNIPAM (DP=8) in D_2O by SET-LRP at 0 °C.	170
Figure 5. 40. MALDI-ToF MS spectrum of PNIPAM (DP=8) by SET-LRP at 0 °C. The MALDI-ToF MS analysis was done as soon as possible after taking sample from the reaction.	171
Figure 5. 41. MALDI-ToF MS spectrum of PNIPAM (DP=8) by SET-LRP at ambient temperature (~ 18 °C). The MALDI-ToF MS analysis was done as soon as possible after taking sample from the reaction.....	171
Figure 5. 42. MALDI-ToF MS spectrum of PNIPAM (DP=8) by SET-LRP at ambient temperature (~ 18 °C). The MALDI-ToF MS analysis was done after taking sample from the reaction overnight. Note: The peaks and peak height of PNIPAM in the MALDI-ToF MS spectra may not reveal the total information or right ratio of each component during the reaction and are only supplied as reference for NMR and GPC characterization results.	172
Figure 5. 43. DMF SEC molecular weight distributions for chain extension reaction of SET-LRP of NIPAM in H_2O at 0 °C with [initiator]: [CuBr]: [Me_6TREN] = 1: 0.4: 0.4.....	173
Figure 5. 44. DMF SEC molecular weight distributions for chain extension reaction of SET-LRP of NIPAM in H_2O at 0 °C with [initiator]: [CuBr]: [Me_6TREN] = 1: 0.8: 0.4.....	173
Figure 5. 45. ^1H NMR spectrum of poly (NIPAM) ₂₀ - <i>b</i> -(HEA) ₄₀ by iterative SET-LRP in D_2O . The numbering of the hydrogen atoms used for the NMR peak assignment is shown in the spectrum.	174
Figure 5. 46. FTIR spectrum of poly (NIPAM) ₂₀ - <i>b</i> -(HEA) ₄₀ by iterative SET-LRP.....	175
Figure 5. 47. DMF SEC molecular weight distributions for poly (NIPAM) ₂₀ - <i>b</i> -(HEA) ₄₀ by iterative SET-LRP in H_2O	175
Figure 5. 48. Molecular weight distributions of poly (NIPAM) ₂₀ - <i>b</i> -(HEA) ₄₀ - <i>b</i> -(PEGA ₄₈₀) ₁₀ by iterative SET-LRP in H_2O at 0 °C as measured <i>via</i> SEC employing DMF as eluent.....	176
Figure 5. 49. ^1H NMR spectrum of poly (NIPAM) ₂₀ - <i>b</i> -(HEA) ₄₀ - <i>b</i> -(PEGA ₄₈₀) ₁₀ by iterative SET-LRP in D_2O	176

Figure 5. 50. DMF SEC elution traces for poly (NIPAM) ₂₀ - <i>b</i> - (HEA) ₄₀ - <i>b</i> - (PEGA ₄₈₀) ₁₀ by iterative aqueous SET-LRP at 0 °C. Conditions: a) 1 st block; b) 2 nd block; c) 3 rd block. Red line for refractive index detector; green line for viscosity detector.	177
Figure 5. 51. DMF SEC molecular weight distributions at different time for the SET-LRP of NIPAM (DP=80) in PBS buffer (pH=6.2, left; pH=6.8, right) at 0 °C with [initiator]: [CuBr]: [Me ₆ TREN] = 1: 0.8: 0.4.	178
Figure 5. 52. Visual observation of the disproportionation of CuBr / Me ₆ TREN (a) and SET-LRP of NIPAM (DP=80) in Tequila (b). Conditions: a) Tequila = 2 mL; CuBr = 10 mg, 70 μmol; Me ₆ TREN = 9 μL, 35 μmol. Picture was taken 30 min after mixing the reagents. b) Picture was taken 5 min after transferring the initiator / NIPAM solution into the catalyst solution of (a).	178
Figure 5. 53. DMF SEC molecular weight distributions at different time for the SET-LRP of NIPAM (DP=80) in Tequila at 0 °C with [initiator]: [CuBr]: [Me ₆ TREN] = 1: 0.8: 0.4.	179
Figure 5. 54. ¹ H NMR spectrum for SET-LRP of NIPAM in Tequila at 30 min in D ₂ O.	179
Figure 5. 55. Visual observation of the disproportionation of CuBr / Me ₆ TREN in sheep serum. Conditions: sheep serum= 2 mL; CuBr = 10 mg, 0.07 mmol; Me ₆ TREN = 9 μL, 0.035 mmol. Picture was taken 1 min after mixing CuBr with the other reagents.	180
Figure 5. 56. Molecular weight distributions of poly (NIPAM) ₈₀ and poly(DMA) ₈₀ by SET-LRP in sheep serum at 0 °C as measured <i>via</i> SEC employing DMF as eluent.	181
Figure 5. 57. ¹ H NMR spectra for SET-LRP of NIPAM in sheep serum at 1 h (left) and PNIPAM (right) recovered after dialysis. D ₂ O was used as the NMR solvent.	181
Figure 5. 58. ¹ H NMR spectra for SET-LRP of DMA in sheep serum at 2 h (left) and PDMA (right) recovered after dialysis. D ₂ O was used as the NMR solvent.	181
Figure 5. 59. FTIR spectra of PNIPAM (DP=80, left) and PDMA (DP=80, right) by SET-LRP in serum.	182
Figure 5. 60. ¹ H NMR spectra for SET-LRP of poly (NIPAM) ₈₀ - <i>b</i> - (DMA) ₈₀ in sheep serum during polymerization (left) and product (right) recovered after dialysis. D ₂ O was used as the NMR solvent.	182
Figure 5. 61. ¹ H NMR spectra for SET-LRP of poly (DMA) ₈₀ - <i>b</i> - (NIPAM) ₈₀ in sheep serum during polymerization (left) and product (right) recovered after dialysis. D ₂ O was used as the NMR solvent.	183
Figure 5. 62. Molecular weight distributions for the <i>In situ</i> SET-LRP block copolymerization of poly(NIPAM) (top) and poly(DMA) (bottom) in sheep serum at 0 °C as measured <i>via</i> SEC employing DMF as eluent.	183
Figure 5. 63. FTIR spectrum of poly (NIPAM) ₈₀ - <i>b</i> -(DMA) ₈₀ (left) and poly (DMA) ₈₀ - <i>b</i> -(NIPAM) ₈₀ (right) by SET-LRP in sheep serum.	184

Figure 5. 64. Molecular weight distribution of poly(Mannose) ₁₀ by SET-LRP in H ₂ O at 0 °C <i>via</i> DMF SEC.....	186
Figure 5. 65. ¹ H NMR spectra of poly(Mannose) ₁₀ in D ₂ O.	187
Figure 5. 66. Molecular weight distributions for the copper(0) wire mediated SET-LRP of D-Mannose glyco monomer in H ₂ O at ambient temperature <i>via</i> DMF SEC.	187
Figure 5. 67. Molecular weight distribution of poly(DEGEEA) ₈₀ (left: elution traces; right: after dialysis) by aqueous SET-LRP at 0 °C <i>via</i> DMF SEC.	188
Figure 5. 68. ¹ H NMR spectra of poly(DEGEEA) ₈₀ in DMSO- <i>d</i> ₆	188
Figure 5. 69. Molecular weight distributions of poly (Mannose) ₁₀ - <i>b</i> - (NIPAM) ₈₀ by SET-LRP in H ₂ O at 0 °C <i>via</i> DMF SEC.	190
Figure 5. 70. ¹ H NMR spectrum for the poly (Mannose) ₁₀ - <i>b</i> - (NIPAM) ₈₀ by SET-LRP in H ₂ O at 0 °C. D ₂ O was used as the NMR solvent.	190
Figure 5. 71. FTIR spectra for the poly (Mannose) ₁₀ (top) and poly (Mannose) ₁₀ - <i>b</i> - (NIPAM) ₈₀ (bottom).	191
Figure 5. 72. Cloud point measurements of poly(NIPAM) ₈₀ and poly (Mannose) ₁₀ - <i>b</i> - (NIPAM) ₈₀ by UV/Vis spectroscopy at 500 nm. Sample concentration: 1mg / mL.....	191
Figure 5. 73. Molecular weight distributions of poly (Mannose) ₁₀ - <i>b</i> - (DEGEEA) ₈₀ by SET-LRP in H ₂ O at 0 °C <i>via</i> DMF SEC.	192
Figure 5. 74. ¹ H NMR spectrum for the poly (Mannose) ₁₀ - <i>b</i> - (DEGEEA) ₈₀ by SET-LRP in H ₂ O at 0 °C. D ₂ O was used as the NMR solvent.	193
Figure 5. 75. FTIR spectra for the poly (DEGEEA) ₈₀ (top) and poly (Mannose) ₁₀ - <i>b</i> - (DEGEEA) ₈₀ (bottom).	193
Figure 5. 76. Cloud point measurements of poly(DEGEEA) ₈₀ and poly (Mannose) ₁₀ - <i>b</i> - (DEGEEA) ₈₀ by UV/Vis spectroscopy at 500 nm. Sample concentrations: 1mg / mL	194
Figure 5. 77. Visual observation of the disproportionation of CuBr / Me ₆ TREN in water / ethanol mixture. Conditions: solvent = 12 mL (V _{water} : V _{ethanol} from left to right: 100%: 0% – 75%: 25% – 50%: 50% – 25%: 75% – 0%: 100%); CuBr = 43 mg, 0.3 mmol; Me ₆ TREN = 78 μL, 0.3 mmol. Picture was taken after setting down for a) 5 min; b) 30 min; c) 120 min.	195
Figure 5. 78. Zoom of Figure 5.96 for the disproportionation of CuBr / Me ₆ TREN in water (left) and ethanol (right). Pictures were taken after setting down for 120 min.	196
Figure 5. 79. Optical microscopy images of copper powders from the disproportionation of CuBr / Me ₆ TREN in water.....	196
Figure 5. 80. Optical microscopy images of copper powders from the disproportionation of CuBr / Me ₆ TREN in water / ethanol mixture. Conditions: V _{water} : V _{ethanol} = 75%: 25% (A), 50%: 50% (B); 25%: 75% (C); 0%: 100% (D). The white scale bar is 300 μm.	196
Figure 5. 81. Visual observation of the disproportionation of CuBr / PMDETA (a) and SET-LRP of NIPAM (DP=80) in water (b). Conditions: a) H ₂ O = 2 mL; CuBr = 10 mg, 70 μmol;	

PMDETA = 7.4 μ L, 35 μ mol. Picture was taken 30 min after mixing the reagents. b) Picture was taken 2 min after transferring the initiator / NIPAM solution into the catalyst solution of (a).	197
Figure 5. 82. Visual observation of the disproportionation of CuBr / TREN (a) and SET-LRP of NIPAM (DP=80) in water (b). Conditions: a) H ₂ O = 2 mL; CuBr = 10 mg, 70 μ mol; TREN = 5.3 μ L, 35 μ mol. Picture was taken 30 min after mixing the reagents. b) Picture was taken 2 min after transferring the initiator / NIPAM solution into the catalyst solution of (a).	197
Figure 5. 83. DMF SEC molecular weight distributions at different time for the SET-LRP of NIPAM (DP=80) in H ₂ O at 0 °C with [initiator]: [CuBr]: [PMDETA] = 1: 0.8: 0.4 (left) and [initiator]: [CuBr]: [TREN] = 1: 0.8: 0.4 (right).	198
Figure 5. 80. Molecular weight distributions of PNIPAM by ATRP at 0 °C <i>via</i> DMF SEC. Include tailing peak at high MW position (left); Ignore tailing peak at high MW position (right).	204
Figure 5. 85. Visual observation of the SET-LRP of NIPAM catalyzed by separated Cu (0) powder / Me ₆ TREN (a) and CuBr ₂ / Me ₆ TREN (b) in H ₂ O. Conditions: a) Picture was taken 15 min after starting polymerization. b) Picture was taken 24 after starting polymerization.	208
Figure 5. 86. Molecular weight distributions of PNIPAM (DP=20) catalyzed by Cu (0) powder / Me ₆ TREN (left) and CuBr ₂ / Me ₆ TREN (right) in H ₂ O at ambient temperature <i>via</i> DMF SEC.	208
Figure 5. 87. ¹ H NMR spectra for SET-LRP of NIPAM catalyzed by Cu (0) powder / Me ₆ TREN (left) and CuBr ₂ / Me ₆ TREN (right) in D ₂ O.	208
Figure 5. 88. Visual observation of the disproportionation of CuBr / Me ₆ TREN (a) and SET-LRP of NIPAM (DP=20) in H ₂ O (b). Conditions: a) H ₂ O = 2 mL; CuBr = 14 mg, 0.1 mmol; Me ₆ TREN = 26 μ L, 0.1 mmol. Picture was taken 30 min after mixing the reagents. b) Picture was taken 15 min after transferring the initiator/NIPAM solution into the catalyst solution of (a).	209
Figure 5. 67. FTIR spectrum of poly (NIPAM) ₂₀ - <i>b</i> - (HEA) ₄₀ - <i>b</i> - (PEGA ₄₈₀) ₁₀ by iterative SET-LRP.	219
Figure 5. 86. DMF SEC molecular weight distributions for the SET-LRP of NIPAM (DP=20) in H ₂ O at ambient temperature with [initiator]: [CuBr ₂]: [Me ₆ TREN]: [Ascorbic acid] = 1: 0.4: 0.4: 0.16.	221
Figure 5. 70. DMF SEC molecular weight distributions for the SET-LRP of NIPAM (DP=20) in H ₂ O at ambient temperature with [initiator]: [CuBr ₂]: [Me ₆ TREN]: [Ascorbic acid] = 1: 0.4: 0.8: 0.2.	221
Figure 5. 88. DMF SEC molecular weight distributions for the AGET ATRP of NIPAM (DP=20) in H ₂ O at ambient temperature with [initiator]: [CuBr ₂]: [Me ₆ TREN]: [Ascorbic acid] = 1: 0.4: 0.8: 0.2.	223

List of Schemes

Scheme 2. 1. Scheme for the Fischer-Helferich type glycosylation reaction. ⁹⁹	20
Scheme 2. 2. Scheme representation for the synthesis of alkyne functionalised sugar.	20
Scheme 2. 3. Scheme representation for synthetic approach to end-functionalised glycopolymers.....	23
Scheme 2. 4. Alkyne compounds employed in the study: propargyl alcohol (13), diethylene glycol alkyne (14), mannose alkyne (15) and fucose alkyne (16).	32
Scheme 3. 1. Synthesis of glycomonomers <i>via</i> Fischer glycosylation & CuAAC.	46
Scheme 3. 2. Homo polymerization of D-glucose acrylate monomer with [EBiB] ₀ = 33 mmol/L, [CuBr ₂] ₀ = 3.3 mmol/L, [Me ₆ TREN] ₀ =6 mmol/L in DMSO (3 mL), 25 °C.....	47
Scheme 3. 3. Schematic representation for the synthesis of sequence-controlled multiblock glycopolymer by iterative addition of glyco monomers without intermediate purification (DP=2 for each block).....	49
Scheme 3. 4. Schematic representation for the synthesis of sequence-controlled multiblock glycopolymers by iterative addition of glyco monomers without intermediate purification (DP=4 for each block).....	54
Scheme 3. 5. Schematic representation for the synthesis of multiblock glycopolymers by iterative addition of glyco monomers at defined time period.	56
Scheme 3. 6. Schematic representation for the synthesis of sequence-controlled multiblock glycopolymers by iterative addition of DEGEEA and mannose glycomonomer at defined time period.	57
Scheme 3. 7. Schematic representation for the azido and CuAAC modification of multiblock glycopolymer.	61
Scheme 3. 8. Schematic synthesis approach to 3-azidopropyl acrylate.....	71
Scheme 3. 9. Synthesis of D-glucose glycomonomer <i>via</i> CuAAC.....	72
Scheme 3. 10. Synthesis of D-mannose glycomonomer <i>via</i> CuAAC.....	73
Scheme 3. 11. Synthesis of L-fucose glycomonomer <i>via</i> CuAAC.....	74
Scheme 3. 12. Schematic representation for the synthesis of sequence-controlled multiblock glycopolymers by iterative addition of DEGEEA and glucose glycomonomer at defined time period.	80
Scheme 4. 1. Synthesis of persubstituted β-CD-based glycocluster <i>via</i> CuAAC of per-6-azido β-CD and alkyne sugar.....	90
Scheme 4. 2. Synthesis of β-CD-(Br) ₁₆ , (N ₃) ₇ -β-CD-(Br) ₁₀ and glyco monomer.	92

Scheme 4. 3. Schematic representation for the synthesis of CD-based glyocluster-smart star polymer hybrids <i>via</i> combination of ATRP and CuAAC and their LCST self-assembled behaviour.....	95
Scheme 4. 4. Schematic representation for the synthesis of cyclodextrin-based PNIPAM <i>via</i> ATRP.	96
Scheme 4. 5. Synthesis of β -CD based glycopolymers <i>via</i> SET-LRP and chain extension reaction.....	102
Scheme 4. 6. Synthesis of β -CD based diblock glycopolymer <i>via</i> SET-LRP of DEGEAA and one-pot chain extension reaction with glycomonomer.	106
Scheme 4. 7. Schematic structure of human DC-SIGN lectin.	108
Scheme 4. 8. Molecular structure of $\text{Man}_9\text{GlcNac}_2$, β -CD-(Man) ₇ and β -CD-[(Man) _{9,6}] ₁₆ . ..	109
Scheme 4. 9. Schematic representation of the synthetic approach to β -CD-(Br) ₇	119
Scheme 4. 10. Schematic representation of the synthetic approach to β -CD-(N ₃) ₇	120
Scheme 4. 11. Schematic representation of the synthetic approach to β -CD-(Br) ₁₆	121
Scheme 4. 12. Schematic representation of the synthetic approach to (N ₃) ₇ - β -CD-(Br) ₁₀	122
Scheme 4. 13. Schematic representation of the synthetic approach to β -CD-(Man) ₇	123
Scheme 4. 14. Schematic representation of the synthetic approach to β -CD-(Fuc) ₇	124
Scheme 4. 15. Schematic representation for the CuAAC reaction of cyclodextrin-based PNIPAM with 1-(2'-propargyl) D-mannose.	126
Scheme 4. 16. Schematic representation for the synthesis of cyclodextrin-based PDEGMEMA <i>via</i> ATRP.	127
Scheme 4. 17. Schematic representation for the CuAAC reaction of cyclodextrin-based PDEGEAA with 1-(2'-propargyl) D-mannose.	128
Scheme 4. 18. Schematic representation for the end group transformation of (N ₃) ₇ - β -CD-(PDEGMEMA) ₁₀ -(Br) ₁₀ into (N ₃) ₇ - β -CD-(PDEGMEMA) ₁₀ -(N ₃) ₁₀	128
Scheme 4. 19. Schematic representation for the CuAAC reaction of cyclodextrin-based (N ₃) ₇ - β -CD-(PDEGMEMA) ₁₀ -(N ₃) ₁₀ with 1-(2'-propargyl) D-mannose.	129
Scheme 4. 20. Synthesis of β -CD based glycopolymers <i>via</i> SET-LRP.	131
Scheme 4. 21. Synthesis of β -CD based diblock glycopolymer <i>via</i> SET-LRP of DEGEAA and one-pot chain extension reaction.....	133
Scheme 5. 1. Accepted mechanism for ATRP.....	137
Scheme 5. 2. Schematic representation of procedures for ATRP and SET-LRP <i>via</i> prior disproportionation of CuBr/Me ₆ TREN in water.	144
Scheme 5. 3. Scheme representation of the disproportionation of CuBr/Me ₆ TREN in H ₂ O and separation of copper (0) powder and CuBr ₂ /Me ₆ TREN solution after disproportionation. ...	150
Scheme 5. 4. Scheme representation of hydrolysis and disproportionation termination of chain end of PNIPAM (DP=8) by SET-LRP <i>via</i> disproportionation of CuBr / Me ₆ TREN in H ₂ O.	171

Scheme 5. 5. Schematic representation for synthesis of poly(NIPAM) ₂₀ - <i>b</i> -(HEA) ₄₀ - <i>b</i> -(PEGA ₄₈₀) ₁₀ by iterative SET-LRP in H ₂ O.	175
Scheme 5. 6. Schematic representation for the hydrophilic monomers polymerized by the aqueous SET-LRP.	184
Scheme 5. 7. Schematic representation for the synthesis of poly(Mannose) ₁₀ - <i>b</i> -(NIPAM) ₈₀ via aqueous SET-LRP.	189
Scheme 5. 8. Schematic representation for the synthesis of poly(Mannose) ₁₀ - <i>b</i> -(DEGEEA) ₈₀ via aqueous SET-LRP.	192
Scheme 5. 9. Disproportionation of CuBr / Me ₆ TREN in water.	201
Scheme 5. 10. Disproportionation of CuBr / N-ethyl-2-pyridylmethanimine in water.	203
Scheme 5. 11. ATRP of NIPAM in H ₂ O at ambient temperature.	203
Scheme 5. 12. ATRP of NIPAM in H ₂ O at 0 °C.	204
Scheme 5. 12. SET-LRP of NIPAM in H ₂ O at 0 °C <i>via</i> disproportionation of CuBr / Me ₆ TREN.	205
Scheme 5. 14. Copper (0) wire mediated SET-LRP of NIPAM in H ₂ O at ambient temperature.	206
Scheme 5. 15. Copper (0) wire mediated SET-LRP of PEGA ₄₈₀ in H ₂ O at ambient temperature.	206
Scheme 5. 16. SET-LRP of NIPAM (DP=20) in H ₂ O at ambient temperature <i>via</i> disproportionation of CuBr/Me ₆ TREN.	209
Scheme 5. 17. SET-LRP of NIPAM (DP=8) in H ₂ O at 0 °C and ambient temperature (~18 °C) <i>via</i> disproportionation of CuBr / Me ₆ TREN.	210
Scheme 5. 18. SET-LRP of NIPAM (DP=40) <i>via</i> disproportionation of CuBr / Me ₆ TREN in H ₂ O at ambient temperature.	211
Scheme 5. 19. SET-LRP of NIPAM (DP=80) <i>via</i> disproportionation of CuBr / Me ₆ TREN in H ₂ O at ambient temperature.	211
Scheme 5. 20. SET-LRP of NIPAM (DP = 160) <i>via</i> disproportionation of CuBr / Me ₆ TREN in H ₂ O at ambient temperature.	212
Scheme 5. 21. SET-LRP of NIPAM (DP = 320) <i>via</i> disproportionation of CuBr / Me ₆ TREN in H ₂ O at 0 °C.	214
Scheme 5. 22. Chain extension reaction for SET-LRP of NIPAM <i>via</i> disproportionation of CuBr / Me ₆ TREN in H ₂ O at ambient temperature.	214
Scheme 5. 23. Chain extension reaction for SET-LRP of NIPAM in H ₂ O with [initiator]: [CuBr]: [Me ₆ TREN] = 1: 0.4: 0.4 at 0 °C.	215
Scheme 5. 24. Chain extension reaction for SET-LRP of NIPAM in H ₂ O with [initiator]: [CuBr]: [Me ₆ TREN] = 1: 0.8: 0.4 at 0 °C.	216

Scheme 5. 25. Synthesis of poly (NIPAM) ₂₀ -b- (HEA) ₄₀ by SET-LRP in H ₂ O with [initiator]: [CuBr]: [Me ₆ TREN] = 1: 0.4: 0.4 at 0 °C.	217
Scheme 5. 26. Synthesis of poly (NIPAM) ₂₀ -b- (HEA) ₄₀ -b- (PEGA ₄₈₀) ₁₀ by iterative aqueous SET-LRP with [initiator]: [CuBr]: [Me ₆ TREN] = 1: 0.4: 0.4 at 0 °C.....	218
Scheme 5. 27. Synthesis of PNIPAM by AGET ATRP in H ₂ O with [initiator]: [CuBr ₂]: [Me ₆ TREN]: [Ascorbic acid] = 1: 0.4: 0.4: 0.16 & 1: 0.4: 0.8: 0.2 at ambient temperature.	219
Scheme 5. 28. Synthesis of PNIPAM by SET-LRP in H ₂ O with [initiator]: [CuBr ₂]: [Me ₆ TREN]: [Ascorbic acid] = 1: 0.4: 0.4: 0.16 & 1: 0.4: 0.8: 0.2 at ambient temperature.	220
Scheme 5. 29. Synthesis of PNIPAM by AGET ATRP in H ₂ O with [initiator]: [CuBr ₂]: [Me ₆ TREN]: [Ascorbic acid] = 1: 0.4: 0.4: 0.16 at ambient temperature.....	222
Scheme 5. 30. SET-LRP of NIPAM (DP = 80) <i>via</i> disproportionation of CuBr / Me ₆ TREN in Tequila at 0 °C.	223
Scheme 5. 31. SET-LRP of NIPAM (DP = 80) <i>via</i> disproportionation of CuBr / Me ₆ TREN in PBS buffer at 0 °C.....	224
Scheme 5. 32. SET-LRP of NIPAM in sheep serum at 0 °C <i>via</i> disproportionation of CuBr / Me ₆ TREN.	224
Scheme 5. 33. SET-LRP of DMA in sheep serum at 0 °C <i>via</i> disproportionation of CuBr / Me ₆ TREN.	225
Scheme 5. 34. Synthesis of poly (NIPAM) ₈₀ -b- (DMA) ₈₀ by SET-LRP in sheep serum with [initiator]: [CuBr]: [Me ₆ TREN] = 1: 0.8: 0.4 at 0 °C.	226
Scheme 5. 35. Synthesis of poly (DMA) ₈₀ -b- (NIPAM) ₈₀ by SET-LRP in sheep serum with [initiator]: [CuBr]: [Me ₆ TREN] = 1: 0.8: 0.4 at 0 °C.	227
Scheme 5. 36. SET-LRP of D-mannose glyco monomer in H ₂ O at 0 °C <i>via</i> disproportionation of CuBr / Me ₆ TREN.	228
Scheme 5. 37. Copper(0) wire mediated SET-LRP of D-mannose glyco monomer in H ₂ O at ambient temperature.....	229
Scheme 5. 38. SET-LRP of DEGEEA in MeOH/H ₂ O at 0 °C <i>via</i> disproportionation of CuBr / Me ₆ TREN.	229
Scheme 5. 39. Synthesis of poly (Mannose) ₁₀ -b- (NIPAM) ₈₀ by SET-LRP in H ₂ O with [initiator]: [CuBr]: [Me ₆ TREN] = 1: 0.8: 0.4 at 0 °C.	230
Scheme 5. 40. Synthesis of poly (Mannose) ₁₀ -b- (DEGEEA) ₈₀ by SET-LRP in sheep serum with [initiator]: [CuBr]: [Me ₆ TREN] = 1: 0.8: 0.4 at 0 °C.	231
Scheme 5. 41. SET-LRP of NIPAM (DP = 80) <i>via</i> disproportionation of CuBr / PMDETA or TREN in H ₂ O at 0 °C.....	233

List of Tables

Table 1.1 Specific polymerization conditions for the synthesis of glycopolymers <i>via</i> copper mediated LRP.....	4
Table 1.2 Specific polymerization conditions for the synthesis of glycopolymers <i>via</i> RAFT ..	6
Table 3. 1. Literature reported constants for monosaccharide binding to extracellular domain fragments of DC-SIGN ¹⁷⁴	64
Table 3. 2. The results of inhibition concentration of glycopolymers.	65
Table 4. 1. Polymerization data for CD-centered star glycopolymers via SET-LRP.	104
Table 4. 2. Properties of saquinavir mesylate encapsulation test from CD-based glycoconjugates.....	115
Table 5. 1. Summary of results obtained from the polymerization of hydrophilic monomers via SET-LRP mediated by in situ disproportionation of CuBr / Me ₆ TREN.	185
Table 5. 2. Charging amounts for SET-LRP of NIPAM (DP=8) in H ₂ O at 0 °C and ambient temperature with [initiator]: [CuBr]: [Me ₆ TREN] = 1: 0.4: 0.4.....	210
Table 5. 3. Charging amounts for SET-LRP of NIPAM (DP=40) in H ₂ O at ambient temperature with [initiator]: [CuBr]: [Me ₆ TREN] = 1: 0.4: 0.4.....	211
Table 5. 4. Charging amounts for SET-LRP of NIPAM (DP=80) in H ₂ O at ambient temperature with [initiator]: [CuBr]: [Me ₆ TREN] = 1: 0.4: 0.4.....	211
Table 5. 5. Charging amounts for SET-LRP of NIPAM (DP=80) in H ₂ O at ambient temperature with [initiator]: [CuBr]: [Me ₆ TREN] = 1: 0.8: 0.4.....	212
Table 5. 6. Charging amounts for SET-LRP of NIPAM (DP=160) in H ₂ O at ambient temperature with [initiator]: [CuBr]: [Me ₆ TREN] = 1: 0.4: 0.4.....	212
Table 5. 7. Charging amounts for SET-LRP of NIPAM (DP=160) in H ₂ O at ambient temperature with [initiator]: [CuBr]: [Me ₆ TREN] = 1: 0.8: 0.4.....	213
Table 5. 8. Charging amounts for SET-LRP of NIPAM (DP=160) in H ₂ O at 0 °C with [initiator]: [CuBr]: [Me ₆ TREN] = 1: 0.8: 0.4.....	213
Table 5. 9. Charging amounts for SET-LRP of NIPAM (DP=160) in H ₂ O at ambient temperature with [initiator]: [CuBr]: [Me ₆ TREN] = 1: 1.2: 0.4.....	213
Table 5. 10. Charging amounts for SET-LRP of NIPAM (DP=320) in H ₂ O at 0 °C with [initiator]: [CuBr]: [Me ₆ TREN] = 1: 0.8: 0.4.....	214
Table 5. 11. Charging amounts for SET-LRP of NIPAM (DP=20) in H ₂ O at ambient temperature with [initiator]: [CuBr]: [Me ₆ TREN] = 1: 0.4: 0.4.....	215
Table 5. 12. Charging amounts for SET-LRP of NIPAM (DP=40) in H ₂ O at 0 °C with [initiator]: [CuBr]: [Me ₆ TREN] = 1: 0.4: 0.4.....	216

Table 5. 13. Charging amounts for SET-LRP of NIPAM (DP=40) in H ₂ O at 0 °C with [initiator]: [CuBr]: [Me ₆ TREN] = 1: 0.8: 0.4.....	216
Table 5. 14. Charging amounts for SET-LRP of NIPAM (DP=20) in H ₂ O at 0 °C with [initiator]: [CuBr]: [Me ₆ TREN] = 1: 0.4: 0.4.....	217
Table 5. 15. Charging amounts for SET-LRP of NIPAM (DP=20) in H ₂ O at 0 °C with [initiator]: [CuBr]: [Me ₆ TREN] = 1: 0.4: 0.4.....	218
Table 5. 16. Charging amounts for SET-LRP of DMA (DP=80) in sheep serum at 0 °C with [initiator]: [CuBr]: [Me ₆ TREN] = 1: 0.8: 0.4.....	225
Table 5. 17. Charging amounts for SET-LRP of NIPAM (DP=80) in sheep serum at 0 °C with [initiator]: [CuBr]: [Me ₆ TREN] = 1: 0.8: 0.4.....	226
Table 5. 18. Charging amounts for SET-LRP of DMA (DP=80) in sheep serum at 0 °C with [initiator]: [CuBr]: [Me ₆ TREN] = 1: 0.8: 0.4.....	227
Table 5. 19. Charging amounts for SET-LRP of NIPAM (DP=80) in H ₂ O at 0 °C with [initiator]: [CuBr]: [PMDETA] or [TREN] = 1: 0.8: 0.4.....	233

Abbreviations

AGET	Activators generated by electron transfer
AIBN	Azobisisobutyronitrile
AM	Acryl amide
ARGET	Activator regenerated by electron transfer
ATRP	Atom transfer radical polymerisation
bpy	2,2'-Bipyridine
CBP	Carbohydrate binding proteins
CCTP	Catalytic chain transfer polymerisation
CDs	Cyclodextrins
β CD	β -cyclodextrin
CRP	Controlled radical polymerisation
CLD	Chain length distribution
CTA	Chain transfer agent
CuAAC	Cu(I)-catalysed azide-alkyne cycloaddition
DC	Dendritic cells
DCM	Dichloromethane
DC-SIGN	Dendritic cell-specific intercellular adhesion molecule-3-grabbing non-integrin
DP	Degree of polymerisation
CoBF	Bis(boron difluorodimethylglyoximate) cobalt(II)
DMPP	Dimethylphenylphosphine
DEGMA	Diethylene glycol methacrylate
DMF	Dimethyl formamide
DMSO	Dimethyl sulfoxide
DRI	Differential refractive index
DC-SIGN	Dendritic cell specific ICAM-3 grabbing nonintegrin
eATRP	Electrochemically mediated ATRP
ESI-MS	Electrospray ionisation mass spectrometry
FRP	Free radical polymerisation
FT-IR	Fourier-transform infrared
GPC	Gel permeation chromatography

Gal	Galactose
Glc	Glucose
HIV	Human immunodeficiency virus
HEMA	2-Hydroxyethyl methacrylate
ICAR	Initiators for continuous activator regeneration
LCST	Lower critical solution temperature
MA	Methyl acrylate
MAA	Methacrylic acid
Man	Mannose
MALDI-TOF	Matrix assisted laser desorption ionisation - time of flight
MS	mass spectrometry
M_n	Number average molecular weight
M_w	Weight average molecular weight
MMA	Methyl methacrylate
MA	Methyl acrylate
MIC_{50}	Minimum inhibitory concentration for half-maximum precipitation
NIPAM	<i>N</i> -Isopropyl acrylamide
NMP	Nitroxide mediated polymerisation
NMR	Nuclear magnetic resonance
PDI	Polydispersity index
PCL	Poly(ϵ -caprolactone)
PGMA	Poly(glycidyl methacrylate)
PEG	Poly(ethylene glycol)
PEO	Poly(ethylene oxide)
PS	Polystyrene
ppm	Parts per million
RAFT	Reversible addition fragmentation chain transfer
ROP	Ring-opening polymerisation
siRNA	Short interfering RNA
SET-LRP	Single electron transfer living radical polymerisation
SPR	Surface plasmon resonance
SBA	Solid-phase binding assay

SEC	Size Exclusion Chromatography
SR&NI	Simultaneous reverse and normal initiation
TEA	Triethylamine
TBTA	Tris(benzyltriazolyl)methyl amine
TMS-PMA	TMS-protected propargyl methacrylate
THF	Tetrahydrofuran
TBAF	Tetrabutylammonium fluoride
TMS	Tetramethylsilane
UV-VIS	Ultra violet-visible

Acknowledgements

I would like to thank all the people who helped me in the past three years since I came to the University of Warwick.

First and foremost, I would like to thank my supervisor, Professor David M Haddleton, for the opportunity to be his student, for the guidance and help through my research, for the constant encouragement and generous support he gave me so that I can achieve my objectives. The way he does research and treats his students will be a model for me.

I am lucky to be arranged in an office for post-doctors. During my early beginning of PhD, Dr. Remzi Becer, Nicole Jagielski, Florence Gayet and Julien Rosselgong gave me much help. I would also like to thank Dr. Remzi Becer, Paul Wilson and Ronan Mchale for their useful discussion and great help during my research.

I would like to thank the Haddleton group members during the past three years. First goes to Stacy, Matthew, George, Antony, Jasmin, Kay, Muxiu, Jenifer, Claudia, Athina, Alice and Ronan, who are members of C223, worked together with me and enjoyed playing music and teaching me how to dance. Thanks then go to Guangzhao, Yanzi, Zaidong, Alex, Chris W & S, Jamie, Vasiliki, Raj, James and Paul, for your tolerance allowing me to steal solvents from C222.

Special thanks go to Dr. Stefan Bon and Rachel O'Reilly for evaluating the progress of my PhD study.

I am grateful for the funding sources that allowed me to pursue my PhD study: University of Warwick and China Scholarship Council. I also acknowledge my seven years' bachelor and master experience in Beijing Normal University, which gave me very solid experimental skill, knowledge background and scientific thinking.

I would also like to thank my parents. Without your unconditional love and support throughout these years I cannot make this happen. Finally, I would like to give my special thanks to my wife, who totally trusted me and gave me her great love, suggestion and support throughout these years. This thesis is dedicated to you all!

Declaration

Experimental work contained in this thesis is original research carried out by the author, unless otherwise stated, in the Department of Chemistry at the University of Warwick, between October 2010 and June 2013. No material contained herein has been submitted for any other degree, or at any other institution.

Results from other authors are referenced in the usual manner throughout the text.

Date: _____

Qiang Zhang

Abstract

In chapter one, recent progress in the synthesis of functional glycopolymers was described.

In chapter two, combination of catalytic chain transfer polymerisation (CCTP) with both thiol-ene and copper catalysed alkyne azide coupling (CuAAC) click chemistry has been employed to give a new route to functional glycopolymers for applications in bioconjugation and biological targeting. Ring opening of poly (glycidyl methacrylate) with sodium azide and subsequent reaction with alkyne functional carbohydrates, as prepared by Fischer glycosylation, has been exploited. This combination of a range of efficient chemistry gives a route to multi gram quantities of glycopolymers avoiding the need for living radical polymerisation chemistry.

In chapter three, multi-block glycopolymers made of mannose, glucose, fucose and di(ethylene glycol) ethyl ether acrylate monomers were synthesized by Cu(0) wire mediated single electron transfer living radical polymerization (SET-LRP). These highly narrow disperse glycopolymers were then tested for binding and inhibition of DC-SIGN, a protein important for HIV infection.

In chapter four, a series of cyclodextrin-based glycoconjugates, including glyoclusters and star glycopolymers, were synthesised *via* combination of CuAAC click reaction and copper-mediated living radical polymerization. These glycoconjugates show high affinity in binding with human DC-SIGN lectin and could be used as inhibitor to prevent the binding of HIV envelope protein gp120 to DC-SIGN at nanomolar concentration. The star block glycopolymer show high loading capacity of hydrophobic anti-cancer and anti-HIV drugs, indicating promising application in HIV-therapeutic and smart drug delivery.

In chapter five, a new approach to perform SET-LRP in pure water is described. The key step in this process is to allow full disproportionation of CuBr/Me₆TREN (Me₆TREN = tris(dimethylamino)ethyl amine) to Cu(0) powder and CuBr₂ in water prior to addition of both monomer and initiator. This provides an extremely powerful tool for the synthesis of functional water-soluble polymers with controlled chain length and narrow molecular weight distributions (PDI approx. 1.10), including poly-NIPAM, DMA, PEG acrylate, HEA and glycomonomers. The polymerizations are

performed at or below ambient temperature with quantitative conversions attained in minutes. Polymers have high chain end fidelity capable of undergoing chain extensions to full conversion or multi-block copolymerization via iterative monomer addition after full conversion. Activator generated by electron transfer atom transfer radical polymerization (AGET ATRP) of NIPAM in water was also conducted as a comparison with the SET-LRP system. This shows that the addition sequence of L-ascorbic acid is crucial in determining the onset of disproportionation, or otherwise. This robust technique was applied to polymerizations under biologically relevant conditions (PBS buffer), a complex ethanol/water mixture (Tequila) and a truly biological condition: sheep blood serum. Finally, double hydrophilic diblock glycopolymers composed of mannose glycopolymer block and LCST PNIPAM or PDEGEEA block were successfully synthesized by this aqueous SET-LRP technique.

Chapter 1 Introduction

Glycopolymers are generally considered as synthetic macromolecules featuring sugar moieties, which have showed promise in bio-related applications.¹ This field has benefited from the development of synthetic polymer chemistry and the past two decades has evidenced a dramatical progress in the synthesis of functional glycopolymers. The strategies in the glycopolymer synthesis have been generally carried out as either direct polymerization of glycomonomers or post-glycosylation of pre-formed polymers.² As a special case, glycopolymers can also be synthesised *via* simultaneous Cu(I)-catalysed azide-alkyne cycloaddition reactions (CuAAC) and living radical polymerization, which is in actual fact a hybrid of the previous two strategies.³

By the combination of living polymerization (LP) and click chemistry, different strategies have been developed for the efficient synthesis of glycopolymers with defined structure and function, which have been already discussed in detailed reviews separately by Haddleton, Stenzel, Cameron, Maynard and co-authors.^{1,2,4-6} The applications of glycopolymers such as therapeutic and drug delivery, multivalent recognitions with lectins and signal transduction have been summarized in recent reviews by Cameron, Stenzel, Remzi, Kiessling and co-authors.^{2,7-9} Thus there has been very intensive research on glycopolymers' synthesis and application and most of the research until 2011 has been summarized in previous reviews. However, new strategies are constantly emerging during 2011-2013 and thus introduced as below.

1.1 Novel strategies in the direct polymerization of glycomonomers

1.1.1 Ring-opening polymerization

Ring-opening polymerization, including cationic, anionic and enzymatic ring-opening polymerization which depends on the catalyst type or the reactive centre of the propagating chain is carbocation or carbanion, has a long history since 1950s and widely used for polymerization of different functional cyclic monomers.¹⁰ However, its application in the direct polymerization of carbohydrate-containing cyclic monomers was limited.^{11,12} Recently, the Schubert group synthesized a glucose-

substituted 2-oxazoline monomer (Figure 1.1) *via* CuAAC and used it for cationic ring-opening copolymerization (CROP) with 2-oxazoline-based monomers, yielding well-defined glycopolymers bearing functional groups for thiol-ene reactions to tune the properties.¹³

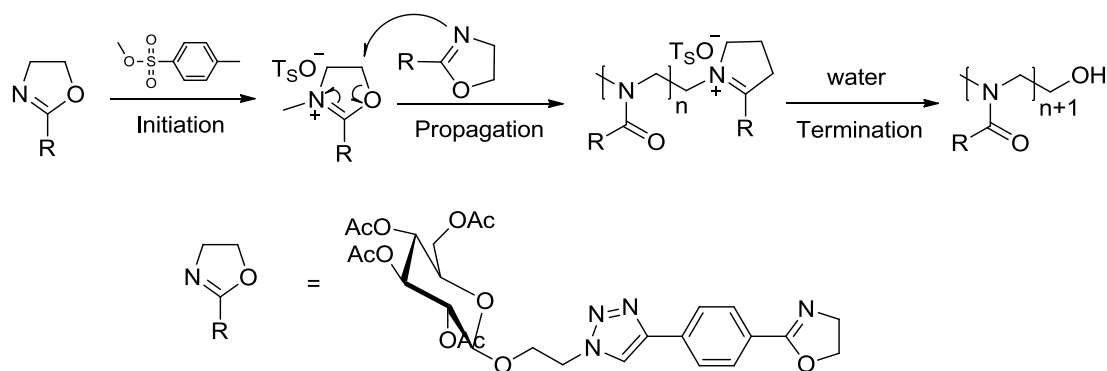


Figure 1.1 Synthesis of glyco-poly(2-oxazoline)s by ring-opening polymerization.

Although the polymerisation of protected glycomonomer require high reaction temperatures ($\sim 120\text{ }^{\circ}\text{C}$) and long reaction times (overnight) for this CROP, final glycopolymers have relatively narrow MW distribution (~ 1.3) and the poly(2-oxazoline) backbones are biocompatible and considered as analogues of poly(amino acids), which may have potential application in drug delivery.

1.1.2 Copper mediated living radical polymerization

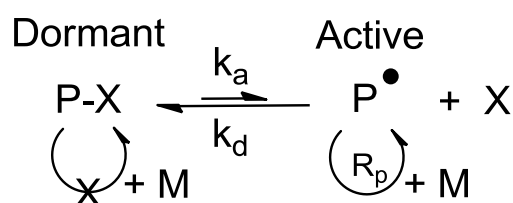


Figure 1.2 Reversible and dynamic equilibrium between active radical growing species and dormant species

Radical species usually have poor chemo- and regio-selectivity in organic reactions and tend to undergo bimolecular termination and disproportionation in polymerizations. Thus in order to get precise control in radical polymerization, a reversible and dynamic equilibrium between active radical growing species and dormant species is necessary to control the concentration of active radicals at low level, while the relatively stable dormant species could avoid side reactions or propagations yet able to generate propagation-active intermediate by dissociation of

the leaving groups *via* chemical catalysis or physical stimuli.¹⁴ Different strategies have been developed to conduct this equilibrium with different leaving groups including halides, stable radicals or thiolcarbonylthio compounds etc. *via* varying dissociation manners such as reversible termination, degenerative chain transfer and addition-fragmentation chain transfer etc. Most of the present methods in living radical polymerizations should be based on this concept.¹⁵

Transition metal-catalyzed living radical polymerization is one of the most popular, versatile and robust polymerization methods for synthesis of various functional polymers with controlled chain length, architecture and molecular weight distribution since its development in late 20th century.¹⁶⁻¹⁸ The initiators are generally organic halides with potentially active carbon-halogen bonds for radical generation or conventional radical initiators, of which both are either commercially available or could be facilely synthesized. The transition-metal catalysts are generally from transition metals of groups 8-11, typically including iron, nickel, ruthenium and copper. Copper catalysts have been the most popular within the transition-metal catalysts, which showed to be easily handled and highly efficient in catalysis.¹⁵

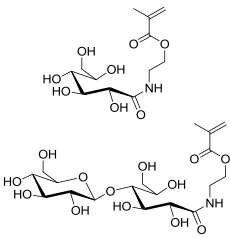
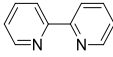
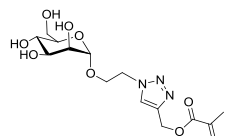
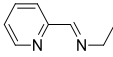
For the copper(I) system, probably the most well-known case is the so-called atom transfer radical polymerization (ATRP), which utilized lower oxidation state copper (I) halide and nitrogen-based ligand complexes as the catalyst. Further research including simultaneous reverse and normal initiation (SR&NI) ATRP, activators generated by electron transfer (AGET) ATRP, activator regenerated by electron transfer (ARGET) ATRP, initiators for continuous activator regeneration (ICAR) ATRP and electrochemically mediated ATRP (eATRP) were developed, in which copper (I) generated by reduction of higher oxidation state copper (II) was believed to be always present in the system and act as the predominant activator.¹⁹

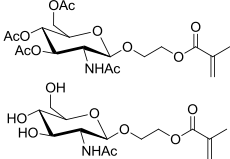
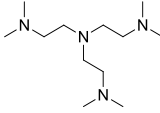
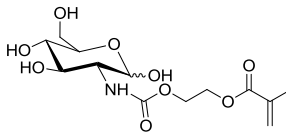
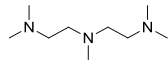
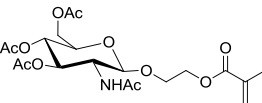
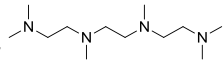
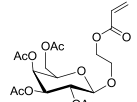
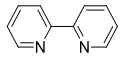
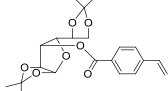
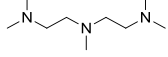
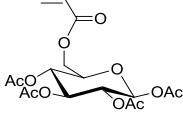
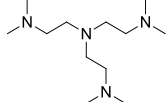
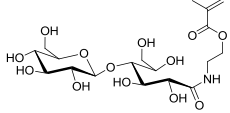
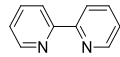
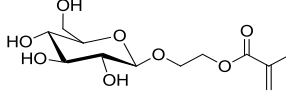
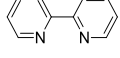
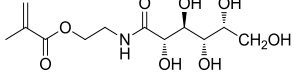
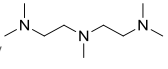
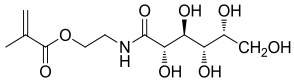
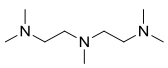
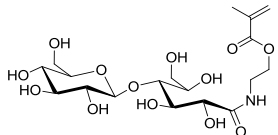
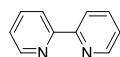
For the copper(0) system, copper(I) was believed as a catalyst precursor to generate copper (0) to react with organic halides for radical generation. Previous research suggested that in polar solvents copper(I) halides and nitrogen-based ligand complexes perform rapid disproportionation into copper(0) and copper (II) halide and this disproportionation facilitates an ultrafast LRP, in which the radicals are generated from the nascent copper (0) atomic species and the deactivation is mediated by copper(II) halide. Both steps proceed *via* low activation energy outer-sphere single-

electron-transfer mechanism and thus the polymerization was named as single electron transfer living radical polymerization (SET-LRP).^{20,21}

Direct polymerization of a protected glycomonomer *via* ATRP was first reported in 1998 using CuBr/4, 4'-Di-n-heptyl-2, 2'-bipyridine catalyst in veratrole at 80 °C,²² Table 1.1, whilst direct copper mediated polymerization of unprotected glycomonomers was generally performed in high polar solvents such as alcohol, DMF, DMSO, NMP or mixtures with water.²³ The main reason choosing such highly polar solvents is to solubilize the glycomonomer and obtained glycopolymer, yet in some cases it showed low initiation efficiency or lack of control.^{23,24} Previous research also revealed that direct aqueous ATRP of unprotected glycomonomers showed poor living character and high ratios of alcohol as the co-solvent were required.^{25,26} The main reason is due to the fast propagation yet inefficient deactivation and side reactions under aqueous condition, such as hydrolysis of initiator and propagating polymer chain terminal groups and more important disproportionation of copper catalysts etc.²⁷ Pure water has only been used as the solvent for surface initiated polymerization, in which cases the chain end fidelity and molecular weight distribution tend to be not easily elucidated.²⁸⁻³⁰ Thus more efforts are necessary to develop a proper catalyst system which could efficiently catalyse the polymerization of glycomonomers under different conditions especially in aqueous media.

Table 1.1 Specific polymerization conditions for the synthesis of glycopolymers *via* copper mediated LRP

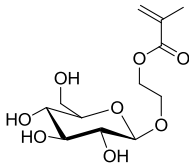
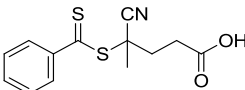
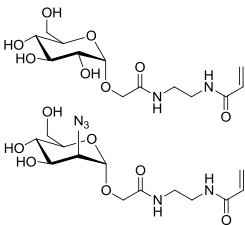
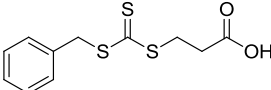
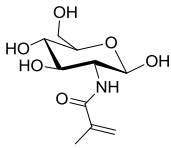
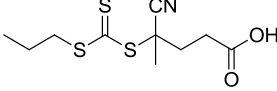
Glycomonomers	Catalysts	Solvents	Reaction temperature	Reference
	CuBr/ 	H ₂ O × MeOH MeOH/ H ₂ O NMP	20 °C	25
	CuBr/ 	MeOH/ H ₂ O (5:2)	25 °C	26

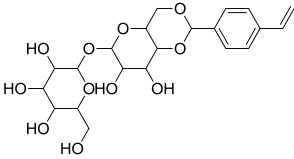
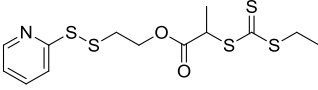
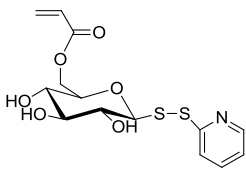
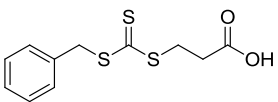
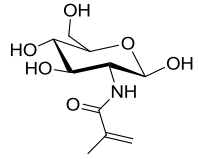
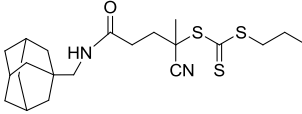
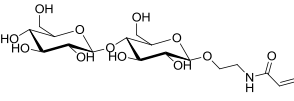
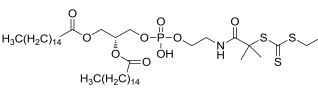
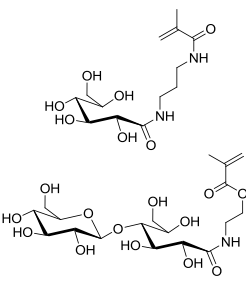
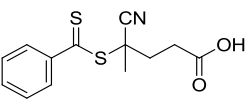
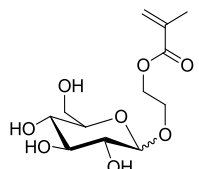
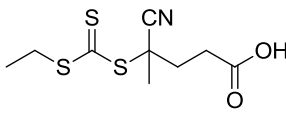
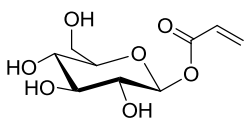
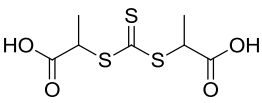
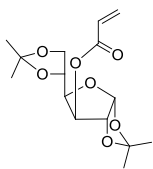
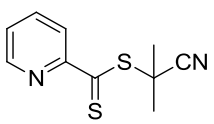
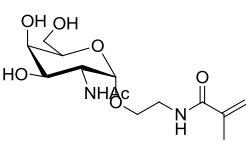
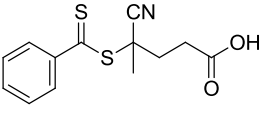
		DMSO MeOH	30 °C	23
	CuBr/ 	DMSO × DMF	40 °C (CuBr) 90 °C (CuCl)	24,31-33
	CuCl / 	Anisole DMSO	25 °C (DMSO) 60 °C (Anisole)	34,35
	CuBr / 	Chlorobenzene	80 °C	36,37
	CuBr / 	THF	60 °C	38,39
	CuBr / 	EtOAc	100 °C	40
	CuBr / CuBr ₂ / 	Pyridine/ H ₂ O	25 °C	41
	CuBr / 	MeOH/ H ₂ O	25 °C	42
	CuCl / CuCl ₂ / 	H ₂ O	30 °C	Surface initiated polymerization ³⁰
	Ascorbic acid / CuCl ₂ / 	H ₂ O	30 °C	Surface initiated polymerization ²⁹
	CuBr / CuBr ₂ / 	H ₂ O NMP	25 °C	Surface initiated polymerization ²⁸

1.1.3 Reversible addition-fragmentation chain transfer (RAFT) polymerization

Since the discovery of RAFT in 1998 it has become one of the most popular living polymerization processes as it is tolerant of a wide variety of functional monomers and reaction conditions and also is promising in bioapplications.^{43,44} For the synthesis of glycopolymers, RAFT is probably the most popular LRP route at present (about twice more published papers than ATRP on the synthesis of glycopolymers) and different strategies have been developed for polymerization of both protected and unprotected glycomonomers.^{2,44} As an interesting case, direct RAFT polymerization of unprotected glycomonomers in pure water was already reported in 2003, at which time it was still a challenge for direct aqueous ATRP of glycomonomers.^{25,45} Thus now most of the RAFT polymerizations of glycomonomers were conducted in aqueous systems with some ratio of organic solvents (DMF, alcohol, DMSO etc.) for the aim to solubilize the RAFT agents and radical sources. As illustrated in Table 1.2, most of the polymerizations were under 60-80 °C, although aqueous RAFT was already reported at room temperature.⁴⁶

Table 1.2 Specific polymerization conditions for the synthesis of glycopolymers *via* RAFT

Glycomonomers	RAFT agent	Solvents	Reaction temperature	Reference
		H ₂ O	70 °C	45
		H ₂ O/DMF (5:1)	70 °C	47
		Acetate buffer : ethanol (4:1)	70 °C	48

		DMF	80 °C	49
		Chlorobenzene	60 °C	50
		D ₂ O/DMSO	70 °C	51
		H ₂ O/DMF (4:1)	70 °C	52
		H ₂ O/DMF (5:1)	70 °C	53-55
		H ₂ O/EtOH (3:1)	70 °C	56
		D ₂ O	60 °C	57
		toluene	75 °C	58
		H ₂ O/DMF (3:7)	75 °C	59

1.2 Novel strategies in the post-glycosylation of pre-formed polymers

1.2.1 Copper-catalyzed azide-alkyne cycloaddition (CuAAC) reaction

CuAAC has been widely used in the post-glycosylation of pre-formed polymers, for which the protected alkyne monomers could be first polymerized by different LRP followed by removal of TMS protection groups using TBAF/acetic acid for click reaction with azido functional sugars (Figure 1.3).^{60,61} This approach avoids the use of hazardous azide-functionalised monomers and utilizes diversity of well-documented azido functional sugars.⁶⁰

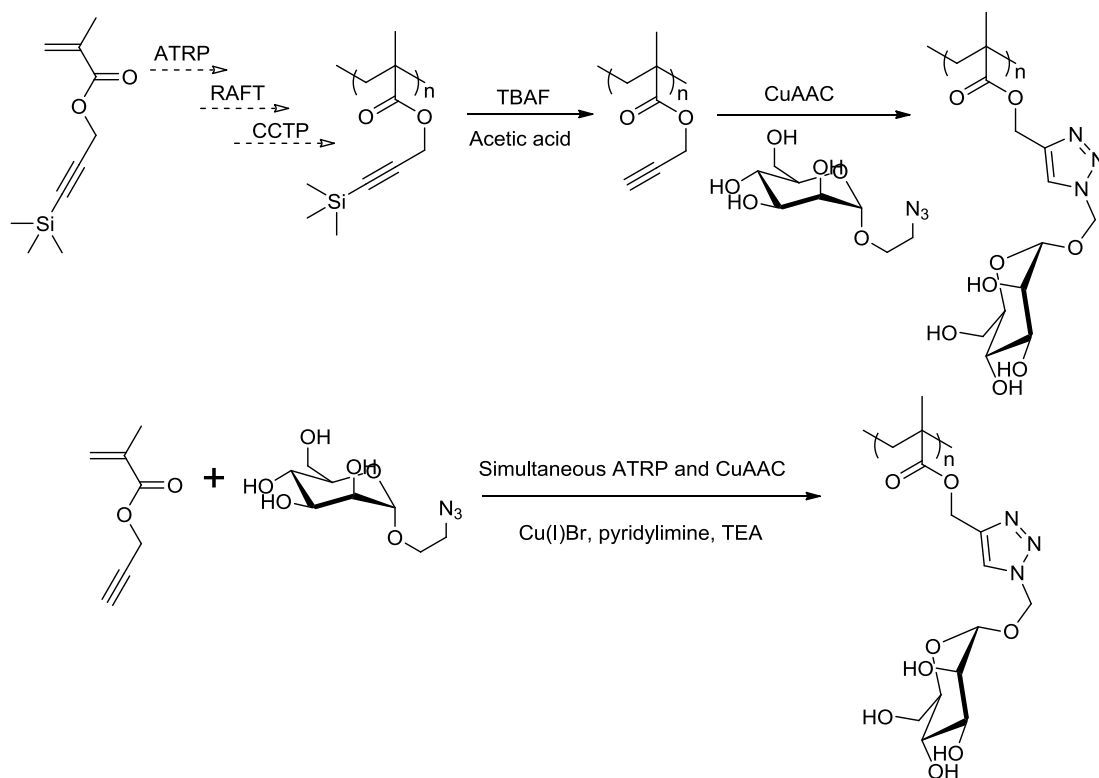


Figure 1.3 Synthesis of glycopolymers via CuAAC of azide sugar with alkyne functional polymer or monomer.

As an inverse approach, an insulin based glycopolymer was synthesized by sequential chemical modification composed of tosylation, azidation and subsequent click reaction with alkyne sugars.⁶² Due to the low ratio of tosylation, the azido functional insulin tends to be safe and obtained insulin-based glycopolymers showed enhanced lectin affinity and gelation properties (Figure 1.4).

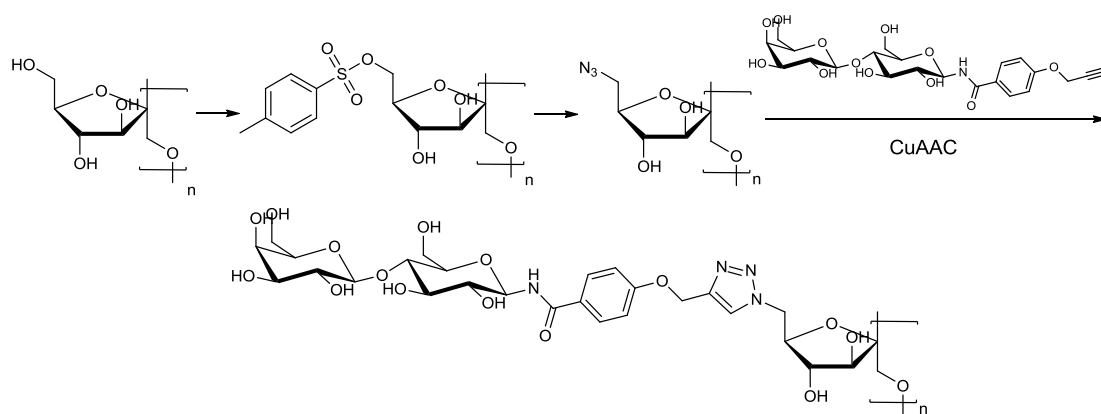


Figure 1.4. Synthesis of glycopolymers via CuAAC of alkyne sugar with azido functional insulin.

Based on the combination of CuAAC and LRP, one-pot simultaneous ATRP and CuAAC was developed as a new tool for synthesis of glycopolymer, which utilized unprotected alkyne monomer and azido sugar (Figure 1.3).³ As an inverse approach, a fluorescent glycopolymer could be synthesized *via* similar one-pot ATRP and CuAAC strategy using 2-azidoethyl methacrylate and alkyne mannose (Figure 1.5).⁶³

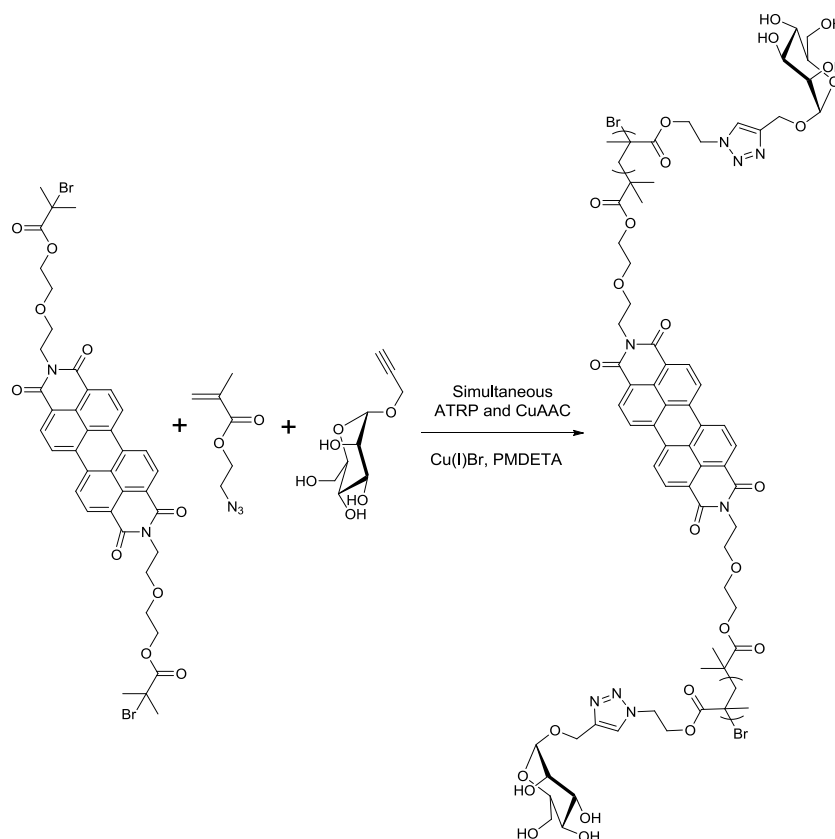


Figure 1.5. Synthesis of glycopolymers via simultaneous ATRP and CuAAC using azido monomer and alkyne sugars.

1.2.2 Thiol-click chemistry

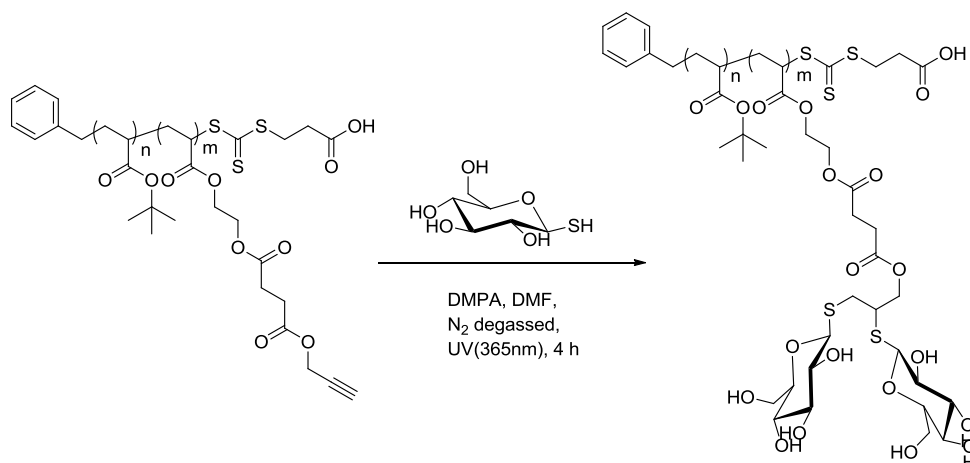


Figure 1.6. Synthesis of glycopolymers via thiol-alkyne click reaction.

Thiol groups can react with many chemical species with high yields under benign conditions and thus many thiol-related reactions, such as thiol-ene, thiol-yne, thiol-epoxy, thiol-isocyanate and thiol-halogen reactions, are considered as click type reactions.⁶⁴

Thiol-yne coupling reaction is versatile, robust and can tolerate different functional groups due to its radical nature. It allows facile addition of two thiols to one alkyne group, which suits for construction of complex polymer structure such as network, dendrimer and hyper-branched polymers.^{64,65} Successful glycosylation of linear polymers and dendrimers can be performed *via* radical-mediated thiol-alkyne click reaction, in which the 1-thiol-β-D-glucose reacted with the alkyne group under the existence of photo-initiator and UV light, Figure 1.6.⁶⁶

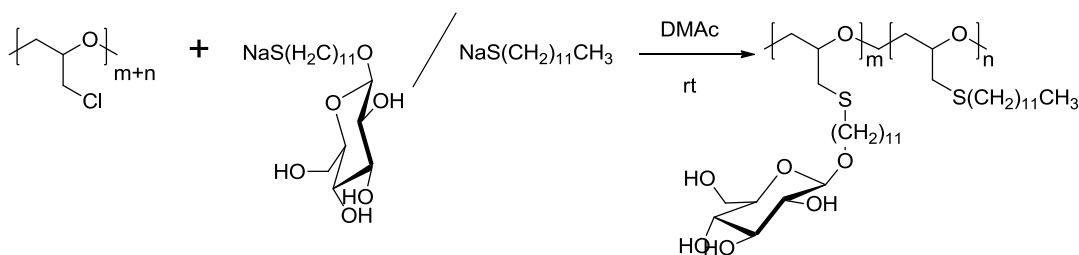


Figure 1.7. Synthesis of glycopolymers via thiol-halogen click reaction

Thiol-halogen reactions, such as nucleophilic substitution reactions of thiocarbohydrate sodium salt with halogen-containing polymers, have been used for direct synthesis of glycopolymers.⁶⁷ This is a relatively slow reaction, however, no

catalyst is needed and hazardous side products are also avoided. Thus further research was reported utilizing a similar method as shown in Figure 1.7.⁶⁸

1.2.3 Amine chemistry

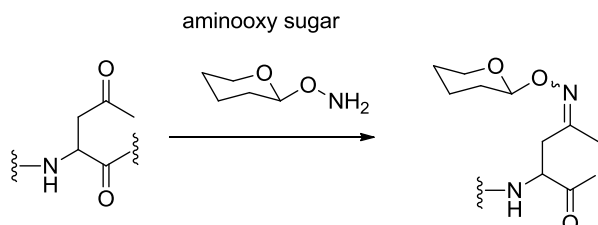


Figure 1.8. Synthesis of glycopolymers by the reaction of ketones with aminooxy sugars.

Condensation reactions between ketone groups and aminooxy sugars have become a tool for synthesis of glycopolymers and glycopeptides (Figure 1.8).⁶⁹⁻⁷¹ Generally the reactions can be performed in acetate buffer or organic solvent/water mixtures at ambient temperature or higher temperatures (up to 95 °C). The reaction conversion is medium at ambient temperature and close to full conversion under high temperature; however, reaction times could be up to 4-7 days.

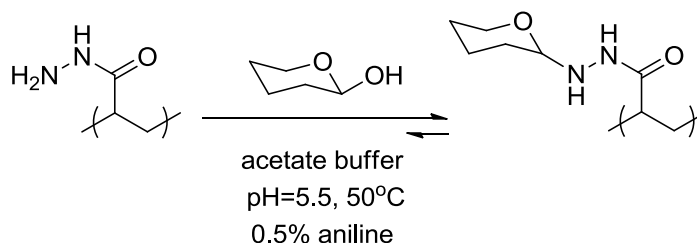


Figure 1.9. Synthesis of glycopolymers by reaction of free reducing sugar with hydrazide functional polymer.

In order to eliminate the multistep reactions required for glycopolymer synthesis, free reducing sugars were directly used for the reaction with hydrazide functional polymer (Figure 1.9) under acidic conditions in the presence of aniline catalyst.⁷² Different sugars including mannose, fucose, lactose, xylose and panose etc. were demonstrated with this reaction giving conversions ranging from 34% to up to 95%.

Poly(pentafluorophenyl methacrylate) (PPFMA) bearing active ester groups could react with a wide variety of functional amines (Figure 1.10). Glycopolymers have been synthesized by direct reaction of PPFMA with glucose amine or first with propargyl amine then with azido sugar *via* CuAAC, in which case glycopolymer with

different linker length and density could be adjusted by the length of propargyl amines.^{73,74}

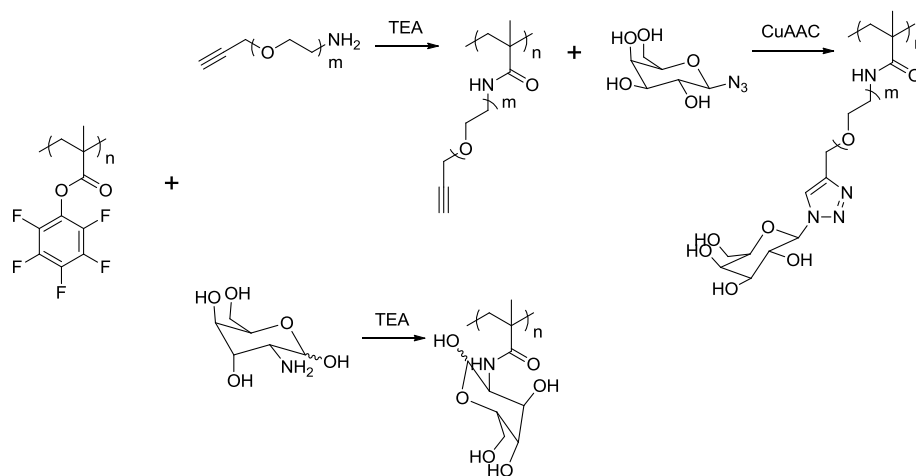


Figure 1.10. Synthesis of glycopolymers by reaction of poly(pentafluorophenyl methacrylate) with functional amines.

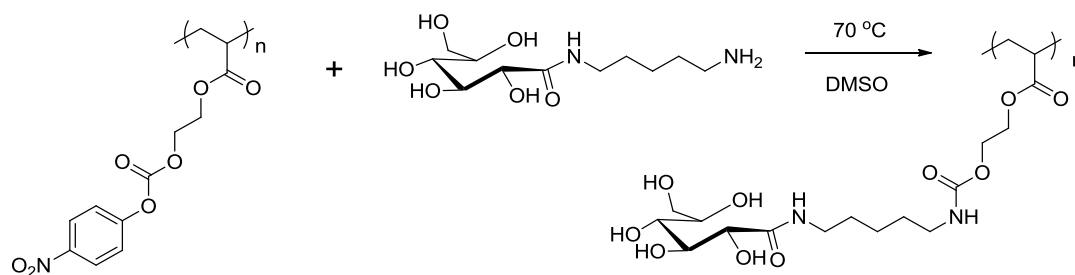


Figure 1.11. Synthesis of glycopolymers by reaction of polymers bearing reactive p-nitrophenyl carbonate with amine functional sugar.

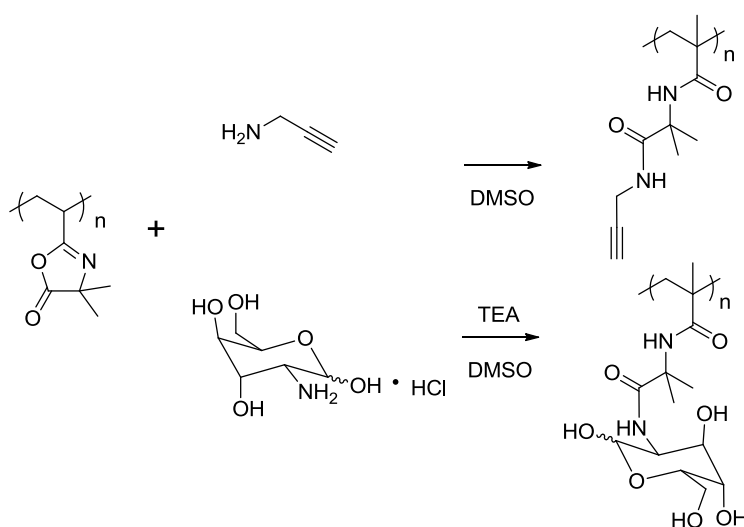


Figure 1.12. Synthesis of glycopolymers by reaction of poly(azlactone) with amine functional sugar.

Other polymers bearing active ester groups, such as highly reactive *p*-nitrophenyl carbonate groups, can also react with amine functional sugar for the synthesis of glycopolymer (Figure 1.11).^{75,76} Utilizing the nucleophilic ring opening reaction of azlactone with amine, poly(galactose) glycopolymers with long linker length between carbohydrate and backbone were synthesized by direct post-polymerization modification of poly(azlactone) scaffold and showed to be very active against the cholera toxin (Figure 1.12).⁷⁷

1.3 Novel applications of glycopolymers

1.3.1 Therapeutic application: Anti-cancer and Anti-HIV

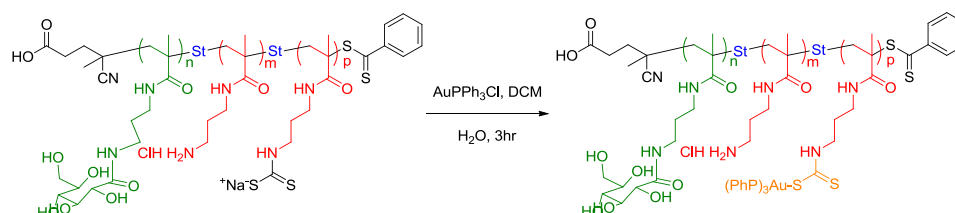


Figure 1.13. Synthesis of glycopolymer-dithiocarbamates gold conjugates.

Carbohydrate based anticancer agents have been explored with the aim of increasing the efficacy and to decrease the side effects of traditional anticancer Pt-based drugs.^{78,79} Recently, glycopolymer based dithiocarbamates conjugates modified with glod(I) phosphine (Figure 1.13) are synthesized and explored for the cytotoxicity profiles, which suggested that the gold conjugates showed higher accumulation and cytotoxicity to cancer cells due to the existence of glycopolymers and the affection to the normal breast cell is not significant.⁸⁰

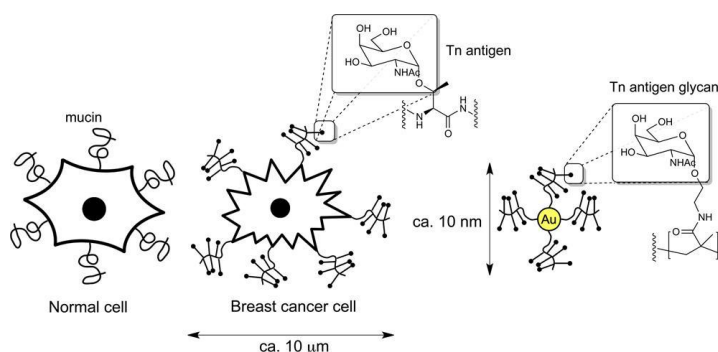


Figure 1.14. Multicopy Multivalent' glycopolymer-stabilized gold nanoparticles as potential synthetic cancer vaccines.⁵⁹

Alison et al synthesized a series of *N*-acetyl-D-glucosamine based glycopolymers by RAFT and subsequently conjugated these glycopolymers to gold nanoparticles yielding a type of multicopy multivalent nanoscale glycoconjugate (Figure 1.14).⁵⁹ These glycopolymer-stabilized gold nanoparticles could generate strong and long-lasting production of antibodies for selective recognition with Tn-antigen thus has the potential as a novel anticancer vaccine.

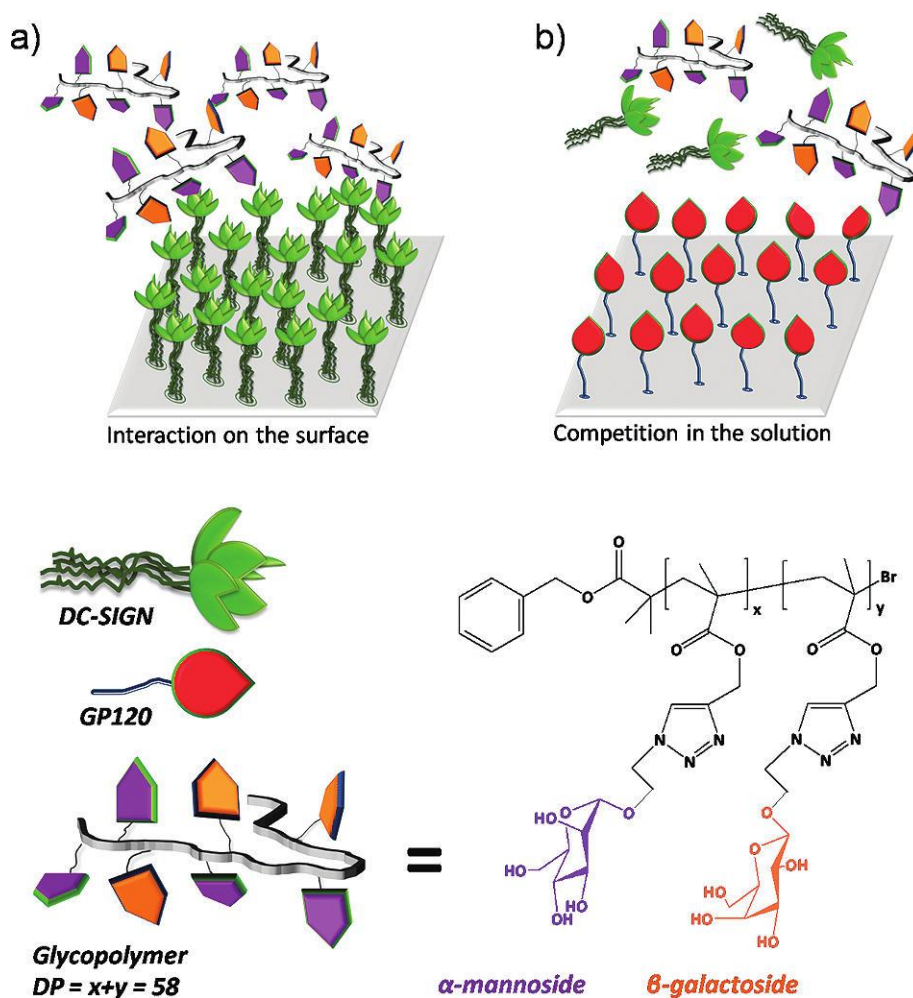


Figure 1.15. High-affinity glycopolymers binding to human-DC-SIGN and disruption of DC-SIGN interactions with gp120.⁸¹

Relatively simple mannose containing glycopolymers can effectively bind to human dendritic cell associated lectin (DC-SIGN) and disrupted the interaction of DC-SIGN interactions with HIV envelope glycoprotein gp120, which could be seen as a new approach for therapeutic (Figure 1.15).⁸¹

1.3.2 Bio-compatible materials

Hyperbranched glycopolymers (Figure 1.16) have been tested for the blood biocompatibility, which revealed that glycopolymers are highly hemocompatible and do not induce clot formation, red blood cell aggregation and immune response suggesting a fine bio-compatible materials.⁵⁴

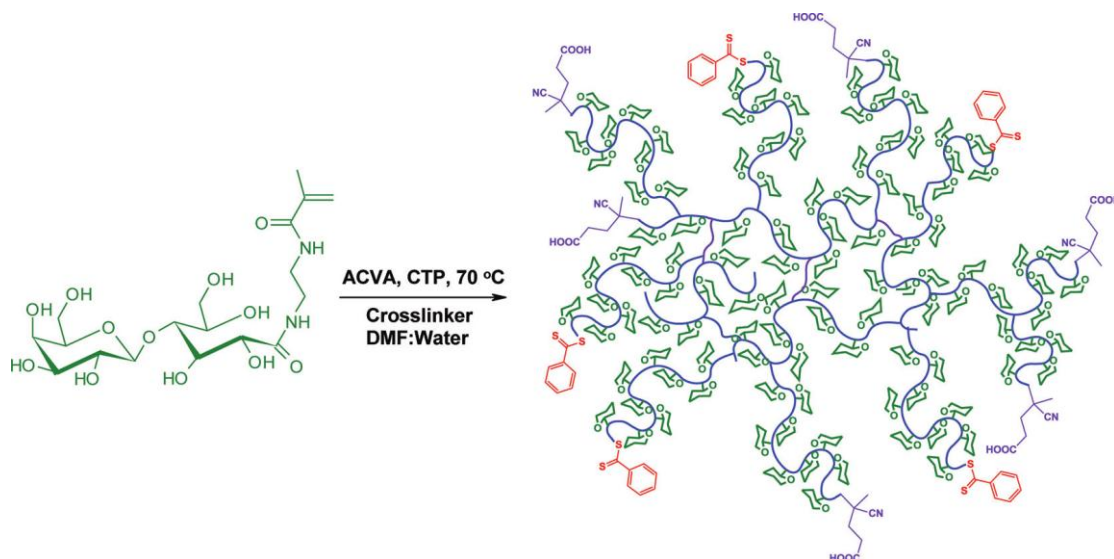


Figure 1.16. Synthesis of hyperbranched glycopolymers via RAFT.⁵⁴

Lactose and biotin-tagged glycopolymer could effectively absorb ricin and the obtained toxin-glycopolymer conjugate could be transferred onto the streptavidin-modified magnetic particles and thus decontamination was obtained (Figure 1.17).⁸²

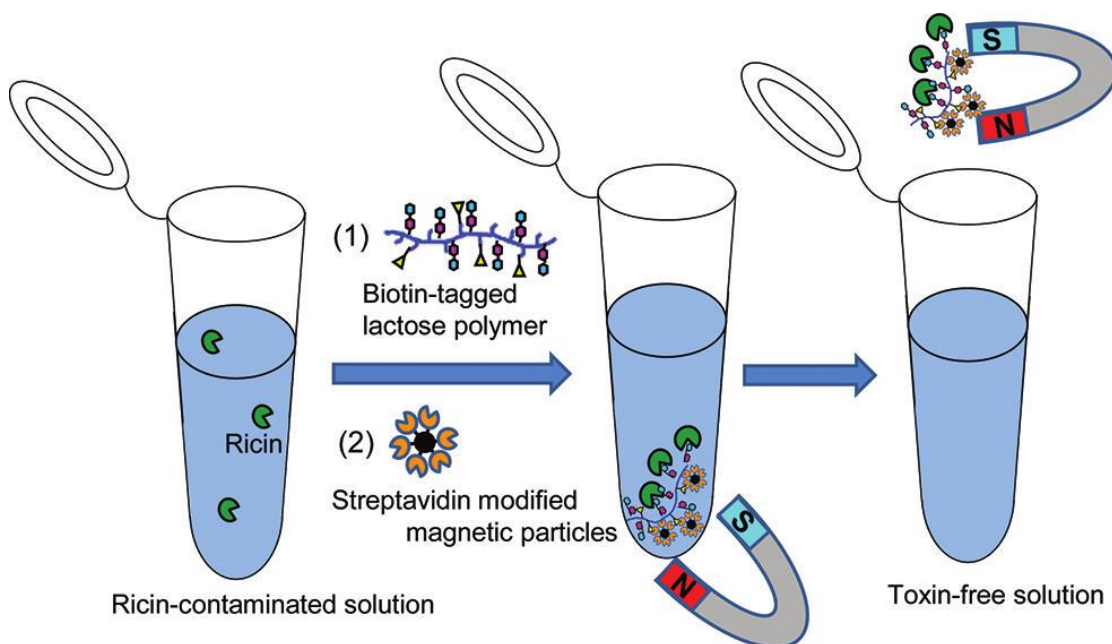


Figure 1.17. Ricin decontamination using biotin-tagged lactose polymer.⁸²

1.4 Conclusion

Although great progress has been achieved in the synthesis of functional glycopolymers, further efforts are still quite necessary for the synthesis of precise glycopolymers with defined structures and functions, including control of sugar sequence and synthesis of star glycopolymers which bear more close structure with cluster/dendritic oligosaccharides.

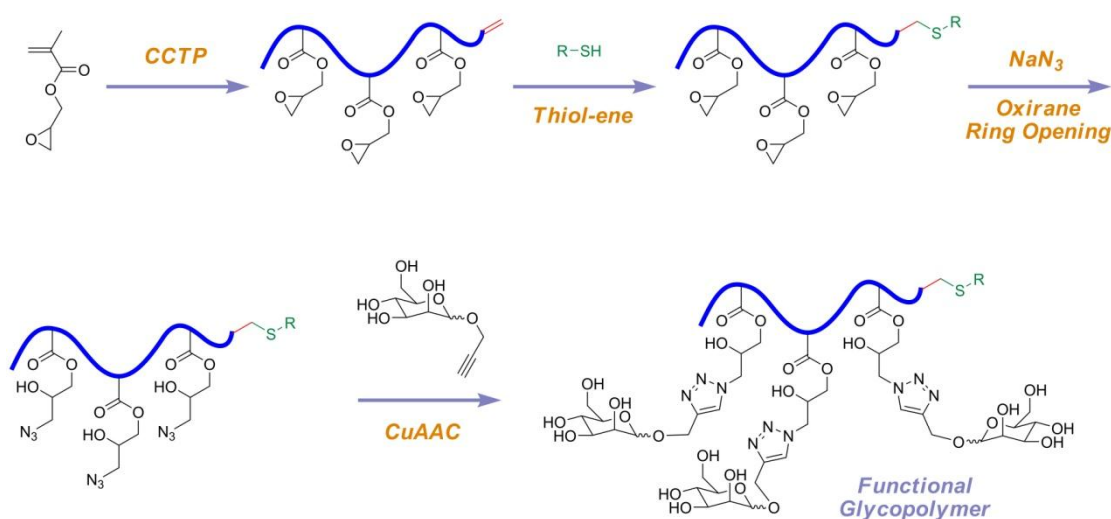
Based on the promising application of glycopolymers, it should be of great importance to make the synthesis more efficient, economy and environmental friendly. New catalyst system and more understanding are still required for copper mediated living radical polymerization in aqueous system.

In chapter two, a combination of CCTP, Fischer glycosylation and three consecutive click reactions was developed as a more commercial strategy for synthesis of glycopolymers.

In chapter three and four, SET-LRP and CuAAC were utilized for control of sugar sequence along polymer backbone and synthesis of complex cyclodextrin based glycoclusters and star glycopolymers.

In chapter five, new strategy was developed for copper mediated living radical polymerization in pure water. Block glycopolymers were then synthesized via aqueous SET-LRP.

Chapter 2 Terminal functional glycopolymers *via* a combination of catalytic chain transfer polymerisation (CCTP) followed by three consecutive click reactions



The combination of catalytic chain transfer polymerisation (CCTP) with both thiol-ene and copper catalysed alkyne azide coupling (CuAAC) click chemistry has been employed to give a new route to functional glycopolymers for applications in bioconjugation and biological targeting. Ring opening of poly (glycidyl methacrylate) with sodium azide and subsequent reaction with alkyne functional carbohydrates, as prepared by Fischer glycosylation, has been exploited. This combination of a range of efficient chemistry gives a route to multi gram quantities of glycopolymers avoiding the need for living radical polymerisation chemistry.

2.1 Introduction

Synthetic glycopolymers are important biological materials and play a vital role in many cell-cell communication events, such as preventing the interactions of human DC-SIGN lectin and the viral envelope glycoprotein gp120.⁸¹ The attachment of glycopolymers to peptides could significantly increase the stability of the conjugates to environmental stress, including lyophilization and heat.⁴⁹ The development of living polymerization and click chemistry have achieved great success in synthesizing many glycopolymers with different function and structure by either direct polymerization of glycomonomers or post polymerization glycosylation reactions.²

Since the introduction of Cu-catalyzed azide-alkyne cycloaddition reaction (CuAAC), it has become a highly versatile tool in polymer science for the design of novel materials and straightforward construction of complex macromolecular structures.⁸³⁻⁸⁵ CuAAC click reaction also provides a variety of new route to synthesizing glycopolymers. For the aim of post polymerization glycosylation, alkyne-functionalised polymers have been first synthesized by a number of techniques including atom transfer radical polymerization (ATRP), reversible addition fragmentation chain transfer polymerization (RAFT), ring opening polymerization (ROP) and catalytic chain transfer polymerisation (CCTP) for click reaction with azide sugar to yield targeted glycopolymers with different carbohydrate functionalities.^{26,60,61,86,87} This approach although effective, generally requires synthesis of monomers and in many cases such as ATRP, RAFT and CCTP it is often necessary to employ the TMS-based protection groups which need to be deprotected prior to a click reaction.

As an alternative approach, it would be possible to first synthesize the azide functionalised polymer and then carry out a click reaction with the alkyne sugar. ROP of 2-bromo- ϵ -caprolactone was carried out to give polymer with side bromide groups in order to avoid using an unstable azide monomer under heating polymerization conditions, which then was transformed into azide groups via substitution reaction with NaN_3 .⁸⁸ However, the multistep reactions were carried out under strict reaction conditions free from water and air prior to click reaction with an alkyne sugar to yield the biodegradable glycopolymers.

In order to search for better strategies for the synthesis of azide functionalised polymers, we noticed that commercial glycidyl methacrylate (GMA) monomer could

be polymerised *via* living radical polymerization which is suitable for a range of post polymerisation modification, including ring opening of the epoxide with NaN_3 for generation of both hydroxyl and azide functionalities.⁸⁹ Previous research reported the synthesis of graft polymers *via* ring opening of GMA based copolymers with NaN_3 and subsequent modification with alkyne-functionalised PEG using CuAAC to yield the desired graft polymer.⁹⁰ This strategy has proven to be an effective route to synthesise polymer brushes and “hairy” polymer nanoobjects.^{91,92} Despite the efficiency of this approach for the introduction of azido-functionality to polymer chains, its application for the synthesis of reactive scaffolds has not yet been explored. GMA could be polymerized via CCTP using low levels of appropriate cobalt(II) catalysts without a requirement for catalyst removal.⁹³ CCTP results in termination of a methacrylate polymerisation *via* abstraction of a hydrogen atom from the propagating chain to give a vinyl terminated product, which is available for subsequent nucleophilic thiol-ene Michael addition with small thiols to give end functional polymers.⁹⁴

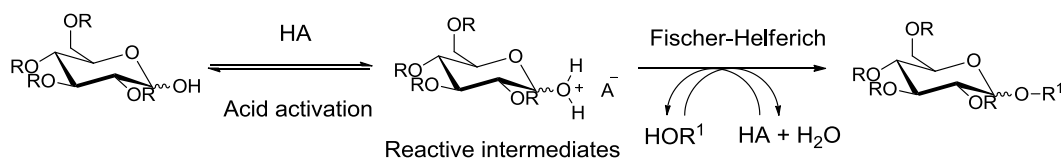
Nurmi et al. previously reported the synthesis of functional glycopolymers using a combination of CCTP, CuAAC and thiol-ene chemistry.⁶¹ This chapter reports an alternative approach to these structures, without the requirement for any protecting group chemistry. Polymerisation of GMA by CCTP, followed by three consecutive click reactions, namely thiol-ene, ring opening of the oxirane and CuAAC were employed as an efficient route to functional glycopolymers.

2.2 Results and discussion

2.2.1 Synthesis of alkyne functionalised sugar *via* Fischer glycosylation

Carbohydrates are one of the most widespread materials in nature. They are found not only in cellulose, starch, sucrose etc. which comprise macroscopic plants but also in cell membrane peptidoglycans and well-known glycoproteins such as ricin etc. which exist in the microscopic cell world. Although modern chemistry has developed for more than one century, since the introduction of quantum mechanics, glycochemistry is still considered as a challenge and a frontier of science, mainly due to the difficulty in the synthesis of complex carbohydrate structures and wide application in glycobiology.^{95,96} Carbohydrate containing polymers are considered to

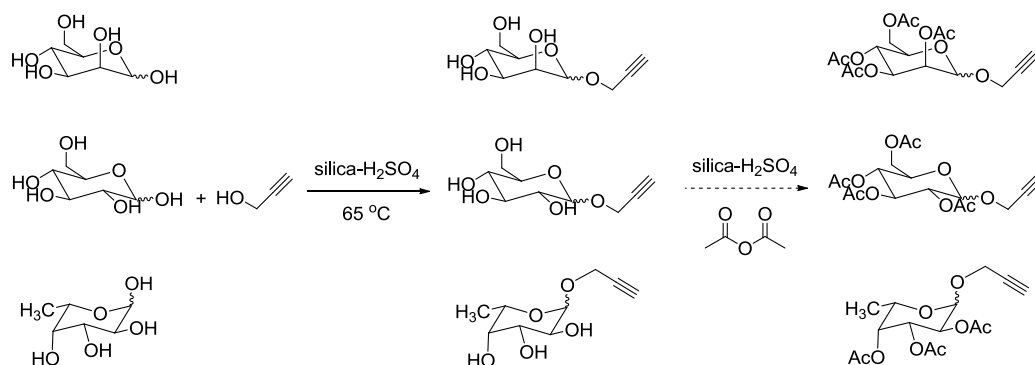
be at the centre of life's origins and the research of glycochemistry and glycobiology are recognized as one key route to find how natural life works.^{97,98}



Scheme 2. 1. Scheme for the Fischer-Helferich type glycosylation reaction.⁹⁹

Synthetic chemists have developed different synthetic protocols for oligosaccharide and glycoprotein synthesis, including chemical, enzymatic and automated solid-phase synthesis.¹⁰⁰⁻¹⁰⁴ Amongst these techniques the Fischer glycosylation reaction (Scheme 2.1), developed by Emil Fischer in 1890s for the acid-catalyzed synthesis of glycosides, still plays important role in the synthesis of simple alkyl and aryl glycosides even now.¹⁰⁵⁻¹⁰⁷ However, this famous reaction has some draw backs, including requirement for strong inorganic acids and excess alcohol at high temperature for relatively long reaction times.^{108,109}

Recently, silica gel supported acid catalysts such as silica-HClO₄ and silica-H₂SO₄ et al have been widely used in carbohydrate chemistry, including glycosylation, functional group transformation and hydrolysis.¹⁰⁹⁻¹¹¹ Silica-H₂SO₄ is a useful form of liquid H₂SO₄ acid as it is easier to handle and also easier to remove after reaction which only requires filtration. Its use in glycosylation has been proved to be an efficient alternative for the required transformation with less reaction time and lower alcohol equivalents.¹⁰⁹ Thus this one-pot Fischer glycosylation reaction was used for the synthesis of alkyne functional sugars from free sugars such as mannose, glucose and fucose with one propargyl alcohol functionality using silica-H₂SO₄ as catalyst at 65 °C (Scheme 2.2).



Scheme 2. 2. Scheme representation for the synthesis of alkyne functionalised sugar.

The glycosylation reactions were performed on a relatively large scale (100 mmol for D-mannose) and flash silica gel column chromatography (CHCl_3 : MeOH = 8: 1) could separate the alkyne sugar product from any excess propargyl alcohol and unreacted free sugar. The desired propargyl glycosides were achieved as white solids as an anomeric mixture due to the thermodynamic equilibrium. ^1H NMR spectroscopy revealed the appearance of doublets at 4.27 and 4.33 ppm which are assigned to the α & β (α : $\beta \approx 4$: 1) anomeric protons of $\text{O}-\text{CH}_2-\text{C}\equiv\text{CH}$ and also overlapped triplets at 2.80-2.90 ppm from the proton of $\text{O}-\text{CH}_2-\text{C}\equiv\text{CH}$, Figure 2.1. ^{13}C NMR spectroscopy showed the presence of a series of propargyl group peaks at 55.0, 56.5 (α & β $\text{O}-\text{CH}_2-\text{C}\equiv\text{CH}$), 72.5 ($\text{O}-\text{CH}_2-\text{C}\equiv\text{CH}$) and 75.3 ($\text{O}-\text{CH}_2-\text{C}\equiv\text{CH}$) ppm. FT-IR also demonstrated propargyl group absorbance at 3285 ($\text{C}\equiv\text{C}-\text{H}$) and 2118 ($\text{C}\equiv\text{C}$) cm^{-1} . ESI-MS analysis confirmed peaks at 241.1 which is in accordance with the theoretical value for $\text{C}_9\text{H}_{14}\text{O}_6$ ($\text{M}+\text{Na}^+$, 241.1). All characterizations proved the successful synthesis of 1-(2'-Propargyl) D-Mannose.

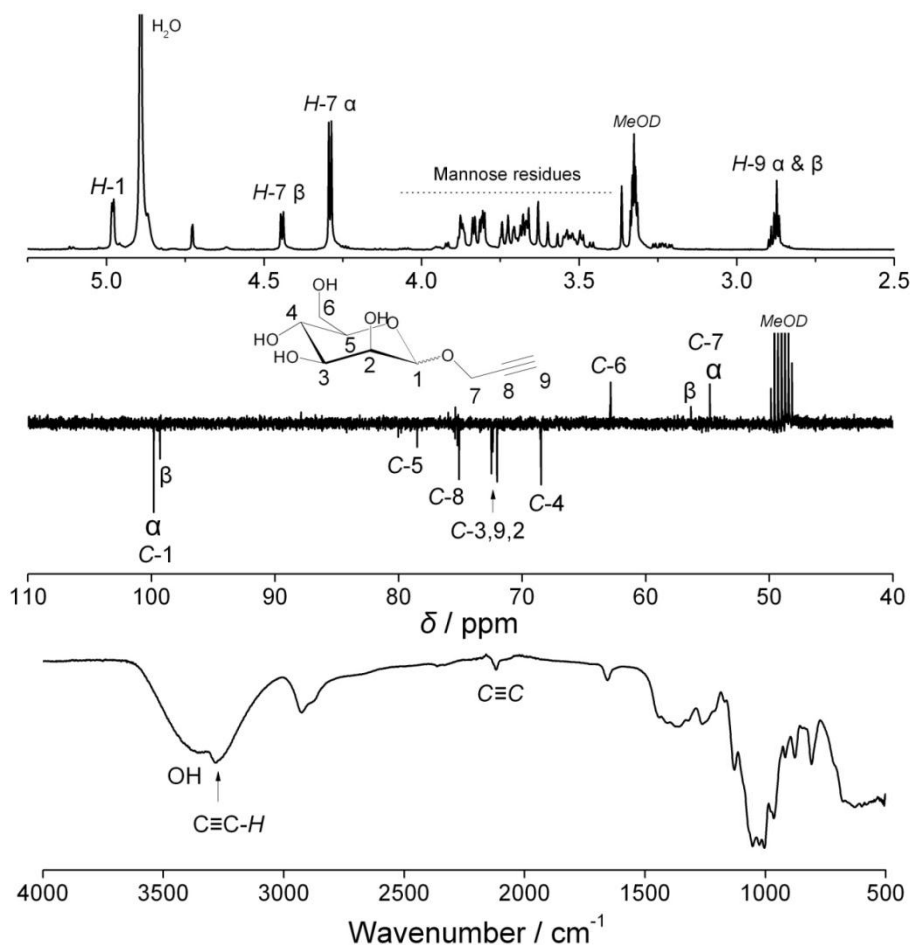


Figure 2. 1. ^1H NMR (top), ^{13}C NMR (middle) and FT-IR (bottom) spectra of 1-(2'-Propargyl) D-Mannose.

For more detailed characterization, the alkyne sugar was per-*O*-acetylated using excess Ac_2O with silica- H_2SO_4 catalysis at ambient temperature. After flash silica gel column chromatography (hexane: ethyl acetate = 8: 1) purification, the anomeric 2, 3, 4, 6-tetra-*O*-acetyl-1-(2'-propargyl)- α -D-mannose and 2, 3, 4, 6-tetra-*O*-acetyl-1-(2'-propargyl)- β -D-mannose could be separated and characterized by NMR, ESI-MS and FT-IR spectroscopies.

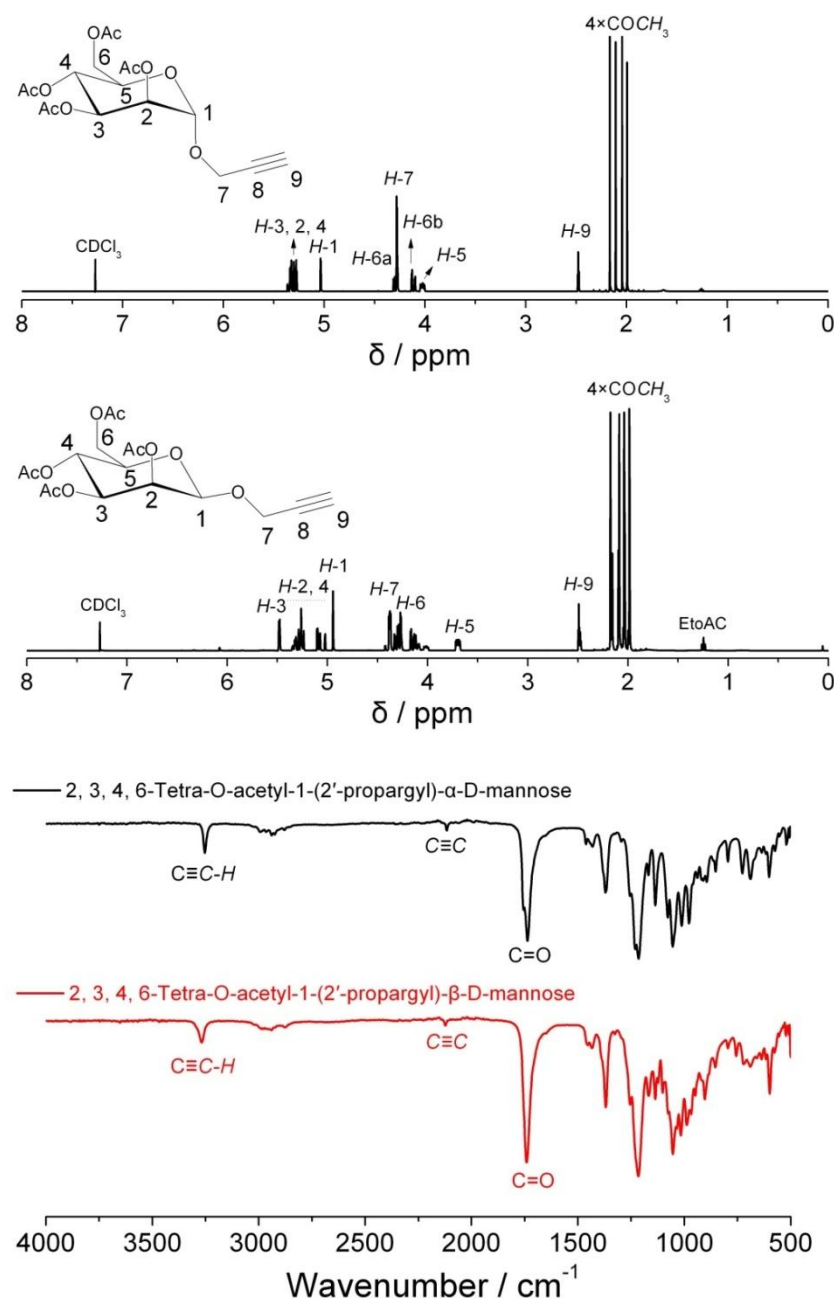
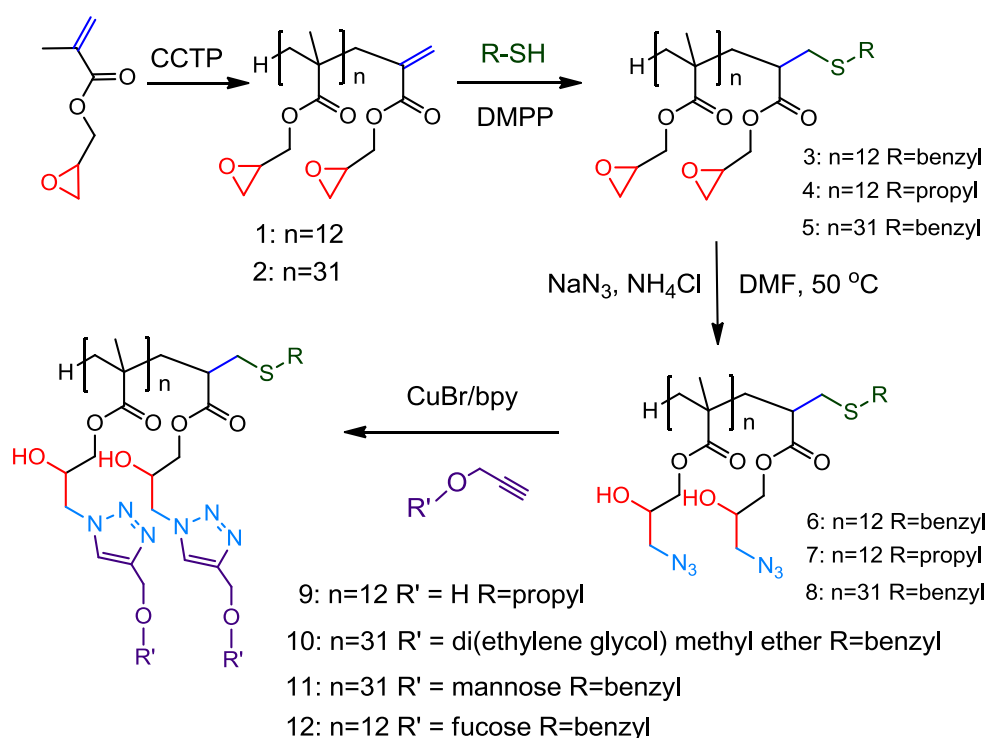


Figure 2. 2. ^1H NMR (top, middle) and FT-IR (bottom) spectra of 2, 3, 4, 6-tetra-*O*-acetyl-1-(2'-propargyl)- α -D-mannose and 2, 3, 4, 6-tetra-*O*-acetyl-1-(2'-propargyl)- β -D-mannose.

^1H NMR spectroscopy clearly revealed the small difference between the 3, 4, 6-tetra-*O*-acetyl-1-(2'-propargyl)- α -D-mannose and 2, 3, 4, 6-tetra-*O*-acetyl-1-(2'-propargyl)- β -D-mannose in detail due to the difference of axial bond and equatorial bond on C-1, Figure 2.2. The FT-IR spectra showed the remaining absorbance peak of alkyne group and the disappearance of the OH absorbance. All these results further proved the structure of the desired alkyne glycoside.

Subsequently, D-glucose and L-fucose were also used for the alkyne glycosylation reaction. The obtained unprotected alkyne glycosides were directly used for the next step click reaction and only partial product were per-*O*-acetylated for detailed characterization. The detailed reaction procedure and characterization data are shown in the experimental section.

2.2.2 Thiol-ene Michael addition reaction of thiol with vinyl terminal CCTP polymers



Scheme 2. 3. Scheme representation for synthetic approach to end-functionalised glycopolymers.

GMA was polymerised via CCTP (by Dr Stacy Slavin and Miss Alice Haddleton) and a polyGMA macromonomer isolated following purification. The presence of the ω -unsaturated end-group was confirmed by both ^1H NMR and MALDI-ToF-MS spectroscopy. Previous work has shown that the thiol-ene addition reaction is highly

efficient for the modification of polymers synthesised by CCTP.^{112,113} A number of amines and phosphines are effective catalysts for this type reaction, in which catalytic amount phosphine can provide relatively fast reaction rates with minimal side reactions. The thiolysis of oxiranes¹¹⁴ can also occur under basic conditions¹¹⁵ or in the presence of a catalyst,¹¹⁶ which was postulated as a competitive reaction for the thiol-ene end-group modification. In order to test this hypothesis, we initially performed a model reaction by reacting GMA with excess benzyl mercaptan in the presence of 5% DMPP in DMSO.

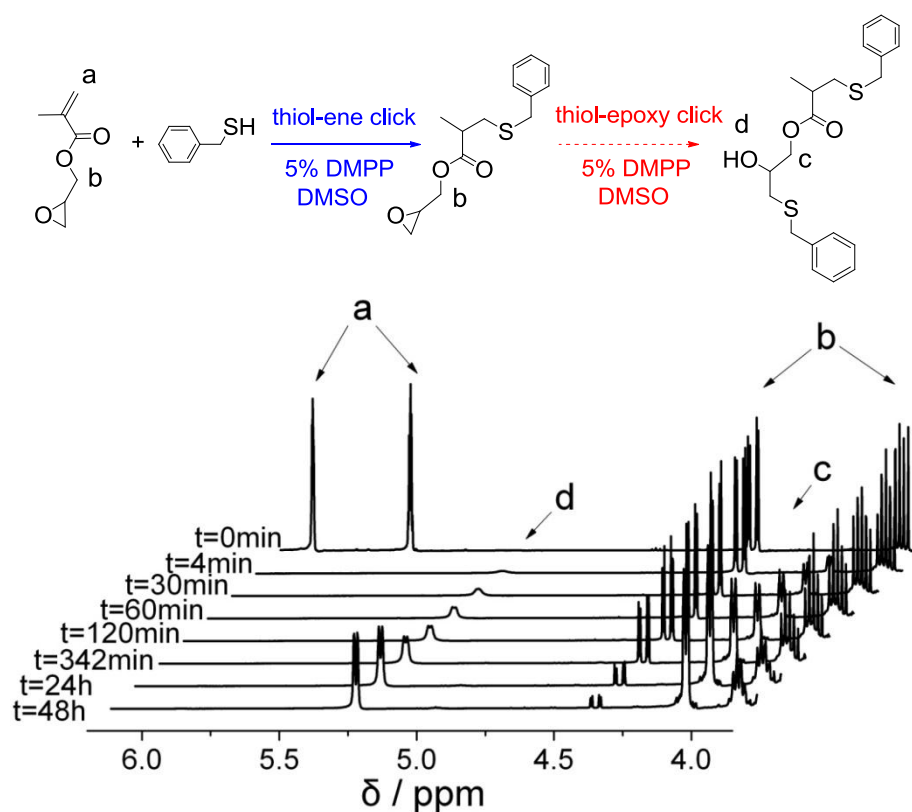


Figure 2. 3. Evolution of the ^1H NMR spectra with time in the reaction of glycidyl methacrylate with benzyl mercaptan (3 equiv) in $\text{DMSO-}d_6$ at $25\text{ }^\circ\text{C}$. The numbering of the typical hydrogen atoms used for the NMR peak assignment is shown in the reaction scheme.

The expected thiol-ene modification was complete in $\leq 4\text{ min}$, which was revealed by the disappearance of the two vinyl signals at 5.71 and 6.07 ppm, Figure 2.3. The thiol-epoxy reaction was also shown to occur, which was confirmed by the gradual disappearance of the signals at 3.92 and 4.46 ppm (the two protons from CO_2CH_2), indicating ring-opening of the oxirane. New peaks were seen at 4.11 ppm (the two protons from CO_2CH_2) and 5.31 ppm (the proton from OH). However, complete ring

opening of the oxirane was not observed for up to 48 h. This indicates that under these conditions, a clear preference for Michael addition was observed by the thiol over ring-opening of the oxirane.

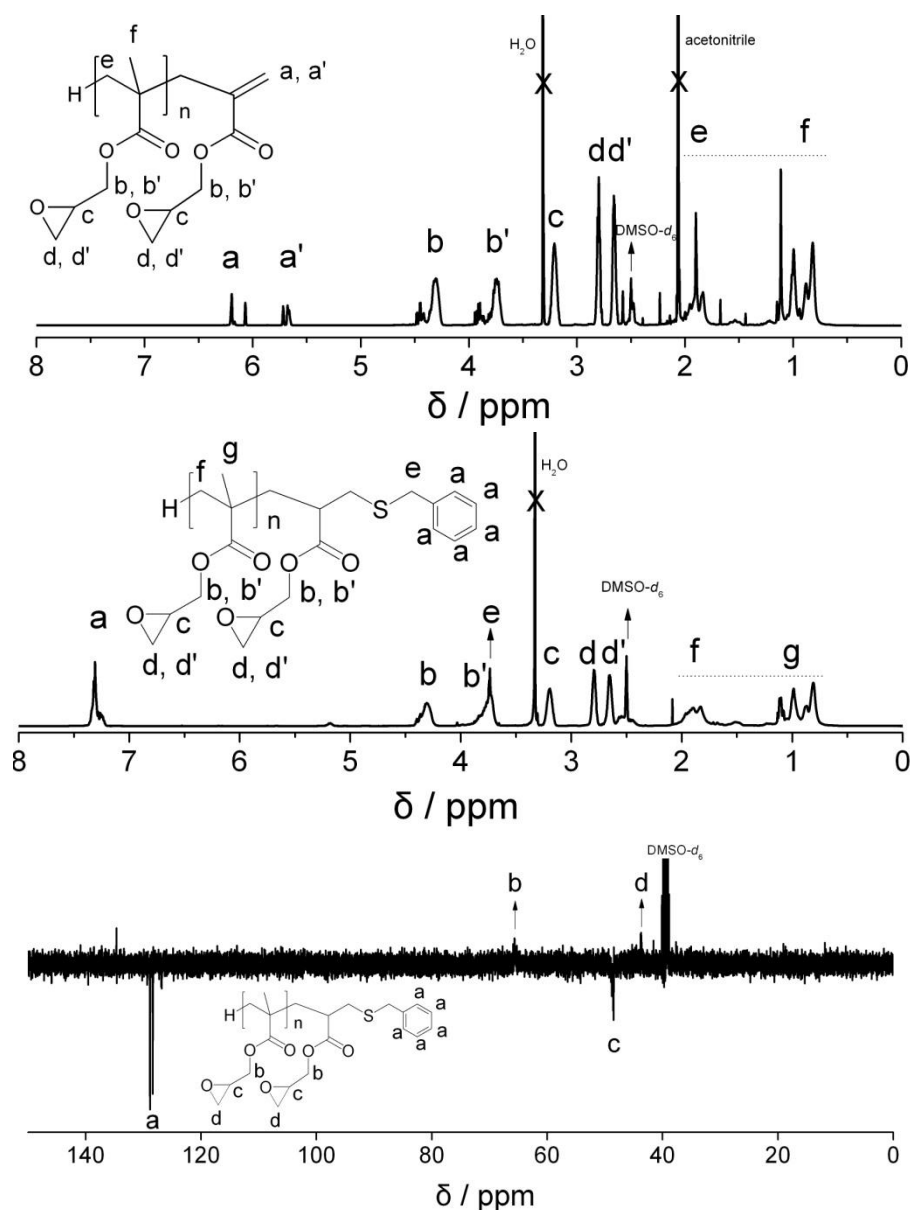


Figure 2. 4. ^1H NMR spectra of PGMA **1** (top), benzyl end-functionalised polymer **3** (middle) and ^{13}C NMR spectrum of benzyl end-functionalised polymer **3** (bottom) in DMSO- d_6 .

The large difference in reactivity of the unsaturated end group relative to the pendant epoxides was exploited in order to selectively modify the vinyl functionality. The PGMA macromonomers were reacted with benzyl mercaptan in DMSO in the presence of DMPP as catalyst. After full conversion of the vinyl groups was observed, the reaction was stopped *via* precipitation into methanol to avoid side-reactions with

the oxiranes. The isolated benzyl end-functionalised product was characterised by NMR, GPC, FT-IR and MALDI-TOF MS spectroscopies.

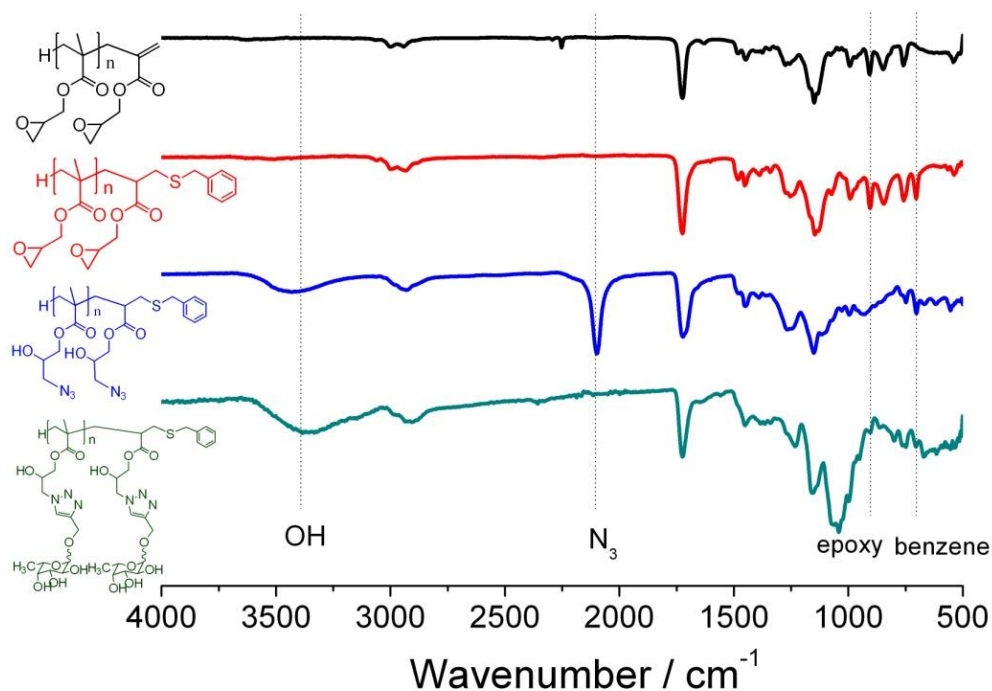


Figure 2. 5. FT-IR spectra of CCTP PGMA **1**, benzyl end-functionalised polymer **3**, azide functionalised polymer **6** and fucose functionalised glycopolymer **12**.

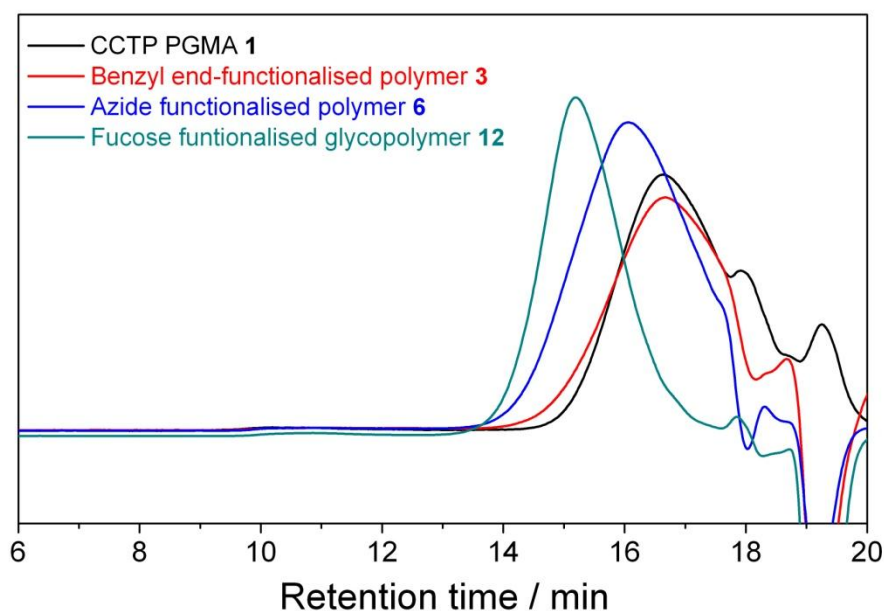


Figure 2. 6. DMF SEC traces (RI detector) of CCTP PGMA **1**, benzyl end-functionalised polymer **3**, azide functionalised polymer **6** and fucose functionalised glycopolymer **12**.

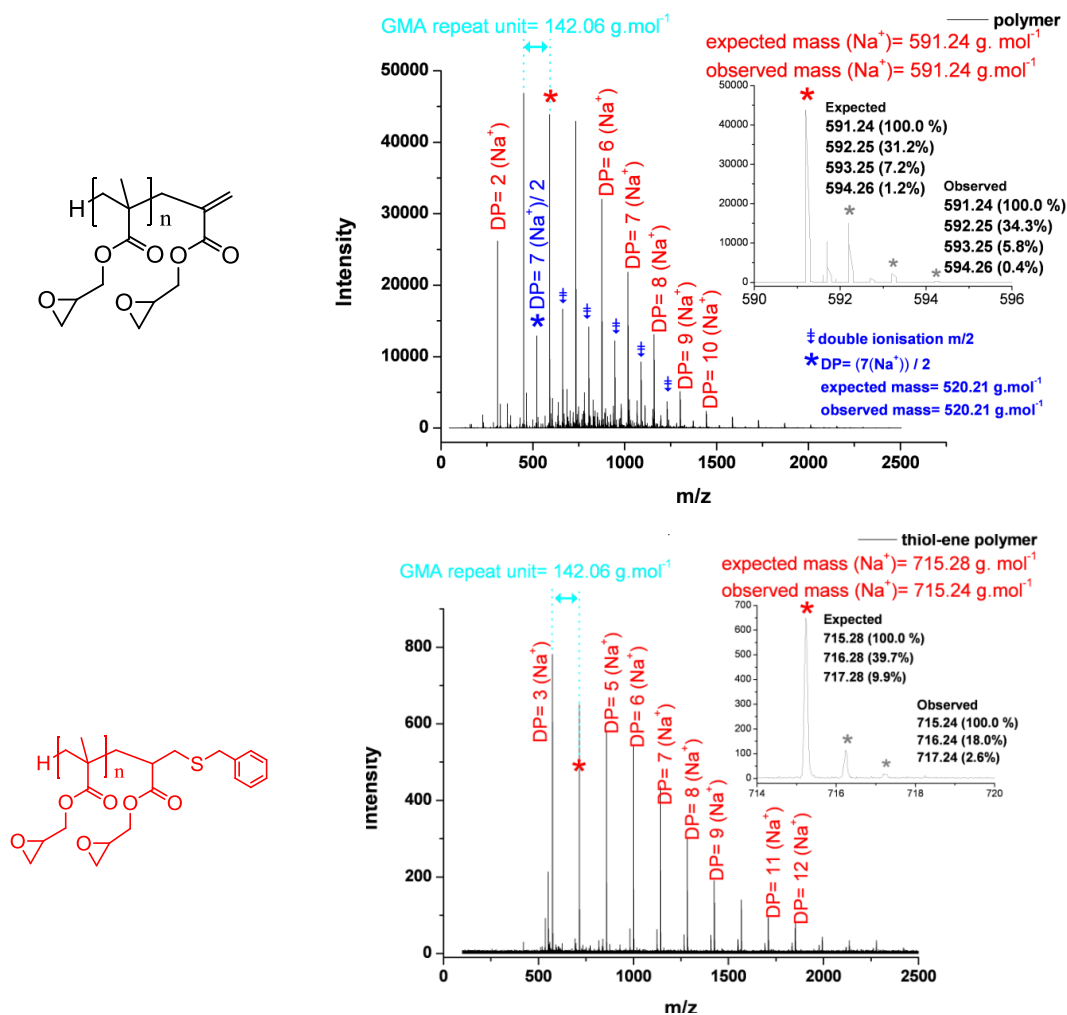


Figure 2. 7. MALDI-ToF MS analysis of CCTP PGMA **1**(top), and benzyl end-functionalised polymer **3** (bottom). (Characterization performed by Dr Stacy Slavin).

The success of the thiol-Michael addition reaction was confirmed by ¹H NMR spectroscopy with the disappearance of the vinyl peaks at 5.7 and 6.2 ppm and appearance of signals corresponding to the benzyl group at 7.2-7.4 ppm, Figure 2.4. Although small peaks at around 4.0 and 5.2 ppm were observed, which could be attributed to the thiol-epoxy reaction, ¹H NMR analysis showed that only less than 3% of the epoxy groups had reacted with the thiol, meaning the thiol-epoxy reaction was limited during this reaction. ¹³C NMR revealed the appearance of benzyl carbons at around 126.7-129.4 ppm and the existence of epoxy ring carbon peaks at 43.8 and 48.5 ppm.

FT-IR spectra revealed the appearance of mono-substituted benzene ring at 703 cm⁻¹ and the remaining of epoxy ring absorbance at around 905 cm⁻¹ after reaction, Figure

2.5. In Figure 2.6, the SEC traces did not move significantly following the thiol-ene reaction due to the slight molecular weight increase.

MALDI-ToF-MS (Figure 2.7) revealed a molecular weight increase of ~120 Da after the reaction, which was attributed to the addition of benzyl mercaptan to the polymer chain-end. MALDI-ToF-MS analysis also showed the molecular weight spacing of each peak remained at 142.06 Da, which remained as the mass of GMA repeating unit and thus confirmed that side thiol-epoxy reaction was not obvious.

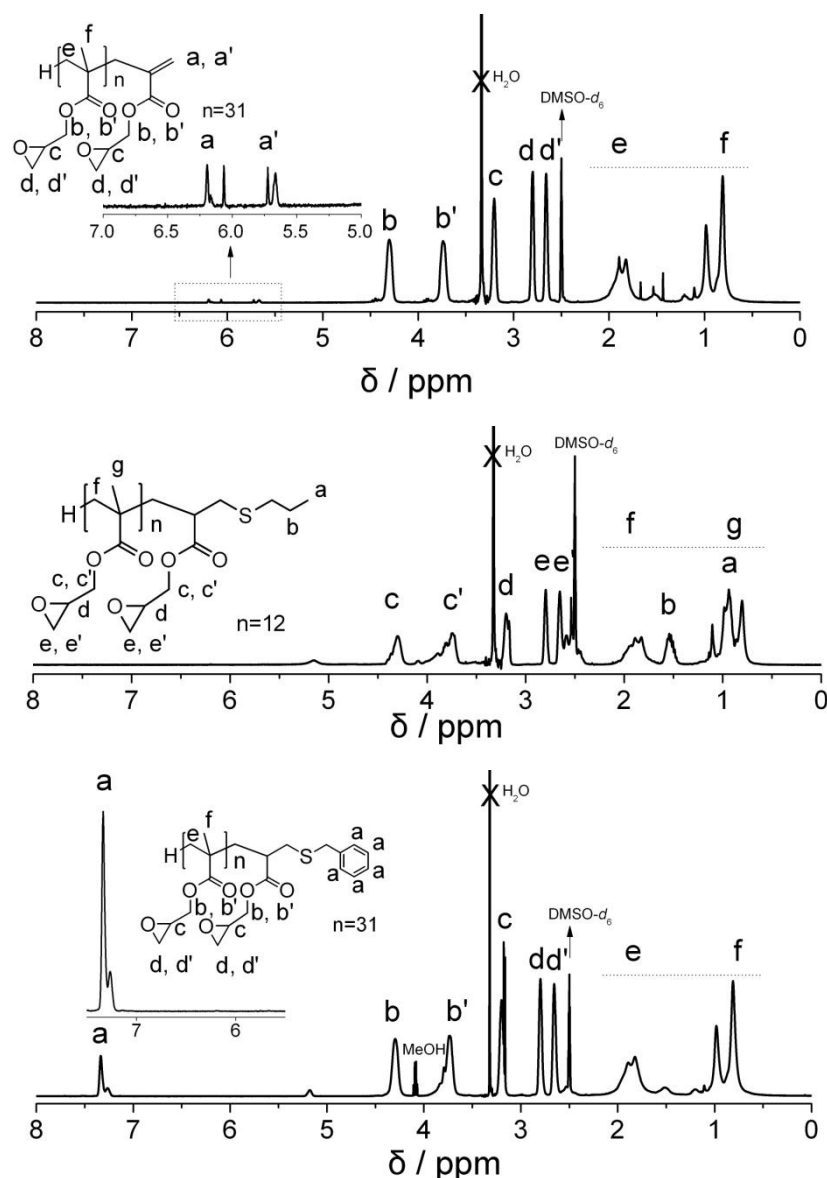


Figure 2. 8. ^1H NMR spectra of PGMA **2** (top), propyl end-functionalised polymer **4** (middle) and benzyl end-functionalised polymer **5** (bottom) in $\text{DMSO-}d_6$.

In order to investigate the versatility of the thiol-Michael addition to CCTP macromonomers, CCTP polymers with different chain lengths were reacted with

different thiols in DMSO, catalysed by DMPP. The PGMA macromonomer **1** (DP=12) and **2** (DP=31) were incubated with 1-propanethiol and benzyl mercaptan respectively (Scheme 2.3). The ^1H NMR spectra of the purified propyl end-functionalised product **4** and benzyl end-functionalised product **5** also showed the disappearance of vinyl peaks and the appearance of corresponded end groups (Figure 2.8), indicating the success of Michael addition reaction for CCTP GPMA with different thiols.

2.2.3 Epoxy ring opening reactions of PGMA with sodium azide

Based on the wide application of CuAAC in polymer science, it is desirable to synthesise polymers bearing pendant azide groups. Due to the potential dangers of the direct synthesis and polymerisation of azide-containing monomers, the ring-opening reaction of epoxides with sodium azide was used to introduce azide to polymer backbone.^{90,117} The ring opening reaction of oxiranes in the presence of ammonium chloride is very efficient and considered a click type reaction.⁹⁰ Similar reaction conditions were employed for the ring opening of the epoxides of the thiol-functionalised PGMA with NaN_3 (Scheme 2.3). Polymer **3** was first used to react with excess sodium azide / ammonium chloride in DMF at 50 °C for 24 h.

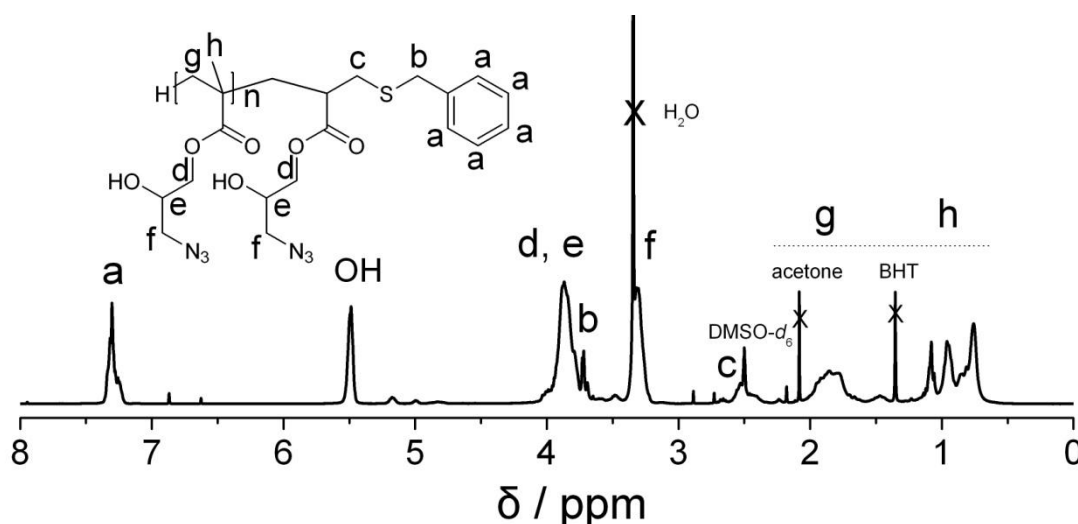


Figure 2. 9. ^1H NMR spectrum of azide functionalised polymer **6** in $\text{DMSO-}d_6$.

Following the reaction, azide functionalised polymer **6** was analysed by SEC, ^1H NMR and FT-IR spectroscopy. The SEC elution trace (Figure 2.6) of **6** ($M_n=3800$ Da, $M_w/M_n = 1.44$) shifted to the higher MW position compared with **3** ($M_n=2800$ Da,

$M_w/M_n = 1.53$), indicating the molecular weight increase due to the addition of azide groups.

Subsequently, the ^1H NMR spectra (Figure 2.9) showed the complete disappearance of the peaks at 3.1-3.3 ppm (the proton of CH from the cycle) and 2.60-2.72 and 2.75-2.82 ppm (the two protons of CH_2 from the cycle), which belong to the protons from the epoxy ring. New peaks were observed at 5.49 ppm (CH-OH), 3.7-4.0 ppm (CO_2CH_2 and CH-OH) and 3.2-3.4 ppm (CH_2N_3), similar as previous report.⁹⁰ FT-IR spectrum of polymer **6** revealed a strong absorbance at 2098 cm^{-1} which was related to the absorbance of azide group and also a broad peak at $3200\text{-}3600\text{ cm}^{-1}$ belonging to the absorbance of OH groups, Figure 2.5. The epoxy ring absorbance of polymer **3** (905 cm^{-1}) was not observed after reaction.

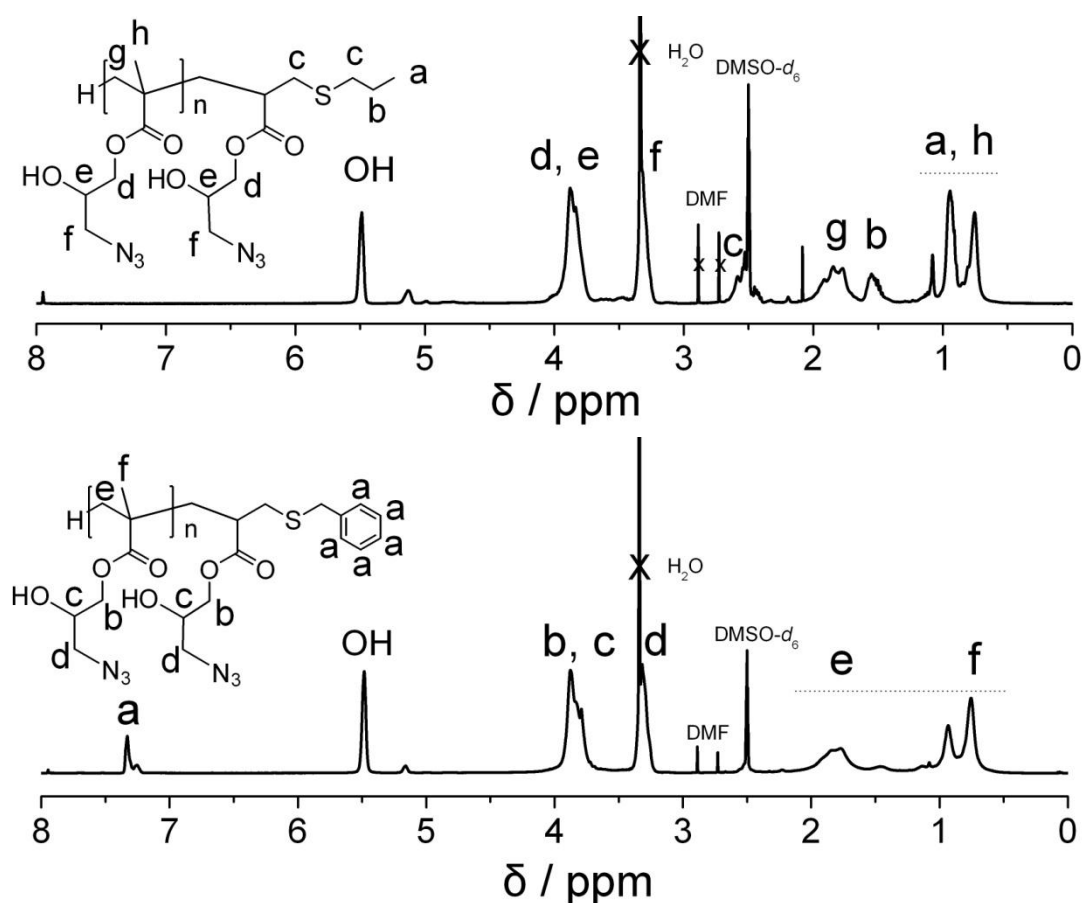


Figure 2. 10. ^1H NMR spectra of azide functionalised polymer **7** (top) and **8** (bottom) in $\text{DMSO-}d_6$.

Different end-functionalised PGMA **4** (DP=12) and **5** (DP=31) were functionalised with azide *via* the same method. ^1H NMR spectra of polymer **7** and **8** (Figure 2.10) showed the proton shifts due to the epoxy ring opening reaction with sodium azide.

FT-IR spectra (Figure 2.11) revealed the corresponding appearance of azide and hydroxyl groups and disappearance of epoxy groups. SEC traces (Figure 2.12, 2.17) also revealed the molecular weight increase after reaction. All these results clearly revealed the efficient reaction of epoxy ring with sodium azide/ammonium chloride, azide grafted polymer was obtained for the subsequent CuAAC reaction.

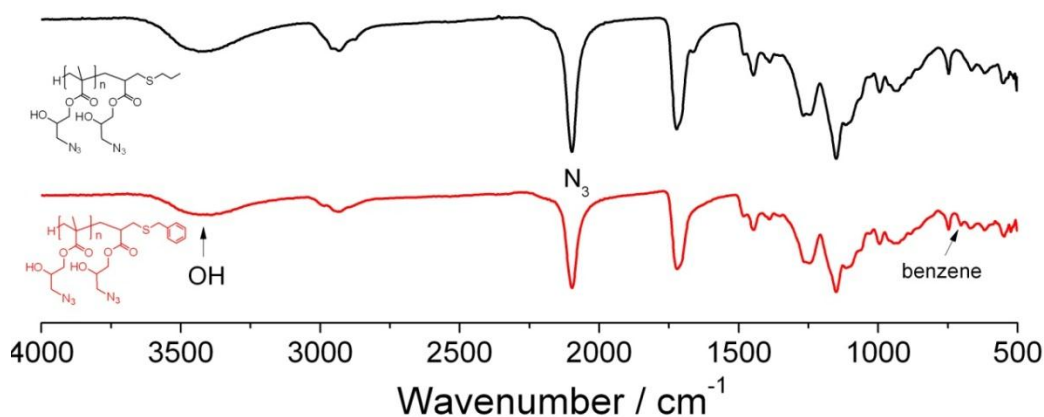


Figure 2. 11. FT-IR spectra of azide functionalised polymer **7** (top) and **8** (bottom).

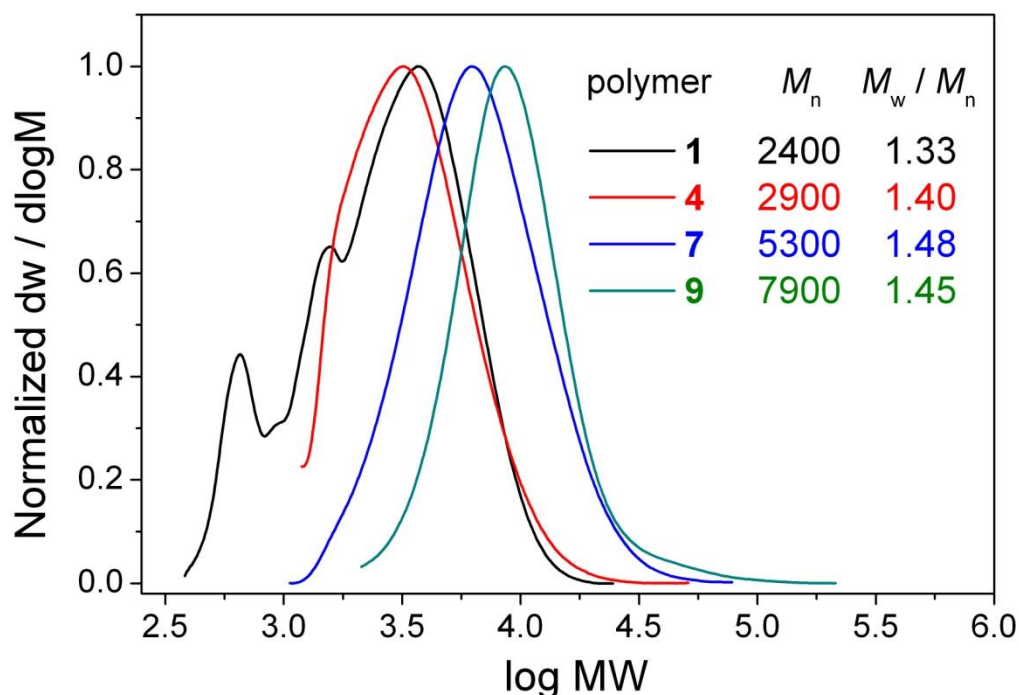
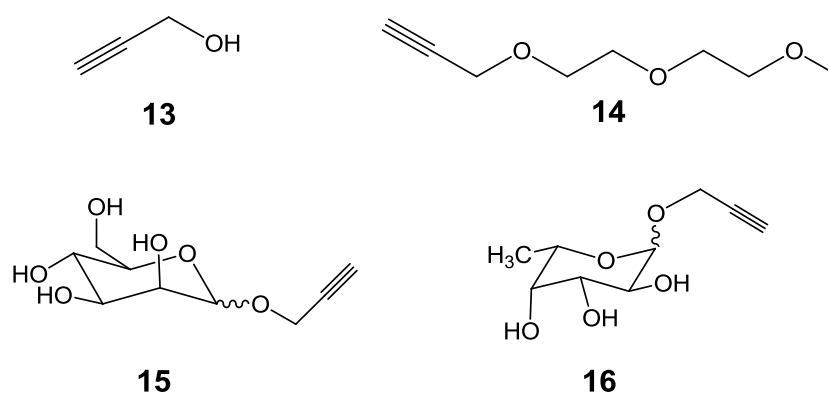


Figure 2. 12. Molecular weight distributions of polymer **1**, **4**, **7** and **9** via SEC employing DMF as the eluent.

2.2.4 CuAAC reactions of azide-containing polymers with alkyne compounds

In order to prepare glycopolymers from azide functionalised polymer *via* CuAAC, sugar alkynes are required. Since the discovery of Fischer glycosylation, it has been widely used in the preparation of simple alkyl or aryl glycosides from free sugars.¹¹⁸⁻¹²⁰ Recently, sulfuric acid immobilised on silica was proved to be an efficient catalyst for the preparation of alkyl glycosides from free sugars *via* Fischer glycosylation.^{121,122} Thus D-mannose and L-fucose were alkyne functionalised in a large scale *via* reacting with propargyl alcohol in the presence of H₂SO₄-silica catalyst at 65 °C. The obtained unprotected sugar alkyne was an anomeric mixture, which could be separated by silica gel column chromatography after per-*O*-acetylation using acetic anhydride.



Scheme 2. 4. Alkyne compounds employed in the study: propargyl alcohol (**13**), diethylene glycol alkyne (**14**), mannose alkyne (**15**) and fucose alkyne (**16**).

The glycopolymers were then synthesised by CuAAC reaction of the azide functionalised polymers with **15** and **16** (Scheme 2.4). Reactions were conducted in DMSO using CuBr / bpy as catalyst. Polymer **6** was reacted with fucose alkyne **16** to yield glycopolymer **12**, which was characterised by SEC, ¹H NMR and FT-IR spectroscopies.

After the reaction the SEC trace (Figure 2.6) of **12** (M_n =8300 Da, M_w/M_n =1.30) shifted to higher MW relative to **6** (M_n =3800 Da, M_w/M_n =1.44), indicating the molecular weight increase due to of the addition of fucose groups. ¹H NMR spectra of **12** (Figure 2.13) showed the appearance of triazole peak at 8.03 ppm, which confirmed the success of CuAAC reaction. Peaks at 1.08 and 1.15 ppm (from CH₃ of the fucose sugar) and multiple peaks from 3.0 to 5.0 ppm (protons from the rest of fucose alkyne, overlapped with polymer backbone protons) confirmed the existence of

fucose. The benzyl proton peaks at 7.2-7.4 ppm still exist, indicating that CuAAC didn't affect the end group. FT-IR spectra (Figure 2.5) showed the complete disappearance of azide absorbance at 2098 cm^{-1} , indicating the success of CuAAC reaction. Due to the addition of fucose, the absorbance strength of OH at $3100\text{-}3600\text{ cm}^{-1}$ enhanced compared with the $\text{C}=\text{O}$ absorbance at 1725 cm^{-1} .

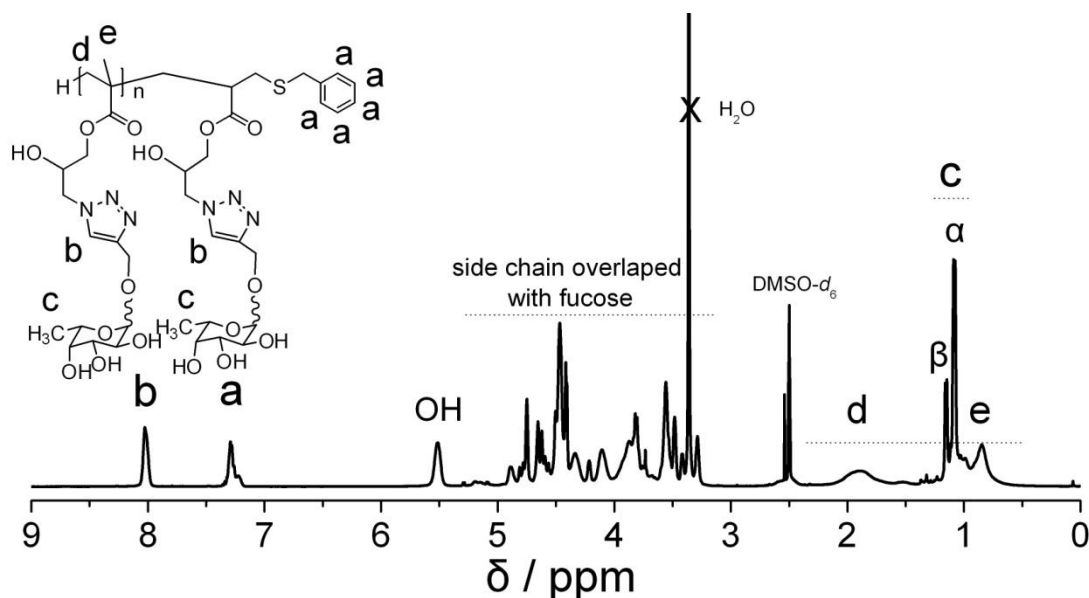


Figure 2. 13. ^1H NMR spectrum of benzyl terminal fucose-functional glycopolymer **12** in $\text{DMSO-}d_6$.

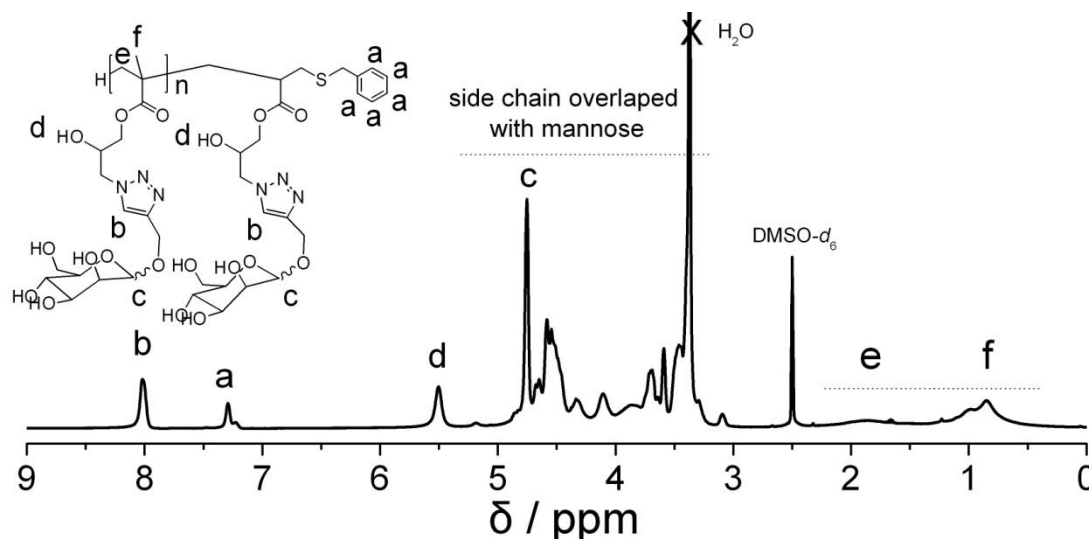


Figure 2. 14. ^1H NMR spectrum of benzyl terminal mannose-functional glycopolymer **11** in $\text{DMSO-}d_6$.

Polymer **8** was reacted with mannose alkyne **15** to yield glycopolymer **11**. After reaction, the SEC trace (Figure 2.17) of **11** ($M_n=23100\text{ Da}$, $M_w/M_n=2.08$) shifted to

higher MW compared with **8** ($M_n=18000$ Da, $M_w/M_n=2.11$), indicating the molecular weight increase due to the addition of mannose moieties. ^1H NMR spectra of **11** (Figure 2.14) showed the appearance of triazole peak at 8.02 ppm, which confirmed the success of CuAAC reaction. FT-IR spectra (Figure 2.16) also revealed the disappearance of azide absorbance and enhancement of the OH absorbance. The results presented above clearly demonstrate the efficient reaction of sugar alkyne with azide functionalised polymer.

In order to investigate the versatility of the CuAAC reaction to these azide functionalised polymers, propargyl alcohol **13** and diethylene glycol alkyne **14** were used to react with different azide functionalised polymers **7** and **8**.

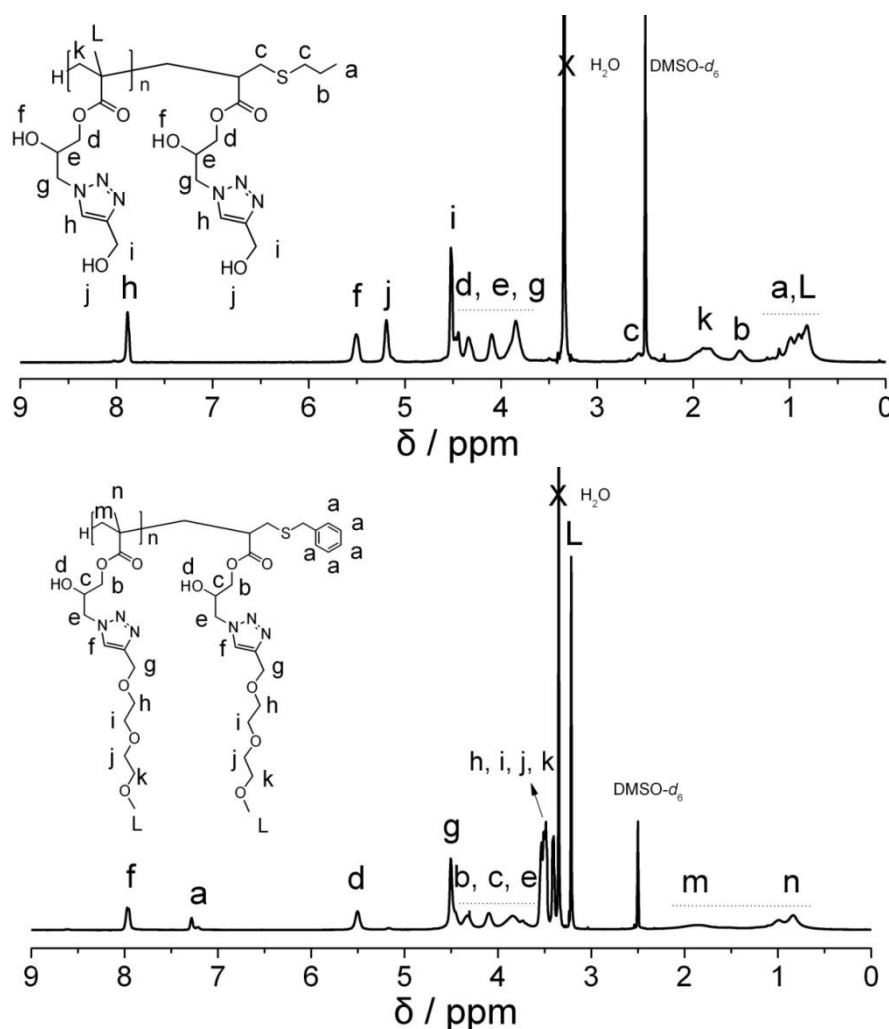


Figure 2. 15. ^1H NMR spectra of polymer **9** (top) and **10** (bottom) in $\text{DMSO-}d_6$.

Following the reaction the ^1H NMR spectra of **9** and **10** (Figure 2.15) showed the appearance of triazole peak at 7.89 and 7.97 ppm respectively, which confirmed the success of CuAAC reaction. SEC traces of **9** and **10** (Figure 2.12, 2.17) showed the

molecular weight increase after reaction. FT-IR (Figure 2.16) revealed the disappearance of azide absorbance and enhancement of OH or methyl and methylene absorbance respectively. Functional polymer **10** showed a concentration dependant LCST behaviour at 46 °C (10 mg/mL) and 63 °C (5 mg/mL).¹²³

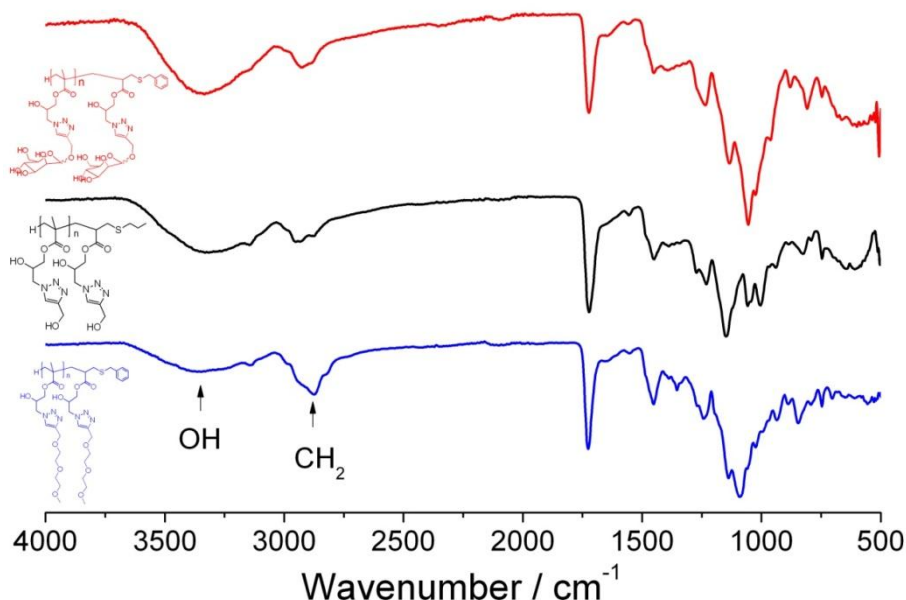


Figure 2. 16. FT-IR spectra of polymer **11** (top), **9** (middle) and **10** (bottom).

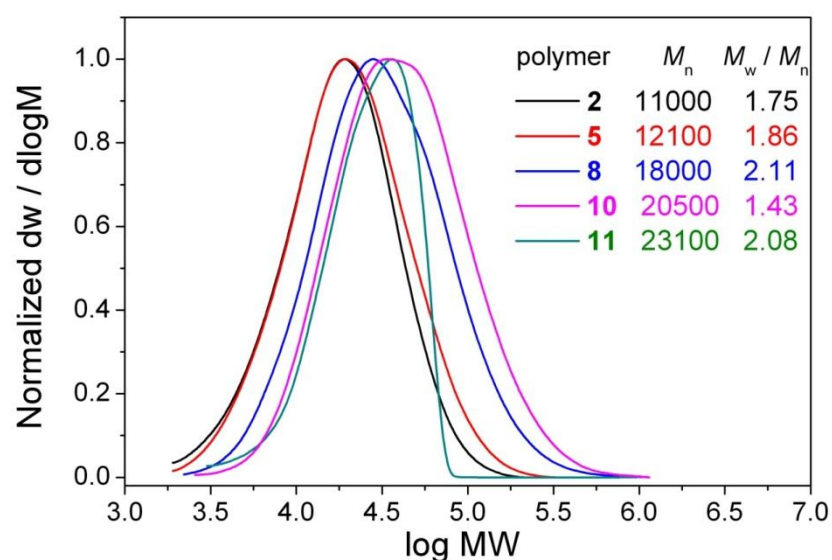


Figure 2. 17. Molecular weight distributions of polymer **2**, **5**, **8**, **10** and **11** via SEC employing DMF as the eluent.

2.2.5 Conclusions

In summary, CCTP has been used to synthesise polymers with ω -vinyl terminal groups and epoxide side groups. These have been functionalised with three different click-type reactions. The ω -polymer end group was transformed *via* Michael thiol-ene addition with different thiols to obtain a range of ω -end-functionalised polymers. The side epoxy ring was reacted with sodium azide in the presence of ammonium chloride to yield the corresponding azide functionalised polymers in high yield. Sugar alkynes were prepared from free sugar *via* a one-step Fisher type glycosylation using a H_2SO_4 -silica catalyst. Glycopolymers were produced by the CuAAC reaction of sugar alkyne with azide functionalised polymer. This is a method based on free radical polymerisation which leads to a diverse range of glycopolymers. The combination of a range of efficient chemistry gives a route to multi gram quantities of glycopolymers which avoids the need for living radical polymerisation and some of the potential problems this can introduce. CCTP as a route to control free radical polymerisation has been shown to be a very scalable and commercialisable process. The chemistry described has the potential to be a very powerful route to targeting polymers in a range of therapeutic applications.

2.3 Experimental

2.3.1 Materials

Glycidyl methacrylate (GMA, 97%) was obtained from Sigma-Aldrich and the inhibitor was removed by passing the monomer through a column filled with neutral alumina prior to use. Copper (I) bromide (98%, Sigma-Aldrich) was washed sequentially with acetic acid and ethanol and dried under vacuum so as to remove residual Cu(II)Br_2 . Dimethylphenylphosphine (DMPP, 97%, Sigma-Aldrich) was stored under nitrogen. D-Mannose (99%, Sigma-Aldrich), L-fucose (98%, Sigma-Aldrich), propargyl alcohol (99%, Sigma-Aldrich), 2, 2'-bipyridyl (bpy, 99%, Sigma-Aldrich), benzyl mercaptan (99%, Sigma-Aldrich), 1-propanethiol (99%, Sigma-Aldrich), sodium azide (99%, Sigma-Aldrich) were used as received.

The H_2SO_4 -silica catalyst was prepared according to the literature procedure.¹²¹ Vinyl terminal polymers were synthesised by Dr Stacy Slavin and Miss Alice Haddleton of

Haddleton group. Diethylene glycol alkyne (3-(2-(2-methoxyethoxy)ethoxy)prop-1-yne) was synthesised by Dr Mathew W. Jones as described by Fitch *et al.*¹²⁴

All other reagents and solvents were obtained at the highest purity available from Sigma-Aldrich and used without further purification unless otherwise stated.

2.3.2 Instruments and analysis

¹H and ¹³C NMR spectra were recorded on Bruker DPX-300 and DPX-400 spectrometers using deuterated solvents obtained from Aldrich. Mass spectra were recorded on an Esquire2000 using electrospray ionisation (ESI) in positive mode.

FTIR spectra were recorded on a Bruker VECTOR-22 FTIR spectrometer using a Golden Gate diamond attenuated total reflection cell.

SEC was conducted on Varian 390-LC system in DMF (1 g/L LiBr) at 50 °C, equipped with refractive index and viscometry detectors, 2 × PLgel 5 mm mixed-D columns (300 × 7.5 mm), 1 × PLgel 5 mm guard column (50 × 7.5 mm) and autosampler. PGMA molar mass distributions were measured on a SEC system equipped with two PL gel 3 µm mixed E-columns (300 × 7.5 mm) and one PL gel 5 mm guard column (50 × 7.5 mm) (Polymer Laboratories) with differential refractive index detection using THF as eluent.

MALDI-ToF data was collected using a Bruker Ultraflex II MALDI ToF Instrument which has a mass range up to 500 kDa and analysed using FlexAnalysis software. The MALDI contains a 337 nm wavelength N₂ (pulse energy of 100 µJ) at a maximum repetition rate 50 Hz. The system is kept inside a vacuum at 5 × 10⁻⁶ Torr to avoid contamination of the sample reading. A matrix was used (DHTB) to protect the product from being destroyed from direct laser beam and to facilitate vaporisation and ionisation. ToF-MS instrument, Bruker MaXis with proxeon easy-nLC and Dionex RS3000 HPLC was used for high resolution mass spectrometry analysis.

2.3.3 Synthesis of alkyne functionalised sugar *via* Fischer glycosylation

2.3.3.1 Synthesis of 1-(2'-Propargyl) D-Mannose

A suspension solution of D-mannose (18.02 g, 100 mmol), propargyl alcohol (29.1 mL, 500 mmol) and H₂SO₄-silica (500 mg) was stirred at 65°C until all reagents completely dissolved (~3 h). Stirring was continued at 65 °C for an additional 3 h

after complete dissolution. After cooling to ambient temperature, a part of the reaction mixture (8.00 g) was transferred to a silica gel column and eluted with CHCl_3 -MeOH (8:1) to remove the excess propargyl alcohol. 1-(2'-Propargyl) D-mannose was obtained as white solid after drying under vacuum (Yield: 26.7%). ^1H and ^{13}C NMR revealed formation of the desired glycoside anomeric mixture.

FT-IR ν (cm^{-1}): 3347 (OH), 3285 ($\text{C}\equiv\text{C-H}$), 2118 ($\text{C}\equiv\text{C}$).

ESI-MS m/z : calcd for $\text{C}_9\text{H}_{14}\text{O}_6$ ($\text{M}+\text{Na}^+$), 241.1; found, 241.1.

For detailed characterisation, a part of the product was per-O-acetylated using acetic anhydride. A suspension solution of 1-(2'-propargyl) D-mannose (218 mg, 1.0 mmol), acetic anhydride (3.0 mL, 32.0 mmol), H_2SO_4 -silica (6 mg) was stirred at ambient temperature for 48 h. After completion of the reaction, the solution was diluted with CH_2Cl_2 (20 mL) and washed sequentially with saturated aq. NaHCO_3 solution and water twice. The extract was dried over MgSO_4 and concentrated under vacuum. The crude anomeric mixture was then separated by silica gel column chromatography using hexane-ethyl acetate (8:1) as eluent. 2, 3, 4, 6-tetra-O-acetyl-1-(2'-propargyl)- α -D-mannose (298 mg) and 2, 3, 4, 6-tetra-O-acetyl-1-(2'-propargyl)- β -D-mannose (37 mg) were obtained after drying under vacuum (Yield: 86.7%).

2, 3, 4, 6-Tetra-O-acetyl-1-(2'-propargyl)- α -D-mannose

^1H NMR (CDCl_3 , 298 K, 400 MHz): δ (ppm) = 5.34 (dd, 1H, J 3.3, 6.5 Hz, H-3), 5.25-5.32 (m, 2H, H-2, H-4), 5.02 (d, 1H, J 1.8 Hz, H-1), 4.28 (dd, 1H, J 5.2, 7.1 Hz, H-6^a), 4.27 (d, 2H, J 2.4 Hz, $\text{CH}_2\text{-C}\equiv\text{CH}$), 4.10 (dd, 1H, J 2.5 Hz, 9.8 Hz, H-6^b), 3.98-4.05 (m, 1H, H-5), 2.47 (t, 1H, $\text{CH}_2\text{-C}\equiv\text{CH}$), 2.16, 2.10, 2.03, 1.98 (4s, 12H, 4 $\times\text{COCH}_3$).

^{13}C NMR (CDCl_3 , 298 K, 400 MHz): δ (ppm) = 170.7, 170.0, 169.9, 169.8 (4 $\times\text{COCH}_3$), 96.3 (C-1), 78.0 ($\text{CH}_2\text{-C}\equiv\text{CH}$), 75.7 ($\text{CH}_2\text{-C}\equiv\text{CH}$), 69.4, 69.1, 69.0, 66.1, 62.4 (C-6), 55.0 ($\text{CH}_2\text{-C}\equiv\text{CH}$), 20.9, 20.8 (2), 20.7 (4 $\times\text{COCH}_3$).

FT-IR ν (cm^{-1}): 3253 ($\text{C}\equiv\text{C-H}$), 2117 ($\text{C}\equiv\text{C}$), 1737 (C=O).

ESI-MS m/z : calcd for $\text{C}_{17}\text{H}_{22}\text{O}_{10}$ ($\text{M}+\text{Na}^+$), 409.1; found, 409.0.

2, 3, 4, 6-Tetra-O-acetyl-1-(2'-propargyl)- β -D-mannose

^1H NMR (CDCl_3 , 298 K, 400 MHz): δ (ppm) = 5.49 (dd, 1H, J 1.0, 2.3 Hz, H-3), 5.06-5.31 (m, 2H, H-2, H-4), 4.95 (d, 1H, J 1.0 Hz, H-1), 4.35-4.45 (m, 2H, $\text{CH}_2\text{-C}\equiv\text{CH}$), 4.31 (dd, 1H, J 5.3, 7.0 Hz, H-6^a), 4.16 (dd, 1H, J 2.6, 9.7 Hz, H-6^b), 3.66-

3.74 (m, 1H, H-5), 2.48 (t, 1H, CH₂-C≡CH), 2.18, 2.10, 2.04, 1.99 (4s, 12H, 4×COCH₃).

¹³C NMR (CDCl₃, 298 K, 400 MHz): δ (ppm) = 170.8, 170.4, 170.1, 169.7 (4×COCH₃), 95.7 (C-1), 77.9 (CH₂-C≡CH), 76.1 (CH₂-C≡CH), 72.6, 71.2, 68.8, 66.0, 62.4 (C-6), 55.9 (CH₂-C≡CH), 20.9 (2), 20.8, 20.7 (4×COCH₃).

FT-IR ν (cm⁻¹): 3268 (C≡C-H), 2123 (C≡C), 1741 (C=O).

ESI-MS *m/z*: calcd for C₁₇H₂₂O₁₀ (M+Na⁺), 409.1; found, 409.0.

2.3.1.2 Synthesis of 1-(2'-Propargyl) L-Fucose

A suspension solution of L-fucose (2.46 g, 15.0 mmol), propargyl alcohol (4.4 mL, 75.0 mmol) and H₂SO₄-silica (75 mg) was stirred at 65 °C for 5 h. After cooling down to ambient temperature, the reaction mixture was transferred to a silica gel column and eluted with CHCl₃-MeOH (10:1) to remove the excess propargyl alcohol. 1-(2'-Propargyl) L-fucose was obtained as white solid after drying under vacuum. (Yield: 50.1%) ¹H and ¹³C NMR revealed formation of the desired glycoside in a 10:4 (α/β) ratio.

FT-IR ν (cm⁻¹): 3360 (OH), 3254 (C≡C-H), 2125 (C≡C).

ESI-MS *m/z*: calcd for C₉H₁₄O₆ (M+Na⁺), 225.1; found, 225.1.

For detailed characterisation, a part of the product was per-*O*-acetylated using acetic anhydride. A suspension solution of 1-(2'-propargyl) L-fucose (202 mg, 1.00 mmol), acetic anhydride (1.42 mL, 15.0 mmol), I₂ (2 mg, 7.88×10⁻³ mmol) was stirred at ambient temperature for 48 h. After completion of the reaction, the obtained yellow solution was diluted with CH₂Cl₂ (20 mL) and washed sequentially with 5% aq. Na₂S₂O₃ solution, saturated aq. NaHCO₃ solution and water. The extract was dried over MgSO₄ and concentrated under vacuum. The crude anomeric mixture was then separated by silica gel column chromatography using hexane-ethyl acetate (8:1) as eluent. 2, 3, 4-tri-*O*-acetyl -1-(2'-propargyl)-α-L-fucose (60 mg) and 2, 3, 4-tri-*O*-acetyl -1-(2'-propargyl)-β-L-fucose (22 mg) were obtained after drying under vacuum. (Yield: 25.0%)

2, 3, 4-Tri-*O*-acetyl-1-(2'-propargyl)-α-L-fucose

^1H NMR (CDCl_3 , 298 K, 400 MHz): δ (ppm) = 5.34 (dd, 1H, J 3.4 Hz, 7.5 Hz H-3), 5.28 (dd, 1H, J 1.0 Hz, 2.3 Hz, H-4), 5.23 (d, 1H, J 3.8 Hz, H-1), 5.14 (dd, 1H, J 3.7 Hz, 7.1 Hz, H-2), 4.24 (d, 2H, J 2.4 Hz, $\text{CH}_2\text{-C}\equiv\text{CH}$), 4.18 (q, 1H, J 6.4 Hz, H-5), 2.42 (t, 1H, $\text{CH}_2\text{-C}\equiv\text{CH}$), 2.15, 2.07, 1.97 (3s, 9H, $3\times\text{COCH}_3$), 1.13 (d, 3H, J 6.6 Hz, H-6).

^{13}C NMR (CDCl_3 , 298 K, 400 MHz): δ (ppm) = 170.7, 170.5, 170.1 ($3\times\text{COCH}_3$), 95.2 (C-1), 78.7 ($\text{CH}_2\text{-C}\equiv\text{CH}$), 75.0 ($\text{CH}_2\text{-C}\equiv\text{CH}$), 71.2, 67.9 (2), 65.1, 55.3 ($\text{CH}_2\text{-C}\equiv\text{CH}$), 20.9, 20.8, 20.7 ($3\times\text{COCH}_3$), 15.9 (C-6).

FT-IR ν (cm^{-1}): 3276 ($\text{C}\equiv\text{C-H}$), 2121 ($\text{C}\equiv\text{C}$), 1740 (C=O).

ESI-MS m/z : calcd for $\text{C}_{15}\text{H}_{20}\text{O}_8$ ($\text{M}+\text{Na}^+$), 351.1; found, 351.1.

2, 3, 4-Tri-*O*-acetyl-1-(2'-propargyl)- β -L-fucose

^1H NMR (CDCl_3 , 298 K, 400 MHz): δ (ppm) = 5.24 (dd, 1H, J 1.0 Hz, 2.5 Hz, H-3), 5.19 (dd, 1H, J 8.1 Hz, 2.4 Hz, H-4), 5.05 (dd, 1H, J 3.5 Hz, 6.9 Hz, H-2), 4.70 (d, 1H, J 7.9 Hz, H-1), 4.37 (t, 2H, $\text{CH}_2\text{-C}\equiv\text{CH}$), 3.83 (q, 1H, J 6.4 Hz, H-5), 2.44 (t, 1H, $\text{CH}_2\text{-C}\equiv\text{CH}$), 2.17, 2.06, 1.98 (3s, 9H, $3\times\text{COCH}_3$), 1.22 (d, 3H, J 6.4 Hz, H-6).

^{13}C NMR (CDCl_3 , 298 K, 400 MHz): δ (ppm) = 170.8, 170.4, 169.8 ($3\times\text{COCH}_3$), 98.6 (C-1), 78.6 ($\text{CH}_2\text{-C}\equiv\text{CH}$), 75.2 ($\text{CH}_2\text{-C}\equiv\text{CH}$), 71.4, 70.3, 69.5, 68.7, 55.8 ($\text{CH}_2\text{-C}\equiv\text{CH}$), 20.9, 20.8, 20.7 ($3\times\text{COCH}_3$), 16.2 (C-6).

FT-IR ν (cm^{-1}): 3274 ($\text{C}\equiv\text{C-H}$), 2121 ($\text{C}\equiv\text{C}$), 1742 (C=O).

ESI-MS m/z : calcd for $\text{C}_{15}\text{H}_{20}\text{O}_8$ ($\text{M}+\text{Na}^+$), 351.1; found, 351.1.

2.3.1.3 Synthesis of 1-(2'-Propargyl) D-Glucose

A suspension solution of D-glucose (12 g, 67 mmol), propargyl alcohol (19.4 mL, 333 mmol) and H_2SO_4 -silica (333 mg) was stirred at 65°C overnight. After cooling to ambient temperature, a part of the reaction mixture (14 g) was transferred to a silica gel column and eluted with CHCl_3 -MeOH (8:1) to remove the excess propargyl alcohol. 1-(2'-Propargyl) D-glucose was obtained as white solid after drying under vacuum (3.7 g, yield: 56 %).

FT-IR ν (cm^{-1}): 3347 (OH), 3285 ($\text{C}\equiv\text{C-H}$), 2118 ($\text{C}\equiv\text{C}$).

ESI-MS m/z : calcd for $\text{C}_9\text{H}_{14}\text{O}_6$ ($\text{M}+\text{Na}^+$), 241.1; found, 241.1.

For detailed characterisation, a part of the product was per-*O*-acetylated using acetic

anhydride. A suspension solution of 1-(2'-propargyl) D-glucose (218 mg, 1.00 mmol), acetic anhydride (3.0 mL, 32.0 mmol), H₂SO₄-silica (6 mg) was stirred at ambient temperature for 48 h. After completion of the reaction, the solution was diluted with CH₂Cl₂ (20 mL) and washed sequentially with saturated aq. NaHCO₃ solution and water twice. The extract was dried over MgSO₄ and concentrated under vacuum. ¹H NMR spectrum revealed the formation of the desired glycoside anomeric mixture in a ratio of 100:43 (α/β). The crude anomeric mixture was then separated by silica gel column chromatography using hexane-ethyl acetate (10:1) as eluent. 2, 3, 4, 6-tetra-*O*-acetyl-1-(2'-propargyl)-α-D-glucose (170 mg) and 2, 3, 4, 6-tetra-*O*-acetyl-1-(2'-propargyl)-β-D-glucose (70 mg) were obtained after drying under vacuum (Yield: 62.2%).

2, 3, 4, 6-Tetra-*O*-acetyl-1-(2'-propargyl)-α-D-glucose

¹H NMR (CDCl₃, 298 K, 400 MHz): δ (ppm) = 5.47 (t, 1 H, J 9.9 Hz, H-3), 5.27 (d, 1 H, J 3.9 Hz, H-1), 5.07 (t, 1 H, J 9.9 Hz, H-4), 4.89 (dd, 1 H, J 3.8, 6.6 Hz, H-2), 4.20-4.30 (m, 3 H, CH₂-C≡CH, H-6^a), 3.92-4.13 (m, 2 H, H-5, H-6^b), 2.44 (t, 1 H, J 2.4 Hz, CH₂-C≡CH), 2.08, 2.06, 2.01, 2.00 (4s, 12H, 4×COCH₃).

¹³C NMR (CDCl₃, 298 K, 400 MHz): δ (ppm) = 170.8, 170.2, 170.1, 169.7 (4×COCH₃), 94.7 (C-1), 78.3 (CH₂-C≡CH), 75.4 (CH₂-C≡CH), 70.5, 70.0, 68.5, 67.9, 61.8 (C-6), 55.5 (CH₂-C≡CH), 20.8 (3), 20.7 (4×COCH₃).

FT-IR ν (cm⁻¹): 3268 (C≡C-H), 2123 (C≡C), 1741 (C=O).

ESI-MS *m/z*: calcd for C₁₇H₂₂O₁₀ (M+Na⁺), 409.1; found, 409.1.

2, 3, 4, 6-Tetra-*O*-acetyl-1-(2'-propargyl)-β-D-glucose

¹H NMR (CDCl₃, 298 K, 400 MHz): δ (ppm) = 5.22 (d, 1 H, J 9.5 Hz, H-3), 4.95-5.13 (m, 2 H, H-2, H-4), 4.72 (d, 1 H, J 8.0 Hz, H-1), 4.22-4.38 (m, 3 H, CH₂-C≡CH, H-6^a), 4.02-4.12 (m, 1 H, H-6^b), 3.69-3.75 (m, 1 H, H-5), 2.46 (t, 1 H, J 2.5 Hz, CH₂-C≡CH), 2.07, 2.04, 2.01, 1.99 (4s, 12H, 4×COCH₃) ppm.

¹³C NMR (CDCl₃, 298 K, 400 MHz): δ (ppm) = 170.4, 169.7, 169.5 (2) (4×COCH₃), 98.2 (C-1), 78.3 (CH₂-C≡CH), 75.6 (CH₂-C≡CH), 72.9, 72.0, 71.1, 68.4, 61.9 (C-6), 56.0 (CH₂-C≡CH), 19.7, 19.6 (3) (4×COCH₃) ppm.

FT-IR ν (cm⁻¹): 3268 (C≡C-H), 2123 (C≡C), 1741 (C=O).

ESI-MS *m/z*: calcd for C₁₇H₂₂O₁₀ (M+Na⁺), 409.1; found, 409.1.

2.3.4 Michael addition reactions of glycidyl methacrylate and PGMA with thiols

The reactions were carried out at ambient temperature and monitored by ^1H NMR spectroscopy. In a typical reaction of GMA with thiol, (71 mg, 0.5 mmol, 1 eq) GMA, (186 mg, 1.5 mmol, 3 eq) benzyl mercaptan, DMPP (3.6 μL , 2.5×10^{-2} mmol, 0.05 eq) and 0.4 mL $\text{DMSO-}d_6$ were added into a NMR tube for ^1H NMR analysis. In a typical reaction of CCTP PGMA with thiol, 1.02 g PGMA ($M_n=1700$ Da, 0.6 mmol of vinyl groups) was dissolved in DMSO (4 mL). Benzyl mercaptan (149 mg, 1.2 mmol) and DMPP (4.1 μL , 0.03 mmol) were added to this solution, and the mixture was stirred at ambient temperature. A part of the solution (0.1 mL) was taken out for ^1H NMR analysis. After conversion of the vinyl groups was achieved, the reaction was stopped by precipitation in methanol and purified *via* dialysis in methanol for one day. The benzyl end-functionalised product was dried under vacuum. (Yield: 42.2%)

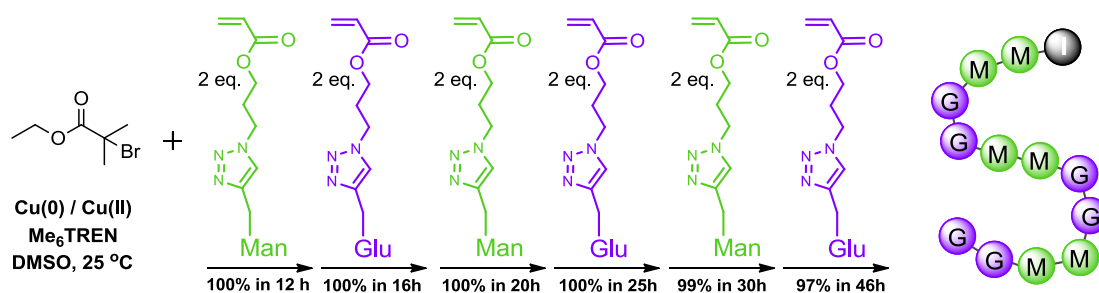
2.3.5 Epoxy ring opening reaction of PGMA with sodium azide

The polymers containing 2-hydroxy-3-azidopropyl methacrylate (HAZPMA) units were prepared according to previous procedure.⁹⁰ In a typical reaction, benzyl end-functionalised PGMA (0.42 g, 2.75 mmol of epoxide groups) was dissolved in DMF (8 mL). Sodium azide (0.358 g, 5.50 mmol) and ammonium chloride (0.294 g, 5.50 mmol) were added to the solution and stirred at 50 $^{\circ}\text{C}$ for 24 h. After cooling down to ambient temperature, the mixture was directly transferred to dialysis tubing and dialysed against water for two days. 0.484 g product was obtained after drying under vacuum.

2.3.6 CuAAC reactions of azide-containing polymers with alkyne compounds

A general procedure is shown as follows. A solution of 1-(2'-propargyl) L-fucose (0.225 g, 1.11 mmol), benzyl end-functionalised PHAZPMA (0.150 g, 0.78 mmol of azide groups), bpy (30 mg, 0.20 mmol) in DMSO (5 mL) was deoxygenated by three freeze-pump-thaw cycles. The solution was then transferred *via* cannula under nitrogen into a Schlenk tube, previously evacuated and filled with nitrogen, containing CuBr (14 mg, 0.10 mmol). The resulting solution was stirred at 30 $^{\circ}\text{C}$ for 24 h. Upon the reaction was completed, the reaction mixture was diluted with water (20 mL) and purged with air for 1 h and then dialysed against water for two days after which the glycopolymer (0.226 g) could be recovered by freeze drying.

Chapter 3 Sequence-Controlled Multi-Block Glycopolymers to Inhibit DC-SIGN-gp120 Binding



Multi-block glycopolymers made of mannose, glucose, fucose and di(ethylene glycol) ethyl ether acrylate monomers were synthesized by $\text{Cu}(0)$ wire mediated single electron transfer living radical polymerization (SET-LRP). These highly narrow disperse glycopolymers were then tested for binding and inhibition of DC-SIGN, a protein important for HIV infection.

3.1 Introduction

Glycan-protein interactions are essential for many physiological processes including cell-cell recognition, cell adhesion, cell signalling, pathogen identification and differentiation. These interactions also play a critical role in infectious disease processes such as pathogen-cell interactions and immune responses. Dendritic cells (DC) are the most antigen presenting cells and form a major component of the immune system. DCs act as messengers between the innate and adaptive immunity and their main function is to process antigen material and present it on the surface to other cells of immune systems such as T-cells. Dendritic cell-specific intercellular adhesion molecule-3-grabbing non-integrin (DC-SIGN; CD209) is a C-type lectin (carbohydrate-binding protein) present on both macrophages and dendritic cell subpopulations. DC-SIGN binds to microorganisms and host molecules by recognizing surface rich mannose containing glycans through multivalent glycan-protein interactions and notably serves a target molecule for several viruses such as human immunodeficiency virus (HIV) and hepatitis C virus (HCV).^{125,126} Both gp120 and gp41 are heavily glycosylated and it is estimated that gp120 consists of glycans, which account for almost 50% of its molecular weight. Carbohydrate binding proteins (CBP) have been suggested as potential candidate microbicides for the prevention of HIV infection.^{127,128} However, the isolation of natural CBPs is relatively difficult due to their hydrophilic nature and they show notably low affinities to virus.^{129,130} Therefore, synthetic lectins are of interest for carbohydrate recognition and Davis *et. al.* have reported the discovery of a simple monocyclic host, which was prepared in 5 steps and 23% overall yield instead of 21 steps and 0.1% yield.¹³¹ Alternatively, non-carbohydrate inhibitors of mammalian lectins can be used to prevent the interaction between DC-SIGN and gp120.¹³²⁻¹³⁴ Borrock and Kiessling have reported IC₅₀ values of 1.6-10 μ M for monovalent small molecule inhibitors. Monovalent ligands have access to a limited number of binding mechanisms and typically bind to a single glycan-binding domain. However, multivalent ligands can interact with receptors through chelate effect, subsite binding, steric stabilization, statistical rebinding, and receptor clustering. The architectures of the multivalent ligands can have a large effect on carbohydrate binding to lectins and the use of linear polymers on effective lectin binding has been demonstrated by several research groups.^{8,26,135-138}

Carbohydrate sequence and conformation potentially supply a vast source of information and could act as biological information transfer beyond genetic code, namely “sugar code” or “glyco code”, which has been proved to play critical role during evolution.¹³⁹⁻¹⁴¹ Sequence control in polymer synthesis had been largely ignored mainly due to the difficulty in precise control and characterization during monomer sequencing.¹⁴² Since the important breakthrough of solid-phase synthesis in the 1960’s, it has been widely utilized in synthesis of many important high-ordered biopolymers and non-biological polymers.^{143,144} Template polymerization and step-growth polymerization could also result in sequence-specific polymers.¹⁴⁵⁻¹⁴⁷ Chain-growth copolymerization tends to be more promising for complex monomer sequence construction, including random, block, alternate and gradient microstructures.¹⁴⁷

Synthetic polymer chemistry has developed rapidly in the last decades owing to much to the discovery of controlled/living radical polymerization and more recently in combination with efficient click reactions.^{15,148-151} Currently, polymerization of functional monomers with desired chain length, architecture and composition is straightforward whereas sequence controlled structures^{146,152} and controlled folding of synthetic macromolecules are current important challenges in polymer chemistry.¹⁵³ There are a few recent reports where sufficient control has been achieved in controlling the monomer sequence along the polymer chain.^{24,154-157} Noteworthy, a successful sequence controlled polymerization technique, single electron transfer living radical polymerization (SET-LRP)^{21,156,158,159}, allows facile synthesis of high-order multiblock copolymers *via* iterative monomer addition in an one-pot reaction featuring high yield, high chain end fidelity and requiring purification only at the last step.¹⁵⁶

The synthesis of glycopolymers featuring well-defined macromolecular architectures has been developed by using different polymerization techniques and click reactions.^{2,4} However, direct transition metal-catalyzed polymerization of unprotected glyco monomers is still limited mainly due to the difficulty in synthesis of unprotected glyco monomers and optimization of polymerization conditions.^{23,24,26,160-162}

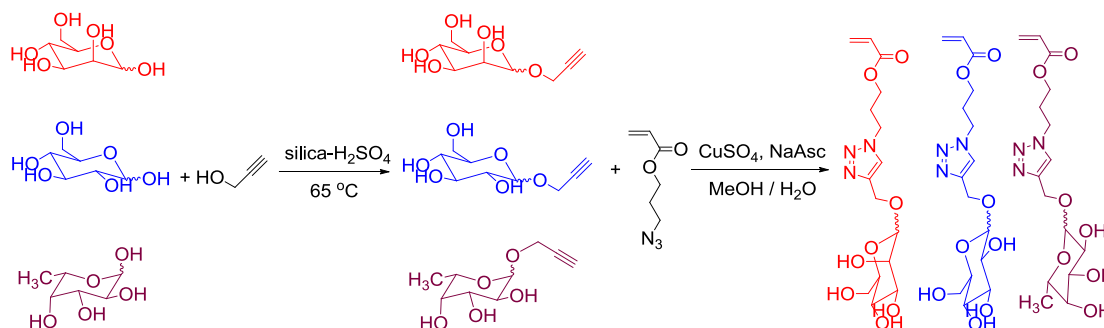
This inspired us to introduce SET-LRP into synthesis of sequence-controlled glycopolymers for a glycopolymer code. To the best of our knowledge this is the first

report on the preparation of sequence controlled glycopolymers and the demonstration of their binding to the human lectin DC-SIGN.

3.2 Results and discussion

3.2.1 Synthesis of glycomonomers via CuAAC click reaction

In order to get a sugar sequence, different carbohydrate units should be inserted along the polymer backbone either through polymerization of different sugar monomers or via post-modification after polymerization. Based on the demand of carbohydrate diversity, direct polymerization of different functional glyco monomers is the first choice compared with multistep chemical modification after polymerization.



Scheme 3. 1. Synthesis of glycomonomers *via* Fischer glycosylation & CuAAC.

CuAAC has supplied a facile route for the synthesis of glycomonomers. From an azide functionalized sugar, methacrylate type sugar monomers and novel 4-vinyl-1, 2, 3-triazole type sugar monomers could be synthesized *via* reaction with alkyne compounds in MeOH/H₂O or THF/H₂O under the catalysis of CuSO₄/sodium ascorbate.^{26,163} For an alternative approach, one-pot Fischer type glycosylation reaction was first conducted to prepare alkyne-functionalised sugars, which were then reacted with one azide acrylate intermediate *via* CuAAC reaction in MeOH/H₂O under the catalysis of CuSO₄/sodium ascorbate. Three different stable solid acrylate glyco monomers could be obtained through this protocol, Scheme 3.1.

¹H NMR clearly revealed the appearance of triazole ring proton at ~7.9 ppm and vinyl peaks at 5.5-6.5 ppm after click reaction, Figure 3.1. ¹³C NMR spectrum showed the existence of D-glucose C-1 peaks at 99.6 & 103.6 ppm, suggesting that the monomer is an anomeric mixture. Combination with further ESI-MS and FT-IR analysis proved that targeted glyco monomer has been successfully synthesized.

D-mannose and L-fucose acrylate monomers were also synthesized in same way and detailed synthesis and characterization were shown in the experimental section.

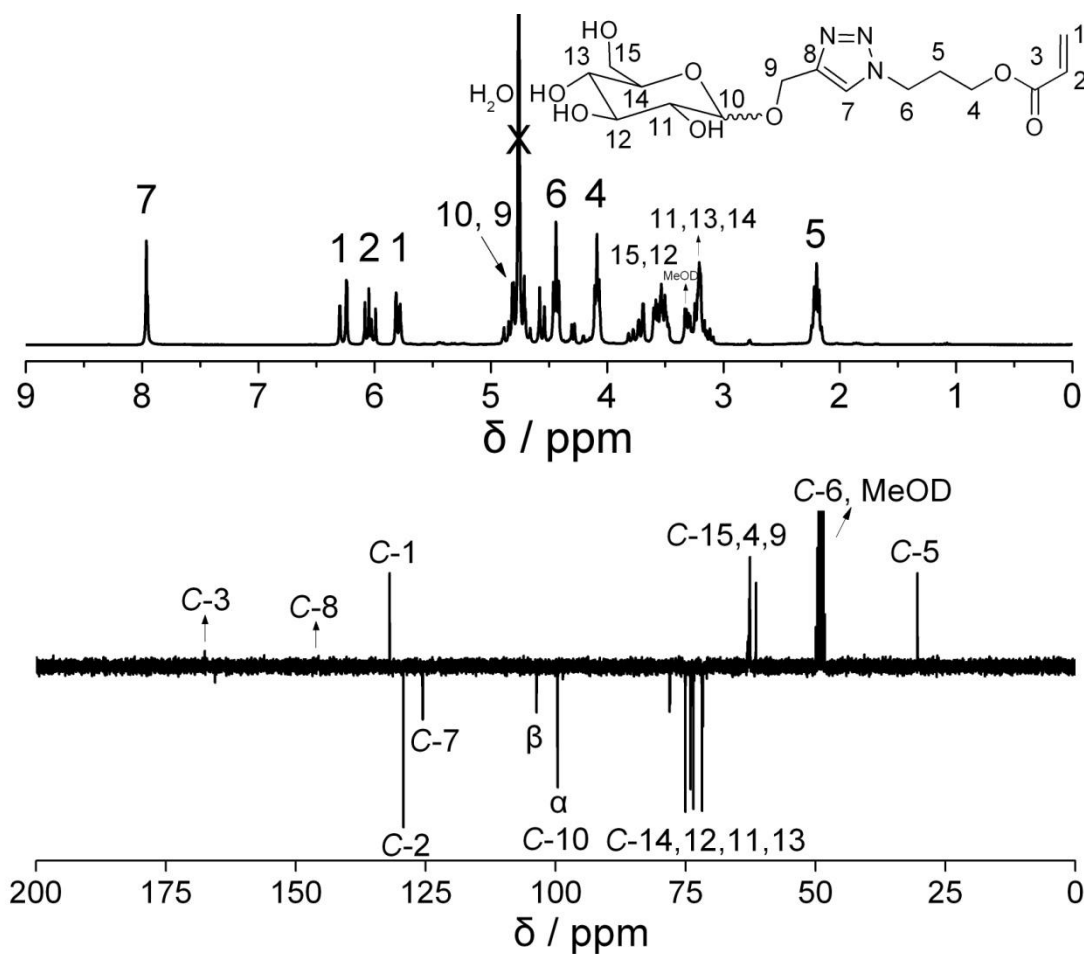
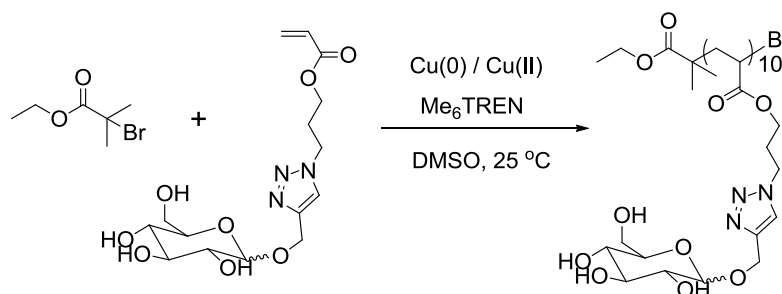


Figure 3. 1. ^1H (top) and ^{13}C (bottom) NMR spectra of D-glucose acrylate monomer in MeOD.

3.2.2 Homopolymerization of glycomonomers by SET-LRP in DMSO at ambient temperature



Scheme 3. 2. Homo polymerization of D-glucose acrylate monomer with $[\text{EBiB}]_0 = 33 \text{ mmol/L}$, $[\text{CuBr}_2]_0 = 3.3 \text{ mmol/L}$, $[\text{Me}_6\text{TREN}]_0 = 6 \text{ mmol/L}$ in DMSO (3 mL), 25 °C.

The glycomonomers have good solubility in DMSO and were polymerized at ambient temperature via the catalysis with Cu(0)/Cu(II)/Me₆TREN system with EBiB as initiator and DMSO as solvent (Scheme 3.2).

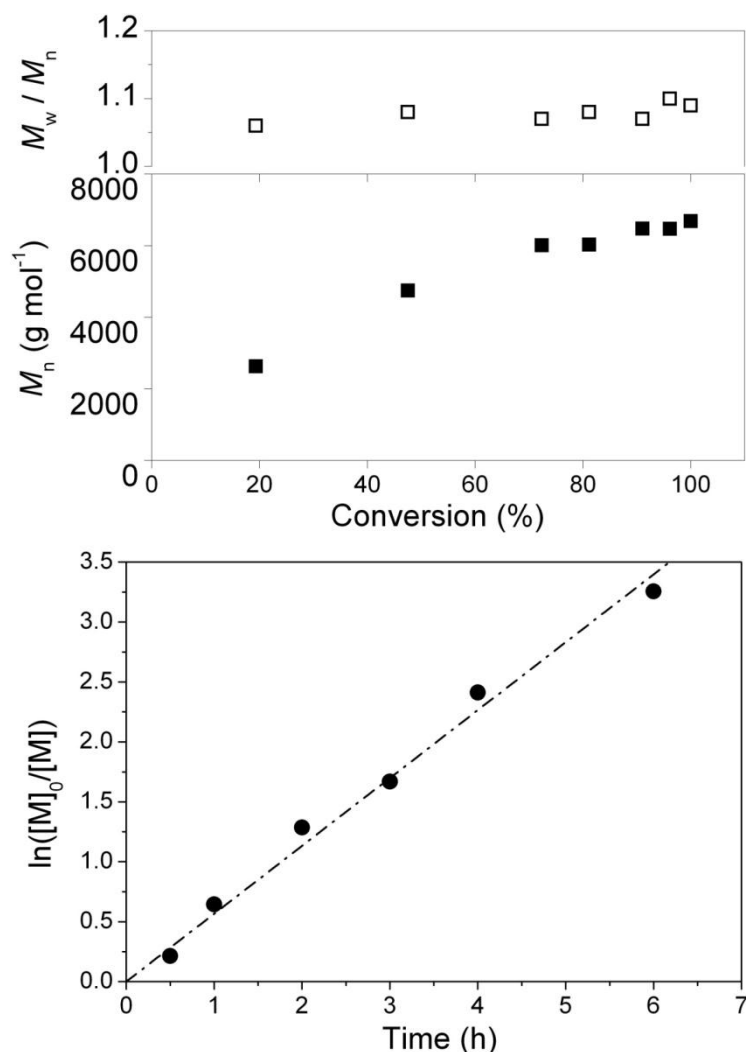


Figure 3. 2. Dependence of M_n and M_w/M_n on conversion (top) and first order kinetic plots (bottom) for the polymerization of D-glucose glycomonomer via SET-LRP in DMSO.

Monomer conversion reached 91% in 4 h and after 24 h full conversion could be obtained, Figure 3.2. Number average molecular weight (M_n) by DMF SEC generally increased linearly with monomer conversion. However, the M_n by SEC is higher than theoretical molecular weight mainly due to the different structure of glycopolymer with PMMA calibration standard, which would cause a significant difference of hydrodynamic volume of polymer in DMF. The molecular weight distribution kept narrow ($M_w/M_n < 1.10$) through the whole polymerization, even after full conversion

no significant bimolecular termination could be detected by SEC, which revealed high chain end fidelity. A linear agreement in the plot of $\ln[M]_0/[M]$ versus time was observed, which indicates that the concentration of growing radicals remains constant during propagation and termination is not significant.

From the ^1H NMR spectrum, Figure 3.3, the resonance of the broad triazole ring protons at 8.1 ppm and D-glucose protons from 2.8 to 5.2 ppm indicated that glucose units have been linked to the polymer backbone. Furthermore, the ratio of integral for the triazole ring protons at 8.11 ppm with EBiB methyl groups at 1.04 to 1.12 is approximately 10: 9.4, which is in good agreement with the theoretical value (10: 9), suggesting the successful and efficient synthesis of D-glucose glycopolymer by SET-LRP.

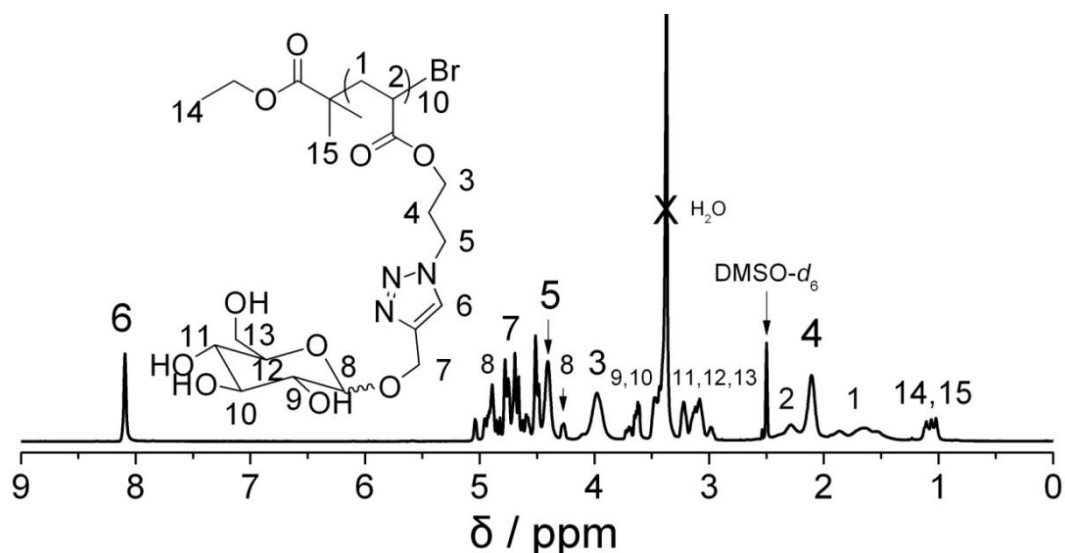
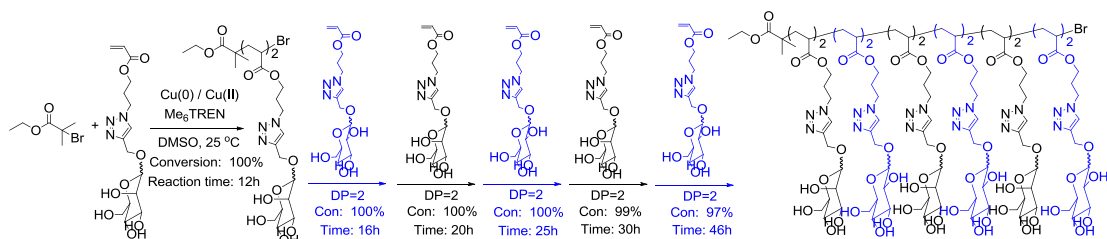


Figure 3. 3. ^1H NMR spectrum of D-glucose glycopolymer in $\text{DMSO-}d_6$.

3.2.3 Synthesis of multiblock glycopolymers *via* iterative monomer addition by SET-LRP



Scheme 3. 3. Schematic representation for the synthesis of sequence-controlled multiblock glycopolymer by iterative addition of glyco monomers without intermediate purification (DP=2 for each block).

Synthesis of high-order multiblock glycopolymers with very short blocks (DP=2 for each block, (mannose)₂-(glucose)₂-(mannose)₂-(glucose)₂-(mannose)₂-(glucose)₂) was first explored by SET-LRP via iterative chain extension under similar reaction condition, as shown in Scheme 3.3.

Long reaction times were employed to ensure monomer conversion of each block was close to full conversion such that no purification procedure was necessary for the next step reaction. The conversion of first four blocks by NMR showed close to 100% as evidenced by disappearance of vinyl groups at 5.7-6.5 ppm. With the addition of monomer in DMSO for chain extension, the system became more diluted and traces of vinyl groups could be detected since 5th and 6th block (conversion is 99%, 97% in turn).

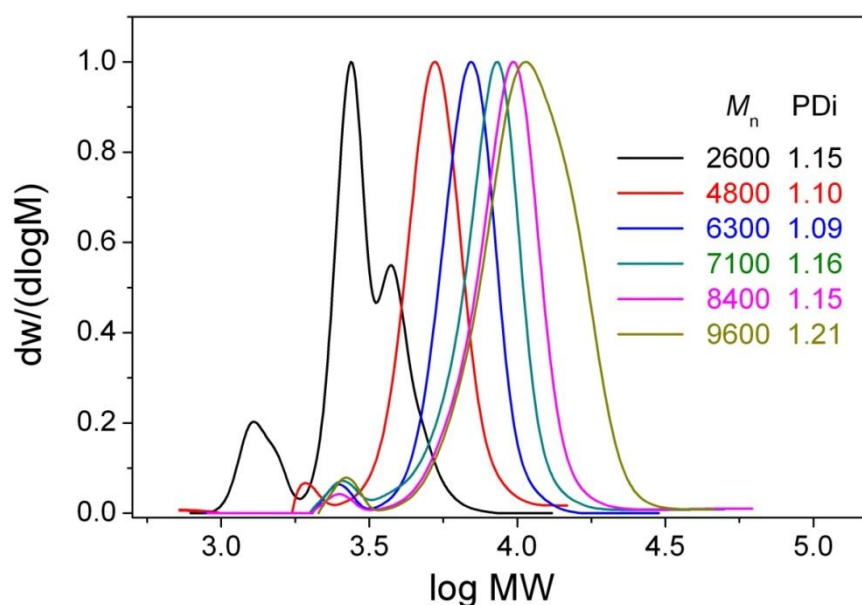


Figure 3. 4. Molecular weight distributions (normalized to peak height) of multiblock glycopolymer obtained by SET-LRP *via* iterative chain extensions (DP=2 for each block).

During the first five blocks, SEC traces (Figure 3.4) almost shift totally after chain extension and M_w/M_n kept narrow (for the 5th block $M_w/M_n = 1.15$, even including the tailing peak), confirming the polymerizations are well-controlled. A small tailing peak at low molecular weight position which may be caused by termination reaction could be detected; however, compared with propagating polymer peak this ratio is very small. After the 6th block, SEC trace became much broader and the M_w/M_n has a significant increase to 1.21. Although no significant shoulder peak at high MW

position was found, the SEC trace didn't shift totally compared with the 5th block, suggesting possible termination happened and reaction was then stopped.

High resolution ESI-MS (Figure 3.5, 3.6) and MALDI-ToF MS analysis (Figure 3.7) were performed to characterize the exact structure of glycopolymer during polymerization.

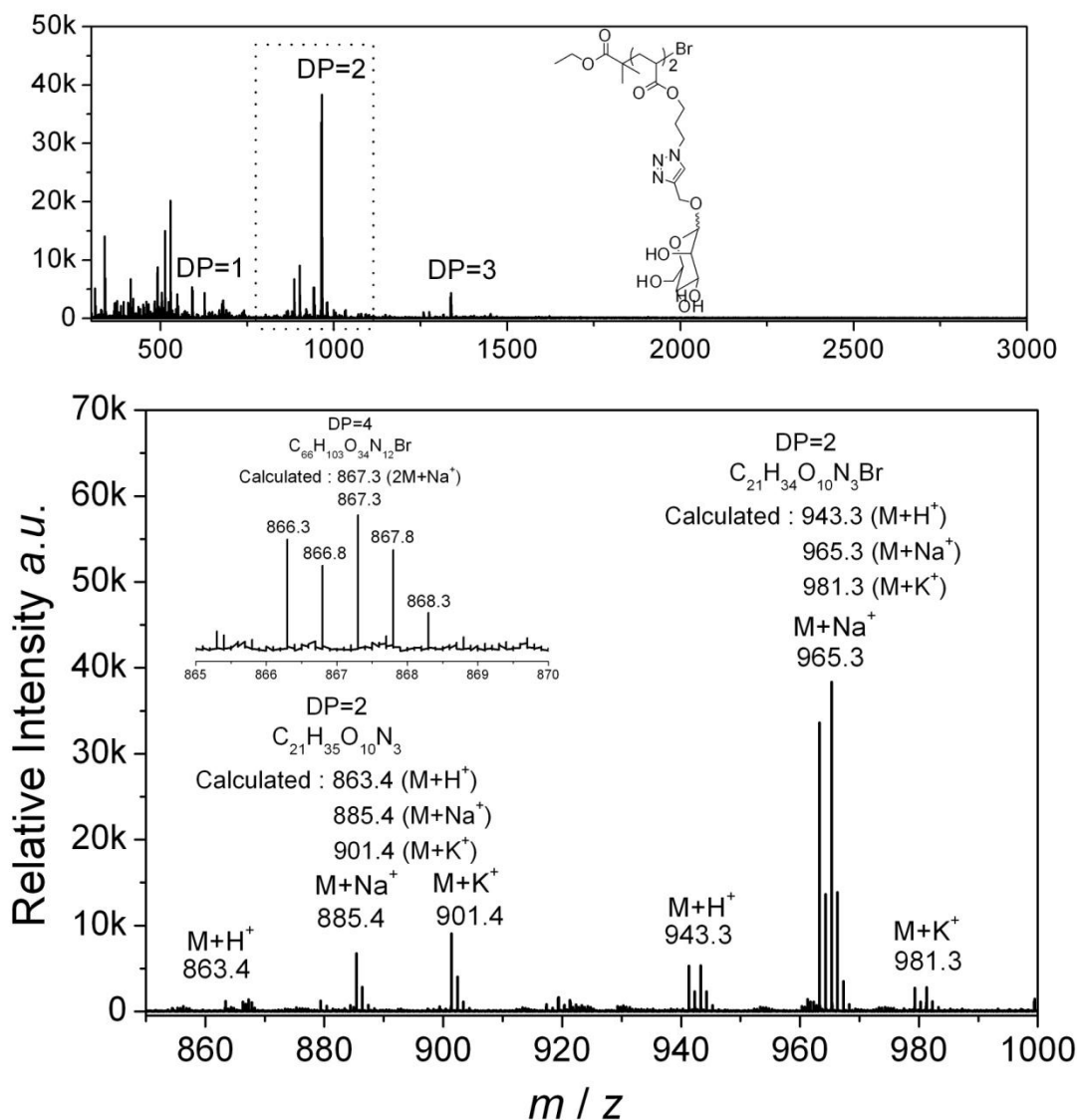


Figure 3. 5. ESI-MS spectra of the 1st block poly(mannose)₂ by SET-LRP(top: whole spectra; bottom: zoom of 800-1000 region).

High resolution ESI-MS spectra, Figure 3.5, clearly show peaks belonging to the 1st block poly(mannose)₂, which reveal the exact structure of extremely low DP glycopolymer with only 1, 2, 3 and 4 mannose units initiated with EBiB and

terminated with bromine. Typically, Figure 3.5, DP = 2 showed mass peaks at 943.3, 965.3 and 981.3 (m/z), which is cationised with H^+ , Na^+ and K^+ respectively.

Peaks at 863.4, 885.4 and 901.4 (m/z) were attributed to dead polymer chains with terminal hydrogen, which were mainly caused by disproportionation and chain transfer side reaction and thus leading to lose of terminal bromine. However, the signal strength of these peaks was weaker than that of propagating polymer chains.

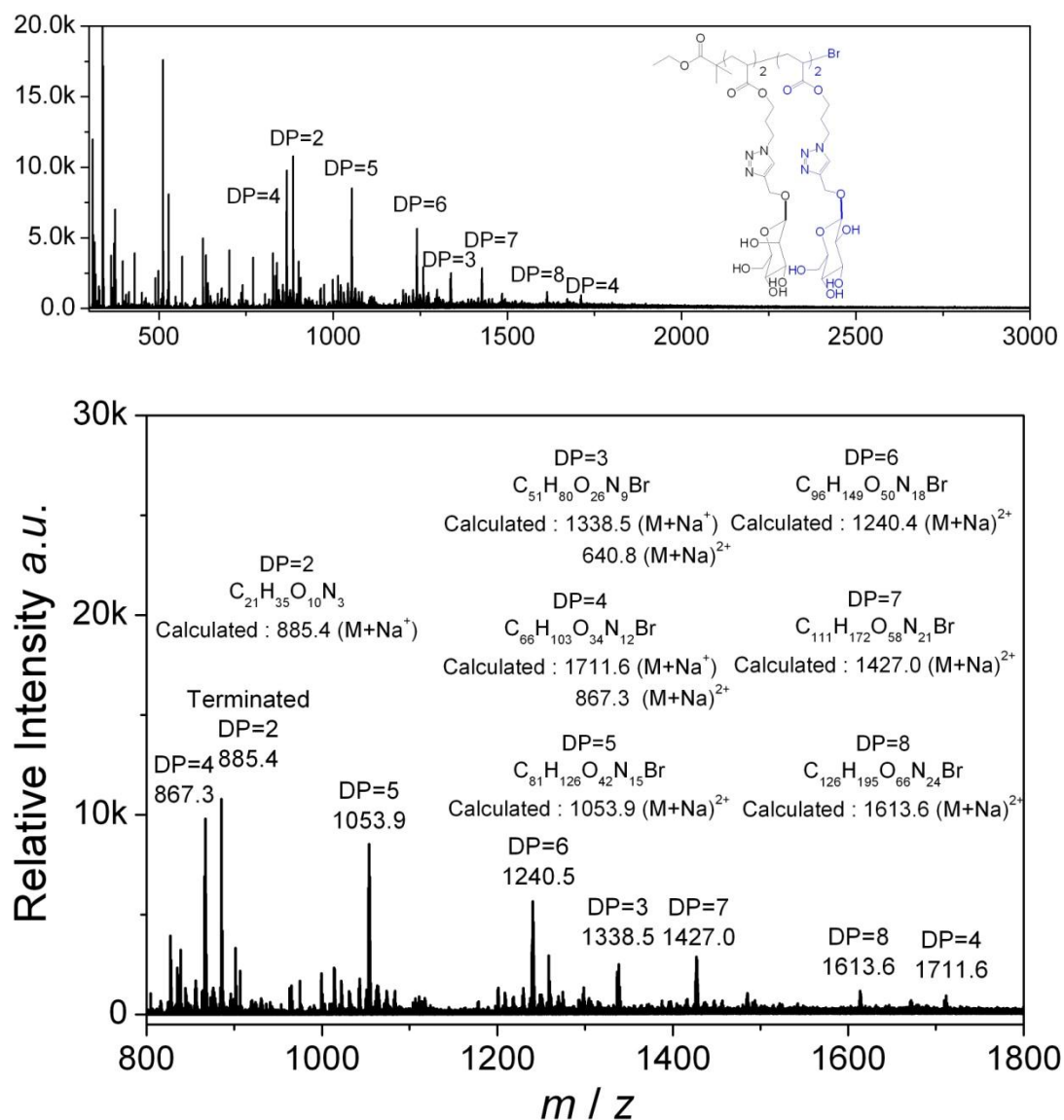


Figure 3. 6. ESI-MS spectra of the 2nd block poly(mannose)₂-(glucose)₂ by SET-LRP(top: whole spectra; bottom: zoom of 800-1800 region).

After the chain extension reaction, the main peaks (Figure 3.6) clearly shifted to higher MW region by 2-3 units, which are in accord with theoretical values and SEC results.

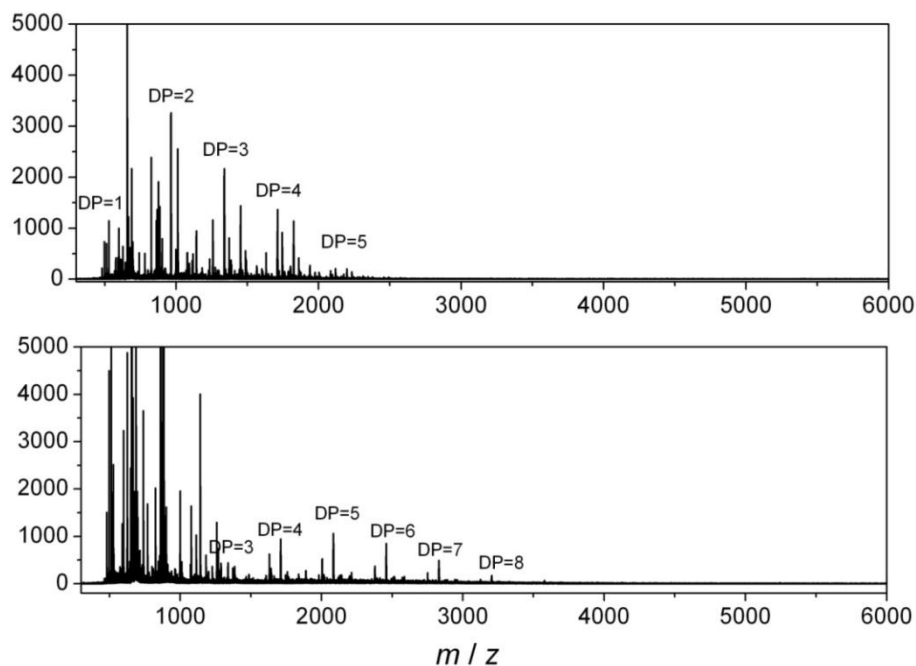


Figure 3. 7. MALDI-ToF MS spectra of the 1st block poly(mannose)₂ (top) and 2nd block poly(mannose)₂-(glucose)₂ (bottom) glycopolymers obtained by SET-LRP.

As comparison, MALDI-ToF MS was also used for the characterization of these glycopolymers, which showed similar results as in the ESI-MS analysis. Following the block copolymerization the polymer peaks have a significant shift to higher MW region, Figure 3.7, suggesting the success of block copolymerization. However, with the increase of MW and incorporation of more sugar units, the ionization of the glycopolymer tends to become more difficult. Thus the resolution of the spectra decreased and became unable to define the exact structure after the 3rd block polymerization or even cannot be detected after 4th block polymerization.

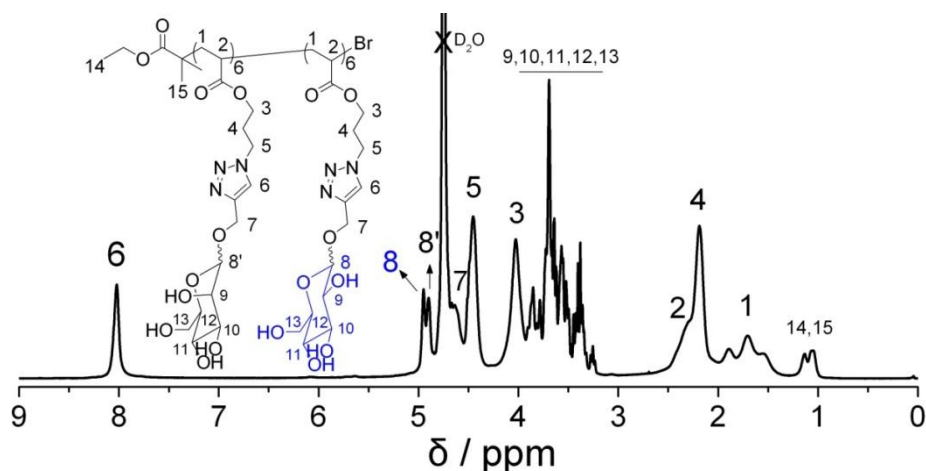
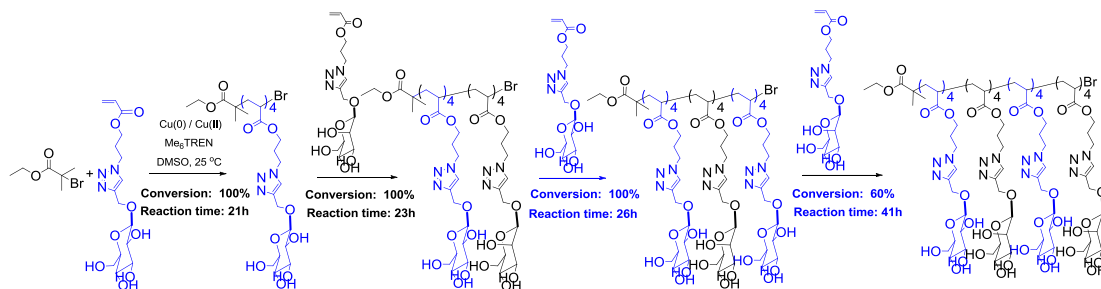


Figure 3. 8. ¹H NMR spectrum of multiblock D-mannose/D-Glucose glycopolymer in D₂O.

^1H NMR spectrum of final polymer product also revealed peaks from mannose and glucose units, typically shown as peaks of C-1 protons at 4.8 and 4.9 ppm (Figure 3.8).

Thus, the above results clearly proved the successful synthesis of multiblock glycopolymer and the microstructure is highly controlled.



Scheme 3. 4. Schematic representation for the synthesis of sequence-controlled multiblock glycopolymers by iterative addition of glyco monomers without intermediate purification (DP=4 for each block).

The chain length of each block was then increased to DP=4 with overnight reaction conditions to ensure full conversion (the first three blocks) was achieved (Scheme 3.4).

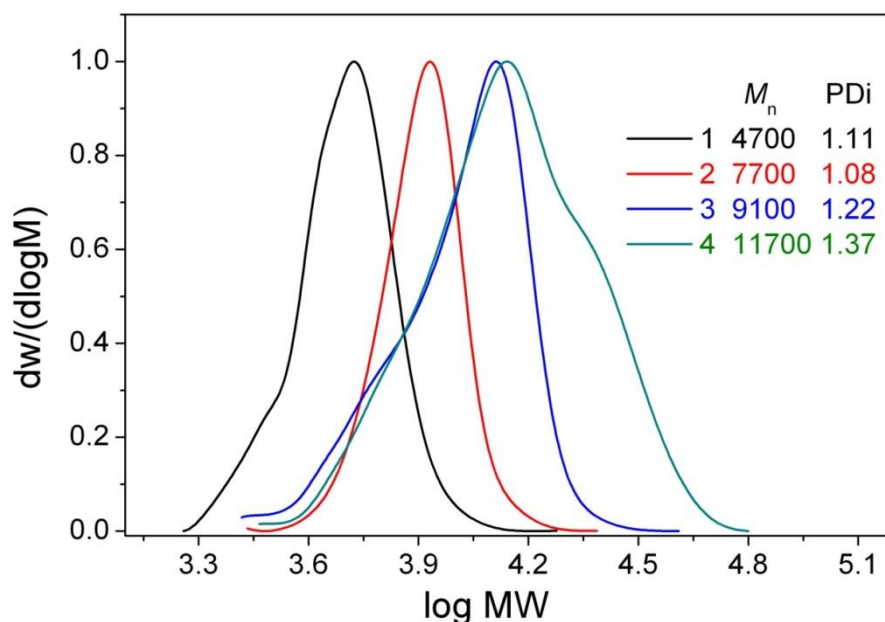


Figure 3. 9. Molecular weight distributions (normalized to peak height) of multiblock glycopolymer obtained by SET-LRP via iterative chain extensions (DP=4 for each block).

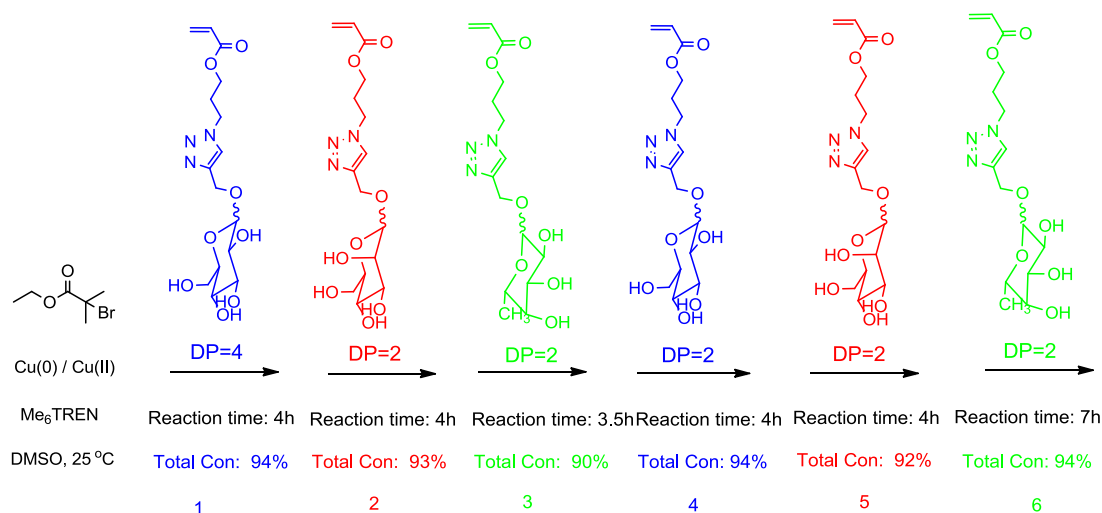
The SEC traces shift totally after the 2nd block polymerization and no significant tailing or coupling peaks were found, Figure 3.9. However, after the 3rd monomer addition the PDI increased to 1.22 and tailing peaks at lower MW position were seen. After the 4th block with a conversion of 60% the PDI increased to 1.37 and double peaks were noticed, including the one overlapped with the 3rd peak due to termination and the shoulder peak at higher MW region due to on-going chain propagation.

To summarize, these experiments demonstrated the successful synthesis of multiblock glycopolymers *via* a facile iterative monomer addition. However, after multiblock full conversion polymerization termination still happened and chain propagation thus stopped. Further research especially on the reaction mechanism is necessary for full understanding of such phenomenon.

3.2.4 Control of sugar sequence in glycopolymers *via* iterative monomer addition before full conversion by SET-LRP

Cu(II) has been used as a deactivator to reduce the rate of SET-LRP and remove the period of slow reaction rate at the start of the reaction.^{159,164} Initially added Cu (II) has also been proved to play an important role in maintaining the chain end fidelity during one-pot multiblock copolymerization^{156,165} and preventing the star-star coupling in the synthesis of star copolymers.¹⁶⁶ Livingness for a decablock copolymer could be kept up to more than 50% according to SEC, although tailing peaks caused by dead polymers in each block could be detected.¹⁶⁵

In previous experiments, radical coupling termination was not significant in the presence of initially added Cu(II), however, termination by disproportionation and chain transfer still occurred during the polymerization. In order to reach full conversion, the reaction time was prolonged with the addition of new monomer which unavoidably diluted the reaction system. The total reaction time was even more than one week, which is generally uncommon and possibly would lead to increased termination side reaction. However, due to the complexity of this reaction system the exact reason is still not perfectly understood.



Scheme 3. 5. Schematic representation for the synthesis of multiblock glycopolymers by iterative addition of glyco monomers at defined time period.

In order to solve this problem it was thought better to add the new monomer prior to full conversion. To test this strategy, new monomer was added after a period of around four hour in a one-pot polymerization, Scheme 3.5.

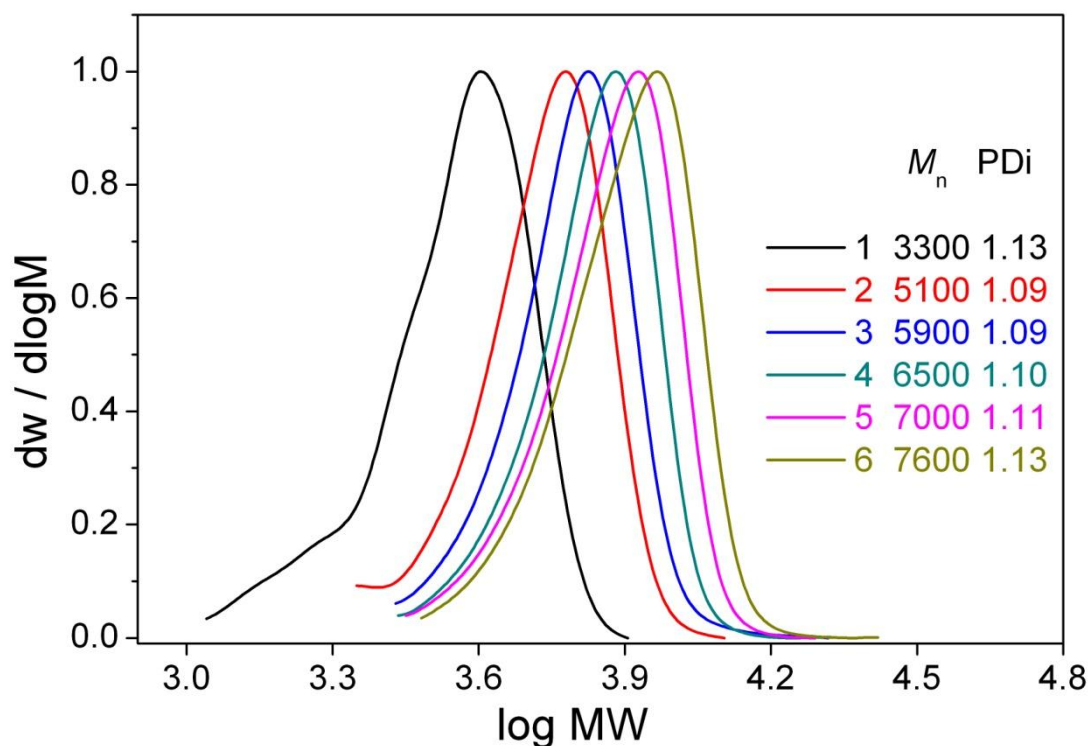
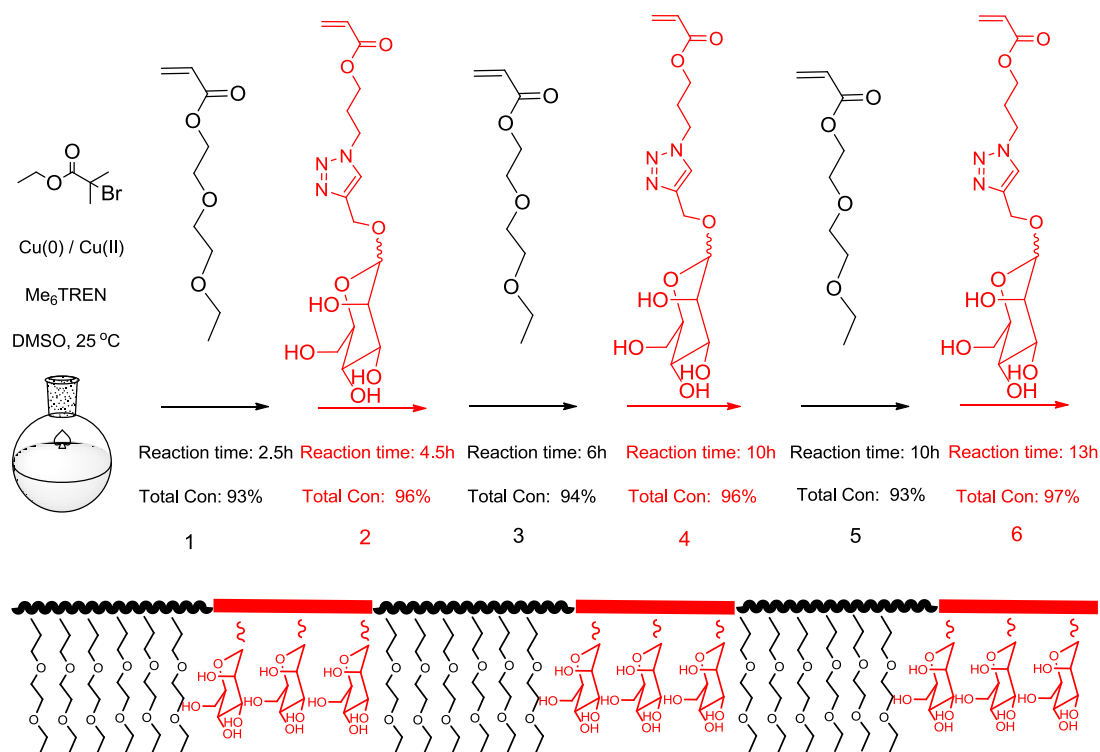


Figure 3. 10. Molecular weight distributions (normalized to peak height) of multiblock glycopolymers obtained by SET-LRP via iterative addition of glyco monomers at defined time period.

^1H NMR showed that total conversion is around 90%-94% and after 5th block reaction time need to be prolonged to 7 h in order to reach a similar conversion. The high conversion means that the obtained glycopolymer is still highly sequence-controlled, although seriously speaking it is not multiblock copolymer. SEC analysis (Figure 3.10) revealed the total shift of elution traces after each monomer addition and final M_w/M_n is ≈ 1.13 and no significant tailing or coupling peaks were detected during the polymerization, indicating that the chain end fidelity is better than the long time scale full conversion reaction.

These results revealed that it's possible to control the glyco code during polymerization *via* controlled addition of different glyco monomers at high conversion.



Scheme 3. 6. Schematic representation for the synthesis of sequence-controlled multiblock glycopolymers by iterative addition of DEGEEA and mannose glycomonomer at defined time period.

The “cluster glycoside effect” is defined as “*an affinity enhancement over and beyond what would be expected from the concentration increase of the determinant sugar in a multivalent ligand*”.¹⁶⁷ Glycopolymers as a typical class of polyvalent glycosidic ligands could dramatically increase the affinity during the multivalent carbohydrate-

protein interaction.¹⁶⁸ The dense sugar units along polymer backbone create cluster glycoside effect and the binding ability of glycopolymer with lectin compared with monosaccharide was thus dramatically enhanced. It has been shown that the sugar number, sugar density, ligand shape, size and linker spacing strongly contribute to the specific binding behaviour.^{74,169-171} In order to further understand the multivalent binding of polymeric ligands, it would be of great importance to control the density, distance and distribution of sugar units along the polymer chain.

Thus SET-LRP was utilized to synthesize a multiblock glycopolymer bearing sequential lectin-binding and lectin-non-binding segments. DEGEAA and mannose glycomonomer were used as monomers for the non-binding and binding blocks and the DP was controlled as 6 and 3 for the aid of characterization. As shown in Scheme 3.6, reaction time was kept longer after each chain extension to gain a high conversion (total conversion was 93%-97% according to ¹H NMR) yet new monomer was added before full conversion in order to keep high chain end fidelity.

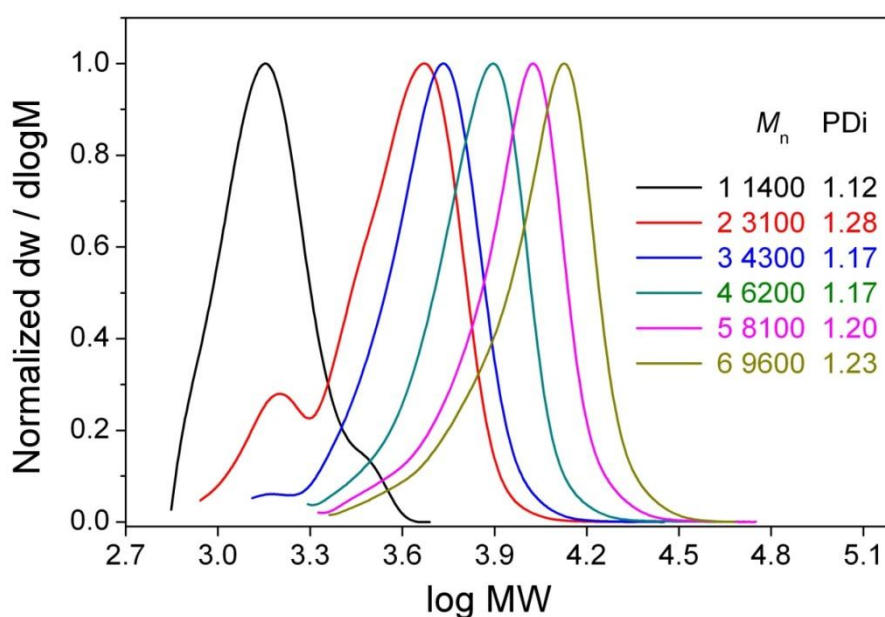


Figure 3. 11. Molecular weight distributions of multiblock glycopolymer obtained by SET-LRP *via* iterative addition of DEGEAA and mannose glycomonomer at defined time period.

SEC analysis confirmed the MW increase after each chain extension, Figure 3.11. Although it still showed tailing after chain extension (especially after the 4th block polymerization) causing slight PDI increase, the final dispersity was still relatively narrow (~1.2), indicating high chain end fidelity. The ¹H NMR spectrum (Figure

3.12) of the final product clearly showed resonance and correct ratio from mannose and DEGEEA units, such as 8.1 ppm (triazole ring proton) & 4.9 ppm (C-1 proton) for the mannose and 3.4 - 3.8 ppm (ethylene glycol protons) for the DEGEEA.

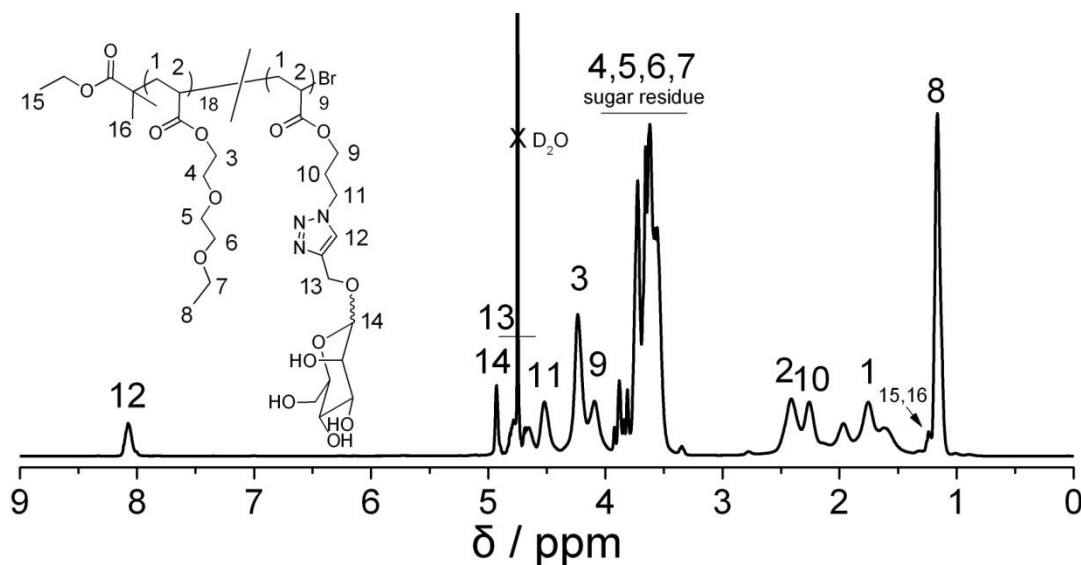


Figure 3. 12. ^1H NMR spectrum of multiblock DEGEEA-mannose glycopolymer in D_2O .

MALDI-ToF MS analysis supported a successful block structure and the MW increased after chain extension, Figure 3.13. Due to the close MW between polymers with different DP, such as $\text{poly}(\text{DEGEEA})_5\text{-}b\text{-(mannose)}_2$ and $\text{poly}(\text{DEGEEA})_7\text{-}b\text{-(mannose)}_1$, higher resolution ESI-MS was utilized to confirm the right structure (Figure 3.18). As previous characterization, resolution of the spectra decreased with incorporation of more sugar units. However, MADLI-ToF MS under linear flight model still revealed appearance of polymer peaks at higher MW region although exact structure cannot be defined (Figure 3.22).

In order to demonstrate the versatility of this synthetic protocol, the multiblock copolymerization of DEGEEA and D-glucose monomer was conducted in the same way and similar results were obtained (see experimental section). Homo mannose glycopolymer and random DEGEEA-Mannose glycopolymer with similar chain length and DEGEEA-mannose ratio were also synthesised in order to compare the different lectin-binding behaviour with sequence-controlled multiblock glycopolymer (see experimental part).

These results show the successful synthesis of multiblock DEGEEA-Mannose glycopolymer, which means that sugar density and distribution along polymer chain can be adjusted by the control of monomer addition during SET-LRP.

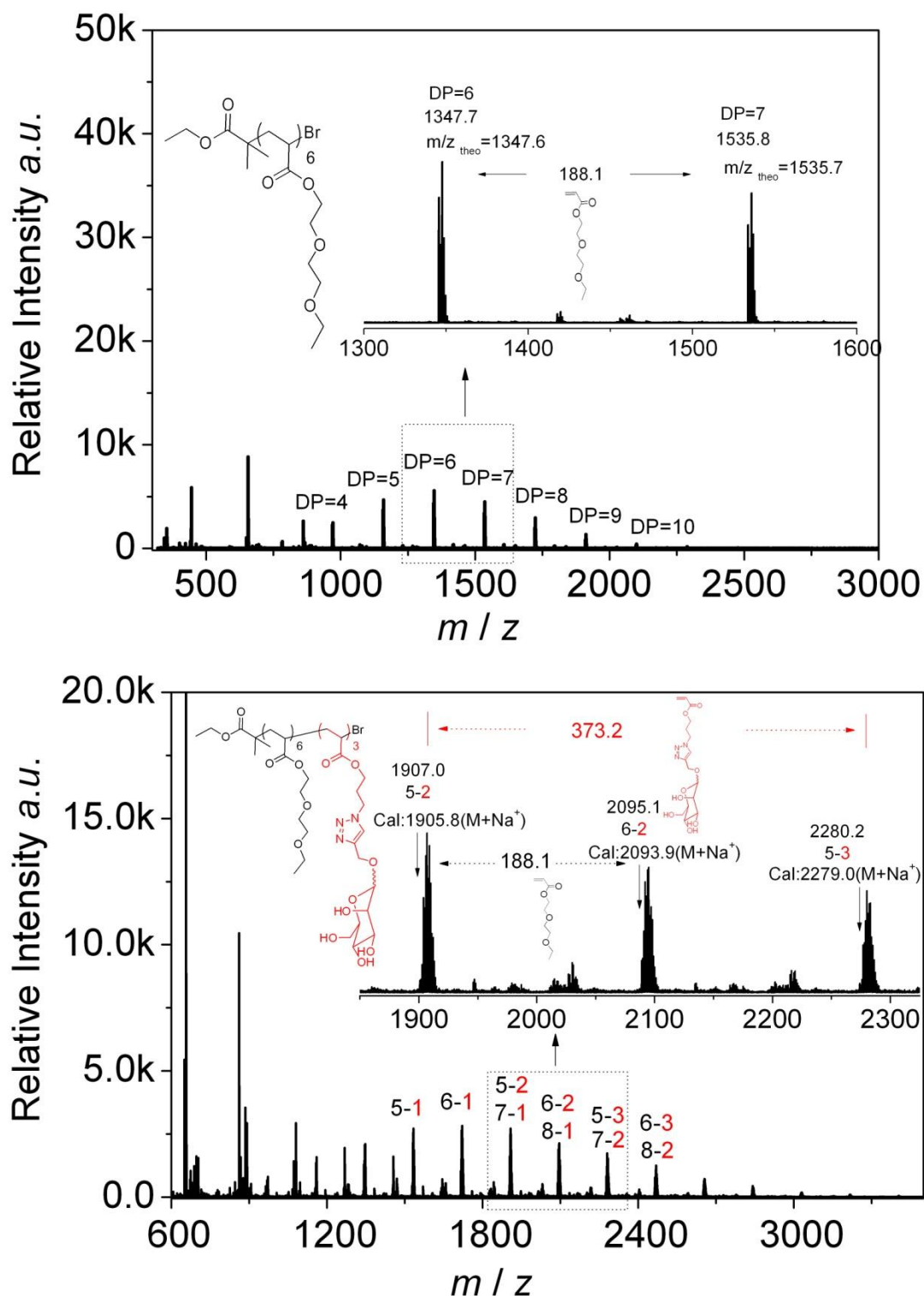
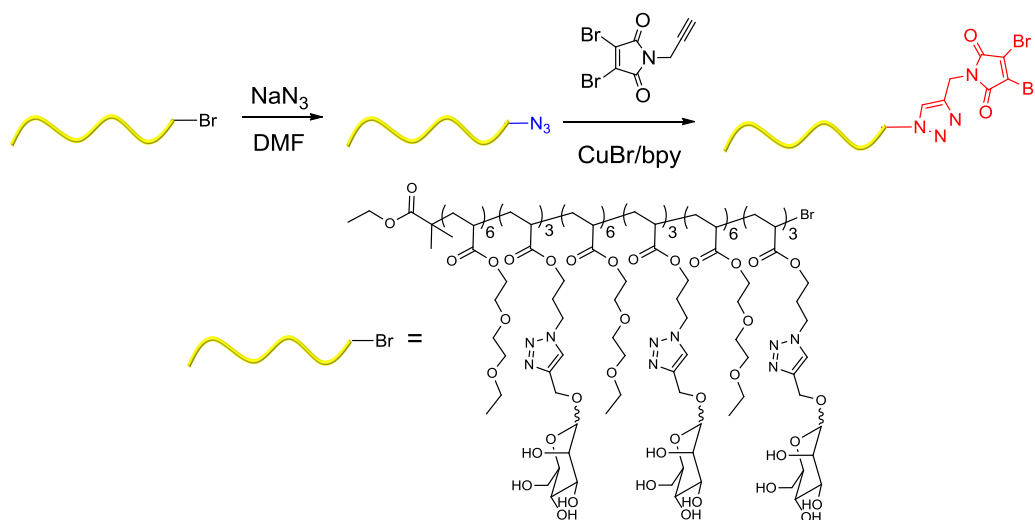


Figure 3. 13. MALDI-ToF MS spectra of the 1st block poly(DEGEEA)₆ (top) and 2nd block poly(DEGEEA)₆-b-(mannose)₃ (bottom) glycopolymers obtained by SET-LRP.

3.2.5 Chain end group functionalization of multiblock glycopolymer by CuAAC

High chain end fidelity was kept during SET-LRP and could be used for further modification.¹⁵⁶ In order to obtain a terminal end functional glycopolymer for bio-conjugation, the bromine end group of a multiblock DEGEEA-Mannose glycopolymer was transformed into azido group and then used for CuAAC reaction with alkyne-functionalised dibromomaleimide, Scheme 3.7.



Scheme 3. 7. Schematic representation for the azido and CuAAC modification of multiblock glycopolymer.

FT-IR spectra (Figure 3.14) showed the appearance and disappearance of an azide absorbance at 2116 cm^{-1} , indicating the successful reaction with NaN_3 and further CuAAC reaction.

The dibromomaleimide modified polymer following the CuAAC reaction was characterized *via* DMF SEC equipped with RI and UV detectors (Figure 3.15, 3.16). The elution traces by UV detector at 400 nm showed a significant absorbance peak compared with azide-functionalised polymer, which is attributed to the clicked dibromomaleimide group according to previous research.^{172,173} The elution time of the peak in UV detector is the same as in RI detector, which means that it is maleimide-functionalised polymer not small molecules that caused the absorbance.

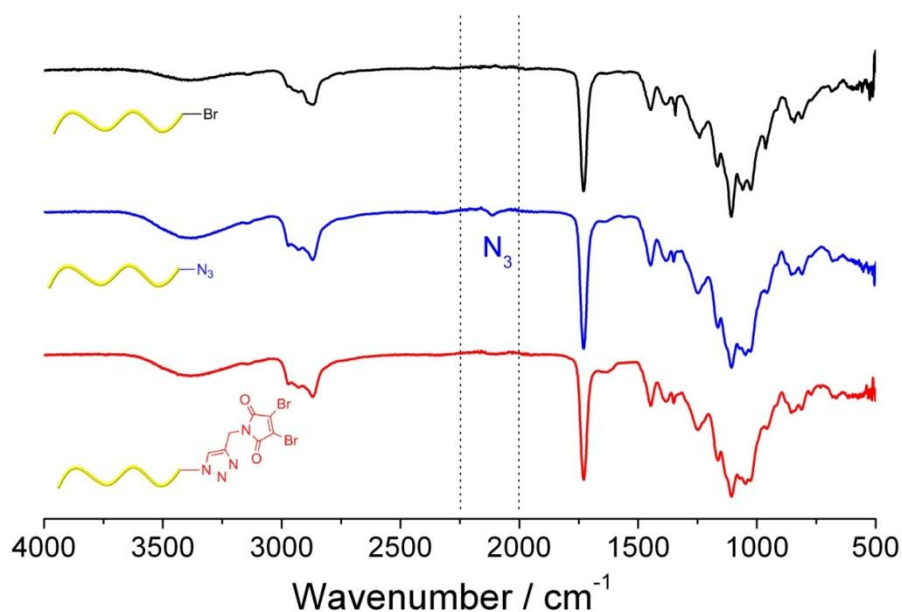


Figure 3. 14. FT-IR spectra of azide and dibromomaleimide modified multiblock glycopolymer.

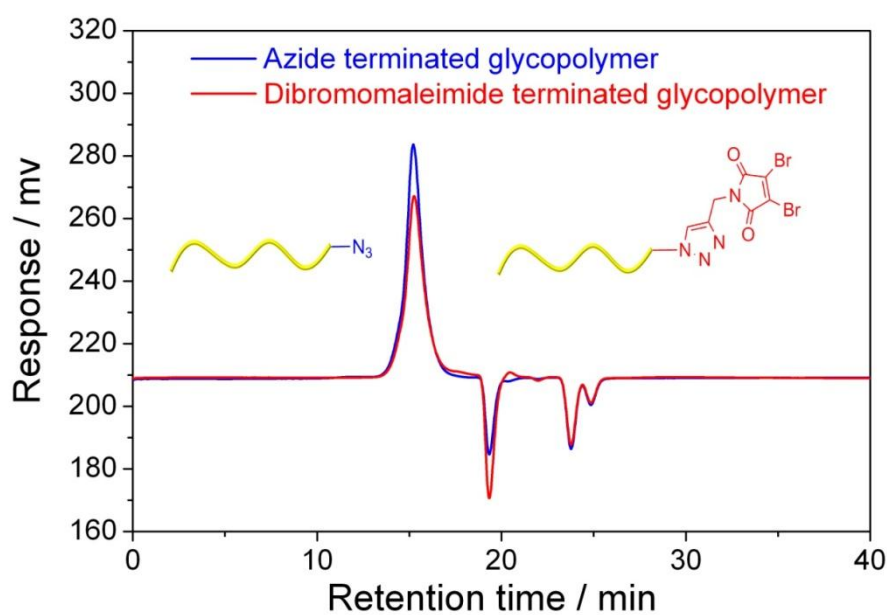


Figure 3. 15. DMF SEC elution traces of the azide and dibromomaleimide modified glycopolymer *via* RI detector.

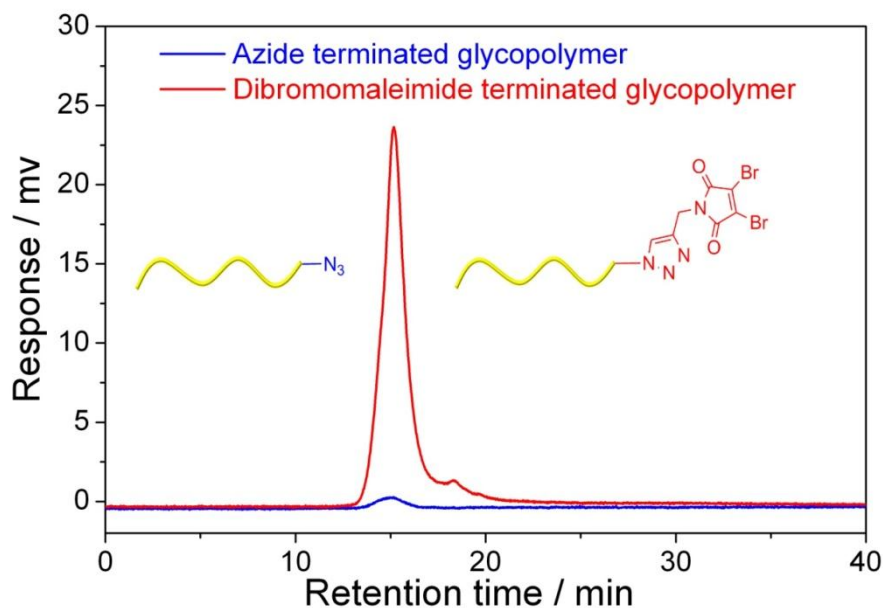


Figure 3. 16. DMF SEC elution traces of the azide and dibromomaleimide modified glycopolymer *via* UV detector at 400 nm.

All these results show that the terminal bromine end groups have been successfully modified into dibromomaleimide groups *via* CuAAC reaction, which could be potentially used for conjugation with thiol-containing peptide and protein.

3.2.6 Interactions between glycopolymers and DC-SIGN

Detailed research has been conducted on the preference of DC-SIGN binding to monosaccharide, Table 3.1, which suggested that DC-SIGN bind with monosaccharides by recognition of C-3 and C-4 hydroxyl groups as other C-type ligands do.¹⁷⁴ Inhibition by mannose is 2- and 7-fold more effective than inhibition by glucose and galactose, but 2-fold less effective than inhibition by L-fucose, which suggested that L-fucose glycopolymer may be a good inhibitor for the binding of DC-SIGN with gp120 as gp120 has a mannose-rich oligosaccharide cluster.

It also suggested that DC-SIGN show preference for axial C-2 substituents in which case N-acetylmannosamine showed higher efficiency than mannose, which revealed that the hydrophobic interaction of the C-2 substituents may contribute for the binding.

It also revealed that mannose and methyl α -mannoside almost has the same binding constant with DC-SIGN, Table 3.1. This showed that C-1 methyl substituted groups did not contribute much for the binding with DC-SIGN compared with C-1 hydroxyl groups.

Although mannose has an anomeric structure, its binding compared with methyl α -mannoside did not reveal any significant difference. This prove that the anomeric specificity may did not affect the binding of mannose with DC-SIGN. However, it's worth trying to synthesize the pure α or β mannose homopolymers in order to verify the difference in binding with DC-SIGN.

Table 3. 1. Literature reported constants for monosaccharide binding to extracellular domain fragments of DC-SIGN¹⁷⁴

Monosaccharide	k_I	$k_{I,sugar}/k_{I,Man}$
Mannose	13.1 \pm	1
Methyl α -mannoside	12.5 \pm 0.5	1.0 \pm 0.1
N-acetylmannosamine	8.7 \pm 0.2	0.7 \pm 0.1
Galactose	72 \pm 5	6.7 \pm 0.5
Methyl α -galactose	270 \pm 10	27 \pm 3
Glucose	23 \pm 1	1.9 \pm 0.3
Methyl α -glucose	32 \pm 1	2.6 \pm 0.3
N-acetylglucosamine	32 \pm 4	2.5 \pm 0.3
2-Deoxyglucose	28 \pm 4	2.9 \pm 0.6
L-fucose	6.7 \pm 0.5	0.50 \pm 0.03

Inhibition constants (k_I) for each monosaccharide were determined by solid-phase competition assay.

Interactions between the glycopolymers and DC-SIGN were measured using surface plasmon resonance spectroscopy (SPR) in a high-throughput multichannel mode.

In the concentration experiments, ManMA₅₈, a methacrylate mannose homopolymer previously synthesized by ATRP by Haddleton group and gp120, the HIV virus glycoprotein, were used as control for binding.⁸¹ All glycopolymers and gp120 were measured at 6-10 different concentrations, in which the buffer was flowed over the chip alone before (90 s) and after (650 s) injection of the analyte (900 s). Glycopolymers with higher mannose content showed higher affinities during binding with DC-SIGN than glycopolymers with non-binding DEGEEA or glucose, Figure 3.17, which reflects the preference of DC-SIGN for mannose over glucose.

Competition experiments were performed by flowing 4 nM of DC-SIGN in buffer with varying amounts of glycopolymers over immobilized gp120. The highest R_{max} is

observed when DC-SIGN is passed over gp120 in the absence of glycopolymer, thus representing maximal binding, Figure 3.18. DC-SIGN binding decreases upon addition of more glycopolymer as carbohydrate moieties of the polymer block binding sites on the lectin.

IC50 values of each of the polymers were determined as the concentration required to reduce DC-SIGN binding to 50% of the maximal level, Table 3.2. The lowest IC50 value observed was for solution-phase gp120 (11 nM). Impressive inhibition was also observed for ManMA₅₈, ManA₂₃ and ManA₁₃-*b*-OEGA₂, only 10-30-fold weaker than for gp120. S3, S4, S5 and S6 showed little inhibition over the measured concentration range, possibly due to the low mannose content. Favourable binding of ManA₂₃ over ManMA₅₈, despite its shorter chain length may reflect differences in acrylic and methacrylic polymer backbones and also the linker structure, which could lead to different behaviour in chain folding and lectin binding (Figure 3.19).

Table 3. 2. The results of inhibition concentration of glycopolymers.

DC-SIGN binding		
Code	Sequence	IC50 (nM)
gp120	gp120	11
C1	ManMA ₅₈	230
S1	ManA ₂₃	153
S2	ManA ₁₃ - <i>b</i> -OEGA ₂	380
S3	ManA ₉ - <i>r</i> -DEGEEA ₁₈	>1000
S4	ManA ₉ - <i>s</i> -DEGEEA ₁₈	>1000
S5	GluA ₆ - <i>s</i> -ManA ₄ - <i>s</i> -FucA ₄	>1000
S6	GluA ₄ - <i>s</i> -ManA ₄ - <i>s</i> -GluA ₄	n/a

[a] *-b-*, *-r-*, and *-s-* stand for block, random, and sequence controlled, respectively.

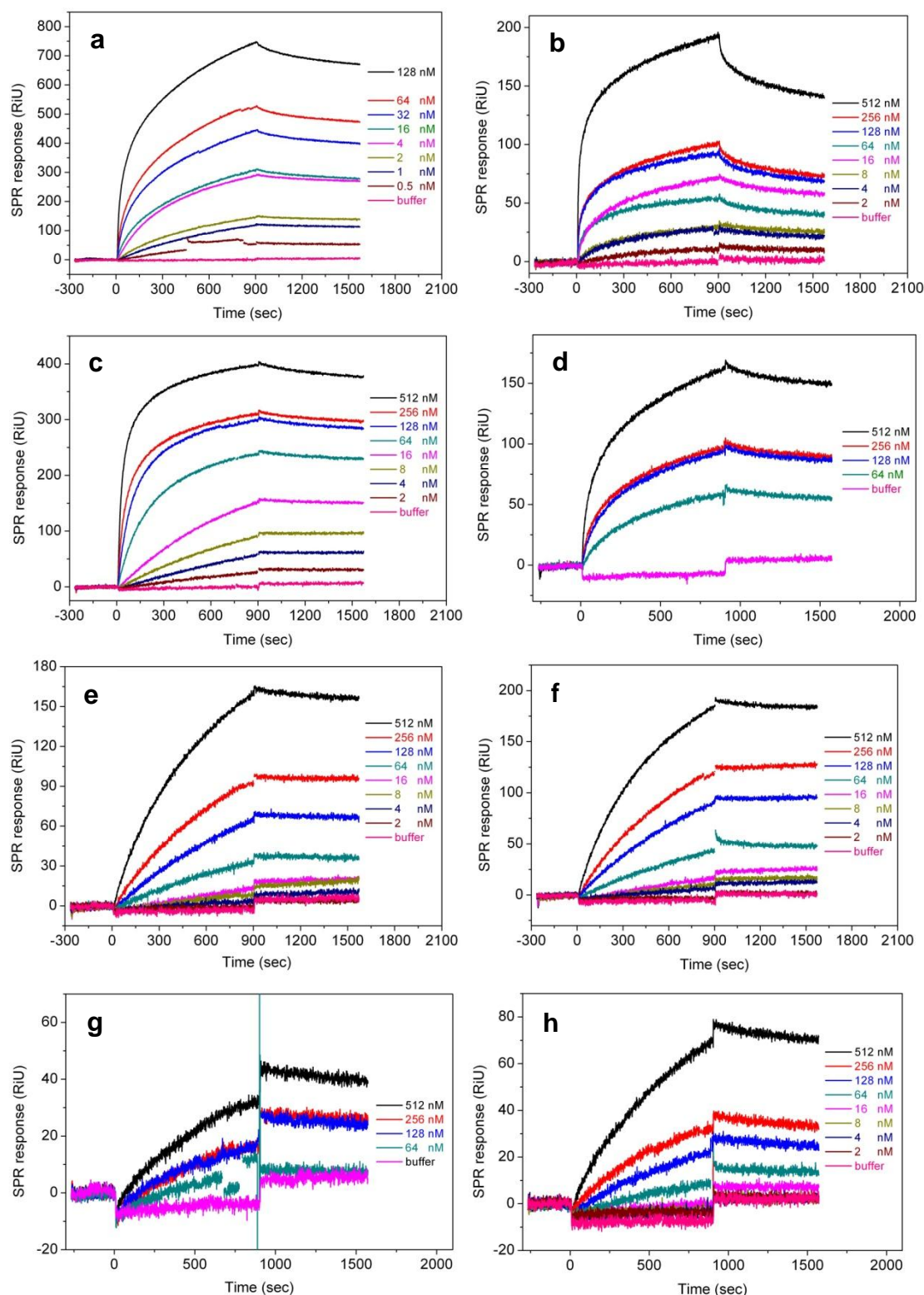


Figure 3. 17. SPR sensorgrams showing the binding of (a) *gp120*; (b) *C1 ManMA₅₈*; (c) *S1 ManA₂₃*; (d) *S2 ManA₁₃-b-OEGA₂*; (e) *S3 ManA₉-r-DEGEAA₁₈*; (f) *S4 ManA₉-s-DEGEAA₁₈*; (g) *S5 GluA₆-s-ManA₄-s-FucA₄*; (h) *S6 GluA₄-s-ManA₄-s-GluA₄* onto DC-SIGN functionalized surfaces.

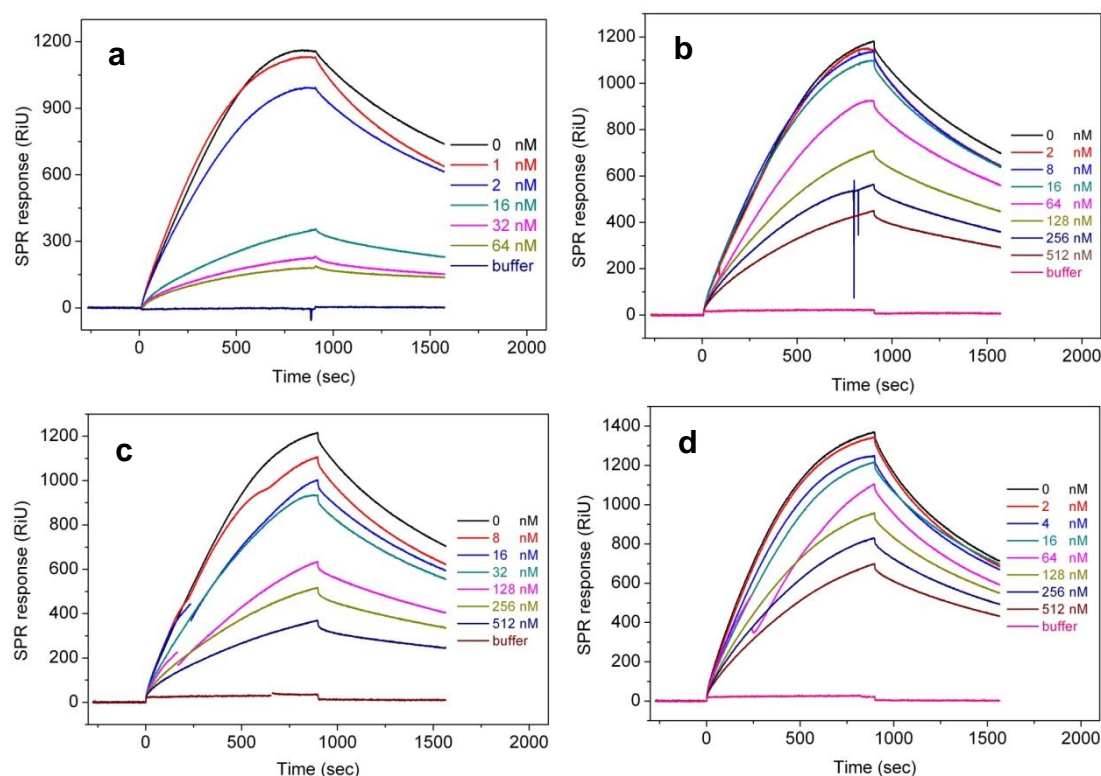


Figure 3. 18. Competition experiments on gp120 functionalized surface between DC-SIGN and (a) *gp120*; (b) *C1 ManMA₅₈*; (c) *S1 ManA₂₃*; (d) *S2 ManA₁₃-b-OEGA₂* at a concentration range of 0-64 nM for gp120, 0-512 nM for glycopolymer and 4 nM for DC-SIGN.

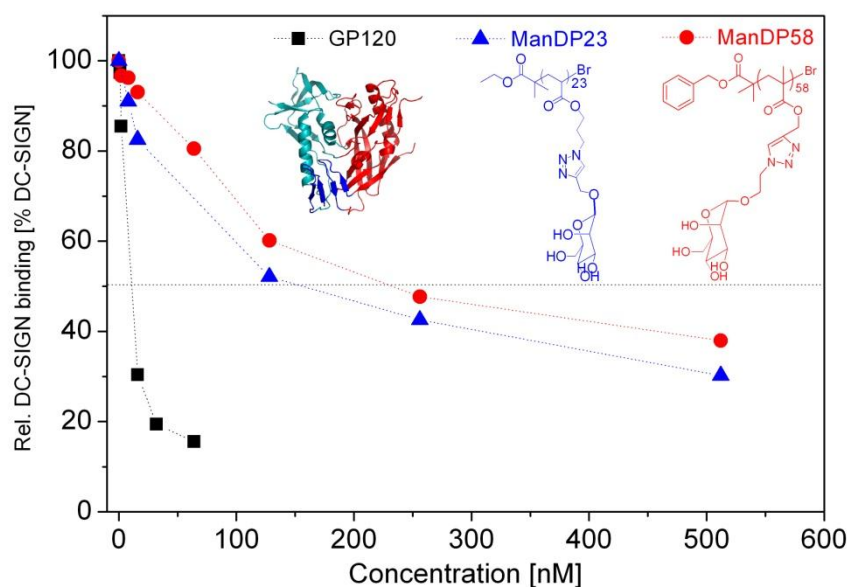


Figure 3. 19. Competition binding experiments on gp120 functionalized surface between DC-SIGN and of gp120 (black), *S1 ManA₂₃* (blue) and *C1 ManMA₅₈* (red) at 4 nM DC-SIGN and different concentration for gp120 and the glycopolymers.

Based on previous results, we observed higher affinity binding for the polymers with higher mannose content. However, we could not conclude any effect of sequence on binding in this system, most likely because DC-SIGN preferentially recognises a range of high-mannose structures whilst other DC-SIGN binding glycans of mixed monosaccharide character possess very defined glycosidic branching.¹⁷⁵ Thus, inhibition is likely to occur only if all (or most) of the binding sites on DC-SIGN are blocked by sugar moieties of the polymer. This in turn will be dependent on the sequence and structure of the polymer highlighting the potential importance of this synthetic strategy.

It has been suggested by Prof Daniel Mitchell that further work should be performed using lectin libraries and sequence controlled polymer libraries to evaluate the sugar sequence or distance and their impact on specific lectin binding properties, in addition to the polymerization of small disaccharide and oligosaccharide units such as Man- α -(1,2)-Man and blood group antigens.¹⁷⁶

3.2.7 Conclusion

In conclusion, we have prepared sequence controlled multi-block glycopolymers in various compositions by the polymerization of glycomonomers via SET-LRP. Glycomonomers containing mannose, glucose and fucose moieties were synthesized by the CuAAC click reaction of a sugar alkyne and azide acrylate, which were subsequently copolymerized in different sequences. Polymerizations were followed by ^1H NMR, SEC and HR ESI-MS or MALDI-ToF MS to obtain information on the products. This technique provides very precise control over the monomer sequence along the polymer chain. Moreover, the polymerization is performed in one pot by sequential addition of the subsequent monomers in a relatively a large scale, which is critical when compared with the preparation of synthetic glycans or lectins. The obtained sequence controlled glycopolymers were then examined for their binding behaviour to DC-SIGN. The synthesized polymers reported here show distinct binding properties to DC-SIGN and an inhibition of the DC-SIGN binding to HIV gp120 using nano molar concentrations. We believe the approach presented here will open new avenues not only in polymer science but also in chemical biology and dendritic cell physiology.

3.3 Experimental

3.3.1 Materials

Di(ethylene glycol) ethyl ether acrylate (DEGEEA, $\geq 90\%$) was obtained from Sigma-Aldrich and the inhibitor was removed by passing the monomer through a column of activated basic alumina prior to use. Cu(I)Br (98%, Sigma-Aldrich) was washed sequentially with acetic acid and ethanol and dried under vacuum. *tris*(2-(Dimethylamino)ethyl)amine (Me₆TREN) was synthesized according to literature procedure and stored under a nitrogen atmosphere prior to use.^{177,178} Copper wire (diameter=0.25 mm) was pre-treated by washing in hydrochloric acid for 15 min and rinsed thoroughly with MiliQ water, dried under nitrogen and used immediately. 1-(2'-Propargyl) D-mannose¹²³, 1-(2'-propargyl) L-fucose¹²³ and 3-azido-propan-1-ol¹⁷⁹ were synthesised as previous report. The H₂SO₄-silica catalyst was prepared according to the literature procedure.¹⁰⁹ Ethyl α -bromoisobutyrate (EBiB, 98%, Sigma-Aldrich), D-(+)-glucose (99.5%, Sigma-Aldrich), propargyl alcohol (99%, Sigma-Aldrich), 2, 2'-bipyridyl (bpy, 99%, Sigma-Aldrich) and (+)-sodium L-ascorbate (98%, Sigma-Aldrich) were used as received. Membrane dialysis (1K MWCO) was obtained from Spectrum Laboratories.

3.3.2 Instruments and analysis

¹H and ¹³C NMR spectra were recorded on Bruker DPX-300 and DPX-400 spectrometers using deuterated solvents obtained from Aldrich. Monomer conversion for glycomonomer polymerization was calculated by comparing the integral of vinyl protons with triazole ring proton or EBiB methyl protons. Mesitylene was used as an internal standard to calculate the conversion for the copolymerization of glycomonomer with DEGEEA.

SEC was conducted on Varian 390-LC system in DMF (1 g/L LiBr) at 50 °C, equipped with refractive index and viscometry detectors, 2 \times PLgel 5 mm mixed-D columns (300 \times 7.5 mm), 1 \times PLgel 5 mm guard column (50 \times 7.5 mm) and autosampler. Narrow linear PMMA standards in range of 200 to 1.0×10^6 g·mol⁻¹ were used to calibrate the system.

High resolution ESI-MS was recorded on Bruker UHR-Q-TOF MaXis equipped with electrospray ionisation source in positive mode; samples were directly infused at 2

mL min⁻¹ with a syringe pump. Nitrogen was used as nebulizer gas (0.4 bar) and dry gas (4 L min⁻¹ at 180 °C). The capillary voltage was set at -3000 V and data were acquired in the 50–3000 *m/z* range. Calibration was carried out with sodium formate solution (10 mM in 50% IPA).

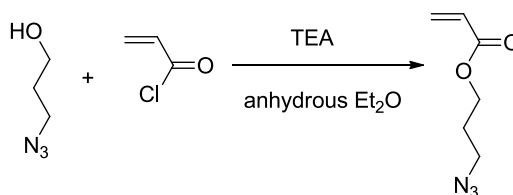
MALDI-ToF MS was recorded in linear or reflex mode on a Bruker Daltonics Ultraflex II MALDI-ToF mass spectrometer, equipped with a nitrogen laser delivering 2 ns laser pulses at 337 nm with positive ion ToF detection performed using an accelerating voltage of 25 kV. The matrix solution was prepared by dissolving α -cyano-4-hydroxycinnamic acid (CHCA) or sinapic acid in THF (20 mg/mL solution). Sodium iodide was added at a 0.1% overall concentration to improve the ionization. Polymer analytes were dissolved to a concentration of 1 mg/mL. Samples were prepared by layering matrix solution and analyte solution on the stainless steel side. Calibration was performed with different linear poly(ethylene glycol) methyl ether standards.

Infrared absorption spectra were recorded on a Bruker VECTOR-22 FTIR spectrometer using a Golden Gate diamond attenuated total reflection cell.

SPR Sensorgrams were recorded in a Biorad ProteOn XPR36 SPR biosensor (Biorad, Hercules CA). Soluble DC-SIGN and gp120 were immobilized to 6000 response units (RU) on discrete channels within Biorad GMC sensor chips via amine coupling. Soluble-phase analytes were prepared in 25 mM HEPES pH 7.4, 150 mM NaCl, 5 mM CaCl₂, 0.01% Tween-20 and flowed over the immobilized materials at a rate of 25 μ L/min at 25°C. Regeneration of the sensor chip surfaces was performed using 10 mM glycine pH 2.5. Datasets were exported to BIAcore BIAevaluation software for kinetic calculations.

Note: Miss Jennifer Collins of Haddleton group contributed in the synthesis of three glyco monomers.

3.3.3 Synthesis of 3-azidopropyl acrylate



Scheme 3. 8. Schematic synthesis approach to 3-azidopropyl acrylate.

A solution of 3-azido-propan-1-ol (3.12 g, 3.0 mmol), TEA (5.8 mL, 4.2 mmol), hydroquinone (30 mg) and anhydrous diethyl ether (200 mL) was cooled in an ice-water bath. Acryloyl chloride (3 mL, 3.6 mmol) in 20 mL diethyl ether was added dropwise into the solution over a period of ca. 30 min. The mixture was stirred in the ice bath for 1 h and then at ambient temperature overnight. The ammonium salts were removed by filtration and the residue was extracted sequentially with aqueous solution of hydrochloric acid (1/10 v/v, 2x 50 mL), water (2x 50 mL), 5 wt% aqueous NaOH (2x 50 mL) and water (2x 50 mL) and dried over magnesium sulphate. The organic solvent was removed under vacuum. The product was recovered as yellow liquid and used directly (yield: 53%).

^1H NMR (CDCl_3 , 298 K, 400 MHz): δ (ppm) = 6.40 (dd, 1 H, J 1.4, 15.9 Hz, $\text{CH}_2=\text{CH}$), 6.11 (dd, 1 H, J 10.5, 6.9 Hz, $\text{CH}_2=\text{CH}$), 5.84 (dd, 1 H, J 1.4, 9.0 Hz, $\text{CH}_2=\text{CH}$), 4.24 (t, 2 H, J 6.2 Hz, $\text{O}-\text{CH}_2$), 3.40 (t, 2 H, J 6.7 Hz, CH_2N_3), 1.95 (m, 2 H, CCH_2C).

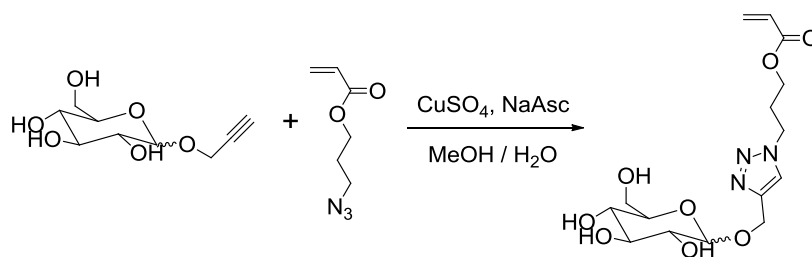
^{13}C NMR (CDCl_3 , 298 K, 400 MHz): δ (ppm) = 166.1 ($\text{C}=\text{O}$), 131.2 ($\text{CH}_2=\text{CH}$), 128.3 ($\text{CH}_2=\text{CH}$), 61.5 ($\text{O}-\text{CH}_2$), 48.3 (CH_2-N_3), 28.3 ($\text{C}-\text{CH}_2-\text{C}$).

FT-IR ν (cm^{-1}): 2095 ($-\text{N}_3$), 1722 ($\text{C}=\text{O}$).

ESI-MS m/z : calcd for $\text{C}_6\text{H}_9\text{N}_3\text{O}_2$ ($2\text{M}+\text{H}^+$), 311.1; found, 311.1.

Note: The organic azide is a very sensitive compound and it should be handled with great care. After synthesis this intermediate was directly used for the next step reaction without further purification. Long period storage even in the fridge is not recommended.

3.3.4 Synthesis of D-glucose glycomonomer via CuAAC



Scheme 3. 9. Synthesis of D-glucose glycomonomer *via* CuAAC.

To a solution of 3-azidopropyl acrylate (2.68 g, 17.3 mmol) and 1-(2'-propargyl) D-glucose (3.45 g, 15.8 mmol) in MeOH/H₂O (2:1 vol/vol, 100 mL), aqueous solution of CuSO₄·5H₂O (312 mg, 1.2 mmol) and (+)-sodium L-ascorbate (313 mg, 1.6 mmol) were sequentially added. The mixture was stirred at ambient temperature for 24 h. The methanol was removed via rotary evaporator and residue mixture was freeze dried to remove water. The obtained green solid was purified by silica gel column chromatography using dichloromethane-MeOH (10:1) as eluent. The relevant fractions were collected and after removal of solvent pure 3-(4-(((3R,4S,5S,6R)-3,4,5-trihydroxy-6-(hydroxymethyl)tetrahydro-2H-pyran-2-yl)oxy)methyl)-1H-1,2,3-triazol-1-yl)propyl acrylate (D-glucose glycomonomer) was isolated as white solid (3.57 g, yield: 60.6%).

The obtained unprotected D-glucose glycomonomer is anomeric mixture ($\alpha/\beta=10/4$, by comparing the integration area of H-1 proton of glucose, almost the same ratio as 1-(2'-propargyl) D-glucose), which has been confirmed by ¹H and ¹³C NMR characterization.

¹H NMR (MeOD, 298 K, 400 MHz): δ (ppm) = 8.07, 8.06 (s, overlaped, 1 H, NCH=C), 6.38 (dd, 1 H, J=1.6, 15.6 Hz, CH₂=C), 6.14 (dd, 1 H, J=10.4, 6.9 Hz, CH₂=CHC=O), 5.90 (dd, 1 H, J=1.5, 8.9 Hz, CH₂=C), 4.97 (d, J=12.6 Hz, CH₂-OH, β anomeric), 4.91 (d, 1 H, J=3.7 Hz, H-1 of glucose, α anomeric), 4.65-4.90 (m, C-CH₂-O, C=O-O-CH₂ β anomeric, overlap with H₂O), 4.54 (t, 2 H, J=6.9 Hz, CH₂-N), 4.39 (d, J=7.7 Hz, H-1 of glucose, β anomeric), 4.12-4.24 (m, 2 H, C=O-O-CH₂), 3.15-4.00 (m, H residues of glucose), 2.30 (m, 2H, CH₂-CH₂-CH₂).

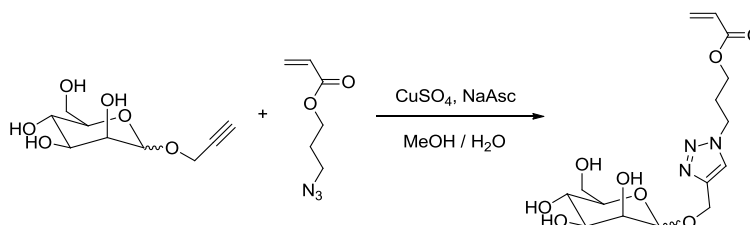
¹³C NMR (MeOD, 298 K, 400 MHz): δ (ppm) = 167.5 (C=O), 145.6 (N-CH=C), 131.9 (CH₂=C), 129.2 (CH₂=C), 125.5 (N-CH=C), 103.6 (β anomeric, C 1 of glucose), 99.6 (α anomeric, C 1 of glucose), 78.0, 77.9, 75.0, 74.0, 73.5, 71.8, 71.6

(carbons of anomeric glucose), 62.7(CH₂-OH), 62.5 (C=O-O-CH₂), 61.4 (C-CH₂-O), 49.0 (CH₂-CH₂-N, overlap with MeOD, confirmed by HMQC), 30.3(CH₂-CH₂-CH₂).

FT-IR ν (cm⁻¹): 3350.6 (OH), 2901.6 (C=C-H), 1720.5 (C=O).

ESI-MS m/z : calcd for C₁₅H₂₃N₃O₈ (M+Na⁺), 396.1; found, 396.1.

3.3.5 Synthesis of D-Mannose Glycomonomer via CuAAC



Scheme 3. 10. Synthesis of D-mannose glycomonomer *via* CuAAC.

To a solution of 3-azidopropyl acrylate (2.46 g, 15.9 mmol) and 1-(2'-propargyl) D-mannose (3.16 g, 14.5 mmol) in MeOH/H₂O (2:1 vol/vol, 100 mL), aqueous solution of CuSO₄·5H₂O (224mg, 0.90 mmol) and (+)-sodium L-ascorbate (225 mg, 1.1 mmol) were sequentially added. The mixture was stirred at ambient temperature for 24 h. The methanol was removed via rotary evaporator and residue mixture was freeze dried to remove water. The obtained green solid was purified by silica gel column chromatography using dichloromethane-MeOH (10:1) as eluent. The relevant fractions were collected and after removal of solvent pure 3-(4-(((3S,4S,5S,6R)-3,4,5-trihydroxy-6-(hydroxymethyl)tetrahydro-2H-pyran-2-yl)oxy)methyl)-1H-1,2,3-triazol-1-yl)propyl acrylate (D-mannose glycomonomer) was isolated as white solid (3.85 g, yield: 71.2%).

The obtained unprotected D-mannose glycomonomer is an anomeric mixture ($\alpha/\beta=10/2.1$), which has been confirmed by ¹H and ¹³C NMR characterization.

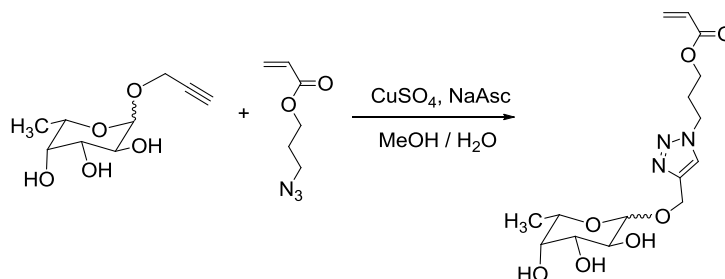
¹H NMR (MeOD, 298 K, 400 MHz): δ (ppm) =8.07, 8.06 (s, overlaped, 1 H, NCH=C), 6.37 (dd, J=1.8, 15.5 Hz), 6.36 (dd, J=1.6, 15.7 Hz) (anomeric 1 H, CH₂=C), 6.14 (dd, J=10.4, 6.9 Hz), 6.13(dd, J=10.4, 7.0 Hz) (anomeric, 1 H, CH₂=CHC=O), 5.89 (dd, 1 H, J=1.5, 8.9 Hz, CH₂=C), 4.70-5.05 (m, CH₂-OH, H-1 of mannose, overlap with H₂O), 4.64 (d, 1 H, J=12.3 Hz, CH₂-OH), 4.55 (t, 2 H, J=6.9 Hz, CH₂-N), 4.19 (t, 2 H, J=6.0 Hz, C=O-O-CH₂), 3.40-3.92 (m, H residues of mannose), 2.30 (m, 2H, CH₂-CH₂-CH₂).

^{13}C NMR (MeOD, 298 K, 400 MHz): δ (ppm) = 167.4 (C=O), 145.4 (N-CH=C), 131.9 ($\text{CH}_2=\text{C}$), 129.2 ($\text{CH}_2=\text{C}$), 125.6 (N-CH=C), 100.8 (β anomeric, C 1 of mannose), 100.7 (α anomeric, C 1 of mannose), 78.4, 75.2, 75.0, 72.5, 72.3, 72.0, 68.6, 68.4 (carbons of anomeric mannose), 63.0 ($\text{CH}_2\text{-OH}$), 62.6 (C=O-O- CH_2), 60.7 (C- $\text{CH}_2\text{-O}$), 48.5 ($\text{CH}_2\text{-CH}_2\text{-N}$, overlap with MeOD), 30.3 ($\text{CH}_2\text{-CH}_2\text{-CH}_2$).

FT-IR ν (cm^{-1}): 3350.6 (OH), 2901.6 (C=C-H), 1720.5 (C=O).

ESI-MS m/z : calcd for $\text{C}_{15}\text{H}_{23}\text{N}_3\text{O}_8$ ($\text{M}+\text{Na}^+$), 396.1; found, 396.1.

3.3.6 Synthesis of L-Fucose Glycomonomer via CuAAC



Scheme 3. 11. Synthesis of L-fucose glycomonomer *via* CuAAC.

To a solution of 3-azidopropyl acrylate (0.83 g, 5.4 mmol) and 1-(2'-propargyl) L-fucose (0.99 g, 4.9 mmol) in MeOH/ H_2O (2:1 vol/vol, 50 mL), aqueous solution of $\text{CuSO}_4 \cdot 5\text{H}_2\text{O}$ (97 mg, 0.39 mmol) and (+)-sodium L-ascorbate (97 mg, 0.49 mmol) were sequentially added. The mixture was stirred at ambient temperature for 24 h. The methanol was removed via rotary evaporator and residue mixture was freeze dried to remove water. The obtained green solid was purified by silica gel column chromatography using dichloromethane-MeOH (10:1) as eluent. The relevant fractions were collected and after removal of solvent pure 3-(4-(((3S,4R,5S,6S)-3,4,5-trihydroxy-6-methyltetrahydro-2H-pyran-2-yl)oxy)methyl)-1H-1,2,3-triazol-1-yl)propyl acrylate (L-fucose glycomonomer) was isolated as white solid (1.29 g, yield: 73.7%).

The obtained unprotected L-fucose glycomonomer is an anomeric mixture ($\alpha/\beta=10/1.6$, by comparing the integration area of CH_3 protons of fucose), which has been confirmed by ^1H and ^{13}C NMR characterization.

^1H NMR (MeOD, 298 K, 400 MHz): δ (ppm) = 8.04, 8.02 (s, overlaped, 1 H, NCH=C), 6.37 (dd, 1 H, $J=1.6$, 15.7 Hz, $\text{CH}_2=\text{C}$), 6.14 (dd, 1 H, $J=10.3$, 6.9 Hz, $\text{CH}_2=\text{CHC}=\text{O}$), 5.89 (dd, 1 H, $J=1.6$, 8.8 Hz, $\text{CH}_2=\text{C}$), 4.88 (d, 1 H, $J=1.6$ Hz, H-1 of

fucose, α anomeric), 4.86 (s, OH, overlap with H_2O), 4.70 (dd, 2 H, $J=12.4$, 28.8 Hz, C- CH_2 -O), 4.54 (t, 2 H, $J=6.9$ Hz, CH_2 -N), 4.32 (d, $J=7.3$ Hz, H-1 of glucose, β anomeric), 4.19 (t, 2 H, $J=6.1$ Hz, C=O-O- CH_2), 3.89-4.02 (m, 1 H, CHOH-CHOH-CHOH), 3.39-3.85 (m, H residues of fucose), 2.30 (m, 2H, CH_2 - CH_2 - CH_2), 1.28 (d, $J=6.5$ Hz, CH- CH_3 , β anomeric), 1.19 (d, $J=6.7$ Hz, CH- CH_3 , α anomeric).

^{13}C NMR (MeOD, 298 K, 400 MHz): δ (ppm) = 167.4 (C=O), 145.8 (N-CH=C), 131.8 (CH_2 =C), 129.3 (CH_2 =C), 125.4 (N-CH=C), 104.0 (β anomeric, C 1 of fucose), 100.2 (α anomeric, C 1 of fucose), 75.0, 73.6, 72.9, 72.2, 72.0, 71.6, 69.9, 67.8 (carbons of anomeric fucose), 62.5 (C=O-O- CH_2), 61.7 (C- CH_2 -O), 48.4 (CH_2 - CH_2 -N, overlap with MeOD), 30.3 (CH_2 - CH_2 - CH_2), 16.8 (CH- CH_3 , β anomeric), 16.6 (CH- CH_3 , α anomeric).

FT-IR ν (cm^{-1}): 3350.6 (OH), 2901.6 (C=C-H), 1720.5 (C=O).

ESI-MS m/z : calcd for $C_{15}H_{23}N_3O_7$ ($M+Na^+$), 380.1; found, 380.1.

3.3.7 Homopolymerization of D-glucose acrylate glycomonomer via SET-LRP

All polymerizations were carried out using standard Schlenk techniques under an inert atmosphere of oxygen-free nitrogen, unless otherwise stated. All obtained glycopolymer products should be stored in the fridge ($-18\text{ }^{\circ}C$) if stored for more than three months.

To a Schlenk tube fitted with a magnetic stir bar and a rubber stopper, glucose glycomonomer (373 mg, 1 mmol, 10 eq), $CuBr_2$ (2 mg, 0.01 mmol, 0.1 eq) and DMSO (3 mL) were charged and the mixture was bubbled with nitrogen for 15 min. Pre-degassed Me_6TREN (4.2 μL , 0.018 mmol, 0.18 eq) and $EBiB$ (14.7 μL , 0.1 mmol, 1 eq) were then added via gas tight syringe sequentially. After that, pre-activated copper wire (3 cm, 14 mg, 0.21 mmol) was carefully added under nitrogen protection. The Schlenk tube was sealed and the light green solution was allowed to polymerize at $25\text{ }^{\circ}C$. Samples of the reaction mixture were carefully removed at suitable time periods for analysis. The sample for 1H NMR was directly diluted with $DMSO-d_6$. Catalyst residues were removed by filtering through a column of neutral alumina prior to SEC analysis. After 24 h, the reaction was stopped via exposure to the air and the mixture was diluted with water and dialysed against water for two days after which the glycopolymer could be recovered by freeze drying.

3.3.8 Synthesis of multiblock glycopolymer by iterative addition of glycomonomers after full conversion polymerization

For the synthesis of (mannose)₂-(glucose)₂-(mannose)₂-(glucose)₂-(mannose)₂-(glucose)₂, the procedure is shown as below.

To a Schlenk tube fitted with a magnetic stir bar and a rubber stopper, mannose glycomonomer (187 mg, 0.5 mmol, 2 eq), CuBr₂ (6 mg, 0.025 mmol, 0.1 eq) and DMSO (2 mL) were charged and the mixture was bubbled with nitrogen for 15 min. Pre-degassed Me₆TREN (10.4 μL, 0.045 mmol, 0.18 eq) and EBiB (36.7 μL, 0.25 mmol, 1 eq) were then added via gas tight syringe sequentially. After that, pre-activated copper wire (3 cm, 14 mg, 0.21 mmol) was carefully added under nitrogen protection. The Schlenk tube was sealed and the light green solution was allowed to polymerize at 25 °C. After reaction overnight, sample was carefully removed for characterization. For chain extension, a further solution of glucose glycomonomer (187 mg, 0.5 mmol) in 1 mL DMSO previously degassed via nitrogen sparging for 20 min, was then transferred via cannula under nitrogen into the Schlenk reaction tube. The solution was allowed to polymerize at 25 °C overnight with stirring. The above polymerization-sampling-extension procedure was repeated as required.

For the synthesis of (glucose)₄-(mannose)₄-(glucose)₄-(mannose)₄, the procedure is the same as above with only changed charging amounts.

To a Schlenk tube fitted with a magnetic stir bar and a rubber stopper, glucose glycomonomer (248 mg, 0.67 mmol, 4 eq), CuBr₂ (4 mg, 0.017 mmol, 0.1 eq) and DMSO (2 mL) were charged and the mixture was bubbled with nitrogen for 15 min. Pre-degassed Me₆TREN (7 μL, 0.03 mmol, 0.18 eq) and EBiB (24.5 μL, 0.17 mmol, 1 eq) were then added via gas tight syringe sequentially. After that, pre-activated copper wire (3 cm, 14 mg, 0.21 mmol) was carefully added under nitrogen protection. The Schlenk tube was sealed and the light green solution was allowed to polymerize at 25 °C. For chain extension, a further solution of mannose glycomonomer (248 mg, 0.67 mmol) in 1 mL DMSO previously degassed via nitrogen sparging for 20 min, was then transferred via cannula under nitrogen into the Schlenk reaction tube. The solution was allowed to polymerize at 25 °C overnight with stirring. The above polymerization-sampling-extension procedure was repeated as required.

3.3.9 Synthesis of multiblock glycopolymer by controlled addition of glyco monomers

For the synthesis of multiblock glucose-mannose-fucose glycopolymer by controlled addition of glyco monomers, the procedure is shown as below.

To a Schlenk tube fitted with a magnetic stir bar and a rubber stopper, glucose glycomonomer (248 mg, 0.67 mmol, 4 eq), CuBr_2 (4 mg, 0.017 mmol, 0.1 eq) and DMSO (2.5 mL) were charged and the mixture was bubbled with nitrogen for 15 min. Pre-degassed Me_6TREN (7 μL , 0.03 mmol, 0.18 eq) and EBiB (24.5 μL , 0.17 mmol, 1 eq) were then added via gas tight syringe sequentially. Subsequently, pre-activated copper wire (3 cm) was carefully added under nitrogen protection. The Schlenk tube was sealed and the light green solution was allowed to polymerize at 25 °C. After reaction for 4h, sample was carefully removed for characterization. For chain extension, a further solution of mannose glycomonomer (124 mg, 0.33 mmol) in 1 mL DMSO, or glucose glycomonomer (124 mg, 0.33 mmol) in 1 mL DMSO, or fucose glycomonomer (119 mg, 0.33 mmol) in 1 mL DMSO which has been degassed via nitrogen sparging for 20 min, was then transferred via cannula under nitrogen into the Schlenk reaction tube. The solution was allowed to polymerize at 25 °C for 4h with stirring. The above polymerization-sampling-extension procedure was repeated as required.

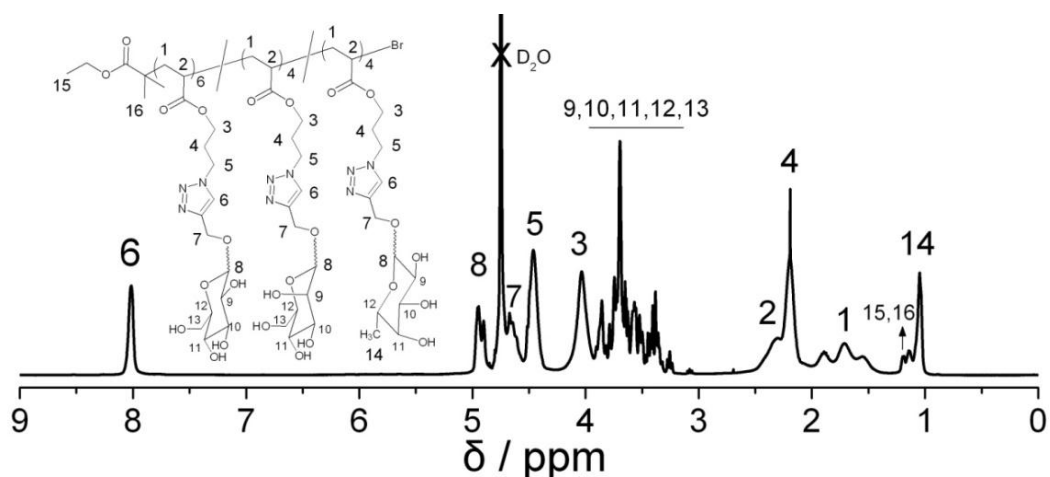


Figure 3. 20. ^1H NMR spectrum of multiblock glucose-mannose-fucose glycopolymer in D_2O obtained by SET-LRP.

3.3.10 Multiblock copolymerization of DEGEEA and mannose glycomonomer *via* SET-LRP

For the multiblock copolymerization, DEGEEA (565 mg, 3 mmol) and mesitylene (18 mg, 0.15 mmol, used as internal standard for ^1H NMR conversion calibration) were soluble in DMSO (4.5 mL) and each time 1/3 of the solution was used for polymerization. Mannose glycomonomer (560 mg, 1.5 mmol) and mesitylene (9 mg, 0.075 mmol) were soluble in DMSO (4.5 mL) and each time 1/3 of the solution was also used for chain extension.

To a Schlenk tube fitted with a magnetic stir bar and a rubber stopper, DEGEEA-DMSO solution (188 mg, 1 mmol, 6 eq), CuBr_2 (4 mg, 0.017 mmol, 0.1 eq) were charged and the mixture was bubbled with nitrogen for 15 min. Pre-degassed Me_6TREN (7 μL , 0.03 mmol, 0.18 eq) and EBiB (24.5 μL , 0.17 mmol, 1 eq) were then sequentially added via gas tight syringe. Subsequently, pre-activated copper wire (3 cm) was carefully added under nitrogen protection. The Schlenk tube was sealed and the light green solution was allowed to polymerize at 25 $^\circ\text{C}$. After reaction for 2.5 h, sample was carefully removed for characterization.

For chain extension, a further mannose glycomonomer-DMSO solution (186 mg, 0.5 mmol) which has been degassed via nitrogen sparging for 20 min was then transferred via cannula under nitrogen into the Schlenk reaction tube. The solution was allowed to polymerize at 25 $^\circ\text{C}$ for 4.5 h with stirring.

The above polymerization-sampling-extension procedure was repeated at defined reaction time, Scheme 3.6.

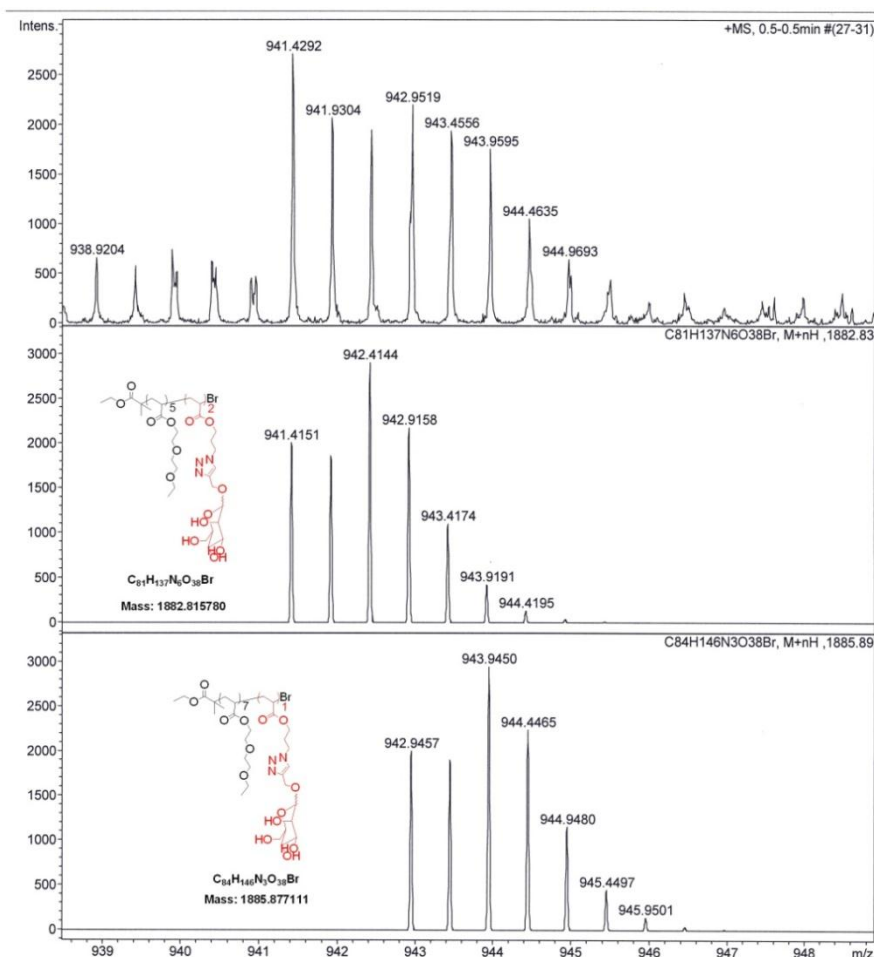
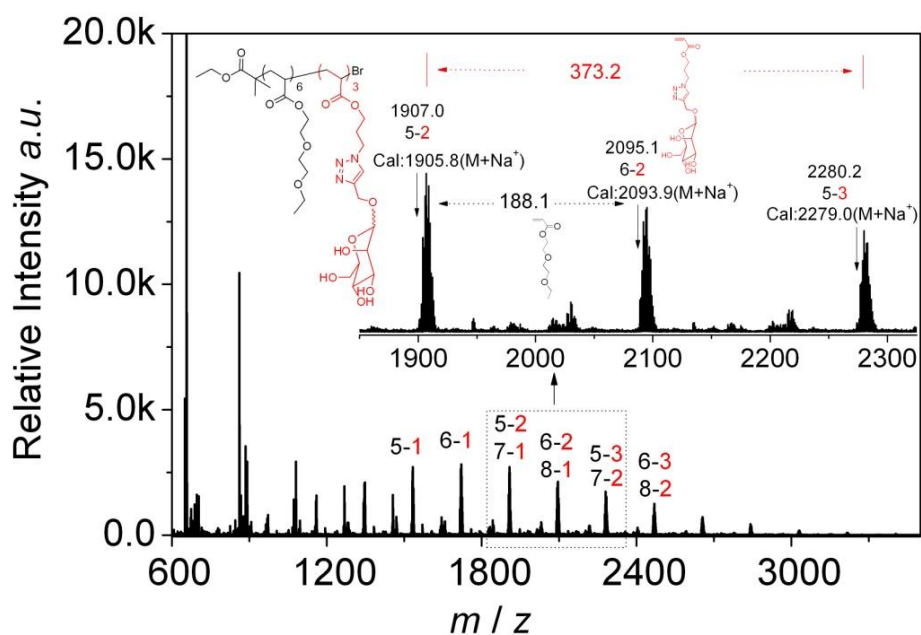
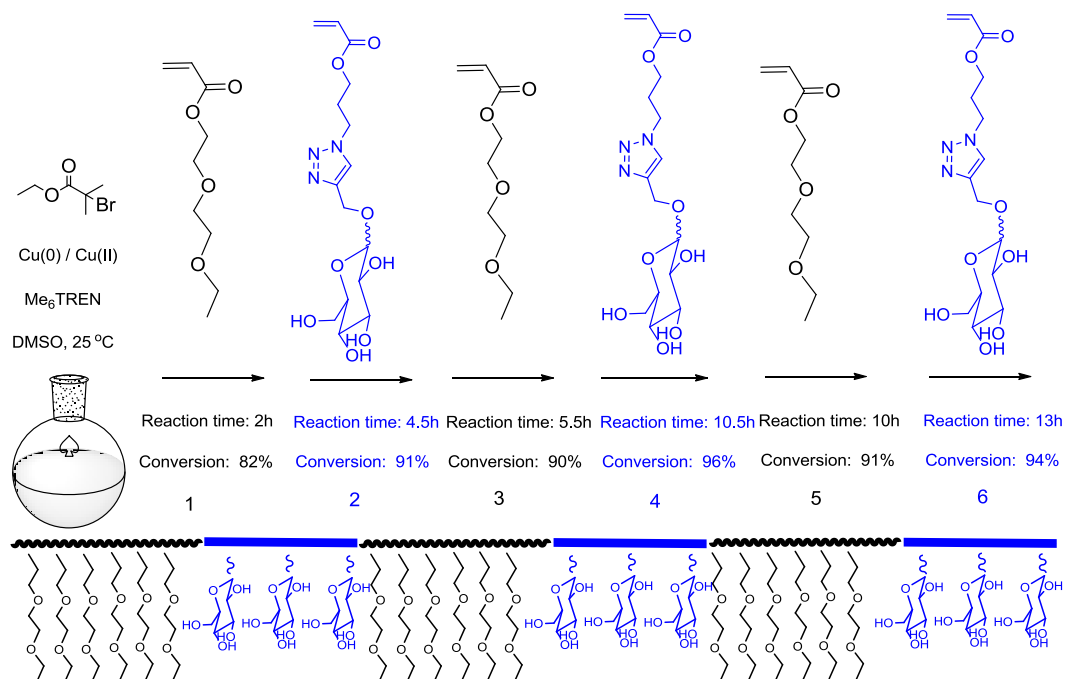


Figure 3. 21. MALDI-ToF MS (top) and high resolution ESI-MS (bottom) zooming spectra of the 2nd block (DEGEEA)₆-(mannose)₃ glycopolymers obtained by SET-LRP.

3.3.11 Multiblock copolymerization of DEGEAA and glucose glycomonomer via SET-LRP



Scheme 3. 12. Schematic representation for the synthesis of sequence-controlled multiblock glycopolymers by iterative addition of DEGEAA and glucose glycomonomer at defined time period.

For the multiblock copolymerization, DEGEAA (565 mg, 3 mmol) mesitylene (18 mg, 0.15 mmol, used as internal standard for ^1H NMR conversion calibration) were soluble in DMSO (4.5 mL) and each time 1/3 of the solution was used for polymerization. Glucose glycomonomer (560 mg, 1.5 mmol) and mesitylene (9 mg, 0.075 mmol) were soluble in DMSO (4.5 mL) and each time 1/3 of the solution was also used for chain extension. To a Schlenk tube fitted with a magnetic stir bar and a rubber stopper, DEGEAA-DMSO solution (188 mg, 1 mmol, 6 eq), CuBr_2 (4 mg, 0.017 mmol, 0.1 eq) were charged and the mixture was bubbled with nitrogen for 15 min. Pre-degassed Me_6TREN (7 μL , 0.03 mmol, 0.18 eq) and EBiB (24.5 μL , 0.17 mmol, 1 eq) were then added via gas tight syringe sequentially. After that, pre-activated copper wire (3 cm) was carefully added under nitrogen protection. The Schlenk tube was sealed and the light green solution was allowed to polymerize at $25\text{ }^\circ\text{C}$. After reaction for 2 h, sample was carefully removed for characterization. For chain extension, a further glucose glycomonomer-DMSO solution (186 mg, 0.5 mmol) which has been degassed via nitrogen sparging for 20 min was then transferred

via cannula under nitrogen into the Schlenk reaction tube. The solution was allowed to polymerize at 25 °C for 4.5 h with stirring. The above polymerization-sampling-extension procedure was repeated at defined reaction time.

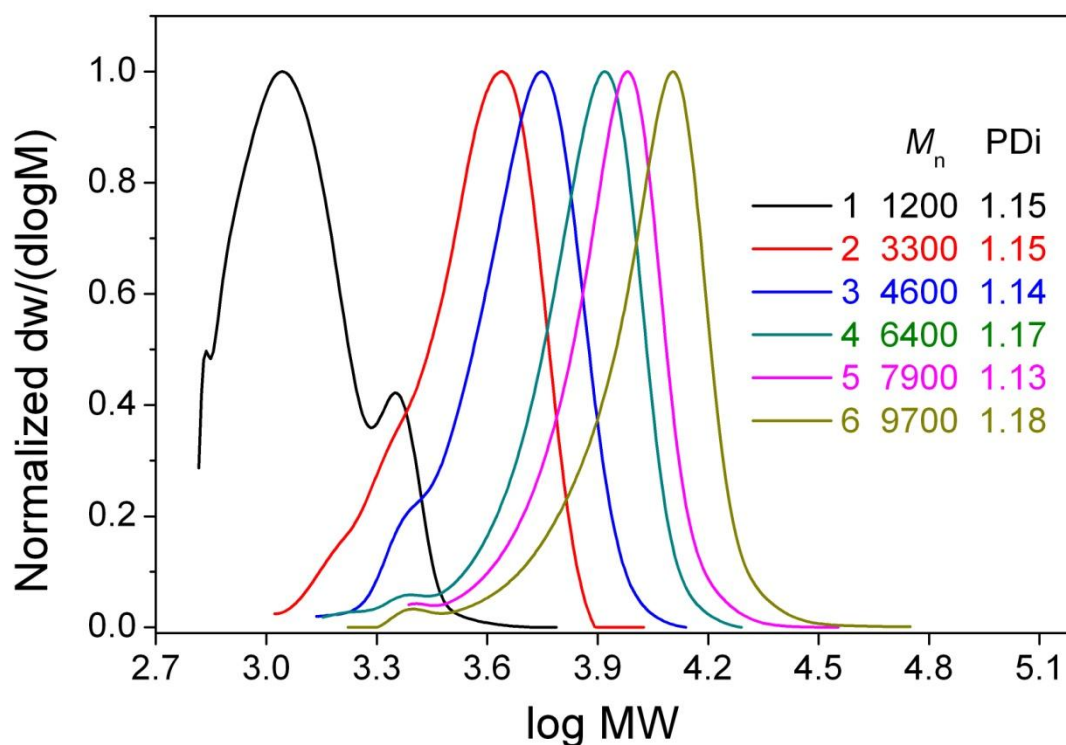


Figure 3. 22. Molecular weight distributions of multiblock DEGEEA-glucose glycopolymer obtained by SET-LRP via iterative monomer addition at defined time period.

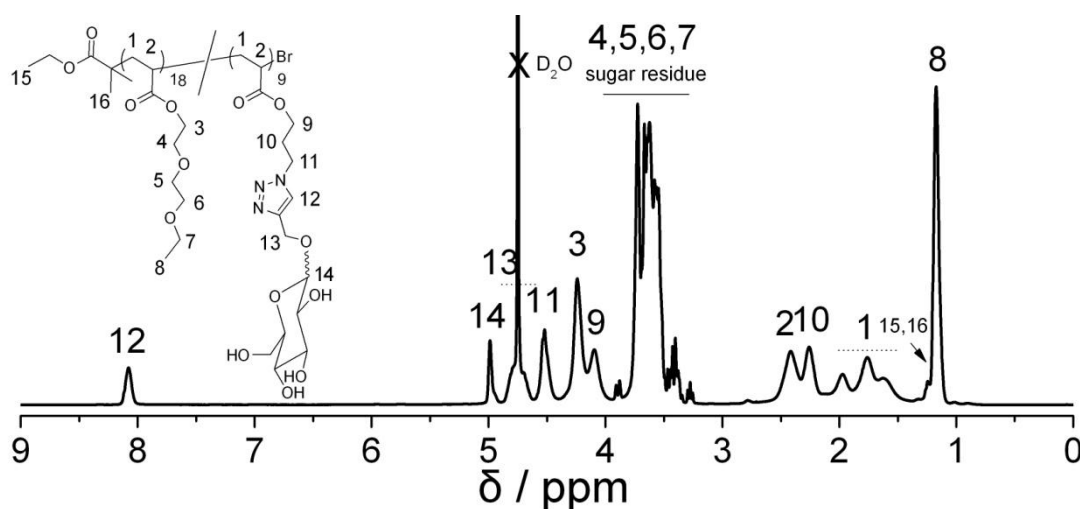


Figure 3. 23. ^1H NMR spectrum of multiblock DEGEEA-glucose glycopolymer in D_2O .

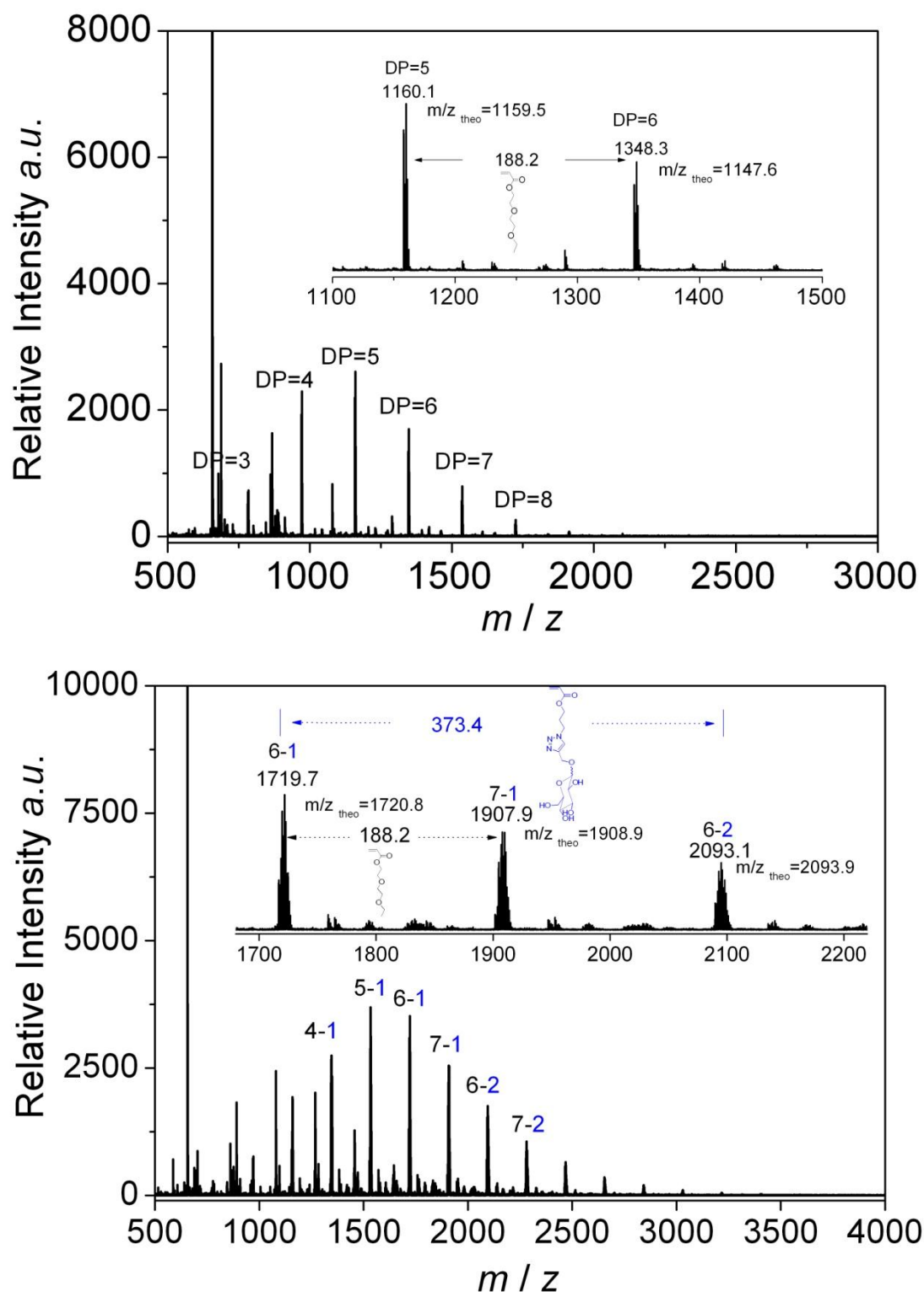


Figure 3. 24. MALDI-ToF MS spectra (RP model) of the 1st block poly(DEGEEA)₆ (top) and 2nd block poly(DEGEEA)₆-b-(glucose)₃ (bottom) glycopolymers obtained by SET-LRP.

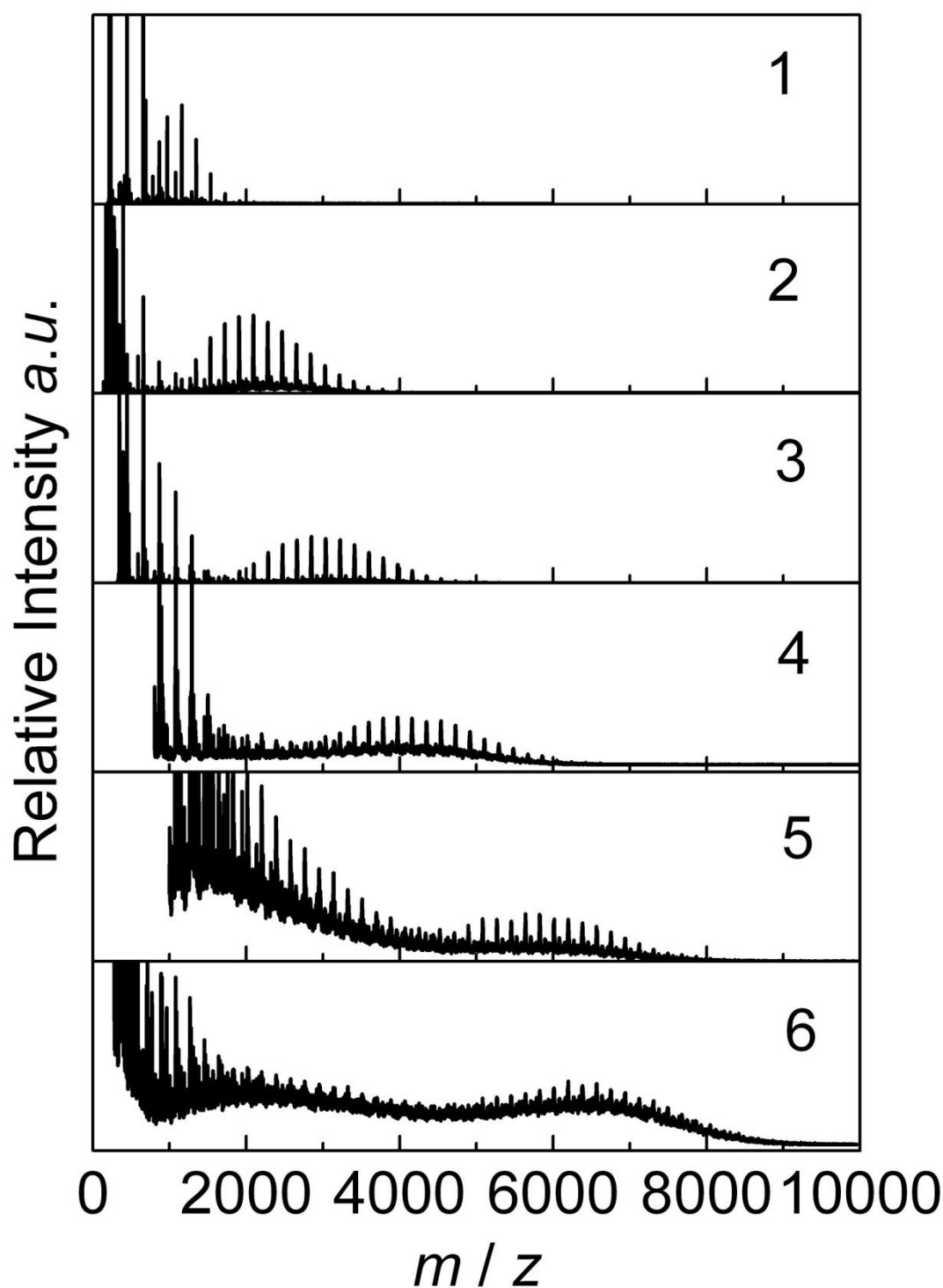


Figure 3. 25. MALDI-ToF MS spectra (LP model) of the 1st block to 6th block DEGEAA/glucose (from top to bottom) glycopolymers obtained by SET-LRP. Due to incorporation of more sugar which causes the loss of resolution under LP model, definition of exact structure after 3rd block is difficult and is for reference only.

3.3.12 Homopolymerization of mannose acrylate glycomonomer via SET-LRP

To a Schlenk tube fitted with a magnetic stir bar and a rubber stopper, mannose glycomonomer (248 mg, 0.67 mmol) and DMSO (1.5 mL) were charged and the mixture was bubbled with nitrogen for 15 min. A quarter of pre-degassed Me₆TREN (4 μ L, 0.018 mmol), EBiB (14.4 μ L, 0.1 mmol), CuBr₂ (2.2 mg, 0.01 mmol) in 6 mL DMSO solution were then added via gas tight syringe sequentially. After that, pre-activated copper wire (1 cm) was carefully added under nitrogen protection. The Schlenk tube was sealed and the light green solution was allowed to polymerize at 25 °C. After 23h, reaction was directly stopped and ¹H NMR analysis revealed a conversion of 85%, which means that the average DP is 23. The rest reaction mixture was dialysed against water for two days after which the glycopolymer could be recovered by freeze drying. SEC analysis confirmed $M_n = 8400$ and $M_w/M_n = 1.10$ of final product.

¹H NMR analysis indicated the expected structure of homo mannose glycopolymer and the integral ratio of triazole ring proton at 8 ppm to methyl groups of EBiB at 1.1 ppm is 10: 4.3, according to which the calculated DP is 21 thus in accordance with the value expected from conversion.

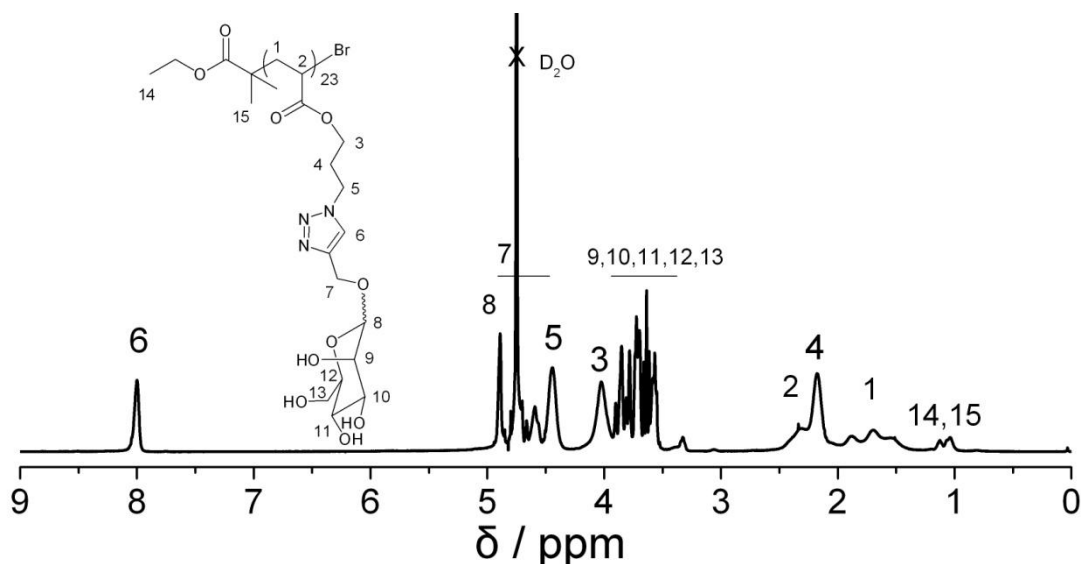


Figure 3. 26. ¹H NMR spectrum of home D-mannose glycopolymer in D₂O.

3.3.13 Statistical copolymerization of DEGEEA and mannose glycomonomer via SET-LRP

To a Schlenk tube fitted with a magnetic stir bar and a rubber stopper, DEGEEA (564 mg, 3 mmol, 18 eq), mannose glycomonomer (560 mg, 1.5 mmol, 9 eq), CuBr_2 (4 mg, 0.017 mmol, 0.1 eq) were charged and the mixture was bubbled with nitrogen for 15 min. Pre-degassed Me_6TREN (7 μL , 0.03 mmol, 0.18 eq) and EBiB (24.5 μL , 0.17 mmol, 1 eq) were then added via gas tight syringe sequentially. After that, pre-activated copper wire (3 cm) was carefully added under nitrogen protection. The Schlenk tube was sealed and the light green solution was allowed to polymerize at 25 $^\circ\text{C}$. After reaction for 22.5 h, ^1H NMR analysis showed total disappearance of vinyl groups. Reaction was then stopped via exposure to the air and the mixture was dialysed against water for two days after which the glycopolymer could be recovered by freeze drying. SEC analysis confirmed $M_n = 6200$ and $M_w/M_n = 1.16$ of the final product.

^1H NMR spectrum of the random copolymer showed broader peaks from mannose and DEGEEA units compared with the block copolymer and the ratio between mannose and DEGEEA is also similar with that in the block copolymer.

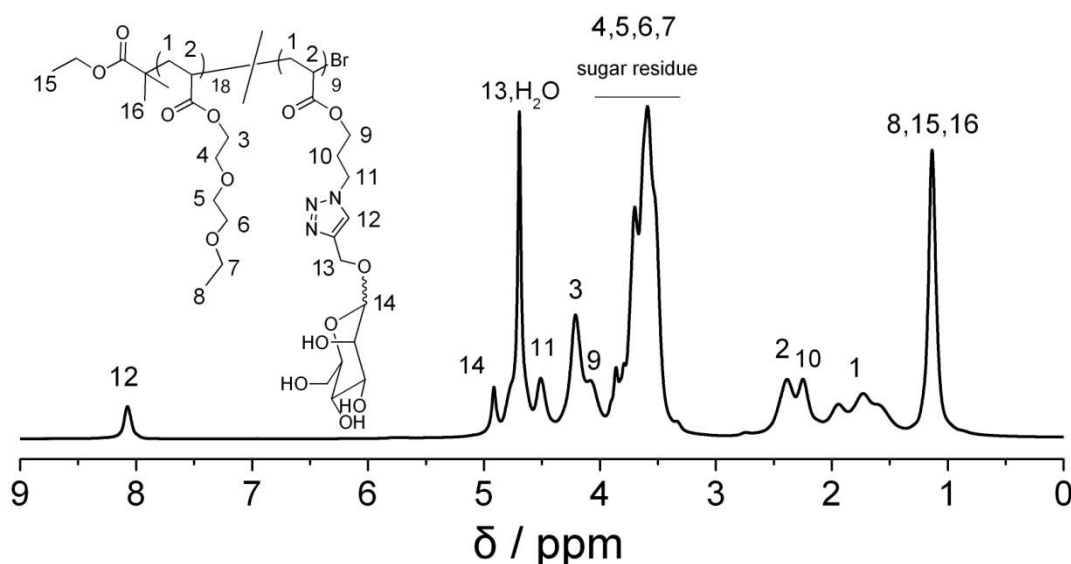


Figure 3. 27. ^1H NMR spectrum of random DEGEEA-mannose glycopolymer in D_2O .

3.3.14 Terminal end group modification

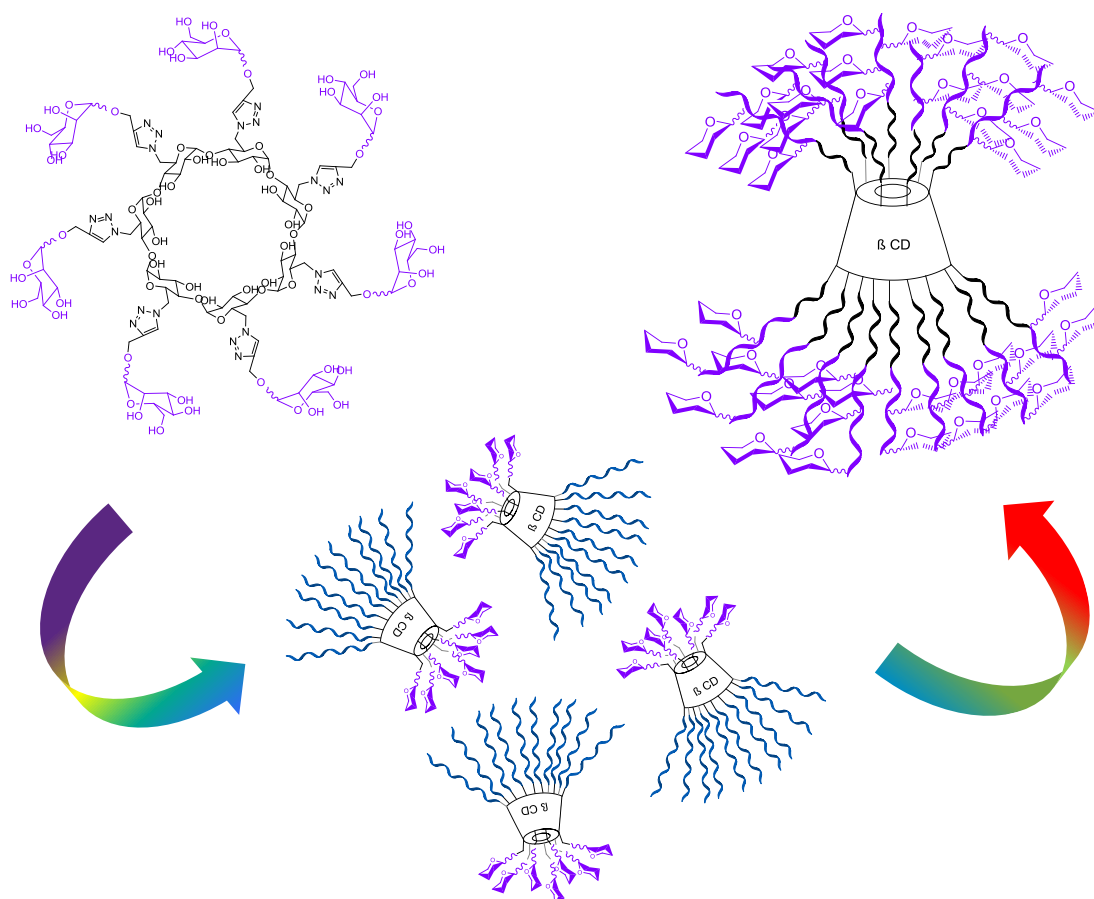
3.3.14.1 *Reaction of terminal the bromide with sodium azide*

In a typical reaction, the multiblock DEGEEA/mannose glycopolymer (400 mg, ~0.06 mmol) was dissolved in DMF (10 ml). Sodium azide (20 mg, 0.3 mmol) was added to the solution and stirred at 25 °C for 24 h. After reaction, the mixture was directly transferred to one dialysis tubing and dialyzed against water for 3 days. 320 mg product was obtained after freeze drying.

3.3.14.2 *CuAAC click reaction with alkyne-functionalised dibromomaleimide*

The general procedure is shown as follow. A solution of azido-terminated glycopolymer (200 mg, ~0.03 mmol), 3, 4-dibromo-1-(prop-2-ynyl)-1H-pyrrole-2, 5-dione (26 mg, 0.09 mmol), bpy (56 mg, 0.36 mmol) in DMF (5 ml) was deoxygenated by three freeze-pump-thaw cycles. The solution was then transferred via cannula under nitrogen into a Schlenk tube, previously evacuated and filled with nitrogen, containing CuBr (26 mg, 0.18 mmol). The resulting solution was stirred at 25 °C for 48 h. When the reaction was completed, the reaction mixture was directly dialysed against MeOH for 2 days and subsequently with water for a further 2 days in order to remove small molecule impurities. After dialysis the glycopolymer (170 mg) was recovered by freeze drying.

Chapter 4 High-affinity cyclodextrin-based glycoconjugates for HIV-therapeutic and drug delivery



A series of cyclodextrin-based glycoconjugates, including glycoclusters and star glycopolymers, were synthesised via combination of CuAAC click reaction and copper-mediated living radical polymerization. These glycoconjugates showed high affinity in binding with human DC-SIGN lectin and could be used as inhibitor to prevent the binding of HIV envelope protein gp120 to DC-SIGN at nanomolar concentration. The star block glycopolymer showed high loading capacity of hydrophobic anti-cancer and anti-HIV drugs, indicating promising application in HIV-therapeutic and smart drug delivery.

4.1 Introduction

Dendritic cell specific ICAM-3 grabbing nonintegrin (DC-SIGN) is a C-type lectin present on the surface of dendritic cell and plays a key role in the immune response, including capturing HIV-1 and enhancing trans-infection of T cells.¹²⁵ The oligosaccharides on the HIV envelope protein gp120 could be recognized by the DC-SIGN and this carbohydrate-protein interaction is considered as the main promotion of viral infection.¹⁸⁰ In addition to the research into the HIV inhibitor, anti-adhesion therapy has been developed as a new avenue for anti-HIV therapy, which focuses on the application of carbohydrates to interfere with the binding between the lectin and pathogen.^{7,81,181,182} Multivalent carbohydrate ligands have been proved to show high-avidity interaction with lectins due to the clustering of glycans, which gives a “Cluster Glycoside Effect”.¹⁸³ Considerable interest has been generated in cyclodextrin (CD)-based glycoclusters, not only due to its highly branched carbohydrate-containing structure for protein binding but also its potential to act as host for the complexation of drug molecules, which can be considered as a kind of intelligent drug delivery system.¹⁸⁴⁻¹⁸⁶ Different synthetic methodologies have been developed, however, multistep reactions are generally required to prepare these glycoclusters with complex structures.¹⁸⁷⁻¹⁹⁰ Compared to oligosaccharides, glycopolymers can also undergo similar recognition events with lectins and could be obtained in a relatively facile manner, which have been considered as alternative structures for oligosaccharides.^{1,2} Well-defined CD-based star polymers could be synthesised *via* core-first approach from functional CD initiators for different controlled radical polymerization, including ATRP, RAFT and NMP.¹⁹¹⁻¹⁹³ However, reports on synthesis of CD-based glycopolymers are very limited and RAFT polymerization did not work.¹⁹⁴

In order to synthesize an intelligent drug delivery system for therapeutic application, this system needs to bear a glycoconjugate structure, either glycocluster or glycopolymer, and can specifically bind to the DC-SIGN lectin and thus used as inhibitor to prevent the binding of HIV gp120. Besides, this system should be able to load anti-HIV drug in order to deliver the drug to the target area and also release the drug under control.

As our first try, β -CD-based glycoclusters with seven mono saccharides on the primary face were synthesized *via* CuAAC. Subsequently, β -CD-based

glycoconjugates with seven mono saccharides on the primary face and thermoresponsive polymers on the secondary face were synthesized. Finally, we will describe our approach to synthesize β -CD-based homo and diblock star glycopolymers *via* SET-LRP.

The different binding ability of these synthesised glycoconjugates with DC-SIGN was characterized by SPR, which revealed the tendency of proper glycoconjugate as high-affinity inhibitor for HIV gp120-DC-SIGN interaction. The drug delivery ability of obtained glycoconjugates for hydrophobic anti-cancer and anti-HIV drug was also tested.

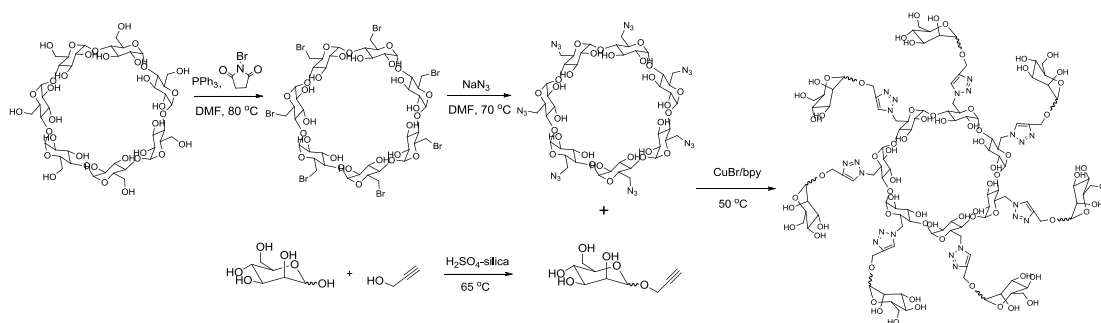
4.2 Results and Discussion

4.2.1 Synthesis and characterization of glycoclusters

Persubstituted CD-based glycoclusters with multivalent monosaccharides showed binding behaviour with different lectins at much lower concentration compared with monosaccharides.^{184,185,190} These promising results inspired us to develop similar structures with glycoclusters on the primary face as recognition sites and secondary face unmodified so that the CD host can still encapsulate drugs. However, this is a complicated process for the synthesis of CD-based glycoclusters according to the previous synthetic route, which used multistep organic reactions, protection, deprotection chemistry and chromatographic purification.¹⁸⁷⁻¹⁹⁰

The development of click chemistry supplies routes to potentially simplify this process, which fulfils the property of modular, stereospecific, wide in scope, quantitative yields and by-products could be easily removed by non-chromatographic methods.¹⁴⁸ Different click chemistry has been applied into the modification of CD in relatively facile manner and we are inspired to use click chemistry to prepare complex CD-based glycoclusters.¹⁹⁵⁻¹⁹⁷

Herein, the synthesis of core moiety, per-6-azido- β -CD and its click reaction with alkyne monosaccharides are first presented (Scheme 4.1). Starting from raw β -CD and free monosaccharides, target glycoclusters could be obtained in high conversion through four step reactions, which allowed us to avoid the tedious multistep reaction and protection chemistry.



Scheme 4. 1. Synthesis of persubstituted β -CD-based glycocluster *via* CuAAC of per-6-azido β -CD and alkyne sugar.

First, the per-6-azido β -CD core was synthesized in 90% yield, according to a modification of the previous method.¹⁹⁸ Secondly, unprotected alkyne monosaccharides were synthesized *via* a one pot Fischer type glycosylation reaction using H_2SO_4 -silica catalyst (Scheme 4.1).^{109,123}

The CuAAC of azide CD and alkyne mannose was then carried out using CuBr/bpy catalyst in DMSO solvent to yield the persubstituted β -CD-(Man)₇ glycocluster (Scheme 4.1). The product was precipitated in methanol and washed with methanol without further chromatographic purification. The final product was characterized using different techniques to prove total substitution and pure product formation. The ^1H NMR spectrum showed the presence of a triazole ring proton at approximately 7.9 ppm and CD residues at around 6.0 ppm (OH) and 5.2 ppm (H-1) and the integral ratio is consistent with theoretical values, Figure 4.1, which indicated the success of the CuAAC. The MALDI-ToF spectrum (Figure 4.1) showed peaks corresponding to the fully substituted product at ~ 2860 (m/z). The FT-IR spectra (Figure 4.2) confirmed the total disappearance of azide functionalities at around 2100 cm^{-1} following the click reaction. Even DMF SEC analysis (Figure 4.2) revealed the shift of elution traces after reaction due to the change of hydrodynamic volume. All these data support the synthesis of pure β -CD-based mannose glycocluster decorated through 1, 2, 3-triazole linker with seven mannose units on the primary face and unmodified secondary face.

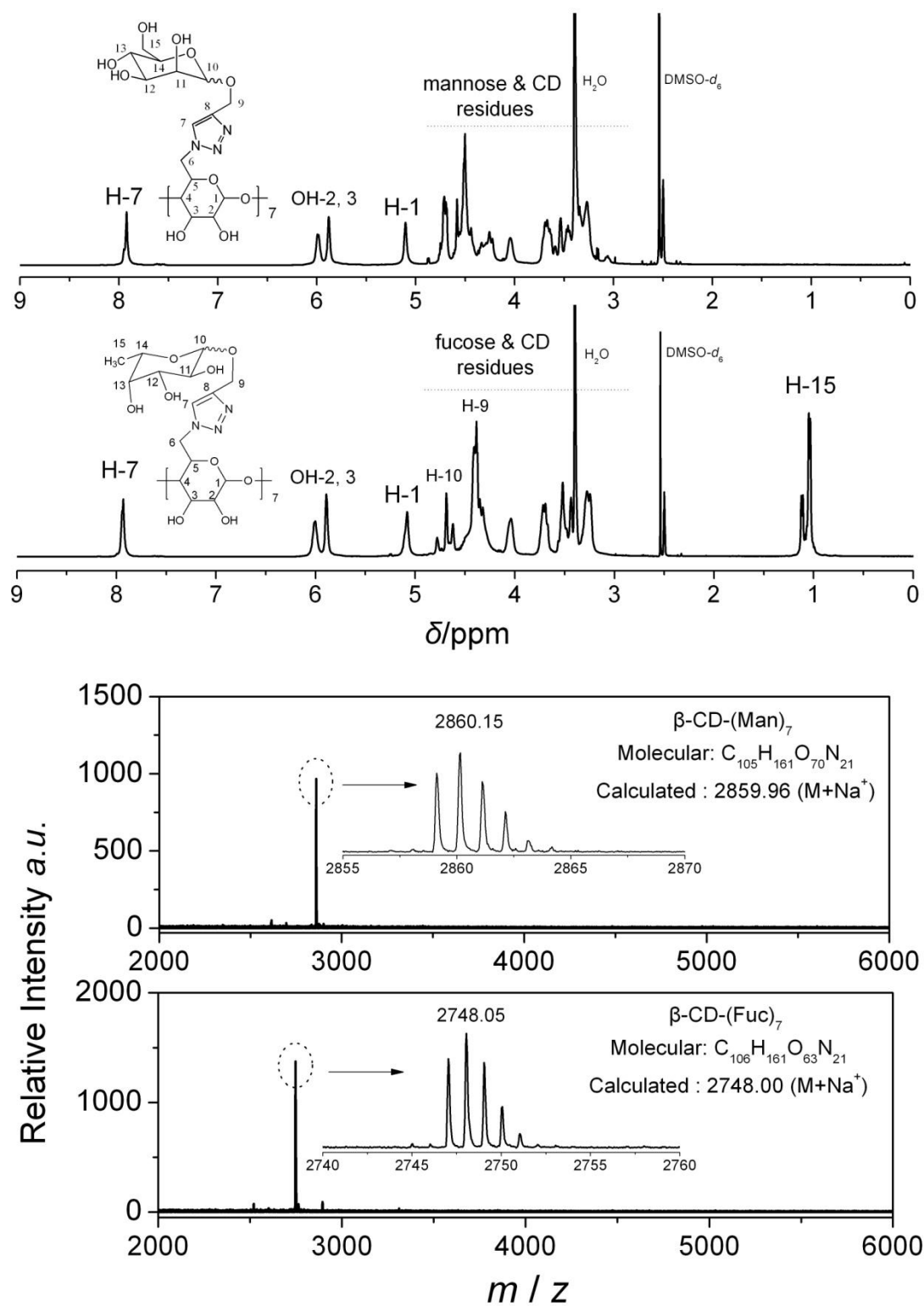


Figure 4. 1. ^1H NMR (top) and MALDI-ToF MS (bottom) spectra of $\beta\text{-CD}-(\text{Man})_7$ & $\beta\text{-CD}-(\text{Fuc})_7$ glycoclusters.

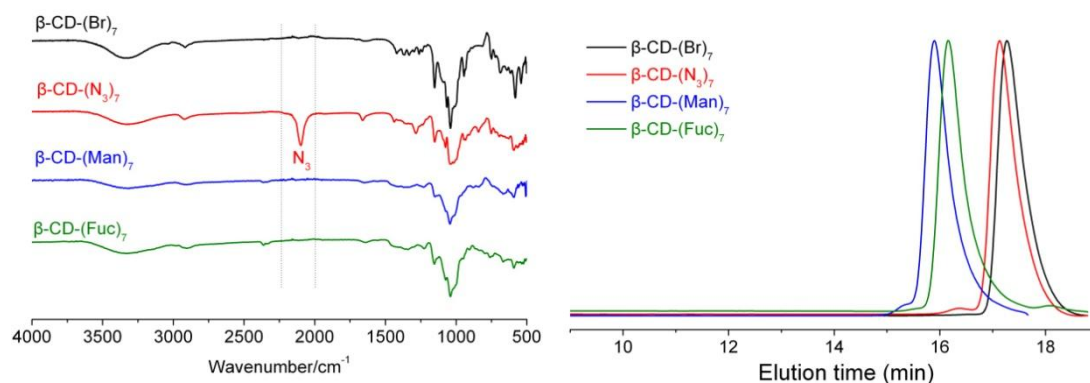
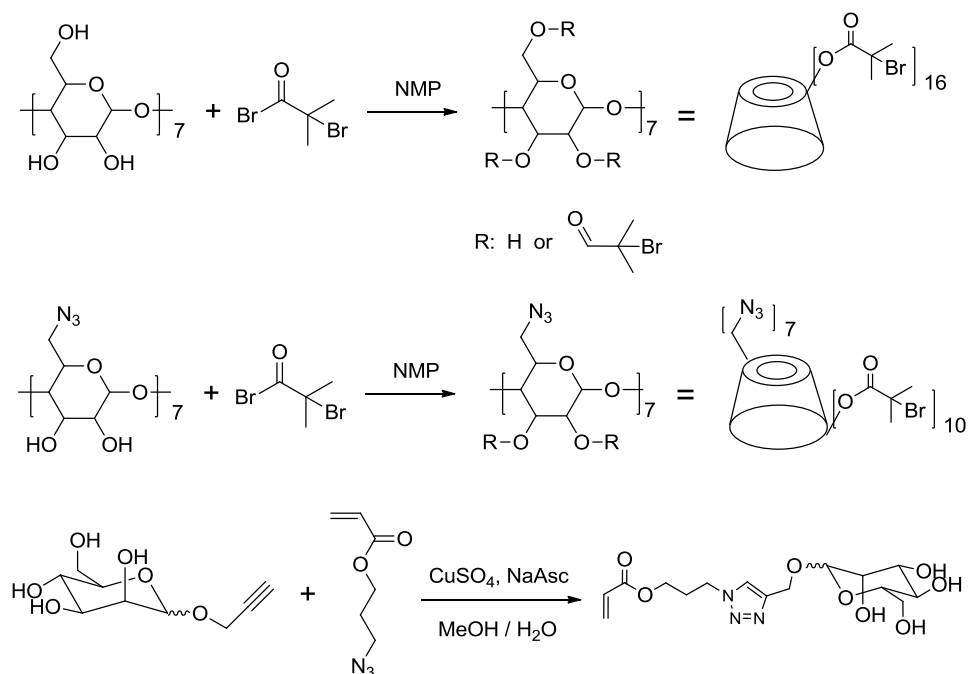


Figure 4. 2. FT-IR (left) spectra and normalized SEC elution traces (right) of β -CD-(Man)₇ & β -CD-(Fuc)₇ glycoclusters.

In order to verify the versatility of this approach, a β -CD-based fucose glycocluster was also synthesized according to same procedure. ¹H NMR, MALDI-ToF MS, FT-IR and SEC analysis revealed similar results as mannose glycocluster and confirmed the right target structure, Figure 4.1 & 4.2. In summary, persubstituted β -CD-based glycoclusters were prepared by Huisgen 1, 3 dipolar cycloaddition of appropriate sugar alkynes with β -CD bearing azide groups on the primary face.

4.2.2 Synthesis of CD-based initiators and glyco monomers for SET-LRP



Scheme 4. 2. Synthesis of β -CD-(Br)₁₆, (N₃)₇- β -CD-(Br)₁₀ and glyco monomer.

The CD-based initiator was synthesized *via* a one pot esterification reaction according to a previous report.¹⁹⁹ Under these experimental conditions, this esterification

reaction cannot reach full conversion and ^1H NMR and MALDI-ToF MS analysis (Figure 4.3, 4.4) confirmed the average degree of substituted hydroxyl groups at the periphery CD was approximately 16, which is given the descriptor $\beta\text{-CD-(Br)}_{16}$.

A further CD-based initiator bearing seven azide groups on the primary face was also synthesised in same way from the $\beta\text{-CD-(N}_3)_7$ with the average degree of substituted hydroxyl groups at the secondary CD ≈ 10 , $(\text{N}_3)_7\text{-}\beta\text{-CD-(Br)}_{10}$. Compared to that of $\beta\text{-CD-(N}_3)_7$, the ^1H NMR spectrum of $(\text{N}_3)_7\text{-}\beta\text{-CD-(Br)}_x$ revealed the appearance of a new signal at 1.92 ppm, which can be ascribed to the methyl groups of $\text{BrC}(\text{CH}_3)_2$. The ^{13}C NMR spectrum of $(\text{N}_3)_7\text{-}\beta\text{-CD-(Br)}_x$ showed the appearance of signals at 30.5, 51.2 and 171.2 ppm, which can be ascribed to methyl and methane carbons and carbonyl groups, respectively. However, as in the synthesis of $\beta\text{-CD-(Br)}_{16}$, the esterification reaction was not 100% complete. According to the peak integral ratio of resonance signals at 1.92 ppm to those in the range of 3.2-5.8 ppm, the average degree of substituted bromines was approximately 10. MALDI-TOF MS analysis (Figure 4.5.) also confirmed the existence of $(\text{N}_3)_7\text{-}\beta\text{-CD-(Br)}_{8-12}$, which meant that the obtained product was in actual fact a mixture of $(\text{N}_3)_7\text{-}\beta\text{-CD-(Br)}_x$ with different degrees of substitution. Silica gel column chromatography with dichloromethane (0.2% ethanol) as eluent could not separate these similar chemicals from each other, so the multifunctional initiator, $(\text{N}_3)_7\text{-}\beta\text{-CD-(Br)}_{10}$, which contains 7 azido groups on the primary face and on average 10 bromine moieties on the secondary face of $\beta\text{-CD}$, was directly used for the next step of the reaction.

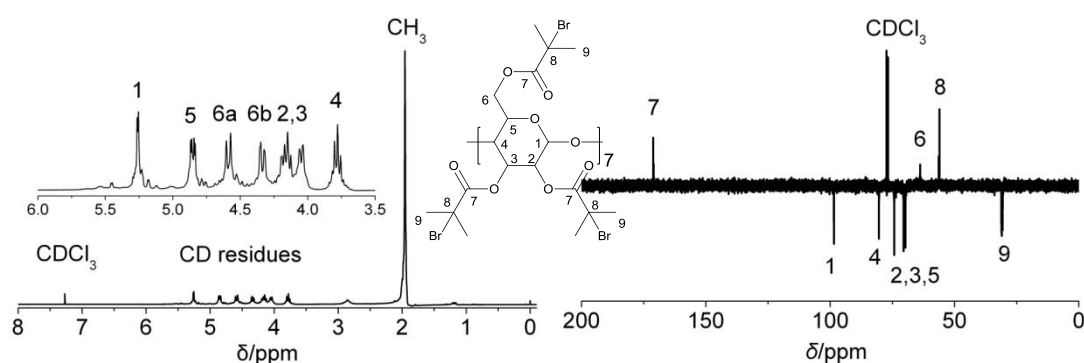


Figure 4. 3. ^1H (left) and ^{13}C (right) NMR spectra of $\beta\text{-CD-(Br)}_{16}$ in $\text{DMSO-}d_6$.

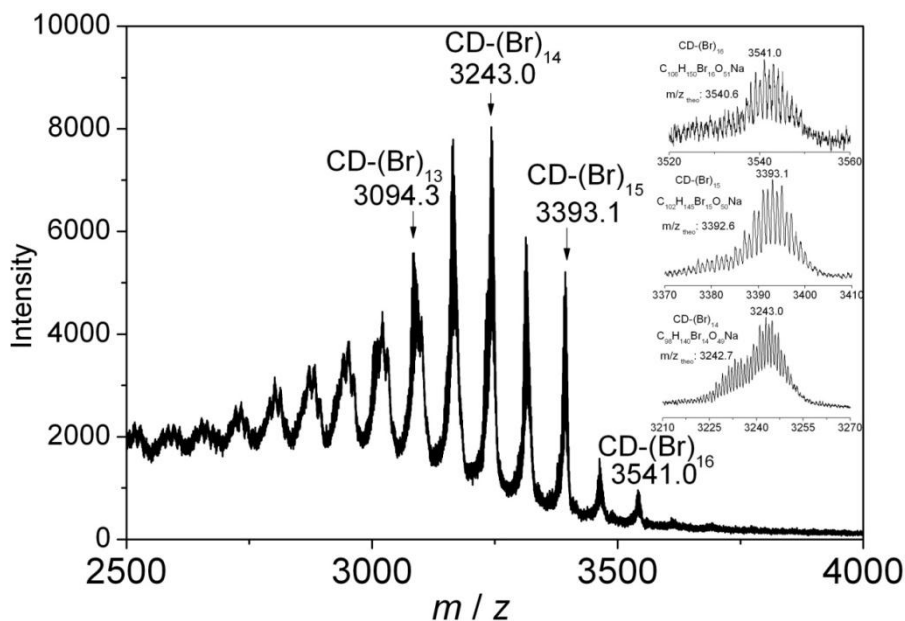


Figure 4. 4. MALDI-ToF MS spectrum of β -CD-(Br)₁₆.

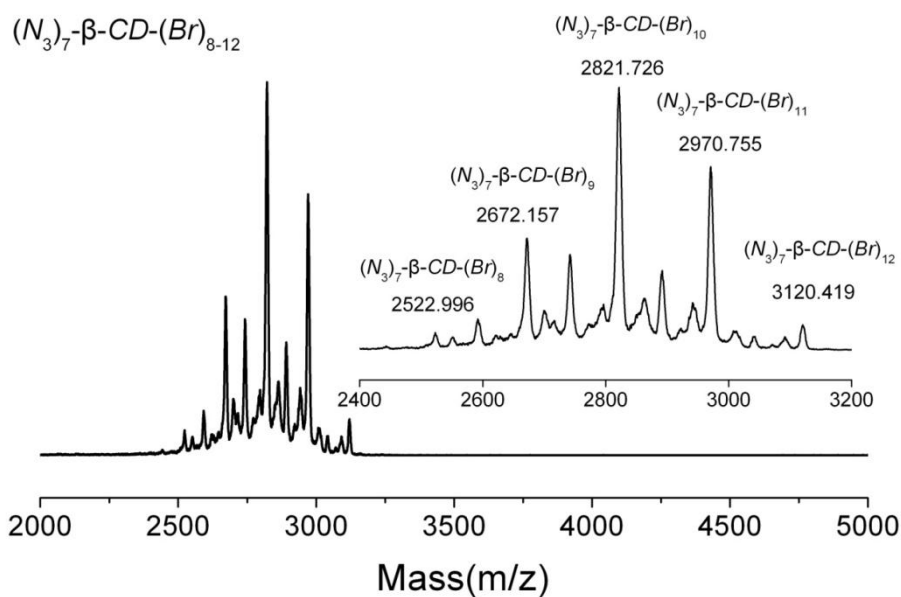
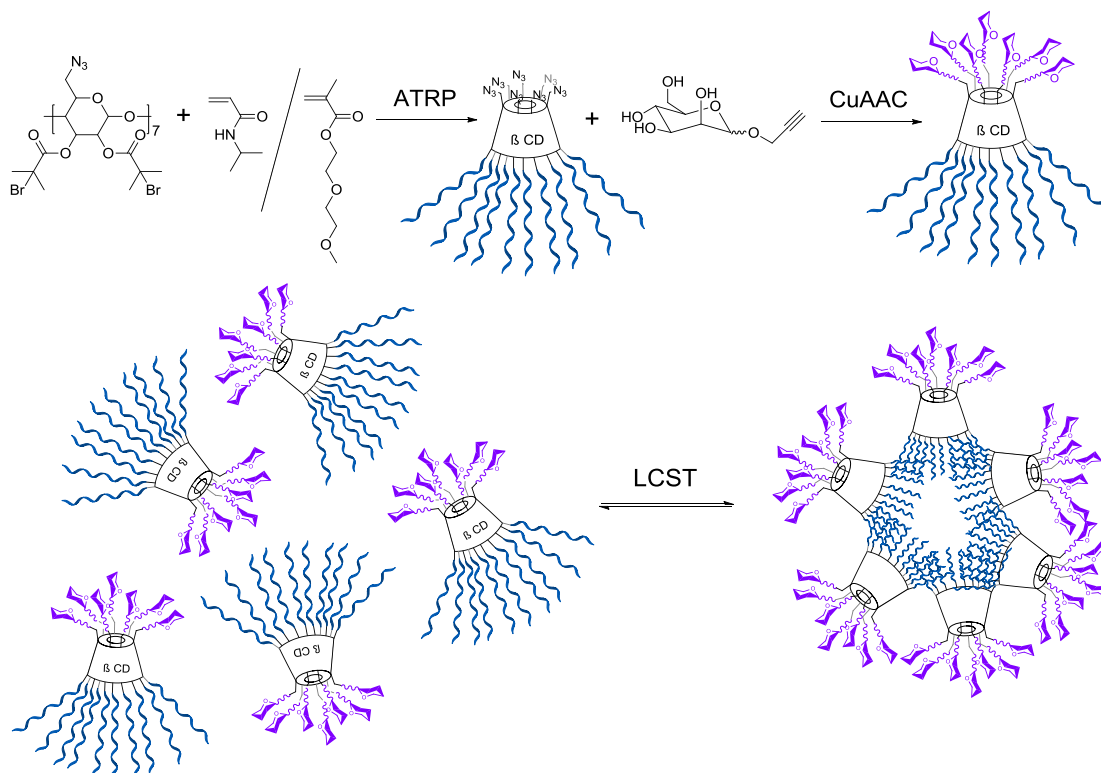


Figure 4. 5. MALDI-ToF MS spectrum of $(N_3)_7$ - β -CD-(Br)₈₋₁₂ in linear model.

CuAAC was used to synthesize glycomonomers *via* reaction of alkyne sugar with azide acrylate intermediate in MeOH/H₂O under catalysis of CuSO₄/sodium ascorbate.¹⁷⁶ Acrylate mannose and glucose glyco monomers were prepared and used for SET-LRP, Scheme 4.2.

4.2.3 Synthesis of CD-based glycocluster-smart star polymer hybrids via combination of ATRP and CuAAC



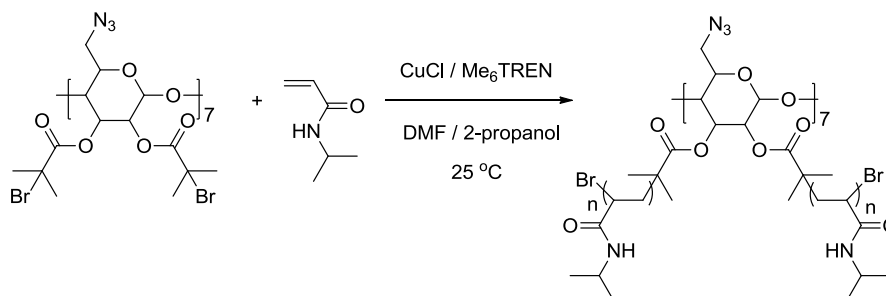
Scheme 4. 3. Schematic representation for the synthesis of CD-based glycocluster-smart star polymer hybrids *via* combination of ATRP and CuAAC and their LCST self-assembled behaviour.

CD-centered star responsive polymers have interesting self-assembling behaviours and could form different type vesicles by tuning solution pH or temperature, which has potential application in controlled drug delivery.²⁰⁰ Star-shaped block copolymers have also been applied as universal hydrophobic drug carriers using the host-guest interaction.^{201,202} Thus this inspired us to synthesize such Janus-type star responsive polymers with sugar moieties for conjugation and potential drug delivery, through which the surface sugar intensity should also be increased *via* specific self-assembly in water by tuning the temperature.

The strategy was to first use the azide functionalised CD-based initiator for ATRP of NIPAM or DEGEEA and to subsequently use CuAAC to attach the monosaccharide on the primary face of cyclodextrin, Scheme 4.3.

The polymerization of NIPAM was performed under the catalysis of CuCl/Me₆TREN in a propanol/DMF mixture as solvent *via* adding CuCl last such that there will be

enough Cu(I) in the system to initiate ATRP at ambient room temperature, in Scheme 4.4.



Scheme 4. 4. Schematic representation for the synthesis of cyclodextrin-based PNIPAM *via* ATRP.

In a similar to a previous report²⁰³, the first-order kinetic plots (Figure 4.6) show significant curvature and in that report this was attributed to the 2-propanol solvent, which was thought to hydrogen-bond to monomer and polymer and thus reduce the deactivation of the polymerization catalyst. However, low dispersities were obtained during the reaction and GPC analysis of the final polymer showed $M_{n,SEC} = 21.6$ kDa and $M_w/M_n = 1.25$.

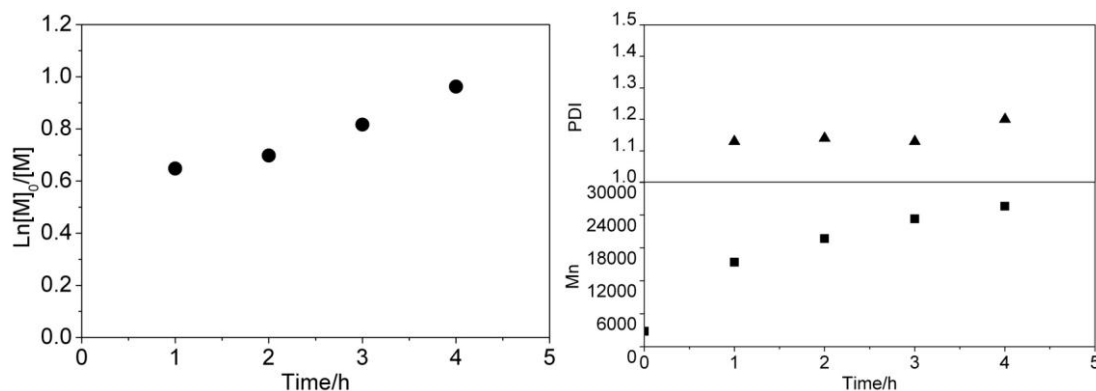


Figure 4. 6. Semi-logarithmic kinetic plots (left) and molecular weight and PDI *vs* reaction time plots for polymerization of NIPAM from $(N_3)_7\text{-}\beta\text{-CD-(Br)}_{10}$.

The polymerization of diethylene glycol methyl ether methacrylate (DEGEEA) was conducted in toluene under the catalysis of CuBr/ *N*-ethyl-2-pyridylmethanimine at 60 °C. The kinetic results showed the linear dependence of $\text{Ln}[M]_0/[M]$ versus time in Figure 4.7, which indicated that the chain radical concentration remained constant during the polymerization. The molecular weight of obtained polymer increase linearly with time and the PDI remained low (~ 1.2) during the polymerization, which indicated the living nature for the polymerization of DEGMEMA.

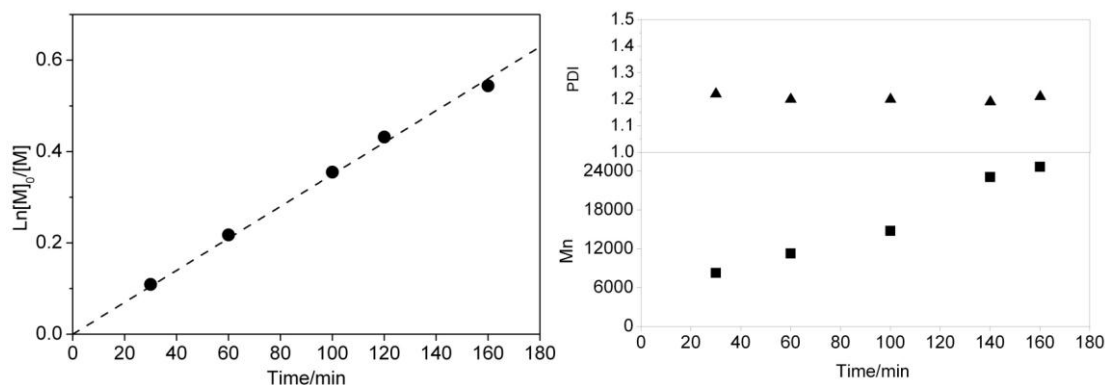


Figure 4. 7. Semi-logarithmic kinetic plots (left) and molecular weight and PDI vs reaction time plots (right) for ATRP of DEGMEMMA from $(N_3)_7\text{-}\beta\text{-CD-(Br)}_{10}$.

Subsequently, the CD-centered PNIPAM with azide groups on the primary face of the CD was used for the CuAAC with 1-(2'-propargyl) D-mannose in DMSO under the catalysis of CuBr/bpy. The success of the click reaction was demonstrated by the disappearance of azide group absorbance at 2100 cm^{-1} in the FT-IR spectrum (Figure 4.8) and the LCST temperature shifting from 31.8 to $36.9\text{ }^\circ\text{C}$ due to the very hydrophilic sugar hydroxyl groups (Figure 4.9).

The SEC and NMR analysis did not reveal significant change due to the low content of mannose moieties compared with PNIPAM. The elution traces only changed slightly after click reaction, Figure 4.10. M_n calculated from PMMA standards showed that it increased from 21600 to 21800 and the PDI kept the same at 1.25. Due to the low ratio of mannose compared with PNIPAM component and also the overlap between N-H and tri-azole ring proton at $7 - 9\text{ ppm}$, ^1H NMR only revealed PNIPAM components and did not show significant peaks from mannose, Figure 4.11.

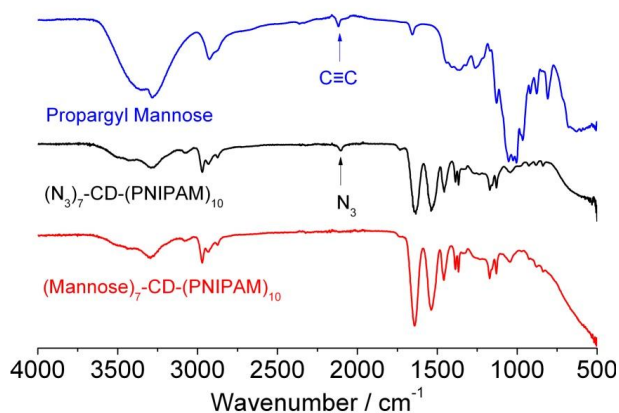


Figure 4. 8. FT-IR spectra obtained for propargyl mannose, $(N_3)_7\text{-}\beta\text{-CD-(PNIPAM)}_{10}$ and $(\text{Mannose})_7\text{-}\beta\text{-CD-(PNIPAM)}_{10}$.

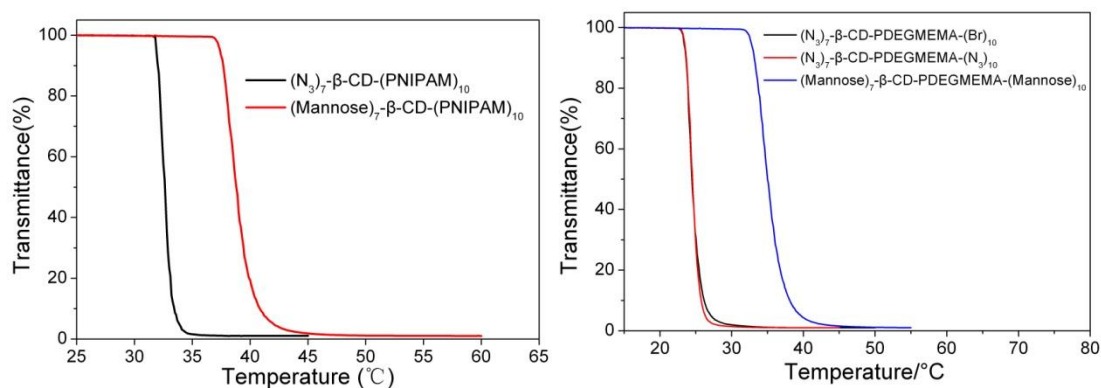


Figure 4. 9. Cloud point measurements of $(N_3)_7\beta\text{-CD}-(\text{PNIPAM})_{10}$, $(\text{Mannose})_7\beta\text{-CD}-(\text{PNIPAM})_{10}$ (left) and $(N_3)_7\beta\text{-CD}-(\text{PDEGMEMA})_{10}-(\text{Br})_{10}$, $(N_3)_7\beta\text{-CD}-(\text{PDEGMEMA})_{10}-(N_3)_{10}$ and $(\text{Mannose})_7\beta\text{-CD}-(\text{PNIPAM})_{10}-(\text{Mannose})_{10}$ (right) by UV/Vis spectroscopy at 500 nm. The analytes concentrations in water are all 1 mg/mL.

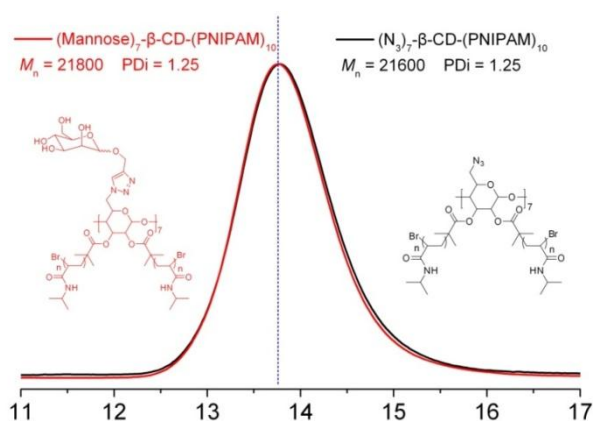


Figure 4. 10. Normalized SEC elution traces for $(N_3)_7\beta\text{-CD}-(\text{PNIPAM})_{10}$ and $(\text{Mannose})_7\beta\text{-CD}-(\text{PNIPAM})_{10}$ via RI detector. The two samples were injected in sequence at the same time.

The click reaction of CD-centered PDEGMEMA with 1-(2'-propargyl) D-mannose was first conducted under the same conditions. However, after the reaction SEC (Figure 4.12) showed a significant star-star coupling shoulder peak at higher MW region, which is probably due to the similar click and ATRP reaction conditions.

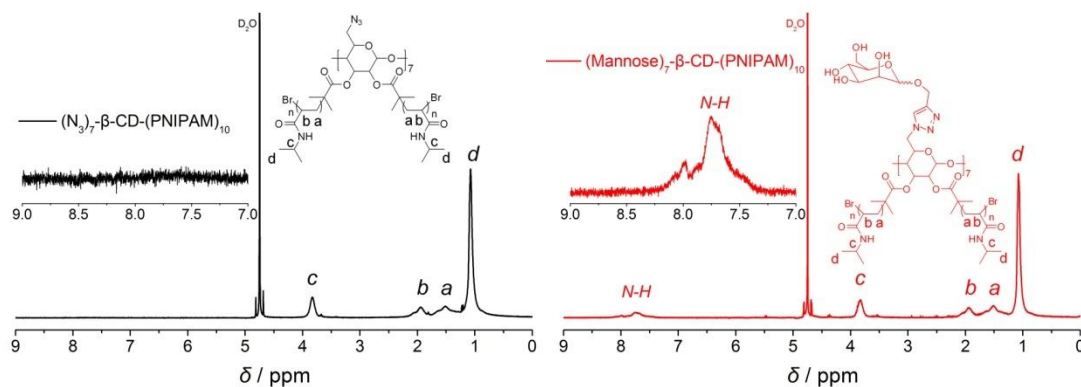


Figure 4. 11. ^1H NMR spectra recorded in D_2O for $(\text{N}_3)_7\text{-}\beta\text{-CD-(PNIPAM)}_{10}$ (left) and $(\text{Mannose})_7\text{-}\beta\text{-CD-(PNIPAM)}_{10}$ (right).

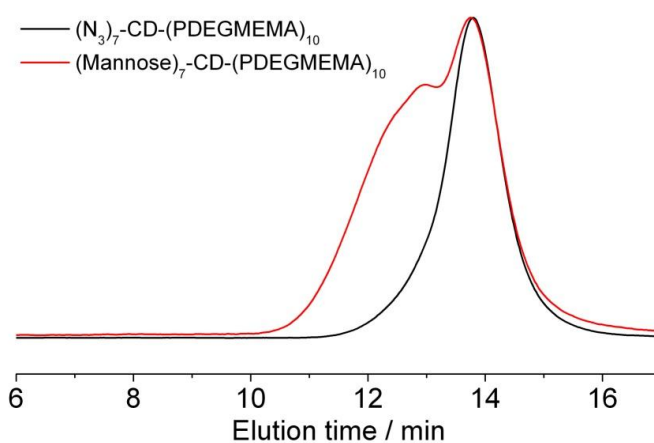


Figure 4. 12. Normalized DMF SEC traces of $(\text{N}_3)_7\text{-}\beta\text{-CD-(PDEGMEMA)}_{10}$ and $(\text{Mannose})_7\text{-}\beta\text{-CD-(PNIPAM)}_{10}$.

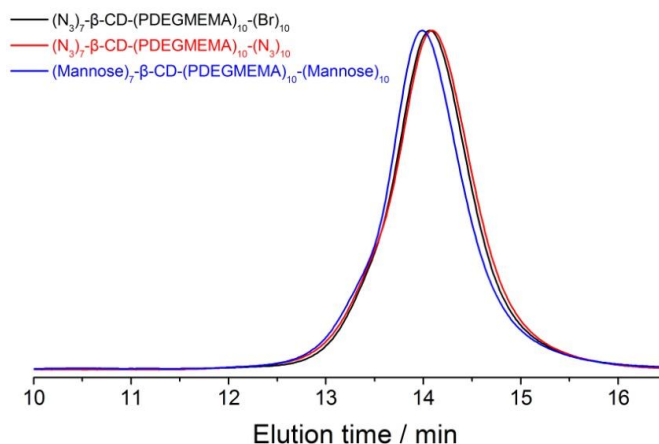


Figure 4. 13. Normalized DMF SEC traces of $(\text{N}_3)_7\text{-}\beta\text{-CD-(PDEGMEMA)}_{10}(\text{Br})_{10}$, $(\text{N}_3)_7\text{-}\beta\text{-CD-(PDEGMEMA)}_{10}(\text{N}_3)_{10}$ and $(\text{Mannose})_7\text{-}\beta\text{-CD-(PNIPAM)}_{10}(\text{Mannose})_{10}$. These three samples were injected in sequence at the same time.

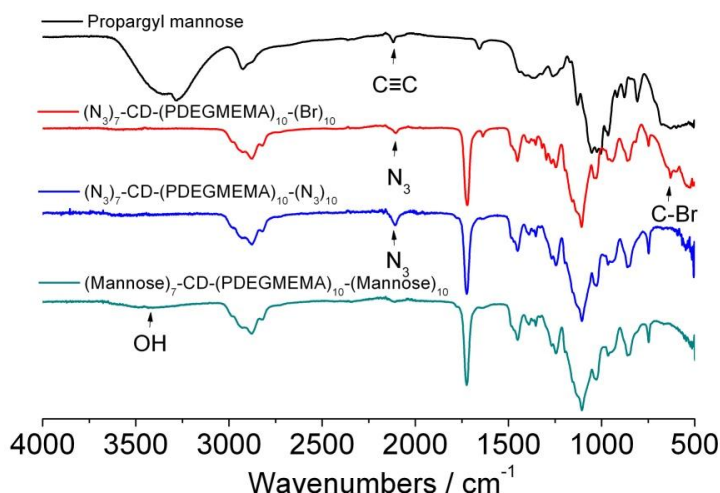


Figure 4. 14. FT-IR spectra obtained for propargyl mannose, $(N_3)_7\beta$ -CD-(PDEGMEMA) $_{10}$ -(Br) $_{10}$, $(N_3)_7\beta$ -CD-(PDEGMEMA) $_{10}$ -(N $_3$) $_{10}$ and (mannose) $_7\beta$ -CD-(PNIPAM) $_{10}$ -(mannose) $_{10}$.

Thus the terminal bromine groups were first transformed into azide groups to avoid the star-star coupling which will also attach more sugar on the star polymers. After reaction, DMF SEC analysis (Figure 4.13) revealed $M_n = 22.0$ KDa and PDI = 1.23 for $(N_3)_7\beta$ -CD-(PDEGMEMA) $_{10}$ -(N $_3$) $_{10}$, which almost has no change compared with $(N_3)_7\beta$ -CD-(PDEGMEMA) $_{10}$ -(Br) $_{10}$. FT-IR analysis (Figure 4.14) confirmed the disappearance of absorbance at ~ 630 cm^{-1} (C-Br). The absorbance peak at ~ 2100 cm^{-1} , which is characteristic of azide moieties, became stronger than that of $(N_3)_7\beta$ -CD-(PDEGMEMA) $_{10}$ -(Br) $_{10}$, which may be attributed to the increase of azide moieties.

Following the click reaction, the coupling phenomenon disappeared and SEC (Figure 4.13) showed slight MW increase and ^1H NMR spectroscopy (Figure 4.15) proved slight triazole ring peak at ~ 8 ppm, indicating the successful addition of mannose. FT-IR (Figure 4.14) revealed the absorbance increase at ~ 2100 cm^{-1} after reaction with sodium azide and total disappearance of the azide peak after click reaction with a new absorbance at ~ 3000 - 3600 cm^{-1} showing the existence of mannose sugar hydroxyl groups. The LCST temperature increased from 23.2 to 32.6 $^\circ\text{C}$ (Figure 4.9), which further showed the success of the click reaction.

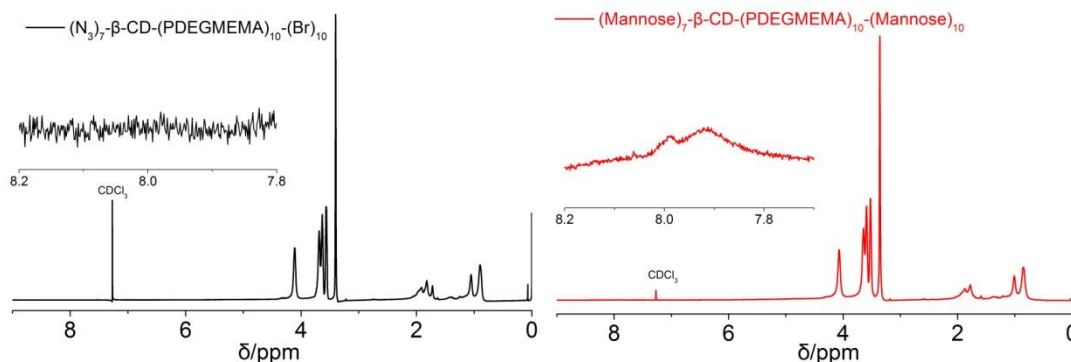


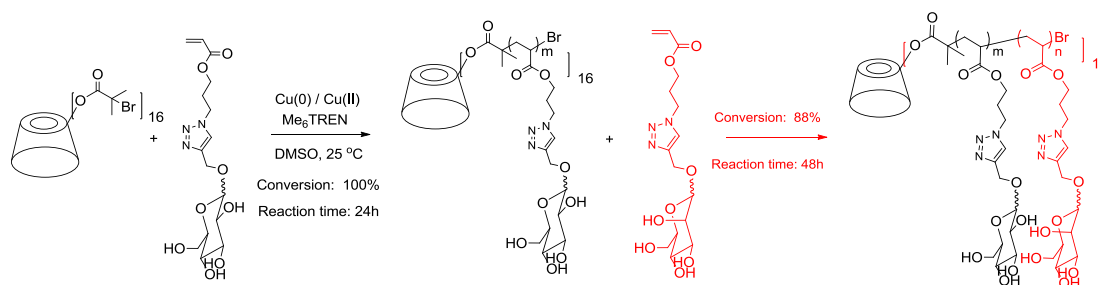
Figure 4. 15. ^1H NMR spectra recorded in CDCl_3 for $(\text{N}_3)_7\text{-}\beta\text{-CD-(PDEGMEMA)}_{10}\text{-(Br)}_{10}$ (left) and $(\text{Mannose})_7\text{-}\beta\text{-CD-(PDEGMEMA)}_{10}\text{-(Mannose)}_{10}$ (right).

All the above results demonstrated that the CD-based glycocluster - star polymer hybrids have been successfully synthesized by the combination of ATRP and CuAAC. The obtained glycoclusters and glycocluster-star polymer hybrids were then tested for the binding with DC-SIGN.

DC-SIGN is a tetrameric transmembrane protein and has a cluster structure. We are interested in whether these CD-centered glycocluster structures could bind with this lectin. Interestingly, SPR characterization showed that the binding between the mannose glycocluster and DC-SIGN tends to be very weak, although this supermolecule bears seven mono mannose units in a cluster shape. SPR revealed a slight response up to 10 Riu after injection of the analytes with flowing over the gold chip bearing DC-SIGN lectin on the surface for 900 seconds, Figure 4.23; however, after a further buffer flush the response decreased to close to the buffer line, suggesting that the previous response was not from the binding of glycocluster to DC-SIGN. The competition test also revealed a very weak inhibition effect between gp120 and DC-SIGN even under very high concentrations (4096 nM), as shown in Figure 4.24. Similarly, the glycocluster-star polymer hybrids showed very weak binding with DC-SIGN (Figure 4.23 & 4.24), which further indicates that the special cluster structure is not good for binding with DC-SIGN. This phenomenon maybe related to the narrow and crowded cluster structure, which cannot block all or most of the binding sties of complex DC-SIGN, thus the bindings are seen to be weak.

4.2.4 Synthesis of cyclodextrin-based star glycopolymers

Based on the above experiments, it is apparent that the design of glycocluster or glycocluster-star polymer hybrid needs to be improved. The sugar density should be increased enough to allow for efficient binding with DC-SIGN. Glycopolymers are a good alternative due to the increase in the sugar density. In order to attach glycopolymers onto the CD core, two synthetic routes are available. The first route is to synthesize alkyne functionalised glycopolymers from a TMS-protected alkyne initiator for click reaction with the previously synthesized azide CD. The second route is the direct polymerization of glycomonomers from CD-based initiator. The Haddleton group has previous experience in synthesis and polymerization from CD-based initiator, which made the second synthetic route the first choice.¹⁹¹



Scheme 4. 5. Synthesis of β -CD based glycopolymers *via* SET-LRP and chain extension reaction.

CD-based star glycopolymers were synthesised *via* direct SET-LRP of glycomonomers, Scheme 4.5. The polymerization of glucose monomer was first conducted at ambient temperature under the catalysis of Cu(0)/Cu(II)/Me₆TREN system with β -CD-(Br)₁₆ as initiator and DMSO as the solvent. The polymerization was continued for 24 h, which led to full conversions according to ¹H NMR analysis revealed by the disappearance of vinyl groups at 5.8-6.4 ppm. DMF SEC analysis showed a narrow dispersity polymer with $M_n=9300$ and $M_w/M_n=1.16$ was obtained (Figure 4.16). The M_n by SEC is lower than the theoretical molecular weight which is ascribed to a lower hydrodynamic volume of a star polymer when compared with a linear polymer of the same molar mass. It is worth noting that no significant star-star coupling termination, which would lead to a shoulder peak at higher molecular weight was detected even after polymerization to full conversion overnight. This phenomenon is mainly attributed to the initially added Cu (II) which possibly aids in the preservation of high chain end fidelity.^{166,204}

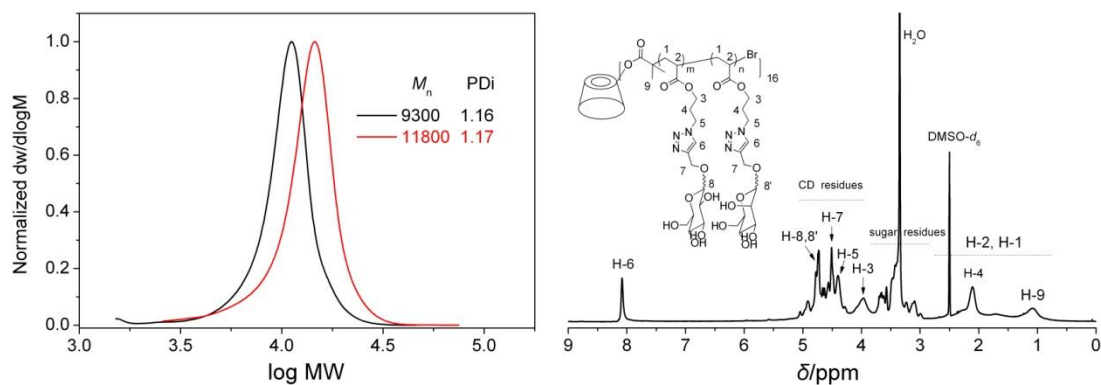


Figure 4. 16. DMF SEC molecular weight distributions (normalized to height, left; black trace: before chain extension; red trace: after chain extension) and ^1H NMR spectra (right) of the diblock CD-based glucose-mannose glycopolymer by SET-LRP.

For the chain extension ability test, another equivalence of mannose glycomonomer was directly added into the reaction mixture and allowed to polymerize for another 48 h. Following the reaction, ^1H NMR spectrum showed a conversion of 88% by comparing the integral of triazole proton area at 7.9-8.2 ppm with the vinyl groups at 5.9-6.4 ppm. SEC analysis revealed the increase of M_n to 11800 and M_w/M_n to 1.17 (Figure 4.16), which is still a quite narrow dispersity for such a multiarm star polymer. The elution traces almost shift totally and no coupling peaks were detected at this stage. ^1H NMR analysis of the final product showed broad resonance from the triazole protons at 8.1 ppm, overlapped CD and sugar units from 3 to 5 ppm and typical initiator methyl groups at 1.1 ppm, Figure 4.16, which supported the structure of CD-based star glycopolymer bearing sugar units with 1, 2, 3-triazole linker. All of the previous results clearly indicated that CD-based star glycopolymer with controlled structure and high chain end fidelity could be synthesized by SET-LRP.

This inspired us to prepare a library of β -CD-based mannose star glycopolymers as binding inhibitors between DC-SIGN and HIV gp120. Three polymerizations with target DP=2, 5, 10 were conducted and long reaction times were kept to give a high conversion. Under these reaction conditions, Table 4.1, polymerization with DP=2 could reach full conversion after 24 h, while conversion of polymerization with DP=5 and 10 only reached 86% and 96% after 48 h.

Table 4. 1. Polymerization data for CD-centered star glycopolymers via SET-LRP.

Target DP	β -CD-(Br) ₁₆ ^a (μ mol of Br)	Monomer (mmol)	Conversion ^b (24 h) / %	Conversion ^b (46 h) / %	M_w/M_n ^c (SEC)	M_n ^c (SEC) / Da	M_n ^d (Theory) / Da
2	170	0.33	100		1.07	10300	15500
5	68	0.33	75	86	1.11	13700	29200
10	68	0.67	87	96	1.17	20000	60800

^a Polymerization conditions: [Br]₀: [Me₆TREN]₀: [CuBr₂]₀ = 1 : 0.18 : 0.08 (mol/mol); Cu wire: length 1 cm / 0.08 mmol; DMSO: 3 mL; ^b calculated *via* ¹H NMR spectroscopy; ^c calculated *via* DMF SEC with RI detector and linear PMMA standard. ^d calculated according to conversion from ¹H NMR spectroscopy.

Sampling analysis of polymerization with DP=10 revealed that conversion already reached > 80% in the first 10 h (Figure 4.17), suggesting that with the monomer consumption, reaction rate decreased, mainly due to the highly diluted reaction condition.

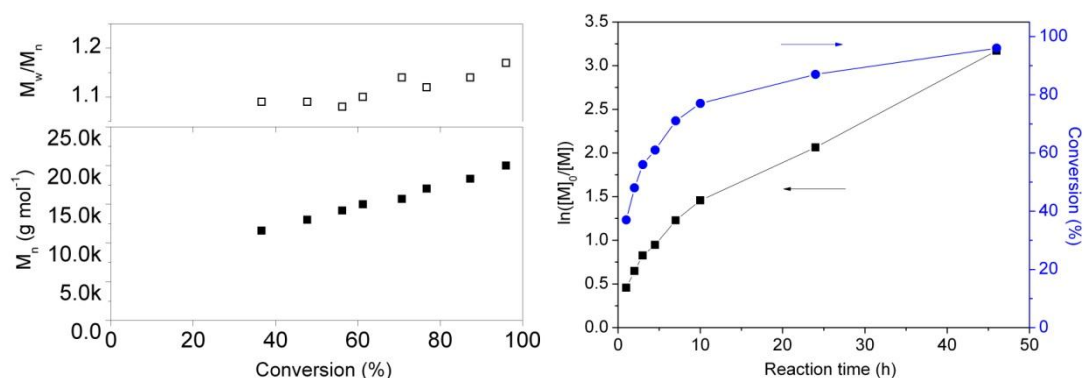


Figure 4. 17. Molecular weight and PDI vs conversion plots (left) and semi-logarithmic kinetic plots (right) for the SET-LRP of mannose glycomonomer from β -CD-(Br)₁₆.

SEC analysis revealed that narrow dispersity star glycopolymers with different chain length were prepared, Figure 4.18. The M_w/M_n is approximately 1.1 and the tailing peak in glycopolymer DP=10 may be caused by sampling during the polymerization, which may introduce air into the reaction system and cause some termination.

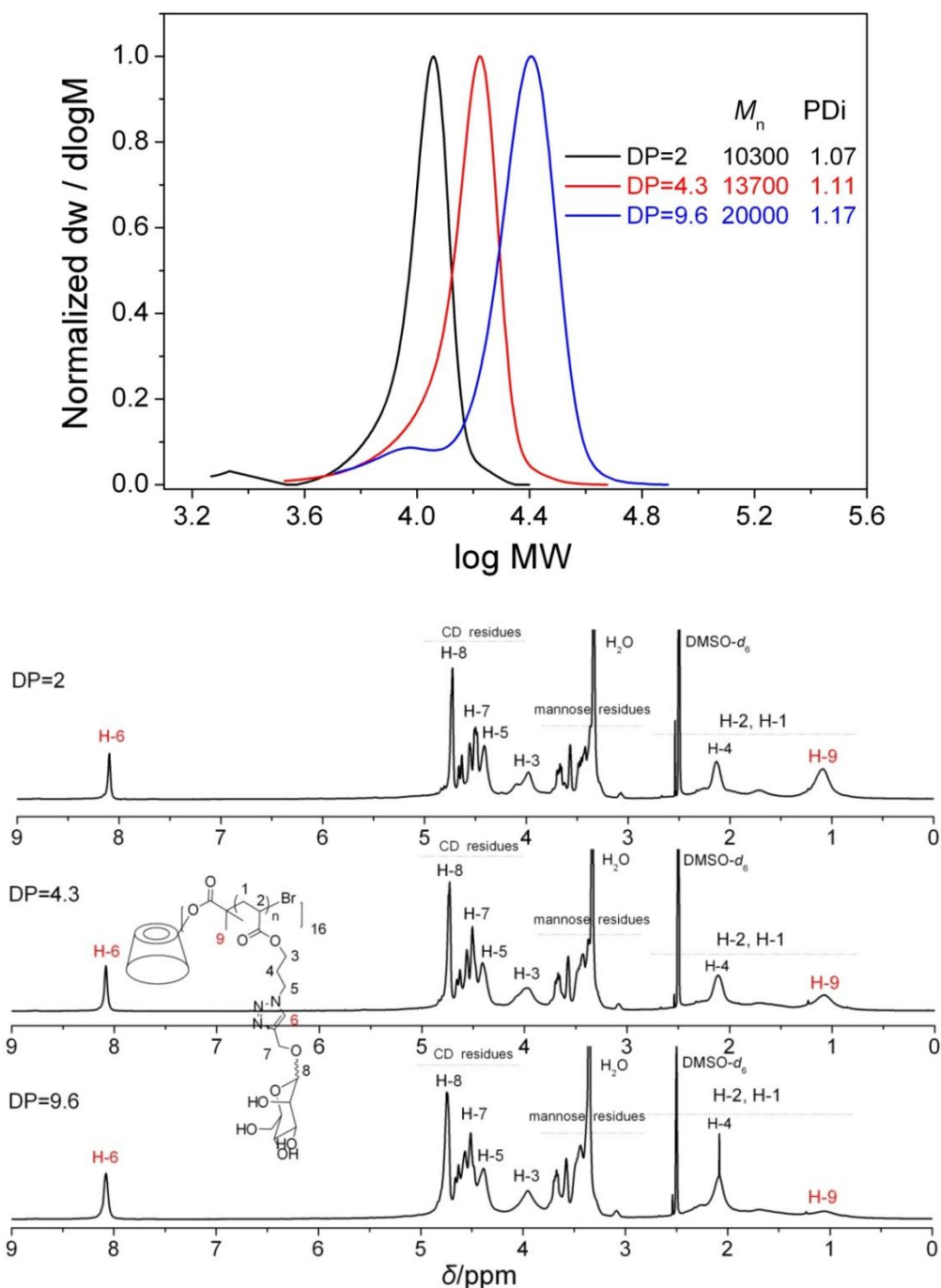


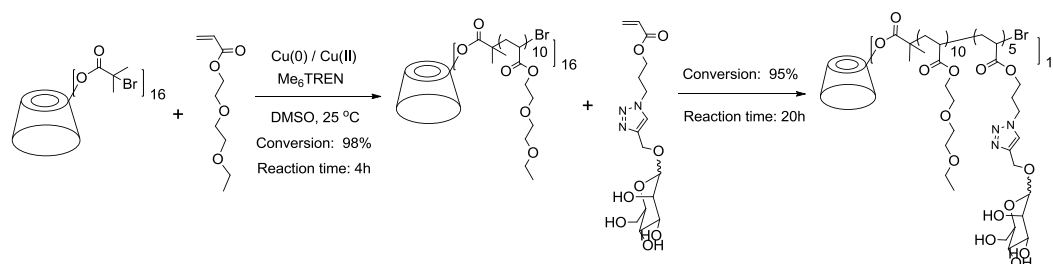
Figure 4. 18. DMF SEC molecular weight distributions (normalized to height, top) and ¹H NMR spectra (bottom) of CD-based mannose glycopolymers obtained by SET-LRP.

¹H NMR analysis (Figure 4.18) revealed the ratio decreased for the integral of initiator methyl groups (H-9) at 1.1 ppm relative to the triazole proton units at 8.1 ppm when the DP increased from 2 to 10, which showed the incorporation of more sugar units. Due to the overlap between initiator residues (H-9), polymer backbone protons (H-1, 2), monomer units (H-4) and DMSO-*d*₆, calculations from the

equivalence of $\int \text{H-6}^{7.9-8.3 \text{ ppm}} : \int \text{H-1, 2, 4, 9}^{0.7-2.5 \text{ ppm}} = \text{DP: (5DP+6)}$ leads to values of DP = 1.6, 3.0 and 8.5, which are close to the values of DP = 2, 4.3 and 9.6 according to the conversion. However, this still proved the successful synthesis of star glycopolymers with different chain lengths. Nevertheless, according to the previous results three β -CD-based mannose star glycopolymers with defined structures have been successfully prepared for the lectin binding tests.

4.2.5 Synthesis of cyclodextrin-based diblock glycopolymers

Water soluble star shaped polymers have been applied as useful polymeric nanocontainers with high loading capacity of hydrophobic drugs.^{201,202} With the synthesis of highly water soluble CD based star glycopolymers, the CD core became surrounded with dense sugar units at the outside shell, which would make the inclusion of drug molecular into CD host more difficult. To construct an intelligent drug delivery system with carbohydrate recognition sites at the outside sphere, hydrophobic core area was necessary to be built for drug loading through the host-guest interaction.



Scheme 4. 6. Synthesis of β -CD based diblock glycopolymer *via* SET-LRP of DEGEAA and one-pot chain extension reaction with glycomonomer.

A β -CD based diblock glycopolymer was synthesized by SET-LRP with a one-pot chain extension reaction. Polymerization of DEGEAA initiated from $\beta\text{-CD}(\text{Br})_{16}$ with the $\text{Cu(0)/Cu(II)/Me}_6\text{TREN}$ catalyst system in DMSO could reach almost full conversion (98% according to ^1H NMR) in 4 h, Scheme 4.6, after which a part of the solution was removed for characterization and another portion of mannose glyco monomer was directly added into the system for chain extension reaction without purification.

After reaction for further 20 h, conversion was up to 95% and the reaction was then stopped. SEC and NMR analysis confirmed the synthesis of $\beta\text{-CD}[(\text{DEGEAA})_{10}]_{16}$

and β -CD-[(DEGEEA)₁₀-*b*-(mannose)₅]₁₆ featuring narrow molecular weight distributions, Figure 4.19.

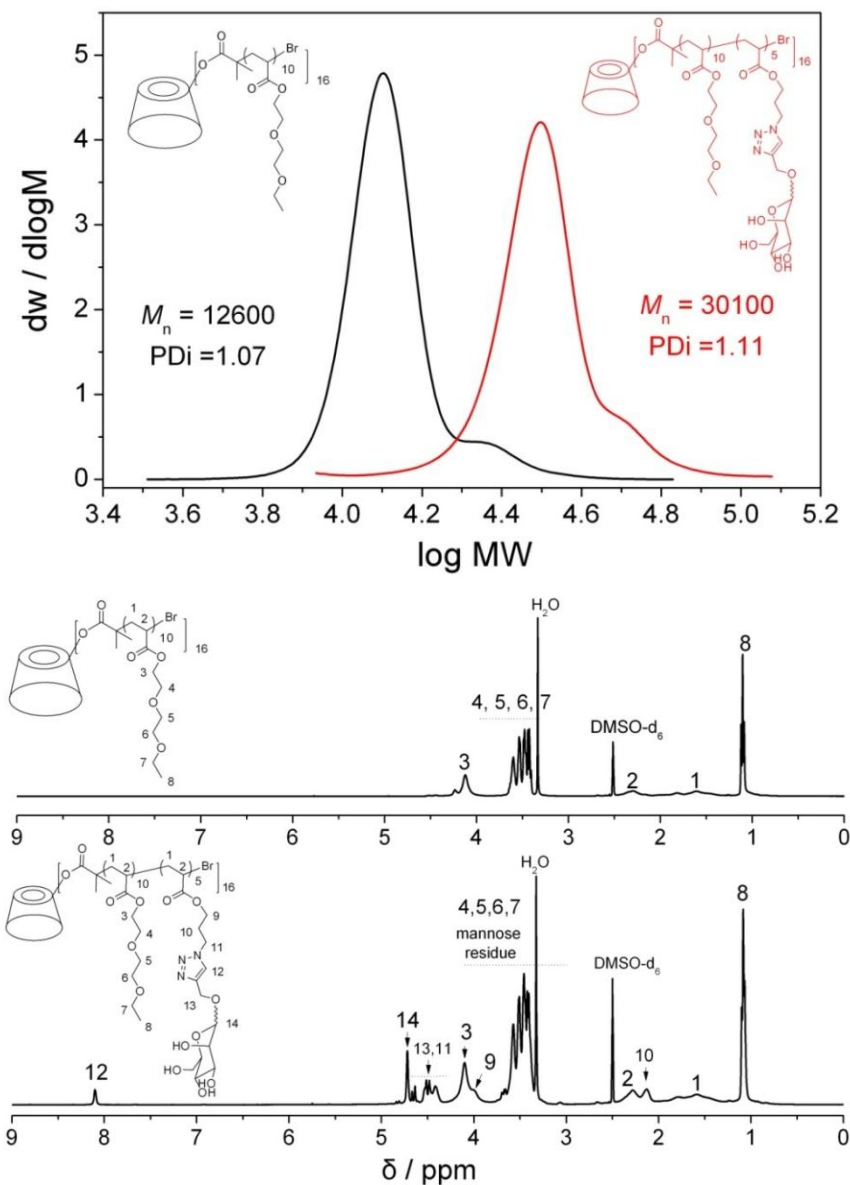


Figure 4. 19. DMF SEC molecular weight distributions (top) and ¹H NMR spectra (bottom) of CD-based diblock glycopolymer obtained by SET-LRP.

For the synthesis of the first block β -CD-[(DEGEEA)₁₀]₁₆, it is noted that the M_w/M_n is as low as 1.07 at almost full conversion, even when the small shoulder peak is included, which may be caused by the star-star coupling or diacrylate impurities in the DEGEEA monomer. Following this chain extension, the SEC elution trace almost shifted totally which revealed that high chain end fidelity was maintained during the polymerization. The M_n increased from 12600 to 30100 g·mol⁻¹ and the M_w/M_n had a slight increase from 1.07 to 1.11. Although the shoulder peak at higher molecular

weight region became more obvious after reaction overnight, the ratio relative to the main peak was still small.

^1H NMR analysis of the final product (Figure 4.19) showed resonances from mannose monomer units after chain extension, including triazole ring protons at 8.1 ppm and typical mannose protons at 3.0-5.0 ppm. FT-IR spectra (Figure 4.20) also revealed strong OH absorbance due to the addition of mannose units. All these data clearly proved the successful synthesis of diblock $\beta\text{-CD-}[(\text{DEGEEA})_{10}\text{-}b\text{-(mannose)}_5]_{16}$ glycopolymer.

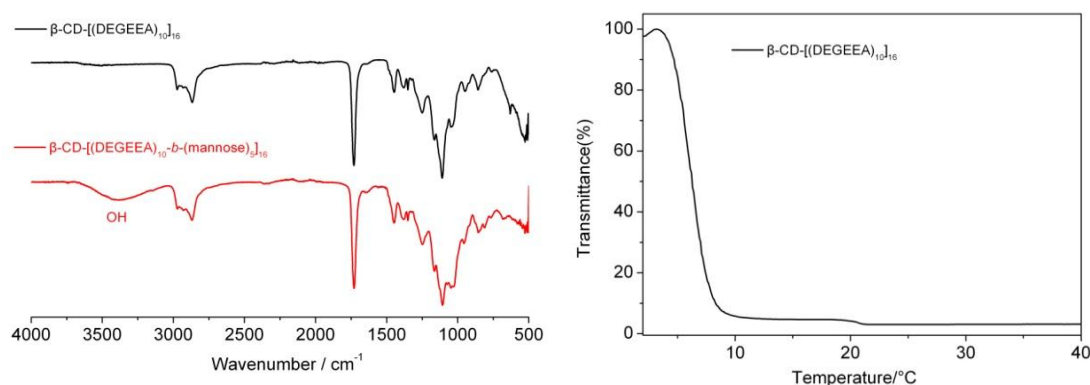
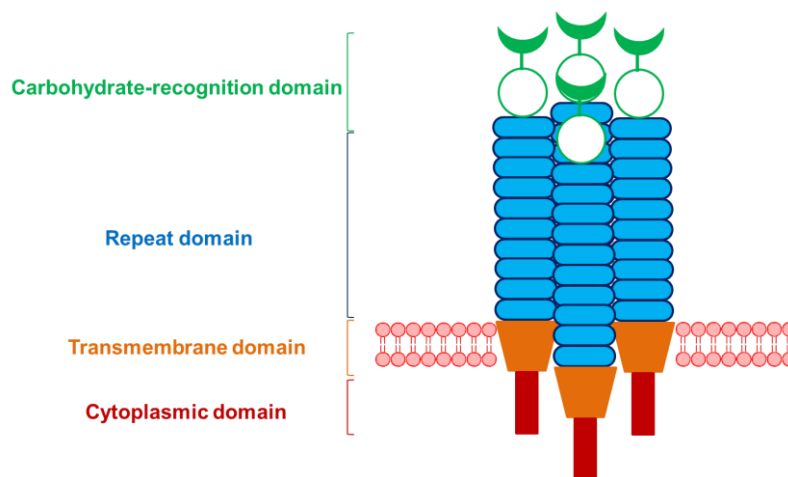
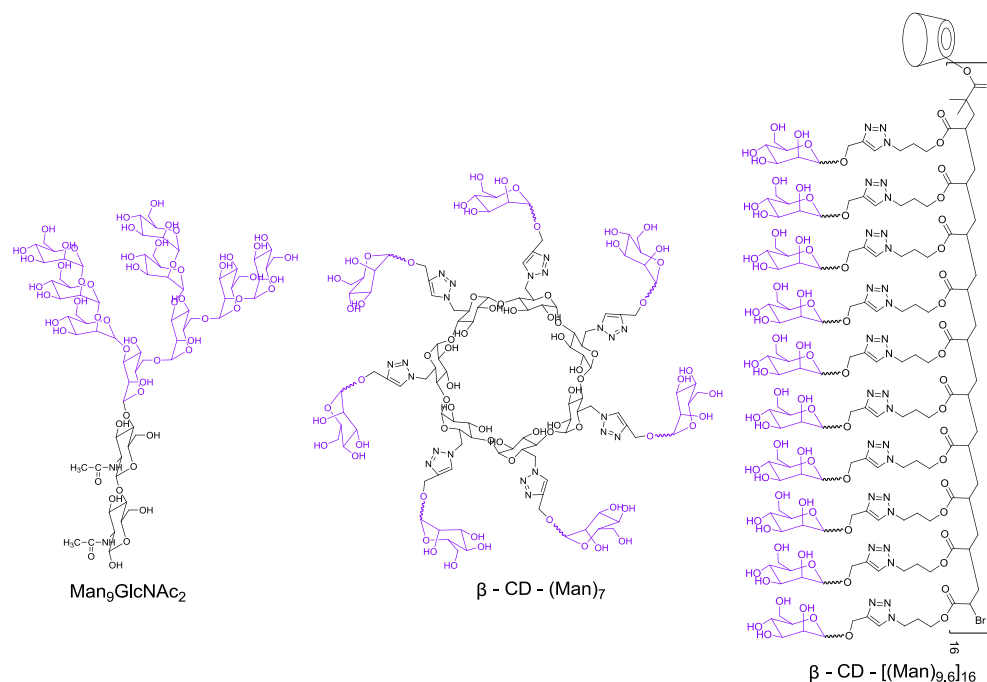


Figure 4. 20. FT-IR spectrum (left) of CD-based diblock glycopolymers obtained by SET-LRP and cloud point measurement (right) of $\beta\text{-CD-}[(\text{DEGEEA})_{10}]_{16}$ by UV/vis spectroscopy at 500nm and 1 mg/mL.

4.2.6 SPR binding test of CD-based glycoconjugates with DC-SIGN



Scheme 4. 7. Schematic structure of human DC-SIGN lectin.



Scheme 4. 8. Molecular structure of $\text{Man}_9\text{GlcNac}_2$, $\beta\text{-CD}-(\text{Man})_7$ and $\beta\text{-CD}-[(\text{Man})_{9,6}]_{16}$.

C-type (calcium dependent) animal lectins participates in many cell-surface carbohydrate-recognition events, in which Ca^{2+} proved to form a coordination bond with the carbohydrate ligand.²⁰⁵ As a typical C-type ligand, DC-SIGN is composed of a carbohydrate-recognition domain (CRD), connected with a neck repeat domain and tailed with a cytoplasmic domain and functions as a cluster structure, as shown in Scheme 4.7.²⁰⁶

The CRD is a tightly folded modular unit with a diameter of ~ 4 nm.^{207,208} It was suggested that the individual CRDs in the tetramers possess high affinity for mannose-containing oligosaccharides by binding with the mannose spaced at appropriate distances.¹⁷⁴ The repeat domain is seven and a half tandem repeat units of 23 amino acids with a length of $\sim 20\text{-}30$ nm.²⁰⁸ Although this neck region did not contain any carbohydrate-recognition units, it plays important role in stabilizing the tetramer nanocluster of DC-SIGN, enabling the formation of multibinding sites and increases ligand-binding avidity.²⁰⁶

In previous research, $\text{Man}_9\text{GlcNac}_2$ (Scheme 4.8) has been widely used as a model oligosaccharide for the binding with CRDs of DC-SIGN, in which it showed 130-fold increase relative to the binding of a single mannose.^{174,208,209} Compared with dendritic $\text{Man}_9\text{GlcNac}_2$, $\beta\text{-CD}-(\text{Man})_7$ also has a cluster structure; notably, with different linker

length and space for the terminal mannose. β -CD-(Man)₇ even under high concentration showed weak binding during the concentration test, Figure 4.20 & 4.23. Under competition test (Figure 4.21 & 4.24), the binding of gp120 with DC-SIGN was inhibited only ~ 12% in the existence of 4096 nM β -CD-(Man)₇. Thus the limited number of mannose units, crowded structure and short linker length between mannose units and β -CD may be not a proper structure for each mannose to reach the binding sites.

However, for the CD-based star glycopolymer, even with only DP=2, the binding affinity with DC-SIGN is much higher than that of the CD-based glycocluster. The total mannose units were increased to ~32, about 4-5-fold than the β -CD-(Man)₇. It is noted that for each chain of the star glycopolymer, average DP=2 means that each chain should contain 1, 2, 3, 4 et al mannose units, which makes it more like the structure of Man₉GlcNac₂ (Scheme 4.8) and thus we see a much better binding effect.

With an increase of DP to ~4, the concentration test showed higher RiU value when compared with DP=2; however, the IC₅₀ value only decreased slightly from 436 nM to 389 nM (Figure 4.21 & 4.24), suggesting that the slight increase in DP did not affect the binding too much.

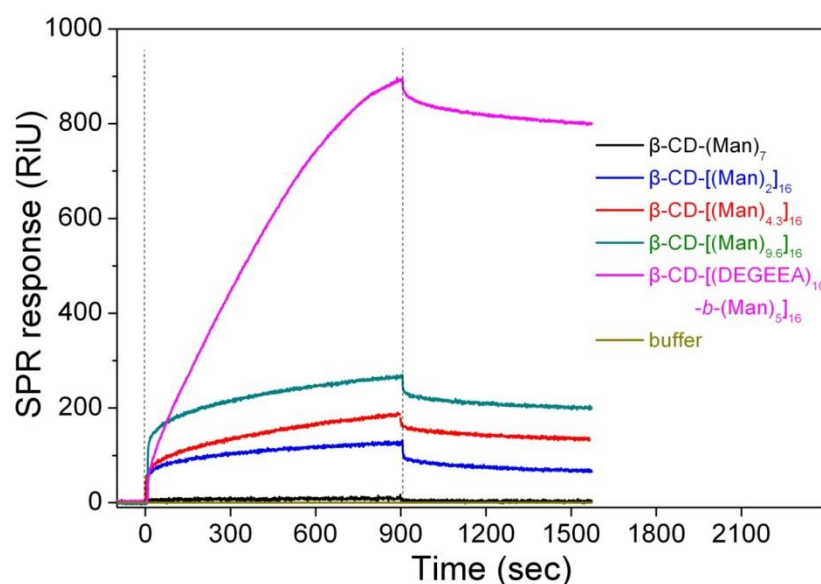


Figure 4. 21. SPR sensorgrams showing the binding of β -CD based glycol conjugates onto DC-SIGN functionalized surfaces. The concentration for β -CD based glycol conjugates was 4096 nM.

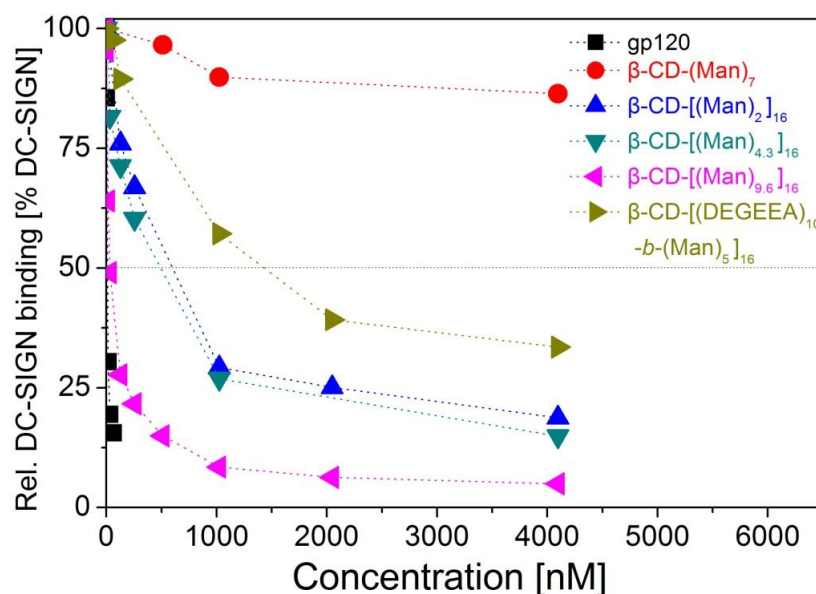


Figure 4. 22. Competition experiments on gp120 functionalized surface between DC-SIGN and β -CD based glycol conjugates at a concentration range of 0-4096 nM for glycol conjugates and 4 nM DC-SIGN.

With an increase of DP to ~ 10 , the concentration test showed an increasing RiU value relative to both DP=2 and 4. In the competition test, β -CD-[(Man)_{9.6}]₁₆ showed unpredictable IC₅₀ values as low as ~ 30 nM, which is only slightly higher than that of gp120 (~ 11 nM) under same test conditions. This dramatic difference indicates that the linker length and spacer is very important for binding with DC-SIGN. It also reveals that there should be multiple binding sites on the DC-SIGN CRDs and tandem mannose units in a cluster structure with enough density are necessary to increase the chance to block all the binding sites.

Interestingly, the block star polymer β -CD-[(DEGEEA)₁₀-b-(mannose)₅]₁₆, which bears a similar number of mannose units as β -CD-[(Man)_{4.3}]₁₆, it showed higher IC₅₀ value (~ 1420 nM), Figure 4.21. With the addition of the poly(DEGEEA) core, the space of the mannose units between each chain should become bigger, which may not favour the binding.

In summary, the above SPR experiments demonstrated the high affinity for the binding of CD-based conjugates between DC-SIGN. The low IC₅₀ value of β -CD-[(Man)_{9.6}]₁₆ to inhibit the binding of gp120 to DC-SIGN is as low as ~ 30 nM, suggesting the potential application in HIV therapeutic.

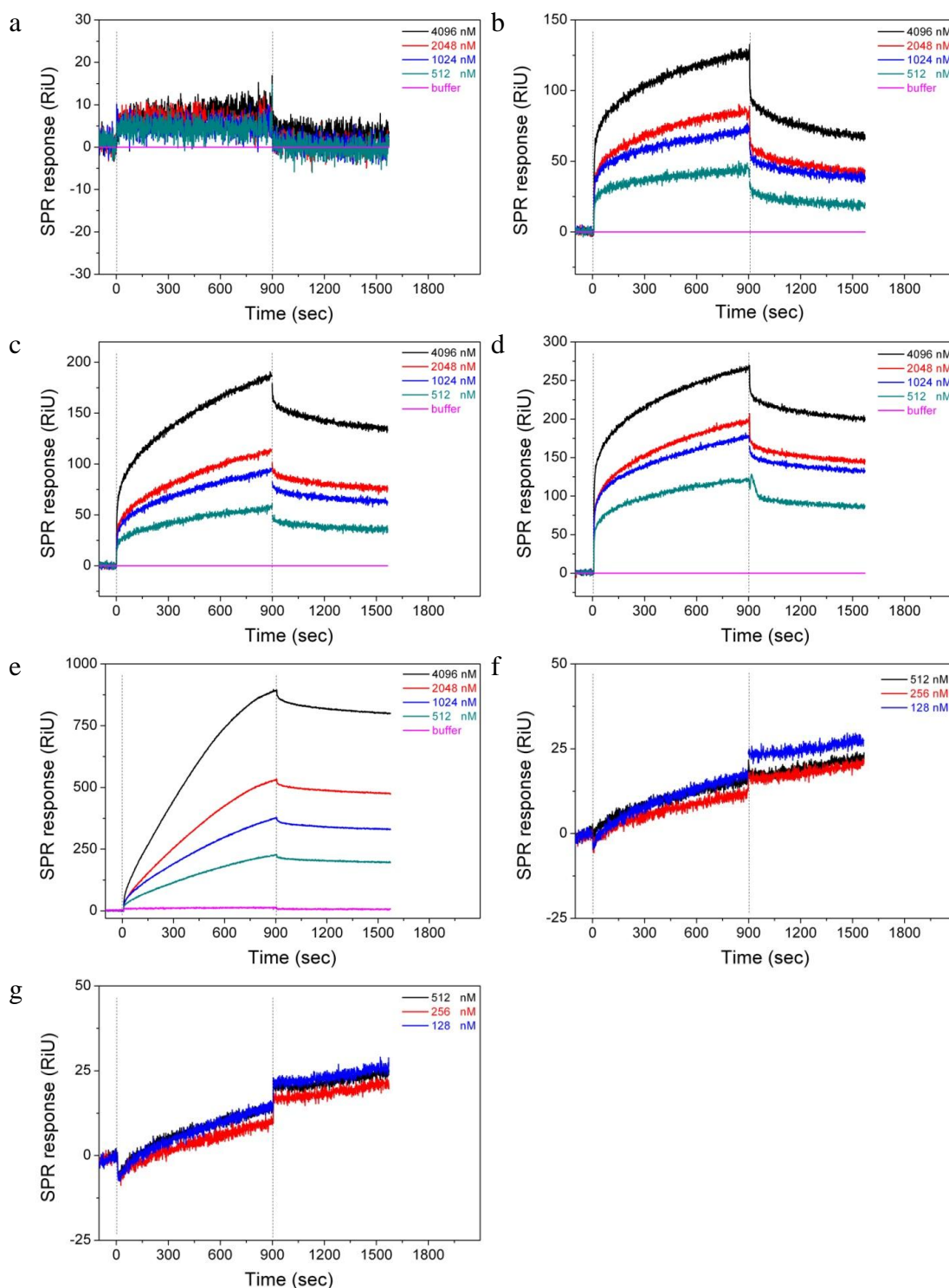


Figure 4. 23. SPR sensorgrams showing the binding of β -CD-(Man)₇ (a), β -CD-[(Mannose)₂]₁₆ (b), β -CD-[(Mannose)_{4,3}]₁₆ (c), β -CD-[(Mannose)_{9,6}]₁₆ (d), β -CD-[(DEGEEA)₁₀-b-(Mannose)₅]₁₆ (e), β -CD-(Fuc)₇ (f) and (Man)₇- β -CD-(PNIPAM)₁₀ (g) onto DC-SIGN functionalized surfaces. The concentration ranges for all the glycoconjugates were 128-4096 nM. Characterization of sample f and g was performed by Dr Remzi Becer.

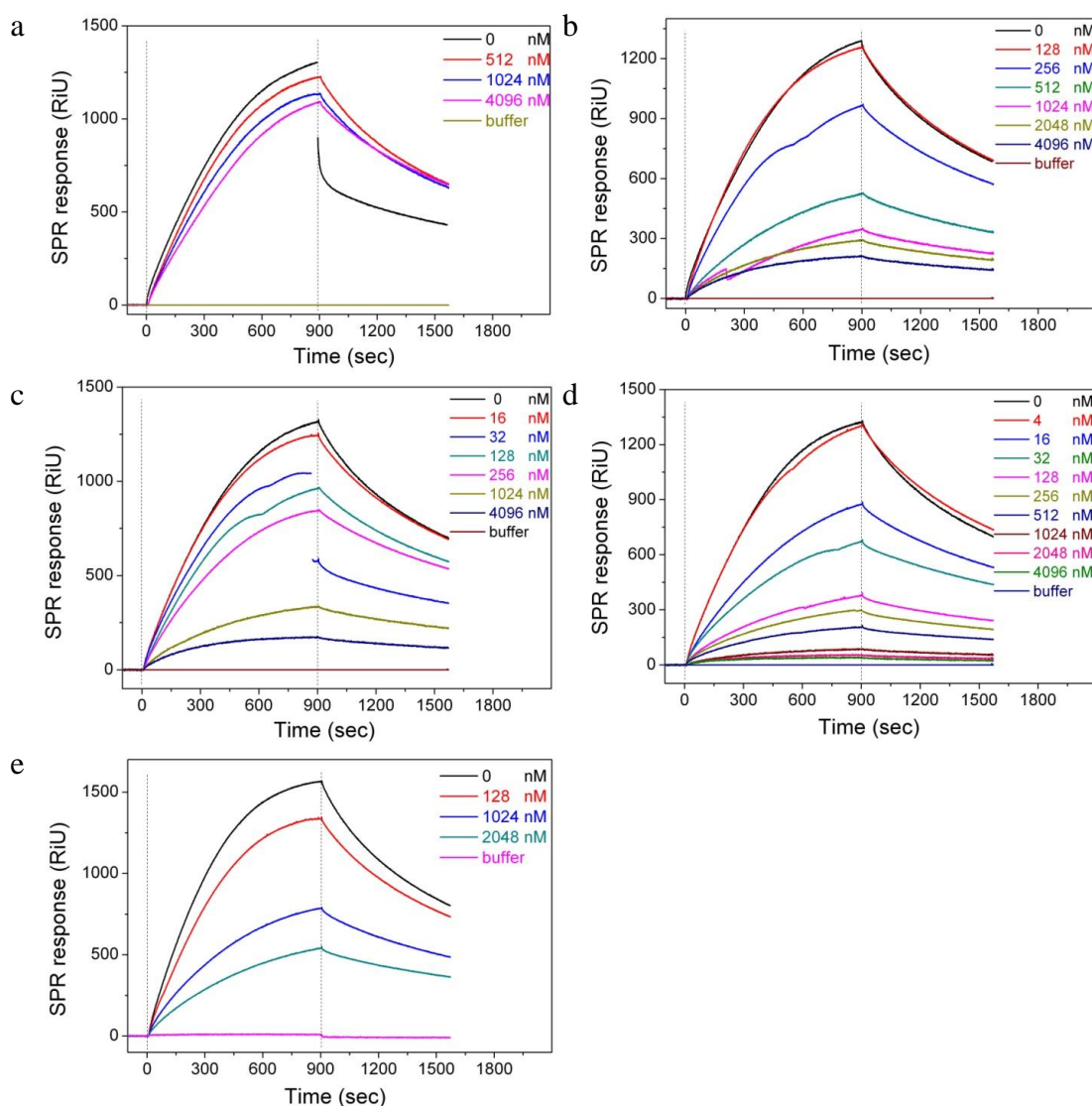


Figure 4. 24. Competition experiments on gp120 functionalized surface between DC-SIGN and β -CD-(*Man*)₇ (a), β -CD-[(*Mannose*)₂]₁₆ (b), β -CD-[(*Mannose*)_{4.3}]₁₆ (c), β -CD-[(*Mannose*)_{9.6}]₁₆ (d) and β -CD-[(*DEGEEA*)₁₀-*b*-(*Mannose*)₅]₁₆ (e). The concentration ranges for all the glycoconjugates were 4-4096 nM and 4 nM for the DC-SIGN.

4.2.7 Encapsulation ability of the CD-based glycoconjugates

Molecular encapsulation behaviours of the obtained cyclodextrin-based glycoconjugates were first characterized by UV-Vis spectroscopy using 1,4-dihydroxyanthraquinone (DHA) as guest molecule, which is considered as a potential anticancer chemotherapeutic agent.²¹⁰ DHA has been chosen as a model compound for CD encapsulation test since this hydrophobic drug possesses sensitive UV-Vis absorbance.²¹¹

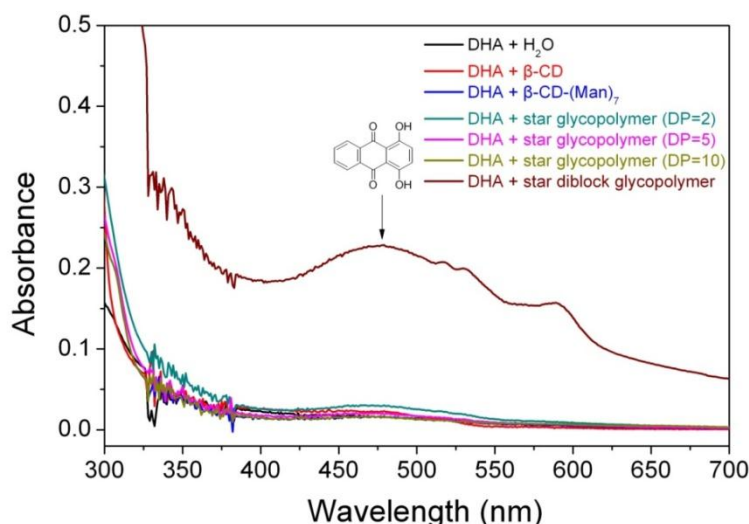


Figure 4. 25. UV-Vis spectra of DHA solution in the presence of different cyclodextrin products. All measurements with β -CD, β -CD-(Man)₇ and glycopolymers were performed at a concentration of 1 mg/mL.

Due to the poor solubility in water, only very weak absorbance could be detected for DHA in water without addition of CD conjugates. After addition of β -CD, β -CD-(Man)₇, β -CD-[(Man)₂]₁₆, β -CD-[(Man)_{4.3}]₁₆ and β -CD-[(Man)_{9.6}]₁₆, the absorbance is still at the same level and no significant increase could be detected, which revealed that no stable inclusion could be formed between DHA and β -CD, β -CD-(Man)₇ and β -CD-based homo glycopolymers. Upon addition of DHA to the aqueous solution of β -CD-[(DEGEEA)₁₀-*b*-(Mannose)₅]₁₆, the absorption at 479 nm (λ_{max}) significantly increased (Figure 4.25), indicating the encapsulation and solubilisation of DHA by the diblock copolymer. The homo β -CD-[(DEGEEA)₁₀]₁₆ exhibited a LCST = 6.2 °C (Figure 4.20), after attachment to the glycopolymer the LCST phenomenon disappeared between 0-80 °C. Thus it is assumed that the core of β -CD-[(DEGEEA)₁₀-*b*-(Mannose)₅]₁₆ acted as a hydrophobic area at ambient temperature in aqueous solution and could encapsulate hydrophobic molecule based on the host-guest interaction. Due to the larger hydrophobic core area compared with β -CD, β -CD-based glycocluster and homo glycopolymers, the star block copolymer could encapsulate more guest molecules and thus showed more significant absorbance in UV-Vis spectroscopy.

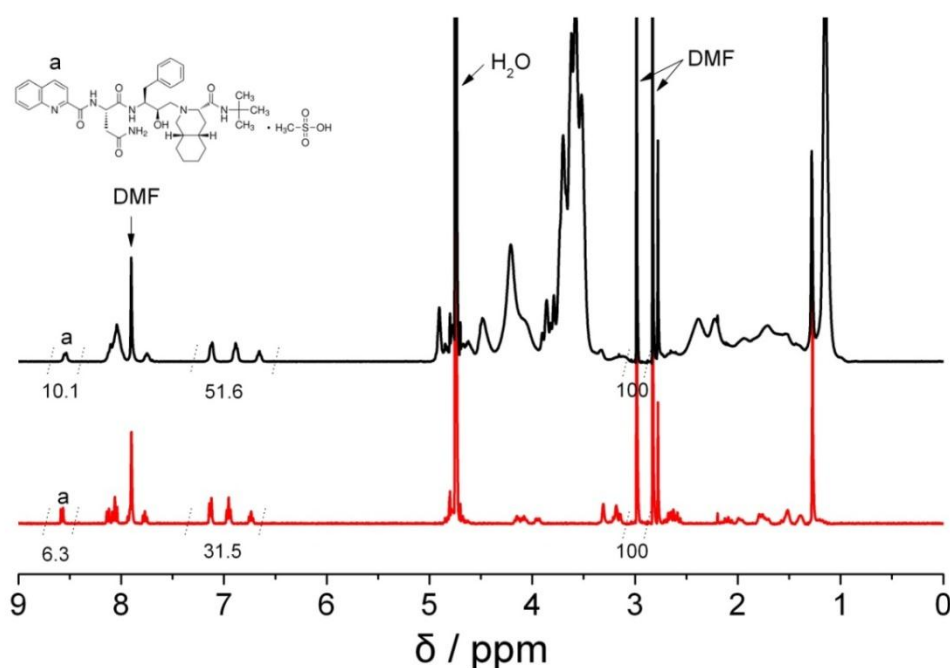


Figure 4. 26. ^1H NMR spectra of saquinavir mesylate (bottom) and of saquinavir mesylate encapsulated into polymer $\beta\text{-CD-}[(\text{DEGEEA})_{10}\text{-}b\text{-(Mannose)}_5]_{16}$ (top). Both measurements were performed in D_2O with 10 mM DMF as an internal standard.

Table 4. 2. Properties of saquinavir mesylate encapsulation test from CD-based glycoconjugates.

Sample name	[CD glycoconjugate] $_0$ ^a (mM)	[saquinavir mesylate] $_0$ ^b (mM)
D_2O	/	1.9
$\beta\text{-CD}$	16	4.0
$\beta\text{-CD-(Man)}_7$	1.0	2.3
$\beta\text{-CD-}[(\text{Man})_2]_{16}$	0.3	2.0
$\beta\text{-CD-}[(\text{Man})_{4.3}]_{16}$	0.3	2.1
$\beta\text{-CD-}[(\text{Man})_{9.6}]_{16}$	0.3	2.0
$\beta\text{-CD-}[(\text{DEGEEA})_{10}\text{-}b\text{-(Man)}_5]_{16}$	0.3	3.0

^a Concentrations of CD or CD-based conjugates were calculated from [mass]/[molecular weight]. The molecular weights of glycopolymer were theoretical value based on conversion from ^1H NMR. ^b Solubility of saquinavir mesylate was determined by ^1H NMR using DMF (10 mM) as internal standard.

This motivated us to investigate if this system could be applied in anti-HIV drug delivery. Saquinavir is an important class of archetypal HIV protease inhibitor, however, its poor aqueous solubility results in low and variable bioavailability.²¹² $\beta\text{-CD}$ derivatives have been applied to enhance the aqueous solubility of saquinavir base

and mesylate salt.²¹² Thus saquinavir mesylate was also used as guest molecules to test the encapsulation ability of CD-based glycoconjugates by NMR.

For the quantitative evaluation of the encapsulated drug by ^1H NMR spectroscopy, several solutions of CD-based glycoconjugates were prepared in D_2O , with excess of the guest saquinavir mesylate and DMF as internal standard (10 mM).

Firstly, a control measurement was performed in order to detect the intrinsic water solubility of drug (C_i) in the absence of glycoconjugates, which revealed a water solubility of saquinavir mesylate of $C_i = 1.9$ mM (Figure 4.26). With the addition of β -CD and β -CD-(Man)₇, the solubility of saquinavir mesylate was also increased, suggesting that inclusion of CD host with saquinavir mesylate could be obtained. Following the addition of β -CD-based homo glycopolymer, the solubility of saquinavir mesylate was almost at the same level, indicating that larger hydrophobic core area was needed in order to increase the solubility even with low concentrations of polymer.

Following the addition of block copolymer the peaks integral of saquinavir mesylate clearly increased compared with the DMF standard, indicating that the solubility of saquinavir mesylate could be increased due to the encapsulation of star block copolymer, Figure 4.26. The solubility of saquinavir mesylate increased to 3.0 mM as calculated from the ratio of the integrated DMF signal with the characteristic peaks of guest molecule, Table 4.2. Followed by a subtraction of the intrinsic concentration in water, the encapsulated drug concentration was calculated as 1.1 mM. The maximum loading capacity of the block copolymer was then determined as ~4 by dividing the mole ratio of drug with the mole ratio of polymer, which means that each star block copolymer can encapsulate up to 4 saquinavir mesylate molecule on average.

In summary, all of these results show that CD-based glycoconjugates, and especially the star block copolymer, could be potentially used as universal anti-cancer and anti-HIV drug carriers.

4.2.8 Conclusion

Cyclodextrin-based mannose and fucose clusters were synthesized *via* the CuAAC reaction of azide-functionalised CD with relative alkyne sugar following precipitation in methanol without the need of protection chemistry and column chromatography purification. Different glycocluster-smart star polymer hybrids were then synthesised *via* combination of ATRP and CuAAC. For the design of high affinity lectin-glycoprotein binding inhibitor, star-shaped glycopolymers containing cyclodextrin core and oligosaccharide chains were synthesized by direct SET-LRP of glycomonomers from CD-based initiator, which also allowed facile synthesis of diblock glycopolymer *via* in-situ monomer addition.

SPR analysis revealed that these glycoconjugates have high affinity in binding with human DC-SIGN lectin and could be used as inhibitor to prevent the binding of HIV envelope protein gp120 to DC-SIGN at nanomolar concentration. From different binding phenomenon of glycoclusters and star glycopolymers with varying DP, it can be concluded that sugar density, linker length and space between sugars contribute much in the binding with cluster CRDs of DC-SIGN.

Encapsulation test of these glycoconjugates *via* UV/Vis and NMR revealed that star diblock glycopolymer bearing a hydrophobic core area showed high loading capacity of hydrophobic anti-cancer and anti-HIV drugs, indicating promising application in HIV-therapeutic and smart drug delivery.

4.3 Experimental

4.3.1 Materials

β -Cyclodextrin (β -CD, 97%, Sigma-Aldrich) was recrystallized twice from water and dried in a vacuum oven at 100 °C for two days prior to use. Di (ethylene glycol) ethyl ether acrylate (DEGEEA, $\geq 90\%$) was obtained from Sigma-Aldrich and the inhibitor was removed by passing the monomer through a column filled with activated basic aluminium prior to use. Copper (I) Bromide (98%, Sigma-Aldrich) was washed sequentially with acetic acid and ethanol and dried under vacuum. Copper wire (diameter=0.25 mm) was activated by washing in hydrochloric acid for 15 min and rinsed thoroughly with MiliQ water and dried under nitrogen. The copper wire was used immediately. 1-(2'-propargyl) D-mannose¹²³, 1-(2'-propargyl) L-fucose¹²³ and

the mannose and glucose acrylate glycomonomers¹⁷⁶ were synthesised as in a previous report. Sodium methoxide (5.4 M in methanol), α -bromoisobutyryl bromide (BIBB, 98%, Sigma-Aldrich), triphenyl phosphine (Ph_3P , 98.5%, Sigma-Aldrich), *N*-bromosuccinimide (NBS, 99%, Sigma-Aldrich), 2, 2'-bipyridyl (bpy, 99%, Sigma-Aldrich), (+)-sodium L-ascorbate (98%, Sigma-Aldrich), saquinavir mesylate (98%, Sigma-Aldrich) and 1, 4-dihydroxyanthraquinone (DHA, 98%, Sigma-Aldrich) were used as received.

4.3.2 Instruments and analysis

SEC in this work was conducted on a Varian 390-LC system in DMF (1 g/L LiBr) at 50 °C, equipped with refractive index and viscometry detectors, 2 \times PLgel 5 mm mixed-D columns (300 \times 7.5 mm), 1 \times PLgel 5 mm guard column (50 \times 7.5 mm) and autosampler.

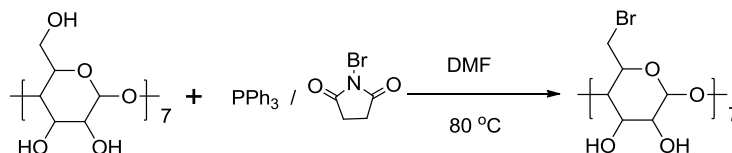
MALDI-ToF MS was recorded in linear or reflex mode on a Bruker Daltonics Ultraflex II MALDI-ToF mass spectrometer, equipped with a nitrogen laser delivering 2 ns laser pulses at 337 nm with positive ion ToF detection performed using an accelerating voltage of 25 kV. The matrix solution was prepared by dissolving α -cyano-4-hydroxycinnamic acid (CHCA) or *trans*-2-[3-(4-*tert*-butylphenyl)-2-methyl-2 propenylidene] malononitrile (DCTB) in THF (10 mg/mL solution). Sodium iodide was added at a 0.1% overall concentration to improve the ionization. CDs or polymer analytes were dissolved to a concentration of 1 mg/mL. Samples were prepared by layering matrix solution and analyte solution on the stainless steel side. Calibration was performed with different linear poly (ethylene glycol) methyl ether standards.

UV-vis spectroscopy measurement was performed on a PerkinElmer Lambda 35 UV-VIS spectrometer. The transmittance of the solution at a concentration of 1 mg/mL was measured at $\lambda=500$ nm through 10 mm path length cuvettes with a micro-stir bar and total volumes = 2 mL.

SPR Sensorgrams were recorded in a Biorad ProteOn XPR36 SPR biosensor (Biorad, Hercules CA). Soluble DC-SIGN and gp120 were immobilized to 6000 response units (RU) on discrete channels within Biorad GMC sensor chips via amine coupling. Soluble-phase analytes were prepared in 25 mM HEPES pH 7.4, 150 mM NaCl, 5 mM CaCl_2 , 0.01% Tween-20 and flowed over the immobilized materials at a rate of 25 $\mu\text{L}/\text{min}$ at 25°C. Regeneration of the sensor chip surfaces was performed using 10

mM glycine pH 2.5. Datasets were exported to BIAcore BIAevaluation software for kinetic calculations. Kinetic parameters were obtained by fitting curves to a 1:1 Langmuir model with correction for baseline drift where necessary. Competition assays were evaluated using Origin software.

4.3.3 Synthesis of *Heptakis* (6-deoxy-6-bromine)- β -cyclodextrin (β -CD-(Br)₇)



Scheme 4. 9. Schematic representation of the synthetic approach to β -CD-(Br)₇.

β -CD-(Br)₇ was prepared via a modification of procedures reported by Defaye *et al.*¹⁹⁸

Ph₃P (7.35 g, 28 mmol) was dissolved in anhydrous DMF (30 mL) under stirring and cooled to 0 °C. NBS (4.99 g, 28 mmol) dissolved in anhydrous DMF (10 mL) was added dropwise to the Ph₃P solution under N₂ atmosphere and then stirred at ambient temperature for 30 min. To a solution of anhydrous β -CD (2.27 g, 2 mmol) in anhydrous DMF (30 mL), the obtained Ph₃P/NBS solution was added dropwise at ambient temperature. The solution temperature was increased to 80 °C after the addition was completed. The mixed brown solution was stirred under N₂ atmosphere for 5 h at 80 °C. After completion (TLC, 7:7:5:4 EtOAc-2-propanol-25% aq NH₄Cl-water), methanol (5 mL) was added at ambient temperature and stirring was continued for 30 min. The reaction mixture was then cooled to -15 °C and the pH was adjusted to 9 with sodium methoxide, while stirring for further 1 h. The reaction mixture was then poured into stirred ice-water (1 L) resulting the formation of a precipitate which was filtered and washed with MeOH. β -CD-(Br)₇ (3.02 g, 95.8%; $M_{n,SEC}$ = 1.4 KDa, M_w/M_n = 1.05) was obtained as white solids and dried under vacuum for 1 day.

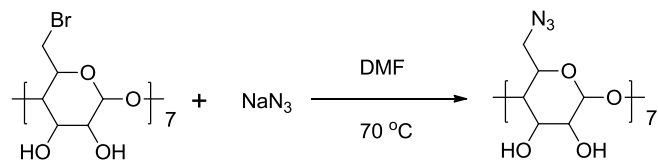
¹H NMR (DMSO-*d*₆, 298 K, 400 MHz): δ (ppm) = 6.03 (d, *J* = 6.7 Hz, 7 H, OH-2), 5.90 (d, *J* = 1.5 Hz, 7 H, OH-2), 4.98 (d, *J* = 3.4 Hz, 7 H, H-1), 4.01 (d, *J* = 9.8 Hz, 7 H, H-6a), 3.82 (t, *J* = 9.0 Hz, 7 H, H-5), 3.54-3.74 (m, 14 H, H-3, H-6b), 3.24-3.46 (m, 14 H, H-2, H-4, overlap with H₂O).

¹³C NMR (DMSO-*d*₆, 298 K, 400 MHz): δ (ppm) = 102.1 (C-1), 84.6 (C-4), 72.3 (C-3), 72.1 (C-2), 71.0 (C-5), 34.4 (C-6).

FT-IR ν (cm^{-1}): 3334(OH); 2916 (CH) cm^{-1} .

MALDI-ToF MS m/z : calcd for $\text{C}_{42}\text{H}_{63}\text{Br}_7\text{O}_{28}$ ($\text{M}+\text{Na}^+$), 1596.8; found, 1596.9.

4.3.4 Synthesis of *Heptakis*-(6-deoxy-6-azido)- β -cyclodextrin (β -CD-(N_3)₇)



Scheme 4. 10. Schematic representation of the synthetic approach to β -CD-(N_3)₇.

β -CD-(Br)₇ (4.73 g, 3 mmol) was dissolved in anhydrous DMF (40 ml) and NaN_3 (2.73 g, 42 mmol) was added. The resulting suspension was stirred at 70 °C under N_2 atmosphere for 24h. The suspension was then concentrated under reduced pressure before precipitation into large excess of water. The precipitate was filtered and washed with water. The obtained white powder (3.51g, 90%; $M_{n,\text{SEC}} = 1.7$ KDa, $M_w/M_n = 1.06$) was dried under vacuum at ambient temperature for 24 h.

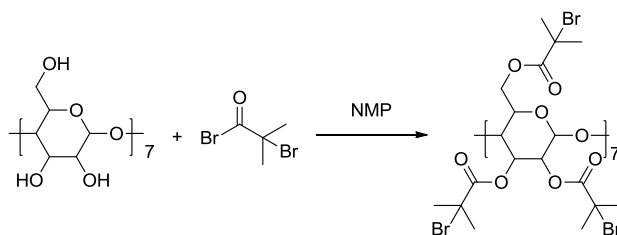
^1H NMR ($\text{DMSO}-d_6$, 298 K, 400 MHz): δ (ppm) = 5.89 (d, $J=6.8$ Hz, 7 H, OH-2), 5.75 (d, $J=1.7$ Hz, 7 H, OH-3), 4.91(d, $J=3.3$ Hz, 7 H, H-1), 3.67-3.86 (m, 14 H, H-6a, H-5), 3.50-3.66 (m, 14 H, H-3, H-6b), 3.26-3.44 (m, 14 H, H-2, H-4, overlap with H_2O).

^{13}C NMR ($\text{DMSO}-d_6$, 298 K, 400MHz): δ (ppm) = 102.1 (C-1), 83.2 (C-4), 72.6 (C-3), 72.0(C-2), 70.3(C-5), 51.3 (C-6).

FT-IR $\nu(\text{cm}^{-1})$: 3334(OH); 2922 (CH); 2098 (N_3) cm^{-1} .

MALDI-ToF MS m/z : calcd for $\text{C}_{42}\text{H}_{63}\text{N}_{21}\text{O}_{28}$ ($\text{M}+\text{Na}^+$), 1332.4; found, 1332.7.

4.3.5 Synthesis of Hepkis-(2, 3, 6-tri-O-(2-bromo-2-methylpropionyl)- β -cyclodextrin (β -CD-(Br)₁₆)



Scheme 4. 11. Schematic representation of the synthetic approach to β -CD-(Br)₁₆.

The cyclodextrin-centred initiator was synthesized *via* the esterification reaction of β -CD with BIBB in 1-methyl-2-pyrrolidone (NMP) according to a previous report.¹⁹⁹ Anhydrous β -CD (3.41 g, 3 mmol) was dissolved in 30 mL anhydrous NMP and was cooled to 0 °C. BIBB (29.0 mL, 235 mmol) dissolved in anhydrous NMP (15 mL) at 0 °C was then added dropwise to the β -CD solution with magnetic stirring. The reaction temperature was maintained at 0 °C for 2h and then was allowed to rise slowly to ambient temperature after which the reaction was allowed to continue for another 56 h. The brown solution was then concentrated under vacuum for 16 h. The obtained syrup was diluted with 100 mL dichloromethane and subsequently washed sequentially with saturated NaHCO₃ aqueous solution (2×100 mL) and water (2×100 mL). The dichloromethane was removed by rotary evaporator and the syrup obtained was diluted with 10 mL acetone and then poured into 1 L water to obtain a precipitate. The product was purified by repeating the precipitation procedure for three times. Fine white powder was obtained after drying under vacuum (8.75 g, yield: 68.5%).

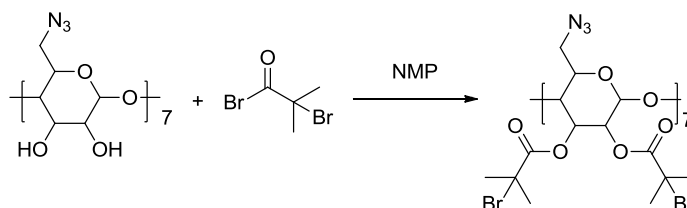
¹H NMR (CDCl₃, 298 K, 400 MHz): δ (ppm) = 5.15-5.35 (m, 7 H, H-1), 4.72-4.95 (m, 7 H, H-5), 4.45-4.68 (m, 7 H, H-6_a), 4.25-4.40 (m, 7 H, H-6_b), 3.90-4.24 (m, 14 H, H-2, 3), 3.65-3.85 (m, 7 H, H-4), 5.15-5.35 (broad s, 102 H, CH₃).

¹³C NMR (CDCl₃, 298 K, 400MHz): δ (ppm) = 171.2, 171.0 (C=O), 98.45 (C-1), 80.4 (C-4), 74.3 (C-5), 70.5 (C-3), 69.7 (C-2), 63.8 (C-6), 56.1 (C-Br), 30.7-31.2 (CH₃).

FT-IR ν (cm⁻¹): 2976, 2931 (CH); 1738(C=O) cm⁻¹.

MALDI-ToF MS m/z : calcd for C₁₀₆H₁₅₀Br₁₆O₅₁ (M+Na⁺), 3539.60; found, 3539.12; calcd for C₁₀₂H₁₄₅Br₁₅O₅₀, 3391.64; found, 3391.04; calcd for C₉₈H₁₄₀Br₁₄O₄₉, 3243.69; found, 3243.04.

4.3.6 Synthesis of Heptkis-(2, 3-di-O-(2-bromo-2-methylpropionyl)-6-azido)- β -cyclodextrin ((N₃)₇- β -CD-(Br)₁₀)



Scheme 4. 12. Schematic representation of the synthetic approach to (N₃)₇- β -CD-(Br)₁₀.

In one 250 ml three-neck round-bottom flask, heptkis (6-deoxy-6-azido)- β -cyclodextrin (2.62 g, 2 mmol) was dissolved in anhydrous NMP (30 ml) under stirring and cooled to 0 °C. 2-Bromo-isobutyryl bromide (13.9 ml, 112 mmol) was dissolved in anhydrous NMP (10 ml) and added dropwise over 2 h *via* a dropping funnel. The reaction temperature was maintained at 0 °C for 2h and then was then allowed to rise slowly to ambient temperature after which the reaction was allowed to continue for further 2 days. The brown solution was then concentrated under vacuum for 1 day. The obtained syrup was dissolved with 100 ml dichloromethane and washed sequentially with 1 N HCl (2×50 ml), saturated NaHCO₃ aqueous solution (2×100 ml), saturated NaCl aqueous solution (2×100 ml) and water (2×100 ml). The dichloromethane was removed by rotary evaporator and the pale yellow solid was further purified by silica gel column chromatography using dichloromethane (0.2% ethanol) as eluent, yielding a white powder (3.70 g, 53.4%).

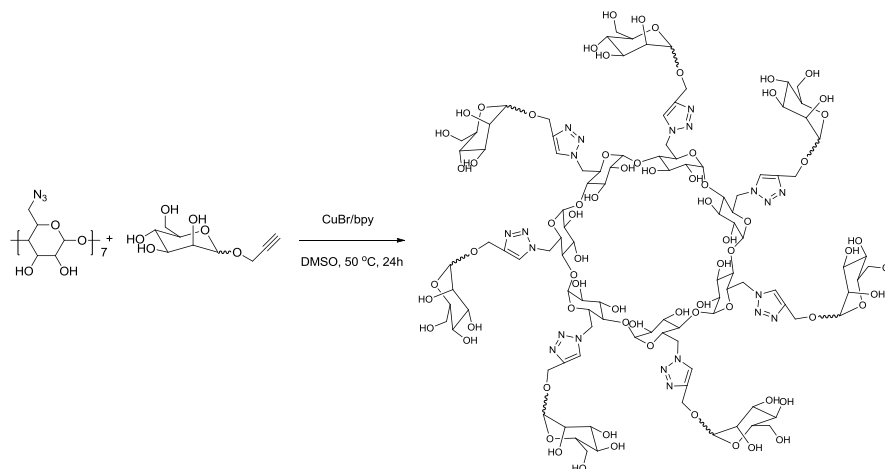
¹H NMR (CDCl₃, 298K, 400MHz): δ (ppm) =3.2-5.8 (70H, sugar residues), 1.92 (s, 84H, CH₃).

³C NMR (CDCl₃, 298K, 400MHz): δ (ppm) =171.2 (C=O), 98.4 (C-1), 73.6, 69.5-71.0 (C-2, C-3, C-4, C-5), 55.7 (C-6), 51.2 (C-Br), 30.5 (CH₃).

FT-IR ν (cm⁻¹): 2977, 2930 (ν_{C-H}); 2101 (ν_{N_3}); 1739($\nu_{C=O}$).

MALDI-TOF MS m/z : calcd for C₉₀H₁₂₃Br₁₂N₂₁O₄₀ (M+Na⁺), 3119.83; found, 3120.42; calcd for C₈₆H₁₁₈Br₁₁N₂₁O₃₉, 2969.88; found, 2970.76; calcd for C₈₂H₁₁₃Br₁₀N₂₁O₃₈, 2821.93; found, 2921.73; calcd for C₇₈H₁₀₈Br₉ N₂₁O₃₇, 2673.98; found, 2673.16.

4.3.7 Synthesis of persubstituted cyclodextrin-based mannose glycocluster via CuAAC (β -CD-(Man)₇).



Scheme 4. 13. Schematic representation of the synthetic approach to β -CD-(Man)₇.

A solution of 1-(2'-propargyl) D-mannose (349 mg, 1.6 mmol, $\alpha/\beta=5/1$), β -CD-(N₃)₇ (262 mg, 0.2 mmol), bpy (50 mg, 0.32 mmol) in DMSO (5 ml) was deoxygenated by three freeze-pump-thaw cycles. The solution was then transferred via cannula under nitrogen into a Schlenk tube, previously evacuated and filled with nitrogen, containing CuBr (23mg, 0.16 mmol). The resulting solution was stirred at 50 °C for 24 h. When the reaction was completed, the reaction mixture was purged with air for 1 h. Most of the DMSO could be removed either under high vacuum or by compressed air blowing overnight. Anhydrous methanol was then added into this concentrated deep blue solution to get a precipitate. The upper layer blue solution was removed and the precipitate was carefully collected and washed with anhydrous methanol to get a white powder. To increase the isolated conversion, the solution was collected and concentrated via rotary evaporator and precipitated into methanol again. The above procedure was repeated at least five times in order to remove DMSO, excess alkyne mannose and Cu/bpy residues. The collected precipitate was soluble in water and passed through a short neutral alumina column to remove the residue copper and the final product could be recovered as white powder after freeze drying (432 mg, yield: 76%).

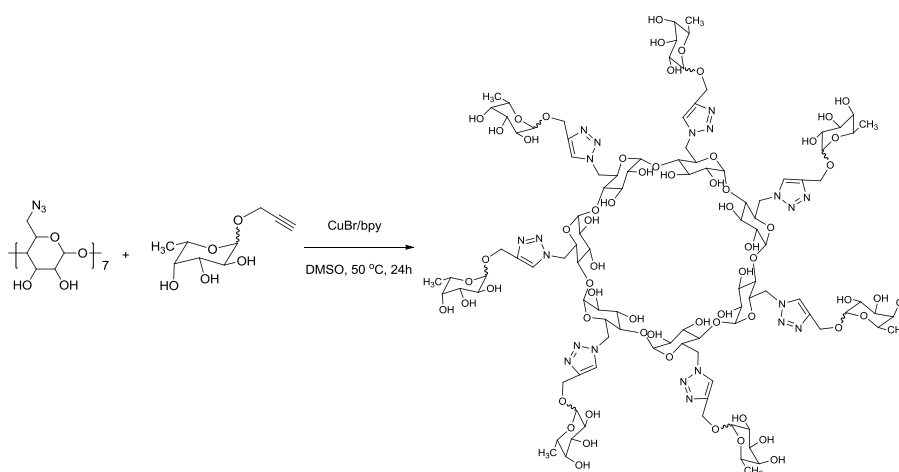
¹H NMR (DMSO-*d*₆, 298 K, 400 MHz): δ (ppm) = 7.95, 7.92 (s, overlaped, 7 H, NCH=C), 5.80-6.10 (m, 14 H, OH-2, OH-3 of CD), 5.10 (s, 7 H, H-1), 3.00-5.00 (m, CD & mannose residues, overlap with H₂O).

^{13}C NMR ($\text{DMSO-}d_6$, 298 K, 400 MHz): δ (ppm) = 143.3 (N-CH=C), 125.8 (N-CH=C), 101.7 (C-1 of CD), 99.4 (β anomeric, O-CH-O of mannose), 99.0 (α anomeric, O-CH-O of mannose), 82.6 (C-4 of CD), 77.4, 74.0, 72.5, 71.9, 71.0, 70.2, 67.0 (carbons of mannose and CD residues), 61.5, 61.2 (C-CH₂-O), 58.9 (CH₂-OH), 49.4(CH₂-N).

FT-IR ν (cm^{-1}): 3326(OH); 2910 (CH) cm^{-1} .

MALDI-ToF MS m/z : calcd for $\text{C}_{105}\text{H}_{161}\text{N}_{21}\text{O}_{70}$ ($\text{M}+\text{Na}^+$), 2859.96; found, 2860.15.

4.3.8 Synthesis of persubstituted cyclodextrin-based fucose glycocluster via CuAAC (β -CD-(Fuc)₇).



Scheme 4. 14. Schematic representation of the synthetic approach to β -CD-(Fuc)₇.

The general procedure is shown as follows. A solution of 1-(2'-propargyl) L-fucose (323 mg, 1.6 mmol, $\alpha/\beta=6/1$), β -CD-(N₃)₇ (262 mg, 0.2 mmol), bpy (50 mg, 0.32 mmol) in DMSO (5 ml) was deoxygenated by three freeze-pump-thaw cycles. The solution was then transferred via cannula under nitrogen into a Schlenk tube, previously evacuated and filled with nitrogen, containing CuBr (23mg, 0.16 mmol). The resulting solution was stirred at 50 °C for 24 h. When the reaction was completed, the reaction mixture was purged with air for 1 h. Most of the DMSO was removed by compressed air blowing overnight. Anhydrous methanol was then added into the concentrated deep blue solution to get a precipitate. The upper layer blue solution was removed and the precipitate was carefully collected and washed with anhydrous methanol to get a white powder. To increase the isolated conversion, the solution was collected and concentrated via rotary evaporator and precipitated into methanol again. The above procedure was repeated at least five times in order to remove DMSO,

excess alkyne fucose and Cu/bpy residues. The collected precipitate was soluble in water and passed through a short neutral alumina column to remove the residue copper and the final product could be recovered as white powder after freeze drying (355 mg, yield: 65%).

^1H NMR (DMSO- d_6 , 298 K, 400 MHz): δ (ppm) = 7.95 (s, overlaped, 7 H, NCH=C), 5.91 (br s, 7 H, OH-2 of CD), 5.91 (s, 7 H, OH-3 of CD), 5.10 (s, 7 H, H-1 of CD), 3.10-4.90 (m, CD & fucose residues, overlap with H_2O), 1.13 (d, J = 6.1 Hz, CH_3 , β anomeric), 1.06 (d, J = 6.3 Hz, CH_3 , α anomeric).

^{13}C NMR (DMSO- d_6 , 298 K, 400 MHz): δ (ppm) = 143.8 (N-CH=C), 125.6 (N-CH=C), 102.2 (β anomeric, O-CH-O of fucose), 101.7 (C-1 of CD), 98.6 (α anomeric, O-CH-O of fucose), 82.6 (C-4 of CD), 73.6, 72.4, 71.9, 71.6, 71.1, 70.2, 70.1, 69.6, 68.1, 66.1 (carbons of fucose and CD residues), 60.0 (C- CH_2 -O), 49.5 (CH_2 -N), 16.6 (β anomeric, CH_3), 16.5 (α anomeric, CH_3).

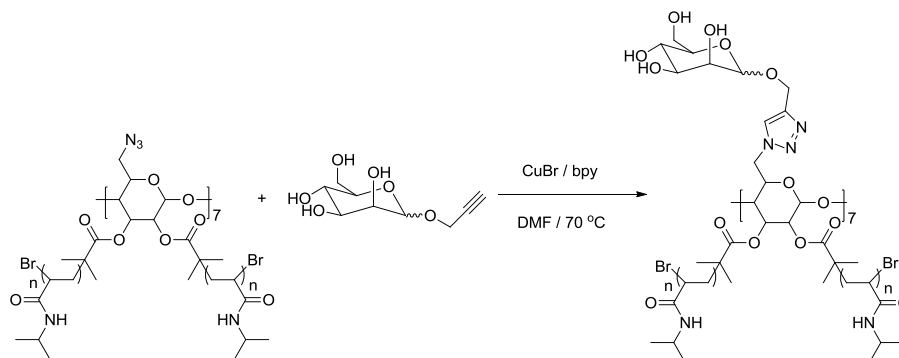
FT-IR ν (cm^{-1}): 3326(OH); 2908 (CH) cm^{-1} .

MALDI-ToF MS m/z : calcd for $\text{C}_{105}\text{H}_{161}\text{N}_{21}\text{O}_{63}$ ($\text{M}+\text{Na}^+$), 2748.00; found, 2748.05.

4.3.9 Synthesis of cyclodextrin-based mannose cluster-star PNIPAM hybrid *via* combination of ATRP and CuAAC.

Ambient temperature polymerization of NIPAM was carried out according to the literature.^{200,203} NIPAM (3.39 g, 30 mmol), tris[2-(dimethylamino)ethyl]amine (Me_6TREN) (0.19 mL, 0.7 mmol), $(\text{N}_3)_7\text{-CD-(Br)}_{10}$ (0.193 g, ~ 0.7 mmol Br moieties) were charged into a dry Schlenk tube along with 2-propanol (6.0 mL) and DMF (4.0 mL) as solvent. The tube was sealed with a rubber septum and subjected to five freeze-pump-thaw cycles. This solution was subsequently cannulated under nitrogen into a second Schlenk tube, previously evacuated and filled with nitrogen, containing Cu(I)Cl (0.069 g, 0.7 mmol) and a magnetic follower. The temperature was adjusted at 25 °C with constant stirring ($t = 0$). Samples were removed using a degassed syringe for molecular weight and conversion analysis. The reaction was allowed to stir at 25°C under N_2 protection for 4 h, reaching a monomer conversion of $\sim 64.4\%$. After diluting with 20 mL of THF, air was bubbled through for 1 h. The reaction mixture was passed through a short neutral alumina column and subsequently washed with THF. The volatiles were removed under reduced pressure and the residues

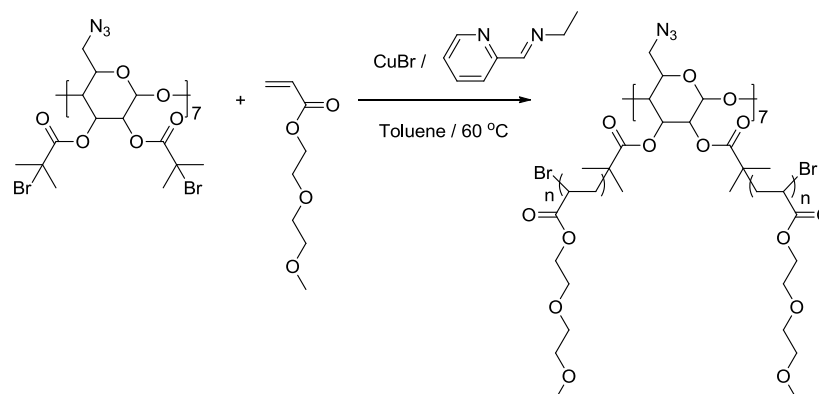
dissolved in THF (ca. 5 mL) prior to precipitation into diethyl ether (ca. 500 mL). The white solid was isolated by filtration, washed with additional diethyl ether and the volatiles removed under reduced pressure. The apparent molecular weight and molecular weight distribution of $(N_3)_7\text{-}\beta\text{-CD-(PNIPAM)}_{10}$ were determined by SEC using PMMA standards: $M_{n,SEC} = 21.6\text{KDa}$, $M_w/M_n = 1.25$.



Scheme 4. 15. Schematic representation for the CuAAC reaction of cyclodextrin-based PNIPAM with 1-(2'-propargyl) D-mannose.

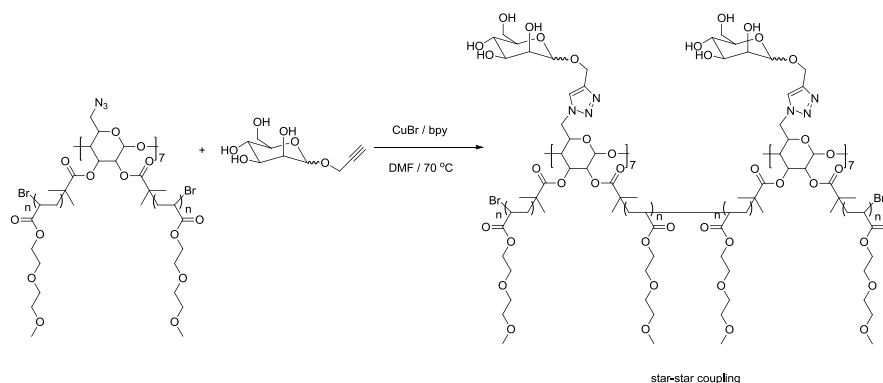
Into a dry Schlenk tube containing a magnetic follower, 1-(2'-propargyl) D-mannose (0.018 g, 0.08 mmol), $(N_3)_7\text{-}\beta\text{-CD-(PNIPAM)}_{10}$ (0.21 g, 0.04 mmol azido moieties), 2, 2'-bipyridyl (bpy) (0.050 g, 0.32 mmol) and DMF (5 ml) were added. The tube was sealed with a rubber septum and subjected to five freeze-pump-thaw cycles. This solution was then cannulated under nitrogen into a second Schlenk tube, previously evacuated and filled with nitrogen, containing Cu(I)Br (0.023 g, 0.16 mmol) and a magnetic follower and placed in an oil bath thermostated at 70°C. The reaction was allowed to stir at 70°C under N_2 protection for 48 h, and then cooled to ambient temperature. DMF was removed under reduced pressure and 20ml deionised water was added in and the solution was bubbled with air for 2 h. Then it was directly transferred into a dialysis tubing (NMWCO 1,000 Da) and dialyzed against water for 24 hours with the water being changed 4 times. The dialysed solution was then freeze-dried to give the glycopolymer as a white solid (0.16 g, yield: 76.2%). The apparent molecular weight and molecular weight distribution of $(N_3)_7\text{-}\beta\text{-CD-(PNIPAM)}_{10}$ were determined by SEC using PMMA standards: $M_{n,SEC} = 21.8\text{KDa}$, $M_w/M_n = 1.25$.

4.3.10 Synthesis of cyclodextrin-based mannose cluster-star PDEGMEMA hybrid *via* combination of ATRP and CuAAC.



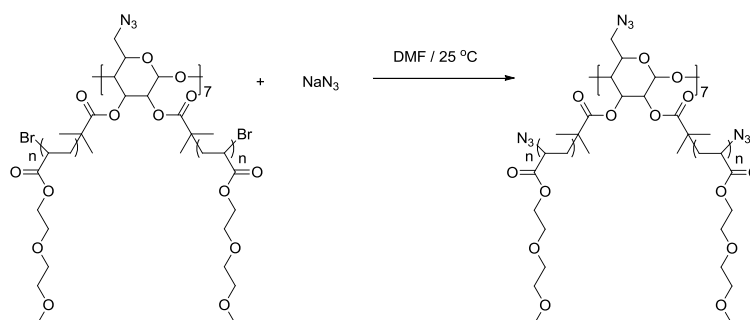
Scheme 4. 16. Schematic representation for the synthesis of cyclodextrin-based PDEGMEMA *via* ATRP.

DEGMEMA (3.2 ml, 17.2mmol), *N*-ethyl-2-pyridylmethanimine (0.108g, 0.8 mmol), (N₃)₇-β-CD-(Br)₁₀ (0.193 g, ~0.4 mmol Br moieties) were charged into a dry Schlenk tube along with toluene (10.0 ml) as solvent. The tube was sealed with a rubber septum and subjected to five freeze-pump-thaw cycles. This solution was then cannulated under nitrogen into a second Schlenk tube, previously evacuated and filled with nitrogen, containing Cu(I)Br (0.057 g, 0.4 mmol) and a magnetic follower. The temperature was adjusted at 60 °C with constant stirring (t = 0). Samples were removed using a degassed syringe for molecular weight and conversion analysis. The reaction was allowed to stir at 60 °C under N₂ protection for 160 min, reaching a monomer conversion of 42%. After diluting with 20 mL of THF, air was bubbled through for 1 h. The reaction mixture was passed through a short neutral alumina column and subsequently washed with THF. The volatiles were removed under reduced pressure and the residues dissolved in THF (ca. 5 mL) prior to precipitation into cold hexane (ca. 500 mL). The polymer precipitate was isolated by filtration, washed with additional cold hexane and volatiles removed under reduced pressure. DMF SEC analysis based on PMMA standards revealed a single peak with an apparent $M_n = 24.7\text{KDa}$ and $M_w/M_n = 1.21$ (Figure. 4.18).



Scheme 4. 17. Schematic representation for the CuAAC reaction of cyclodextrin-based PDEGEEA with 1-(2'-propargyl) D-mannose.

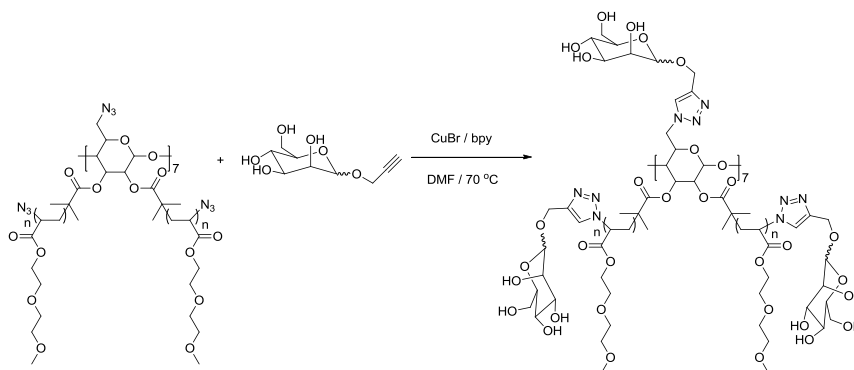
Into a dry Schlenk tube containing a magnetic follower, α -propargyl mannose (0.060 g, 0.27 mmol), $(N_3)_7$ - β -CD-(PDEGMEMA) $_{10}$ -(Br) $_{10}$ (0.500 g, 0.09 mmol azido moieties), 2, 2'-bipyridyl (bpy) (0.172 g, 1.09 mmol) and DMF 10 mL were added. The tube was sealed with a rubber septum and subjected to five freeze-pump-thaw cycles. This solution was then cannulated under nitrogen into a second Schlenk tube, previously evacuated and filled with nitrogen, containing Cu(I)Br (0.078 g, 0.54 mmol) and a magnetic follower and placed in an oil bath thermostated at 70 °C. The reaction was allowed to stir at 70 °C under N₂ protection for 24 h, and then cooled to ambient temperature. 20 mL deionised water was added in and the solution was bubbled with air for 2 h. Then it was directly transferred into a dialysis tubing (NMWCO 1,000 Da) and dialyzed against water for one day with the water being changed 4 times. The dialysed solution was then freeze-dried to give the solid glycopolymers.



Scheme 4. 18. Schematic representation for the end group transformation of $(N_3)_7$ - β -CD-(PDEGMEMA) $_{10}$ -(Br) $_{10}$ into $(N_3)_7$ - β -CD-(PDEGMEMA) $_{10}$ -(N₃) $_{10}$.

In order to avoid the coupling reaction during click reaction, the bromide end group was first transformed into an azide group via reaction with NaN₃.

In a 50 ml round-bottom bottle, $(\text{N}_3)_7\text{-CD-(PDEGMEMA)}_{10}$ (0.300 g, 0.065 mmol Br moieties, $M_{n, \text{SEC}} = 22.1\text{KDa}$, $M_w/M_n=1.21$) and NaN_3 (0.022 g, 0.33 mmol) was dissolved in DMF (10 mL) and stirred at 25°C for 24 h. After reaction, water (20 mL) was added into the solution and then directly transferred into a dialysis tubing (NMWCO 1,000 Da) and dialyzed against water for 1 day with the water being changed 4 times. The dialysed solution was then freeze-dried to give the azide-terminated polymer (0.200 g, yield: 66.7%).



Scheme 4. 19. Schematic representation for the CuAAC reaction of cyclodextrin-based $(\text{N}_3)_7\text{-}\beta\text{-CD-(PDEGMEMA)}_{10}\text{-(N}_3\text{)}_{10}$ with 1-(2'-propargyl) D-mannose.

Into a dry Schlenk tube containing a magnetic follower, α -propargyl mannose (0.018 g, 0.08mmol), $(\text{N}_3)_7\text{-}\beta\text{-CD-(PDEGMEMA)}_{10}\text{-(N}_3\text{)}_{10}$ (0.105 g, ~ 0.04 mmol azido moieties), 2, 2'-bipyridyl (bpy) (0.025g, 0.16 mmol) and DMF (10ml) were added. The tube was sealed with a rubber septum and subjected to five freeze-pump-thaw cycles. This solution was then cannulated under nitrogen into a second Schlenk tube, previously evacuated and filled with nitrogen, containing Cu(I)Br (0.012 g, 0.08 mmol) and a magnetic follower and placed in an oil bath thermostated at 70°C . The reaction was allowed to stir at 70°C under N_2 protection for 24 h, and then cooled to ambient temperature. 20mL deionised water was added and the solution was bubbled with air for 2h. Then it was directly transferred into a dialysis tubing (MWCO 1,000 Da) and dialyzed against water for 1 day with the water being changed 4 times. The dialysed solution was then freeze-dried to give the solid glycopolymer. The apparent molecular weight and molecular weight distribution of $(\text{Mannose})_7\text{-}\beta\text{-CD-(PNIPAM)}_{10}\text{-(Mannose)}_{10}$ were determined by GPC using PMMA standards: $M_{n, \text{SEC}} = 23.7\text{ KDa}$, $M_w/M_n=1.19$.

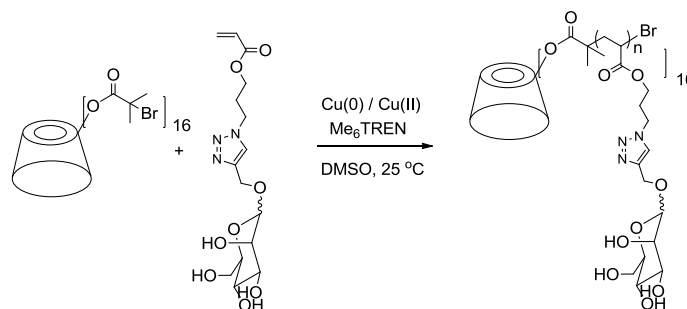
4.3.11 Cyclodextrin-based star glycopolymers *via* SET-LRP and chain extension ability test

All polymerizations were carried out using standard Schlenk techniques under an inert atmosphere of oxygen-free nitrogen, unless otherwise stated. All obtained glycopolymer products were stored in the cold room (4 °C) or fridge (-18 °C) if stored for more than three months.

To a Schlenk tube fitted with a magnetic stir bar and a rubber stopper, β -CD-(Br)₁₆ (48 mg, 0.22 mmol Br, 1 eq), glucose glycomonomer (124 mg, 0.33 mmol, 1.5 eq), CuBr₂ (4 mg, 0.018 mmol, 0.08 eq) and DMSO (2 mL) were charged and the mixture was bubbled with nitrogen for 15 min. Pre-degassed Me₆TREN (9.2 μ L, 0.04 mmol, 0.18 eq) and pre-activated copper wire (1.5 cm, 7 mg, 0.11 mmol) were then carefully added into the bottle sequentially under nitrogen. Subsequently, the Schlenk tube was sealed and the light green solution was allowed to polymerize at 25 °C for 24 h. Sample of the reaction mixture was then carefully removed for analysis. The sample for ¹H NMR was directly diluted with DMSO-*d*₆. Catalyst residues were removed by filtering through a column of neutral alumina prior to SEC analysis.

A further solution of mannose glycomonomer (124 mg, 0.33 mmol) in 1 mL DMSO which has been pre-degassed via nitrogen sparging for 20 min, was then transferred via cannula under nitrogen into the Schlenk reaction tube. The solution was allowed to polymerize at 25 °C for another 48 h with stirring. After the reaction a sample was removed for analysis. The reaction mixture was directly diluted with water and bubbled with air for 1 h and then passed through a short neutral alumina column. The collected aqueous solution was dialysed against water for two days after which the glycopolymer (111 mg) could be recovered by freeze drying.

4.3.12 Synthesis of cyclodextrin-centred star mannose glycopolymers (β -CD-[(Mannose)₂]₁₆, β -CD-[(Mannose)₅]₁₆, β -CD-[(Mannose)₁₀]₁₆)



Scheme 4. 20. Synthesis of β -CD based glycopolymers *via* SET-LRP.

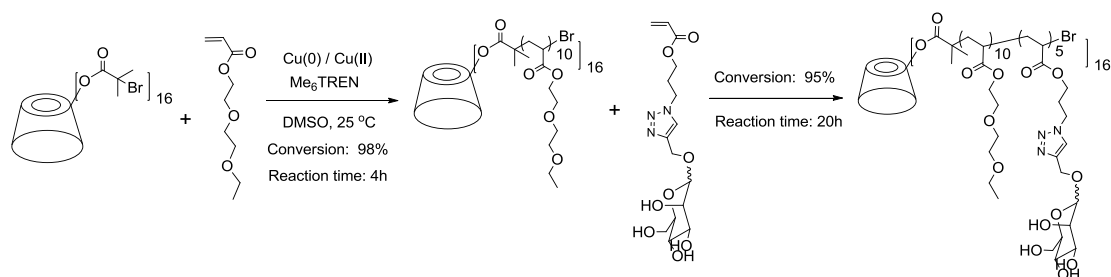
For the synthesis of β -CD-[(Mannose)₂]₁₆, the general procedure is shown as follows. To a Schlenk tube fitted with a magnetic stir bar and a rubber stopper, β -CD-(Br)₁₆ (37 mg, 0.17 mmol Br, 1 eq), mannose glycomonomer (124 mg, 0.33 mmol, 2 eq), CuBr₂ (3 mg, 0.013 mmol, 0.08 eq) and DMSO (3 mL) were charged and the mixture was bubbled with nitrogen for 15 min. Pre-degassed Me₆TREN (6.9 μ L, 0.03 mmol, 0.18 eq) and pre-activated copper wire (1 cm, 5 mg, 0.08 mmol) were then carefully added into the bottle sequentially under nitrogen protection. Subsequently, the Schlenk tube was sealed and the light green solution was allowed to polymerize at 25 °C for 24 h. After reaction, sample of the reaction mixture was removed for ¹H NMR and SEC analysis. ¹H NMR spectrum revealed a conversion of 100% from the disappearance of vinyl groups at 5.8-6.4 ppm. The reaction mixture was then diluted with water and bubbled with air for 1 h and then passed through a short neutral alumina column. The collected aqueous solution was then dialysed against water for two days after which the glycopolymer (110 mg) could be recovered by freeze drying.

For the synthesis of β -CD-[(Mannose)₅]₁₆, the procedure is similar as previously described. To a Schlenk tube fitted with a magnetic stir bar and a rubber stopper, β -CD-(Br)₁₆ (15 mg, 68 μ mol Br, 1 eq), mannose glycomonomer (124 mg, 0.33 mmol, 5 eq), CuBr₂ (1.2 mg, 5.4 μ mol, 0.08 eq) and DMSO (3 mL) were charged and the mixture was bubbled with nitrogen for 15 min. Pre-degassed Me₆TREN (2.8 μ L, 12 μ mol, 0.18 eq) and pre-activated copper wire (1 cm, 5 mg, 0.08 mmol) were then carefully added into the bottle sequentially under nitrogen protection. Subsequently, the Schlenk tube was sealed and the light green solution was allowed to polymerize at 25 °C for 46 h. After reaction, sample of the reaction mixture was removed for ¹H NMR and SEC analysis. ¹H NMR spectrum revealed a conversion of 86%. The

reaction mixture was then diluted with water and bubbled with air for 1 h and then passed through a short neutral alumina column. The collected aqueous solution was then dialysed against water for two days after which the glycopolymer (85 mg) could be recovered by freeze drying.

For the synthesis of β -CD-[(Mannose)₁₀]₁₆, the procedure is similar as previously described. To a Schlenk tube fitted with a magnetic stir bar and a rubber stopper, β -CD-(Br)₁₆ (15 mg, 68 μ mol Br, 1 eq), mannose glycomonomer (248 mg, 0.67 mmol, 10 eq), CuBr₂ (1.2 mg, 5.4 μ mol, 0.08 eq) and DMSO (3 mL) were charged and the mixture was bubbled with nitrogen for 15 min. Pre-degassed Me₆TREN (2.8 μ L, 12 μ mol, 0.18 eq) and pre-activated copper wire (1 cm, 5 mg, 0.08 mmol) were then carefully added into the bottle sequentially under nitrogen protection. Subsequently, the Schlenk tube was sealed and the light green solution was allowed to polymerize at 25 °C for 46 h. During the reaction, samples of the reaction mixture were carefully removed for ¹H NMR and SEC analysis. After reaction, ¹H NMR spectrum revealed a conversion of 96%. The reaction mixture was then diluted with water and bubbled with air for 1 h and then passed through a short neutral alumina column. The collected aqueous solution was then dialysed against water for two days after which the glycopolymer (113 mg) could be recovered by freeze drying.

4.3.13 Synthesis of cyclodextrin-based star diblock mannose glycopolymer (β -CD-[(DEGEEA)₁₀-*b*-(Mannose)₅]₁₆)



Scheme 4. 21. Synthesis of β -CD based diblock glycopolymer *via* SET-LRP of DEGEEA and one-pot chain extension reaction.

To a Schlenk tube fitted with a magnetic stir bar and a rubber stopper, β -CD-(Br)₁₆ (66 mg, 0.3 mmol Br, 1 eq), DEGEEA (565 mg, 3 mmol, 10 eq), CuBr₂ (8 mg, 0.036 mmol, 0.12 eq) and DMSO (7 mL) were charged and the mixture was bubbled with nitrogen for 15 min. Pre-degassed Me₆TREN (12.5 μ L, 0.054 mmol, 0.18 eq) and pre-activated copper wire (5 cm, 25 mg, 0.4 mmol) were then carefully added into the bottle sequentially under nitrogen protection. Subsequently, the Schlenk tube was sealed and the light green solution was allowed to polymerize at 25 °C for 4 h. After that, 2/3 volume of the reaction mixture (5.7 mL) was carefully removed from the bottle under nitrogen protection and sample was taken for ¹H NMR and SEC analysis. The sample for ¹H NMR was directly diluted with CDCl₃. Conversion at this stage was calculated by comparing the integral of vinyl groups at 5.4-6.2 ppm with integral of oligo ethylene glyco groups at 3.2-4.6 ppm, CD initiator residues at this region cannot be detected due to the high total DP and thus were overlooked. Catalyst residues were removed by filtering through a column of neutral alumina prior to SEC analysis. The rest mixture was diluted with acetone and bubbled with air for 1 h and then passed through a short neutral alumina column. The collected solution was dialysed against acetone for two days after which the DEGEEA polymer (160 mg) could be recovered for characterization after drying under vacuum.

A further solution of mannose glycomonomer (186 mg, 0.5 mmol) in 2 mL DMSO which has been pre-degassed via nitrogen sparging for 20 min, was then transferred via cannula under nitrogen into the Schlenk reaction tube. The solution was allowed to polymerize at 25 °C for another 20 h with stirring. After reaction, sample was also removed for ¹H NMR and SEC analysis. The sample for ¹H NMR was directly diluted

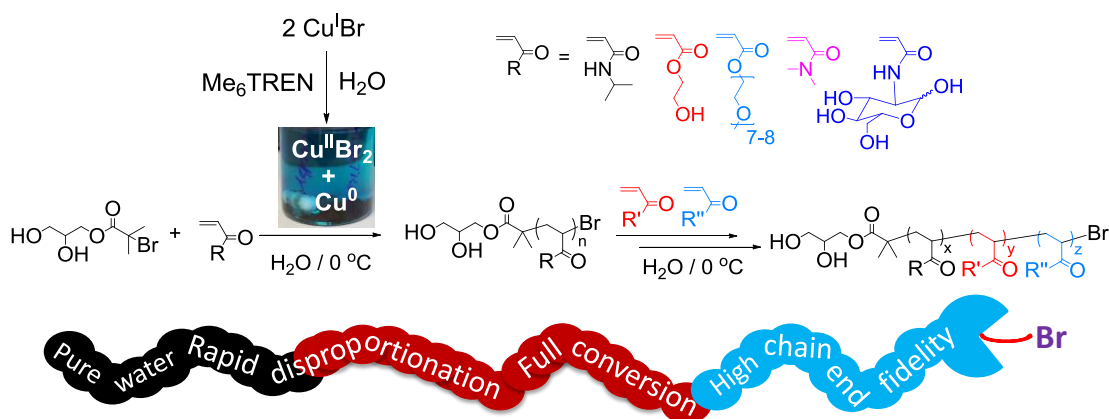
with DMSO- d_6 . Conversion at this stage was calculated by comparing the integral of vinyl groups at 5.9-6.4 ppm with integral of triazole protons at 8.0-8.2 ppm. The reaction mixture was directly diluted with water and bubbled with air for 1 h and then passed through a short neutral alumina column. The collected aqueous solution was dialysed against methanol/water (1:1) and then water for three days after which the glycopolymer (260 mg) could be recovered after drying.

4.3.14 Drug encapsulation ability of the cyclodextrin-based glycoconjugates

The general procedure for the encapsulation test of DHA is shown as follow. To a vial with a magnetic stir, 5 mL CD glycoconjugate solution (1 mg/mL) and excess DHA (10 mg) was added. After ultrasonication for 30 min, the mixture was vigorously stirred for 12 h under ambient temperature and then was passed through a 0.45 μ m filter to remove any insoluble drug. The obtained clear solution was directly used for UV-Vis test.

The typical procedure for the encapsulation test of saquinavir mesylate is shown as follows. To a vial with a magnetic stir and 0.6 mL D₂O (with 10 mM DMF as internal standard), 6 mg β -CD-[(DEGEEA)₁₀-(Mannose)₅]₁₆ and excess saquinavir mesylate (6 mg) were added. After ultrasonication for 30 min, the mixture was vigorously stirred for 12 h under ambient temperature and then was carefully passed through a 0.45 μ m filter to remove any insoluble drug. The obtained clear solution was directly transferred into a NMR tube for ¹H NMR test (400 M, proton weak).

Chapter 5 Aqueous Copper Mediated Living Polymerization: Exploiting Rapid Disproportionation of CuBr with Me₆TREN



A new approach to perform single-electron transfer living radical polymerization (SET-LRP) in water is described. The key step in this process is to allow full disproportionation of $\text{CuBr}/\text{Me}_6\text{TREN}$ (Me_6TREN = tris(dimethylamino)ethyl amine) to $\text{Cu}(0)$ powder and CuBr_2 in water prior to addition of both monomer and initiator. This provides an extremely powerful tool for the synthesis of functional water-soluble polymers with controlled chain length and narrow molecular weight distributions (PDI approx. 1.10), including poly- NIPAM, DMA, PEG acrylate, HEA and glyco monomers. The polymerizations are performed at or below ambient temperature with quantitative conversions attained in minutes. Polymers have high chain end fidelity capable of undergoing chain extensions to full conversion or multi-block copolymerization via iterative monomer addition after full conversion. Activator generated by electron transfer atom transfer radical polymerization (AGET ATRP) of NIPAM in water was also conducted as a comparison with the SET-LRP system. This shows that the addition sequence of L-ascorbic acid is crucial in determining the onset of disproportionation, or otherwise. This robust technique was applied to polymerizations under biologically relevant conditions (PBS buffer), a complex ethanol/water mixture (Tequila) and a truly biological condition: sheep blood serum. Finally, double hydrophilic diblock glycopolymers composed of mannose glycopolymer block and LCST PNIPAM or PDEGEEA block are successfully synthesized by this aqueous SET-LRP technique.

5.1 Introduction

Controlled and living radical polymerisation methods have evolved to become almost routine. However, in the majority of cases they still prove problematic in water. Given the expanding interest in hydrophilic and biocompatible polymers in an ever widening array of applications, this deficiency in the synthetic toolbox needs to be addressed.

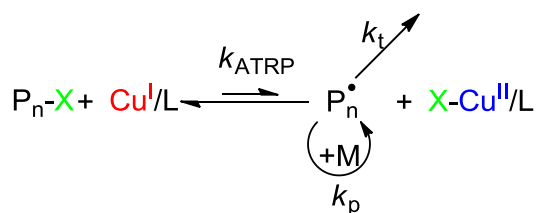
Copper mediated living polymerisation remains one of the most widely applied and useful methods of controlling vinyl polymerization. Thus, a greater understanding and development of very well controlled Cu-mediated polymerization in water and other aqueous media is required. All existing protocols are encumbered by important, and often overlooked, competing reactions that can reduce the polymerisation control, broadening PDI values which can generally fall between 1.2->1.4. However, living anionic polymerisation, a standard bearer in living polymerization, allows facile access to polymers with PDI values < 1.10. As many applications are increasingly in biological and therapeutic fields, there is a pressing requirement for better control over both PDI and end group fidelity.

As polymerisation initiators and propagating chains are usually secondary or tertiary alkyl halides in Cu-mediated radical polymerization (typically bromide or chloride, X), hydrolysis or elimination of HX can occur at an appreciable rate leading to chain termination. Although conceptually a simple reaction, hydrolysis usually requires a base and, as a result, this reaction is seldom used for synthetic organic purposes. However, it has been reported that tertiary alkyl α -halocarbonyls can be efficiently converted to alcohols with silver oxide in aqueous acetonitrile.²¹³

The use of copper complexes - as polymerisation catalysts - extends the likelihood of competing side reactions via possible removal of a halide anion or homolytic bond cleavage. With respect to controlled polymerization reactions in aqueous media, any such aqua-mediated side reactions which occur at an appreciable rate relative to initiation and/or propagation, will lead to loss of active species, low initiation efficiency and/or premature termination. The overall consequence of this is a loss of both molecular weight control and the inability to chain extend to block copolymers and introduce desirable chain end functionality. Despite Cu(I) retaining a full complement of d-electrons (d^{10}) it is very unstable with respect to oxidation and readily undergoes rapid disproportionation to Cu(0) and Cu(II) in aqueous and polar

media. The equilibrium constants for the disproportionation vary considerably depending on the ligands, temperature, counter anions and solvent composition. Unless there is a stabilising effect such as a π -acceptor orbital on the ligand, as in pyridine imines,²¹⁴⁻²¹⁶ diazabutadienes,²¹⁷ tripyridylmethyamine (TPMA),²¹⁸ and bipyridine,^{17,219} or other stabilising effects such as solvation by acetonitrile, these equilibrium constants can be high, particularly in water (approaching 10^6).

The occurrence, or not, of disproportionation is also highly dependent on ligand geometry. Many sterically constrained ligands, such as Me₆TREN, cause deviations away from a preferred geometry, exposing coordination sites to water, monomer and other ligation. Although this does not seem to be fully understood, it is ascribed in inorganic text books to be in part due to greater lattice and solvation energetics as well as higher formation constants for Cu(II) complexes relative to Cu(I). Thus there is a very large thermodynamic driving force towards disproportionation under appropriate conditions e.g. in water. Matyjaszewski *et al.* have reported that atom transfer radical polymerisation (ATRP)^{17,220} can be influenced by a conditional disproportionation constant²²¹. This knowledge, they suggest, can be used to select an appropriate ligand for ATRP which should exhibit high activity towards activation and deactivation processes but remain stable with respect to disproportionation.²²² Using this rationale, it is clear that aqueous ATRP employing Cu(I) in conjunction with tertiary amine ligands that distort complex geometry (Me₆TREN or PMDETA) is not a favoured approach. A well accepted mechanism for Cu(I) mediated ATRP, which is reproduced in many publications, is shown in Scheme 5.1:²²³



Scheme 5. 1. Accepted mechanism for ATRP.

The mechanism is often discussed in terms of the equilibrium constant, K_{ATRP} which has been measured during polymerisation of methyl acrylate (MA) under a range of conditions and in a variety of polar solvents. Considering the contrasting stability of Cu(I) under these conditions, it is notable that the additional equilibrium between Cu(I) and Cu(0)/Cu(II) is often omitted from reaction schemes. As the equilibrium

lies very much to the left, with measured K_{ATRP} values in the order of $10^{-9} - 10^{-8}$, there should be very significant amounts of Cu(I) in solution. In DMSO, in the presence of Me₆TREN, there is a significant level of disproportionation,^{224,225} thus, there are many different complexes present during propagation. The removal of Cu(I) from this equation *via* disproportionation increases complexity and should not be ignored when considering the reaction mechanism.

The ATRP of acrylamide monomers has proven problematic with Brittain concluding that ATRP of *N,N*-dimethylacrylamide (DMA) was not controlled.²²⁶ This was purported to be due to complexation of the amido group at the chain ends, which stabilized the propagating radicals. It was suggested that this retarded the deactivation step in ATRP, giving an unacceptably high concentration of radicals and leading to bimolecular termination. Additionally, cyclization involving nucleophilic Br displacement by the penultimate amide nitrogen was invoked and hydrolysis of the resulting onium intermediate furnished hydroxyl-terminated polymers.

Greater success has been achieved in the polymerisation of *N*-isopropylacrylamide (NIPAM) under apparent ATRP conditions²²⁷. It is worthwhile to note that most Cu-mediated LRP of NIPAM have usually been performed using chloro-based initiators with CuCl/CuCl₂/Me₆TREN catalyst in high polarity organic solvents (alcohol, DMF or DMSO) or binary mixtures of water and organic solvents.²²⁸⁻²³⁶ The only example of ATRP of NIPAM in water with no added co-solvent required a high ratio of Cu(II) salts for effective deactivation in order to retain good control.²³⁷ Likewise, in the expanding field of nano-medicine, NIPAM containing (block) copolymers are desirable for the formation of responsive, dynamic assemblies. Statistical copolymerisation and in-situ chain extension of NIPAM have been conducted, however, due to the complex nature of (meth)acrylamide systems, examples of block copolymerizations *via* Cu-mediated methods are limited.^{233,236,238} Nitroxide mediated polymerisation (NMP) and reversible addition fragmentation chain transfer polymerization (RAFT), are therefore often employed for the (co)polymerisation of NIPAM.²³⁹⁻²⁴²

SET-LRP employs Cu(0) as the activator and cites the disproportionation of *in situ* formed Cu(I) into highly active ‘nascent’ Cu(0) and Cu(II) as a key step in the mechanism.^{20,21,243,244} Percec *et al* have conducted numerous investigations towards identifying the degree, rate, location and effect of the disproportionation phenomenon

under assumed SET-LRP conditions.^{158,224,244-248} The presence of ‘nascent’ Cu(0) has been microscopically verified²⁴⁹ and the enhanced activity of these species has been demonstrated via polymerisation mediated by Cu(0) particles prepared *in situ* from disproportionation [L_nCu(I)X] in polar solvents and their binary mixtures in water.²⁵⁰ Intentional termination and reactivation experiments have also been used to ascertain the activating species and highlight the ‘living’ nature of this process.^{251,252}

Thus there are currently conflicting reports in the literature regarding the effectiveness and mechanism of Cu-mediated polymerisation in aqueous media (particularly for acrylamide monomers). Herein, we report the SET-LRP polymerisation of a variety of water soluble monomers using Cu(0) and CuBr₂ as the activator and deactivator respectively. The catalyst is prepared, for the first time, by *in situ* disproportionation of CuBr/Me₆TREN in pure water prior to addition of monomers and initiator. Careful experimental design allowed the use of hydrolytically labile bromine containing initiator and propagating species. Optimisation of the reaction conditions also provides near quantitative end-group fidelity which is exemplified by iterative chain extension towards the synthesis of well-defined multiblock copolymers.

5.2 Results and discussion

5.2.1 Disproportionation of Cu(I)X (X = Br, Cl) / N-ligand complexes in water.

Cu(I)X/N-ligand complexes are frequently employed in living radical polymerization, either as catalysts in ATRP or activator precursors in SET-LRP.^{150,151} The disproportionation of Cu(I)X/N-ligand complexes into nascent Cu(0) and Cu(II) is considered the crucial step in SET-LRP, which has been demonstrated to occur in a series of polar solvents and monomers.²⁴⁴ Many papers report that the disproportionation is a *slow* process relative to propagation and overall chain formation. As such, SET-LRP has also been considered in some of the literature as ARGET ATRP or SARA ATRP.¹⁹ In order to conduct successful polymerization in water, it is important to define more precisely the nature of Cu(I)X/N-ligand complexes in water.

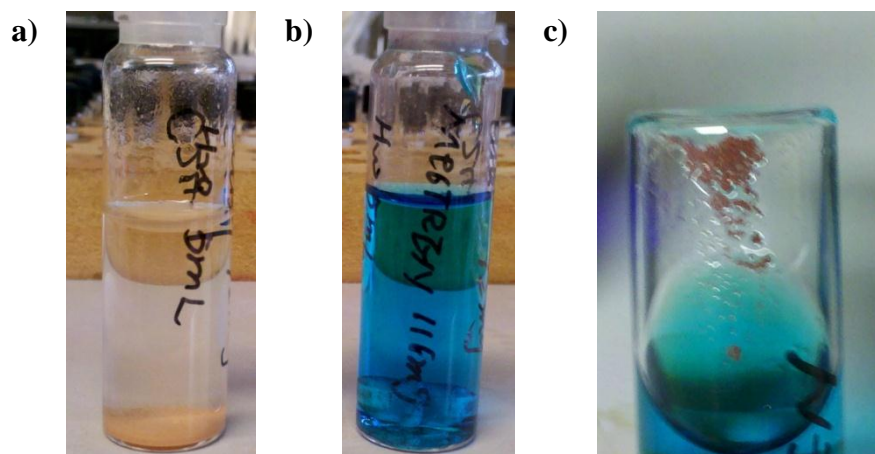


Figure 5. 1. Visual observation of the disproportionation of CuBr/Me₆TREN in H₂O. Conditions: H₂O = 5 mL, (a) CuBr = 72 mg, 0.5 mmol; (b) CuBr = 72 mg, 0.5 mmol; Me₆TREN = 130 μ L, 0.5 mmol; (c) zoom of the bottom copper (0) powder of (b). Pictures were taken 1 h after mixing the reagents.

Disproportionation of Cu(I) in water in the absence of *N*-donor ligands proceeds efficiently (with an equilibrium constant of $\sim 10^6$) when non-coordinating ClO₄⁻ and SO₄²⁻ counter ions are present.²⁵³ However, Cu (I) halides, which are widely used in both ATRP and SET-LRP, have low solubility in water. Consequently, the disproportionation to Cu (0) and Cu(II) halides, which should lead to a slightly blue color in water, is not significant at ambient temperature when ligands are absent (Figure 5.1).

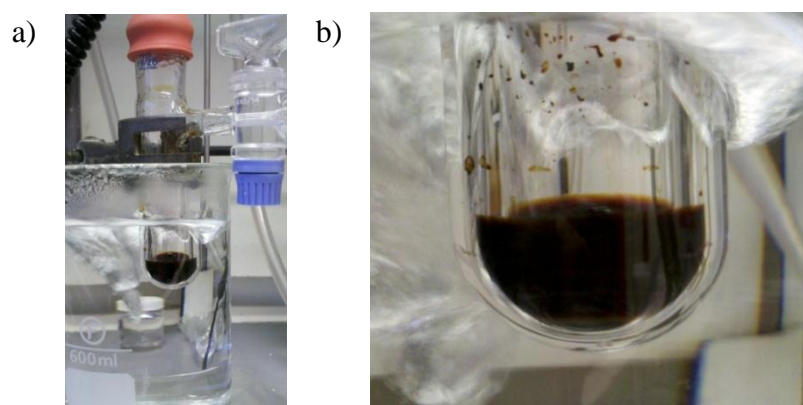


Figure 5. 2. Visual observation of the disproportionation of CuBr/*N*-ethyl-2-pyridylmethanimine in H₂O. Conditions: H₂O = 2 mL, (a) CuBr = 14 mg, 0.1 mmol; *N*-ethyl-2-pyridylmethanimine = 27 mg, 0.2 mmol; (b) zoom of (a). Pictures were taken 1 h after mixing the reagents.

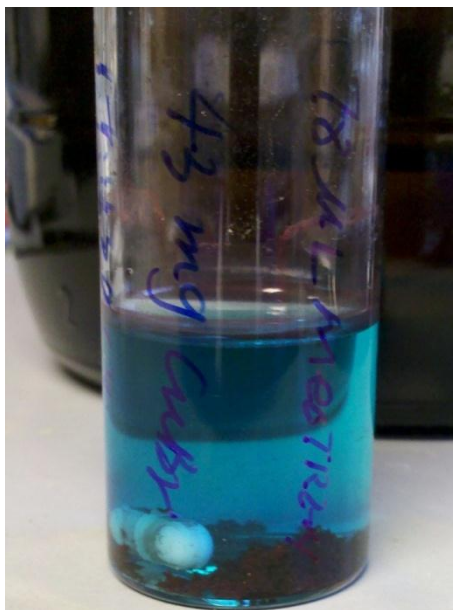


Figure 5. 3. Visual observation of the disproportionation of CuBr/Me₆TREN in H₂O. Conditions: H₂O = 12 mL; CuBr = 43 mg, 0.3 mmol; Me₆TREN = 78 μ L, 0.3 mmol; nitrogen protection. Picture was taken 45 min after mixing the reagents.

With the addition of *N*-donor ligands, Cu(I) halides coordinate to form water-soluble complexes²⁵⁴. As Cu(I) can be stabilized in water by ligands that have π -acceptor orbitals both *N*-ethyl-2-pyridylmethanimine and CuBr were added to water to form a stable water-soluble complex which is dark brown in colour, due to metal to ligand charge transfer. No precipitate or color change resulting from disproportionation was observed even when the mixture was heated to 50 °C for 1 h (Figure 5.2).

Me₆TREN is a widely-used tetradentate tertiary amine-based ligand in both ATRP and SET-LRP. Previously it has been reported that this ligand does not stabilize Cu(I) in aqueous solution with disproportionation proceeding with an equilibrium constant of $\sim 1.4 \times 10^3$.^{224,254} In our hands, when CuBr was added to an aqueous solution of Me₆TREN, the solution instantly became blue and Cu(0) powder is formed even in the presence of air (Figure 5.1). Under oxygen-free conditions, disproportionation of CuBr /Me₆TREN in water is fast and significant, yielding an obvious purple-red colored Cu(0) precipitate and a bright blue solution (Figure 5.3). Careful separation of the blue solution from the Cu(0) precipitate and UV/Vis characterization, by way of comparison with known concentrations of CuBr₂/Me₆TREN/H₂O solutions (Figure 5.4), confirmed the existence of CuBr₂ from disproportionation and the results were in accordance with the literature.^{224,255} Concurrent mass measurement of Cu(0)

precipitate and concentration calculations *via* UV/Vis showed that the extent of disproportionation is close to 100% (Figure 5.5), implying that stable, detectable CuBr / Me₆TREN complexes cannot exist in a water solution for any significant period of time. Indeed, visual and quantitative analysis of the suspension formed after mixing CuBr with Me₆TREN in water revealed the existence of newly formed Cu(0) powder and CuBr₂/Me₆TREN/H₂O complexes.

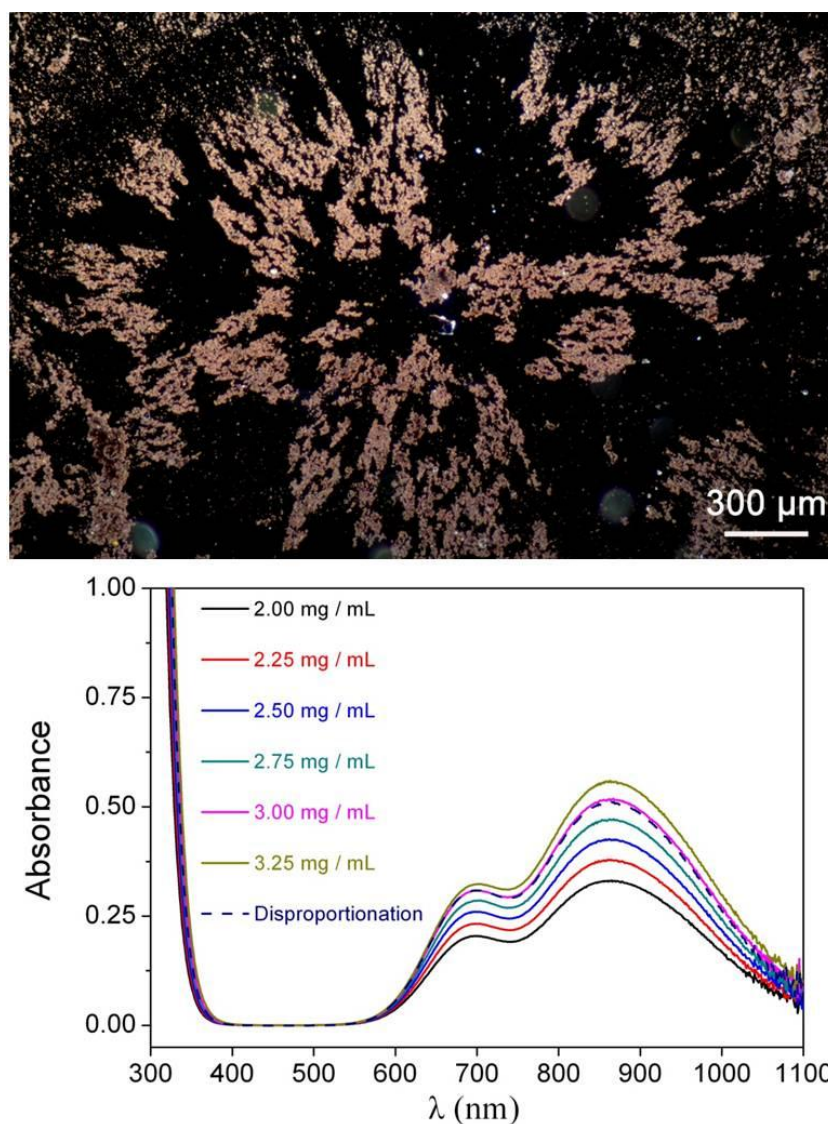


Figure 5. 4. Optical microscopy image (top) of copper powders from disproportionation of CuBr/Me₆TREN in H₂O and UV-Vis spectra (bottom) of the solution of CuBr₂/Me₆TREN and filtered disproportionation solution (dashed line). All the samples were diluted ten times before analysis (0.5 mL sample solution into 4.5 mL degassed H₂O). The optical microscopy analysis was helped by Dr Yunhua Chen.

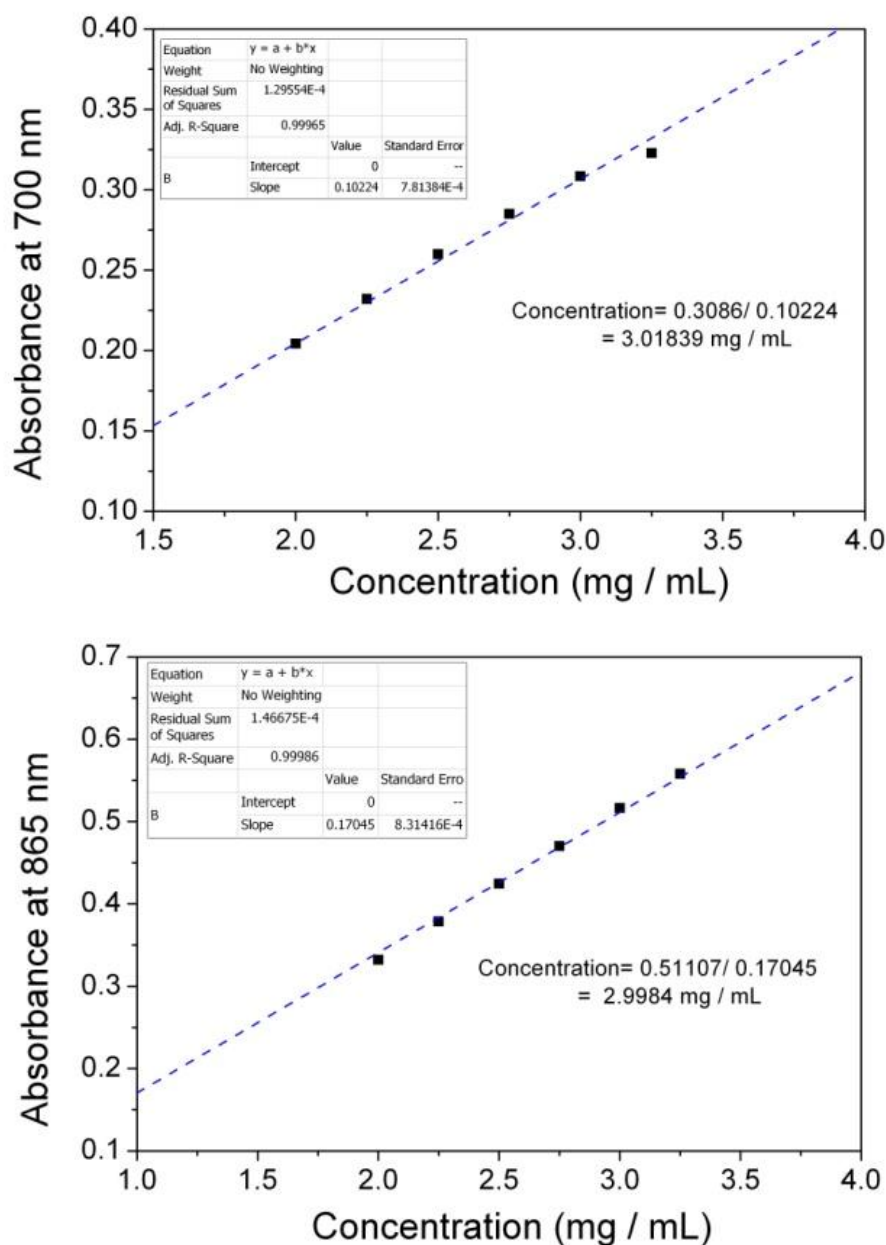
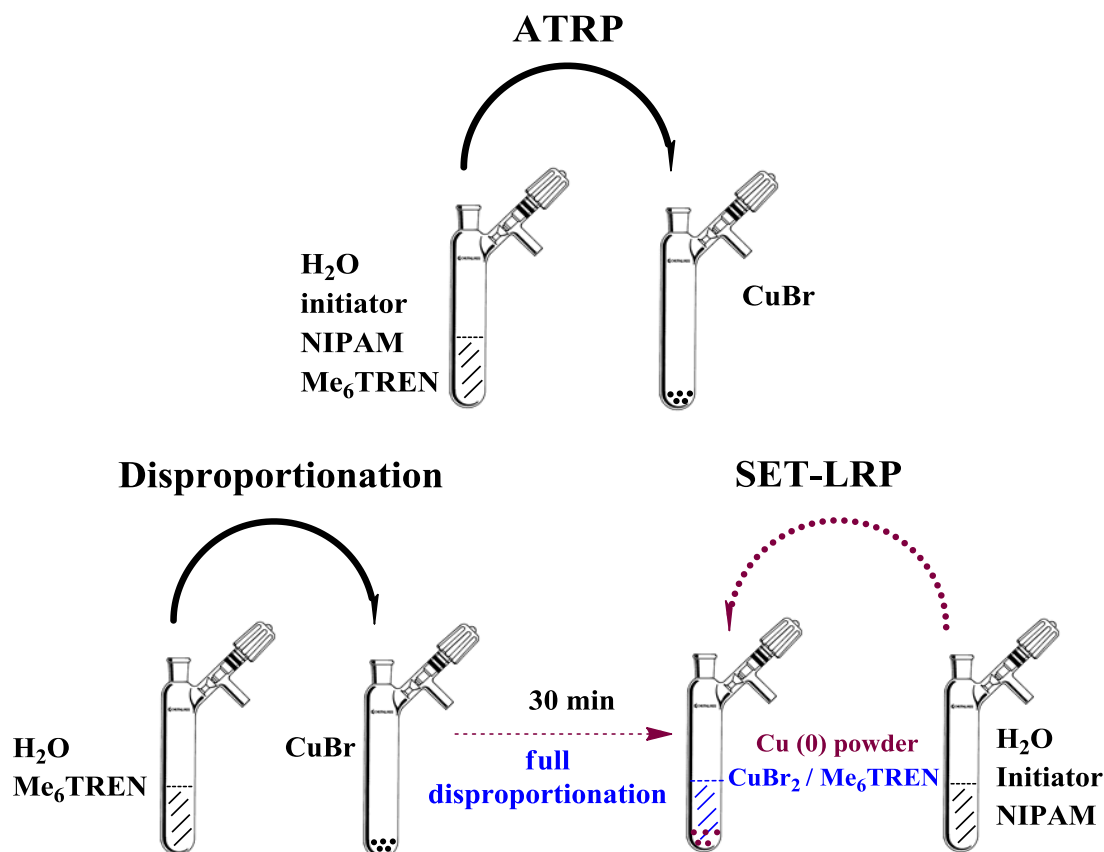


Figure 5. 5. Calibration curve based on UV-Vis absorbance at 700 nm (top) and 865 nm (bottom). The intercept for the linear fit was set as 0.

In a previous report regarding the ATRP of NIPAM, a catalyst stock solution of CuCl/Me₆TREN in water was used without reference to any observation of this disproportionation reaction.²²⁸ However, upon addition of CuCl to aqueous Me₆TREN, we predictably observed significant existence of purple-red colored Cu(0) precipitate and a blue solution, indicative of rapid disproportionation.

5.2.2 Synthesis of PNIPAM by ATRP in water.



Scheme 5. 2. Schematic representation of procedures for ATRP and SET-LRP *via* prior disproportionation of $\text{CuBr}/\text{Me}_6\text{TREN}$ in water.

The challenges in performing ATRP in protic media are often attributed to inefficient deactivation, relative to activation and propagation, and the existence of side reactions with both the catalyst and chain end.²⁵⁶ As a useful reference point for the present study, we first investigated the ATRP of NIPAM in water using a traditional experimental approach.

In order to avoid the direct disproportionation of Cu(I)Br promoted by Me_6TREN in water, a degassed initiator/NIPAM/ Me_6TREN aqueous solution was transferred to a second Schlenk tube containing CuBr under nitrogen for ATRP (Scheme 5.2). In a polymerization using a ratio of $[\text{initiator}]: [\text{CuBr}]: [\text{Me}_6\text{TREN}] = 1: 1: 1$ at ambient temperature, fast polymerization resulted in a gel precipitate with $\text{PDI} = 2.60$ and 100% conversion in 30 min (Figure 5.6). CuBr was observed to diminish during the polymerization as exemplified by the blue color of the solution becoming more intense (Figure 5.7).

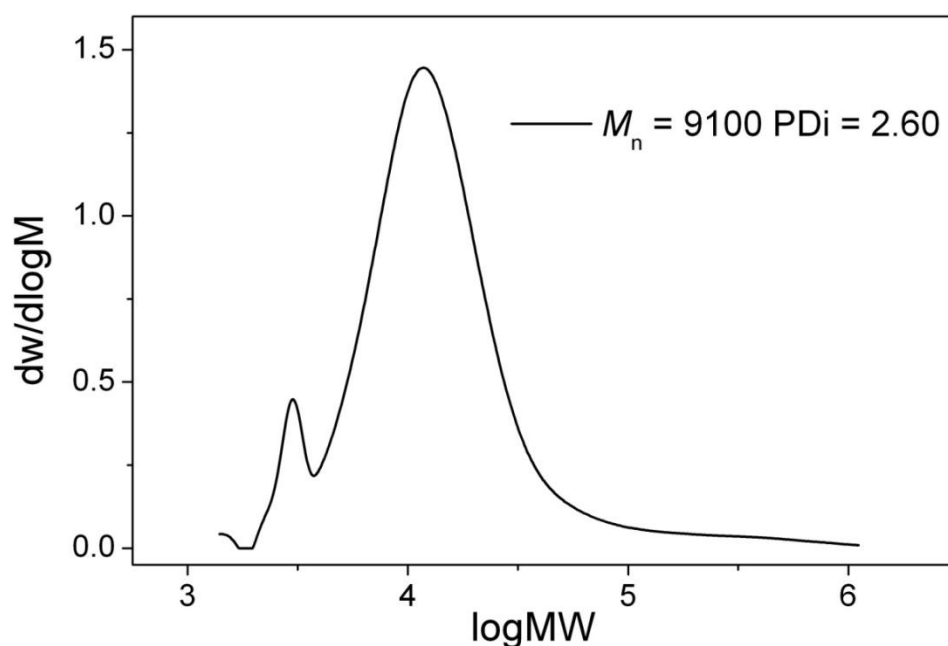
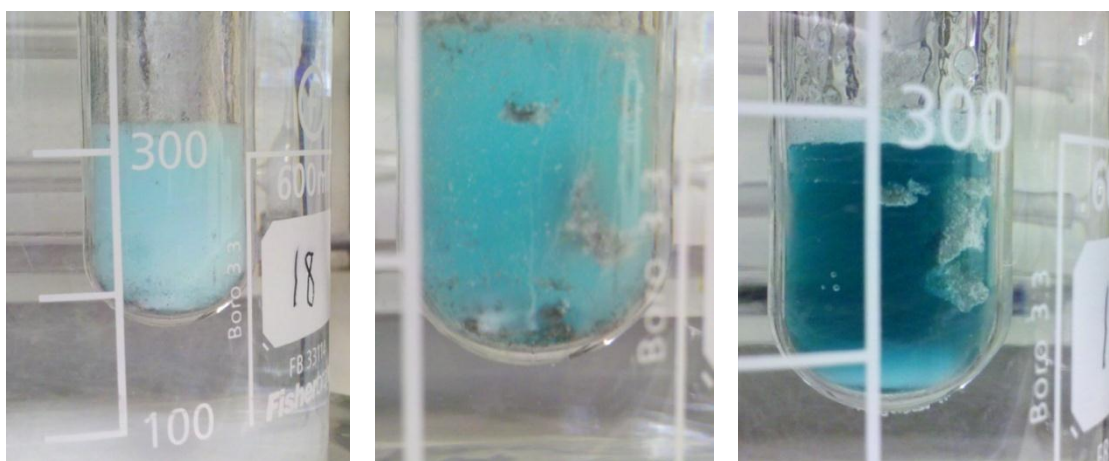


Figure 5. 6. Molecular weight distributions of PNIPAM by ATRP at ambient temperature *via* DMF SEC. Reaction conditions: H₂O = 5 mL; NIPAM = 1.13 g, 10 mmol; 2, 3-dihydroxypropyl 2-bromo-2-methylpropanoate = 60 mg, 0.25 mmol; Me₆TREN = 65 μ L, 0.25 mmol; CuBr = 36 mg, 0.25 mmol. Note: The gel was not soluble in DMF and was removed by filtration before analysis. So SEC did not reveal the MW of the gel.



a) 10 s

b) 2 min

c) 30 min

Figure 5. 7. Visual observation of the ATRP of NIPAM in H₂O under ambient temperature (~18 °C). Pictures were taken at different time after mixing the reagents. (a) 10 seconds; (b) 2 min; c) 30 min.

Optimization of polymerization conditions with a lower ratio of [initiator]: [CuBr]: [Me₆TREN] = 1: 0.8: 0.4 in an ice/water bath allowed polymerization without gel formation attaining 100% conversion in 30 min but the PDI was still high (2.70) (Figure 5.8). The high molecular weight tail may be caused by the fast initiation and propagation due to the highly reactive catalyst in water and also ineffective deactivation due to the absence of additional Cu(II) halides. To summarize, the ATRP of NIPAM in water *via* the traditional ATRP approach of adding degassed ligand, monomer and initiator to CuBr under an inert blanket does not yield a controlled/living system.

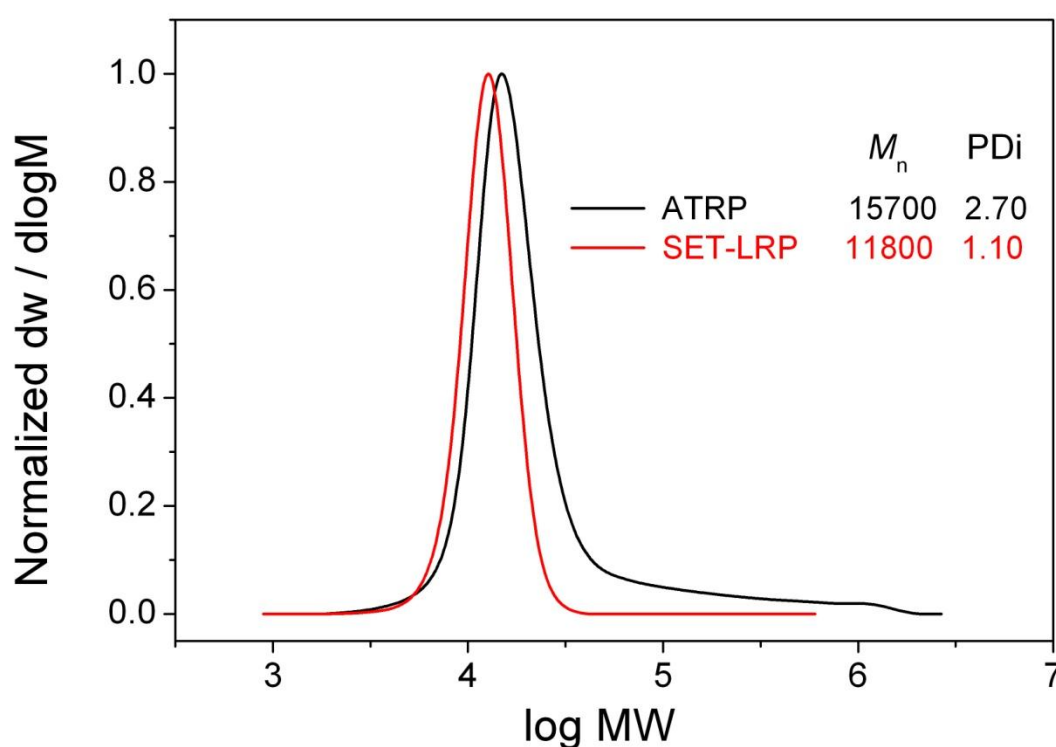


Figure 5. 8. Molecular weight distributions of PNIPAM by ATRP and SET-LRP with [NIPAM]: [initiator]: [CuBr]: [Me₆TREN] = 80: 1: 0.8: 0.4 at 0 °C as measured *via* SEC employing DMF as eluent.

5.2.3 Cu(0) wire mediated SET-LRP of NIPAM and PEGA₄₈₀ in water.

Cu(0) wire-mediated SET-LRP of NIPAM and PEGA₄₈₀ was performed in both dipolar aprotic and protic solvents.^{158,225,250} Addition of Cu(II) halides proved to be required for deactivation and suppression of an induction period. As a further reference point, the SET-LRP of NIPAM and PEGA₄₈₀ were performed using a Cu(0) wire/CuBr₂/Me₆TREN catalyst system in water.

For NIPAM polymerization, there tends to be an induction period > 2 h prior to monomer conversion reaching > 99% in a further 2 h, resulting in a final polymer with $M_n = 7200$ and dispersity = 1.13 (Figure 5.9, 5.10).

For the analogous polymerization of PEGA₄₈₀, the polymerization rate is moderate without significant induction period, reaching approximately 99% conversion in 5h and resulting in a final polymer with $M_n = 6500$ and dispersity = 1.11 (Figure 5.11). The results attained are in accordance with a previous report.¹⁵⁸

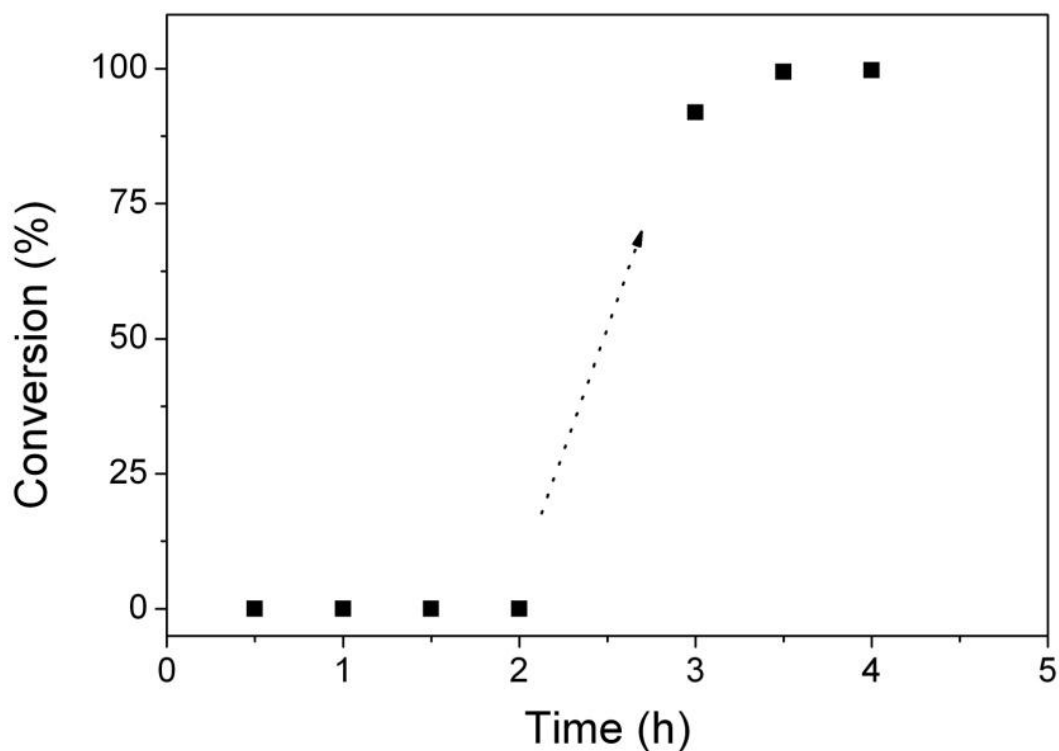


Figure 5. 9. Dependence of conversion on time for the copper (0) wire mediated SET-LRP of NIPAM in H₂O at ambient temperature.

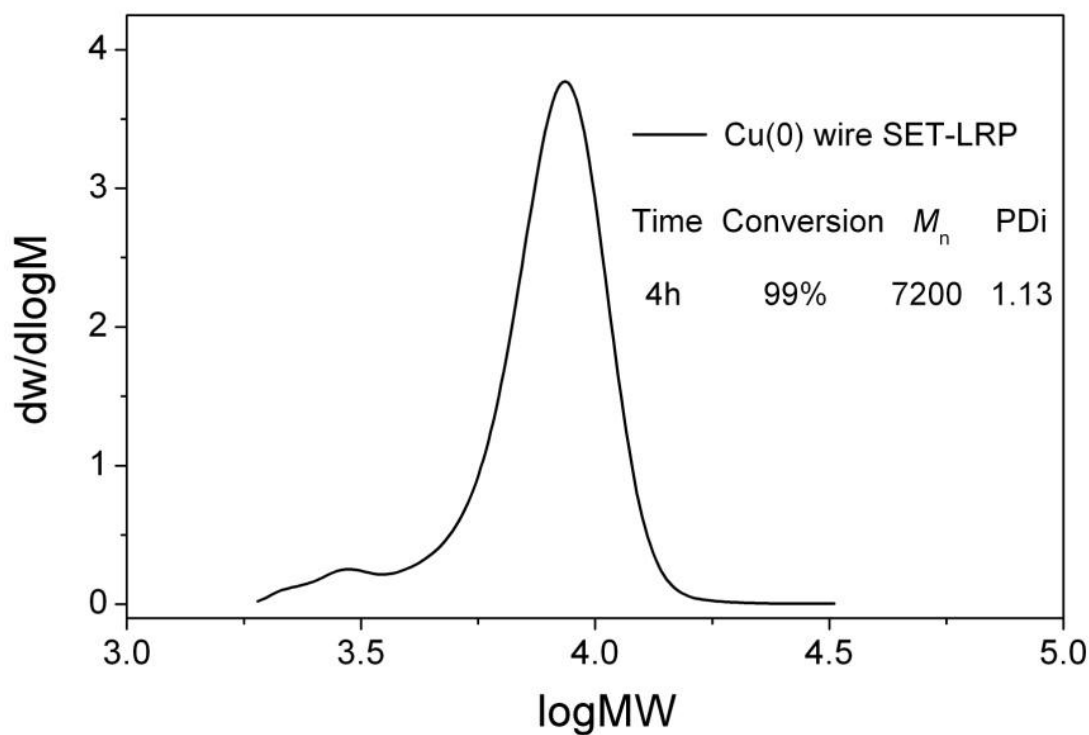


Figure 5. 10. Molecular weight distributions of PNIPAM by copper (0) wire mediated SET-LRP at ambient temperature via DMF SEC.

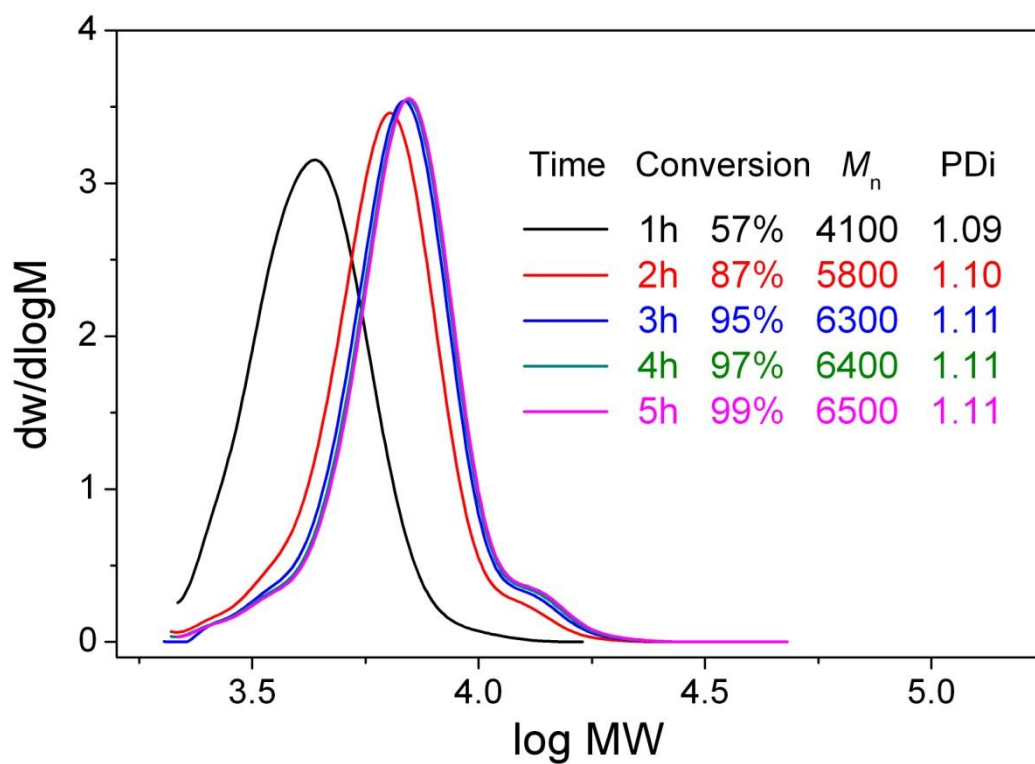


Figure 5. 11. Molecular weight distributions of poly (PEGA₄₈₀)₁₀ by copper (0) wire mediated SET-LRP at ambient temperature *via* DMF SEC.

5.2.4 Generation of Cu(0) powder and CuBr₂ via disproportionation of CuBr/Me₆TREN in water for SET-LRP of NIPAM under apparent ATRP conditions.

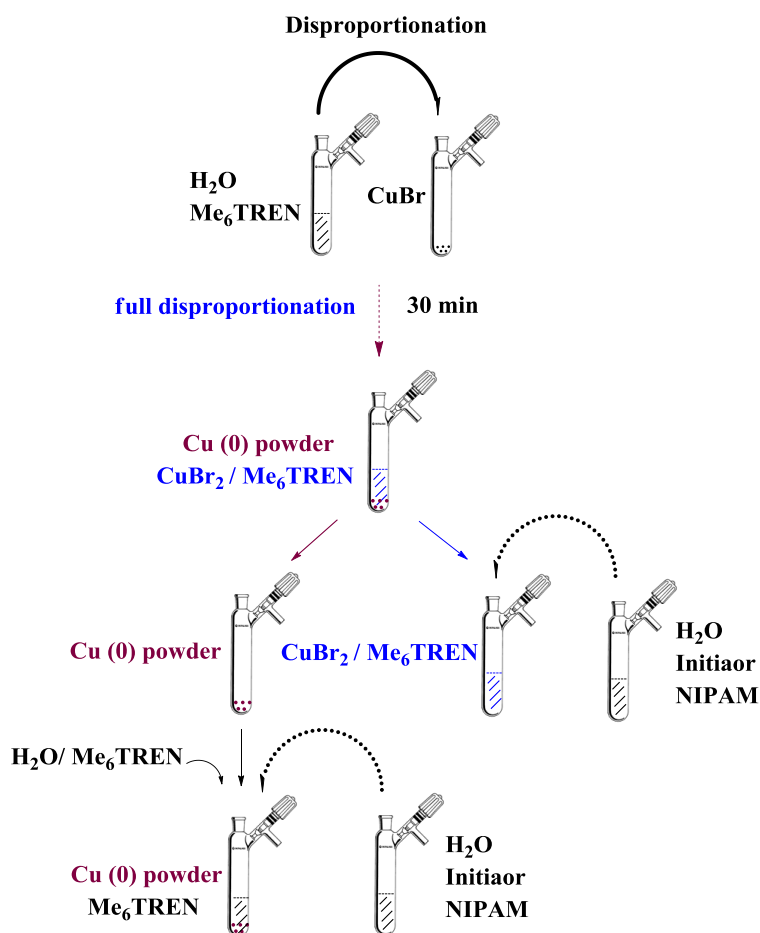
Disproportionation of CuBr promoted by Me₆TREN in water yields a purple-red colored precipitate of Cu(0) powder and CuBr₂/Me₆TREN aqua complexes (Figure 5.12). The fine Cu(0) powders should be highly active toward reaction with the initiator while CuBr₂ in solution is necessary in mediating the deactivation step, particularly at the beginning of the polymerization.



Figure 5. 12. Visual observation of the disproportionation of CuBr/Me₆TREN in H₂O under strict freeze-pump-thaw degas procedure. Conditions: H₂O = 2 mL; CuBr = 10 mg, 0.07 mmol; Me₆TREN = 9 μ L, 0.035 mmol. Picture was taken 1 min after mixing the reagents *via* cannula.

Previous work describing ATRP using stock solutions of CuCl/Me₆TREN and *in-situ* SET-LRP of NIPAM seem to have either ignored the above phenomena or did not discuss the occurrences nor consequences. This could be due to the use of mixed water/organic solvents where the organic solvents act as dispersants for the Cu(0) or the additional complexity associated with employing mixed initiator/Cu(I) halogen/ligand/monomer/solvent systems together, which likely has an effect on the rate and extent of disproportionation.^{228,233,236}

In order to investigate the potential of the suspension arising from disproportionation to control polymerization, we injected a degassed solution of initiator and NIPAM into the obtained blue suspension and left the mixture to react in an ice/water bath for 30 min. It is noteworthy that the reagent quantities and conditions used mirror those applied to the ATRP procedure discussed above with the only change being the precursory disproportionation reaction. ^1H NMR analysis confirmed full conversion according to the disappearance of the vinyl peaks. Surprisingly, SEC characterization revealed a very symmetrical Poisson-shaped distribution with $M_n = 11800$ and dispersity = 1.10 without tailing at either high or low molecular weight (MW) (Figure 5.8).



Scheme 5. 3. Scheme representation of the disproportionation of CuBr/Me₆TEN in H₂O and separation of copper (0) powder and CuBr₂/Me₆TREN solution after disproportionation.

In order to identify the synergistic nature of the disproportionation products the Cu (0) precipitate was carefully separated from the blue solution, washed with water

repeatedly and added to equivalent amounts of Me₆TREN/H₂O (Scheme 5.3). Initiator/NIPAM solutions were then injected separately into both the Cu(0) / Me₆TREN and CuBr₂ / Me₆TREN systems to test for polymerization activity.

The polymerization catalyzed by the separated Cu(0) (and additional Me₆TREN), reached 96 % conversion in 15 min according to ¹H NMR. However, the reaction solution had an observable high viscosity and SEC showed a very broad peak with $M_n = 5400$ and dispersity = 13.25 (Figure 5.13). Addition of an initiator/NIPAM solution to the bright blue CuBr₂ / Me₆TREN solution showed no detectable polymerization after 24 h according to both ¹H NMR and SEC analysis.

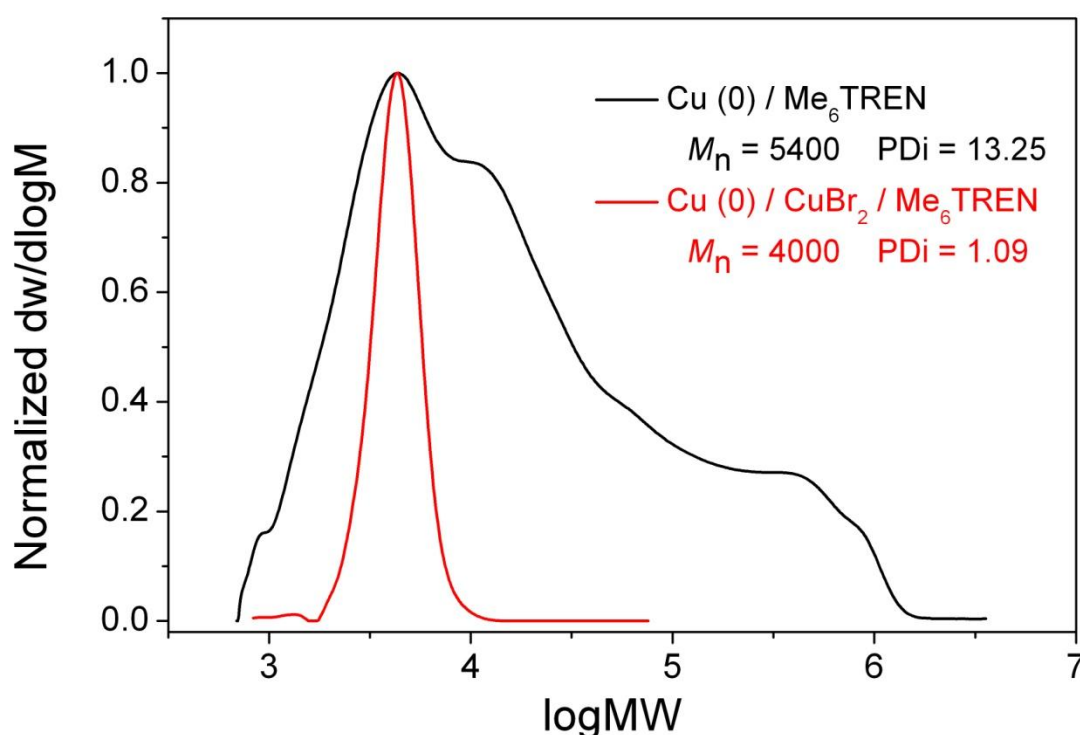


Figure 5. 13. Molecular weight distributions of PNIPAM (DP=20) catalyzed by separated Cu(0) powder/Me₆TREN (black) or Cu (0) powder/CuBr₂/Me₆TREN (red) in H₂O at ambient temperature as measured *via* SEC employing DMF as eluent.

For the polymerization catalyzed by the Cu(0)/CuBr₂/Me₆TREN suspension resulting from the initial disproportionation, full conversion was obtained in 30 min and SEC showed a final polymer with $M_n = 4000$ and dispersity = 1.09 (Figure 5.13). These experiments indicate it is unlikely CuBr/Me₆TREN complexes exist under these conditions or any minute quantities present are incapable of efficiently catalyzing

ATRP. Crucially, the *in-situ* generated Cu(0) powders and CuBr₂ are required to be present in tandem for a controlled SET-LRP polymerization.

5.2.5 Synthesis of PNIPAM by AGET ATRP in water.

AGET ATRP utilizes water-soluble reducing agents (typically L-ascorbic acid) to reduce higher oxidation state Cu(II) / ligand complexes and generate Cu(I) / ligand complexes which are claimed to have higher catalytic stability. This allows for reduced catalytic loadings, and hence, more applicability in heterogeneous systems.^{257,258}

In order to check the stability and behavior of the obtained Cu(I) / ligand complexes for AGET ATRP, we polymerized NIPAM using CuBr₂/Me₆TREN and L-ascorbic acid at ambient temperature. Initial experiments were carried out according to the literature reported procedure using slightly less reducing reagent with a ratio of [CuBr₂]:[Me₆TREN]:[L-ascorbic acid] = 1: 1: 0.4, resulting in only 60% conversion after 16 h to give a product with $M_n = 2500$ and dispersity = 1.11 (Figure 5.14). Under more optimized conditions, with a ratio of [CuBr₂]: [Me₆TREN]: [L-ascorbic acid] = 1: 2: 0.5 the polymerization rate was increased and conversion reached 85% in 15 min with full conversion obtained with a final $M_n = 4000$ and dispersity = 1.10 (Figure 5.15). Interestingly, the initially blue solution remained clear throughout the polymerization when L-ascorbic acid was added and no significant visible Cu(0) precipitation was observed (Figure 5.16), suggesting that disproportionation of the reduced Cu(I) / ligand complexes possibly does not occur under these conditions.

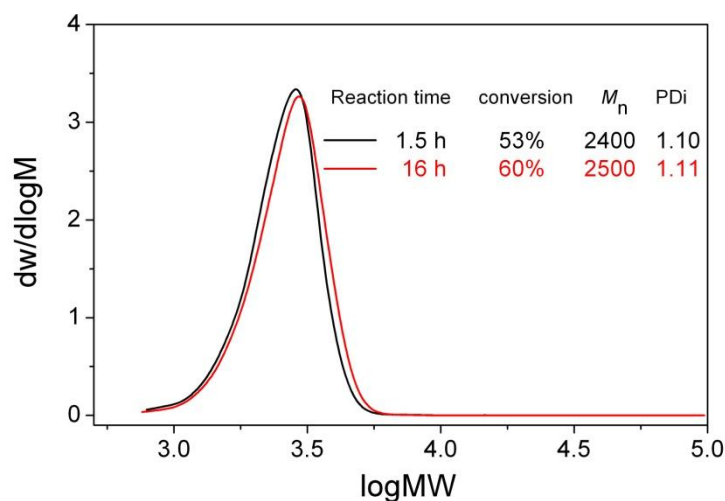


Figure 5. 14. DMF SEC molecular weight distributions for the ARGET ATRP of NIPAM (DP=20) in H₂O at ambient temperature with [initiator]: [CuBr₂]: [Me₆TREN]: [Ascorbic acid] = 1: 0.4: 0.4: 0.16.

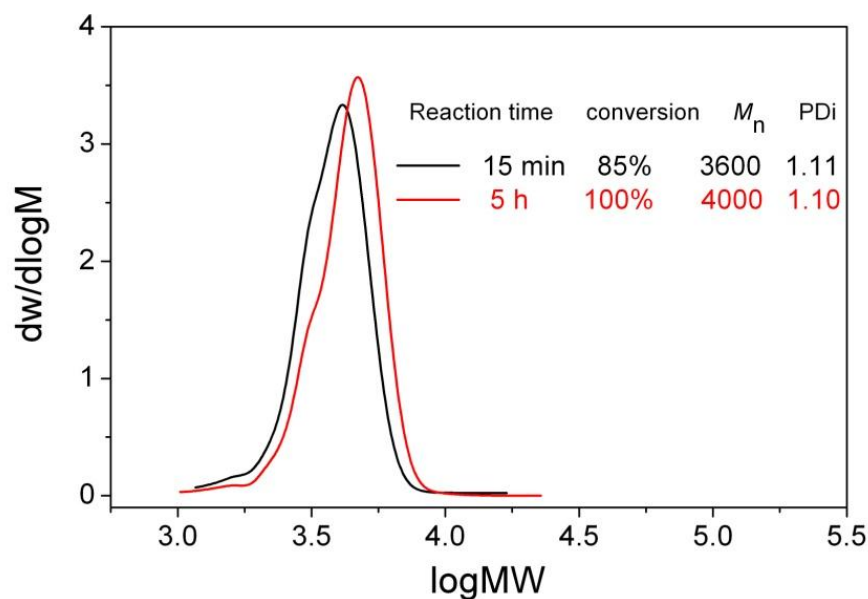


Figure 5. 15. DMF SEC molecular weight distributions for the ARGET ATRP of NIPAM (DP=20) in H₂O at ambient temperature with [initiator]: [CuBr₂]: [Me₆TREN]: [Ascorbic acid] = 1: 0.4: 0.8: 0.2.

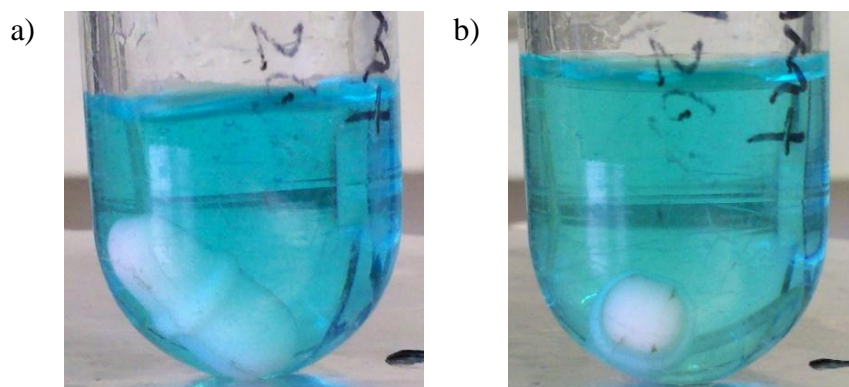


Figure 5. 16. Visual observation of the AGET ATRP of NIPAM in H₂O with [initiator]: [CuBr₂]: [Me₆TREN]: [Ascorbic acid] = 1: 0.4: 0.4: 0.16 before (a) and after (b) addition of L-ascorbic acid. Conditions: a) Picture was taken 15 min after nitrogen bubbling. b) Picture was taken 1 min after addition of L-ascorbic acid.

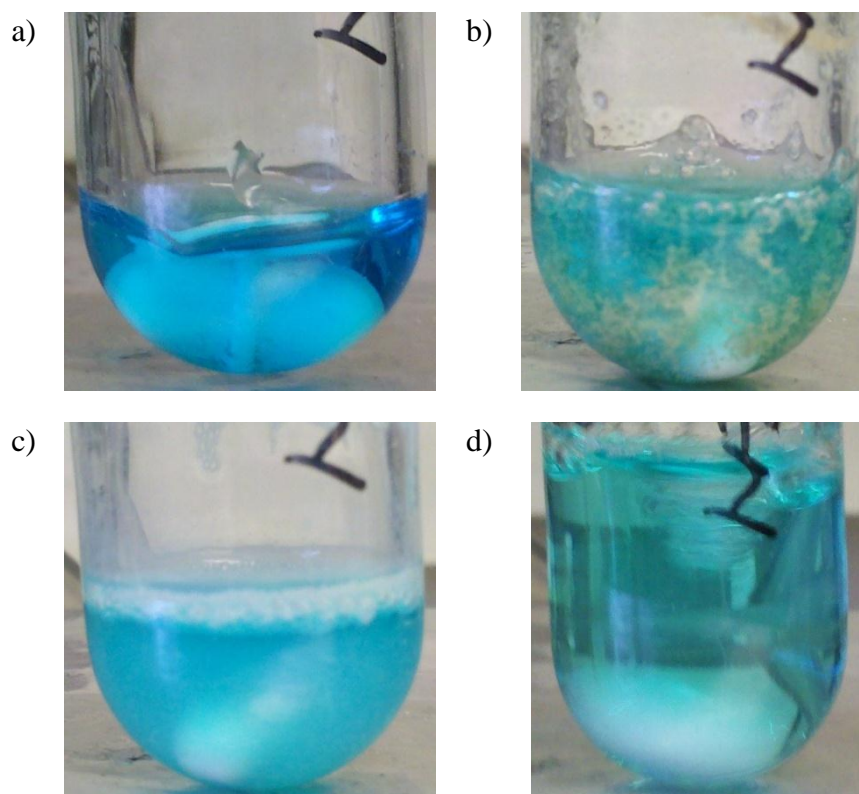


Figure 5. 17. Visual observation of the reduction of CuBr₂/Me₆TREN complex by L-ascorbic acid for AGET ATRP of NIPAM in H₂O under ambient temperature with [initiator]: [CuBr₂]: [Me₆TREN]: [Ascorbic acid] = 1: 0.4: 0.4: 0.16. Conditions: a) CuBr₂ / Me₆TREN in H₂O; b) picture was taken 1 min after addition of L-Ascorbic acid; c) picture was taken 15 min after addition of L-Ascorbic acid; d) picture was taken 1 min after addition of initiator and monomer.

In order to distinguish the Cu(I)/ligand complexes from the polymerization solution, we first made a solution of Cu(I)/ligand prior to addition of initiator and monomer, either by addition of the L-ascorbic acid to the $\text{CuBr}_2/\text{Me}_6\text{TREN}$ solution or addition of Me_6TREN after mixing $\text{CuBr}_2/\text{L-ascorbic acid}$. Interestingly, foaming occurred when L-ascorbic acid was added to the clear blue solution of $\text{CuBr}_2/\text{Me}_6\text{TREN}$, resulting in a turbid white suspension. Following the injection of monomer and initiator, the suspension immediately became clear (Figure 5.17). ^1H NMR spectroscopy showed that polymerization stopped at conversion = 36% and SEC analysis revealed an asymmetric peak with $M_n = 1800$ and dispersity = 1.10.

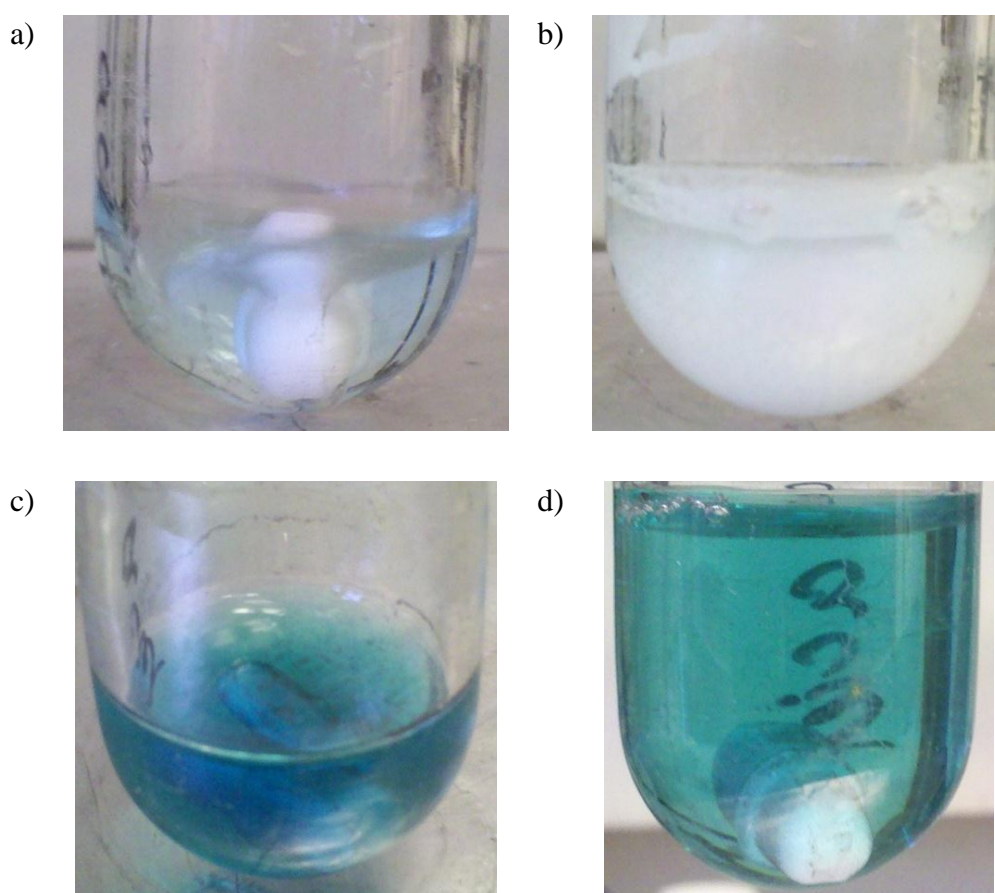


Figure 5. 18. Visual observation of the reduction of CuBr_2 by L-ascorbic acid into CuBr following disproportionation into Cu (0) & CuBr_2 for SET-LRP of NIPAM in H_2O under ambient temperature with [initiator]: $[\text{CuBr}_2]$: $[\text{Me}_6\text{TREN}]$: [Ascorbic acid] = 1: 0.4: 0.4: 0.16. Conditions: a) CuBr_2 in H_2O ; b) after addition of L-Ascorbic acid; c) after addition of Me_6TREN ; d) after addition of initiator and monomer; All pictures were taken 1 min after relative reaction.

A white precipitate of CuBr was obtained when L-ascorbic acid was added to the light blue solution of CuBr₂ disappearing when Me₆TREN was added leave a bright blue solution and the appearance of a red Cu(0) precipitate, indicative of disproportionation (Figure 5.18). Subsequently, initiator and monomer was added to start polymerization. When a ratio of [CuBr₂]: [Me₆TREN]: [L-ascorbic acid] = 1: 1: 0.4 was used polymerization stopped at 61 % conversion with final $M_n = 2500$ and dispersity = 1.08. With [CuBr₂]: [Me₆TREN]: [L-ascorbic acid] = 1: 2: 0.5, polymerization was fast and full conversion was attained in 15 min with final $M_n = 4000$ and dispersity = 1.12.

These experiments further underline the complexity inherent in Cu-mediated LRP, which showed that the copper aquo ion behaves very differently to the Cu(I, II) / ligand complexes. L-ascorbic acid has been shown to coordinate with copper even in the presence of *N*-ligands.²⁵⁹⁻²⁶¹ The reduction of CuBr₂ also releases HBr into the solution and it is still not clear whether this protonates Me₆TREN or affects the disproportionation. Thus, the catalyst in this AGET ATRP system does not seem to be a CuBr / Me₆TREN / H₂O complex or disproportionation does not proceed under such conditions. Further research is required for full understanding.

5.2.6 Synthesis of PNIPAM with varying DP by SET-LRP in water.

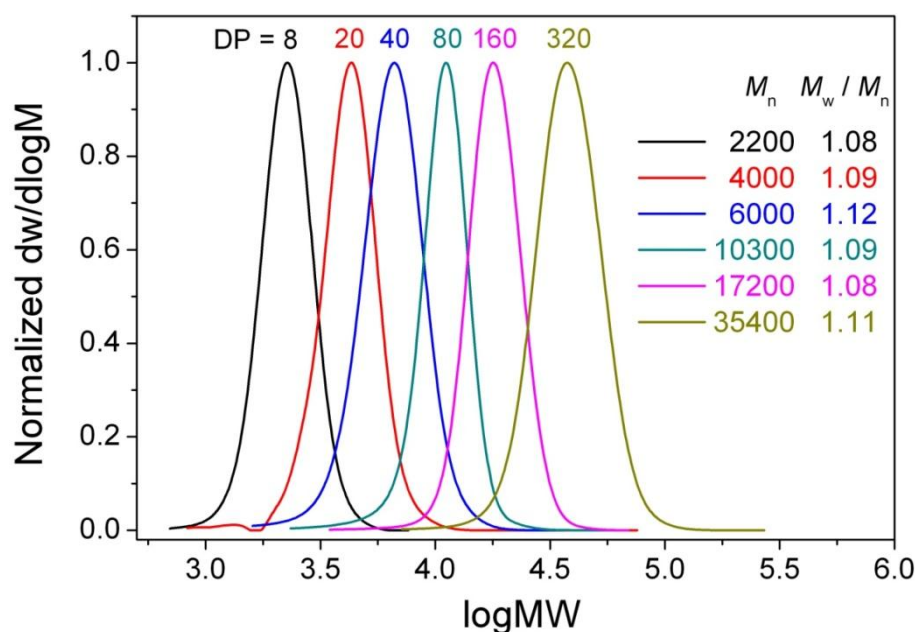


Figure 5. 19. Molecular weight distributions of PNIPAM (DP=8, 20, 40, 80, 160, 320) catalyzed by the in-situ generated Cu(0) powders/CuBr₂/Me₆TREN in H₂O as measured *via* SEC employing DMF as eluent.

SET-LRP catalyzed by *in-situ* generated Cu(0) and CuBr₂ formed *via* disproportionation of CuBr/Me₆TREN in water was used for the synthesis of PNIPAM with DP between 8 and 320. Polymerizations were conducted under strict degassing procedures using either repeated freeze-pump-thaw procedures or, more conveniently, nitrogen bubbling. For DP = 8, 20 and 40, polymerizations were conducted at ambient temperature (~18 °C) using a ratio of [CuBr]: [Me₆TREN] = 1:1. ¹H NMR analysis of the polymerization (DP=40) showed conversion reached 93% in 5 min, 99% in 10 min and 99.9% in 15 min, with full conversion obtained in < 30 min (Figure 5.20 & 5.21). SEC characterization of all final polymer products revealed narrow molecular weight distributions (dispersity~ 1.10, Figure 5.19) with symmetrical peaks without tailing.

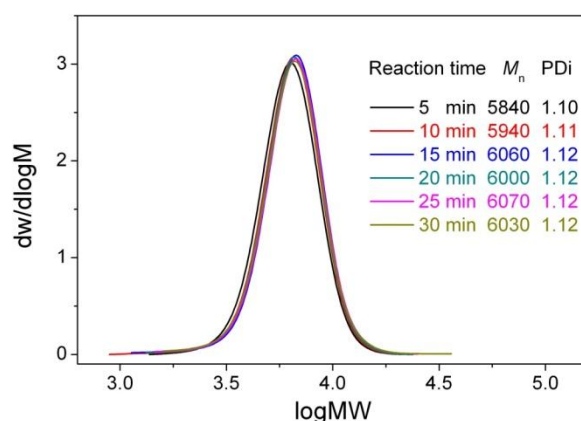


Figure 5. 20. DMF SEC molecular weight distributions at different time for the aqueous SET-LRP of NIPAM (DP=40) at ambient temperature.

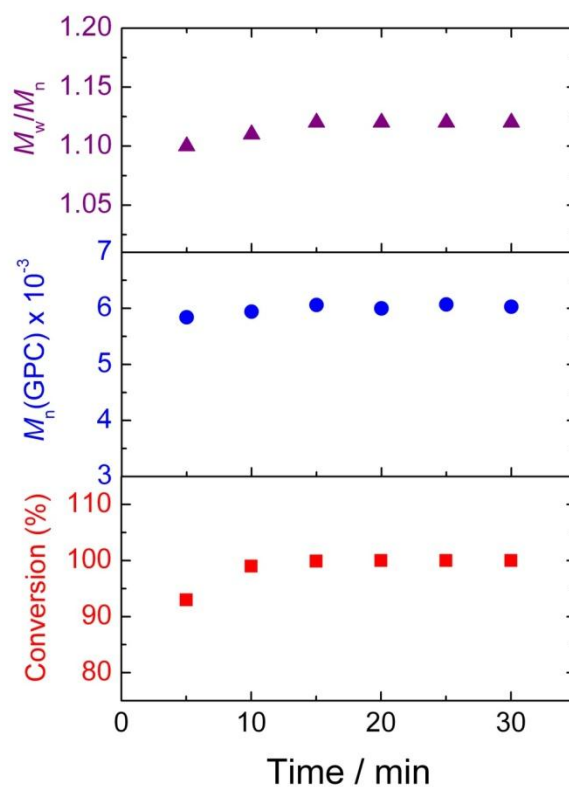


Figure 5. 21. Dependence of conversion, M_n and M_w / M_n on time for the SET-LRP of NIPAM (DP=40) *via* disproportionation of CuBr / Me₆TREN in H₂O at ambient temperature.

When using the same ratio of [CuBr]: [Me₆TREN] = 1: 1 for polymerizations targeting higher DP (80 & 160), increased amounts of water and NIPAM were used (lower overall catalyst concentration). In this case, inefficient deactivation was

observed. The dispersity observed during the early stages of polymerization was approximately 3.0 with final values > 1.4 (Figure 5.22). Consequently, we changed the ratio of $[\text{CuBr}]: [\text{Me}_6\text{TREN}]$ to 2: 1, which should provide more CuBr_2 and thus more efficient deactivation. Polymerization of $\text{DP} = 80$ under ambient temperature reached 99% conversion in 30 min with $M_n = 10300$ and dispersity = 1.08 (Figure 5.23) a significantly improved control. Interestingly, previous reports also suggested that a ratio of $[\text{CuBr}]: [\text{Me}_6\text{TREN}] = 2: 1$ showed maximum degree of disproportionation in DMSO.²²⁴

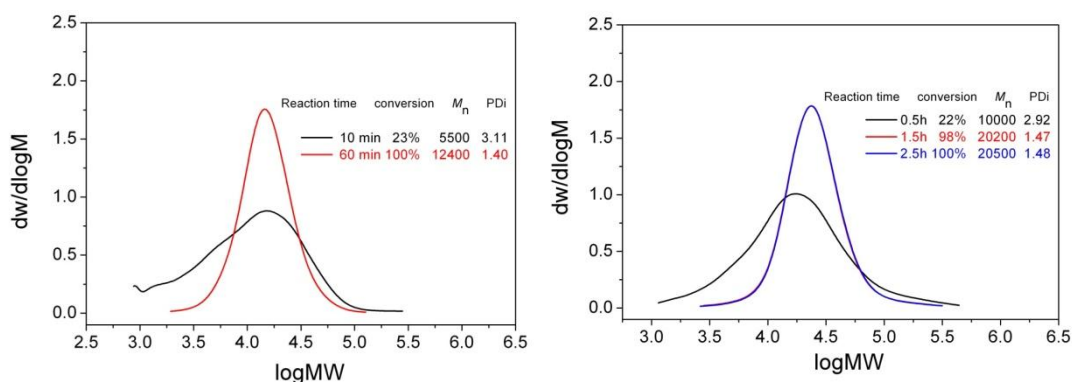


Figure 5. 22. DMF SEC molecular weight distributions at different time for the SET-LRP of NIPAM ($\text{DP}=80$, left; $\text{DP}=160$, right) in H_2O at ambient temperature with $[\text{initiator}]: [\text{CuBr}]: [\text{Me}_6\text{TREN}] = 1: 0.4: 0.4$.

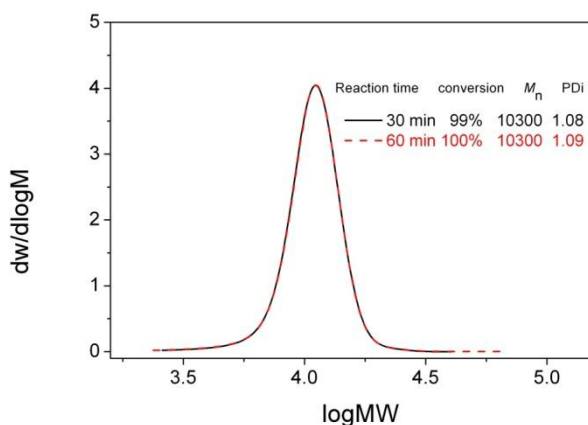


Figure 5. 23. DMF SEC molecular weight distributions at different time for the SET-LRP of NIPAM ($\text{DP}=80$) in H_2O at ambient temperature with $[\text{initiator}]: [\text{CuBr}]: [\text{Me}_6\text{TREN}] = 1: 0.8: 0.4$.

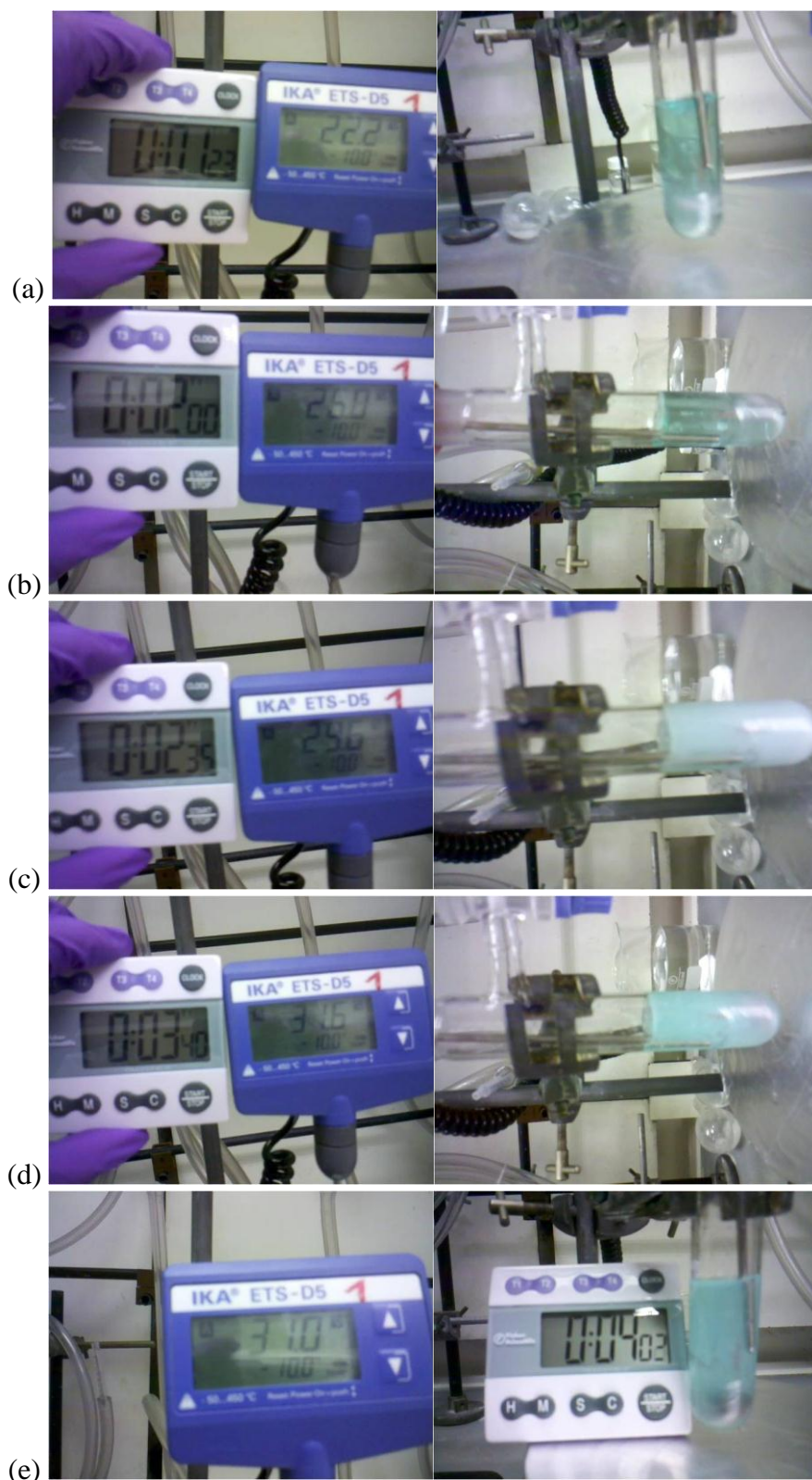


Figure 5. 24. Visual observations for SET-LRP of NIPAM (DP=160) in H₂O at ambient temperature (~18 °C) with [initiator]: [CuBr]: [Me₆TREN] = 1: 0.8: 0.4. Conditions: white equipment = time meter; blue equipment = IKA electronic contact thermometer. Video screenshot (d) shows highest temperature as 31.6 °C (3 min 40 s).

When applying the same conditions in a polymerization targeting $DP = 160$ under ambient temperature, an interesting LCST phenomenon was observed after approximately 3 min. This was manifested by way of a cloudy suspension and precipitation of polymer, caused by an enhanced exotherm associated with the larger scale reaction. A temperature profile revealed that the temperature increased from $\sim 18\text{ }^{\circ}\text{C}$ to $\sim 31\text{ }^{\circ}\text{C}$ over the first 3 min, bringing it close to the LCST temperature of PNIPAM. This further illustrated that there is no significant induction period and the polymerization rate was fast (Figure 5.24). Although conversion reached 93% in 60 min with $M_n = 18200$ and dispersity = 1.13, a tailing peak at low molecular weight was observed (Figure 5.25).

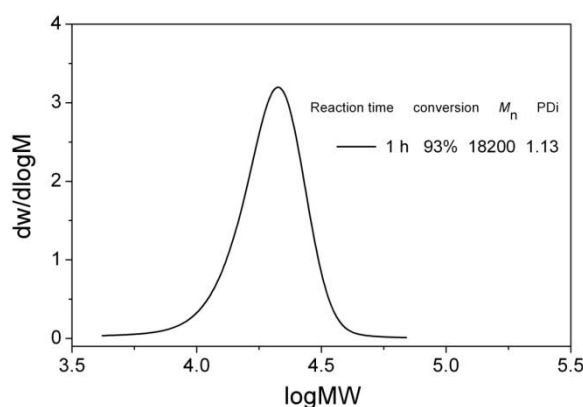


Figure 5. 25. DMF SEC molecular weight distributions at 1 h for the SET-LRP of NIPAM ($DP=160$) in H_2O at ambient temperature with [initiator]: [CuBr]: [Me₆TREN] = 1: 0.8: 0.4.

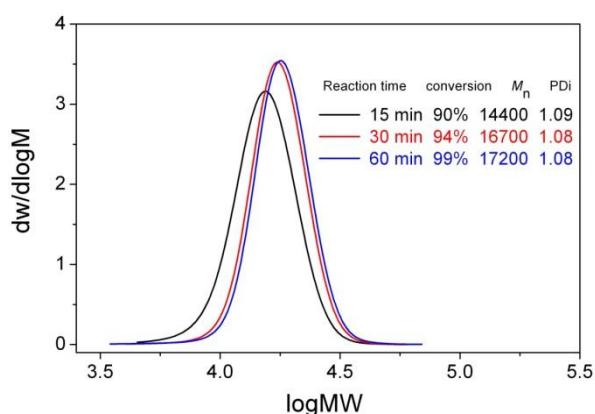


Figure 5. 26. DMF SEC molecular weight distributions at different time for the SET-LRP of NIPAM ($DP=160$) in H_2O at $0\text{ }^{\circ}\text{C}$ with [initiator]: [CuBr]: [Me₆TREN] = 1: 0.8: 0.4.

The polymerization was repeated in an ice/water bath, which eliminated the previously observed LCST phenomenon and resulted in 99% conversion in 60 min and a final $M_n = 17200$ and dispersity = 1.08 (Figure 5.26).

Successful polymerization targeting a DP = 320 under the same reaction conditions resulted in 99.9% conversion in 60 min, $M_n = 35400$ and dispersity = 1.11 (Figure 5.27). At a higher ratio of [CuBr]: [Me₆TREN] = 3: 1 (DP = 160) at ambient temperature the polymerization was slower, reaching only 70% conversion in 150 min and $M_n = 12900$ and dispersity = 1.20, indicative of increased termination during the polymerization (Figure 5.28).

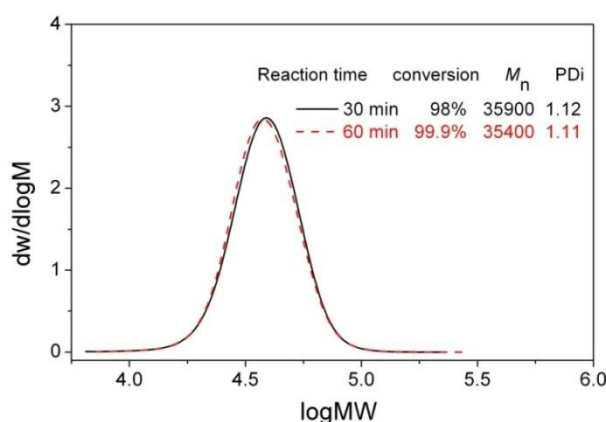


Figure 5. 27. DMF SEC molecular weight distributions at different time for the SET-LRP of NIPAM (DP=320) in H₂O at 0 °C with [initiator]: [CuBr]: [Me₆TREN] = 1: 0.8: 0.4.

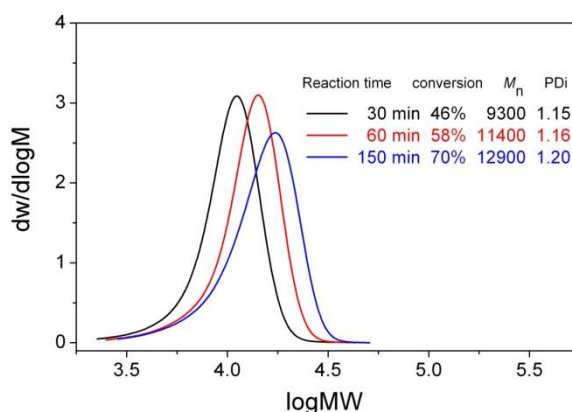


Figure 5. 28. DMF SEC molecular weight distributions at different time for the SET-LRP of NIPAM (DP=160) in H₂O at ambient temperature with [initiator]: [CuBr]: [Me₆TREN] = 1: 1.2: 0.4.

5.2.7 Chain end fidelity and chain extension of PNIPAM by SET-LRP in water.

It is normally difficult to maintain high chain end fidelity under aqueous polymerization conditions, mainly due to the facile hydrolysis of the terminal halogen group via a cyclic onium intermediate.^{226,262} Significant termination and very broad MW distributions have been observed when employing ATRP procedures for block copolymerization of NIPAM in water.²⁶³

Previous reports suggested that chlorine-containing initiator/CuCl systems were preferable in invoking good control and high chain end fidelity. Interestingly, while we used a bromide initiator with CuBr for all polymerizations we did not observe any deleterious effects in employing the more labile halide.^{250,262} Narrow dispersity was maintained throughout all SET-LRP polymerizations from low conversion to full conversion. No detectable coupling peaks were observed, even when reactions were left overnight. Chain extension polymerization was initially performed at ambient temperature as a qualitative assessment of the terminal bromide. The polymerization to produce the first block was allowed to proceed for 2 h, although ¹H NMR spectroscopy showed 100% conversion already at 30 min. After addition of new monomer and reaction for a further 3 h, total conversion reached 87%. However, SEC revealed a bimodal peak which overlapped with the initial polymer trace, implying significant loss of the terminal bromide (Figure 5.29).

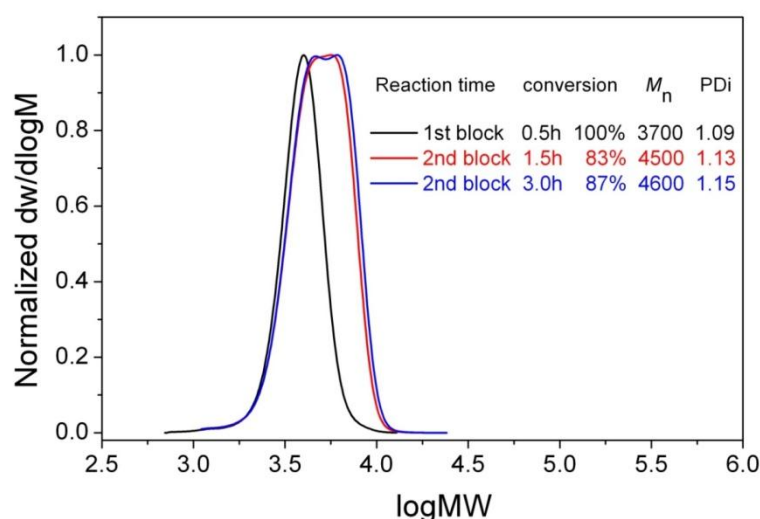


Figure 5. 29. Molecular weight distributions of PNIPAM by SET-LRP for chain extension in H₂O under ambient temperature as measured *via* SEC employing DMF as eluent.

As a more quantitative assessment of bromo- functionality, DMF SEC, high resolution NMR and MALDI-ToF MS analysis were used to characterize low MW PNIPAM samples (DP=8) obtained by SET-LRP at both ambient temperature (~ 18 °C) and 0 °C.

SEC spectroscopy revealed similar MW and MW distribution, Figure 5.30. FT-IR showed same peak absorbance for PNIPAM obtained at both ambient temperature (~ 18 °C) and 0 °C, Figure 5.31.

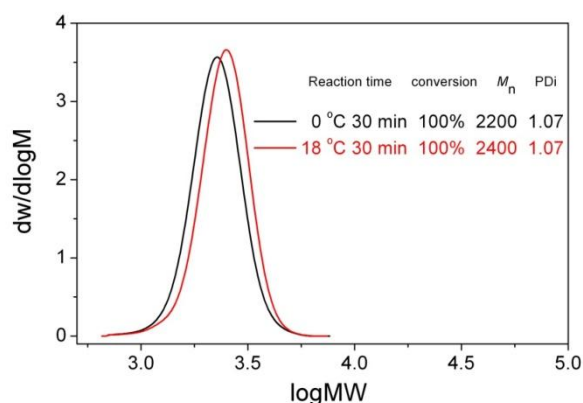


Figure 5. 30. Molecular weight distributions of PNIPAM (DP=8) by SET-LRP at 0 °C and ambient temperature *via* DMF SEC.

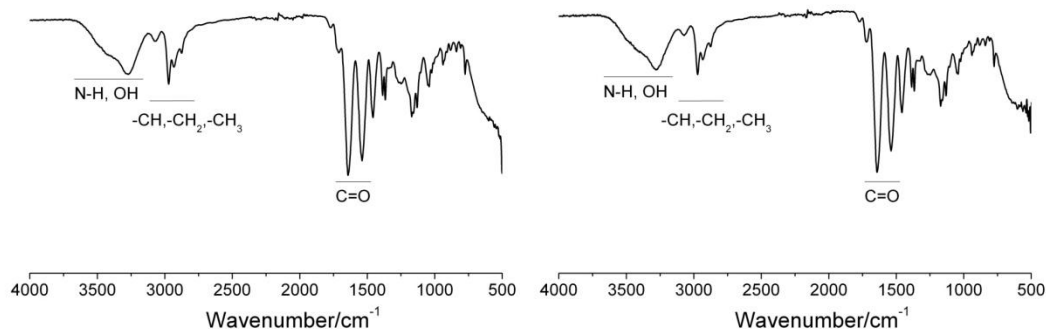


Figure 5. 31. FTIR spectra of PNIPAM (DP=8) by SET-LRP at 0 °C (left) and ambient temperature (right).

^1H , ^{13}C , COSY and HSQC NMR spectra showed that the bromide end groups of PNIPAM obtained at ambient temperature underwent quantitative hydrolysis to yield terminal hydroxyl (OH) groups (3.75 ppm (^1H NMR) and 69 ppm (^{13}C NMR)). The relative correlation with polymer backbone on COSY and clear overlap with initiator residue at 3.9 ppm & 69 ppm on HSQC was also observed, Figure 5.32-5.35.

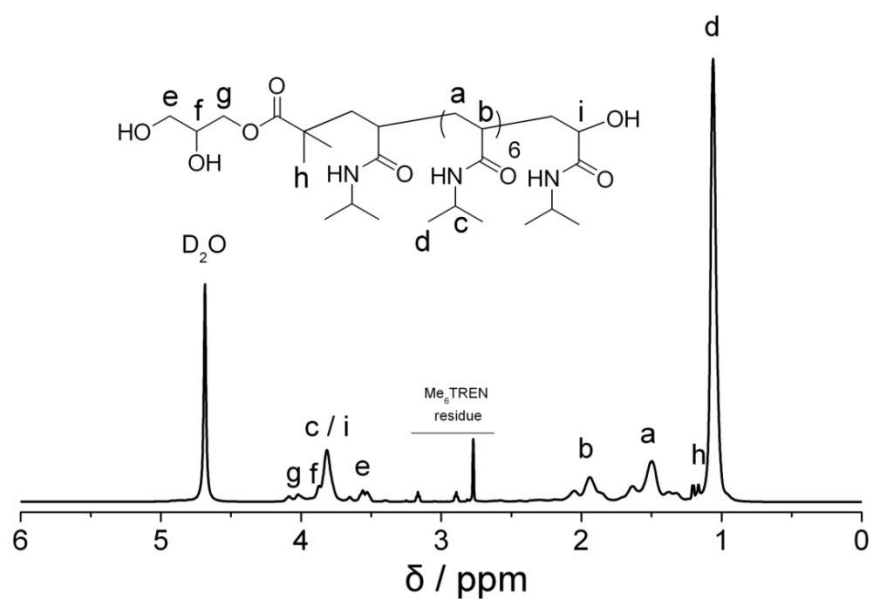


Figure 5. 32. ^1H NMR spectrum of PNIPAM (DP=8) in D_2O by SET-LRP at ambient temperature. The numbering of the hydrogen atoms used for the NMR peak assignment is shown in the spectrum. Peak i is overlapped with peak c.

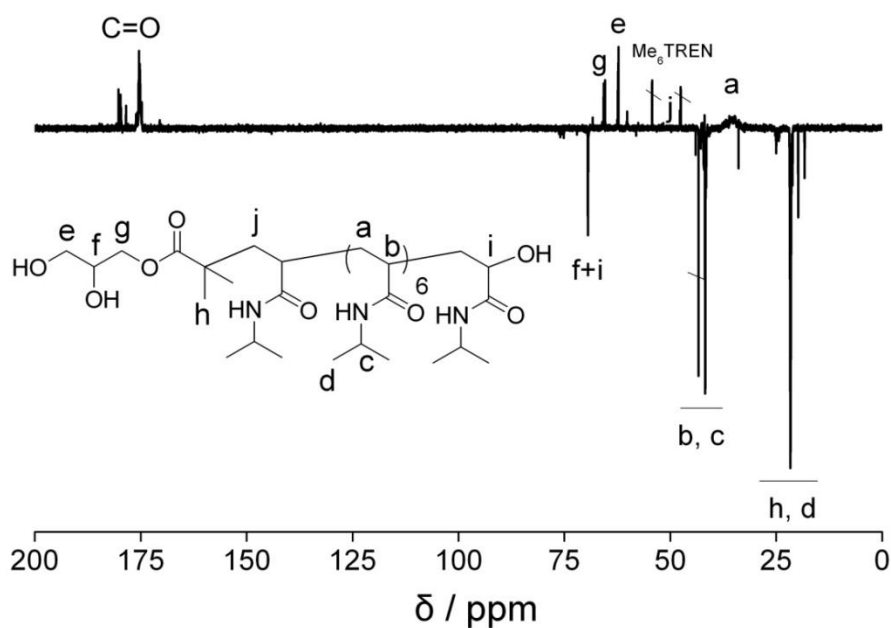


Figure 5. 33. ^{13}C NMR spectrum of PNIPAM (DP=8) in D_2O by SET-LRP at ambient temperature. The numbering of the carbon atoms used for the NMR peak assignment is shown in the spectrum. Peak f is overlapped with peak i.

THE UNIVERSITY OF
WARWICK

C46-2 in D2O @ 298°K 1H-1H COSY Spectrum

QZC46-2 18°C DP=8 PNIPAM.

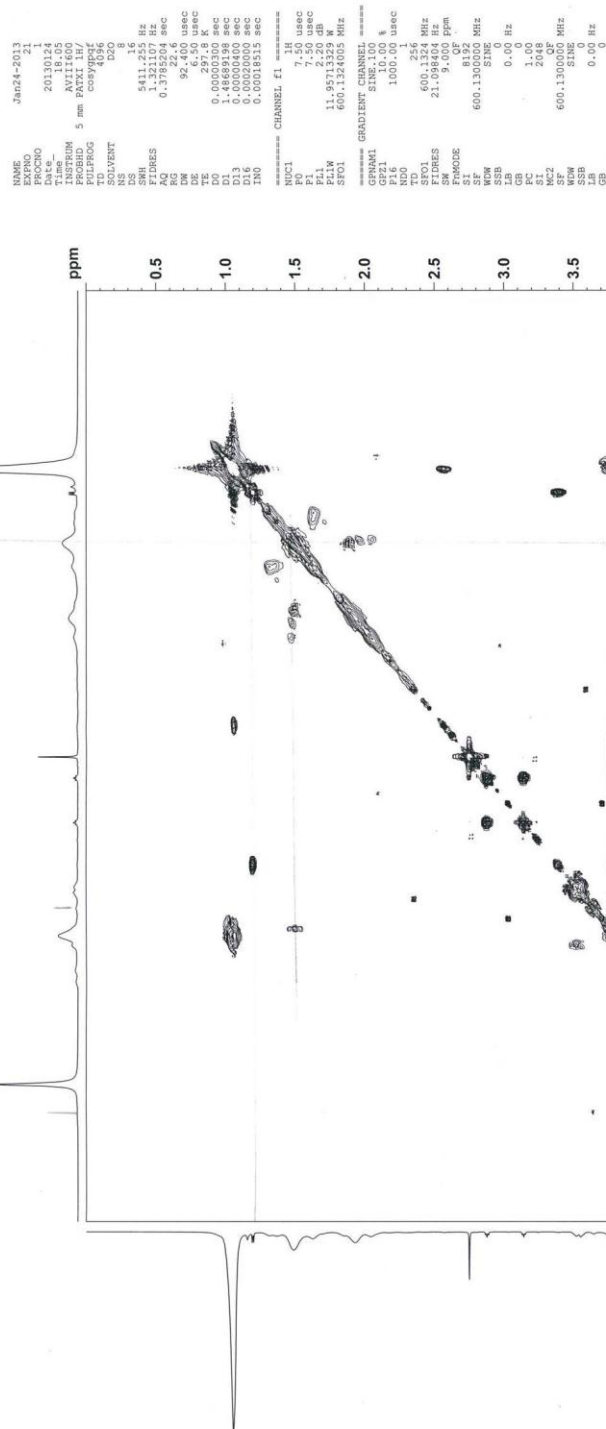


Figure 5. 34. ^1H - ^1H COSY NMR spectrum of PNIPAM (DP=8) in D_2O by SET-LRP at ambient temperature.



Hydrolysis was also found in PNIPAM polymerized at 0 °C. However, in this case we were able to identify some bromo- functional PNIPAM, via a resonance at 3.95

(terminal *CH*-Br) and appropriate correlation with the polymer backbone from COSY spectroscopy, Figure 5.36-5.39.

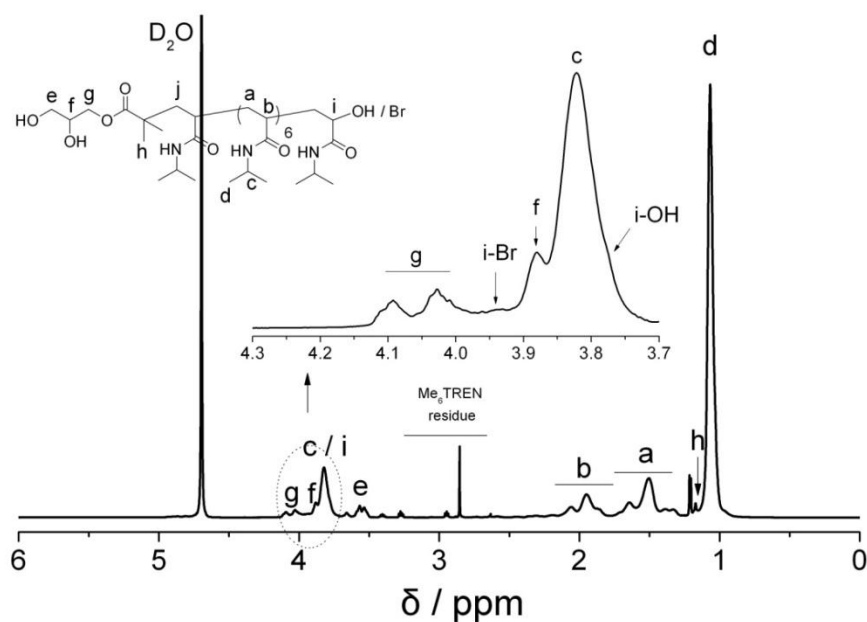


Figure 5. 36. ^1H NMR spectrum of PNIPAM (DP=8) in D_2O by SET-LRP at $0\text{ }^\circ\text{C}$. The numbering of the hydrogen atoms used for the NMR peak assignment is shown in the spectrum. Peak i-OH is overlapped with peak c.

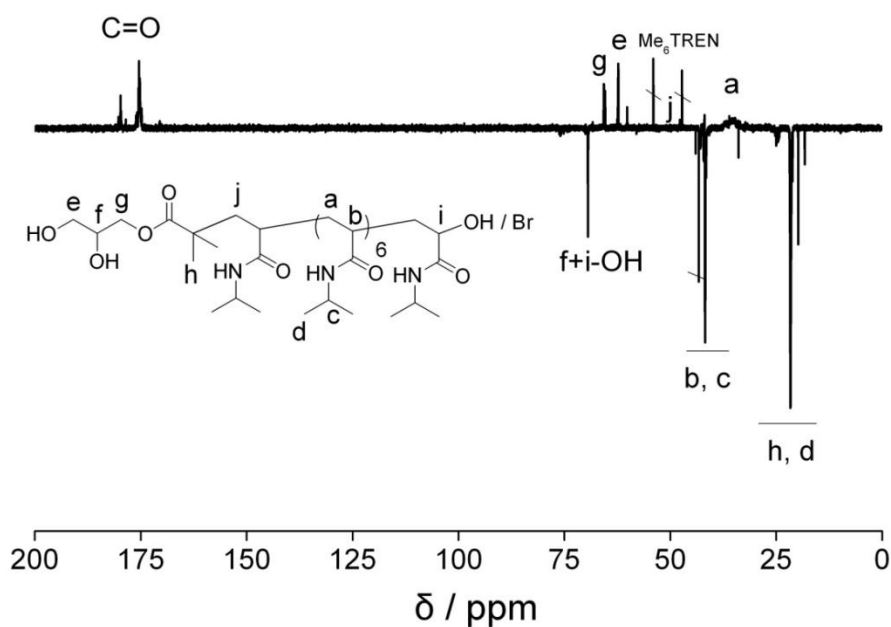


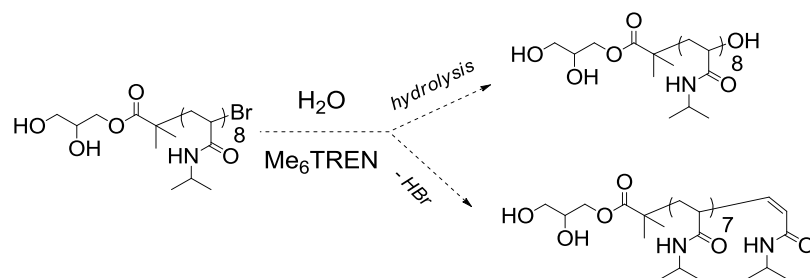
Figure 5. 37. ^{13}C NMR spectrum of PNIPAM (DP=8) in D_2O by SET-LRP at $0\text{ }^\circ\text{C}$. The numbering of the carbon atoms used for the NMR peak assignment is shown in the spectrum. Peak f is overlapped with peak i-OH.



QZC46-1 0°C DP=8 DNZDAM.



Figure 5. 39. ^1H - ^{13}C HSQC NMR spectrum of PNIPAM (DP=8) in D_2O by SET-LRP at 0 °C.



Scheme 5. 4. Scheme representation of hydrolysis and disproportionation termination of chain end of PNIPAM (DP=8) by SET-LRP *via* disproportionation of CuBr / Me₆TREN in H₂O.

MALDI-ToF MS analysis (Figure 5.40-5.42) of the same sample (0 °C) confirmed peaks of PNIPAM with terminal bromide groups, OH groups from hydrolysis, and also internal vinyl groups, as a result of HBr elimination, Scheme 5.4.

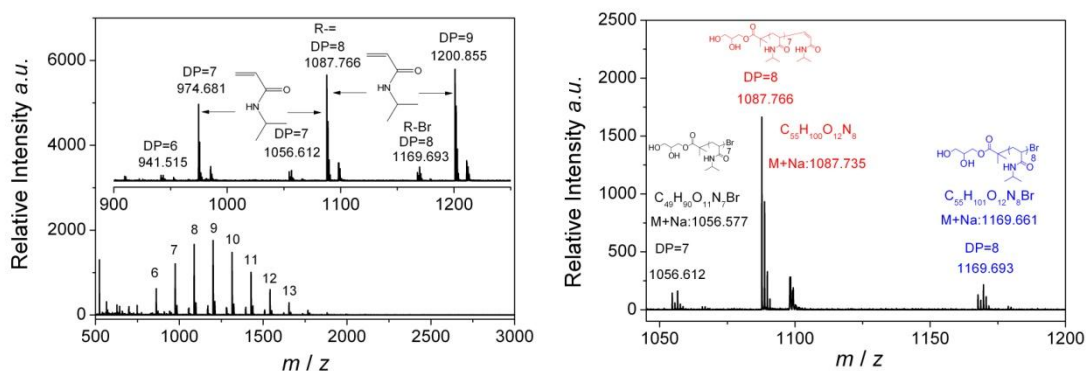


Figure 5. 40. MALDI-ToF MS spectrum of PNIPAM (DP=8) by SET-LRP at 0 °C. The MALDI-ToF MS analysis was done as soon as possible after taking sample from the reaction.

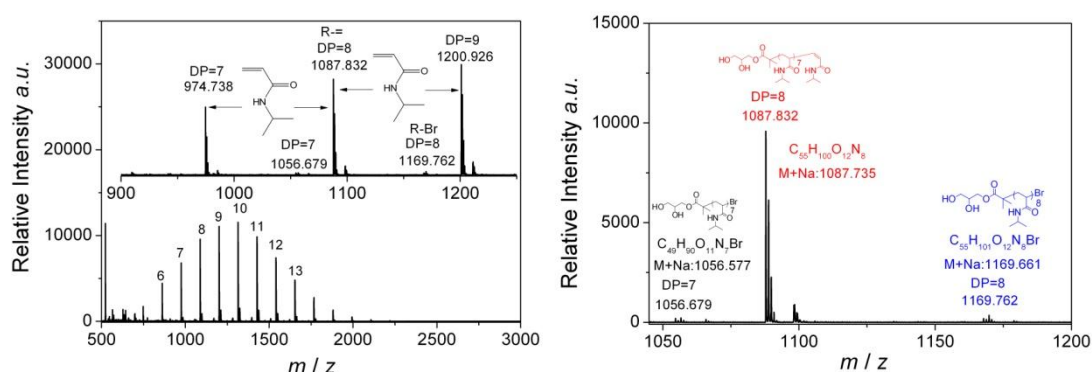


Figure 5. 41. MALDI-ToF MS spectrum of PNIPAM (DP=8) by SET-LRP at ambient temperature (~ 18 °C). The MALDI-ToF MS analysis was done as soon as possible after taking sample from the reaction.

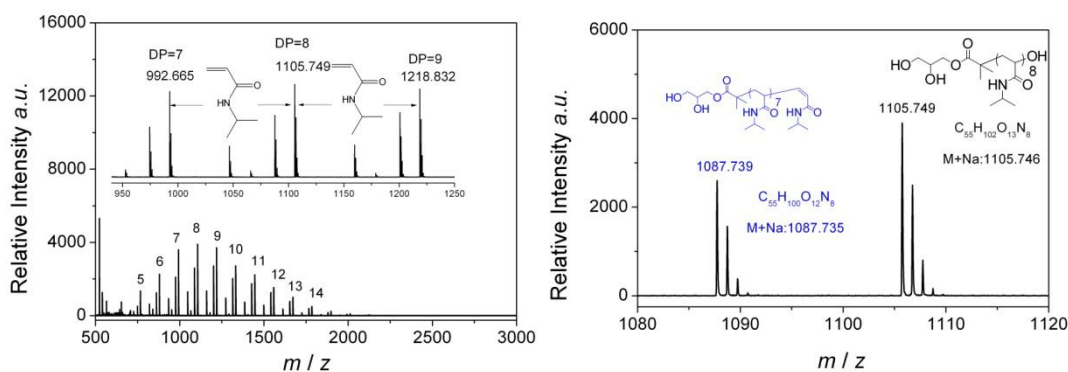


Figure 5. 42. MALDI-ToF MS spectrum of PNIPAM (DP=8) by SET-LRP at ambient temperature ($\sim 18\text{ }^{\circ}\text{C}$). The MALDI-ToF MS analysis was done after taking sample from the reaction overnight. **Note:** The peaks and peak height of PNIPAM in the MALDI-ToF MS spectra may not reveal the total information or right ratio of each component during the reaction and are only supplied as reference for NMR and GPC characterization results.

From 600 MHz NMR we can conclude that the hydrolysis of bromine is the predominant termination reaction. The hydrolysis reaction becomes more obvious subsequent to full conversion but lower reaction temperatures (i.e. ice / water bath) suppress the rate.

Given the above end group fidelity, both initial polymerization and chain extension was carried out at $0\text{ }^{\circ}\text{C}$ using a ratio of $[\text{CuBr}]: [\text{Me}_6\text{TREN}] = 1: 1$ or $2: 1$. Successful chain extensions were carried out to very near full conversions (96-99%). The ratio of $[\text{CuBr}]/[\text{Me}_6\text{TREN}]$ influenced the MW distribution of the first block and also affected the reaction rate, whereby $[\text{CuBr}] / [\text{Me}_6\text{TREN}] = 1: 1$ showed worse control but a faster reaction rate.

For the polymerization under the reaction ratio of $[\text{CuBr}]: [\text{Me}_6\text{TREN}] = 1: 1$, after 30 min, NMR confirmed 100% conversion of the first block polymerization and new NIPAM monomer was added for chain extension. Reaction time for the second, third and fourth block polymerization was extended to 30 min, 60 min and 80 min. Conversion was all $>99\%$ according to ^1H NMR spectroscopy. The control of the “first block” polymerization was not good, which led to a high PDI value (1.63). However, SEC revealed increase of M_n from 6600 to 19100, 31300 and 43300 and also decrease of M_w / M_n from 1.63 to 1.27, 1.21 and 1.20 for the second, third and fourth block polymerization, Figure 5.43.

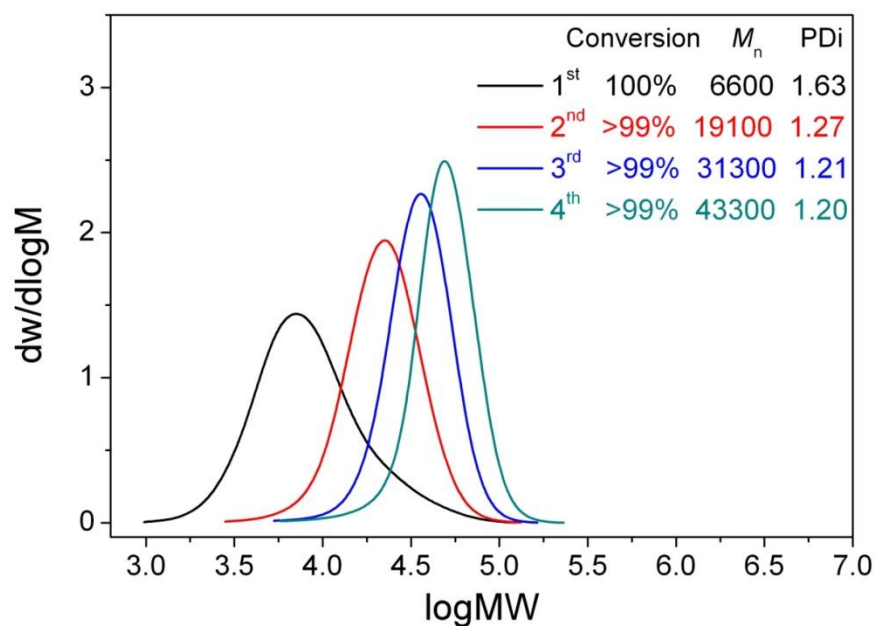


Figure 5. 43. DMF SEC molecular weight distributions for chain extension reaction of SET-LRP of NIPAM in H₂O at 0 °C with [initiator]: [CuBr]: [Me₆TREN] = 1: 0.4: 0.4.

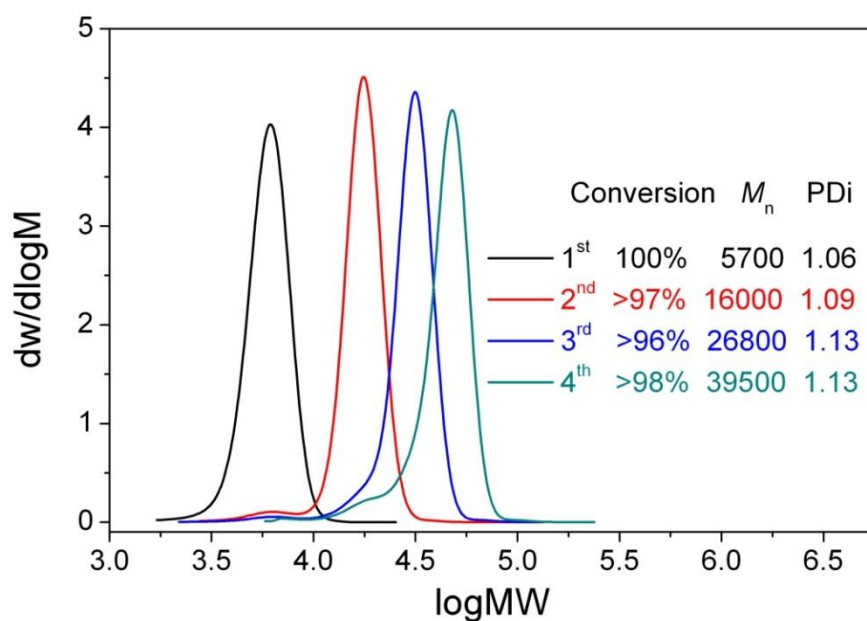


Figure 5. 44. DMF SEC molecular weight distributions for chain extension reaction of SET-LRP of NIPAM in H₂O at 0 °C with [initiator]: [CuBr]: [Me₆TREN] = 1: 0.8: 0.4.

For the polymerization under the reaction ratio of [CuBr]: [Me₆TREN] = 2: 1, After 80 min, NMR confirmed 100% conversion for the first block polymerization and new NIPAM monomer was added for chain extension. Reaction time for the second, third

and fourth block polymerization was extended to 75 min, 150 min and overnight. Conversion was separately calculated as only >97%, >96% and >98% according to ^1H NMR spectroscopy. SEC revealed increase of M_n from 5700 to 16000, 26800 and 39500 and also slight increase of M_w / M_n from 1.06 to 1.09, 1.13 and 1.13 for the second, third and fourth block polymerization, and even included small tailing peak at low molecular weight position, Figure 5.44.

Nevertheless, the clear MW shift after chain extension and only slight increase of dispersity to 1.13 (including small tailing peaks at low MW) showed that high chain end fidelity could be maintained under these conditions.

5.2.8 Multiblock copolymers by SET-LRP in water.

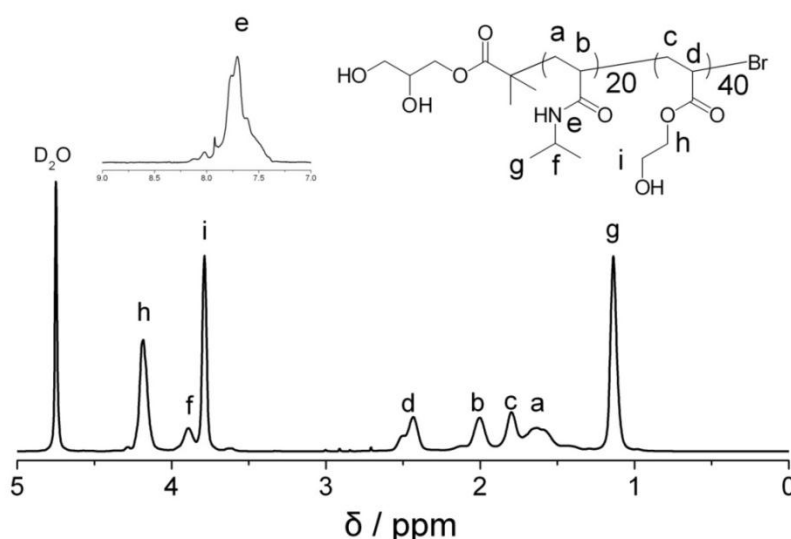


Figure 5. 45. ^1H NMR spectrum of poly (NIPAM)₂₀-b-(HEA)₄₀ by iterative SET-LRP in D_2O . The numbering of the hydrogen atoms used for the NMR peak assignment is shown in the spectrum.

We subsequently applied this technique for the preparation of di-block copolymer poly(NIPAM)₂₀-b-(HEA)₄₀. Block co-polymerization was performed by *in situ* addition of monomers to the reaction solution at full conversion with respect to the first block, negating the need for purification between each block and further highlighting the high versatility of this one-pot reaction. ^1H NMR analysis confirmed 100% conversion of each block according to the total disappearance of vinyl groups and the expected ratios of each component in the product (Figure 5.45), which is in agreement with FT-IR analysis (Figure 5.46). SEC characterization revealed a clear

and total MW shift after block co-polymerization and a final dispersity < 1.2 (Figure 5.47).

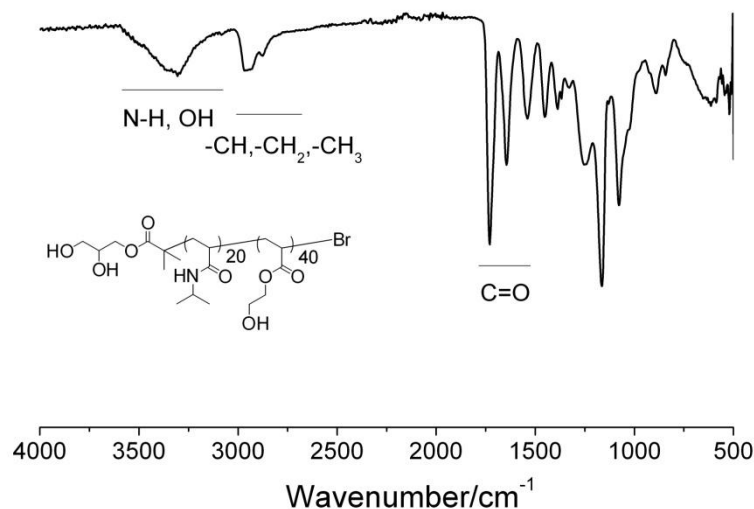


Figure 5. 46. FTIR spectrum of poly (NIPAM)₂₀-b- (HEA)₄₀ by iterative SET-LRP.

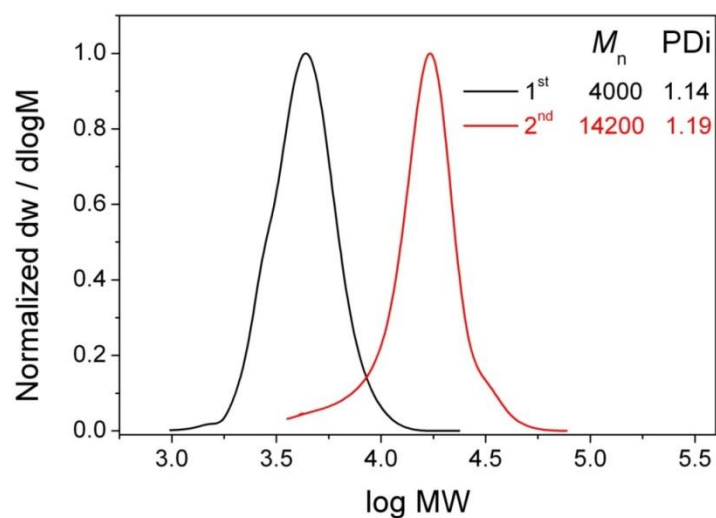
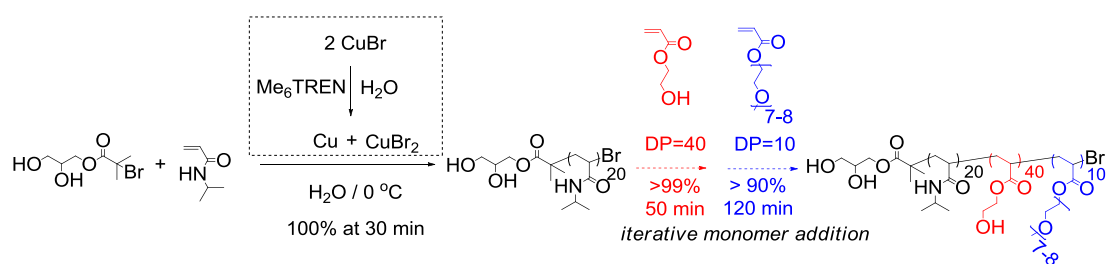


Figure 5. 47. DMF SEC molecular weight distributions for poly (NIPAM)₂₀-b- (HEA)₄₀ by iterative SET-LRP in H₂O.



Scheme 5. 5. Schematic representation for synthesis of poly(NIPAM)₂₀-b-(HEA)₄₀-b-(PEGA₄₈₀)₁₀ by iterative SET-LRP in H₂O.

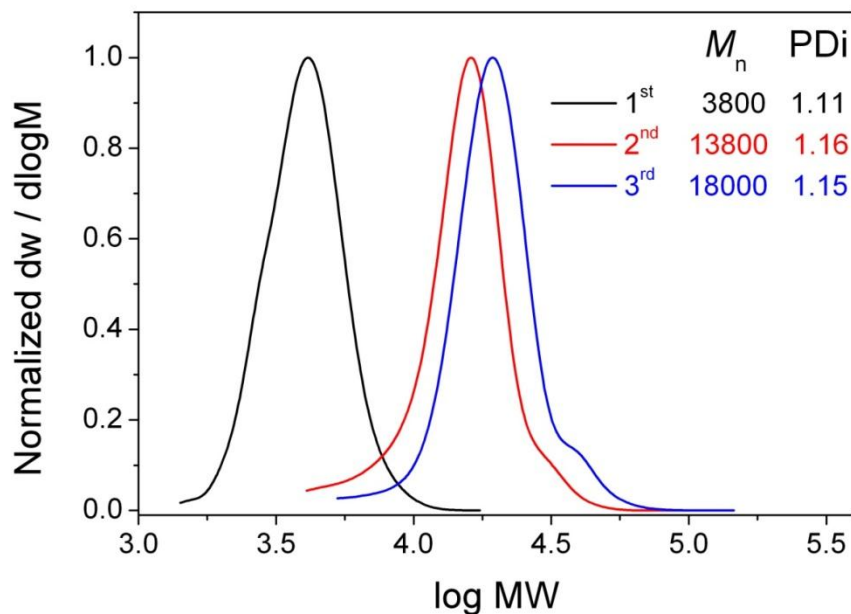


Figure 5. 48. Molecular weight distributions of poly (NIPAM)₂₀-*b*-(HEA)₄₀-*b*-(PEGA₄₈₀)₁₀ by iterative SET-LRP in H₂O at 0 °C as measured *via* SEC employing DMF as eluent.

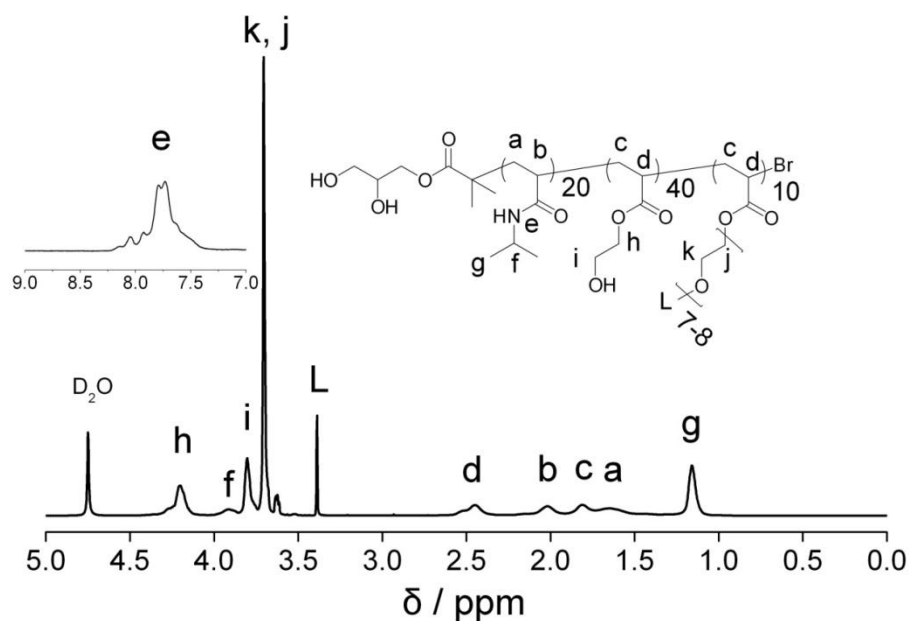


Figure 5. 49. ¹H NMR spectrum of poly (NIPAM)₂₀-*b*-(HEA)₄₀-*b*-(PEGA₄₈₀)₁₀ by iterative SET-LRP in D₂O.

Furthermore, a tri-block copolymer was synthesized *via* iterative monomer addition (Scheme 5.5). Aqueous solutions of HEA and PEGA₄₈₀ were sequentially added to the reaction solution of PNIPAM at full conversion. SEC characterization using RI and viscosity detector again revealed a MW shift after each block polymerization with

only a slight increase of dispersity to 1.15 (Figure 5.48, 5.50). SEC revealed a higher M_n than the theoretical target for the second poly(NIPAM)₂₀-*b*-(HEA)₄₀ copolymer, which is likely due to the different hydrodynamic volume of HEA block with narrow PMMA calibration standard. ¹H NMR spectrum of the final product confirmed the correct ratio of NIPAM – HEA – PEGA (Figure 5.49).

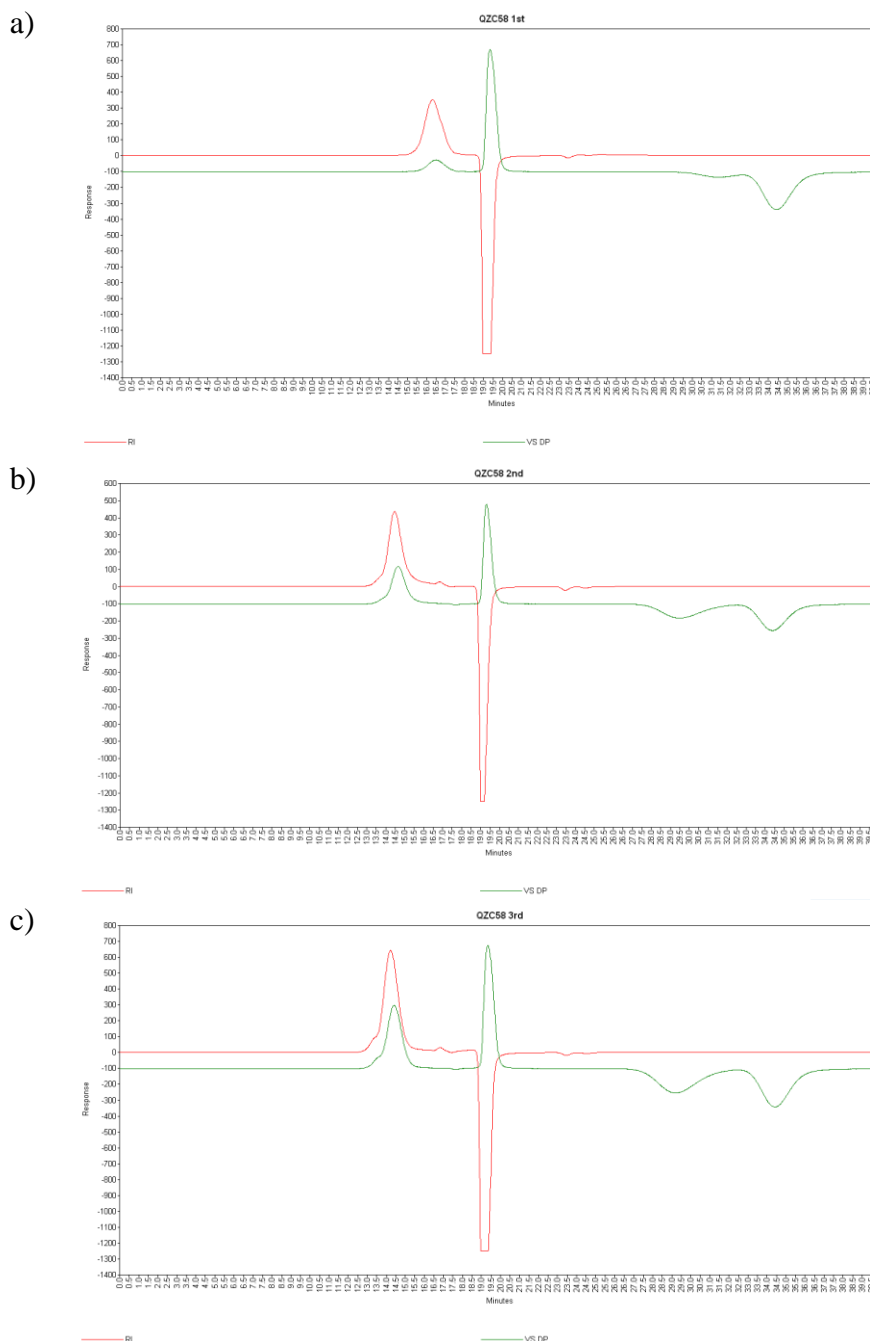


Figure 5. 50. DMF SEC elution traces for poly (NIPAM)₂₀ -*b*- (HEA)₄₀ -*b*- (PEGA₄₈₀)₁₀ by iterative aqueous SET-LRP at 0 °C. Conditions: a) 1st block; b) 2nd block; c) 3rd block. Red line for refractive index detector; green line for viscosity detector.

5.2.9 SET-LRP in PBS buffer, ethanol/water (Tequila) and sheep blood serum.

PBS buffer is a medium used to mimic biological conditions and alcohol/water mixtures can extend the scope of this process to less hydrophilic initiators and monomers. Accordingly, we conducted SET-LRP, with prior disproportionation, in these solvents. In PBS buffer (pH = 6.2 and 6.8) disproportionation of CuBr/Me₆TREN was observed, although with a slower rate than in pure water. SET-LRP in PBS buffer tended to be slower than that in pure water and resulted in final polymers with higher dispersity = 1.21 and 1.29, suggesting that the buffer affected the catalyst and polymerization (Figure 5.51).

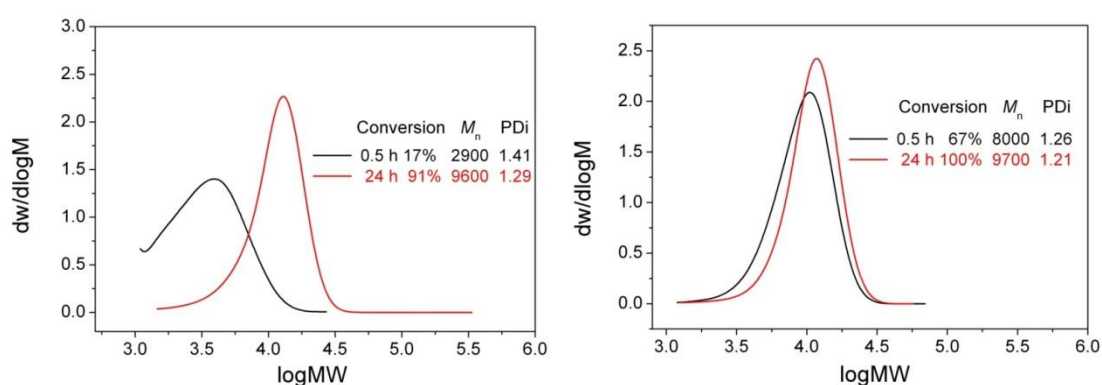


Figure 5. 51. DMF SEC molecular weight distributions at different time for the SET-LRP of NIPAM (DP=80) in PBS buffer (pH=6.2, left; pH=6.8, right) at 0 °C with [initiator]: [CuBr]: [Me₆TREN] = 1: 0.8: 0.4.

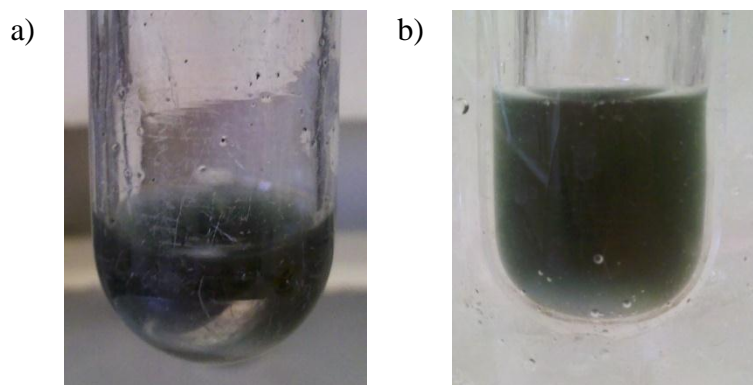


Figure 5. 52. Visual observation of the disproportionation of CuBr / Me₆TREN (a) and SET-LRP of NIPAM (DP=80) in Tequila (b). Conditions: a) Tequila = 2 mL; CuBr = 10 mg, 70 μ mol; Me₆TREN = 9 μ L, 35 μ mol. Picture was taken 30 min after mixing the reagents. b) Picture was taken 5 min after transferring the initiator / NIPAM solution into the catalyst solution of (a).

For SET-LRP in an alcohol/water mixture, we directly used commercial Tequila (38% ethanol) as the solvent. Disproportion of CuBr/Me₆TREN resulted in a deep green solution with insoluble Cu(0) precipitate (Figure 5.52). The SET-LRP of NIPAM in Tequila showed similar results as in pure water, with 99% conversion obtained in 30 minutes ($M_n = 9900$ and dispersity = 1.08 for the final polymer, Figure 5.53-5.54). This finding intimates that previous reports on ATRP of NIPAM using water / alcohol mixture as the solvent, especially when stock solutions of CuCl/Me₆TREN have been employed prior to addition of initiator/NIPAM, are likely proceeding *via* SET-LRP rather than ATRP.

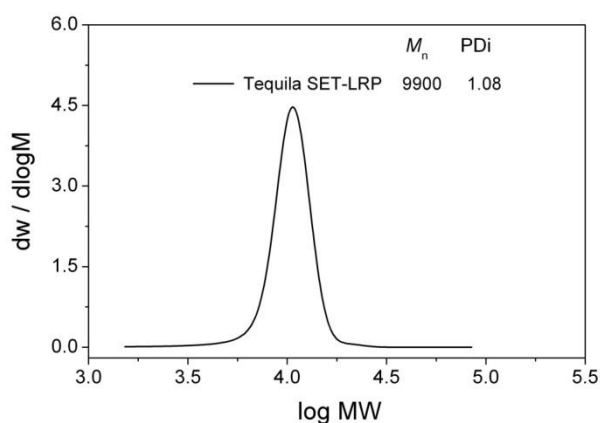


Figure 5. 53. DMF SEC molecular weight distributions at different time for the SET-LRP of NIPAM (DP=80) in Tequila at 0 °C with [initiator]: [CuBr]: [Me₆TREN] = 1: 0.8: 0.4.

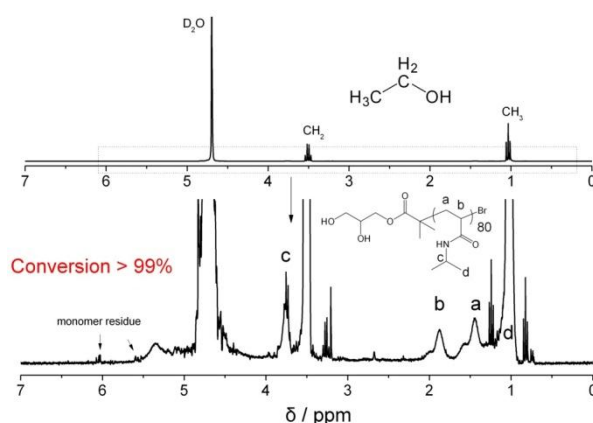


Figure 5. 54. ¹H NMR spectrum for SET-LRP of NIPAM in Tequila at 30 min in D₂O.

After that, we moved on to perform the aqueous SET-LRP under a truly biological system: sheep serum. Mammals' blood serum generally contains a series of inorganic constituents, amino acids, proteins, carbohydrates, fats, vitamins and hormones et al. in water, which is considered as a preferred solvent for biochemical experiment.^{264,265} Upon addition of CuBr to a degassed solution of Me₆TREN in sheep serum a blue suspension prevailed instantaneously containing a purple, metallic copper precipitate (Figure 5.55), which indicated the occurrence of disproportionation.



Figure 5. 55. Visual observation of the disproportionation of CuBr / Me₆TREN in sheep serum. Conditions: sheep serum= 2 mL; CuBr = 10 mg, 0.07 mmol; Me₆TREN = 9 μ L, 0.035 mmol. Picture was taken 1 min after mixing CuBr with the other reagents.

The polymerization of NIPAM and DMA was then investigated in the serum media according to previous procedure. NIPAM was found to undergo efficient polymerization resulting in a slightly broader dispersity (1.26) compared with ~1.10 in pure water, Figure 5.56. The drift in PDI is caused by low molecular weight tailing as a result of side reactions producing unidentified small molecule by-products during the early part of the reaction which could be removed after polymerization by precipitation and dialysis.

The polymerization of DMA exhibited optimum control reaching full conversion within 2 hours to yield poly(DMA) with agreement between theoretical and observed molecular weights and narrow, symmetrical molecular weight distribution (PDI = 1.09, Figure 5.56). Crude reaction mixtures were isolated from the serum solution by precipitation of the biological macromolecules into DMF followed by centrifugation.

Dialysis of the polymer containing supernatant against water removed any remaining unwanted soluble material, furnishing the desired pure polymers, Figure 5.57-5.59.

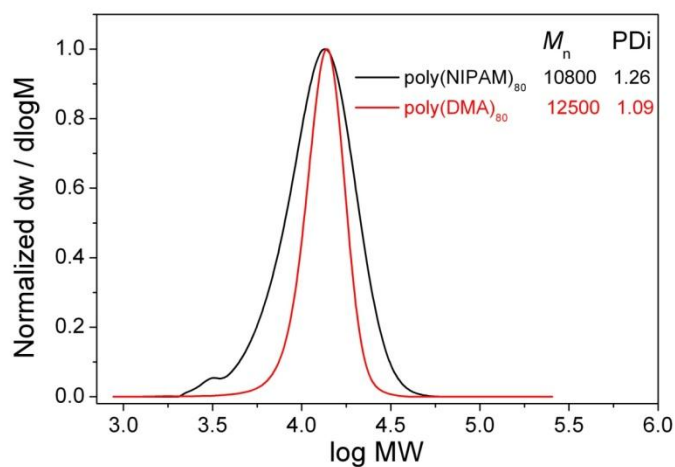


Figure 5. 56. Molecular weight distributions of poly (NIPAM)₈₀ and poly(DMA)₈₀ by SET-LRP in sheep serum at 0 °C as measured *via* SEC employing DMF as eluent.

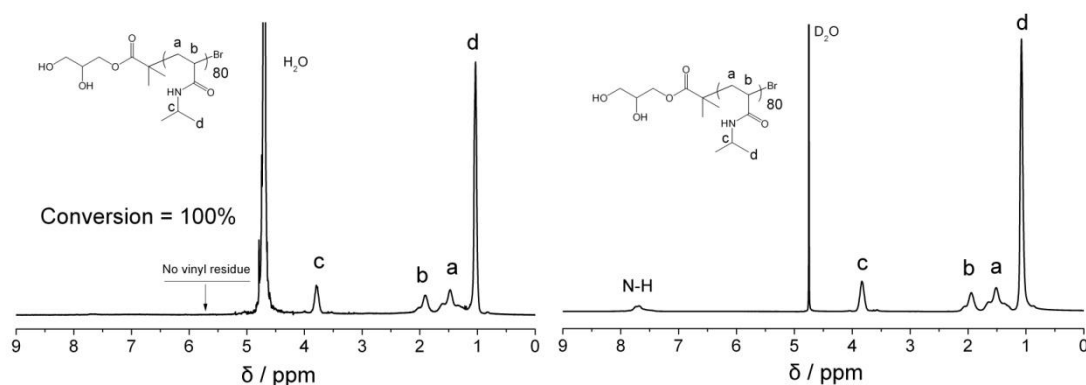


Figure 5. 57. ¹H NMR spectra for SET-LRP of NIPAM in sheep serum at 1 h (left) and PNIPAM (right) recovered after dialysis. D₂O was used as the NMR solvent.

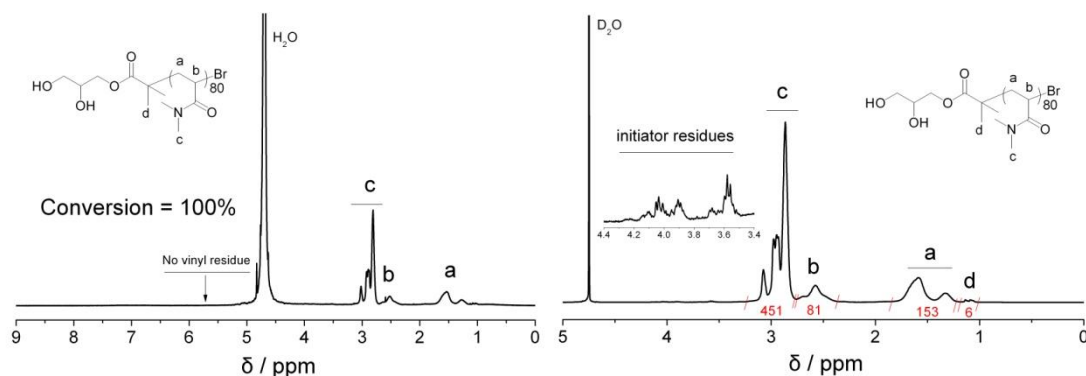


Figure 5. 58. ¹H NMR spectra for SET-LRP of DMA in sheep serum at 2 h (left) and PDMA (right) recovered after dialysis. D₂O was used as the NMR solvent.

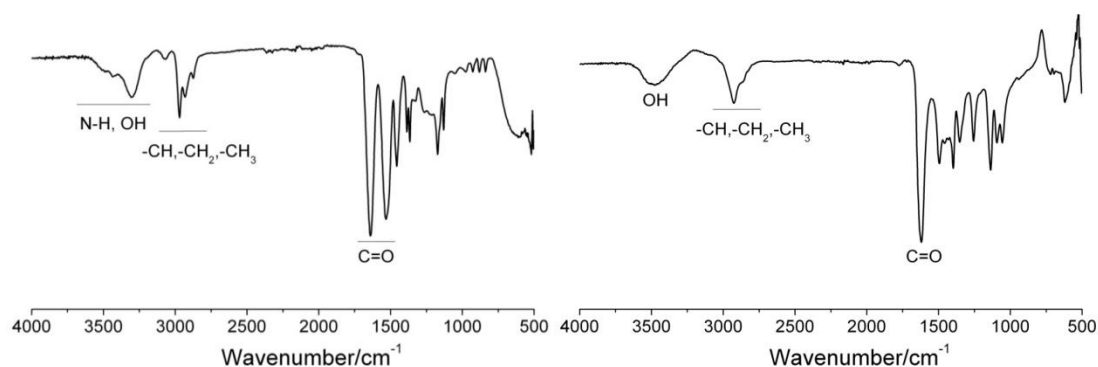


Figure 5. 59. FTIR spectra of PNIPAM (DP=80, left) and PDMA (DP=80, right) by SET-LRP in serum.

In serum, poly(NIPAM) was attained using established reaction conditions [NIPAM]: [I]: [CuBr]: [Me₆TREN] = 80: 1: 0.8: 0.4 at 0 °C within 1 hour. At this time DMA (80 eq), as a degassed serum solution (4 mL) was injected into the reaction mixture. ¹H NMR analysis after 18 hours revealed complete consumption of the vinyl peaks from DMA (Figure 5.60) and SEC analysis revealed a complete shift in molecular weight distribution (Figure 5.62). A final PDI of 1.30 was obtained for the poly(NIPAM)-*b*-(DMA) which is broader than related blocks obtained previously in our aqueous system.

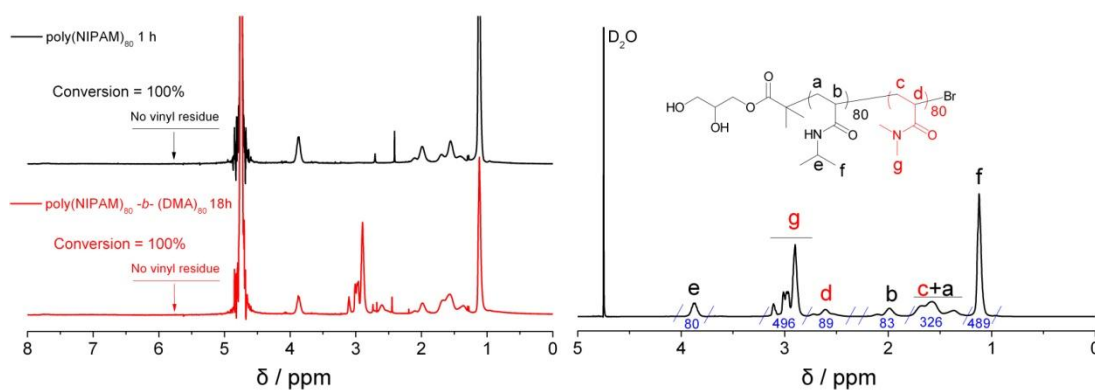


Figure 5. 60. ¹H NMR spectra for SET-LRP of poly (NIPAM)₈₀ -*b*- (DMA)₈₀ in sheep serum during polymerization (left) and product (right) recovered after dialysis. D₂O was used as the NMR solvent.

Considering the results obtained for the homopolymerization of NIPAM in serum, the effect of the order of monomer addition was investigated. Under the same conditions poly(DMA) homopolymer was obtained with near quantitative conversion after 1 hour at which point NIPAM (80 eq) as a degassed serum solution (4 mL) was injected. Near quantitative conversion (>97%, Figure 5.61) was observed after 22

hours and the final poly(DMA)-*b*-(NIPAM) molecular weight distribution was improved (PDI=1.21, Figure 5.62). In this example a small, low molecular weight, shoulder peak, attributed to premature termination as a result of chain end hydrolysis *etc.*, was observed in the SEC chromatogram of the final block copolymer (Figure 5.62).

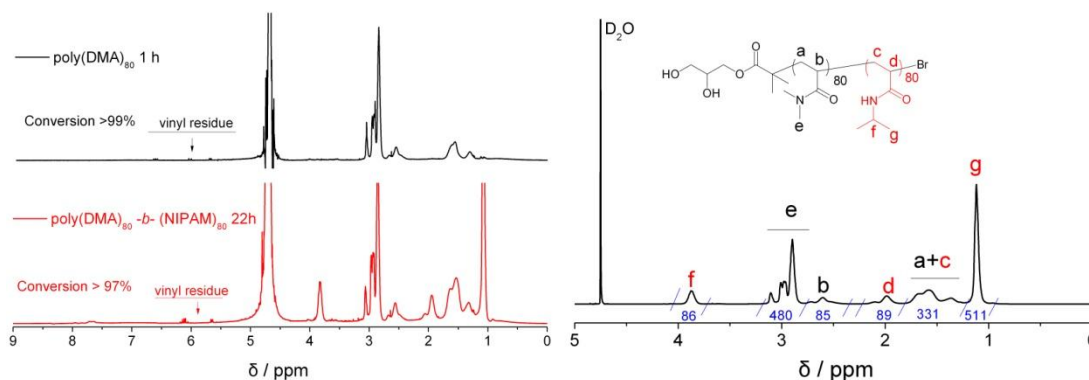


Figure 5. 61. ^1H NMR spectra for SET-LRP of poly (DMA)₈₀-*b*-(NIPAM)₈₀ in sheep serum during polymerization (left) and product (right) recovered after dialysis. D_2O was used as the NMR solvent.

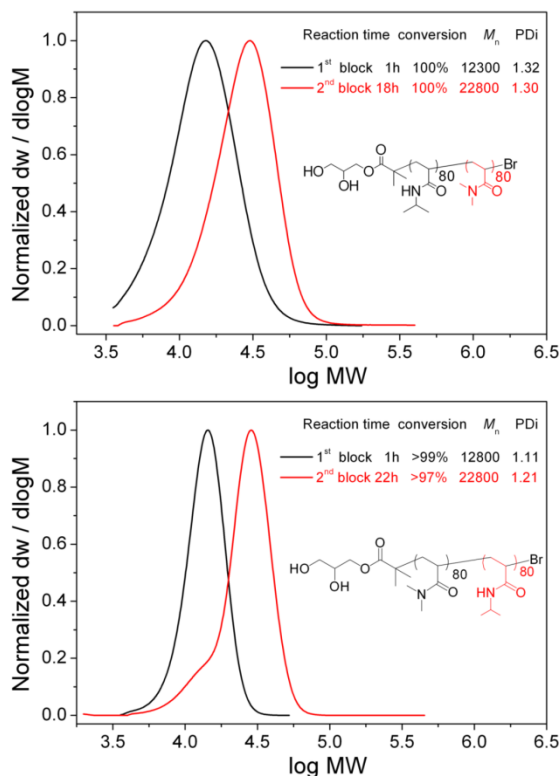


Figure 5. 62. Molecular weight distributions for the *In situ* SET-LRP block copolymerization of poly(NIPAM) (top) and poly(DMA) (bottom) in sheep serum at 0 °C as measured *via* SEC employing DMF as eluent.

^1H NMR spectra of final block copolymers revealed ratio of NIPAM/DMA close to theoretical values (Figure 5.60, 5.61) and FT-IR spectra confirmed absorbance from both NIPAM and DMA compared with homopolymers, Figure 5.63.

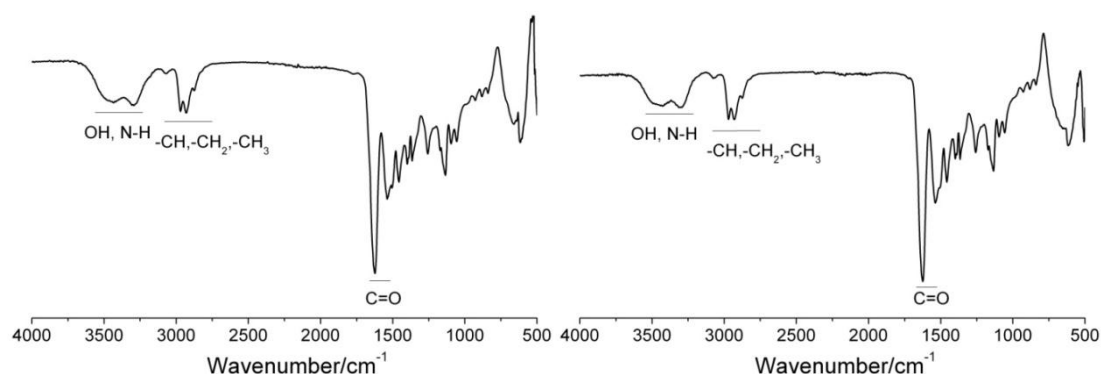
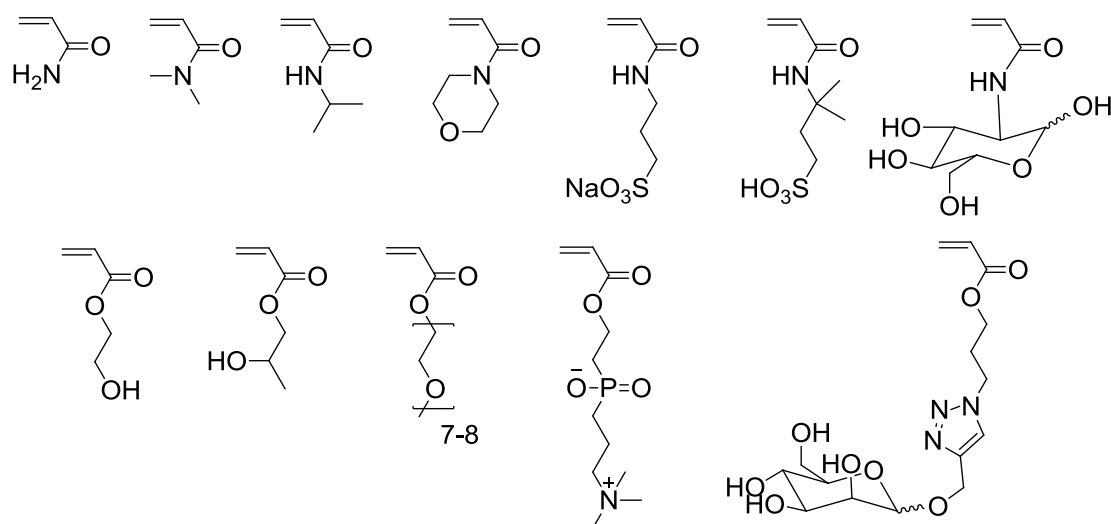


Figure 5. 63. FTIR spectrum of poly (NIPAM)₈₀-*b*-(DMA)₈₀ (left) and poly (DMA)₈₀-*b*-(NIPAM)₈₀ (right) by SET-LRP in sheep serum.

In summary, SET-LRP has been conducted for the first time in biological media without any additional aqueous dilution. The controlled nature of the polymerizations performed in this media was exemplified by *in situ* block copolymerization of poly(NIPAM) and poly(DMA) macroinitiators with DMA and NIPAM respectively.

5.2.10 SET-LRP of hydrophilic monomers mediated by *prior* disproportionation of CuBr/Me₆TREN in pure water.



Scheme 5. 6. Schematic representation for the hydrophilic monomers polymerized by the aqueous SET-LRP.

The initial scope of this approach to SET-LRP has been extended to the polymerization of common hydrophilic monomers including PEGA, HEA, DMA and synthesized acrylamide based glycomonomer, glucose acrylamide (GAm) et al, as shown in Scheme 5.6. The general procedure for NIPAM polymerization was followed, with variations in temperature and [CuBr]/[Me₆TREN] ratios dependent on the targeted DP. For each monomer, the polymerizations reached quantitative conversion within 1 hour. Pleasingly, narrow molecular weight distributions were attained and good agreement between theoretical and observed molecular weights were obtained, indicative of controlled polymerization. A part of the results were reported as shown in Table 5.1.²⁶⁶

Table 5. 1. Summary of results obtained from the polymerization of hydrophilic monomers via SET-LRP mediated by in situ disproportionation of CuBr / Me₆TREN.

	[M]: [I]: [CuBr]: [L]	Conv ¹ / %	M _{n,th} / Da	M _{n,GPC} ² / Da	PDi
DMA ³	80: 1: 0.8: 0.4	>99%	8200	9700	1.18
HEA	20: 1: 0.4: 0.4	97%	2600	8800	1.07
PEGA	10: 1: 0.4: 0.4	>99%	5000	7600	1.07
PEGA	20: 1: 0.4: 0.4	>99%	10000	11300	1.09
GAm	10: 1: 0.4: 0.4	>99%	2600	2800	1.15

¹ Measured by ¹H NMR; ² DMF eluent, PMMA standards; ³ Performed at T = 0 °C. These polymerizations were performed by members from Haddleton group.

5.2.11 Synthesis of double hydrophilic diblock glycopolymers via aqueous SET-LRP.

Synthetic carbohydrate-containing block copolymers are being increasingly explored as novel biocompatible and biodegradable materials for wide use in self-assembly, drug & nucleic acids delivery and lectin recognition.^{32,48,267,268} The glycopolymer segments are hydrophilic to impart water-solubility and recognized as alternative to poly(ethylene glycol) (PEG) for avoiding aggregation.⁴⁸ The combination with hydrophobic segments could form amphiphilic block copolymers and have been intensively studied due to the interesting aggregation behavior in aqueous solution.²⁵ While the combination with thermo-responsive or pH-responsive hydrophilic block segments could assemble into interesting vesicles or aggregates for association with bacteria and pDNA & siRNA, which showed a promising application in cell sensing

and delivery et al.^{48,269} Living radical polymerization, such as atom transfer living radical polymerization (ATRP) and reversible addition-fragmentation chain transfer polymerization (RAFT), combined with click chemistry has supplied a facile route for the synthesis of diblock glycopolymers.² However, previous research on direct aqueous ATRP of unprotected glycomonomer showed poor living character and has to use high ratio alcohol as the co-solvent.^{25,26} Alternatively acetyl protected glycomonomers were frequently used for ATRP and even RAFT in organic solvents.²⁷⁰⁻²⁷² For the aim of atom-efficiency and environment-friendly consideration, aqueous RAFT was tried for the polymerization of unprotected glycomonomers.⁴⁵ However, it still suffered from loss of control during chain extension which represents as significant increase of PDI to as high as 1.63.

We recently developed a new approach to perform SET-LRP in pure water under ambient temperature or below and high chain end fidelity was maintained in this system for multiblock copolymerization.²⁶⁶

Thus we use this polymerization technique for the polymerization of unprotected glycomonomer in pure water. At first, a relatively low DP poly(Mannose)₁₀ was prepared by transferring the initiator/Mannose acrylate monomer solution into a catalyst suspension containing Cu(0)/CuBr₂/Me₆TREN, resulting from prior rapid disproportionation of CuBr/Me₆TREN in water, starting fast polymerization even under 0 °C and reached 100% in 1 h.

SEC characterization of final polymer revealed $M_n=7100$ and dispersity=1.09, Figure 5.64, which is higher than theoretical molecular weight due to the different hydrodynamic volume of glycopolymer with PMMA calibration standard in DMF.

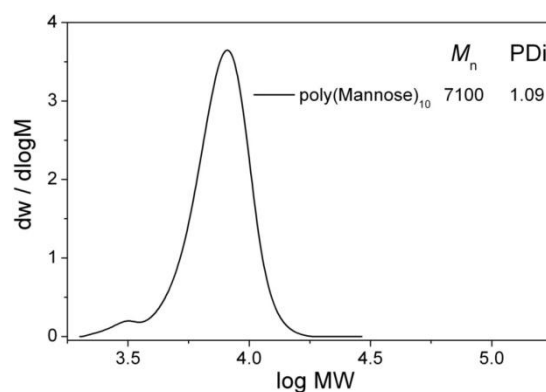


Figure 5. 64. Molecular weight distribution of poly(Mannose)₁₀ by SET-LRP in H₂O at 0 °C *via* DMF SEC.

^1H NMR analysis (Figure 5.65) confirmed the right structure of targeted glycopolymer and right DP by comparing the integral of triazole ring proton at around 8.1 ppm with the initiator methyl groups at around 1.1 ppm.

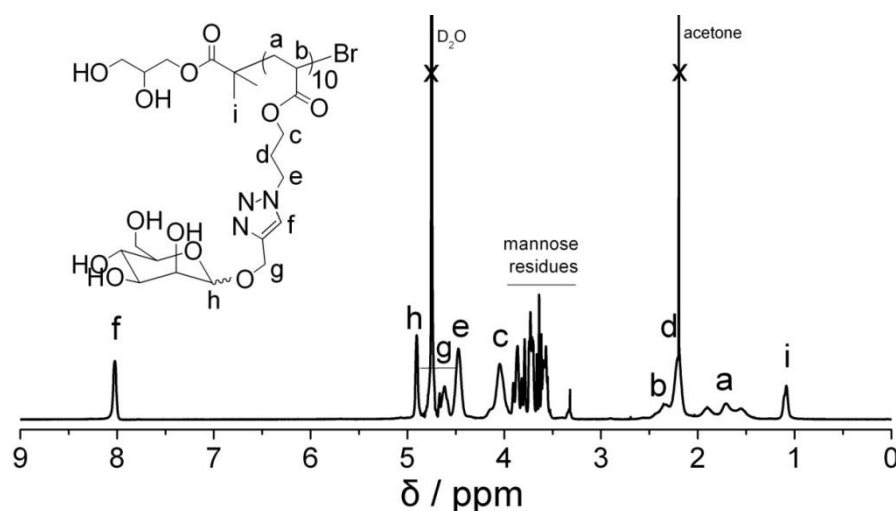


Figure 5. 65. ^1H NMR spectra of poly(Mannose)₁₀ in D_2O .

Compared with copper(0) wire mediated SET-LRP which resulted in glycopolymers with similar M_n and dispersity, Figure 5.66, the reaction rate was much faster, possibly due to the much larger surface area of the fine copper powders with copper wire.

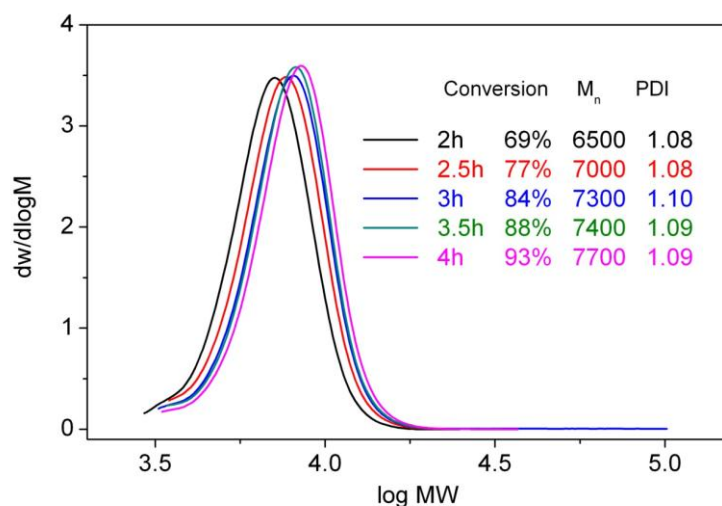


Figure 5. 66. Molecular weight distributions for the copper(0) wire mediated SET-LRP of D-Mannose glyco monomer in H_2O at ambient temperature *via* DMF SEC.

For the polymerization of DEGEAA, which could form another thermal-responsive polymer, MeOH/ H_2O mixture was utilized to make sure the monomer is soluble in the

system. The polymerization was also fast and SEC characterization showed the final polymer with $M_n=13200$ which is close to the theoretical value. The final dispersity is as low as 1.12 even with a shoulder peak at high MW position, which may be caused by diacrylate residue in the DEGEEA monomer. An unidentified very small peak at low MW position via RI detector was noticed before dialysis, Figure 5.67, which may be caused by side reaction of catalyst or monomer under aqueous polymerization condition according to previous report.^{27,273-275} Due to the low content and challenge for separation from the polymer, its exact structure has not yet been confirmed by NMR under clear and high resolution; however, this could be removed by precipitation or dialysis purification. Nevertheless, the fast polymerization showed similar results as previous research and targeted polymer with defined molecular weight and narrow polydispersity could be successfully synthesized.

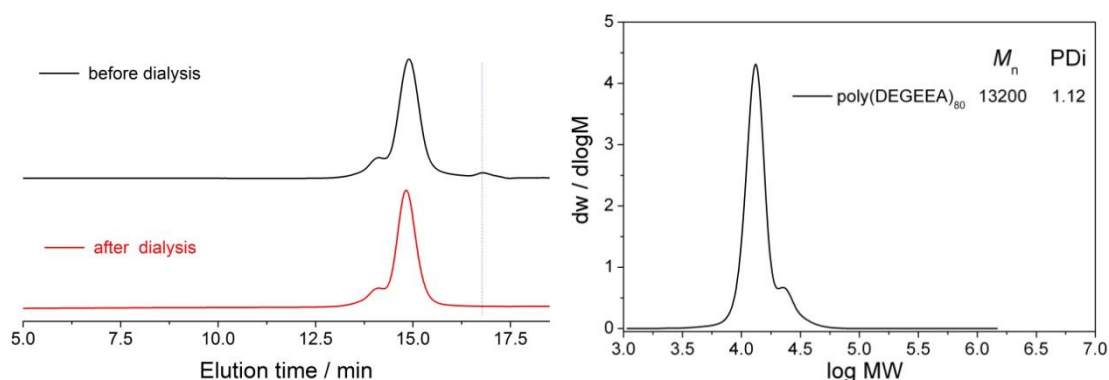


Figure 5. 67. Molecular weight distribution of poly(DEGEEA)₈₀ (left: elution traces; right: after dialysis) by aqueous SET-LRP at 0 °C *via* DMF SEC.

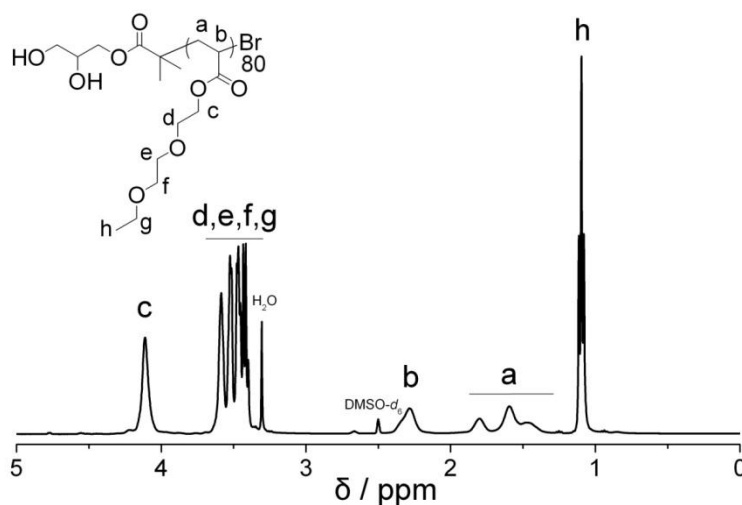
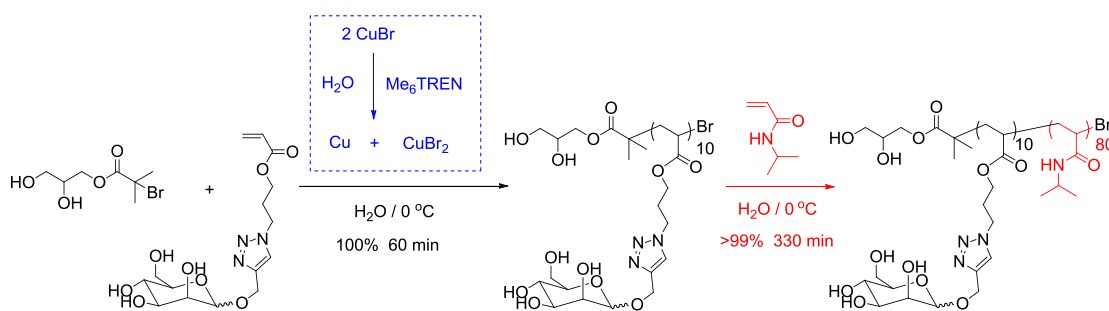


Figure 5. 68. ^1H NMR spectra of poly(DEGEEA)₈₀ in DMSO- d_6 .



Scheme 5. 7. Schematic representation for the synthesis of poly(Mannose)₁₀-b-(NIPAM)₈₀ via aqueous SET-LRP.

After that two different double hydrophilic diblock copolymers containing poly(mannose) segments and thermoresponsive PNIPAM and PDEGEEA segments were facilely synthesized via a one-pot iterative monomer addition.

As shown in Scheme 5.7, new degassed NIPAM monomer solution was directly added to the reaction tube after full conversion of the 1st block polymerization for chain extension at 0 °C. After 330 min, reaction was directly stopped for characterization.

As shown in Figure 5.69, the elution traces shifted totally after block copolymerization and the dispersity only increased slightly from 1.06 to 1.13, although there is a small shoulder peak at low MW position overlapped with peak of the first block glycopolymers, which could be attributed to the unavioded termination during polymerization including disproportionation and terminal bromine hydrolysis et al.

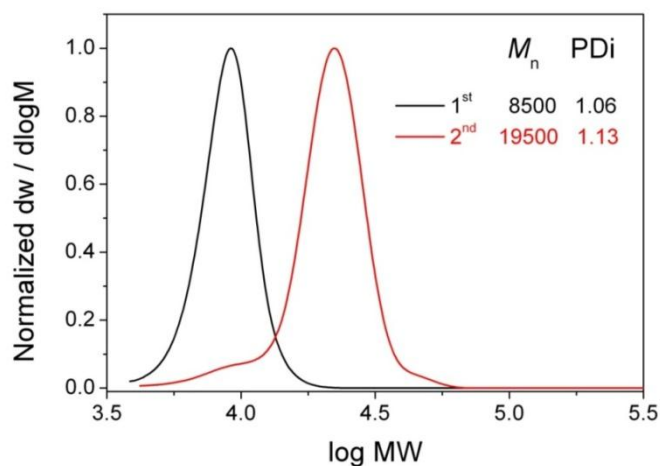


Figure 5. 69. Molecular weight distributions of poly (Mannose)₁₀ -*b*- (NIPAM)₈₀ by SET-LRP in H₂O at 0 °C *via* DMF SEC.

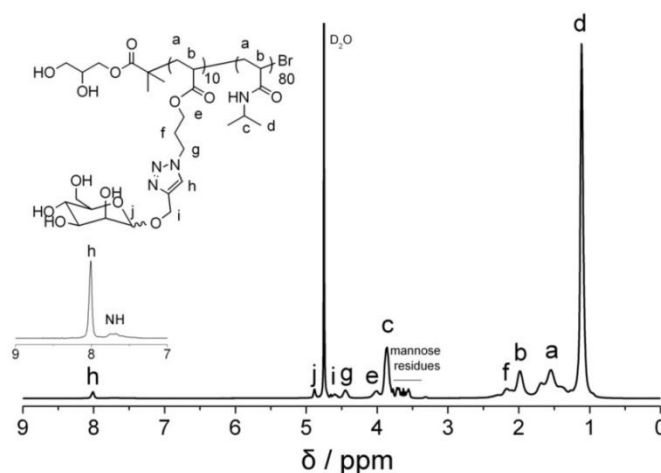


Figure 5. 70. ¹H NMR spectrum for the poly (Mannose)₁₀ -*b*- (NIPAM)₈₀ by SET-LRP in H₂O at 0 °C. D₂O was used as the NMR solvent.

¹H NMR spectrum (Figure 5.70) clearly revealed peaks from glycopolymer components, such as triazole ring protons at around 8 ppm and mannose residues at 3.5-5.0 ppm and also typical PNIPAM peaks at 1.1 and 3.8 ppm. The ratio of NIPAM to Mannose is ~1:10, which is higher than theoretical value 1:8. This is due to the sampling during the first block polymerization for SEC and NMR analysis, which unavoidably took the 1st block macro initiator from the system.

FT-IR spectrum (Figure 5.71) also revealed peak absorbance from both components, typically shown as different C=O absorbance between 1500-1750 cm⁻¹.

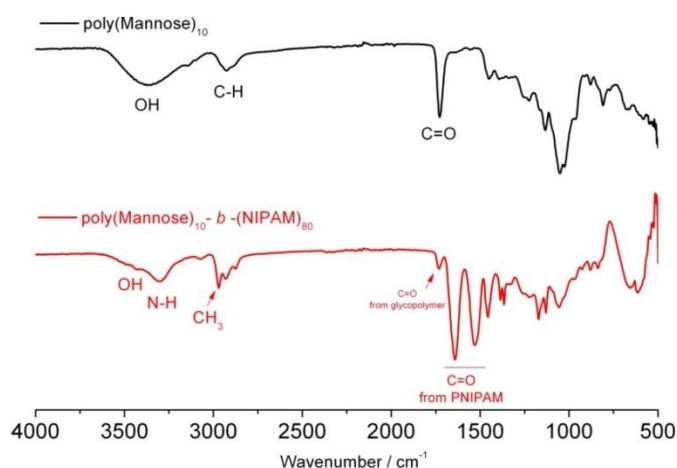


Figure 5. 71. FTIR spectra for the poly (Mannose)₁₀ (top) and poly (Mannose)₁₀ -*b*-(NIPAM)₈₀ (bottom).

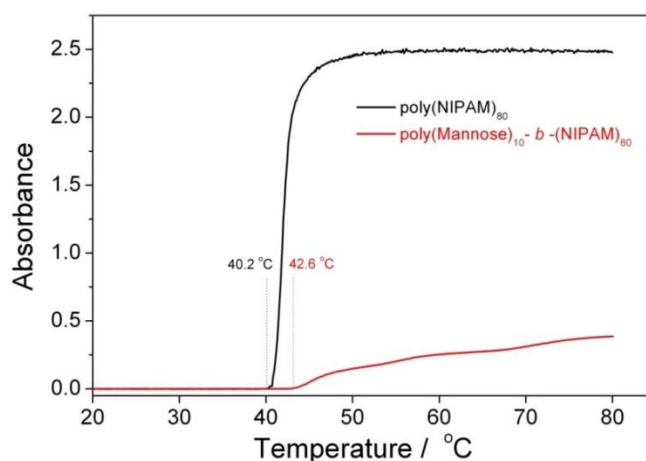
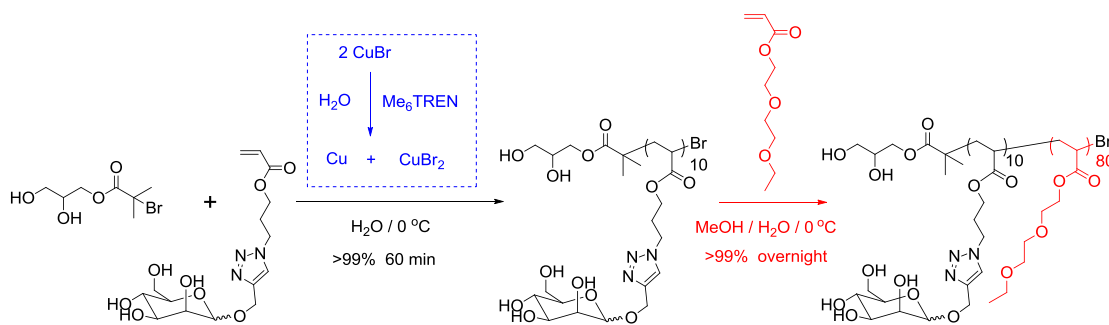


Figure 5. 72. Cloud point measurements of poly(NIPAM)₈₀ and poly (Mannose)₁₀ -*b*-(NIPAM)₈₀ by UV/Vis spectroscopy at 500 nm. Sample concentration: 1 mg / mL.

Interestingly, the poly(NIPAM)₈₀ with initiator residue OH groups and terminal OH groups due to the hydrolysis of terminal bromine showed a LCST temperature of ~40.2 °C (1 mg/mL), which is higher than typical LCST temperature of PNIPAM (~32 °C), as shown in Figure 5.72. The diblock glycopolymer at same concentration showed even higher LCST temperature at ~42.6 °C due to more hydrophilic sugar components. The absorbance value at same concentration is also significantly lower than the PNIPAM, which could be attributed to the self-assemble behaviour of the block copolymer in water.



Scheme 5. 8. Schematic representation for the synthesis of poly(Mannose)₁₀-b-(DEGEEA)₈₀ via aqueous SET-LRP.

After that, a different block copolymer bearing poly(DEGEEA) segment was synthesized in similar way. For chain extension with DEGEEA monomer, MeOH/H₂O mixture was used as the solvent. As shown in Figure 5.73, the SEC traces also showed total shift and after block copolymerization the dispersity increased slightly to 1.13 with a shoulder peak at higher MW region, which is similar as poly(DEGEEA) homopolymer.

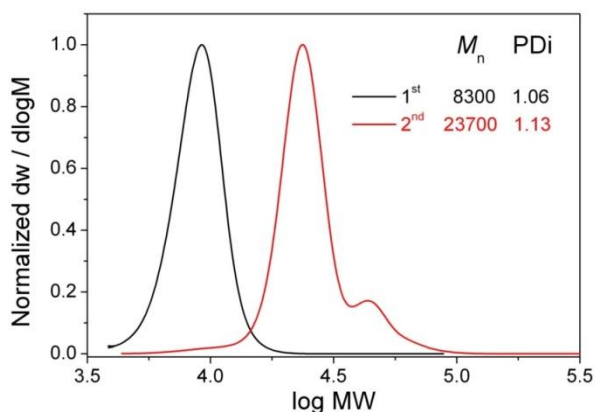


Figure 5. 73. Molecular weight distributions of poly (Mannose)₁₀ -b- (DEGEEA)₈₀ by SET-LRP in H₂O at 0 °C via DMF SEC.

¹H NMR spectrum (Figure 5.74) showed peaks from glycopolymer components and also typical PDEGEEA peaks at 1.1 (methyl groups) and 3.2-3.8 (methylene groups) ppm. The ratio of DEGEEA to Mannose is ~1:9 due to sampling during the 1st block polymerization, which is higher than theoretical value 1:8.

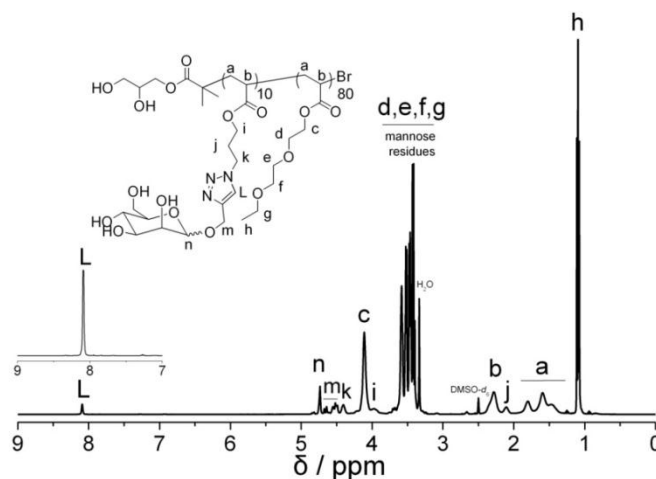


Figure 5. 74. ^1H NMR spectrum for the poly (Mannose)₁₀-*b*-(DEGEEA)₈₀ by SET-LRP in H_2O at 0 °C. D_2O was used as the NMR solvent.

FT-IR spectrum (Figure 5.75) did not reveal significant absorbance peak from the mannose glycopolymer block, mainly due to the high ratio of poly(DEGEEA) block and similar functional groups. The diblock glycopolymer at same concentration showed thoroughly different LCST temperature compared with poly(DEGEEA), Figure 5.76. The absorbance value of the glycopolymer at concentration of 1mg/mL is significantly lower than that of Poly(DEGEEA), which could be attributed to the mannose content making the block copolymer more hydrophilic.

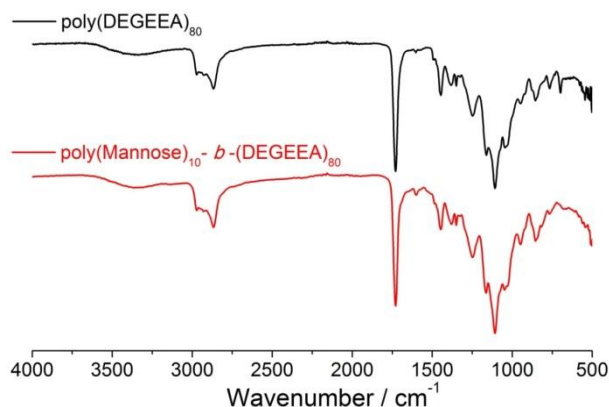


Figure 5. 75. FTIR spectra for the poly (DEGEEA)₈₀ (top) and poly (Mannose)₁₀-*b*-(DEGEEA)₈₀ (bottom).

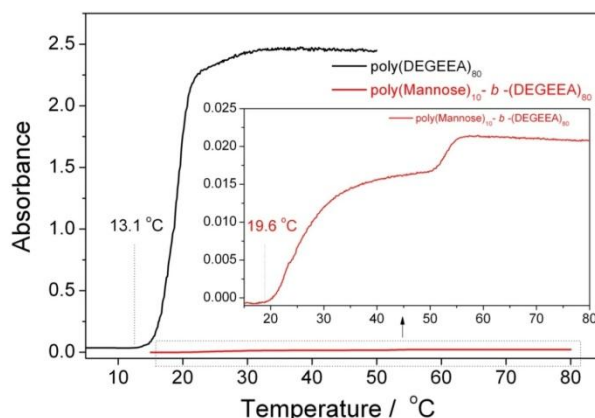


Figure 5. 76. Cloud point measurements of poly(DEGEEA)₈₀ and poly (Mannose)₁₀ - *b*- (DEGEEA)₈₀ by UV/Vis spectroscopy at 500 nm. Sample concentrations: 1mg / mL

In summary, two different double hydrophilic diblock glycopolymer have been successfully synthesized by the aqueous SET-LRP and one-pot chain extension. Full conversion and low dispersity was maintained even after block copolymerization. The targeted block copolymer showed different LCST temperature due to the presence of glycopolymer segment, which favors interesting self-assemble behavior in water.

5.2.12 Exploration of ligand and solvent effect on the in-situ SET-LRP.

Previous research has pointed out that solvent and ligand play vital role in mediating the disproportionation of Cu(I)X into Cu(0) and Cu(II)X₂.^{21,224} Solvents, such as water and ethanol, do not stabilize colloidal Cu(0) and thus give large particulate precipitates. In our hands, water strongly facilitates the disproportionation of CuBr/Me₆TREN with agglomeration of Cu(0), which resulted in apparent clumps of Cu(0) particles easily separating from a blue aqueous solution (Figure 5.77, 5.78). However, with the addition of ethanol, the Cu (0) precipitate became finer with a reduction in particle size (Figure 5.79, 5.80).

Figure 5.77-80 clearly showed the disproportionation of CuBr mediated by Me₆TREN and water/ethanol, which yielded purple-red Cu (0) precipitate in the blue or green CuBr₂/Me₆TREN containing solution. Both water and ethanol proved to facilitate the agglomeration of Cu (0) particles, which could be visually observed clearly.

In pure water, the aggregation tends to be very fast; causing a big lump of random Cu (0) precipitate and the solution became clear in less than 5 min. However, with the addition of ethanol, the Cu (0) particles tend to become more even and fine and it

needs up to more than 120 min for the fine Cu (0) particles to precipitate in pure ethanol, as shown in Figure 5.77.

The copper particles dispersed in solvents were observed using a Leica DM2500M optical microscope equipped with a Nikon D5100 camera under dark field. As shown in Figure 5.79 & 5.80, Cu (0) particles obtained from disproportionation in 100% water assemble together randomly. With the addition of ethanol from 25% to 75%, the size of the aggregates became much smaller, however, could still be observed by optical microscopy. The particle size can go down to 1 μm in 100% ethanol.

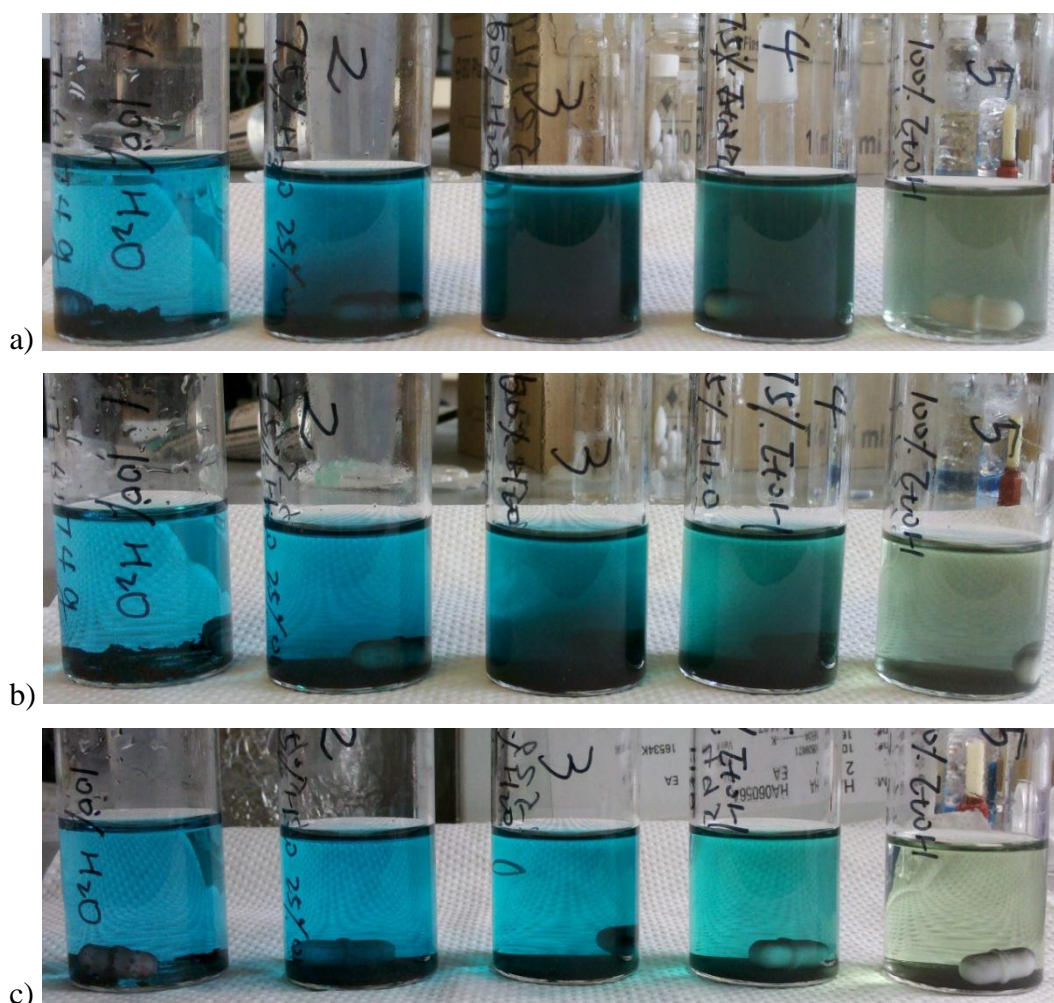


Figure 5. 77. Visual observation of the disproportionation of CuBr / Me₆TREN in water / ethanol mixture. Conditions: solvent = 12 mL (V_{water} : V_{ethanol} from left to right: 100%: 0% – 75%: 25% – 50%: 50% – 25%: 75% – 0%: 100%); CuBr = 43 mg, 0.3 mmol; Me₆TREN = 78 μL , 0.3 mmol. Picture was taken after setting down for a) 5 min; b) 30 min; c) 120 min.

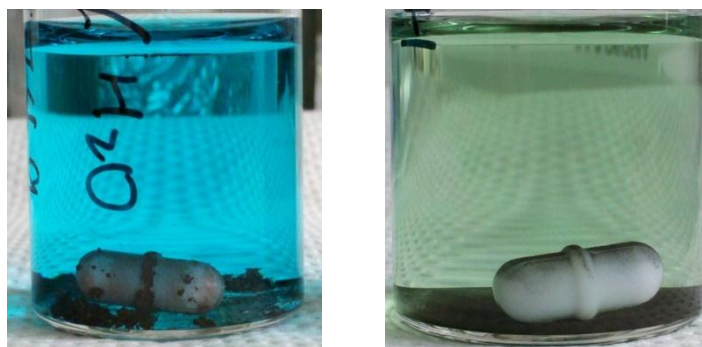


Figure 5. 78. Zoom of Figure 5.96 for the disproportionation of CuBr / Me₆TREN in water (left) and ethanol (right). Pictures were taken after setting down for 120 min.

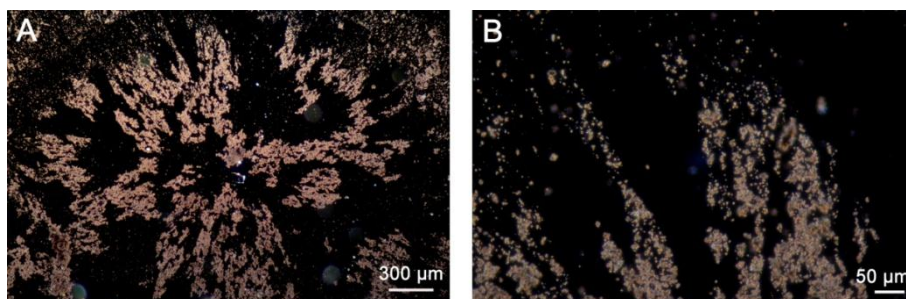


Figure 5. 79. Optical microscopy images of copper powders from the disproportionation of CuBr / Me₆TREN in water.

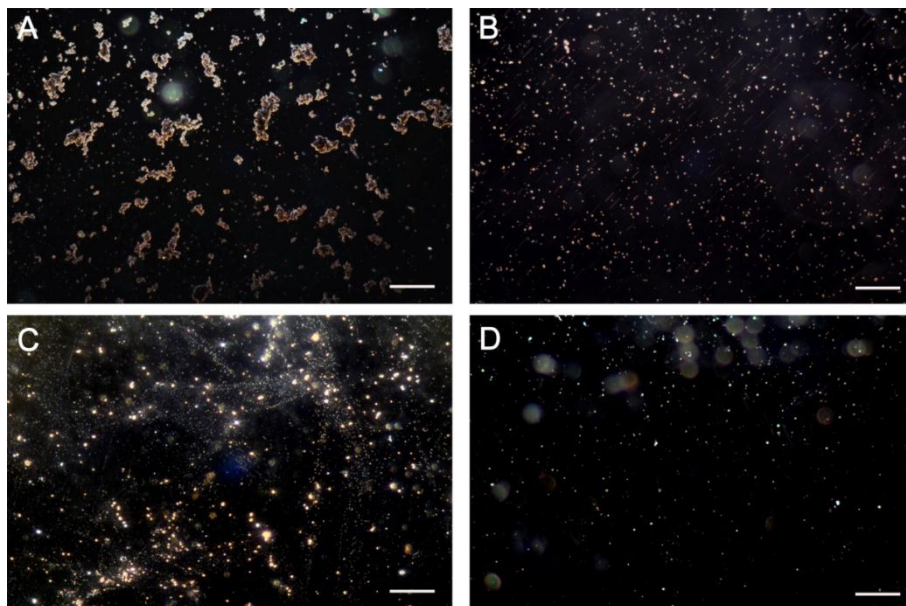


Figure 5. 80. Optical microscopy images of copper powders from the disproportionation of CuBr / Me₆TREN in water / ethanol mixture. Conditions: $V_{\text{water}}:V_{\text{ethanol}} = 75\%:25\%$ (A), $50\%:50\%$ (B); $25\%:75\%$ (C); $0\%:100\%$ (D). The white scale bar is 300 μm .

In order to investigate the versatility of this system we further investigated two ligands which have been previously widely utilized in SET-LRP, Tris(2-aminoethyl)amine (TREN) and *N, N, N', N'', N'''*-Pentamethyldiethylenetriamine (PMDETA), for the polymerization of NIPAM, HEA and PEGA.

Disproportionation tests showed that both TREN and PMDETA favor the disproportionation of CuBr in water, Figure 5.81, 5.82, purple red colour copper precipitates were found on the inside wall of reaction tubes with a deep blue (for PMDETA) or light blue (for TREN) solution.

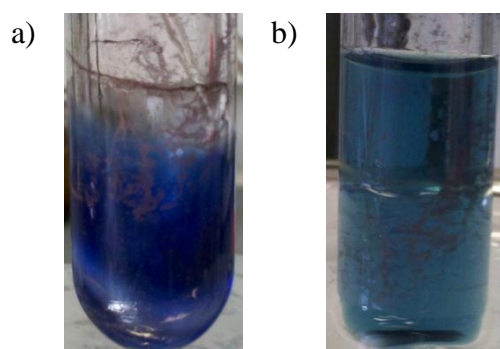


Figure 5. 81. Visual observation of the disproportionation of CuBr / PMDETA (a) and SET-LRP of NIPAM (DP=80) in water (b). Conditions: a) H_2O = 2 mL; CuBr = 10 mg, 70 μmol ; PMDETA = 7.4 μL , 35 μmol . Picture was taken 30 min after mixing the reagents. b) Picture was taken 2 min after transferring the initiator / NIPAM solution into the catalyst solution of (a).

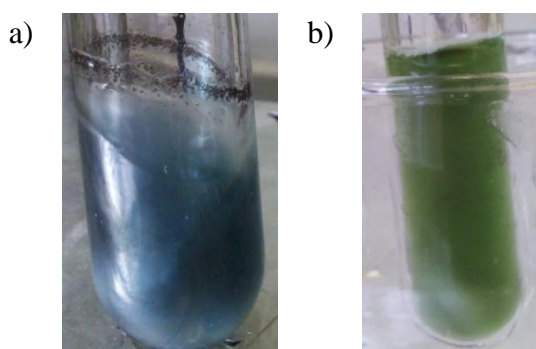


Figure 5. 82. Visual observation of the disproportionation of CuBr / TREN (a) and SET-LRP of NIPAM (DP=80) in water (b). Conditions: a) H_2O = 2 mL; CuBr = 10 mg, 70 μmol ; TREN = 5.3 μL , 35 μmol . Picture was taken 30 min after mixing the reagents. b) Picture was taken 2 min after transferring the initiator / NIPAM solution into the catalyst solution of (a).

Polymerization of NIPAM using PMDETA and TREN resulted in final polymer with dispersity ≈ 1.50 , showing worse control than Me₆TREN (Figure 5.83). However, polymerizations of HEA and PEGA using PMDETA and TREN under similar reaction conditions gave better control and the dispersity of final polymer was as low as 1.16, suggesting that NIPAM may coordinate with the copper catalyst and thus affects the polymerization. Thus choice of ligand is important to mediate a living/controlled polymerization and future work is underway to optimize reaction conditions.

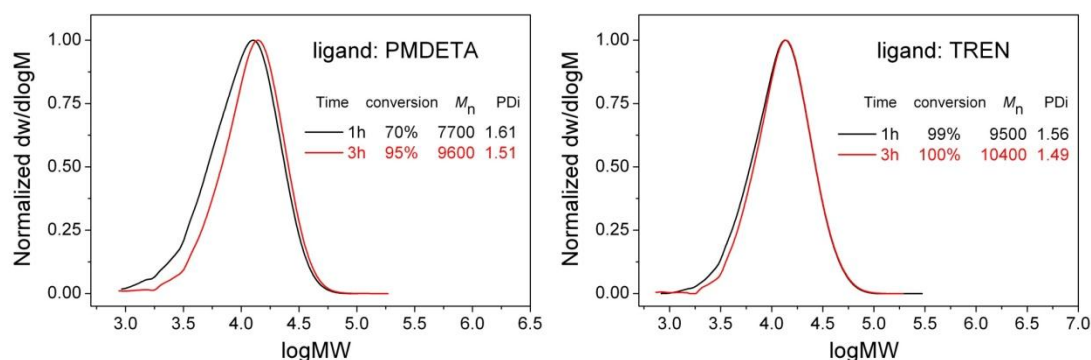


Figure 5. 83. DMF SEC molecular weight distributions at different time for the SET-LRP of NIPAM (DP=80) in H₂O at 0 °C with [initiator]: [CuBr]: [PMDETA] = 1: 0.8: 0.4 (left) and [initiator]: [CuBr]: [TREN] = 1: 0.8: 0.4 (right).

5.2.13 Conclusion

The *prior* disproportionation of CuBr/Me₆TREN in water has been exploited for the SET-LRP of hydrophilic monomers. Reactions proceed faster and with no induction periods when compared to SET-LRP mediated by commercial Cu(0) sources without any compromise in polymerization control.

Thorough analysis of model and reaction mixtures confirmed complete disproportionation of CuBr/Me₆TREN in the water system. Attempted polymerization with the separated products of disproportionation revealed the synergistic character of the products of the disproportionation reaction. Comparison with L-ascorbic acid mediated aqueous AGET-ATRP revealed the sensitive and complex nature of all Cu-mediated systems, as observations were found to be highly dependent on the order of reagent addition. The SET-LRP polymerization of NIPAM was investigated and careful selection of catalyst ratio and reaction temperature provided access to a range of molecular weights (DP = 8-320). Full characterization of the low molecular weight

PNIPAM resulted in identification of the end-group functionality. Suppression of hydrolysis, leading to premature termination, permitted preparation of block copolymers. Iterative, *in situ* chain extension up to a triblock copolymer was also tolerated without appreciable loss of polymerization control.

The robustness of this procedure has been further exemplified by performing SET-LRP of NIPAM in biologically relevant media (PBS pH 6.2 and 6.8) and in a commercial water-alcohol mixture (Tequila) and finally under a truly biological condition: sheep blood serum. A small library of acrylamide and acrylate monomers was then polymerized to provide an indication of the potential scope of this procedure.

Two different double hydrophilic diblock glycopolymer were synthesized by this aqueous SET-LRP and chain extension after full conversion. It is our belief that this process could be applied to a wide range of hydrophilic monomers and less hydrophilic monomers in mixed solvent systems.

5.3 Experimental

5.3.1 Materials

N-Isopropylacrylamide (NIPAM, 97%) was obtained from Sigma-Aldrich and was recrystallized from hexane to remove the inhibitor. 2-Hydroxyethyl acrylate (HEA, 96%, Sigma-Aldrich), Poly (ethylene glycol) methyl ether acrylate (PEGA₄₈₀, average M_n 480, Sigma-Aldrich), *N*, *N*-Dimethylacetamide (DMA, 99.5%, Sigma-Aldrich) were de-inhibited by passing through a column of basic alumina prior to use. Glucose acrylamide was synthesised according to a previously reported procedure.²⁷⁶

HPLC grade water (H₂O, VWR international, LLC) was directly used as the solvent for polymerizations unless otherwise stated. Tequila (Jose Cuervo Gold Tequila, 38% v/v, TESCO) was used as received. Sheep serum (USA origin, sterile-filtered, suitable for cell culture, Sigma-Aldrich) was directly used as the solvent for polymerization unless otherwise stated. The sheep serum was stored under -20 °C in the freezer and transferred to the cold room to defreeze under 4 °C overnight before use.

Tris(2-(dimethylamino)ethyl)amine (Me₆TREN) was synthesized according to literature procedure and stored under a nitrogen atmosphere prior to use.^{177,178} *N*-Ethyl-2-pyridylmethanimine was synthesized according to literature procedure and

stored under a nitrogen atmosphere prior to use.²⁷⁷ *N, N, N', N'', N''*-Pentamethyldiethylenetriamine (PMDETA, 99%, Sigma-Aldrich) and Tris(2-aminoethyl)amine (TREN, 96%, Sigma-Aldrich) was used as received. Water soluble initiator 2, 3-dihydroxypropyl 2-bromo-2-methylpropanoate was synthesized according to literature procedure.²¹⁵

Copper (I) bromide (CuBr, 98%, Sigma-Aldrich) was washed sequentially with acetic acid and ethanol and dried under vacuum. Copper(II) bromide (CuBr₂, 99%, Sigma-Aldrich) was used as received. Copper wire (diameter=0.25 mm) was pre-treated by washing in hydrochloric acid for 15 min and rinsed thoroughly with MiliQ water, dried under nitrogen and used immediately. Membrane dialysis (1K MWCO) was obtained from Spectrum Laboratories.

5.3.2 Instruments and analysis

¹H and ¹³C NMR spectra were recorded on Bruker DPX-300, DPX-400 and DPX-600 spectrometers using deuterated solvents obtained from Aldrich. Monomer conversion for NIPAM polymerization was calculated by comparing the integral of vinyl protons with isopropyl protons.

SEC was conducted on Varian 390-LC system in DMF (5 mM NH₄BF₄) at 50 °C, equipped with refractive index, UV and viscometry detectors, 2 × PLgel 5 mm mixed-D columns (300 × 7.5 mm), 1 × PLgel 5 mm guard column (50 × 7.5 mm) and autosampler. Narrow linear poly (methyl methacrylate) standards in range of 200 to 1.0 × 10⁶ g·mol⁻¹ were used to calibrate the system. All samples were passed through 0.45 μm PTFE filter before analysis.

UV/Vis spectra were recorded on Agilent Technologies Cary 60 UV-Vis in the range of 200-1100 nm using a cuvette with 10 mm optical length.

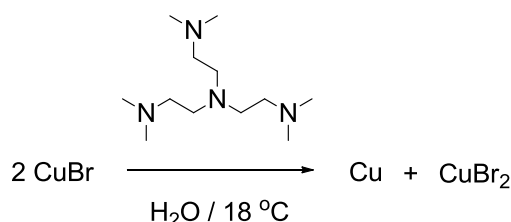
MALDI-ToF MS was recorded in linear or reflex mode on a Bruker Daltonics Ultraflex II MALDI-ToF mass spectrometer, equipped with a nitrogen laser delivering 2 ns laser pulses at 337 nm with positive ion ToF detection performed using an accelerating voltage of 25 kV. The matrix solution was prepared by dissolving α-cyano-4-hydroxycinnamic acid (CHCA) or *trans*-2-[3-(4-*tert*-butylphenyl)-2-methyl-2-propenylidene]malononitrile (DCTB) in THF (20 mg/mL solution). Sodium iodide was added at a 0.1% overall concentration to improve the ionization. Polymer analytes were dissolved to a concentration of 1 mg/mL. Samples were prepared by

layering matrix solution and analyte solution on the stainless steel side. Calibration was performed with different linear poly (ethylene glycol) methyl ether standards. The MALDI-ToF MS characterization in this chapter was performed by Miss Athina Anastasaki of Haddleton group.

Infrared absorption spectra were recorded on a Bruker VECTOR-22 FTIR spectrometer using a Golden Gate diamond attenuated total reflection cell.

The copper particles dispersed in solvents were observed using a Leica DM2500M optical microscope equipped with a Nikon D5100 camera under dark field. This analysis was performed by Dr Yunhua Chen of Bon's group.

5.3.3 Disproportionation of CuBr / Me₆TREN into Cu (0) and CuBr₂ in H₂O



Scheme 5. 9. Disproportionation of CuBr / Me₆TREN in water.

For the disproportionation test in the presence of air, to one vial with 5 mL H₂O and a magnetic stir bar, Me₆TREN (130 μL, 0.5 mmol) and CuBr (72 mg, 0.5 mmol) were sequentially added and the mixed solution was allowed to stir for 1 h under the existence of air.

To calculate the degree of disproportionation of CuBr / Me₆TREN in H₂O, another experiment was carried out under oxygen-free condition to avoid possible side oxidation reaction of the in-situ generated copper (0) powders. One typical experiment was shown as follow.

A magnetic stir bar, H₂O (12 mL) and Me₆TREN (78 μL, 0.3 mmol) were charged to a vial fitted with a rubber septum and the mixture was degassed via nitrogen sparging for 15 min. CuBr (43 mg, 0.3 mmol) was then carefully added into the solution under stirring. The solution became blue at once after the addition of CuBr and massive purple red powders could be observed in the suspension, but the stirring was allowed to continue for 30 min under nitrogen protection. After that, the stirring was stopped to allow the powders settle down (for 15 min) and the blue aqueous solution was carefully transferred through a gas tight syringe and 0.45 μm PTFE filter to another

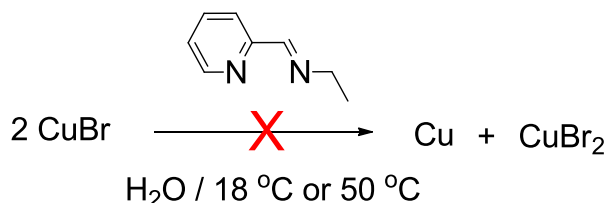
vial, previously filled with nitrogen. The residue copper (0) powders were washed with degassed water carefully for 6 times until the water became colourless. The vial with copper (0) powders was then directly transferred to a vacuum oven and dried under vacuum for two days. After that the total weight increase of the vial and stir bar was measured and it revealed the weight of copper (0) powder as 9.4 mg, which is very close to the theoretical value of 9.5 mg when 100% disproportionation happened. (Note: the readability of the balance is 0.1 mg)

The filtered blue solution was diluted in order to get an accurate UV-Vis spectrum. 0.5 mL of the solution was transferred to a vial filled with 4.5 mL degassed water. Then 3 mL of the diluted solution was transferred to a UV-Vis cuvette (optical length, 10 mm), which was fitted with a rubber septum and previously filled with nitrogen. The cuvette was directly taken for UV-Vis measurements.

To calculate the concentration of CuBr_2 in disproportionation solution, a series of $\text{CuBr}_2/\text{Me}_6\text{TREN}$ solution, with same amount of Me_6TREN (78 μL , 0.3 mmol) and different amounts of CuBr_2 (24, 27, 30, 33, 36, 39 mg) in 12 mL water, were made for UV-Vis measurements according to the same procedure as the disproportionation of $\text{CuBr} / \text{Me}_6\text{TREN}$ in H_2O .

As shown in Figure 5.4, the UV-Vis spectrum of the solution from disproportionation of $\text{CuBr} / \text{Me}_6\text{TREN}$ in H_2O is the same as the spectra of $\text{CuBr}_2 / \text{Me}_6\text{TREN}$ in H_2O , which proved the existence of CuBr_2 due to the disproportion of CuBr . Its trace is almost overlapped with one spectrum of $\text{CuBr}_2 / \text{Me}_6\text{TREN}$ in H_2O (3.00 mg / mL). The CuBr_2 concentration from the disproportionation of $\text{CuBr} / \text{Me}_6\text{TREN}$ in H_2O was then calculated as 3.00 ± 0.01 mg / mL, which was according to the calibration curves based on UV-Vis absorbance at 700 and 865 nm. This value is slightly higher than the theoretical value (2.79 mg / mL) if 100% disproportionation happened, which was first thought as experimental error due to limit of equipment (balance and UV-Vis) or artificial factor during dilution. However, we notice that such phenomenon also happened when higher ratio Me_6TREN (2.0-3.0 equivalents to CuBr) was used in the disproportionation of CuBr in H_2O , which was attributed that high level Me_6TREN could help water stabilize Cu (0) colloids.²²⁴ However, combined with the results of Cu (0) amount and CuBr_2 concentration, $\text{CuBr} / \text{Me}_6\text{TREN}$ in water tends to disproportionate fast and totally into Cu (0) and CuBr_2 . Stable $\text{CuBr} / \text{Me}_6\text{TREN}$ complex could hardly exist in water or cannot be detected by previous experiments.

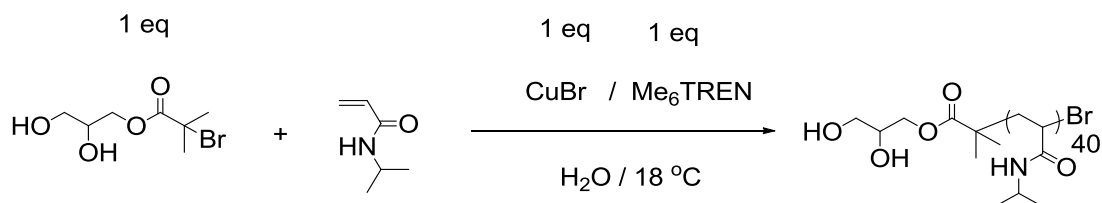
5.3.4 Disproportionation test of the CuBr / *N*-ethyl-2-pyridylmethanimine complex in H₂O



Scheme 5. 10. Disproportionation of CuBr / *N*-ethyl-2-pyridylmethanimine in water.

A magnetic stir bar, H₂O (2 mL) and *N*-ethyl-2-pyridylmethanimine (27 mg, 0.1 mmol) were charged to a vial fitted with a rubber septum and the mixture was degassed via nitrogen sparging for 15 min. CuBr (14 mg, 0.1 mmol) was then carefully added into the solution under stirring and nitrogen protection. The solution became dark brown at once after the addition of CuBr. The tube was then sealed and immersed in a thermostated water bath at 50 °C and kept stirring for 1 h.

5.3.5 Atom transfer radical polymerization of NIPAM in H₂O at ambient temperature

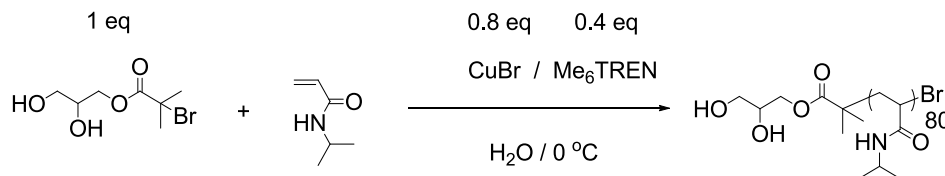


Scheme 5. 11. ATRP of NIPAM in H₂O at ambient temperature.

A magnetic stir bar, H₂O (5 mL), 2, 3-dihydroxypropyl 2-bromo-2-methylpropanoate (60 mg, 0.25 mmol), NIPAM (1.13 g, 10 mmol) and Me₆TREN (65 μL, 0.25 mmol) were charged to a Schlenk tube fitted with a rubber septum and the solution was deoxygenated via freeze-pump-thaw for six times. The degassed solution was then transferred via cannula to another Schlenk tube, previously evacuated and filled with nitrogen, containing CuBr (36 mg, 0.25 mmol) and a magnetic stir bar. The resulting solution became turbid immediately and massive gel was also found. The reaction mixture was allowed to stir at ambient temperature (~ 18 °C) for 30 min. Sample of the reaction mixture was then removed for analysis. The sample for ¹H NMR was directly diluted with D₂O, which confirmed 100% conversion according to the total

disappearance of vinyl groups. Catalyst residues were removed by filtering through a column of neutral alumina prior to DMF SEC analysis.

5.3.6 Atom transfer radical polymerization of NIPAM in H₂O at 0 °C



Scheme 5. 12. ATRP of NIPAM in H₂O at 0 °C.

A magnetic stir bar, H₂O (5.5 mL), 2, 3-dihydroxypropyl 2-bromo-2-methylpropanoate (21 mg, 0.087 mmol), NIPAM (0.79 g, 7 mmol) and Me₆TREN (9 μ L, 0.035 mmol) were charged to a Schlenk tube fitted with a rubber septum and the solution was deoxygenated via freeze-pump-thaw for six times. The degassed solution was then transferred via cannula to another Schlenk tube, previously evacuated and filled with nitrogen, containing CuBr (10 mg, 0.07 mmol) and a magnetic stir bar, which has already been immersed in ice / water bath. The resulting solution became blue immediately and no significant gel was noticed, although system viscosity tends to be high. The reaction mixture was allowed to stir at 0 °C for 30 min. Sample of the reaction mixture was then removed for analysis. The sample for ¹H NMR was directly diluted with D₂O, which confirmed 100% conversion according to the total disappearance of vinyl groups. Catalyst residues were removed by filtering through a column of neutral alumina prior to DMF SEC analysis.

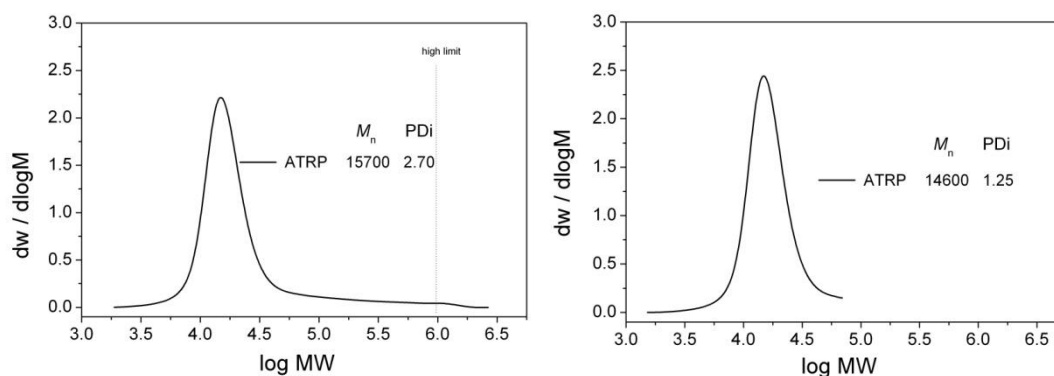
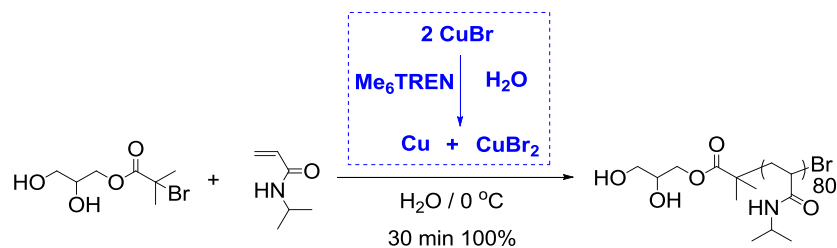


Figure 5. 84. Molecular weight distributions of PNIPAM by ATRP at 0 °C *via* DMF SEC. Include tailing peak at high MW position (left); Ignore tailing peak at high MW position (right).

5.3.7 SET-LRP of NIPAM in H₂O at 0 °C *via* disproportionation of CuBr / Me₆TREN

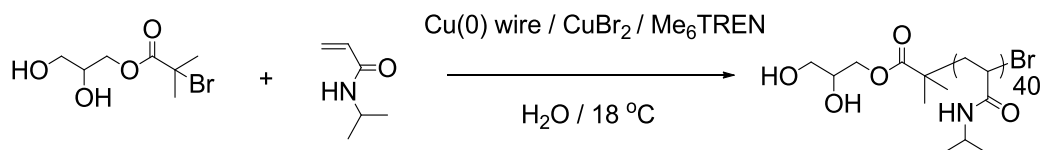


Scheme 5. 13. SET-LRP of NIPAM in H₂O at 0 °C *via* disproportionation of CuBr / Me₆TREN.

A magnetic stir bar, H₂O (2 mL) and Me₆TREN (9 µL, 0.035 mmol) were charged to a Schlenk tube (**No. 1**) fitted with a rubber septum and the solution was deoxygenated via freeze-pump-thaw for six times. The degassed solution was then transferred via cannula to another Schlenk tube (**No. 2**), previously evacuated and filled with nitrogen, containing CuBr (10 mg, 0.07 mmol) and a magnetic stir bar. The mixed suspension became blue immediately after cannula transfer and massive purple red colour copper (0) powder was found in the suspension. The reaction mixture was allowed to stir at ambient temperature (~ 18 °C) for 30 min under nitrogen protection. After that, Schlenk tube (**No. 2**) was immersed into ice/water bath.

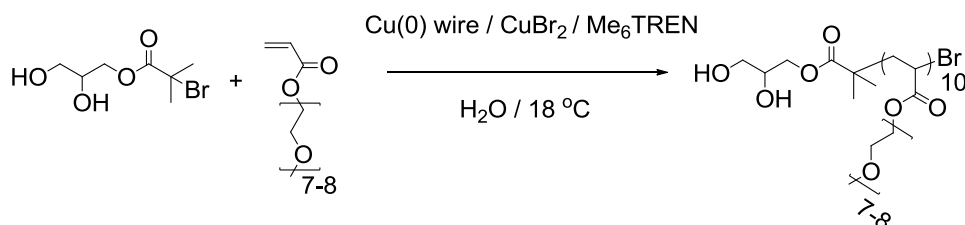
A magnetic stir bar, H₂O (3.5 mL), 2, 3-dihydroxypropyl 2-bromo-2-methylpropanoate (21 mg, 0.087 mmol), and NIPAM (0.79 g, 7 mmol) were charged to a Schlenk tube (**No. 3**) fitted with a rubber septum and the solution was deoxygenated via freeze-pump-thaw for six times. The degassed initiator / monomer solution was then transferred via cannula to Schlenk tube (**No. 2**), which has already been immersed in the ice / water bath. The mixed solution was allowed to stir at 0 °C for 30 min. Sample of the reaction mixture was then removed for analysis. The sample for ¹H NMR was directly diluted with D₂O, which confirmed 100% conversion according to the total disappearance of vinyl groups. Catalyst residues were removed by filtering through a column of neutral alumina prior to DMF SEC analysis.

5.3.8 Copper (0) wire mediated SET-LRP of NIPAM and PEGA₄₈₀ in H₂O at ambient temperature



Scheme 5. 14. Copper (0) wire mediated SET-LRP of NIPAM in H₂O at ambient temperature.

To a Schlenk tube fitted with a magnetic stir bar and a rubber septum, 2, 3-dihydroxypropyl 2-bromo-2-methylpropanoate (60 mg, 0.25 mmol), NIPAM (1.13 g, 10 mmol), CuBr₂ (12 mg, 0.05 mmol) and H₂O (5 mL) were charged and the mixture was bubbled with nitrogen for 15 min. Pre-degassed Me₆TREN (26 μL, 0.1 mmol) were then added via gas tight syringe. After that, pre-activated copper wire (4 cm, 18 mg, 0.28 mmol) was carefully added under nitrogen protection. The Schlenk tube was sealed and the blue solution was allowed to polymerize at ambient temperature (~18 °C). Samples of the reaction mixture were carefully removed at suitable time periods for analysis. The sample for ¹H NMR was directly diluted with D₂O. Catalyst residues were removed by filtering through a column of neutral alumina prior to SEC analysis.



Scheme 5. 15. Copper (0) wire mediated SET-LRP of PEGA₄₈₀ in H₂O at ambient temperature.

The polymerization procedure is the same as copper (0) wire mediated SET-LRP of NIPAM in H₂O at ambient temperature. The charging amounts of each component are listed below: 2, 3-dihydroxypropyl 2-bromo-2-methylpropanoate (120 mg, 0.5 mmol), PEGA₄₈₀ (2.4 g, 5 mmol), CuBr₂ (22 mg, 0.1 mmol), H₂O (3 mL), Me₆TREN (26 μL, 0.1 mmol) and copper wire (4 cm, 18 mg, 0.28 mmol).

5.3.9 Test polymerizations of NIPAM in H₂O at ambient temperature *via* separated copper(0) powder and CuBr₂/Me₆TREN solution from disproportionation of CuBr/Me₆TREN

A magnetic stir bar, H₂O (2 mL) and Me₆TREN (26 μ L, 0.1 mmol) were charged to a Schlenk tube (**No. 1**) fitted with a rubber septum and the solution was deoxygenated *via* freeze-pump-thaw for six times. The degassed solution was then transferred *via* cannula to another Schlenk tube (**No. 2**), previously evacuated and filled with nitrogen, containing CuBr (14 mg, 0.1 mmol) and a magnetic stir bar. The mixed suspension became blue immediately after cannula transfer and massive purple red colour copper (0) powder was found in the suspension. The reaction mixture was allowed to stir at ambient temperature ($\sim 18\text{ }^{\circ}\text{C}$) for 30 min under nitrogen protection. After that, stirring was stopped for static settlement about 15 min to allow all the copper (0) powders to precipitate at the bottom of tube. A gas tight syringe was then carefully used to take the blue solution out and transferred through a 0.45 μm PTFE filter to another Schlenk tube (**No. 3**), previously evacuated and filled with nitrogen.

In order to remove the residue CuBr₂ / Me₆TREN, degassed water ($\sim 3\text{ mL}$) was then transferred *via* cannula to Schlenk tube **No. 2**, stir for 1 min to wash the copper (0) powders, static settlement for 2 min and then the water was removed *via* gas tight syringe. The above procedure was repeated for five times until the solution became totally colourless. After that a solution of H₂O (2 mL) and Me₆TREN (26 μ L, 0.1 mmol), previously degassed *via* freeze-pump-thaw for three times, was transferred *via* cannula to Schlenk tube **No. 2**.

To test polymerizations catalyzed by copper (0) powder / Me₆TREN or CuBr₂ / Me₆TREN, two same solutions of H₂O (2.5 mL), 2, 3-dihydroxypropyl 2-bromo-2-methylpropanoate (60 mg, 0.25 mmol) and NIPAM (0.57 g, 5 mmol), previously degassed *via* freeze-pump-thaw for at least three times, were then transferred separately *via* cannula to Schlenk tube **No. 2** and **No. 3**. The mixed solutions were then allowed to stir at ambient temperature ($\sim 18\text{ }^{\circ}\text{C}$). Samples of the reaction mixtures were carefully removed at suitable time periods for analysis. The sample for ¹H NMR was directly diluted with D₂O. Catalyst residues were removed by filtering through a column of neutral alumina prior to SEC analysis.

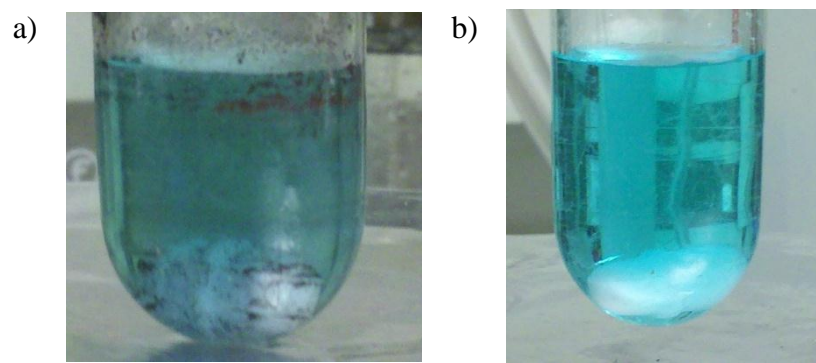


Figure 5. 85. Visual observation of the SET-LRP of NIPAM catalyzed by separated Cu (0) powder / Me₆TREN (a) and CuBr₂ / Me₆TREN (b) in H₂O. Conditions: a) Picture was taken 15 min after starting polymerization. b) Picture was taken 24 after starting polymerization.

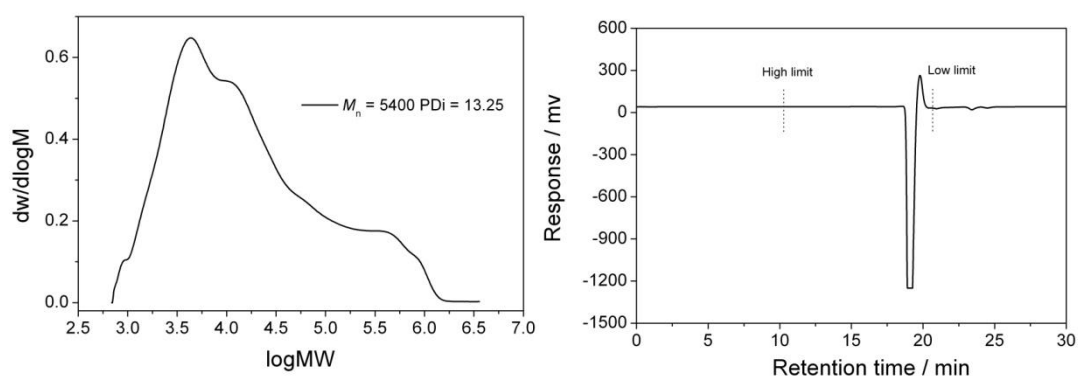


Figure 5. 86. Molecular weight distributions of PNIPAM (DP=20) catalyzed by Cu (0) powder / Me₆TREN (left) and CuBr₂ / Me₆TREN (right) in H₂O at ambient temperature *via* DMF SEC.

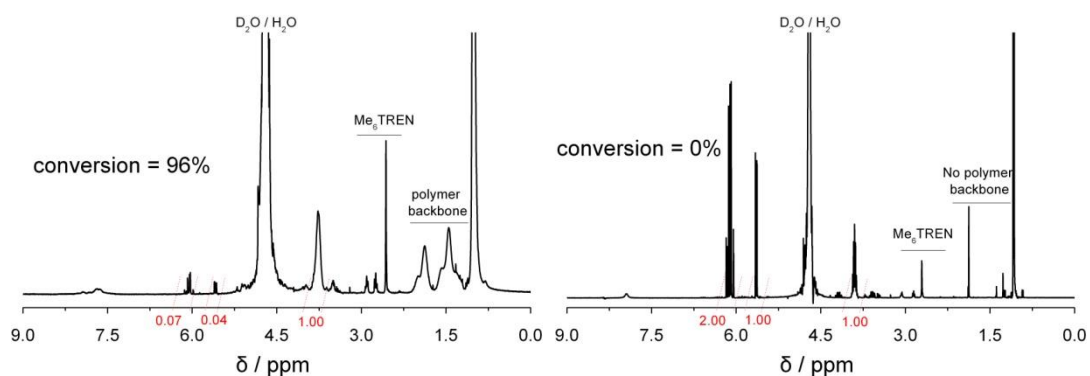
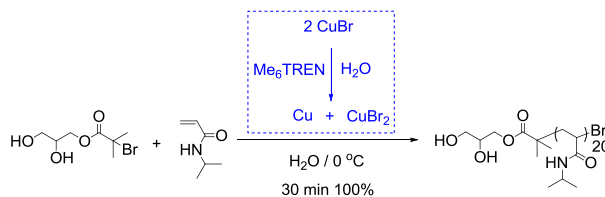


Figure 5. 87. ¹H NMR spectra for SET-LRP of NIPAM catalyzed by Cu (0) powder / Me₆TREN (left) and CuBr₂ / Me₆TREN (right) in D₂O.

5.3.10 SET-LRP of NIPAM (DP=20) in H₂O at ambient temperature *via* disproportionation of CuBr / Me₆TREN



Scheme 5. 16. SET-LRP of NIPAM (DP=20) in H₂O at ambient temperature *via* disproportionation of CuBr/Me₆TREN.

To a Schlenk tube fitted with a magnetic stir bar and a rubber septum, H₂O (2 mL) and Me₆TREN (26 μ L, 0.1 mmol) were charged and the mixture was bubbled with nitrogen for 10 min. CuBr (14 mg, 0.1 mmol) was then carefully added under slight positive pressure of nitrogen. The nitrogen bubbling was continued for another 10 min and then the blue suspension with purple red colour copper (0) powder was allowed to stir at ambient temperature under nitrogen protection for 15 min. At the same time, to another vial fitted with a magnetic stir bar and a rubber septum, H₂O (2.5 mL), 2, 3-dihydroxypropyl 2-bromo-2-methylpropanoate (60 mg, 0.25 mmol) and NIPAM (0.57 g, 5 mmol) were charged and the mixture was bubbled with nitrogen for 15 min. After that, the degassed monomer/initiator aqueous solution was transferred *via* cannula to the Schlenk tube with Cu(0)/CuBr₂/Me₆TREN catalyst. The Schlenk tube was sealed and allowed to polymerize at ambient temperature (~ 18 °C) for 30 min. Sample of the reaction mixture was then removed for analysis. The sample for ¹H NMR was directly diluted with D₂O, which confirmed 100% conversion according to the total disappearance of vinyl groups. Catalyst residues were removed by filtering through a column of neutral alumina prior to DMF SEC analysis.

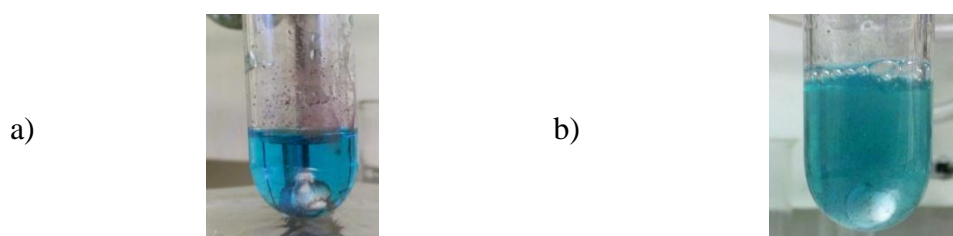
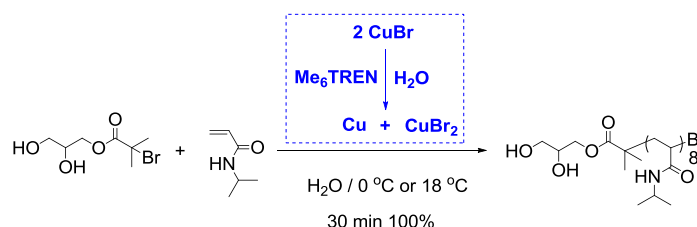


Figure 5. 88. Visual observation of the disproportionation of CuBr / Me₆TREN (a) and SET-LRP of NIPAM (DP=20) in H₂O (b). Conditions: a) H₂O = 2 mL; CuBr = 14 mg, 0.1 mmol; Me₆TREN = 26 μ L, 0.1 mmol. Picture was taken 30 min after mixing

the reagents. b) Picture was taken 15 min after transferring the initiator/NIPAM solution into the catalyst solution of (a).

5.3.11 SET-LRP of NIPAM (DP=8) in H₂O at 0 °C and ambient temperature *via* disproportionation of CuBr/Me₆TREN



Scheme 5. 17. SET-LRP of NIPAM (DP=8) in H₂O at 0 °C and ambient temperature (~18 °C) *via* disproportionation of CuBr / Me₆TREN.

The polymerization procedure is the same as described in SET-LRP of NIPAM (DP=20). The charging amount for each component is listed below.

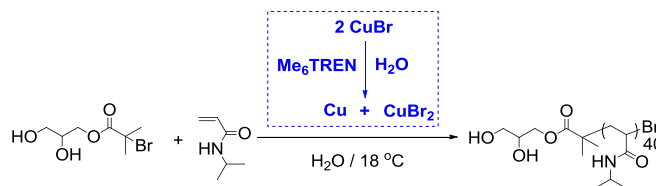
Table 5. 2. Charging amounts for SET-LRP of NIPAM (DP=8) in H₂O at 0 °C and ambient temperature with [initiator]: [CuBr]: [Me₆TREN] = 1: 0.4: 0.4.

Initiator / monomer system			Catalyst system		
Initiator	NIPAM	H ₂ O	CuBr	Me ₆ TREN	H ₂ O
0.25 mmol	2 mmol	2 mL	0.1 mmol	0.1 mmol	2 mL

After 30 mins, sample of the reaction mixture was removed for NMR, SEC and MALDI-ToF MS analysis. The sample for ¹H NMR was directly diluted with D₂O, which confirmed 100% conversion for both polymerizations under 0 °C or ambient temperature (~18 °C) according to the total disappearance of vinyl groups. The sample for MALDI-ToF MS analysis was diluted with THF first. Catalyst residues were removed by filtering through a column of neutral alumina prior to DMF SEC analysis.

The rest solution was diluted with more water and passed through a basic alumina column to remove the copper catalyst. Then the PNIPAM products could be recovered by freezing dry. **Note:** Due to the high polarity of water, basic alumina was not able to remove all the copper catalyst. If high purity was demanded, diluted with THF for alumina column or dialysis against water will result in better results.

5.3.12 SET-LRP of NIPAM (DP=40) in H₂O at ambient temperature *via* disproportionation of CuBr / Me₆TREN



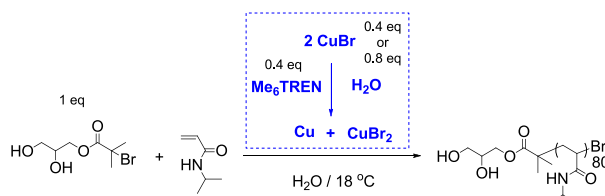
Scheme 5. 18. SET-LRP of NIPAM (DP=40) *via* disproportionation of CuBr / Me₆TREN in H₂O at ambient temperature.

The polymerization procedure is the same as described in SET-LRP of NIPAM (DP=20). The charging amount for each component is listed below.

Table 5. 3. Charging amounts for SET-LRP of NIPAM (DP=40) in H₂O at ambient temperature with [initiator]: [CuBr]: [Me₆TREN] = 1: 0.4: 0.4.

Initiator / monomer system			Catalyst system		
Initiator	NIPAM	H ₂ O	CuBr	Me ₆ TREN	H ₂ O
125 μmol	5 mmol	2.5 mL	50 μmol	50 μmol	2 mL

5.3.13 SET-LRP of NIPAM (DP = 80) in H₂O at different ratios of CuBr / Me₆TREN under ambient temperature



Scheme 5. 19. SET-LRP of NIPAM (DP=80) *via* disproportionation of CuBr / Me₆TREN in H₂O at ambient temperature.

The polymerization procedure is the same as described in SET-LRP of NIPAM (DP=20). The charging amount for each component is listed below.

Table 5. 4. Charging amounts for SET-LRP of NIPAM (DP=80) in H₂O at ambient temperature with [initiator]: [CuBr]: [Me₆TREN] = 1: 0.4: 0.4.

Initiator / monomer system			Catalyst system		
Initiator	NIPAM	H ₂ O	CuBr	Me ₆ TREN	H ₂ O
87 μmol	7 mmol	3.5 mL	35 μmol	35 μmol	1 mL

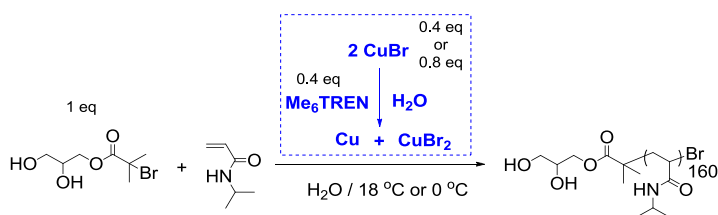
For polymerization with [initiator]: [CuBr]: [Me₆TREN] = 1: 0.4: 0.4, after transfer of initiator / monomer solution into the catalyst solution, the solution became turbid at once and then became clear after 10 min. After 1 h, the conversion reached 100% according to ¹H NMR analysis.

Table 5. 5. Charging amounts for SET-LRP of NIPAM (DP=80) in H₂O at ambient temperature with [initiator]: [CuBr]: [Me₆TREN] = 1: 0.8: 0.4.

Initiator / monomer system			Catalyst system		
Initiator	NIPAM	H ₂ O	CuBr	Me ₆ TREN	H ₂ O
87 μmol	7 mmol	3.5 mL	70 μmol	35 μmol	2 mL

For polymerization with [initiator]: [CuBr]: [Me₆TREN] = 1: 0.8: 0.4, after transfer of initiator / monomer solution into the catalyst solution, the solution kept clear through the reaction and the conversion reached 99% in 30 min and 100% in 60 min.

5.3.14 SET-LRP of NIPAM (DP = 160) in H₂O at different ratios of CuBr / Me₆TREN under ambient temperature and 0 °C.



Scheme 5. 20. SET-LRP of NIPAM (DP = 160) *via* disproportionation of CuBr / Me₆TREN in H₂O at ambient temperature.

The polymerization procedure is the same as described in SET-LRP of NIPAM (DP=20). The charging amounts for each component are listed below.

Table 5. 6. Charging amounts for SET-LRP of NIPAM (DP=160) in H₂O at ambient temperature with [initiator]: [CuBr]: [Me₆TREN] = 1: 0.4: 0.4.

Initiator / monomer system			Catalyst system		
Initiator	NIPAM	H ₂ O	CuBr	Me ₆ TREN	H ₂ O
87 μmol	14 mmol	7 mL	35 μmol	35 μmol	1 mL

For polymerization with [initiator]: [CuBr]: [Me₆TREN] = 1: 0.4: 0.4 at ambient temperature, after transfer of initiator / monomer solution into the catalyst solution, the solution became turbid at once with a small amount of gel noticed and then the

system became clear after 10 min. After 2.5 h, the conversion reached 100% according to ^1H NMR analysis.

Table 5. 7. Charging amounts for SET-LRP of NIPAM (DP=160) in H_2O at ambient temperature with [initiator]: [CuBr]: [Me_6TREN] = 1: 0.8: 0.4.

Initiator / monomer system			Catalyst system		
Initiator	NIPAM	H_2O	CuBr	Me_6TREN	H_2O
87 μmol	14 mmol	7 mL	70 μmol	35 μmol	2 mL

For polymerization with [initiator]: [CuBr]: [Me_6TREN] = 1: 0.8: 0.4 at ambient temperature, after transfer of initiator / monomer solution into the catalyst solution, no turbid phenomenon was noticed at first, however, after about 2.5 min, the solution became turbid and lots of polymer gel was noticed to precipitate on the magnetic stir. After about 10 min, the system became clear again. ^1H NMR analysis of sample at 1 h showed that conversion reached 93%.

Table 5. 8. Charging amounts for SET-LRP of NIPAM (DP=160) in H_2O at 0 °C with [initiator]: [CuBr]: [Me_6TREN] = 1: 0.8: 0.4.

Initiator / monomer system			Catalyst system		
Initiator	NIPAM	H_2O	CuBr	Me_6TREN	H_2O
87 μmol	14 mmol	7 mL	70 μmol	35 μmol	2 mL

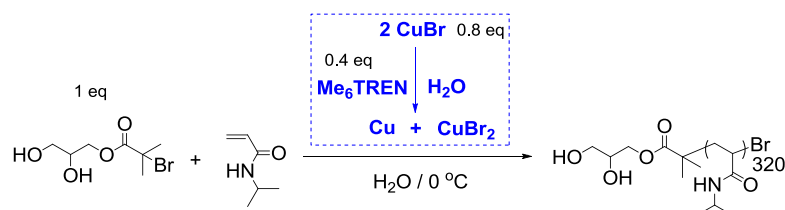
For polymerization with [initiator]: [CuBr]: [Me_6TREN] = 1: 0.8: 0.4 at 0 °C, the solution kept clear and no precipitate was noticed through the reaction period.

For polymerization with [initiator]: [CuBr]: [Me_6TREN] = 1: 1.2: 0.4 at ambient temperature, after transfer of initiator / monomer solution into the catalyst solution, no turbid phenomenon was noticed.

Table 5. 9. Charging amounts for SET-LRP of NIPAM (DP=160) in H_2O at ambient temperature with [initiator]: [CuBr]: [Me_6TREN] = 1: 1.2: 0.4.

Initiator / monomer system			Catalyst system		
Initiator	NIPAM	H_2O	CuBr	Me_6TREN	H_2O
87 μmol	14 mmol	7 mL	105 μmol	35 μmol	2 mL

5.3.15 SET-LRP of NIPAM (DP = 320) *via* disproportionation of CuBr / Me₆TREN in H₂O at 0 °C.



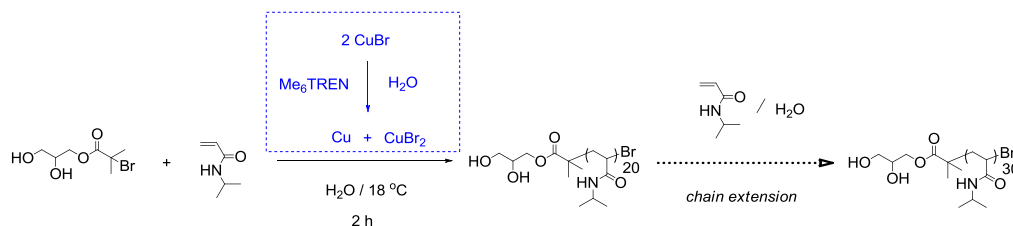
Scheme 5. 21. SET-LRP of NIPAM (DP = 320) *via* disproportionation of CuBr / Me₆TREN in H₂O at 0 °C.

The polymerizations were performed at the ratio of initiator / CuBr / Me₆TREN = 1: 08: 0.4 in H₂O at 0 °C according to previous procedure. The charging amounts for each component are listed below.

Table 5. 10. Charging amounts for SET-LRP of NIPAM (DP=320) in H₂O at 0 °C with [initiator]: [CuBr]: [Me₆TREN] = 1: 0.8: 0.4.

Initiator / monomer system			Catalyst system		
Initiator	NIPAM	H ₂ O	CuBr	Me ₆ TREN	H ₂ O
87 μmol	28 mmol	14 mL	70 μmol	35 μmol	2 mL

5.3.16 Chain extension reaction for SET-LRP of NIPAM in H₂O at ambient temperature.



Scheme 5. 22. Chain extension reaction for SET-LRP of NIPAM *via* disproportionation of CuBr / Me₆TREN in H₂O at ambient temperature.

The “first block” polymerization procedure is the same as described in SET-LRP of NIPAM (DP=20). After full conversion of the first block polymerization, a solution of NIPAM (0.29 g, 2.5 mmol) in 1.5 mL H₂O, previously degassed by nitrogen sparging for 15 min, was directly transferred via cannula to the Schlenk tube under nitrogen protection. Sample of the reaction mixture was removed for analysis at defined time period.

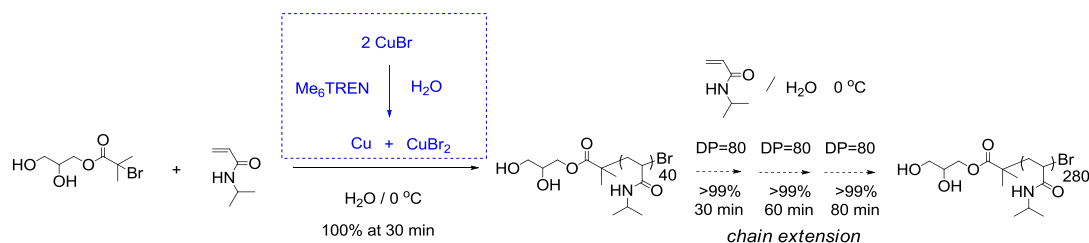
Table 5. 11. Charging amounts for SET-LRP of NIPAM (DP=20) in H₂O at ambient temperature with [initiator]: [CuBr]: [Me₆TREN] = 1: 0.4: 0.4.

Initiator / monomer system			Catalyst system		
Initiator	NIPAM	H ₂ O	CuBr	Me ₆ TREN	H ₂ O
250 μ mol	5 mmol	2.5 mL	100 μ mol	100 μ mol	2 mL

The “first block” polymerization was performed at the ratio of initiator / CuBr / Me₆TREN = 1: 0.4: 0.4 in H₂O at ambient temperature. The charging amounts for each component are listed above.

¹H NMR and SEC analysis of sample at 0.5 h of the first block polymerization confirmed full conversion with $M_n=3700$ and $M_w / M_n=1.09$. However, new monomer for the “second block” was added after stirring for 2 h while waiting for NMR analysis result. ¹H NMR analysis of samples at 1.5 h and 3 h of “second block” polymerization showed that total conversion was only 83% and 87% separately, which means that second block conversion was only about 50% and 61% for the new added monomer.

5.3.17 Chain extension reaction for SET-LRP of NIPAM in H₂O at 0 °C.

**Scheme 5. 23.** Chain extension reaction for SET-LRP of NIPAM in H₂O with [initiator]: [CuBr]: [Me₆TREN] = 1: 0.4: 0.4 at 0 °C.

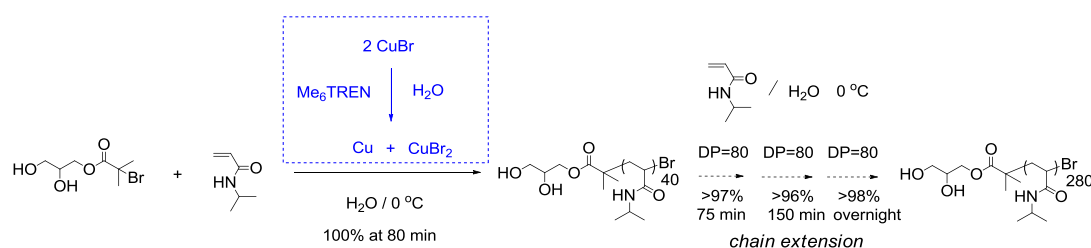
The “first block” polymerization procedure is the same as described in SET-LRP of NIPAM (DP=20).

After full conversion of the first block polymerization, a solution of NIPAM (0.79 g, 7 mmol) in 2 mL H₂O, previously degassed by nitrogen sparging for 15 min, was directly transferred via cannula to the Schlenk tube under nitrogen protection. Sample of the reaction mixture was removed for analysis at defined time periods.

Table 5. 12. Charging amounts for SET-LRP of NIPAM (DP=40) in H₂O at 0 °C with [initiator]: [CuBr]: [Me₆TREN] = 1: 0.4: 0.4.

Initiator / monomer system			Catalyst system		
Initiator	NIPAM	H ₂ O	CuBr	Me ₆ TREN	H ₂ O
87 μmol	3.5 mmol	2 mL	35 μmol	35 μmol	2 mL

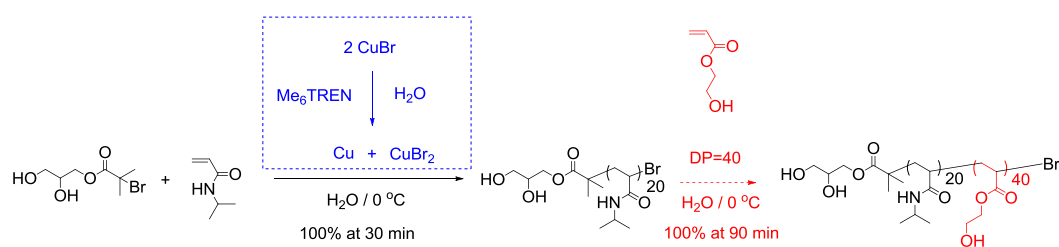
The “first block” polymerization was first performed at the ratio of initiator / CuBr / Me₆TREN = 1: 0.4: 0.4 in H₂O at 0 °C. The charging amounts for each component are listed above.

**Scheme 5. 24.** Chain extension reaction for SET-LRP of NIPAM in H₂O with [initiator]: [CuBr]: [Me₆TREN] = 1: 0.8: 0.4 at 0 °C.

In order to get a good control for the first block polymerization, the amount of CuBr was doubled so that there will be more CuBr₂ to slow down the polymerization. The “first block” polymerization was then performed at the ratio of initiator / CuBr / Me₆TREN = 1: 0.8: 0.4 in H₂O at 0 °C. The charging amounts for each component are listed below.

Table 5. 13. Charging amounts for SET-LRP of NIPAM (DP=40) in H₂O at 0 °C with [initiator]: [CuBr]: [Me₆TREN] = 1: 0.8: 0.4.

Initiator / monomer system			Catalyst system		
Initiator	NIPAM	H ₂ O	CuBr	Me ₆ TREN	H ₂ O
87 μmol	3.5 mmol	2 mL	70 μmol	35 μmol	2 mL

5.3.18 Synthesis of diblock copolymer by SET-LRP in H₂O.

Scheme 5. 25. Synthesis of poly (NIPAM)₂₀ -*b*- (HEA)₄₀ by SET-LRP in H₂O with [initiator]: [CuBr]: [Me₆TREN] = 1: 0.4: 0.4 at 0 °C.

The “first block” polymerization procedure is the same as described in SET-LRP of NIPAM (DP=20) but reaction at 0 °C.

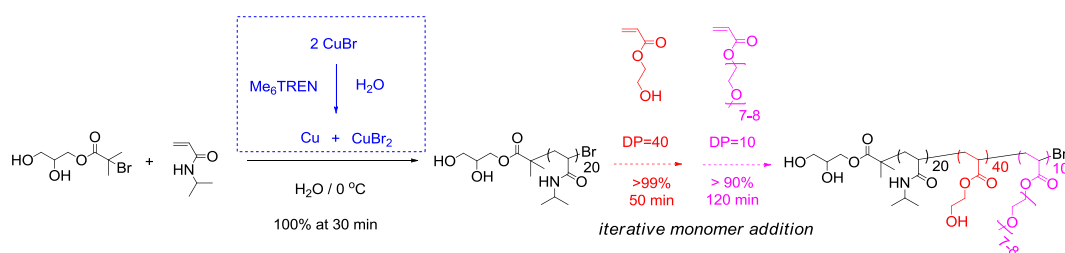
After full conversion of the first block polymerization, a solution of HEA (1.16 g, 10 mmol) in 2 mL H₂O, previously degassed by nitrogen sparging for 15 min, was directly transferred via cannula to the Schlenk tube under nitrogen protection and polymerization for 90 min. Sample of the reaction mixture was removed for analysis at defined time periods.

Table 5. 14. Charging amounts for SET-LRP of NIPAM (DP=20) in H₂O at 0 °C with [initiator]: [CuBr]: [Me₆TREN] = 1: 0.4: 0.4.

Initiator / monomer system			Catalyst system		
Initiator	NIPAM	H ₂ O	CuBr	Me ₆ TREN	H ₂ O
250 μmol	5 mmol	2.5 mL	100 μmol	100 μmol	2 mL

The first block polymerization was performed at the ratio of initiator / CuBr / Me₆TREN = 1: 0.4: 0.4 in H₂O at 0 °C. The charging amounts for each component are listed above.

After 30 min, ¹H NMR confirmed 100% conversion of the first block polymerization and new HEA monomer was added for chain extension. Reaction time for the second block polymerization was 90 min and ¹H NMR revealed 100% conversion was obtained and reaction was then stopped. After reaction, the aqueous solution was directly transferred to a dialysis tube (MWCO = 1000) and dialyzed against water for two days. The product was then recovered as white powder via freezing dry.

5.3.19 Synthesis of tri-block copolymer by iterative SET-LRP in H₂O.

Scheme 5. 26. Synthesis of poly (NIPAM)₂₀ -*b*- (HEA)₄₀ -*b*- (PEGA₄₈₀)₁₀ by iterative aqueous SET-LRP with [initiator]: [CuBr]: [Me₆TREN] = 1: 0.4: 0.4 at 0 °C.

The first block polymerization was performed at the ratio of initiator / CuBr / Me₆TREN = 1: 0.4: 0.4 in H₂O at 0 °C. The charging amounts for each component are listed below.

Table 5. 15. Charging amounts for SET-LRP of NIPAM (DP=20) in H₂O at 0 °C with [initiator]: [CuBr]: [Me₆TREN] = 1: 0.4: 0.4.

Initiator / monomer system			Catalyst system		
Initiator	NIPAM	H ₂ O	CuBr	Me ₆ TREN	H ₂ O
250 μmol	5 mmol	2.5 mL	100 μmol	100 μmol	2 mL

After full conversion of the first block polymerization, a solution of HEA (1.16 g, 10 mmol) in 2 mL H₂O, previously degassed by nitrogen sparging for 15 min, was directly transferred via cannula to the Schlenk tube under nitrogen protection and polymerization for 50 min. ¹H NMR revealed that conversion was over 99%.

After full conversion of the second block polymerization, a solution of PEGA₄₈₀ (1.20 g, 2.5 mmol) in 2 mL H₂O, previously degassed by nitrogen sparging for 15 min, was directly transferred via cannula to the Schlenk tube under nitrogen protection and polymerization for 120 min, conversion of which reached 90% according to ¹H NMR. Reaction was then stopped and product was recovered via direct dialysis and freezing dry.

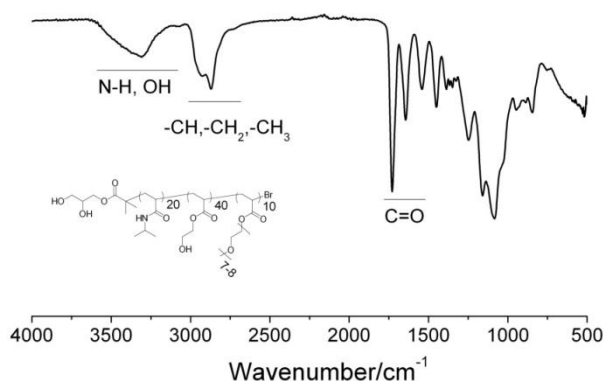
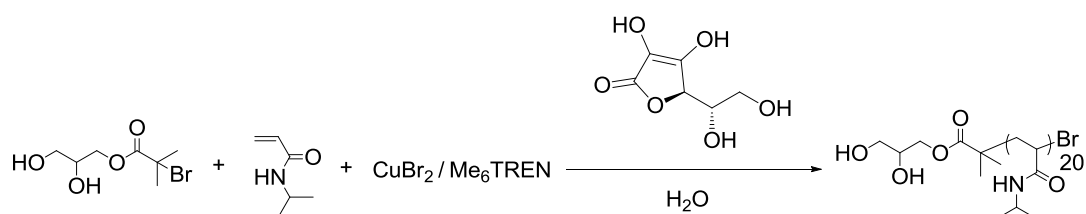


Figure 5. 89. FTIR spectrum of poly (NIPAM)₂₀ -b- (HEA)₄₀ -b- (PEGA₄₈₀)₁₀ by iterative SET-LRP.

5.3.20 Synthesis of PNIPAM by AGET ATRP in H₂O under ambient temperature.



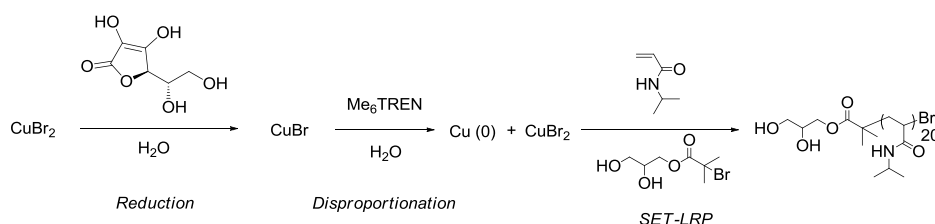
Scheme 5. 27. Synthesis of PNIPAM by AGET ATRP in H₂O with [initiator]: [CuBr₂]: [Me₆TREN]: [Ascorbic acid] = 1: 0.4: 0.4: 0.16 & 1: 0.4: 0.8: 0.2 at ambient temperature.

For the polymerization with [initiator]: [CuBr₂]: [Me₆TREN]: [Ascorbic acid] = 1: 0.4: 0.4: 0.16, the typical procedure is shown as follow. To a Schlenk tube fitted with a magnetic stir bar and a rubber septum, H₂O (3 mL) CuBr₂ (22 mg, 0.1 mmol), Me₆TREN (26 μ L, 0.1 mmol), 2, 3-dihydroxypropyl 2-bromo-2-methylpropanoate (60 mg, 0.25 mmol) and NIPAM (0.57 g, 5 mmol) were charged and the mixture was bubbled with nitrogen for 15 min. At the same time, to another vial fitted with a magnetic stir bar and a rubber septum, H₂O (2mL) and L-ascorbic acid (7 mg, 0.04 mmol) were charged and the solution was bubbled with nitrogen for 15 min. After that, the degassed L-ascorbic acid solution was transferred *via* cannula to the Schlenk tube with initiator / monomer / copper complex. The Schlenk tube was sealed and the mixed solution was allowed to polymerize at ambient temperature (~ 18 °C). Sample of the reaction mixture was removed for analysis at defined time period. The sample

for ^1H NMR was directly diluted with D_2O . Catalyst residues were removed by filtering through a column of neutral alumina prior to DMF SEC analysis.

For the polymerization with [initiator]: $[\text{CuBr}_2]$: $[\text{Me}_6\text{TREN}]$: [Ascorbic acid] = 1: 0.4: 0.8: 0.2, the amount of Me_6TREN was increased to 52 μL , 0.2 mmol and the amount of L-ascorbic acid was increased to 9 mg, 0.05 mmol, without change of the rest components. The polymerization procedure is the same as shown above.

5.3.21 Reduction of CuBr_2 by L-ascorbic acid into CuBr following disproportionation into Cu (0) & CuBr_2 for SET-LRP of NIPAM in H_2O under ambient temperature.



Scheme 5. 28. Synthesis of PNIPAM by SET-LRP in H_2O with [initiator]: $[\text{CuBr}_2]$: $[\text{Me}_6\text{TREN}]$: [Ascorbic acid] = 1: 0.4: 0.4: 0.16 & 1: 0.4: 0.8: 0.2 at ambient temperature.

For the polymerization with [initiator]: $[\text{CuBr}_2]$: $[\text{Me}_6\text{TREN}]$: [Ascorbic acid] = 1: 0.4: 0.4: 0.16, the typical procedure is shown as follow.

To a Schlenk tube fitted with a magnetic stir bar and a rubber septum, H_2O (1 mL) and CuBr_2 (22 mg, 0.1 mmol) were charged and the mixture was bubbled with nitrogen for 10 min. At the same time, to another vial fitted with a magnetic stir bar and a rubber septum, H_2O (1 mL) and L-ascorbic acid (7 mg, 0.04 mmol) were charged and the solution was bubbled with nitrogen for 10 min. After that, the degassed L-ascorbic acid solution was transferred *via* cannula to the Schlenk tube with CuBr_2 solution. White CuBr precipitate was immediately got after addition of L-ascorbic acid. The mixed suspension was allowed to stir under nitrogen protection for 5 min. After that, degassed Me_6TREN (26 μL , 0.1 mmol) was carefully added to the suspension via a gas-tight syringe. The suspension became blue at once with total disappearance of white precipitate and appearance of red colour copper (0) powders. The obtained blue suspension was allowed to stir under nitrogen protection for 15 min. After that, a solution of 2, 3-dihydroxypropyl 2-bromo-2-methylpropanoate (60

mg, 0.25 mmol) and NIPAM (0.57 g, 5 mmol) in 3.5 mL H₂O, previously degassed via nitrogen bubbling for 15 min, was added via cannula under nitrogen protection. The Schlenk tube was sealed and the mixed solution was allowed to polymerize at ambient temperature (~18 °C). Sample of the reaction mixture was removed for analysis at defined time period. The sample for ¹H NMR was directly diluted with D₂O. Catalyst residues were removed by filtering through a column of neutral alumina prior to DMF SEC analysis.

For the polymerization with [initiator]: [CuBr₂]: [Me₆TREN]: [Ascorbic acid] = 1: 0.4: 0.8: 0.2, the amount of Me₆TREN was increased to 52 μL, 0.2 mmol and the amount of L-ascorbic acid was increased to 9 mg, 0.05 mmol, without change of the rest components. The polymerization procedure is the same as shown above.

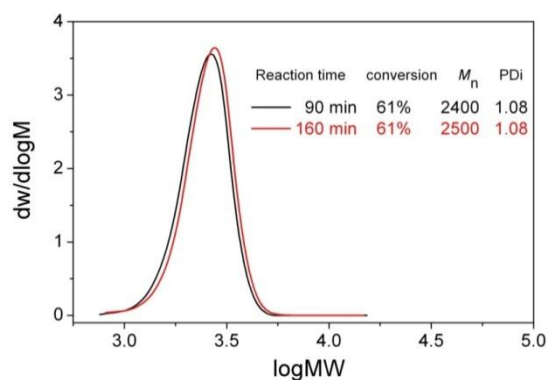


Figure 5. 90. DMF SEC molecular weight distributions for the SET-LRP of NIPAM (DP=20) in H₂O at ambient temperature with [initiator]: [CuBr₂]: [Me₆TREN]: [Ascorbic acid] = 1: 0.4: 0.4: 0.16.

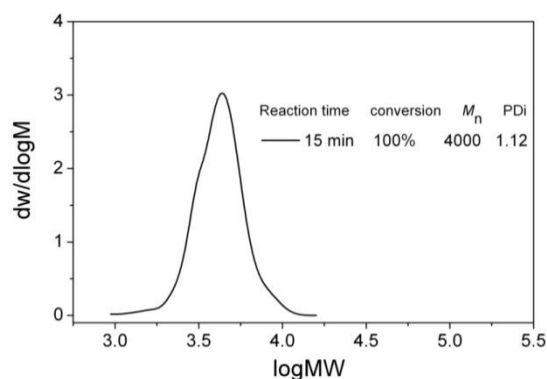
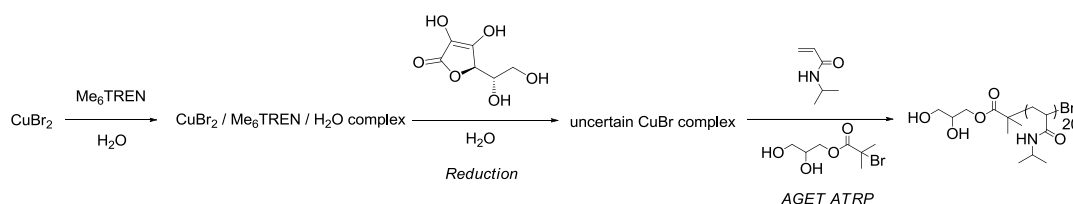


Figure 5. 91. DMF SEC molecular weight distributions for the SET-LRP of NIPAM (DP=20) in H₂O at ambient temperature with [initiator]: [CuBr₂]: [Me₆TREN]: [Ascorbic acid] = 1: 0.4: 0.8: 0.2.



Scheme 5. 29. Synthesis of PNIPAM by AGET ATRP in H₂O with [initiator]: [CuBr₂]: [Me₆TREN]: [Ascorbic acid] = 1: 0.4: 0.4: 0.16 at ambient temperature.

To check what happened during the reduction of CuBr₂ complex by L-ascorbic acid, the reduction reaction without the existence of initiator and monomer was conducted with the ratio of [initiator]: [CuBr₂]: [Me₆TREN]: [Ascorbic acid] = 1: 0.4: 0.4: 0.16, the typical procedure is shown as follow.

To a Schlenk tube fitted with a magnetic stir bar and a rubber septum, H₂O (1 mL) and CuBr₂ (22 mg, 0.1 mmol) were charged and the mixture was bubbled with nitrogen for 10 min. Degassed Me₆TREN (26 µL, 0.1 mmol) was then added to the suspension via a gas-tight syringe. The solution became bright blue and the solution was stirred under nitrogen protection for 5 min. At the same time, to another vial fitted with a magnetic stir bar and a rubber septum, H₂O (1 mL) and L-ascorbic acid (7 mg, 0.04 mmol) were charged and the solution was bubbled with nitrogen for 10 min. After that, the degassed L-ascorbic acid solution was transferred *via* cannula to the Schlenk tube with CuBr₂ / Me₆TREN solution. The solution became a bit cloudy at once and was stirred under nitrogen protection for 15 min. After that, a solution of 2, 3-dihydroxypropyl 2-bromo-2-methylpropanoate (60 mg, 0.25 mmol) and NIPAM (0.57 g, 5 mmol) in 3.5 mL H₂O, previously degassed via nitrogen bubbling for 15 min, was added via cannula under nitrogen protection. The solution became clear at once with total disappearance of white precipitate. The Schlenk tube was sealed and the mixed solution was allowed to polymerize at ambient temperature (~18 °C). Sample of the reaction mixture was removed for analysis at defined time period.

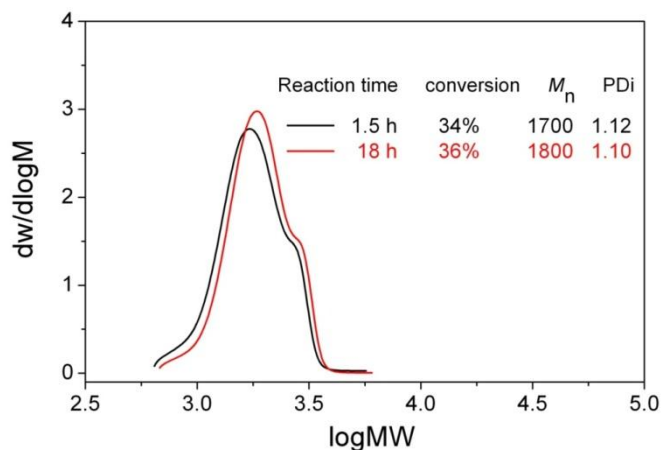
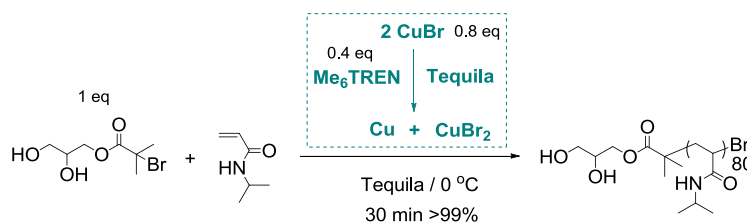


Figure 5. 92. DMF SEC molecular weight distributions for the AGET ATRP of NIPAM (DP=20) in H_2O at ambient temperature with [initiator]: $[CuBr_2]$: $[Me_6TREN]$: $[Ascorbic\ acid]$ = 1: 0.4: 0.8: 0.2.

5.3.22 SET-LRP of NIPAM (DP=80) *via* disproportionation of $CuBr/Me_6TREN$ in Tequila at 0 °C.

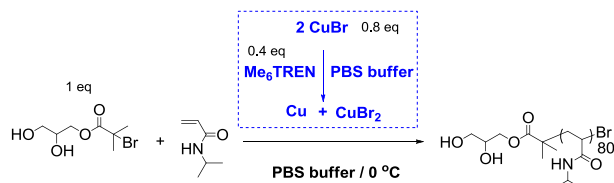


Scheme 5. 30. SET-LRP of NIPAM (DP = 80) *via* disproportionation of $CuBr / Me_6TREN$ in Tequila at 0 °C.

The disproportionation and polymerization procedure is the same as described in SET-LRP of NIPAM (DP=80) with only change of H_2O into Tequila. The polymerization was performed at the ratio of initiator / $CuBr$ / Me_6TREN (1: 0.8: 0.4) in Tequila under ice / water bath (0 °C).

For the disproportionation of $CuBr / Me_6TREN$ in Tequila (mainly water / ethanol mixture), metallic copper (0) powder was also noticed under same procedure when water was used for the solvent. However, the colour of the suspension changed from bright blue into deep green. After 30 min, the reaction was directly stopped and sample was then removed for analysis. The conversion was over 99% according to 1H NMR spectrum.

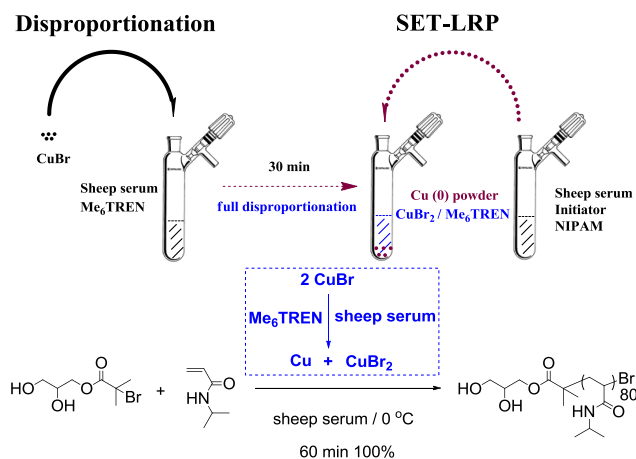
5.3.23 SET-LRP of NIPAM *via* disproportionation of CuBr/Me₆TREN in PBS buffer (pH=6.2 & 6.8) at 0 °C.



Scheme 5. 31. SET-LRP of NIPAM (DP = 80) *via* disproportionation of CuBr / Me₆TREN in PBS buffer at 0 °C.

The disproportionation and polymerization procedure is the same as described in SET-LRP of NIPAM (DP=80) with only change of H₂O into PBS buffer (pH = 6.2 or 6.8).

5.3.24 SET-LRP of NIPAM in sheep serum at 0 °C *via* disproportionation of CuBr/Me₆TREN



Scheme 5. 32. SET-LRP of NIPAM in sheep serum at 0 °C *via* disproportionation of CuBr / Me₆TREN.

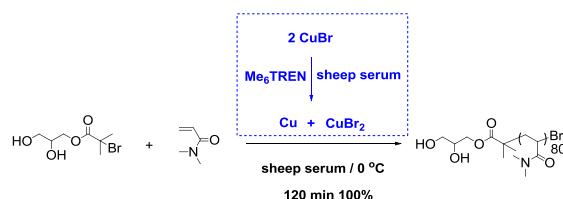
A magnetic stir bar, sheep serum (2 mL) and Me₆TREN (9 μL, 0.035 mmol) were charged to Schlenk tube fitted with a rubber septum and the solution was deoxygenated via nitrogen bubbling for ten minutes. CuBr (10 mg, 0.07 mmol) was then carefully added under slight positive pressure of nitrogen. The nitrogen bubbling was continued for another 10 min and then the blue suspension with purple red colour copper (0) powder was allowed to stir at ambient temperature under nitrogen protection for 15 min. After that, the tube was immersed into ice / water bath.

At the same time, to another 100 mL single neck round bottom bottle fitted with a magnetic stir bar and a rubber septum, sheep serum (4 mL), 2, 3-dihydroxypropyl 2-

bromo-2-methylpropanoate (21 mg, 0.087 mmol) and NIPAM (0.79 g, 7 mmol) were charged and the mixture was bubbled with nitrogen for 15 min. After that, the degassed monomer / initiator serum solution was transferred *via* cannula to the Schlenk tube with Cu (0) / CuBr₂ / Me₆TREN catalyst. The tube was sealed and the mixed solution was allowed to polymerize at 0 °C for 60 min. Sample of the reaction mixture was then removed for analysis. The sample for ¹H NMR was directly diluted with D₂O, which confirmed 100% conversion according to the total disappearance of vinyl groups. Catalyst residues and protein precipitate were removed by filtering through a column of neutral alumina prior to DMF SEC analysis.

Then 20 mL DMF was added to the rest polymer / serum solution, which caused lots of protein precipitate. The suspension was directly transferred to one 50 mL centrifuge tube for centrifuge at 11000 rpm for 20 min. After that the up-layer clear liquid was transferred to one dialysis tube for dialysis against water for 3 days. The polymer product could then be recovered by freeze drying.

5.3.25 SET-LRP of DMA in sheep serum at 0 °C *via* disproportionation of CuBr / Me₆TREN

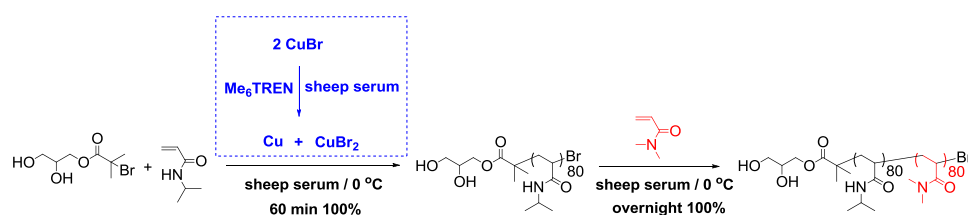


Scheme 5. 33. SET-LRP of DMA in sheep serum at 0 °C *via* disproportionation of CuBr / Me₆TREN.

The polymerization was performed at the ratio of initiator / CuBr / Me₆TREN (1: 0.8: 0.4) under ice / water bath (0 °C) for 2 h according to same procedure described in SET-LRP of NIPAM. The charging amounts for each component are listed below.

Table 5. 16. Charging amounts for SET-LRP of DMA (DP=80) in sheep serum at 0 °C with [initiator]: [CuBr]: [Me₆TREN] = 1: 0.8: 0.4.

Initiator / monomer system			Catalyst system		
Initiator	NIPAM	Sheep serum	CuBr	Me ₆ TREN	Sheep serum
87 μmol	7 mmol	4 mL	70 μmol	35 μmol	2 mL

5.3.26 Synthesis of poly (NIPAM)₈₀-*b*-(DMA)₈₀ by SET-LRP in sheep serum

Scheme 5. 34. Synthesis of poly (NIPAM)₈₀-*b*-(DMA)₈₀ by SET-LRP in sheep serum with [initiator]: [CuBr]: [Me₆TREN] = 1: 0.8: 0.4 at 0 °C.

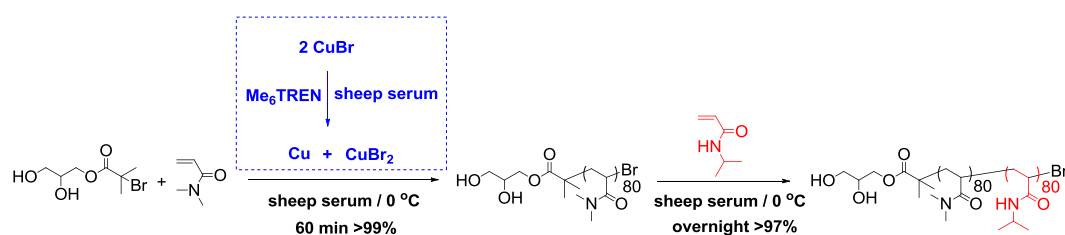
The procedure of the first block polymerization is the same as described in SET-LRP of NIPAM (DP=80). It was performed at the ratio of initiator / CuBr / Me₆TREN = 1: 08: 0.4 in sheep serum at 0 °C for 1 h. The charging amounts for each component are listed below.

Table 5. 17. Charging amounts for SET-LRP of NIPAM (DP=80) in sheep serum at 0 °C with [initiator]: [CuBr]: [Me₆TREN] = 1: 0.8: 0.4.

Initiator / monomer system			Catalyst system		
Initiator	NIPAM	Sheep serum	CuBr	Me ₆ TREN	Sheep serum
87 μmol	7 mmol	4 mL	70 μmol	35 μmol	2 mL

After 1 h, a solution of DMA (0.70 g, 7 mmol) in 4 mL sheep serum, previously degassed by nitrogen sparging for 15 min, was directly transferred via cannula to the Schlenk tube under nitrogen protection and polymerization overnight and the reaction was then stopped. The sample for ¹H NMR was directly diluted with D₂O. Catalyst residues and protein precipitate were removed by filtering through a column of neutral alumina prior to DMF SEC analysis.

After reaction, 30 mL DMF was added to the rest polymer / serum solution, which caused lots of protein precipitate. The suspension was directly transferred to one 50 mL centrifuge tube for centrifuge at 11000 rpm for 20 min. After that the up-layer clear liquid was transferred to one dialysis tube for dialysis against water for 3 days. The polymer product could then be recovered by freeze drying.

5.3.27 Synthesis of poly (DMA)₈₀-*b*-(NIPAM)₈₀ by SET-LRP in sheep serum

Scheme 5. 35. Synthesis of poly (DMA)₈₀-*b*-(NIPAM)₈₀ by SET-LRP in sheep serum with [initiator]: [CuBr]: [Me₆TREN] = 1: 0.8: 0.4 at 0 °C.

The procedure of the first block polymerization is the same as described in SET-LRP of NIPAM (DP=80) in serum. It was performed at the ratio of initiator / CuBr / Me₆TREN = 1: 0.8: 0.4 in sheep serum at 0 °C for 1 h. The charging amounts for each component are listed below.

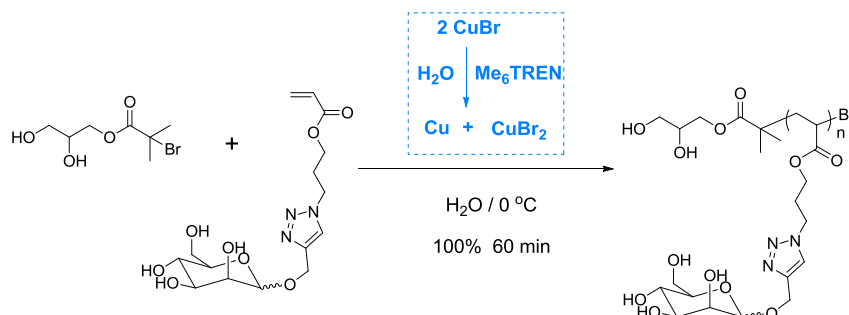
Table 5. 18. Charging amounts for SET-LRP of DMA (DP=80) in sheep serum at 0 °C with [initiator]: [CuBr]: [Me₆TREN] = 1: 0.8: 0.4.

Initiator / monomer system			Catalyst system		
Initiator	DMA	Sheep serum	CuBr	Me ₆ TREN	Sheep serum
87 μmol	7 mmol	4 mL	70 μmol	35 μmol	2 mL

After 1 h, a solution of NIPAM (0.79 g, 7 mmol) in 4 mL sheep serum, previously degassed by nitrogen sparging for 15 min, was directly transferred via cannula to the Schlenk tube under nitrogen protection and polymerization overnight and the reaction was then stopped. The sample for ¹H NMR was directly diluted with D₂O. Catalyst residues and protein precipitate were removed by filtering through a column of neutral alumina prior to DMF SEC analysis.

After reaction, 30 mL DMF was added to the rest polymer / serum solution, which caused lots of protein precipitate. The suspension was directly transferred to one 50 mL centrifuge tube for centrifuge at 11000 rpm for 20 min. After that the up-layer clear liquid was transferred to one dialysis tube for dialysis against water for 3 days. The polymer product could then be recovered by freeze drying.

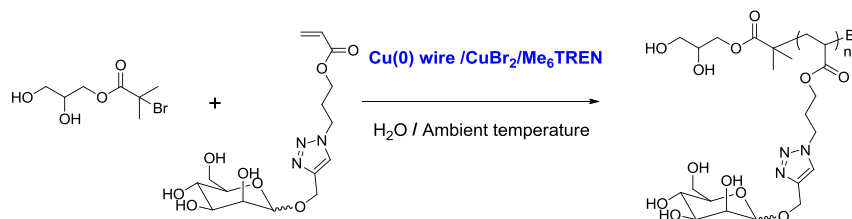
5.3.28 Aqueous SET-LRP of D-Mannose acrylate glycomonomer at 0 °C via disproportionation of CuBr / Me₆TREN



Scheme 5. 36. SET-LRP of D-mannose glyco monomer in H₂O at 0 °C via disproportionation of CuBr / Me₆TREN.

To a Schlenk tube fitted with a magnetic stir bar and a rubber septum, H₂O (1 mL) and Me₆TREN (10.6 μL, 0.04 mmol) were charged and the mixture was bubbled with nitrogen for 5 min. CuBr (11 mg, 0.08 mmol) was then carefully added under slight positive pressure of nitrogen. The nitrogen bubbling was continued for another 10 min and then the blue suspension with purple red colour copper (0) powder was allowed to stir under ice/water bath cool for 15 min. At the same time, to another vial fitted with a magnetic stir bar and a rubber septum, H₂O (2 mL), 2, 3-dihydroxypropyl 2-bromo-2-methylpropanoate (24 mg, 0.1 mmol) and D-Mannose glyco monomer (373 mg, 1 mmol) were charged and the mixture was bubbled with nitrogen for 15 min. After that, the degassed monomer / initiator aqueous solution was transferred *via* cannula to the Schlenk tube with Cu (0) / CuBr₂ / Me₆TREN catalyst. The Schlenk tube was sealed and the mixed solution was allowed to polymerize at 0 °C for 1 h. Sample of the reaction mixture was then removed for analysis. The sample for ¹H NMR was directly diluted with D₂O, which confirmed 100% conversion according to the total disappearance of vinyl groups. Catalyst residues were removed by filtering through a column of neutral alumina prior to DMF SEC analysis. The rest polymer product was purified via dialysis against water for two days and recovered by freeze drying.

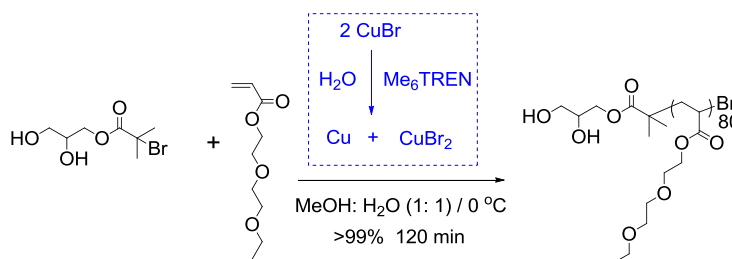
5.3.29 Copper(0) wire mediated SET-LRP of D-mannose glycomonomer in H₂O



Scheme 5. 37. Copper(0) wire mediated SET-LRP of D-mannose glyco monomer in H₂O at ambient temperature.

To a Schlenk tube fitted with a magnetic stir bar and a rubber septum, 2, 3-dihydroxypropyl 2-bromo-2-methylpropanoate (24 mg, 0.1 mmol), D-mannose glyco monomer (373 mg, 1 mmol), CuBr₂ (4.5 mg, 0.02 mmol) in 3 mL H₂O (note: this was performed by using a stock solution of 9 mg CuBr₂ in 6 mL H₂O due to balance limit) were charged and the mixture was bubbled with nitrogen for 15 min. Pre-degassed Me₆TREN (5.2 μL, 0.02 mmol) were then added via gas tight micro syringe. After that, pre-activated copper wire (4 cm, 18 mg, 0.28 mmol) was carefully added under nitrogen protection. The Schlenk tube was sealed and the blue solution was allowed to polymerize at ambient temperature (~18 °C).

5.3.30 Aqueous SET-LRP of DEGEAA at 0 °C *via* disproportionation of CuBr/Me₆TREN



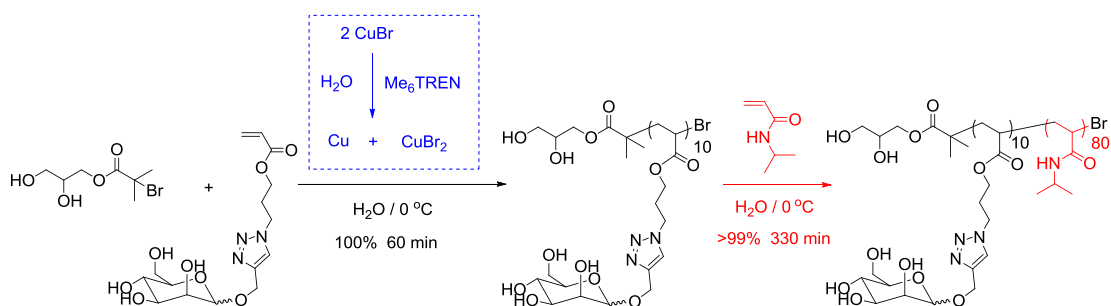
Scheme 5. 38. SET-LRP of DEGEAA in MeOH/H₂O at 0 °C *via* disproportionation of CuBr / Me₆TREN.

To a Schlenk tube fitted with a magnetic stir bar and a rubber septum, H₂O (1 mL) and Me₆TREN (9.1 μL, 35 μmol) were charged and the mixture was bubbled with nitrogen for 5 min. CuBr (10 mg, 0.07 mmol) was then carefully added under slight positive pressure of nitrogen. The nitrogen bubbling was continued for another 10 min

and then the blue suspension with purple red colour copper (0) powder was allowed to stir under ice/water bath cooling for another 15 min.

At the same time, to another vial which is also immersed in ice/water bath and fitted with a magnetic stir bar and a rubber septum, H₂O/MeOH mixture (4 mL, 1:1 in volume ratio), 2, 3-dihydroxypropyl 2-bromo-2-methylpropanoate (21 mg, 87 μ mol) and DEGEEA (1317 mg, 7 mmol) were charged and the mixture was bubbled with nitrogen for 15 min. After that, the degassed monomer / initiator solution was transferred *via* cannula to the Schlenk tube with Cu (0) / CuBr₂ / Me₆TREN catalyst. The Schlenk tube was sealed and the mixed solution was allowed to polymerize at 0 °C for 2 h. Sample of the reaction mixture was then removed for analysis. The sample for ¹H NMR was directly diluted with D₂O, which confirmed >99% conversion according to integral of vinyl groups with that of the O-CH₂ groups at 4.15-4.40 ppm. Catalyst residues were removed by filtering through a column of neutral alumina prior to DMF SEC analysis. The rest polymer product was purified *via* dialysis against MeOH for two days and recovered by drying under vacuum.

5.3.31 Synthesis of poly (Mannose)₁₀-*b*-(NIPAM)₈₀ by aqueous SET-LRP



Scheme 5. 39. Synthesis of poly (Mannose)₁₀-*b*-(NIPAM)₈₀ by SET-LRP in H₂O with [initiator]: [CuBr]: [Me₆TREN] = 1: 0.8: 0.4 at 0 °C.

The procedure and charging amounts for the first block polymerization is the same as described in the SET-LRP of D-Mannose glyco monomer (DP=10).

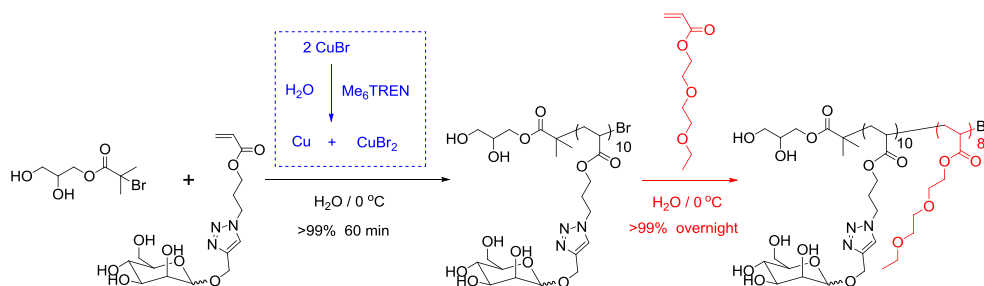
After polymerization for 1 h, sample (0.3 mL of the reaction solution) was taken for ¹H NMR and SEC analysis.

After another 0.5 h (waiting for the NMR results), ¹H NMR analysis confirmed 100% conversion of the glyco monomer and then a solution of NIPAM (905 mg, 8 mmol) in 5 mL H₂O, previously degassed by nitrogen sparging for 15 min, was directly

transferred via cannula to the Schlenk tube under nitrogen protection and polymerization for another 6.5 h. The reaction was then stopped and samples were taken for ^1H NMR and SEC analysis. The sample for ^1H NMR was directly diluted with D_2O , which confirmed >99% conversion according to integral of vinyl groups with that of the $\text{O}-\text{CH}_2$ groups at 4.15-4.40 ppm. Catalyst residues were removed by filtering through a column of neutral alumina prior to DMF SEC analysis.

After that, the rest solution was directly transferred to a dialysis tube (MWCO 1000) for dialysis against water for three days. The diblock glycopolymer product was then recovered as white solid *via* freezing dry.

5.3.32 Synthesis of poly (Mannose)₁₀-*b*-(DEGEEA)₈₀ by aqueous SET-LRP



Scheme 5. 40. Synthesis of poly (Mannose)₁₀-*b*-(DEGEEA)₈₀ by SET-LRP in sheep serum with [initiator]: [CuBr]: [Me₆TREN] = 1: 0.8: 0.4 at 0 °C.

The procedure and charging amounts for the first block polymerization is the same as described in the SET-LRP of D-Mannose glyco monomer (DP=10).

After polymerization for 1 h, sample (~0.3 mL of the reaction solution) was taken for ^1H NMR and SEC analysis.

After another 0.5 h (waiting for the NMR results), ^1H NMR analysis confirmed conversion of the glyco monomer was >99% by comparing the integral of vinyl groups with that of the triazole ring protons as 7.80-8.00 ppm.

Then a solution of DEGEEA (905 mg, 8 mmol) in 6 mL $\text{H}_2\text{O}/\text{MeOH}$ mixture (2 mL H_2O +4 mL MeOH), previously degassed by nitrogen sparging for 15 min, was directly transferred via cannula to the Schlenk tube under nitrogen protection and polymerization was continued overnight. The reaction was then stopped and samples were taken for ^1H NMR and SEC analysis. The sample for ^1H NMR was directly diluted with D_2O , which confirmed >99% conversion according to integral of vinyl

groups with that of the N-H groups at 3.70-3.90 ppm. Catalyst residues were removed by filtering through a column of neutral alumina prior to DMF SEC analysis.

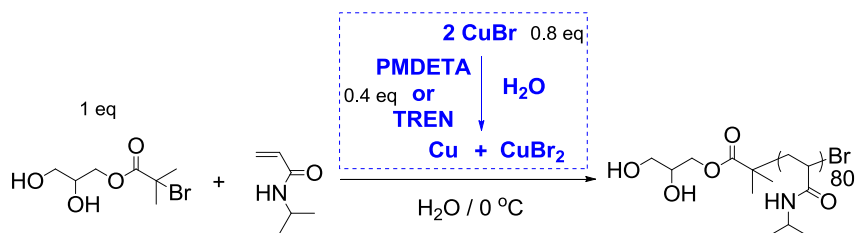
After that, the rest solution was directly transferred to a dialysis tube (MWCO 1000) for dialysis against water for three days. The diblock glycopolymer product was then recovered as white solid *via* freezing dry.

5.3.33 Optical microscopy characterization of Cu (0) powders from the disproportionation of CuBr / Me₆TREN in water and ethanol.

Previous detailed research has pointed out that both water and ethanol are competent solvents to mediate the disproportionation of CuBr / Me₆TREN.²²⁴ The K_{disp} determined by UV/Vis spectroscopy for [CuBr]: [Me₆TREN] = 1:1 is 1.40×10^3 in water and 1.85×10^2 in ethanol, which suggested that ethanol is not as effective as water for mediating the disproportionation of CuBr. Compared with DMSO, DMF, DMAC and NMP which could stabilize Cu (0), it was also demonstrated that ethanol and water facilitate the agglomeration of Cu (0) particles. To further check the disproportionation behaviour of CuBr / Me₆TREN in water and ethanol, a series of disproportionation experiments were conducted in 100% water, 100% ethanol and water-ethanol mixture (75% : 25%, 50% : 50% and 25% : 75% in volume ratio). The typical procedure was shown as follow.

A magnetic stir bar, solvent (12 mL) and Me₆TREN (78 μ L, 0.3 mmol) were charged to a vial fitted with a rubber septum and the mixture was degassed via nitrogen sparging for 15 min. CuBr (43 mg, 0.3 mmol) was then carefully added into the solution under stirring and nitrogen protection. The solution was allowed to stir for 30 min under nitrogen protection. After that, the stirring was stopped to allow the powders settle down for observation. All the samples were stirred at 1000 rpm for 1 min before optical microscopy analysis.

5.3.34 SET-LRP of NIPAM *via* disproportionation of CuBr / PMDETA or TREN in pure water.



Scheme 5. 41. SET-LRP of NIPAM (DP = 80) *via* disproportionation of CuBr / PMDETA or TREN in H₂O at 0 °C.

The polymerization procedure is the same as described in SET-LRP of NIPAM (DP=20). The polymerizations were performed with a ratio of [initiator]: [CuBr]: [PMDETA] or [TREN] = 1: 0.8: 0.4 in H₂O at 0 °C. The charging amounts for each component are listed below.

Table 5. 19. Charging amounts for SET-LRP of NIPAM (DP=80) in H₂O at 0 °C with [initiator]: [CuBr]: [PMDETA] or [TREN] = 1: 0.8: 0.4.

Initiator / monomer system			Catalyst system		
Initiator	NIPAM	H ₂ O	CuBr	PMDETA / TREN	H ₂ O
87 μmol	7 mmol	3.5 mL	70 μmol	35 μmol	2 mL

Chapter 6 Overview and Prospect

Novel strategies in the synthesis of functional glycopolymers were described in this thesis.

From the view of post-glycosylation method, a combination of CCTP with thiol-ene, epoxy ring opening and CuAAC click reactions was utilized as a novel strategy to synthesize terminal functional glycopolymers in chapter two. Fischer glycosylation was used for the synthesis of alkyne functionalized monosaccharides, which were in actual fact an anomeric mixture. Although obtained glycopolymers bearing both α & β type mannose etc. showed high affinity in binding with human DC-SIGN lectin, people questioned that the β type mannose may not contribute in the binding. The author believes that after attached onto polymer backbones both α & β type carbohydrate issues would bind with DC-SIGN as the C-1 substituted functional groups did not participate in the key recognition with the binding sites of lectin. To check this, it is worth trying to synthesize poly(glycidyl acrylate) as a precursor for click reaction with pure or mixed α and β type alkyne functionalised mannose and then test the binding with DC-SIGN or Con A lectin.

The synthesis of glycopolymers benefited from the development of polymer chemistry. As a development of copper mediated living radical polymerization, SET-LRP allowed the direct polymerization of unprotected glycomonomers in DMSO at ambient temperature. The chain end fidelity was kept high for multiblock glycopolymer synthesis via iterative monomer addition under full or high conversion, in chapter 3. The radical-radical coupling side reactions in SET-LRP system even after full conversion polymerizations are not significant. Thus SET-LRP was also utilized for the synthesis of cyclodextrin-centered star glycopolymers, chapter 4, which showed high affinity in binding with DC-SIGN and low IC_{50} values in inhibition the binding of DC-SIGN with HIV glyco protein gp120.

It was also noticed that there was a great debate on the mechanism of SET-LRP, in many cases it was thought as SARA ATRP. Recently detailed research has been conducted on reversible-deactivation radical polymerization in the presence of metallic copper, including comproportionation-disproportionation equilibria and kinetics, kinetic simulation, activation of alkyl halides by Cu^0 and solvent effects on the activation rate constant.²⁷⁸⁻²⁸¹ It revealed that the relative amount of Cu^I at

comproportionation/disproportionation equilibrium increased with ligand concentration, Cu^{I} even represents approximately 99.95% of all soluble Cu species under ratio of $[\text{Me}_6\text{TREN}]_0/[\text{Cu}^{\text{II}}]_0=6/1$ in the presence of copper wire in MA/DMSO = 2/1, in which the authors seem to overlooked the ratio lower than 2.²⁷⁸ It should also be noticed that in this thesis the utilized ratio of $[\text{Me}_6\text{TREN}]_0/[\text{Cu}^{\text{II}}]_0=1.8/1$, thus should not be the same situation and the disproportionation should not be ignored. It also suggested that Cu^0 worked as supplemental activator and a reducing agent, following SARA mechanism rather than SET-LRP mechanism, as the contribution of $\text{Cu}^{\text{I}}\text{Br}/\text{Me}_6\text{TREN}$ to activate the alkyl halides is 99% while the activity of Cu^0 is much less effective.²⁸⁰ Based on these results, both processes of SARA ATRP and SET-LRP may both exist in polymerizations using copper wire $\text{Cu}^0/\text{Cu}^{\text{II}}/\text{Me}_6\text{TREN}/\text{DMSO}$ catalyst system.

It revealed that with the increase of solvent polarity the activation rate is higher, which is also a factor affecting the disproportionation rate of Cu^{I} .²⁸¹ Thus, in water, the disproportionation degree and rate of Cu^{I} could be much higher and faster than in organic solvents, under which case the activation rate of alkyl halides by Cu^0 should be verified more carefully compared with Cu^{I} . The disproportionation rate and degree of $\text{Cu}^{\text{I}}/\text{Me}_6\text{TREN}$ in pure water was being researched utilizing electrochemistry analysis tool by Haddleton group.

Successful aqueous copper mediated living radical polymerization has been performed in chapter five. It suggested that the disproportionation of Cu^{I} to Cu^0 and Cu^{II} is the key step in obtaining good control during polymerization in pure water. A small library of acrylate and acrylamide water-soluble homopolymers and copolymers with low MW distribution could be facilely synthesized via a one-pot reaction and synthesis of diblock glycopolymers also worked under same strategy. The exact detail should be checked more carefully to verify the role of Cu^{I} in this system.

Nevertheless, a tool for copper mediated living radical polymerization under aqueous condition has been developed. It should have wide application in synthesis of a series of hydrophilic polymers under water-containing conditions including bio-related conditions. Further research on surface initiated polymerization under aqueous conditions is in progress.

Chapter 7 References

- (1) Ladmiral, V.; Melia, E.; Haddleton, D. M. *Eur Polym J* **2004**, *40*, 431.
- (2) Ting, S. R. S.; Chen, G.; Stenzel, M. H. *Polym Chem* **2010**, *1*, 1392.
- (3) Geng, J.; Lindqvist, J.; Mantovani, G.; Haddleton, D. M. *Angew Chem Int Ed* **2008**, *47*, 4180.
- (4) Slavin, S.; Burns, J.; Haddleton, D. M.; Becer, C. R. *Eur Polym J* **2011**, *47*, 435.
- (5) Spain, S. G.; Gibson, M. I.; Cameron, N. R. *J Polym Sci A Polym Chem* **2007**, *45*, 2059.
- (6) Vázquez-Dorbatt, V.; Lee, J.; Lin, E.-W.; Maynard, H. D. *Chembiochem* **2012**, *13*, 2478.
- (7) Spain, S. G.; Cameron, N. R. *Polym Chem* **2011**, *2*, 60.
- (8) Becer, C. R. *Macromol Rapid Commun* **2012**, *33*, 742.
- (9) Kiessling, L. L.; Grim, J. C. *Chem Soc Rev* **2013**, *42*, 4476.
- (10) Kamber, N. E.; Jeong, W.; Waymouth, R. M.; Pratt, R. C.; Lohmeijer, B. G. G.; Hedrick, J. L. *Chem Rev* **2007**, *107*, 5813.
- (11) Aoi, K.; Tsutsumiuchi, K.; Aoki, E.; Okada, M. *Macromolecules* **1996**, *29*, 4456.
- (12) Tsutsumiuchi, K.; Aoi, K.; Okada, M. *Macromolecules* **1997**, *30*, 4013.
- (13) Kempe, K.; Weber, C.; Babiuch, K.; Gottschaldt, M.; Hoogenboom, R.; Schubert, U. S. *Biomacromolecules* **2011**, *12*, 2591.
- (14) Kamigaito, M.; Ando, T.; Sawamoto, M. *Chem Rev* **2001**, *101*, 3689.
- (15) Ouchi, M.; Terashima, T.; Sawamoto, M. *Chem Rev* **2009**, *109*, 4963.
- (16) Kato, M.; Kamigaito, M.; Sawamoto, M.; Higashimura, T. *Macromolecules* **1995**, *28*, 1721.
- (17) Wang, J.-S.; Matyjaszewski, K. *J. Am. Chem. Soc.* **1995**, *117*, 5614.
- (18) Wayland, B. B.; Poszmik, G.; Mukerjee, S. L.; Fryd, M. *J Am Chem Soc* **1994**, *116*, 7943.
- (19) Matyjaszewski, K. *Macromolecules* **2012**, *45*, 4015.
- (20) Percec, V.; Popov, A. V.; Ramirez-Castillo, E.; Monteiro, M.; Barboiu, B.; Weichold, O.; Asandei, A. D.; Mitchell, C. M. *J Am Chem Soc* **2002**, *124*, 4940.
- (21) Percec, V.; Guliashvili, T.; Ladislaw, J. S.; Wistrand, A.; Stjerndahl, A.; Sienkowska, M. J.; Monteiro, M. J.; Sahoo, S. J. *Am. Chem. Soc.* **2006**, *128*, 14156.
- (22) Ohno, K.; Tsujii, Y.; Fukuda, T. *J Polym Sci A Polym Chem* **1998**, *36*, 2473.
- (23) Vázquez-Dorbatt, V.; Maynard, H. D. *Biomacromolecules* **2006**, *7*, 2297.
- (24) León, O.; Bordegé, V.; Muñoz-Bonilla, A.; Sánchez-Chaves, M.; Fernández-García, M. *J Polym Sci A Polym Chem* **2010**, *48*, 3623.
- (25) Narain, R.; Armes, S. P. *Biomacromolecules* **2003**, *4*, 1746.
- (26) Geng, J.; Mantovani, G.; Tao, L.; Nicolas, J.; Chen, G.; Wallis, R.; Mitchell, D. A.; Johnson, B. R. G.; Evans, S. D.; Haddleton, D. M. *J Am Chem Soc* **2007**, *129*, 15156.
- (27) Tsarevsky, N. V.; Matyjaszewski, K. *Chem Rev* **2007**, *107*, 2270.
- (28) Yang, Q.; Ulbricht, M. *Macromolecules* **2011**, *44*, 1303.
- (29) Yuan, J.; Meng, J.-q.; Kang, Y.-l.; Du, Q.-y.; Zhang, Y.-f. *Appl Surf Sci* **2012**, *258*, 2856.
- (30) Meng, J.; Yuan, J.; Kang, Y.; Zhang, Y.; Du, Q. *J Colloid Interface Sci* **2012**, *368*, 197.
- (31) Muñoz-Bonilla, A.; León, O.; Bordegé, V.; Sánchez-Chaves, M.; Fernández-García, M. *J Polym Sci A Polym Chem* **2013**, *51*, 1337.

- (32) León, O.; Muñoz-Bonilla, A.; Bordegé, V.; Sánchez-Chaves, M.; Fernández-García, M. *J Polym Sci A Polym Chem* **2011**, *49*, 2627.
- (33) Munoz-Bonilla, A.; Heuts, J. P. A.; Fernandez-Garcia, M. *Soft Matter* **2011**, *7*, 2493.
- (34) Pfaff, A.; Shinde, V. S.; Lu, Y.; Wittemann, A.; Ballauff, M.; Müller, A. H. E. *Macromol Biosci* **2011**, *11*, 199.
- (35) Pfaff, A.; Müller, A. H. E. *Macromolecules* **2011**, *44*, 1266.
- (36) Wang, Y.; Zhang, X.; Mu, J.; Li, C. *New Journal of Chemistry* **2013**, *37*, 796.
- (37) Wang, Y.; Zhang, X.; Yu, P.; Li, C. *Int J Pharm* **2013**, *441*, 170.
- (38) Menon, S.; Ongungal, R. M.; Das, S. *Polym Chem* **2013**, *4*, 623.
- (39) Menon, S.; Das, S. *Polym Chem* **2012**, *3*, 2619.
- (40) Lin, K.; Kasko, A. M. *Biomacromolecules* **2012**, *14*, 350.
- (41) Chernyy, S.; Jensen, B. E. B.; Shimizu, K.; Ceccato, M.; Pedersen, S. U.; Zelikin, A. N.; Daasbjerg, K.; Iruthayaraj, J. *J Colloid Interface Sci* **2013**, *404*, 207.
- (42) Kitano, H.; Saito, D.; Kamada, T.; Gemmei-Ide, M. *Colloids and Surfaces B: Biointerfaces* **2012**, *93*, 219.
- (43) Chiefari, J.; Chong, Y. K.; Ercole, F.; Krstina, J.; Jeffery, J.; Le, T. P. T.; Mayadunne, R. T. A.; Meijs, G. F.; Moad, C. L.; Moad, G.; Rizzardo, E.; Thang, S. H. *Macromolecules* **1998**, *31*, 5559.
- (44) Boyer, C.; Bulmus, V.; Davis, T. P.; Ladmiral, V.; Liu, J.; Perrier, S. b. *Chem Rev* **2009**, *109*, 5402.
- (45) Lowe, A. B.; Sumerlin, B. S.; McCormick, C. L. *Polymer* **2003**, *44*, 6761.
- (46) Convertine, A. J.; Lokitz, B. S.; Vasileva, Y.; Myrick, L. J.; Scales, C. W.; Lowe, A. B.; McCormick, C. L. *Macromolecules* **2006**, *39*, 1724.
- (47) Abdelkader, O.; Moebs-Sanchez, S.; Queneau, Y.; Bernard, J.; Fleury, E. *J Polym Sci A Polym Chem* **2011**, *49*, 1309.
- (48) Smith, A. E.; Sizovs, A.; Grandinetti, G.; Xue, L.; Reineke, T. M. *Biomacromolecules* **2011**, *12*, 3015.
- (49) Mancini, R. J.; Lee, J.; Maynard, H. D. *J Am Chem Soc* **2012**, *134*, 8474.
- (50) Pearson, S.; Scarano, W.; Stenzel, M. H. *Chem Comm* **2012**, *48*, 4695.
- (51) Buckwalter, D. J.; Sizovs, A.; Ingle, N. P.; Reineke, T. M. *ACS Macro Lett* **2012**, *1*, 609.
- (52) Belardi, B.; O'Donoghue, G. P.; Smith, A. W.; Groves, J. T.; Bertozzi, C. R. *J Am Chem Soc* **2012**, *134*, 9549.
- (53) Ahmed, M.; Narain, R. *Mol Pharm* **2012**, *9*, 3160.
- (54) Ahmed, M.; Lai, B. F. L.; Kizhakkedathu, J. N.; Narain, R. *Bioconjug Chem* **2012**, *23*, 1050.
- (55) Ahmed, M.; Narain, R. *Biomaterials* **2013**, *34*, 4368.
- (56) Song, E.-H.; Manganiello, M. J.; Chow, Y.-H.; Ghosn, B.; Convertine, A. J.; Stayton, P. S.; Schnapp, L. M.; Ratner, D. M. *Biomaterials* **2012**, *33*, 6889.
- (57) Albertin, L.; Wolnik, A.; Ghadban, A.; Dubreuil, F. *Macromol Chem Phys* **2012**, *213*, 1768.
- (58) Glassner, M.; Delaittre, G.; Kaupp, M.; Blinco, J. P.; Barner-Kowollik, C. *J Am Chem Soc* **2012**, *134*, 7274.
- (59) Parry, A. L.; Clemson, N. A.; Ellis, J.; Bernhard, S. S. R.; Davis, B. G.; Cameron, N. R. *J Am Chem Soc* **2013**, *135*, 9362.
- (60) Ladmiral, V.; Mantovani, G.; Clarkson, G. J.; Cauet, S.; Irwin, J. L.; Haddleton, D. M. *J Am Chem Soc* **2006**, *128*, 4823.
- (61) Nurmi, L.; Lindqvist, J.; Randev, R.; Syrett, J.; Haddleton, D. M. *Chem Comm* **2009**, *0*, 2727.

- (62) Izawa, K.; Akiyama, K.; Abe, H.; Togashi, Y.; Hasegawa, T. *Bioorg Med Chem* **2013**, *21*, 2895.
- (63) Xu, L. Q.; Huang, C.; Wang, R.; Neoh, K.-G.; Kang, E.-T.; Fu, G. D. *Polymer* **2011**, *52*, 5764.
- (64) Hoyle, C. E.; Lowe, A. B.; Bowman, C. N. *Chem Soc Rev* **2010**, *39*, 1355.
- (65) Lowe, A. B.; Hoyle, C. E.; Bowman, C. N. *J Mater Chem* **2010**, *20*, 4745.
- (66) Kumar, J.; Bousquet, A.; Stenzel, M. H. *Macromol Rapid Commun* **2011**, *32*, 1620.
- (67) Chen, Y.; Chen, G.; Stenzel, M. H. *Macromolecules* **2010**, *43*, 8109.
- (68) Kim, J. C.; Rho, Y.; Kim, G.; Kim, M.; Kim, H.; Kim, I. J.; Kim, J. R.; Ree, M. *Polym Chem* **2013**, *4*, 2260.
- (69) Marcaurelle, L. A.; Shin, Y.; Goon, S.; Bertozzi, C. R. *Org Lett* **2001**, *3*, 3691.
- (70) Rabuka, D.; Parthasarathy, R.; Lee, G. S.; Chen, X.; Groves, J. T.; Bertozzi, C. R. *J Am Chem Soc* **2007**, *129*, 5462.
- (71) Godula, K.; Bertozzi, C. R. *J Am Chem Soc* **2012**, *134*, 15732.
- (72) Godula, K.; Bertozzi, C. R. *J Am Chem Soc* **2010**, *132*, 9963.
- (73) Gibson, M. I.; Fröhlich, E.; Klok, H.-A. *J Polym Sci A Polym Chem* **2009**, *47*, 4332.
- (74) Richards, S.-J.; Jones, M. W.; Hunaban, M.; Haddleton, D. M.; Gibson, M. I. *Angew Chem Int Ed* **2012**, *51*, 7812.
- (75) Muñoz-Bonilla, A.; León, O.; Cerrada, M. L.; Rodríguez-Hernández, J.; Sánchez-Chaves, M.; Fernández-García, M. *J Polym Sci A Polym Chem* **2012**, *50*, 2565.
- (76) Muñoz-Bonilla, A.; Bordegé, V.; León, O.; Cuervo-Rodríguez, R.; Sánchez-Chaves, M.; Fernández-García, M. *Eur Polym J* **2012**, *48*, 963.
- (77) Jones, M. W.; Richards, S.-J.; Haddleton, D. M.; Gibson, M. I. *Polym Chem* **2013**, *4*, 717.
- (78) Huynh, V. T.; Chen, G.; Souza, P. d.; Stenzel, M. H. *Biomacromolecules* **2011**, *12*, 1738.
- (79) Huynh, V. T.; Quek, J. Y.; de Souza, P. L.; Stenzel, M. H. *Biomacromolecules* **2012**, *13*, 1010.
- (80) Ahmed, M.; Mamba, S.; Yang, X.-H.; Darkwa, J.; Kumar, P.; Narain, R. *Bioconj Chem* **2013**, *24*, 979.
- (81) Becer, C. R.; Gibson, M. I.; Geng, J.; Ilyas, R.; Wallis, R.; Mitchell, D. A.; Haddleton, D. M. *J Am Chem Soc* **2010**, *132*, 15130.
- (82) Nagatsuka, T.; Uzawa, H.; Sato, K.; Ohsawa, I.; Seto, Y.; Nishida, Y. *ACS Appl Mater Interfaces* **2012**, *4*, 832.
- (83) Meldal, M.; Tornøe, C. W. *Chem Rev* **2008**, *108*, 2952.
- (84) Lutz, J.-F. *Angew Chem Int Ed* **2007**, *46*, 1018.
- (85) Fournier, D.; Hoogenboom, R.; Schubert, U. S. *Chem Soc Rev* **2007**, *36*, 1369.
- (86) Semsarilar, M.; Ladmiral, V.; Perrier, S. b. *Macromolecules* **2010**, *43*, 1438.
- (87) Xiao, C.; Zhao, C.; He, P.; Tang, Z.; Chen, X.; Jing, X. *Macromol Rapid Commun* **2010**, *31*, 991.
- (88) Xu, N.; Wang, R.; Du, F.-S.; Li, Z.-C. *J Polym Sci A Polym Chem* **2009**, *47*, 3583.
- (89) Gauthier, M. A.; Gibson, M. I.; Klok, H.-A. *Angew Chem Int Ed* **2009**, *48*, 48.
- (90) Tsarevsky, N. V.; Bencherif, S. A.; Matyjaszewski, K. *Macromolecules* **2007**, *40*, 4439.
- (91) Yuan, Y.-Y.; Du, Q.; Wang, Y.-C.; Wang, J. *Macromolecules* **2010**, *43*, 1739.
- (92) Chen, Y. *Macromolecules* **2012**, *45*, 2619.

- (93) McEwan, K. A.; Slavin, S.; Tunnah, E.; Haddleton, D. M. *Polym Chem* **2013**, 4, 2608.
- (94) Li, G.-Z.; Randev, R. K.; Soeriyadi, A. H.; Rees, G.; Boyer, C.; Tong, Z.; Davis, T. P.; Becer, C. R.; Haddleton, D. M. *Polym Chem* **2010**, 1, 1196.
- (95) Galonic, D. P.; Gin, D. Y. *Nature* **2007**, 446, 1000.
- (96) Scanlan, C. N.; Offer, J.; Zitzmann, N.; Dwek, R. A. *Nature* **2007**, 446, 1038.
- (97) Stern, R.; Jedrzejewski, M. J. *Chem Rev* **2008**, 108, 5061.
- (98) Finkelstein, J. *Nature* **2007**, 446, 999.
- (99) Zhu, X.; Schmidt, R. R. *Angew Chem Int Ed* **2009**, 48, 1900.
- (100) Paulsen, H. *Angew Chem Int Ed* **1982**, 21, 155.
- (101) Schmidt, R. R. *Angew Chem Int Ed* **1986**, 25, 212.
- (102) Plante, O. J.; Palmacci, E. R.; Seeberger, P. H. *Science* **2001**, 291, 1523.
- (103) Sears, P.; Wong, C.-H. *Science* **2001**, 291, 2344.
- (104) Seeberger, P. H.; Werz, D. B. *Nature* **2007**, 446, 1046.
- (105) Fittig, R. *Berichte der deutschen chemischen Gesellschaft* **1893**, 26, 40.
- (106) Fischer, E. *Berichte der deutschen chemischen Gesellschaft* **1895**, 28, 1145.
- (107) von Rybinski, W.; Hill, K. *Angew Chem Int Ed* **1998**, 37, 1328.
- (108) Heard, D. D.; Barker, R. *J Org Chem* **1968**, 33, 740.
- (109) Roy, B.; Mukhopadhyay, B. *Tetrahedron Lett* **2007**, 48, 3783.
- (110) Mukhopadhyay, B.; Russell, D. A.; Field, R. A. *Carbohydr Res* **2005**, 340, 1075.
- (111) Tiwari, P.; Misra, A. K. *Tetrahedron Lett* **2006**, 47, 3573.
- (112) Li, G.-Z.; Randev, R. K.; Soeriyadi, A. H.; Rees, G.; Boyer, C.; Tong, Z.; Davis, T. P.; Becer, C. R.; Haddleton, D. M. *Polym. Chem.* **2010**, 1, 1196.
- (113) Soeriyadi, A. H.; Li, G.-Z.; Slavin, S.; Jones, M. W.; Amos, C. M.; Becer, C. R.; Whittaker, M. R.; Haddleton, D. M.; Boyer, C.; Davis, T. P. *Polym. Chem.* **2011**, 2, 815.
- (114) Harvison, M. A.; Davis, T. P.; Lowe, A. B. *Polym. Chem.* **2011**, 2, 1347.
- (115) Behrens, C. H.; Sharpless, K. B. *J. Org. Chem.* **1985**, 50, 5696.
- (116) Fringuelli, F.; Pizzo, F.; Tortoioli, S.; Vaccaro, L. *J. Org. Chem.* **2003**, 68, 8248.
- (117) Sumerlin, B. S.; Tsarevsky, N. V.; Louche, G.; Lee, R. Y.; Matyjaszewski, K. *Macromolecules* **2005**, 38, 7540.
- (118) Heard, D. D.; Barker, R. *J. Org. Chem.* **1968**, 33, 740.
- (119) Capon, B. *Chem. Rev.* **1969**, 69, 407.
- (120) Ferrier, R. J.; Hatton, L. R. *Carbohydr. Res.* **1968**, 6, 75.
- (121) Roy, B.; Mukhopadhyay, B. *Tetrahedron Lett.* **2007**, 48, 3783.
- (122) Mandal, S.; Gaunial, H. M.; Pramanik, K.; Mukhopadhyay, B. *J. Org. Chem.* **2007**, 72, 9753.
- (123) Zhang, Q.; Slavin, S.; Jones, M. W.; Haddleton, A. J.; Haddleton, D. M. *Polym Chem* **2012**, 3, 1016.
- (124) Scates, B. A.; Lashbrook, B. L.; Chastain, B. C.; Tominaga, K.; Elliott, B. T.; Theising, N. J.; Baker, T. A.; Fitch, R. W. *Bioorg. Med. Chem.* **2008**, 16, 10295.
- (125) Geijtenbeek, T. B. H.; Kwon, D. S.; Torensma, R.; van Vliet, S. J.; van Duijnhoven, G. C. F.; Middel, J.; Cornelissen, I. L. M. H. A.; Nottet, H. S. L. M.; KewalRamani, V. N.; Littman, D. R.; Figdor, C. G.; van Kooyk, Y. *Cell* **2000**, 100, 587.
- (126) Marzi, A.; Gramberg, T.; Simmons, G.; Möller, P.; Rennekamp, A. J.; Krumbiegel, M.; Geier, M.; Eisemann, J.; Turza, N.; Saunier, B.; Steinkasserer, A.; Becker, S.; Bates, P.; Hofmann, H.; Pöhlmann, S. *J Virol* **2004**, 78, 12090.

- (127) Balzarini, J. *Antiviral Res* **2006**, 71, 237.
- (128) François, K. O.; Balzarini, J. *Med Res Rev* **2012**, 32, 349.
- (129) Toone, E. J. *Curr Opin Struct Biol* **1994**, 4, 719.
- (130) Ambrosi, M.; Cameron, N. R.; Davis, B. G. *Org Biomol Chem* **2005**, 3, 1593.
- (131) Ke, C.; Destecroix, H.; Crump, M. P.; Davis, A. P. *Nat Chem* **2012**, 4, 718.
- (132) Borrok, M. J.; Kiessling, L. L. *J Am Chem Soc* **2007**, 129, 12780.
- (133) Mahalingam, A.; Geonnotti, A. R.; Balzarini, J.; Kiser, P. F. *Mol Pharm* **2011**, 8, 2465.
- (134) Doores, K. J.; Fulton, Z.; Hong, V.; Patel, M. K.; Scanlan, C. N.; Wormald, M. R.; Finn, M. G.; Burton, D. R.; Wilson, I. A.; Davis, B. G. *Proc Nat Acad Sci USA* **2010**, 107, 17107.
- (135) Gestwicki, J. E.; Cairo, C. W.; Strong, L. E.; Oetjen, K. A.; Kiessling, L. L. *J Am Chem Soc* **2002**, 124, 14922.
- (136) Pieters, R. J. *Org Biomol Chem* **2009**, 7, 2013.
- (137) Ponader, D.; Wojcik, F.; Beceren-Braun, F.; Dervede, J.; Hartmann, L. *Biomacromolecules* **2012**, 13, 1845.
- (138) Miura, Y. *Polym J* **2012**, 44, 679.
- (139) Feizi, T.; Chai, W. *Nat Rev Mol Cell Biol* **2004**, 5, 582.
- (140) Gabius, H. J. *Naturwissenschaften* **2000**, 87, 108.
- (141) Gabius, H.-J.; Siebert, H.-C.; André, S.; Jiménez-Barbero, J.; Rüdiger, H. *Chembiochem* **2004**, 5, 740.
- (142) Badi, N.; Lutz, J.-F. *Chem Soc Rev* **2009**, 38, 3383.
- (143) Merrifield, R. B. *Angew Chem Int Ed* **1985**, 24, 799.
- (144) Seeberger, P. H. *Chem Soc Rev* **2008**, 37, 19.
- (145) Połowiński, S. *Prog Polym Sci* **2002**, 27, 537.
- (146) Ida, S.; Terashima, T.; Ouchi, M.; Sawamoto, M. *J Am Chem Soc* **2009**, 131, 10808.
- (147) Lutz, J.-F. *Polym Chem* **2010**, 1, 55.
- (148) Kolb, H. C.; Finn, M. G.; Sharpless, K. B. *Angew Chem Int Ed* **2001**, 40, 2004.
- (149) Becer, C. R.; Hoogenboom, R.; Schubert, U. S. *Angew Chem Int Ed* **2009**, 48, 4900.
- (150) Rosen, B. M.; Percec, V. *Chem. Rev.* **2009**, 109, 5069.
- (151) Matyjaszewski, K.; Xia, J. *Chem. Rev.* **2001**, 101, 2921.
- (152) Hibi, Y.; Tokuoka, S.; Terashima, T.; Ouchi, M.; Sawamoto, M. *Polym Chem* **2011**, 2, 341.
- (153) Schmidt, B. V. K. J.; Fechler, N.; Falkenhagen, J.; Lutz, J.-F. *Nature Chemistry* **2011**, 3, 234.
- (154) Lutz, J.-F. *Nat Chem* **2010**, 2, 84.
- (155) McHale, R.; Patterson, J. P.; Zetterlund, P. B.; O'Reilly, R. K. *Nat Chem* **2012**, 4, 491.
- (156) Soeriyadi, A. H.; Boyer, C.; Nyström, F.; Zetterlund, P. B.; Whittaker, M. R. *Journal of the American Chemical Society* **2011**, 133, 11128.
- (157) Nakatani, K.; Ogura, Y.; Koda, Y.; Terashima, T.; Sawamoto, M. *J Am Chem Soc* **2012**, 134, 4373.
- (158) Nguyen, N. H.; Kulis, J.; Sun, H.-J.; Jia, Z.; van Beusekom, B.; Levere, M. E.; Wilson, D. A.; Monteiro, M. J.; Percec, V. *Polym. Chem.* **2013**, 4, 144.
- (159) Levere, M. E.; Willoughby, I.; O'Donohue, S.; de Cuendias, A.; Grice, A. J.; Fidge, C.; Becer, C. R.; Haddleton, D. M. *Polym Chem-Uk* **2010**, 1, 1086.
- (160) Dai, X.-H.; Dong, C.-M. *J Polym Sci A Polym Chem* **2008**, 46, 817.

- (161) Mateescu, A.; Ye, J.; Narain, R.; Vamvakaki, M. *Soft Matter* **2009**, *5*, 1621.
- (162) Mizukami, K.; Takakura, H.; Matsunaga, T.; Kitano, H. *Colloids and Surfaces B: Biointerfaces* **2008**, *66*, 110.
- (163) Hetzer, M.; Chen, G.; Barner-Kowollik, C.; Stenzel, M. H. *Macromol Biosci* **2010**, *10*, 119.
- (164) Levere, M. E.; Willoughby, I.; O'Donohue, S.; Wright, P. M.; Grice, A. J.; Fidge, C.; Remzi Becer, C.; Haddleton, D. M. *J Polym Sci A Polym Chem* **2011**, *49*, 1753.
- (165) Boyer, C.; Soeriyadi, A. H.; Zetterlund, P. B.; Whittaker, M. R. *Macromolecules* **2011**, *44*, 8028.
- (166) Boyer, C.; Derveaux, A.; Zetterlund, P. B.; Whittaker, M. R. *Polym Chem* **2012**, *3*, 117.
- (167) Lee, Y. C.; Lee, R. T. *Acc Chem Res* **1995**, *28*, 321.
- (168) Sigal, G. B.; Mammen, M.; Dahmann, G.; Whitesides, G. M. *J Am Chem Soc* **1996**, *118*, 3789.
- (169) Kiessling, L. L.; Pohl, N. L. *Chemistry & Biology* **1996**, *3*, 71.
- (170) Cairo, C. W.; Gestwicki, J. E.; Kanai, M.; Kiessling, L. L. *J Am Chem Soc* **2002**, *124*, 1615.
- (171) Roy, R.; Page, D.; Perez, S. F.; Bencomo, V. V. *Glycoconj J* **1998**, *15*, 251.
- (172) Jones, M. W.; Strickland, R. A.; Schumacher, F. F.; Caddick, S.; Baker, J. R.; Gibson, M. I.; Haddleton, D. M. *J Am Chem Soc* **2011**, *134*, 1847.
- (173) Jones, M. W.; Strickland, R. A.; Schumacher, F. F.; Caddick, S.; Baker, J. R.; Gibson, M. I.; Haddleton, D. M. *Chem Comm* **2012**, *48*, 4064.
- (174) Mitchell, D. A.; Fadden, A. J.; Drickamer, K. *J Biol Chem* **2001**, *276*, 28939.
- (175) Guo, Y.; Feinberg, H.; Conroy, E.; Mitchell, D. A.; Alvarez, R.; Blixt, O.; Taylor, M. E.; Weis, W. I.; Drickamer, K. *Nat. Struct. Mol. Biol.* **2004**, *11*, 591.
- (176) Zhang, Q.; Collins, J.; Anastasaki, A.; Wallis, R.; Mitchell, D. A.; Becer, C. R.; Haddleton, D. M. *Angew Chem Int Ed* **2013**, *52*, 4435.
- (177) Ciampolini, M.; Nardi, N. *Inorg Chem* **1966**, *5*, 41.
- (178) Queffelec, J.; Gaynor, S. G.; Matyjaszewski, K. *Macromolecules* **2000**, *33*, 8629.
- (179) Mantovani, G.; Ladmiral, V.; Tao, L.; Haddleton, D. M. *Chem Comm* **2005**, 2089.
- (180) Feinberg, H.; Mitchell, D. A.; Drickamer, K.; Weis, W. I. *Science* **2001**, *294*, 2163.
- (181) Pieters, R. J. *Med Res Rev* **2007**, *27*, 796.
- (182) Fais, M.; Karamanska, R.; Allman, S.; Fairhurst, S. A.; Innocenti, P.; Fairbanks, A. J.; Donohoe, T. J.; Davis, B. G.; Russell, D. A.; Field, R. A. *Chem Sci* **2011**, *2*, 1952.
- (183) Lundquist, J. J.; Toone, E. J. *Chem Rev* **2002**, *102*, 555.
- (184) André, S.; Kaltner, H.; Furuike, T.; Nishimura, S.-I.; Gabius, H.-J. *Bioconj Chem* **2003**, *15*, 87.
- (185) Gómez-García, M.; Benito, J. M.; Rodríguez-Lucena, D.; Yu, J.-X.; Chmurski, K.; Ortiz Mellet, C.; Gutiérrez Gallego, R.; Maestre, A.; Defaye, J.; García Fernández, J. M. *J Am Chem Soc* **2005**, *127*, 7970.
- (186) Smiljanic, N.; Moreau, V.; Yockot, D.; Benito, J. M.; García Fernández, J. M.; Djedaïni-Pilard, F. *Angew Chem Int Ed* **2006**, *45*, 5465.
- (187) García-López, J. J.; Santoyo-González, F.; Vargas-Berenguel, A.; Giménez-Martínez, J. J. *Chemistry – A European Journal* **1999**, *5*, 1775.
- (188) Fulton, D. A.; Stoddart, J. F. *Org Lett* **2000**, *2*, 1113.

- (189) Carpenter, C.; Nepogodiev, S. A. *Eur. J. Org. Chem.* **2005**, 3286.
- (190) Gómez-García, M.; Benito, J. M.; Butera, A. P.; Mellet, C. O.; Fernández, J. M. G.; Blanco, J. L. J. *J Org Chem* **2011**, 77, 1273.
- (191) Ohno, K.; Wong, B.; Haddleton, D. M. *J Polym Sci A Polym Chem* **2001**, 39, 2206.
- (192) Stenzel, M. H.; Davis, T. P. *J Polym Sci A Polym Chem* **2002**, 40, 4498.
- (193) Kakuchi, T.; Narumi, A.; Miura, Y.; Matsuya, S.; Sugimoto, N.; Satoh, T.; Kaga, H. *Macromolecules* **2003**, 36, 3909.
- (194) Zhang, L.; Stenzel, M. H. *Aust J Chem* **2009**, 62, 813.
- (195) Hoogenboom, R.; Moore, B. C.; Schubert, U. S. *Chem Comm* **2006**, 4010.
- (196) Srinivasachari, S.; Fichter, K. M.; Reineke, T. M. *J Am Chem Soc* **2008**, 130, 4618.
- (197) Zhang, Q.; Li, G.-Z.; Becer, C. R.; Haddleton, D. M. *Chem Comm* **2012**, 48, 8063.
- (198) Chmurski, K.; Defaye, J. *Supramol Chem* **2000**, 12, 221.
- (199) Li, J.; Xiao, H. *Tetrahedron Lett* **2005**, 46, 2227.
- (200) Ge, Z.; Xu, J.; Hu, J.; Zhang, Y.; Liu, S. *Soft Matter* **2009**, 5, 3932.
- (201) Meier, M. A. R.; Gohy, J.-F.; Fustin, C.-A.; Schubert, U. S. *J Am Chem Soc* **2004**, 126, 11517.
- (202) Schramm, O. G.; Meier, M. A. R.; Hoogenboom, R.; van Erp, H. P.; Gohy, J.-F.; Schubert, U. S. *Soft Matter* **2009**, 5, 1662.
- (203) Xia, Y.; Yin, X.; Burke, N. A. D.; Stoeber, H. D. H. *Macromolecules* **2005**, 38, 5937.
- (204) Soeriyadi, A. H.; Boyer, C.; Nyström, F.; Zetterlund, P. B.; Whittaker, M. R. *J Am Chem Soc* **2011**, 133, 11128.
- (205) Weis, W. I.; Drickamer, K.; Hendrickson, W. A. *Nature* **1992**, 360, 127.
- (206) Wu, L.; KewalRamani, V. N. *Nat Rev Immunol* **2006**, 6, 859.
- (207) Weis, W. I.; Kahn, R.; Fourme, R.; Drickamer, K.; Hendrickson, W. A. *Science* **1991**, 254, 1608.
- (208) Menon, S.; Rosenberg, K.; Graham, S. A.; Ward, E. M.; Taylor, M. E.; Drickamer, K.; Leckband, D. E. *Proc Nat Acad Sci USA* **2009**, 106, 11524.
- (209) Calarese, D. A.; Lee, H.-K.; Huang, C.-Y.; Best, M. D.; Astronomo, R. D.; Stanfield, R. L.; Katinger, H.; Burton, D. R.; Wong, C.-H.; Wilson, I. A. *Proc Nat Acad Sci USA* **2005**, 102, 13372.
- (210) Kimler, B. F. *Cancer Res* **1980**, 40, 42.
- (211) Thiele, C.; Auerbach, D.; Jung, G.; Qiong, L.; Schneider, M.; Wenz, G. *Polym Chem* **2011**, 2, 209.
- (212) Buchanan, C. M.; Buchanan, N. L.; Edgar, K. J.; Little, J. L.; Ramsey, M. G.; Ruble, K. M.; Wachter, V. J.; Wempe, M. F. *Biomacromolecules* **2007**, 9, 305.
- (213) Cavicchioni, G. *Synth. Commun.* **1994**, 24, 2223.
- (214) Haddleton, D. M.; Jasieczek, C. B.; Hannon, M. J.; Shooter, A. J. *Macromolecules* **1997**, 30, 2190.
- (215) Perrier, S.; Armes, S. P.; Wang, X. S.; Malet, F.; Haddleton, D. M. *J. Polym. Sci., Part A: Polym. Chem.* **2001**, 39, 1696.
- (216) Perrier, S.; Haddleton, D. M. *Macromol Symp* **2002**, 182, 261.
- (217) Koten, G. V.; Vrieze, K. In *Adv. Organomet. Chem.*; Stone, F. G. A., Robert, W., Eds.; Academic Press: : 1982; Vol. Volume 21, p 151.
- (218) Xia, J.; Matyjaszewski, K. *Macromolecules* **1999**, 32, 2434.
- (219) Percec, V.; Barboiu, B. *Macromolecules* **1995**, 28, 7970.

- (220) Kato, M.; Kamigaito, M.; Sawamoto, M.; Higashimura, T. *Macromolecules* **1995**, 28, 1721.
- (221) Tsarevsky, N. V.; Braunecker, W. A.; Matyjaszewski, K. *J. Organomet. Chem.* **2007**, 692, 3212.
- (222) Tang, W.; Matyjaszewski, K. *Macromolecules* **2006**, 39, 4953.
- (223) Wang, Y.; Kwak, Y.; Buback, J.; Buback, M.; Matyjaszewski, K. *ACS Macro Letters* **2012**, 1, 1367.
- (224) Rosen, B. M.; Jiang, X.; Wilson, C. J.; Nguyen, N. H.; Monteiro, M. J.; Percec, V. *J. Polym. Sci., Part A: Polym. Chem.* **2009**, 47, 5606.
- (225) Rosen, B. M.; Percec, V. *J. Polym. Sci., Part A: Polym. Chem.* **2007**, 45, 4950.
- (226) Rademacher, J. T.; Baum, M.; Pallack, M. E.; Brittain, W. J.; Simonsick, W. J. *Macromolecules* **1999**, 33, 284.
- (227) Heredia, K. L.; Bontempo, D.; Ly, T.; Byers, J. T.; Halstenberg, S.; Maynard, H. D. *J. Am. Chem. Soc.* **2005**, 127, 16955.
- (228) Masci, G.; Giacomelli, L.; Crescenzi, V. *Macromol. Rapid Commun.* **2004**, 25, 559.
- (229) Xia, Y.; Yin, X.; Burke, N. A. D.; Stöver, H. D. H. *Macromolecules* **2005**, 38, 5937.
- (230) Xia, Y.; Burke, N. A. D.; Stöver, H. D. H. *Macromolecules* **2006**, 39, 2275.
- (231) Duan, Q.; Miura, Y.; Narumi, A.; Shen, X.; Sato, S.-I.; Satoh, T.; Kakuchi, T. *J. Polym. Sci., Part A: Polym. Chem.* **2006**, 44, 1117.
- (232) Akiyama, H.; Tamaoki, N. *Macromolecules* **2007**, 40, 5129.
- (233) Appel, E. A.; del Barrio, J.; Loh, X. J.; Dyson, J.; Scherman, O. A. *J. Polym. Sci., Part A: Polym. Chem.* **2012**, 50, 181.
- (234) Bontempo, D.; Li, R. C.; Ly, T.; Brubaker, C. E.; Maynard, H. D. *Chem. Commun.* **2005**, 4702.
- (235) Feng, C.; Shen, Z.; Li, Y.; Gu, L.; Zhang, Y.; Lu, G.; Huang, X. *J. Polym. Sci., Part A: Polym. Chem.* **2009**, 47, 1811.
- (236) Tang, X.; Liang, X.; Yang, Q.; Fan, X.; Shen, Z.; Zhou, Q. *J. Polym. Sci., Part A: Polym. Chem.* **2009**, 47, 4420.
- (237) Millard, P.-E.; Mougin Nathalie, C.; Böker, A.; Müller Axel, H. E. In *Controlled/Living Radical Polymerization: Progress in ATRP*; American Chemical Society: 2009; Vol. 1023, p 127.
- (238) Vachaudes, M.; D'hooge, D. R.; Socka, M.; Libiszowski, J.; Coulembier, O.; Reyniers, M. F.; Duda, A.; Marin, G. B.; Dubois, P. *React. Funct. Polym.* **2013**, 73, 484.
- (239) Bosman, A. W.; Vestberg, R.; Heumann, A.; Fréchet, J. M. J.; Hawker, C. J. *J. Am. Chem. Soc.* **2003**, 125, 715.
- (240) Savariar, E. N.; Thayumanavan, S. *J. Polym. Sci., Part A: Polym. Chem.* **2004**, 42, 6340.
- (241) Moughton, A. O.; Patterson, J. P.; O'Reilly, R. K. *Chem. Commun.* **2011**, 47, 355.
- (242) Moughton, A. O.; O'Reilly, R. K. *Chem. Commun.* **2010**, 46, 1091.
- (243) Percec, V.; Popov, A. V.; Ramirez-Castillo, E.; Weichold, O. *J. Polym. Sci., Part A: Polym. Chem.* **2003**, 41, 3283.
- (244) Levere, M. E.; Nguyen, N. H.; Leng, X.; Percec, V. *Polym. Chem.* **2013**, 4, 1635.
- (245) Nguyen, N. H.; Percec, V. *J. Polym. Sci., Part A: Polym. Chem.* **2011**, 49, 4227.

- (246) Nguyen, N. H.; Rosen, B. M.; Jiang, X.; Fleischmann, S.; Percec, V. *J. Polym. Sci., Part A: Polym. Chem.* **2009**, *47*, 5577.
- (247) Lligadas, G.; Rosen, B. M.; Monteiro, M. J.; Percec, V. *Macromolecules* **2008**, *41*, 8360.
- (248) Lligadas, G.; Percec, V. *J. Polym. Sci., Part A: Polym. Chem.* **2008**, *46*, 6880.
- (249) Nguyen, N. H.; Sun, H.-J.; Levere, M. E.; Fleischmann, S.; Percec, V. *Polym. Chem.* **2013**, *4*, 1328.
- (250) Nguyen, N. H.; Rosen, B. M.; Percec, V. *J. Polym. Sci., Part A: Polym. Chem.* **2010**, *48*, 1752.
- (251) Levere, M. E.; Nguyen, N. H.; Sun, H.-J.; Percec, V. *Polym. Chem.* **2013**, *4*, 686.
- (252) Jiang, X.; Rosen, B. M.; Percec, V. *J. Polym. Sci., Part A: Polym. Chem.* **2010**, *48*, 2716.
- (253) Ciavatta, L.; Ferri, D.; Palombari, R. *J. Inorg. Nucl. Chem.* **1980**, *42*, 593.
- (254) Navon, N.; Cohen, H.; Paoletti, P.; Valtancoli, B.; Bencini, A.; Meyerstein, D. *Industrial & Engineering Chemistry Research* **2000**, *39*, 3536.
- (255) Thaler, F.; Hubbard, C. D.; Heinemann, F. W.; van Eldik, R.; Schindler, S.; Fábíán, I.; Dittler-Klingemann, A. M.; Hahn, F. E.; Orvig, C. *Inorg. Chem.* **1998**, *37*, 4022.
- (256) Tsarevsky, N. V.; Pintauer, T.; Matyjaszewski, K. *Macromolecules* **2004**, *37*, 9768.
- (257) Min, K.; Gao, H.; Matyjaszewski, K. *J. Am. Chem. Soc.* **2005**, *127*, 3825.
- (258) Li, W.; Matyjaszewski, K. *Polym. Chem.* **2012**, *3*, 1813.
- (259) Zumreoglu-Karan, B. *Coord. Chem. Rev.* **2006**, *250*, 2295.
- (260) Ünaleroğlu, C.; Mert, Y.; Zümreoğlu-Karan, B. *Synth. React. Inorg. Met.-Org. Chem.* **2001**, *31*, 1531.
- (261) Yamamoto, Y.; Ishizu, K.; Shimizu, Y. *Chem Lett* **1977**, *6*, 735.
- (262) Teodorescu, M.; Matyjaszewski, K. *Macromolecules* **1999**, *32*, 4826.
- (263) Wever, D. A. Z.; Raffa, P.; Picchioni, F.; Broekhuis, A. A. *Macromolecules* **2012**, *45*, 4040.
- (264) Krebs, H. A. *Annu Rev Biochem* **1950**, *19*, 409.
- (265) Mårtensson, E.; Raal, A.; Svennerholm, L. *Biochim Biophys Acta* **1958**, *30*, 124.
- (266) Zhang, Q.; Wilson, P.; Li, Z.; McHale, R.; Godfrey, J.; Anastasaki, A.; Waldron, C.; Haddleton, D. M. *J Am Chem Soc* **2013**, *135*, 7355.
- (267) Schatz, C.; Lecommandoux, S. *Macromol Rapid Commun* **2010**, *31*, 1664.
- (268) Luo, Y.; Liu, L.; Wang, X.; Shi, H.; Lv, W.; Li, J. *Soft Matter* **2012**, *8*, 1634.
- (269) Pasparakis, G.; Alexander, C. *Angew Chem Int Ed* **2008**, *47*, 4847.
- (270) Li, Z.-C.; Liang, Y.-Z.; Chen, G.-Q.; Li, F.-M. *Macromol Rapid Commun* **2000**, *21*, 375.
- (271) Suriano, F.; Coulembier, O.; Degée, P.; Dubois, P. *J Polym Sci A Polym Chem* **2008**, *46*, 3662.
- (272) Shi, H.; Liu, L.; Wang, X.; Li, J. *Polym Chem* **2012**, *3*, 1182.
- (273) Li, L.; Shu, X.; Zhu, J. *Polymer* **2012**, *53*, 5010.
- (274) Xia, S.; Yang, B.; Li, G.; Zhu, X.; Wang, A.; Zhu, J. *Polym Chem* **2011**, *2*, 2356.
- (275) Tsarevsky, N. V.; Matyjaszewski, K. *J Polym Sci A Polym Chem* **2006**, *44*, 5098.
- (276) Ting, S. R. S.; Min, E. H.; Zetterlund, P. B.; Stenzel, M. H. *Macromolecules* **2010**, *43*, 5211.

- (277) Haddleton, D. M.; Crossman, M. C.; Dana, B. H.; Duncalf, D. J.; Heming, A. M.; Kukulj, D.; Shooter, A. J. *Macromolecules* **1999**, *32*, 2110.
- (278) Wang, Y.; Zhong, M.; Zhu, W.; Peng, C.-H.; Zhang, Y.; Konkolewicz, D.; Bortolamei, N.; Isse, A. A.; Gennaro, A.; Matyjaszewski, K. *Macromolecules* **2013**, *46*, 3793.
- (279) Zhong, M.; Wang, Y.; Krys, P.; Konkolewicz, D.; Matyjaszewski, K. *Macromolecules* **2013**, *46*, 3816.
- (280) Peng, C.-H.; Zhong, M.; Wang, Y.; Kwak, Y.; Zhang, Y.; Zhu, W.; Tonge, M.; Buback, J.; Park, S.; Krys, P.; Konkolewicz, D.; Gennaro, A.; Matyjaszewski, K. *Macromolecules* **2013**, *46*, 3803.
- (281) Horn, M.; Matyjaszewski, K. *Macromolecules* **2013**, *46*, 3350.